University of Warsaw

Faculty of Physics

Doctoral Thesis

Role of gravitational interactions during reheating and dark matter production

---

Author:
Anna Socha

Supervisor:
Prof. Bohdan Grządkowski

June 10, 2023

Abstract

Role of gravitational interactions during reheating and dark matter production

Anna Socha

This work focuses on the minimal model of dark matter, assuming it consists of particles interacting solely through gravity. The considered scenario involves massive vector particles as candidates for dark matter. Such a hypothesis is quite restrictive and, in this sense, extreme, but on the other hand, it captivates with its simplicity and universality. What makes this scenario so compelling is its inevitability and complementarity with cosmological models of the early Universe. Its attractiveness is also evidenced by the rich phenomenology considered in this work. The origin of purely gravitational dark matter is related to gravitational effects occurring in the very early Universe. Hence, its genesis and dynamics are attributable to how the primordial Universe transformed from an inflationary to a radiation-dominated phase.

This thesis aims to shed some light on the unknown physics of the early Universe. We explore the possibility of a non-standard cosmological history by postulating the existence of a non-instantaneous reheating phase. In particular, we focus on the perturbative reheating model induced by direct inflaton coupling to the visible sector or as a result of indirect interactions of gravitational origin. The production of the Standard Model radiation is discussed by considering a time-varying inflaton decay rate, which exhibits a power-law dependence on the scale factor. Such behavior could reflect the non-standard form of the inflaton potential during reheating and/or might be generated by the kinematic effects. The time-dependent inflaton decay width, in general, meaningfully affects the production of the visible sector and thus alters the thermal bath's evolution. In addition, it might also change the duration of the reheating phase. We also study the implications of the non-standard reheating scenario for primordial gravitational waves, showing that the presence of a stiff epoch before the Big Bang nucleosynthesis era might enhance their spectrum. Finally, we use this effect to explore the possibility of probing inflaton-matter couplings in future gravitational wave detectors.

Three different mechanisms of dark matter creation are considered in this work. Namely, we investigate purely gravitational particle production in the expanding Universe, gravitational scattering through graviton exchange in the inflaton background, and the gravitational freeze-in from the thermal bath. Limitations and necessary conditions for their occurrence are discussed. We also determine the parameter space in which each of these mechanisms, individually, as well as all of them combined, saturate the observed amount of dark matter. The presented analysis justifies gravitational production as a viable mechanism for the vector dark matter in a wide range of dark matter mass. Moreover, our results apply to various possible models of the early Universe with non-standard cosmology, demonstrating that reheating dynamics play a crucial role in the gravitational production of dark vectors and cannot be neglected in calculations of their present abundance.

Streszczenie

Role of gravitational interactions during reheating and dark matter production

Anna Socha

W niniejszej rozprawie omówiono minimalny scenariusz ciemnej materii, zakładając, że składa się ona z cząstek posiadających wyłącznie grawitacyjne oddziaływania. Rozważany scenariusz dotyczy masywnych cząstek wektorowych będących kandydatem na ciemną materię. Taka hipoteza jest dość restrykcyjna i w tym sensie ekstremalna, ale z drugiej strony urzeka swoją prostotą i uniwersalnością. To, co czyni ten scenariusz tak interesującym, to jego nieuchronność i komplementarność z kosmologicznymi modelami wczesnego Wszechświata. O jego atrakcyjności świadczy również bogata fenomenologia rozważana w tej pracy. Pochodzenie czysto grawitacyjnej ciemnej materii związane jest z efektami grawitacyjnymi występującymi we wczesnym Wszechświecie. Stąd też jej geneza i ewolucja są odzwierciedleniem dynamiki pierwotnego Wszechświata, a w szczególności tego, w jaki sposób przekształcił się on z fazy inflacyjnej do epoki dominacji promieniowania.

W rozprawie analizowano niestandardowy scenariusz kosmologiczny, zakładając, że okres dominacji promieniowania został poprzedzony epoką "podgrzania" (ang. *reheating*). Szczególną uwagę poświęcono modelowi epoki podgrzania, w którym proces ten zachodzi w wyniku perturbacyjnych bezpośrednich oddziaływań pola inflatonu z materią widzialną, jak również jako wynik oddziaływań grawitacyjnych. Omówiono produkcję cząstek Modelu Standardowego, zakładając, że oddziaływania między tymi ostatnimi a klasycznym polem inflatonu parametryzowane są zależną od czasu szerokością rozpadu. Takie zachowanie może wynikać z niestandardowej postaci potencjału inflatonu podczas fazy podgrzania i/lub być generowane przez efekty kinematyczne, związane z niezerową masą cząstek w stanie końcowym. Zademonstrowano, że zależność szerokości rozpadu od czasu istotnie wpływa na produkcję sektora widzialnego i tym samym przyczynia się do modyfikacji jego ewolucji w okresie podgrzania. Ponadto pokazano, że efekt ten może również zmienić czas trwania epoki podgrzania. Dodatkowo omówione zostały również konsekwencje niestandardowego scenariusza podgrzania w kontekście pierwotnych fal grawitacyjnych. W szczególności pokazano, że obecność wczesnej epoki podgrzania w pewnych przypadkach może wzmocnić widmo fal grawitacyjnych o pierwotnej genezie. Tę obserwację wykorzystano do zbadania możliwości analizowania sprzężeń inflatonu z materią w przyszłych detektorach fal grawitacyjnych.

W tej pracy rozważano trzy różne mechanizmy produkcji ciemnej materii. Zbadano czysto grawitacyjną produkcję cząstek w rozszerzającym się Wszechświecie, rozpraszanie grawitacyjne w tle klasycznego pola inflatonu oraz grawitacyjną anihilację cząstek Modelu Standardowego. Omówiono ograniczenia i warunki konieczne do wystąpienia powyższych procesów. Określono również przestrzeń parametrów, w której każdy z tych mechanizmów, zarówno indywidualnie, jak i w połączeniu, odtwarza obserwowaną ilość ciemnej materii. Uzyskane wyniki mają zastosowanie w różnych modelach kosmologicznych i jednoznacznie wskazują, że dynamika okresu podgrzania odgrywa kluczową rolę w grawitacyjnej produkcji wektorowej ciemnej materii.

Acknowledgements

First and foremost, I would like to express profound gratitude to my advisor, prof. Bohdan Grządkowski for his invaluable guidance and long-term mentoring throughout my master's and doctoral studies. When six years ago he proposed the topic for my master's thesis, I never imagined what would arise from an innocent statement: *Let us suppose that dark matter interacts only gravitationally...* I greatly appreciate his insightful feedback, understanding and unwavering support. I am sincerely grateful for the numerous opportunities he provided me, including collaborations, conference attendance, and networking connections. My supervisor taught me three important things: asking difficult questions, finding answers, and tunneling through the hole in the fence. I am so lucky to be your student, Professor. Thank you so much for everything!

Furthermore, I would like to thank my collaborators, especially Aqeel Ahmed and Basabendu Barman, for many fruitful discussions, your patience with my cascade of questions and remarks, and our fantastic common work. I hope that we can do much more in the future!

Special thanks go to my scientific *partner in crime* Michał Iglicki. I greatly enjoyed our (not only) scientific discussions. I really appreciate that you always find some answer to all my silly questions.

Dziękuję również rodzicom i babci, która ciągle dopytywała się *"Czy dużo mam jeszcze nauki?"* i *"Czy jadłam śniadanie?"*.

Finally, the biggest thanks go to the love of my life, M. and P.B. Without you, all of this would be meaningless, and this work would never have come into existence (and it would never look the way it does, even though you hate LaTeX).

List of publications

- [1] B. Barman, A. Ghoshal, B. Grzadkowski and **A. Socha**, *Measuring Inflaton Couplings via Primordial Gravitational Waves*, [2305.00027].
- [2] A. Ahmed, B. Grzadkowski and **A. Socha**, *Higgs boson induced reheating and ultraviolet frozen-in dark matter*, JHEP 02 (2023) 196 [2207.11218].
- [3] A. Ahmed, B. Grzadkowski and **A. Socha**, *Implications of time-dependent inflaton decay on reheating and dark matter production*, Phys. Lett. B 831 (2022) 137201 [2111.06065].
- [4] A. Ahmed, B. Grzadkowski and **A. Socha**, *Gravitational production of vector dark matter*, JHEP 08 (2020) 059 [2005.01766].

Conference Proceedings

- [5] A. Ahmed, B. Grzadkowski and **A. Socha**, *Higgs Boson-Induced Reheating and Dark Matter Production*, Symmetry 14 (2022) 306.
- [6] A. Ahmed, B. Grzadkowski and **A. Socha**, *Production of Purely Gravitational Vector Dark Matter*, Acta Phys. Polon. B 50 (2019) 1809.

Contents

List of Figures

List of Tables

List of Abbreviations

AS	Anisotropic stress (tensor)
BAO	Baryon acoustic oscillations
BB	Big Bang
BBN	Big Bang Nucleosynthesis
BEq	Boltzmann equation
BSM	Beyond the Standard Model
CCR	Canonical commutation relation
CDM	Cold dark matter
CMB	Cosmic microwave background
DE	Dark energy
DM	Dark matter
dS	de-Sitter
EFT	Effective Field Theory
EoM	Equation of motion
e.o.s	Equation of state
FIMP	Feebly interacting massive particles
FLRW	Friedmann–Lemaître–Robertson–Walker
GP	Purely gravitational production
GR	General relativity
GUT	Grand unified theories
GW	Gravitational waves
HO	Harmonic oscillator
HSR	Hubble slow roll parameters
IG	Gravitational production in the inflaton background
ΛCDM	Lambda cold dark matter concordance model
MACHO	Massive compact halo objects
MD	Matter-dominated era
MOND	Modified Newtonian dynamics
SM	Standard Model of particle physics
SMG	Gravitational freeze-in from the SM bath
PBH	Primordial black holes
PGW	Primordial gravitational waves
PSR	Potential slow roll parameters
RD	Radiation-dominated era
WIMP	Weakly interacting massive particles
QCD	Quantum chromodynamics
QFT	Quantum field theory
vev	Vacuum expectation value

Conventions

Throughout this thesis, we use a mostly negative metric signature $(+1, -1, -1, -1)$, and work with natural units, i.e., $h = 1 = c$.

Chapter 1

Whispers from the Darkness

Dark Matter (DM) : *No one can see what dark matter is.* (pol. *Ciemna materia jaka jest, nikt nie widzi*). This paraphrase of a memorable "definition" of a horse (*Horse: Everyone can see what a horse is.*) from the first Polish-language encyclopedia abbreviated as "New Athens" perfectly describes our (lack of) knowledge of the dominant matter component in the Universe. The unprecedented ignorance and simplemindedness of the above description counterpose the deep truth hidden within. Namely, dark matter cannot be seen. It is not low-luminous; dark matter is rather invisible and hidden. The unseen matter is electrically neutral and thus does not interact with the electromagnetic field. Furthermore, it does not interact via strong nuclear interactions, which makes it hard to detect. Hence, to some extent, the name "dark matter" reflects doubts about the nature of the unseen matter and refers to its elusiveness.

To understand the current status of dark matter, it is instructive to summarize our knowledge. The first four sections are purely of a review nature. We begin in Sec.(1.1) with an introduction to this topic, tracing back the historical arguments leading to the concept of dark matter. Then, in Sec.(1.2), we briefly review the observational evidence for a dark sector. Next, in Sec.(1.3), we present some possible candidates, which nowadays are viewed as alternatives to best-established particle dark matter, on which we elaborate in Sec.(1.4). Here, we briefly describe the most popular scenarios. Our review is equipped with a discussion of properties and characteristic features that dark matter should possess. In section (1.5) we introduce the minimal DM model - purely gravitational dark matter. Finally, we close this chapter in Sec.(1.6) by presenting the motivation for this work.

1.1 A brief history of the dark Universe

The following four sections are based mainly on the references [14–19]. Additional in-text references are directly cited.

One of the earliest traces of invisible matter is dated to the 1600s. Soon after the publication of Newton's opus magnum *Philosophiæ Naturalis Principia Mathematica*, some natural philosophers began to speculate about the possibility of faint, dark objects, whose existence can only be inferred from their gravitational attraction of bright stars or planets. In the 1700s, John Michell and Pierre Laplace argued that some objects, called *corps obscur*, might be so massive that even light cannot escape their gravitational pull and thus is trapped by mysterious dark bodies. Nowadays, this proposal is considered the origin of the black hole concept - yet another invisible object whose existence has already been confirmed experimentally. Next, in 1846, Urbain Le Verrier and John Couch Adams explained gravitational anomalies in the motion of Uranus by proposing the presence of a new faint planet - Neptune. At that time, it became clear that the Universe is rich in eerie, undiscovered objects that do not emit light.

More modern treatment of dark matter can be traced to the beginning of the twentieth century. In 1904 Lord Kelvin proposed to treat stars as a gas of particles interacting via gravity. This approach enabled him to estimate the number of stars in our galaxy ($\sim 10^9$) and find an upper limit on the density of matter from the observed velocity dispersion of stars. In one of his Baltimore Lectures on Molecular Dynamics and the Wave Theory of Light, we can read, *"[..] Many of our stars, perhaps a great majority of them, may be dark bodies."* [20]. The very first mention of the term "dark matter" emanates from Henri Poincaré's work "The Milky Way and Theory of Gases" [21]. In his response to Lord Kelvin's idea, he explicitly used the name *"matiére obscure"* referring to dark bodies. Henri Poincaré's disagreed with Lord Kelvin, claiming that "[..] Then there is no dark matter or at least not so much as there is of shining matter". His conclusion was based on the fact that the velocity dispersion predicted by Kelvin was comparable to the observed value. Next, in 1932 Jan Oort derived an estimate for the local density of matter near the Sun and the amount of dark matter to be about half of the total density [22]. At that time, there was a belief that the unseen matter is composed of faint stars, *"nebulous or meteoric matter"*.

The first observation directly indicated the existence of *"Dunkle Materie"* was made in 1933. This German term was coined by Swiss astronomer Fritz Zwicky widely recognized as a man who first unmasked the dark side of the Universe. Zwicky studied the redshifts of various galaxy clusters. Such objects are the largest gravitationally bound systems in the Universe, containing thousands of galaxies and a hot gas emitting X-ray radiation. Zwicky found that the velocity dispersion exhibited by the Coma Cluster is significantly larger than in other galaxy clusters [23]. He determined the total mass of the Coma Cluster by multiplying the observed number of galaxies (800) by their averaged mass ($10^9 M_\odot$). Zwicky then applied the virial theorem to estimate the velocity dispersion, which was more than an order of magnitude smaller than the observed value. This unexpected discrepancy indicated that Coma must be much heavier; otherwise, there would not be enough visible matter to hold galaxies together. Thus, to explain the cohesion of the Coma Cluster and ensure its stability, one needs to assume the existence of a dark sector that saturates the total mass together with the luminous matter. Although Zwicky's discovery was puzzling, at that time, there existed many observational limitations minimizing this revelation. The most serious doubts concerned inferring the distance to the Coma Cluster and adopting the mass-to-light ratio of the Sun to all stars. Hence, the missing mass problem seemed like a house of cards waiting to be blown down.

A true revolution happened more than four decades later due to the unprecedented progress in radio astronomy and the discovery of the 21 cm line. In the 1970s, Kent Ford, Vera Rubin, and other astronomers began a detailed study of the rotation curves in spiral galaxies, i.e., flattened gravitationally bound systems rotating in a nearly circular fashion around a central concentration of stars called the bulge. Leveraging an image tube spectrograph, Rubin performed spectroscopic observations to determine the rotation curves of stars in the Andromeda Galaxy. Her discovery amazed astronomers and became the most striking evidence of a dark halo around galaxies. The rotation curve illustrates the relation between an object's orbital velocity v and its radial distance r from the central bulge. Such a relation is used to determine the mass distribution in a given stellar system. For example, in spiral galaxies, orbits of rotating objects like stars or clouds of hydrogen gas are approximately circular. Thus, according to Newton's law of gravitation, one can estimate the total mass $M(r)$ inside a radius r once the relation between v and r is known. More precisely, by setting the gravitational force to the centripetal force, we find the following formula for the orbital velocity:

$$v(r) = \sqrt{\frac{GM(r)}{r}}, \tag{1.1}$$

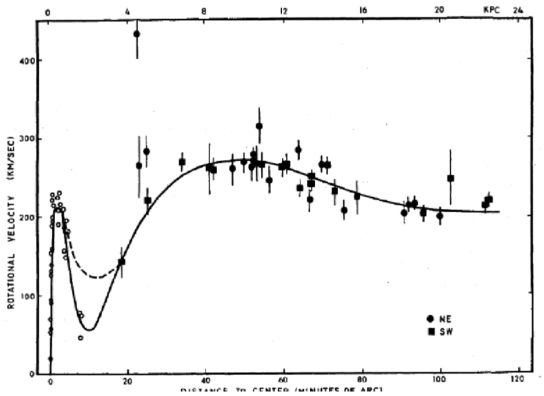

FIGURE 1.1: Rotation Curve of the Andromeda Galaxy as done by Vera Rubin [7]

with G being the gravitational constant. The mass of the whole galaxy is concentrated in its bulge; thus, outside of it, $M(r) \simeq const.$ Hence, formula (1.1) tells us that $v(r)$ should scale as $r^{-1/2}$ for objects whose distance from the center is larger than the size of the galaxy. Instead, Rubin's discovery was in considerable contradiction with this prediction, cf. Fig.(1.1). She found that the rotation curve of Andromeda remains approximately flat and does not decrease with r in the galaxy's outer region [7]. This peculiar behavior has also been observed in many other spiral galaxies. A natural explanation of this puzzling phenomenon was that there must be some additional contribution to the total mass outside the border of observed galaxies. The density profile $\rho(r)$ of the dark halo should decrease as r^{-2}, such that the total mass $M(r) = 4\pi \int r^2 \rho(r) dr$ becomes constant. Another explanation for the flattening of the rotation curves was that Newton's laws could not be applied to such objects. This, in turn, suggested that Newtonian gravity must be modified at the galaxy scales.

At that moment, it became clear that the problem of missing mass cannot be ignored by the astronomical community. Soon after, the dark matter puzzle became an object of theoretical physicists' interest. This resulted from several observations, which we briefly review in the following section.

1.2 Recent evidence for dark matter

Now let us briefly review some observations supporting the existence of a dark sector.

1.2.1 Cosmic microwave background

One of the most compelling pieces of evidence supporting the existence of the dark sector originates from the observation of anisotropies in the cosmic microwave background (CMB). This probe is particularly interesting since it allows us to determine the total abundance of dark matter precisely.

CMB radiation was predicted by Ralph A. Alpher and Robert C. Herman in 1948 based on George Gamow's work [24]. However, Arno Penzias and Robert Woodrow Wilson at Bell Labs observed it for the first time sixteen years later while detecting a persistent and isotropic background 'noise' in the radio-wave spectrum [25]. CMB is a leftover remnant of the early Universe that was created 380,000 years after the Big Bang when the Universe had cooled enough ($T \lesssim 1\,\mathrm{eV}$) to form neutral hydrogen via the following process: $e^- + p^+ \to H + \gamma$. After recombination, photons were no longer scattered off the free electrons since the number density of the latter had decreased rapidly. Instead, at that moment, photons were finally released and started to propagate freely across the Universe, forming the surface of the last scattering. Hence, the CMB map can be viewed as a snapshot of the primeval Universe, i.e., the earliest direct probe of how the Universe looked at its beginning.

The power spectrum of the CMB radiation is almost homogeneous. It is considered the best perfect blackbody spectrum that has ever been seen. Its current temperature has been determined with high precision to be $T_{\text{CMB}} = 2.72547 \pm 0.00057$ K [26]. The first full-sky CMB map from NASA's Cosmic Background Explorer (COBE) mission revealed that the CMB temperature is not entirely uniform but exhibits tiny fluctuations across the sky. This observation has been further confirmed by the COBE's successor - the WMAP satellite, and the WMAP's successor - the Planck satellite. One can distinguish two types of anisotropies: primary and secondary. The former have primordial origins and stemmed from the surface of the last scattering and before. Secondary anisotropies are generated later due to effects emerging between the surface of the last scattering and the observer, e.g., interactions of the CMB radiation with intervening hot gas. The most considerable anisotropies are of the order of $\delta T/T \sim 10^{-3}$. It is the Doppler shift in the temperature caused by our motion with respect to the CMB rest frame. After removing dipole anisotropies and other contamination, it has been revealed that the typical amplitude of the primary CMB fluctuations is of the order $\Delta T/T \approx 10^{-5}$. These tiny anisotropies allow us to directly probe the physics of the very early Universe since they carry a memory about the matter distribution at the time of recombination.

It turns out that the existence of dark matter leaves a noticeable imprint on the amplitude of the CMB temperature anisotropies. More precisely, the presence of the density perturbations $\delta\epsilon$ induce fluctuations of the gravitational potential, $\nabla^2(\delta\Phi) = 4\pi G \cdot \delta\epsilon$, which are related to the temperature fluctuations through the following formula $\delta T/T = \delta\Phi/3$ [27]. The density fluctuations were initially tiny but grew with time, eventually providing the seeds for structure formation. It has been shown that in the Universe without non-baryonic matter, the temperature fluctuations should have been of the order $\Delta T/T \sim 10^{-4}$ to explain the formation of the observed structures. The smaller measured amplitude of anisotropies can only be explained by the existence of the non-baryonic sector.

From the angular size and height of the CMB peaks, one can constrain the value of the cosmological parameters. For instance, the position of the first acoustic peak enables us to determine the geometry of the Universe, see Sec.(2.4). In addition, the character of oscillations in the CMB power spectrum depends on the ratio between matter and radiation. In particular, the high of the acoustic peaks is sensitive to baryonic and dark matter density. The ratio of second to first peak amplitude allows us to find the baryon density parameter [13]:

$$\Omega_{b,0}h^2 = 0.0224 \pm 0.0001. \tag{1.2}$$

Finally, the height of the third peak is sensitive to the energy density of dark matter, which is estimated to be equal [13]

$$\boxed{\Omega^{\text{obs}}_{\text{DM},0}h^2 = 0.120 \pm 0.001, \qquad (68\%, \text{Planck TT, TE, EE} + \text{lowE} + \text{lensing})} \tag{1.3}$$

At this point, let us emphasize that these results leave no room for baryonic dark matter. In particular, data from WMAP and Planck surveys favour the so-called ΛCDM model, which emerged as a concordance model of cosmology. The name is an abbreviation of the two major constituents of the Universe, i.e., a cosmological constant Λ associated with dark energy and cold non-baryonic dark matter (CDM), see Sec.(2.4).

1.2.2 Big Bang Nucleosynthesis

The exotic, i.e., non-baryonic, nature of the dark sector has been further confirmed by the successful predictions of Big Bang Nucleosynthesis (BBN). Primordial nucleosynthesis refers to the light nuclei production in the first few minutes after the very beginning.

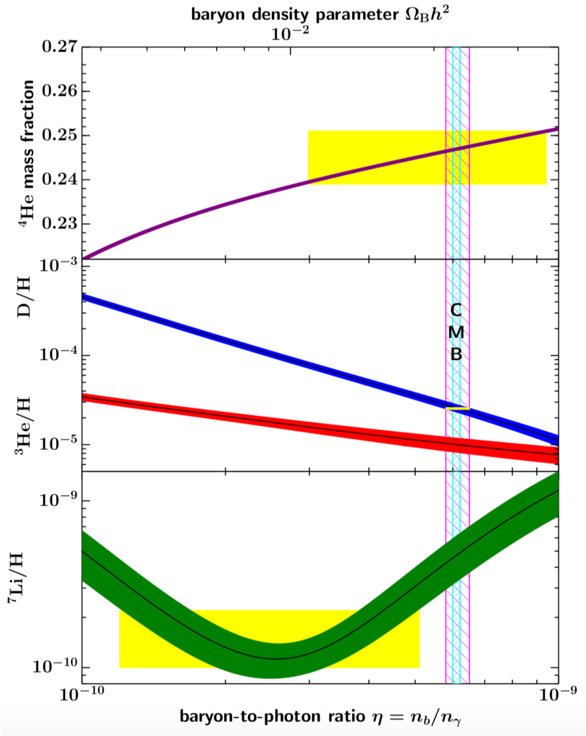

FIGURE 1.2: Primordial abundances of ^{4}He, D, ^{3}He, and ^{7}Li (compared with the hydrogen abundance) as a function of the baryon-to-photon ratio [8]. CMB predictions [9, 10] are shown as narrow vertical bands.

As the temperature of the Universe decreased, nucleons that formed the primordial plasma combined into deuterium nuclei. The latter underwent further nuclear reactions and formed ^{4}He and a tiny fraction of the ^{3}H and ^{7}Li nuclei, see Sec.(2.4). Since the amount of these elements depends on the temperature at the moment of their production, one can probe the ten-minute-old Universe by measuring their present abundances. In particular, the deuterium-to-helium ratio is susceptible to the baryon-to-photon ratio η, which, in turn, is related to baryon abundance through $\Omega_b h^2 = 0.004\eta/10^{-10}$ [19]. Thus, by measuring the relative abundances of these elements, one can determine the overall density of baryons. Figure (1.2) depicts the computed abundances of $^4\text{He}/H$, D/H (^{2}He/H), ^{3}He/H, and ^{7}Li/H as a function of η. BBN estimates are in agreement with the WMAP and Planck data for $\Omega_b h^2 \simeq 0.02$. This result is an important crosscheck of the CMB data.

1.2.3 Gravitational lensing

Other compelling evidence for dark matter has been inferred from gravitational lensing. The gravitational deflection of light caused by the presence of massive bodies is considered one of the most important predictions of general relativity (GR). According to this theory, the deflection angle δ of a light ray bent by a spherically symmetric object of mass M is [19]

$$\delta \simeq \frac{4GM}{bc^2}, \tag{1.4}$$

with b being the impact parameter of the incident photon. The flat metric result, i.e., $\delta \to 0$, is obtained if i) the mass M of the source is small and ii) the impact parameter is large. Typically, one distinguishes three categories of lensing, i.e., *strong lensing*, *weak lensing*, and *microlensing*.

Strong Lensing

Strong lensing corresponds to large deflection angles and creates highly distorted and magnified images of a physical source; for a review, see Ref.[28]. In a rare case, when the source, lens, and observer are located exactly on the same axis, a unique form of gravitational lensing, i.e., an Einstein ring, is generated. Properties of the images, e.g., their number, positions, intensities, etc., are used to map the distribution of dark matter [18]. Data inferred from strong lensing events greatly agrees with other cosmological probes.

Weak Lensing

In the weak lensing regime, deflection angles are small, and the principal signal is a tiny distortion in the shape of distant galaxies; for a review, see Ref.[29]. In the idealized case, the image of the background source is stretched tangentially around a circle centered in the lens. Although the signals of the weak lensing events are typically too weak to be inferred from a signal source, nevertheless, one can use statistical analysis to infer the distribution of a foreground structure [30, 31]. Initially, weak lensing has been used to constrain the amount of dark matter in a given volume. This method has also been adopted to map the distribution of dark matter around galaxy clusters [32]. In addition, a similar technique can also be applied to individual galaxies.

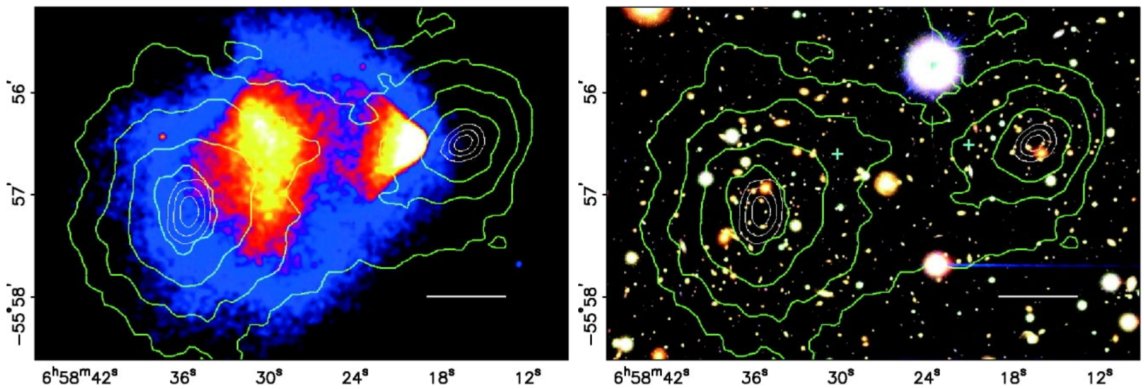

FIGURE 1.3: "*A direct empirical proof of the existence of dark matter*" [11]. Left panel: Optical images from the Magellan telescope of the merging cluster 1E0657-558. Right panel: The same image from the Chandra X-ray telescope. Green contours in both panels represent the spatial distribution of mass reconstructed from gravitational lensing. One can see that matter and plasma are concentrated in distinct areas.

One of the best-established evidence for dark matter has been inferred from the weak lensing mass-contour mapping of the cluster system (1E0657-558), better known as the Bullet Cluster. This object consists of two galaxy clusters that underwent a collision around a hundred million years ago. As a result of the merger, a smaller component of the Cluster has passed unhindered through the main cluster, whereas the hot intergalactic gas has been trapped and emitted the X-ray radiation. Hence, collisionless galaxies have spatially decoupled from the plasma, making it possible to determine the mass profile of the Bullet Cluster [11]. In addition, a gravitational lensing map of this Cluster has been created, indicating that the gravitational potential does not trace the distribution of the plasma. They found that the total mass of the Bullet Cluster is herded around the galaxies. The zero overlap between the concentration of the visible matter, inferred from measurements of the X-rays, and the total mass, mapped by the weak lensing, led to the conclusion that the Bullet Cluster cannot be entirely comprised of the baryonic matter; instead, it must contain a large amount of an invisible non-interacting matter.

Microlensing

Microlensing occurs when the source is temporarily brightened, but the angular separation of images is too small to be resolved. This phenomenon relies on events that, at first sight, appear to be quite rare, in which the source and the lens are perfectly aligned from our viewpoint. However, since there can be relative motion between these two objects, the probability of such an effect is nonzero. When the faint object passes in front of the farther body, which is typically brighter, the gravitational potential of the former causes the light emitted by the source to bend, which in turn results in an enhancement of the lens's brightness. The unique microlensing signature is a temporal brightening of the combined signal from the source and the lens. Gravitational microlensing is broadly employed to study faint or dark objects, e.g., brown stars, planets, white dwarfs, neutron stars, or black holes, that emit little or no light. It is also considered a potentially powerful technique for probing instance, primordial black holes. The typical time scale of such an event ranges from seconds up to years, allowing for the detection of objects with mass in the range $M \in [10^{-7}, 10^{2}]M_{\odot}$.
The term *microlensing* was coined by the Polish astronomer Bohdan Paczynski, who was the first to propose microlensing to probe massive compact halo objects (MACHOs) in the Milky Way [33]. His idea has been employed by several surveys, including MACHO [34, 35], EROS [36, 37] and OGLE collaborations [38, 39]. In 2007, the EROS-2 survey found that dark matter in our Galaxy cannot be in the form of dark compact objects in the mass range $10^{-7}M_{\odot} < M < 15M_{\odot}$ [36]. More recent analyses seem to relax these constraints, allowing MACHOs with the mass $M \sim M_{\odot}$ to be still in the game. However, in light of other evidence, it is hardly possible that dark matter is all made up of these objects.

1.2.4 Large-scale structures

Yet another direct evidence for dark matter comes from mapping large-scale structures. According to our understanding, the primeval density fluctuations serve as a seed for all of the large-scale structures we observe now. Two opposing forces are involved in this process: gravitational attraction and the repulsion force caused by the radiation pressure. The origin of the structure formation is the interplay between these two effects. During the radiation-dominated (RD) epoch, the non-zero pressure resists the gravitational collapse of the baryonic matter. Thus, matter fluctuations are homogenized during this era. After recombination, the radiation pressure is no longer present, and the density fluctuations finally collapse.

The Dark Energy Survey measurements indicate that the locations of the largest structures in the Universe cannot be explained only by the gravitational interactions of baryonic matter [40, 41]. Namely, without dark matter, the structure formation should have been highly suppressed compared to what we observe today. Dark matter serves as a seed of structure formation and allows the distribution of galaxies and their clusters to be what we observe today.

Although large-scale structure observations alone are typically less powerful and accurate in probing cosmological parameters, combining multiple datasets can provide more precise constraints. For example, the Dark Energy Survey combined cosmic shear, galaxy clustering, and galaxy-galaxy lensing to determine the present matter abundance to be $\Omega_m = 0.339^{=0.032}_{-0.031}$ [41]. When this result is further combined with other cosmological datasets, such as Planck, Baryon Acoustic Oscillations (BAO), and BBN, the measurement narrows down to $\Omega_m = 0.306^{+0.004}_{-0.005}$ [41], providing a tighter constraint.

1.3 Alternative dark matter candidates

Over the last decades, many hypotheses have been put forward on dark matter nature. The diversity of the proposed possible explanations is, in fact, somewhat overwhelming. Below, we list the most popular DM scenarios.

1.3.1 Massive Compact Halo Objects

For a long time, Massive Compact Halo Objects (MACHOs) have been considered a plausible explanation for the missing mass problem [42]. According to this hypothesis, galaxies are surrounded by a halo composed of massive, compact astronomical bodies, including black holes (BH), neutron stars (NS), brown dwarfs, faint stars, and unassociated planets. Nowadays, the concept of MACHOs dark matter is somewhat outdated. Namely, it is hardly possible that the existence of massive dim objects can exclusively explain the dark matter puzzle. The main feature that makes this theory untrustworthy is that MACHOs consist of baryonic matter, which alone cannot account for the structure formation.

1.3.2 Primordial Black Holes

Primordial Black Holes (PBHs) are among the most intriguing astronomical objects belonging to the class of MACHOs. Such black holes could have been created in the early radiation-dominated Universe as a result of the gravitational collapse of primordial overdensities. Since the energy density of the Universe scales as $\rho \sim 1/(Gt^2)$, one can estimate the initial mass of PBHs to be [17]

$$M \sim \frac{c^3 t}{G} \sim 10^{15} \left(\frac{t}{10^{-s}} \right) \text{g}, \tag{1.5}$$

where the density of a Schwarzschild black hole, i.e., $\rho = M/V \sim 1/(G^3M^2)$, has been adopted [43]. Using the above relation, we can see that masses of PBHs span over a wide range of scales, i.e., from $M \sim 10^{-5}\,\text{g}$ if they originated at the Planck time (10^{-43} s) up to $M \sim 10^5\, M_\odot$ if they formed at $t \sim 1$ s [17].

The very first mention of PBHs dates back to 1974 from the work of Zeldovich and Novikov [44]. Based on a Bondi accretion, they concluded that the existence of such objects is highly improbable since the mass of PBHs with an initial size comparable to the horizon should be of the order of $10^{17}\, M_\odot$ by the end of RD epoch. Their analysis neglected cosmic expansion, which could significantly suppress the accretion process. More detailed studies were done several years after this work. It is Stephen Hawking who is credited with pioneering research on PBHs. In the paper from 1971 [45], he proposed the existence of electrically charged PBH to explain the low flux of solar neutrinos. Then, in 1974 Stephen Hawking and Bernard Carr argued that the result of Zeldovich and Novikov cannot be applied in GR, showing that the cosmic expansion inhibits the growth of PBHs' mass [46]. In the same year [47] Hawking discovered something generally recognized as one of the most important revelations in theoretical physics. By combining insights from GR, quantum mechanics, and thermodynamics, he figured out that black holes should have a non-zero temperature

$$T_{\text{BH}} = \frac{1}{8\pi G M k_B}, \tag{1.6}$$

with k_B being the Boltzmann constant, as a result of thermal radiation, they should evaporate on a timescale

$$\tau \approx \frac{1}{G^2 M^2}. \tag{1.7}$$

One can show that PBHs with initial mass smaller than $\sim 10^{15}$ g have been evaporated entirely by now. On the other hand, according to these formulas, PBHs with a mass of the order of $\sim 10^{24}$ g have a temperature lower than the temperature of the CMB radiation, and thus the typical evaporation timescale for such objects is larger than the age of the Universe [17]. Although light PBHs, i.e., with mass $M_{\rm BH} < 10^{15}$ g, are the main focus of interest due to the potential of detecting their evaporation, heavier PBHs have recently attracted more attention. This is because the latter objects are unaffected by Hawking radiation and thus could serve as a dark matter candidate. This idea was first discussed in 1975 independently by George Chapline [48] and Péter Mészáros [49]. The notable feature of PBHs, distinguishing them from other MACHOs, is that they are not only dark and non-baryonic. Thus, unlike MACHOs, PBHs are not in tension with, e.g., large-scale structure formation or the anisotropies observed in the CMB spectrum. However, as we have already discussed, microlensing observations provide important constraints on the mass of dim objects. Hence, PBHs with mass in the range $\sim (10^{-7}, 10) M_\odot$ are excluded. Other constraints are being extensively investigated. Such studies see, e.g., [50] show that there are only a few narrow 'mass windows' where the fraction of dark matter in PBHs can be significant. Namely, PBHs with mass in the range $(10^{17}, 10^{23})$ g and $(10^{34}, 10^{35})$ g can saturate the observed dark matter abundance. It is worth noting that although the above bounds are based on monochromatic PBH mass distribution, such conclusions remain robust. Moreover, the detection of a gravitational waves' signal from the binary BH merger the LIGO/Virgo provided a fresh perspective on intermediate-mass PBHs. The estimated mass of black holes is in the range $10 - 50\, M_\odot$, which could suggest its primordial origin. Even though PBHs could provide only a (small) fraction of the dark matter, it would still lead to interesting phenomenology [17].

1.3.3 Modifications of gravity

One of the most immediate elucidations of the missing mass problem is that Newton's Law does not apply at the scales of galaxies. This hypothesis should be considered an alternative to the DM paradigm, which does not invoke the existence of a dark sector. One distinguishes several different models based on modifications of gravity theories.

Mordehai Milgrom was the first who brings this idea to life. In 1983, inspired by the revelation of the flatness of galaxies' rotation curves, he suggested modifying Newton's theory of gravity for objects with extremely low acceleration [51]. The primary premise of his Modified Newtonian Dynamics (MOND) hypothesis was that Newton's laws have never been tested in the low-acceleration regime. Accordingly, Milgrom proposed the following modification of Newton's second law of motion [51]:

$$\vec{F}_{\rm MOND} = m \cdot \mu \left(\frac{|\vec{a}|}{a_0} \right) \vec{a}, \tag{1.8}$$

where m is the gravitational mass of an object, a denotes its acceleration, a_0 is a new fundamental constant connecting the Newtonian and MOND regimes, while μ is the so-called interpolating function, such that $\mu(a/a_0) \to 1$ for $a \gg a_0$, and $\mu(a/a_0) \to a/a_0$ for $a \ll a_0$. Note that the first condition is required to reproduce the Newtonian result at the limit of high acceleration. Milgrom did not specify the exact form of the interpolating function; however, two common choices are: the so-called *simple interpolating function*

$$\mu\left(\frac{|\vec{a}|}{a_0}\right) = \frac{1}{1+\frac{a}{a_0}}\,, \tag{1.9}$$

and the *standard interpolating function*

$$\mu\left(\frac{|\vec{a}|}{a_0}\right) = \sqrt{\frac{1}{1+\left(\frac{a}{a_0}\right)^2}}\,. \tag{1.10}$$

By equating the gravitational force in the "deep-MOND regime" to the centripetal force of an object with mass m rotating at a distance r around a point mass M, Milgrom obtained the Tully-Fisher relation for an asymptotic form of the rotational velocity: $v_\infty^4 = (GMa_0)^{1/4}$ that is independent on r. Next, by applying his law to the rotation curve of a sample of galaxies, Milgrom estimated the value of the universal constant a_0 to be $a_0 \sim 1.2 \times 10^{-10}\,\mathrm{m\,s^{-2}}$. However, recently it has been shown that this prediction is not universal. Namely, the measured mass-to-light ratio for the NGC 1052-DF2 galaxy suggests that this object is devoid of dark matter [52]. This fact poses a challenge to MOND since this theory does not predict the existence of galaxies with no dark-matter halo. Even though this isolated object does not entirely rule out the MOND paradigm, it contradicts several other observations, including the Bullet Cluster. According to the MOND predictions, the gravitational lensing map of the Bullet Cluster should agree with the distribution of the X-ray gas. However, as we have already emphasized, the luminous mass distribution is separated from the total mass mapped by weak lensing. Moreover, MOND is also strongly disfavoured by the Sloan Digital Sky Survey data, indicating that the observed motions of galaxies within clusters do not match the MOND's predictions [53].

A more mature generalization of the MOND paradigm is referred to as the Tensor-Vector-Scalar (TeVeS) gravity and was developed by Jacob Bekenstein in 2004 as a relativistic generalization of Milgrom's theory [54]. One of the main features of TeVeS is that it contains two additional gravitational degrees of freedom: a spin-0 field ϕ and a spin-1 field A_μ. Moreover, it involves two frames: the Bekenstein frame for the gravitational fields and a physical frame for the matter fields. The action for the metric field is the standard Einstein-Hibert action, as in GR see Sec.(2.3), whereas the action for the matter contains a physical metric $\tilde{g}_{\mu\nu}$, given by the following expression:

$$\tilde{g}_{\mu\nu} = e^{2\phi} g_{\mu\nu} - 2A_\mu A_\nu \sinh(2\phi) \tag{1.11}$$

The existence of two extra degrees of freedom leads to the modification of Newtonian dynamics in the low gravitational potential regime. Even though TeVeS, in contrast with MOND, can accommodate gravitational lensing, it appears inconsistent with recent measurements of gravitational waves made by LIGO [55].

Another alternative for dark matter is entropic or emergent gravity. It was originally proposed by Erik Verlinde in 2010 [56] and then developed in 2016 [57]. Entropic gravity emerges from string theory, black hole thermodynamics, and quantum information theory. According to this theory, gravity is not a fundamental interaction but rather an *emergent phenomenon* resulting from the quantum entanglement of spacetime information bits. Although testing Verlinde's proposal seems not feasible, it is challenged on various grounds. For instance, it has been shown that entropic gravity is inconsistent with the observed data on the rotation velocities of dwarf galaxies [58].

1.4 Particle dark matter

Undoubtedly, the best-established and compelling candidate for dark matter is (are) some elementary particle(s). Depending on the specific model, the dark sector might consist of one or more degrees of freedom. It is widely believed that dark matter must be made of new yet undiscovered species (s). The reason why we should go beyond the Standard Model of particle physics is the fact that this theory does not contain any plausible candidate that could play the role of dark matter. The majority of the SM degrees of freedom are highly unstable, with lifetimes far shorter than the age of the Universe. The remaining stable particles, i.e., the electron and the up and down quarks, are either baryonic or charged under the $U_Y(1)$ gauge group. The only SM species with the required properties to explain the missing mass problem are three neutrinos, which are stable, non-baryonic, electrically neutral, and highly elusive. Moreover, the discovery of neutrino oscillations implies that neutrinos have a non-zero mass [59–61]. At first glance, massive neutrinos that are non-relativistic today could be considered an excellent dark matter candidate. Their current density can be estimated as [62]

$$\Omega_\nu h^2 = \frac{\sum_i m_{\nu_i}}{93.14\,\mathrm{eV}}, \tag{1.12}$$

where the summation of all non-relativistic neutrino states is adopted. According to the experimental data, the sum of neutrino masses is constrained as [63]

$$0.06\,\mathrm{eV} \lesssim \sum_i m_{\nu_i} \lesssim 0.15\,\mathrm{eV}. \tag{1.13}$$

The above approximate bounds imply that

$$0.0006 \lesssim \Omega_\nu h^2 \lesssim 0.0016, \tag{1.14}$$

which means that cosmic neutrinos are probably a few percent of the total dark matter in the Universe. Since the rest masses of neutrinos are smaller than the eV scale, they could only contribute to the hot dark matter. The reason for this is the assumption that neutrinos would have been in thermal equilibrium with the thermal plasma in the early hot Universe. Even though neutrinos are non-relativistic at present because their masses are small, they would have decoupled while being relativistic, see Sec.(2.4.1). Therefore, SM neutrinos could only contribute to hot dark matter at the time of structure formation and hence cannot account for all dark matter.

Since there is no viable DM candidate within the Standard Model, dark species are expected to be some new elementary particle(s) accommodated in some SM extension. Any such extension must agree with a broad range of cosmological and astrophysical observations described above. The consistency with the ΛCDM model implies several constraints on properties of dark particles [16]:

- **Almost dark with respect to the SM interactions**
  Since dark species do not interact with the electromagnetic force, viable dark matter candidates must have zero quantum number with respect to the SM $U_Y(1)$ gauge group. Moreover, other possible interactions of DM with the SM sector should be feeble not to spoil the growth of density perturbations.
- **Influenced by gravity**
  The existence of dark matter has been inferred from its gravitational effects. Therefore, dark matter particles must have a non-zero rest mass and interact with the SM species, at least through gravity.

- **Massive**
  Possible masses of DM particles span an enormous range. According to the Tremaine-Gunn bound [64], the mass of fermionic DM species must be larger than $0.27^{+0.30}_{-0.14}$ keV at 95% CL [65]. Such bound comes essentially from the fact that using the Pauli Exclusion Principle, one constraint to which extent fermionic DM could comprise a galactic halo. It is worth noting that this limit does not apply to bosonic dark matter. In this case, one gets a weaker lower bound $m_{\mathrm{DM}} \gtrsim 10^{-22}$ eV originating from the requirement that the de Broglie wavelength of the DM particle, $\lambda_{\mathrm{dB}} = 2\pi/(m_{\mathrm{DM}} v)$, should be large enough in order not to spoil the structure formation [66, 67]. Regardless of the spin of DM species, the upper bound on their mass is 10^{19} GeV [68]. The limit comes from the requirement that DM is not comprised of black holes.
- **Non-relativistic at the time of structure formation**
  The nature of DM species strongly affects the evolution of the density perturbations. *Cold* and *hot* DM are the two limiting cases corresponding to small and large velocity dispersion. To account for the observed structure, DM must be non-relativistic by the redshift $z \sim 10^7$.
- **Collisionless**
  Dark matter species should be nearly collisionless, meaning that they hardly interact with themselves on a large scale except for the gravitational forces. In other words, DM particles do not lose energy through radiation or collisions.
- **(Almost) stable**
  Dark particles must be stable, or at least, their lifetime must be larger than the age of the Universe. This is because only cosmic relics could contribute to the energy density of the Universe, which is 13.8 billion years.
- **Primordial origin**
  The abundance of light elements formed during BBN puts a strong constraint on the dark matter energy density at that time. Hence, dark matter species must have originated well before the BBN epoch.

Among these constraints, probably the most important one is just a single number - the observed abundance of dark matter (1.3) measured by the Planck Collaboration [13]. It is the only DM parameter that has been measured.

Apart from the constraints mentioned above on DM species, our knowledge about the dark sector is relatively poor and highly unsatisfactory. Very little is known about dark particles' basic properties, so the viable theory space is vast. Moreover, depending on the specific model, the dark sector might consist of one or several different kinds of elementary particles or even be in the form of composite objects. To characterize the dark sector, one could address the following issues: What are the spin and the mass of DM species? How do they interact with the SM degrees of freedom? In addition, we also would like to know what is the origin and nature of DM species. What mechanism is responsible for their production in the early Universe? Given that possible masses span an enormous range of scales and that the viable parameter space for DM interaction strength is poorly constrained, a plethora of Beyond the Standard Model (BSM) models are considered a viable possible explanation of the dark matter puzzle. DM candidates can be classified according to several categories described below.

1.4.1 Spin

Dark matter particles could have both bosonic as well as fermionic nature. However, as mentioned above, fermions with mass below the $\sim$ keV scale are not plausible DM candidates.

Among bosons, dark matter scalars and vectors are the most established candidates, whereas spin-1/2 particles are the most popular fermionic DM pretenders. However, it should be stressed that particles with higher spins, e.g., $s = 3/2$ [69–71], $s = 2$ [72–74], or even higher, i.e., $s > 2$ [75–77] could also act as viable DM candidates. The origin of DM scalars, spin-1/2 fermions, and vectors can be very different; however, the Higuchi bound on the mass of higher bosonic spin states [78], $m^2 \geq s(s-1)H^2$, with H being the Hubble rate, implies that such species might have a gravitational origin.

1.4.2 Mass

Depending on mass, one distinguishes several types of dark matter candidates. To saturate the observed DM abundances, particles with different masses typically have very different production mechanisms, which generally are operational in a given mass range.

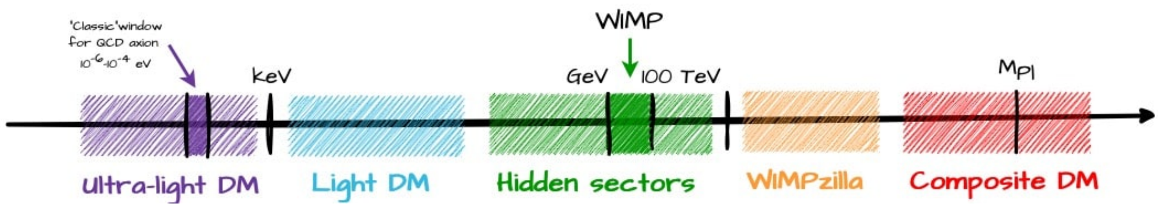

FIGURE 1.4: The mass range of particle DM candidates.

Ultra-light dark matter

Particles with mass below the $\sim$ keV scale are usually ranked as **ultra-light dark matter**, for a comprehensive review, see [79]. These models have gained much attention recently due to their wave properties of forming a Bose–Einstein condensate or a superfluid on galactic scales. **Ultra-light** species collectively behave as a coherent field with a typical the de Broglie wavelength of the order of $\lambda_{\rm dB} \approx 0.4\,{\rm kpc}\,(10^{-22}\,{\rm eV}/m_{\rm DM})$ [16]. Their occupation number, $N = \frac{\rho_{\rm DM}}{m_{\rm DM}}\lambda_{\rm dB}^3$, is quite large, i.e., $N \gg 1$, which indicates that **ultra-light DM** can be effectively described as a classical field.

The evolution of scalar **ultra-light DM** fields is governed by the Schrödinger–Poisson equation. It turns out that **ultra-light** scalar particles behave as condensate on galactic scales, which could address some of the small-scale shortcomings of the CDM, e.g., the cusp-core problem. However, on larger cosmological scales, **ultra-light DM** behaves as a standard CDM. Models with **ultra-light DM** are classified into three main classes.

- **Fuzzy dark matter** refers to a gravitationally bounded ultra-light dark scalar with $m_{\rm DM} \sim 10^{-22}\,$eV, see, e.g., [80, 81]. This model predicts that condensation of the spin-0 field is achieved in galaxies where the quantum pressure counterpoises the gravitational attraction.
- **Self-interacting fuzzy dark matter**, or **repulsive DM, scalar field DM, fluid DM** is a model with a dark scalar field, in the presence of gravity, with a (usually) 2-body self-interaction [79]. The inclusion of this interaction leads to the emergence of superfluid behavior when the scalar field undergoes condensation.
- In **DM superfluidity** models, dark matter is treated as a condensate of axion-like particles that behaves as a special liquid, which lacks viscosity on the galaxy scales [82]. Collective excitations of this superfluid lead to a new long-range interaction, in

addition to gravitational force, which explains the flattening of galaxy rotation curves. On the other hand, dark matter is in a normal phase at the scale of galaxy clusters and behaves as a set of incoherent particles.

Axions

The mass range between $\sim 10^{-6}$ and $\sim 10^{-4}$ eV is known as the "classic" window for the **QCD axions**. The QCD axions a were originally postulated by Peccei and Quinn in 1977 to resolve the strong CP problem in quantum chromodynamics [83, 84]. They proposed a new $U(1)_{\rm PQ}$ symmetry, known now as Peccei-Quinn (PQ) symmetry, that is spontaneously broken at a high energy scale f_a. Steven Weinberg and Frank Wilczek independently realized the existence of a new pseudo-Nambu-Goldstone (pNG) boson emerging from the spontaneous breaking of the global symmetry [85, 86]. The name **axions** was coined by Wilczek after a brand of laundry detergent because axions were supposed to "clean up" the strong CP problem. The density Lagrangian of a proposed model is given by

$$\mathcal{L} \supset \theta_{\rm QCD}\frac{\alpha_S}{8\pi}G^a_{\mu\nu}\tilde{G}^{\mu\nu}_a + \frac{a}{f_a}\frac{\alpha_S}{8\pi}G^a_{\mu\nu}\tilde{G}^{\mu\nu}_a, \tag{1.15}$$

where the first time violates the CP symmetry, whereas the second term is a low energy effective Lagrangian for the pNG of the PQ symmetry. Above, $\theta_{\rm QCD}$ is a QCD parameter which can be understood as an angle determining the vacuum of the theory, α_S is the fine-structure constant, $G^a_{\mu\nu}$ and $\tilde{G}^{\mu\nu}_a$ denote the gluon field strength tensor, and its dual. The second term in Eq.(1.15) effectively replaces the CP-violating term since the axion field can be redefined absorbing $\theta_{\rm QCD}$. The crucial part of the PQ mechanism arises from the fact that the potential of the a field has a minimum at the CP-conserving value $\theta_{\rm QCD} = 0$. Hence, the non-trivial topological configurations of the QCD vacuum generated by the CP-violating term are canceled dynamically, effectively solving the strong CP problem.

Axions acquire a non-zero mass through the mixing with neutral pion and other mesons [87]

$$m_a = 5.70\mu\text{eV}\left(\frac{10^{12}\text{GeV}}{f_a}\right). \tag{1.16}$$

The mass of the axion field should be considered as a QCD effect. Therefore, it vanishes in the early Universe, above the QCD scale. The theory does not fix the scale of the PQ symmetry breaking f_a, and to evade current experimental constraints, it should be higher than 10^7GeV. The moment the phase transition occurs defines the subsequent evolution of axions. One typically distinguishes two types of models, i.e., pre-inflation and post-inflation scenarios, in which the PQ symmetry is broken before and after the inflationary phase, respectively. Depending on the specific model, axions can be produced due to the thermal interactions with the SM bath, via the vacuum realignment mechanism (VR), also known as the misalignment mechanism, and as a result of the decay of topological defects (TD). Axions cannot comprise all DM if they are thermal relics since they contribute to the hot dark matter. Moreover, if axions were topological defects produced prior to inflation, they should have been wiped out by the exponential expansion of the Universe. Vacuum realignment in the pre-inflation scenario would require fine-tuning the initial misalignment angle θ_i. For instance, if we fix $\theta_i \sim 1$, the matching with the observed relic abundance can be achieved for $m_a \sim$ few μeV, but by varying the value of θ_i, such that $\theta_i \in (0.3, 3)$ one widens the allowed mass range $m_a \in (10^{-6} - 10^{-4})$ eV [87]. Finally, to saturate the observed DM relic density, the mass of axions produced through VR and TD mechanisms after inflation could only lie in a narrow window around $\sim 10^{-5}\,\mathrm{eV}$.

The existing constraints for the QCD axions as CDM can be easily relaxed is one generalize the Peccei-Quinn idea to a more generic model in which the mass of the pNG boson is independent of its coupling. The string theory predicts the existence of other light bosons A, dubbed as **axion-like particles (ALPs)**, as a result of the spontaneous breaking of global symmetries at high energies [88]. ALPs could also be produced via the realignment mechanism. Moreover, ALPs, similar to QCD axions, couple to photons via the operator

$$\mathcal{L}_{A\gamma} = -\frac{g_{A\gamma}}{4} A F^{\mu\nu} \tilde{F}_{\mu\nu}, \tag{1.17}$$

with $F_{\mu\nu}$ being the electromagnetic tensor and $\tilde{F}_{\mu\nu}$ its dual. The axion-photon coupling $g_{a\gamma}$ is inversely proportional to f_a, and hence, in the light of Eq.(1.16), it is proportional to axion mass. On the other hand, the ALP-photon coupling $g_{A\gamma}$ is generally unrelated to the ALPs mass, which untightens the existing bounds for QCD DM axions. Depending on the value of $g_{A\gamma}$, ALPs could serve as a viable DM candidate while evading current experimental constraints in a wide range of masses $m_A \lesssim 10^2\,\mathrm{eV}$ [87].

Light dark matter

DM particles with mass in the range keV $-$ 10 GeV traditionally fall into the category of **light dark matter**. The above mass range encompasses **sterile neutrinos** and several **thermal DM candidates called Sub-GeV**. The former has been introduced to resurrect neutrinos as viable candidates for dark matter. This can be done by postulating the existence of an extra heavy "sterile" neutrino with feeble interactions with the SM bath. It is worth noting that this proposal could also provide a simple explanation for the observed oscillations of DM neutrinos via the seesaw mechanism, see, e.g., [89]. Sterile neutrinos could act as viable DM candidates if their mass is of the order of the keV scale [90–92]. Sterile neutrinos do not carry any SM gauge charges; however, they should interact with other species to be efficiently produced in the early Universe. Typically, three different scenarios are taken into account. Namely, sterile neutrinos could have been produced by the weak interaction through mixing θ with the $SU(2)_L$ charged SM neutrinos, see, e.g., [93, 94]. Another possibility is that sterile neutrinos might have had new gauge interactions at high energies and thus could have been produced thermally by these interactions [95, 96]. Finally, sterile neutrinos could also have been created non-thermally by the decay of some heavier state in the early Universe. Depending on the model, sterile neutrinos could be produced either in decays of the SM fields, e.g., pions [97, 98], the Higgs boson [99], and the W boson [100], or in the decay of some new BSM degree of freedom [101, 102]. It should be stressed that the standard keV mass scale is only favored for sterile neutrinos produced via the active-sterile mixing, whereas for the remaining two production channels mass of sterile neutrino can be well above the electroweak scale [89].

Dark or hidden sectors

Another class of DM candidates below the GeV-scale is referred to as **dark or hidden sectors**, containing both the DM species and other light states [103–106]. Apart from a DM candidate, such models involve new light mediator states with sufficiently small couplings to the SM particles. The mediator and DM are part of a secluded sector linked to the SM sector with a portal. SM symmetries allow only a few possibilities [16], e.g., the axions portal, where a pseudoscalar a couples to SM fermions $\frac{\partial_\mu a}{f_a}\bar{f}\gamma^\mu\gamma^5 f$, or to SM gauge bosons $\frac{a}{f_a}G_{\mu\nu}\tilde{G}^{\mu\nu}$, $\frac{a}{f_a}F_{\mu\nu}\tilde{F}^{\mu\nu}$, the Higgs portal, where the coupling of the scalar mediator ϕ to the SM Higgs $\mathbf{h}$ generates Yukawa interactions with SM fermions $y_f\phi\bar{f}f$ after the EW electroweak symmetry breaking, neutrino portal, where the sterile neutrinos serve as a mediator that couples to the SM lepton doublet L via the operator $\bar{L}\mathbf{h}\nu_s$, and the kinetic mixing portal referring to the kinetic mixing of dark photons with the SM photons $\kappa V_{\mu\nu}F^{\mu\nu}$, with κ being the kinetic mixing parameter, and $V_{\mu\nu}$ denoting the field strength tensor of a dark $U(1)$ symmetry. The sub-GeV DM has a rich phenomenology, which is still under active investigation.

WIMPs

Presumably, the most frequently explored mass range spans over the $\mathcal{O}(10)$ GeV scale up to 10 TeV. This is the standard mass window for **weakly interacting massive particles (WIMP)** - one of the leading DM candidates. A comprehensive review can be found in Ref.[107, 108]. Although there is no precise definition of WIMP, this term generally refers to a non-baryonic and non-relativistic massive particle interacting with the SM sector via weak or sub-weak interactions. The WIMP mass typically lies in the range from about 2 GeV (the so-called Lee-Weinberg bound) up to ~ 100 TeV (the unitarity bound) [109]. This relatively old idea emerged from at the turn of the 1970s and 1980s [110, 111], and over the last four decades, it has remained the most common paradigm to explain the DM puzzle.

There are several reasons why the WIMP paradigm is still in vogue. First of all, WIMP species come up in various well-motivated BSM modes. A favorite WIMP candidate arises in the supersymmetric extensions of the SM, e.g., in the Minimal Supersymmetric Standard Model (MSSM), in which each SM species has a supersymmetric partner whose quantum numbers are the same, but a spin is different by a factor of 1/2 from its SM counterpart. Due to the R-parity, the lightest supersymmetric partner is stable and can serve as a WIMP candidate for DM. Moreover, what makes the WIMP scenario particularly attractive is the so-called *"WIMP miracle"*. This catchy term refers to the profound connection, or maybe just a coincidence, between the WIMP annihilation cross section and the observed relic abundance of dark matter. Dark matter in the form of WIMP is supposed to be a thermal relic from the early Universe. When the temperature of the Universe was sufficiently high, WIMPs were in thermal equilibrium with the SM bath, meaning that they interacted with each other efficiently. At that time, WIMPs would have been produced from the annihilations of other particles in the thermal bath. The rate of such interactions was fast enough to maintain WIMPs in thermal and chemical equilibrium with other species. However, as the Universe cooled down, the time scale of such interactions could have decreased faster than the scale of expansion, and the relevant interaction rate became too small to maintain particles in equilibrium. WIMPs then *decoupled* or *froze out* from the thermal bath, and their abundance reached an asymptotic value. In other words, after *freeze-out*, the number of WIMPs per comoving volume remained constant. WIMPs with stronger interactions would have stayed longer in thermal equilibrium and, hence, less abundant. The freeze-out abundance can be related to the DM relic density observed today. Now the "miracle" happens. It turns out that the relic abundance of WIMPs with mass of the order of the electroweak scale, i.e., $m_{\mathrm{WIMP}} \sim 100\,\mathrm{GeV}$, can be estimates as [14]

$$\Omega_{\mathrm{WIMP}}h^2 \approx \frac{3\times 10^{-27}\mathrm{cm}^3\,\mathrm{s}^{-1}}{\langle\sigma v\rangle}. \tag{1.18}$$

Hence, for a cross-section characteristic for electroweak interactions $\sim 10^{-26}\,\mathrm{cm}^3\,\mathrm{s}^{-1}$ one obtains the right relic density for dark matter, i.e., $\Omega_{\mathrm{WIMP}}h^2 \simeq \Omega^{\mathrm{obs}}_{\mathrm{DM}}h^2$. Hence, if the dark sector is made of WIMPs whose mass and coupling scales are close to the SM ones, the observed abundance of DM is achieved intrinsically. At this point, it should be emphasized that the assumption of WIMPs being thermal relics imposes quite strong constrain on their mass. In particular, WIMPs more massive than $\sim$ 100 TeV would be dramatically overabundant, leading to an over-closure problem. The "WIMP miracle" happens only for WIMPs with masses of the order of the TeV scale.

Over the years, the WIMP scenario has been considered a seductive hypothesis due to its (prospective) testability. For a long time, it was expected that WIMPs with masses around the TeV scale should be not only within sight of high-energy colliders [112–114] but also of direct [115–117] and indirect [118, 119] DM searches. The fact that this scenario has many potential implications for various experiments has driven much effort in the search for WIMPs in the last decades. Although this possibility has been extensively studied for many years, no signals have been found yet.

WIMPZILLAs

The assumption of relatively low-mass DM seems quite natural, and therefore, most of the theoretical efforts have been put into such candidates, whereas over the years, the heavier mass region has not been extensively explored in the literature. Thus paradigm was finally questioned by Edward W. Kolb, Daniel Chung, and Antonio Riotto, who claimed that DM might be made of superheavy particles with masses larger than the weak scale by several orders of magnitude [120, 121].

Dark matter particles above the $\mathcal{O}(10)$ TeV scale were christened by the name **WIMPzillas** [68]. The scenario considered by Kolb, Chung, and Riotto was developed in opposition to the WIMP paradigm. They claimed that *"Dark matter may be much more massive than usually assumed, much more massive than wimpy WIMPS, perhaps in the WIMPZILLA class"* [68]. In this alternative proposal, the dark sector is composed of superheavy particles with masses ranging from 10^{12} up to 10^{16} GeV. The main distinguishing feature of WIMPzilla from "wimpy WIMP" is that the former is not a thermal relic. Otherwise, if WIMPzillas were in equilibrium at the freeze-out time, their relic abundance would be much larger than the observed value. Because WIMPzillas particles are not thermal relics, their present abundance is not determined by their cross-section. To reproduce the observed dark matter relic density, the fraction of total DM energy density in the form of WIMPzilla at the time they were produced must be tiny. Therefore, one expects WIMPzillas to have feeble interactions with other species. In the extreme case, one could even consider an extreme scenario where WIMPzillas are coupled directly neither to the SM sector nor to any other hidden sectors. Surprisingly, even if WIMPzillas have only gravitational interactions, numerous non-thermal mechanisms might populate the dark sector. Pure gravitational production is considered one of the most elegant mechanisms for DM production. Kolb, Chung, and Riotto considered the scenario where superheavy DM is produced during the transition between the inflationary phase and a matter-dominated (or radiation-dominated) epoch as a result of the "non-adiabatic expansion of the background spacetime acting on the vacuum quantum fluctuations" [120]. Conceptually, this mechanism has much in common with the inflationary formation of gravitational perturbations and will be discussed in more detail later. The notable feature of this process is the capability of creating particles with a mass of the order of the Hubble scale during inflation, regardless of their other interactions. In addition, they also demonstrated that WIMPzillas particles with mass up to $10^3\,H_e$, with H_e being the scale of Hubble rate at the end of inflation, can be produced via a broad parametric resonance during the preliminary stage of reheating called "preheating" [122–127].

Composite dark matter

Dark matter heavier than the Planck mass scale might be made of macroscopic composite objects, i.e., bound states of lighter species. For instance, it is known that the gravitational collapse of a scalar field condensate could lead to the formation of a **boson star** [128]. Such phenomenon is observed for a collection of axions that condense into an axion star [129]. There is a chance that a significant fraction of dark matter is in the form of such non-luminous stars. A somewhat related possibility is that of **supersymmetric Q-balls** - coherent state of a complex scalar field, or more precisely, stable non-topological solitons carrying baryon or lepton number [130]. Finally, ultra-heavy DM can also be in the form of **nuggets** of quark matter - an exotic phase of "quark matter" that could have been created at high baryon-number density and low-temperature [131]. The authors of Ref.[132] demonstrated that dark quark nuggets are unavoidable in confining gauge theories that generically admit a first-order phase transition and a dark baryon asymmetry. Depending on the confinement scales, their mass can be as large as 10^{23} g with the corresponding radius 10^8 cm.

1.4.3 Thermalization

Dark matter models can be also distinguished depending on whether DM species were or were not in thermal equilibrium with the SM bath, see Appendices (B) and (C). The production mechanism and thus the dynamics of DM species are determined by their strength of their interactions with the visible sector. Namely, the evolution of the dark sector can be described in a model-independent way by its thermally-averaged interaction rate $\langle\sigma|v|\rangle$ with the thermal bath, see (6.177). One singles out three main scenarios.

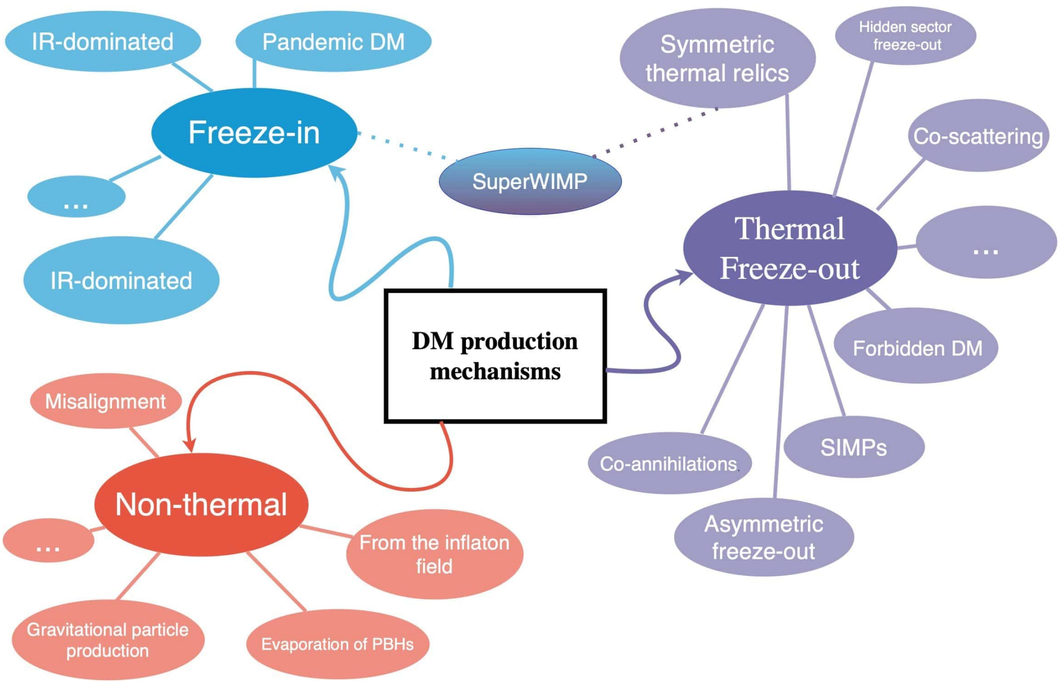

Figure 1.5: Various DM production mechanisms.

Thermal freeze-out

For large enough $\langle\sigma|v|\rangle$, such that the interaction rate $\Gamma \equiv n_X^{\text{eq}}\langle\sigma|v|\rangle$, with n_X^{eq} being the equilibrium number density (for a negligible chemical potential, n_X^{eq} will be defined in Eq.(2.113)), exceeds the Hubble rate H, DM species were in thermal equilibrium with the SM bath at early times. In such models, DM starts its evolution with a large number density. At high temperatures, DM-SM interactions proceed rapidly, relative to the Universe's expansion. As the temperature of the Universe drops, dark species lose their initial abundance, following the equilibrium distribution. When the temperature is of the order of the DM mass, dark species are so dilute that their interaction rate eventually drops below the Hubble rate. The transition between these two regimes, i.e., efficient and inefficient interactions with SM bath, is called *freeze-out*. Around this moment DM interaction rate equalized with the Hubble rate, i.e., $\Gamma \approx H$, and as a result, the comoving number density of dark species becomes fixed and stays constant up to now. The strongest coupling is, the longer DM particles remain in thermal equilibrium with the SM bath, leading to a lower freeze-out abundance, cf. Fig.(1.6).

Note that the present amount of thermal relics have no memory of the initial conditions and does not depend on the details of the production mechanism. This is because thermalization washes out any dependence on initial conditions. The role of the SM sector in this scenario boils down to the suppression of initial (most presumable large) DM abundance.

The best-established realization of thermal freeze-out is the standard WIMP scenario discussed above. However, this is only one of the simplest examples of a much broader class of models. The whole landscape is diverse and rich, as it spans various scenarios, including symmetric thermal relics [111], hidden sector freeze-out [103, 133, 134], forbidden dark matter [135, 136], strongly interacting massive particles (SIMPs) [137, 138], asymmetric dark matter [139, 140], co-annihilations [135], co-scattering [141], and many more.

Freeze-in

If DM interactions with the SM bath are weak, thermal equilibrium cannot be achieved. DM particles starting their evolution with a large abundance would have been overproduced, which, in turn, would have led to the over-closure of the Universe. On the other hand, if the initial abundance of dark particles was tiny, or even zero, feeble interactions with the SM quanta gradually increase the number of dark species whose abundance accumulates with time. The production of DM particles stops when the temperature of the Universe drops below DM mass since thermal plasma no longer has enough energy to create dark particles. The main aim here is to reproduce the exact present abundance.

The above described **thermal freeze-in**[1] scenario [142] can be viewed as the opposite mechanism to thermal freeze-out. Feebly Interacting Massive Particles (FIMPs) never attained thermal equilibrium with the SM sector. The latter's role is now to create DM species, not to decrease its initial abundance, as in the freeze-out mechanism. This process might not be efficient enough for too small couplings to saturate the relic density. On the other hand, if DM-SM couplings are too high, one would end up with too much dark matter. Hence, unlike freeze-out, the abundance of DM produced via freeze-in increases with $\langle\sigma|v|\rangle$, cf. Fig.(1.6).

[1]The term *'thermal'* refers here to SM particles comprising thermal bath, from which DM species originated. It does not refer to dark matter, which is not in thermal equilibrium.

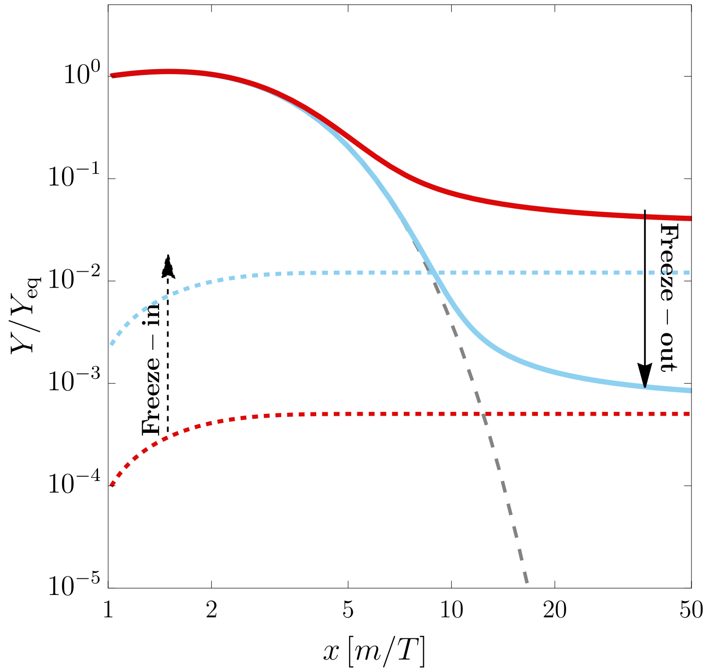

FIGURE 1.6: Schematic comparison of the freeze-out (solid curves) and freeze-in (dashed curves) mechanisms. Red curves correspond to a lower value of $\langle\sigma|v|\rangle$. $Y = n/s$ denotes the DM yield, with s, denotes entropy density (2.136). Gray dashed curve presents the evolution of $Y_{\rm eq} \equiv n_{\rm eq}/s$.

Moreover, the number density of FIMPs initially increases with time and *frozen-in* when $T \sim m_{\rm DM}$, contrary to WIMPs whose abundance exponentially decreases with time up to the point when it *freeze-out* to a constant value. Moreover, let us notice that the relic density of FIMPs depends on the initial conditions and has a memory of the Universe's expansion history.

Several important questions arise, for instance, when, or in other words, at what temperatures WIMPs are produced. Typically this is determined by the ratio Γ/H, or more precisely, the moment at which it is maximized. One distinguishes two possible scenarios. Namely, the **UV freeze-in** [143], in which Γ/H reaches its maximal value at high temperatures, and the **IR dominated freeze-in** for which Γ/H is maximized at low temperatures, typically around the DM mass threshold [142]. Now let us briefly examine what type of interactions could lead to UV and IR freeze-in. To that end, we assume that DM interactions can be described within the effective field theory (EFT) framework. In this case, the temperature dependence of the thermally averaged DM cross section can be parametrized as,

$$\langle\sigma|v|\rangle \sim \frac{T^{2(d-4)-2}}{\Lambda^{2(d-4)}}, \tag{1.19}$$

where Λ denotes the EFT cutoff, and d is the mass dimension of an operator $\mathcal{O}$ which mediates DM-SM interactions. Using the fact that $n_{\rm DM} \sim T^3$, and adopting the following scaling of the Hubble rate $H \sim T^2/M_{\rm Pl}$, one finds

$$\frac{\Gamma}{H} \sim \frac{M_{\rm Pl}}{\Lambda^{2(d-4)}} T^{2(d-4)-1}. \tag{1.20}$$

From the above estimations, one can see that if the operator $\mathcal{O}$ has a mass dimension $d \leq 4$, then the $\frac{\Gamma}{H}$ ratio decreases as T increases. Hence, the IR-dominated freeze-in typically emerges from renormalizable interactions. On the other hand, Eq.(1.20) implies that for $d \geq 5$, the $\frac{\Gamma}{H}$ ratio decreases with T, and therefore, it is maximized at the highest temperature scales. Thus, higher-dimensional interactions lead to the UV type of freeze-in mechanism.

From the above discussion, one infers that DM abundance depends on the history of the early Universe in the UV freeze-in scenario. Hence, it might be very different in various cosmological models, depending on how the Universe evolved at the very early times. The UV sensitivity, in particular, means that DM abundance can access information about the Universe at very high temperatures.

Another key question is what type of interactions could create DM via the freeze-in mechanism. Similar to thermal freeze-out, freeze-in zoology is tremendous. Here we list only a few of them, including portal models, where DM species interactions with the SM bath arise through the so-called Higgs portal [144–146], or as a result of mixing between the hidden $U(1)$ gauge boson and the SM hypercharge [147–149], or via the spin-2 portal [150–153], etc. Another example is the pandemic DM [154, 155]. and superWIMPs [156]. For a comprehensive review, see [157].

Non-thermal production

Finally, let us consider the extreme scenario where DM interactions with the thermal bath are so weak that SM particles cannot produce the observed amount of dark matter. One would naively expect that such a scenario is unrealistic since we observe some signatures of dark matter from which we have inferred its existence. However, we should be aware that the DM's origin is not necessarily related to the SM sector. In fact, there is no profound reason to assume that the genesis of DM is associated with its interactions with the SM particles. If it is, then we are, in some sense, lucky since then we might have some chance to see its imprints in collider or direct searches. If not, then ... a plethora of possible models would still be overwhelming.

This idea is not new, and many models exist in the literature. Among the best-established scenarios are the misalignment mechanism for axion-like-particles [86], non-perturbative gravitational production from the rapidly changing metric [120, 121, 158–173], production from the inflaton field [174–178], DM production via non-minimal couplings to gravity [179–181], the evaporation of PBHs [182–185], etc.

1.5 Gravitational dark matter

Despite unprecedented efforts made to experimentally confirm the existence of dark matter particles, so far, neither on Earth nor in the sky, any single DM imprint has been detected. Even though it is still too early to completely discard the WIMP paradigm, the complete lack of any signal motivates the consideration of alternative, slightly more pessimistic DM scenarios.

The **purely gravitational dark matter** is one of the most elegant and minimal models for a dark sector. Particles interacting with other species only through gravity seems to be an appealing explanation for the dark matter puzzle. Although such a scenario appears very well-motivated and natural, it has not been extensively explored in the literature for many years. The reason for this may be associated with the perceived difficulty of testing it. Even if the observational prospects are not very promising, certain signatures of purely gravitational dark matter are expected [186, 187], and the scenario itself can be ruled out if the inflationary scale is found to be low.

A key question one might raise is what makes gravitational DM production compelling. First and foremost, it is its inevitability. The gravitational coupling is universal and thus irreducible. Hence, the issue to be addressed is not whether dark matter is produced gravitationally but rather when and how many dark particles are created that way. Thus, purely gravitational dark matter production might provide the ultimate lower limit for the DM abundance that should be taken into account in any non-thermal scenario.
Moreover, it is also a complementarity between the dark sector and the primordial Universe. This results from the fact that the produced amount of dark matter is strongly attached to inflationary observables, which we hope to measure in the near future.
Lastly, it is also the minimalism and simplicity that make this scenario so appealing. To fully determine the gravitational production of dark matter species, one should only specify two basic DM characteristics, i.e., its spin and mass, and adopt some inflationary and post-inflationary scenarios. That is all we need to determine the whole dynamics of dark matter. The model-dependent part of this scenario is associated with a choice of the early-Universe model, which determines the background dynamics during and after cosmic inflation. It should be highlighted that no other direct coupling to matter fields or curvature are not required.
We also want to emphasize that this scenario has incredibly rich and involved phenomenology. Many different gravitational processes might contribute to the population of a dark sector.

One of them is related to particle production by the external gravitational field from vacuum (GP). This idea dates back to 1939 when Erwin Schrödinger noticed that "[...] *proper vibrations cannot be rigorously separated in the expanding universe* [...] *With particles it would mean production or annihilation of matter, merely by expansion,* [...] *Alarmed by these prospects, I have examined the matter in more detail."* [188]. Schrödinger called this effect *"alarming phenomenon"* as a bug. It took many years for this phenomenon to be recognized as a reliable mechanism for particle creation. Leonard Parker was one of the first to notice the tremendous cosmological significance of this process. In one of his works, we can read "[...] *for the early stages of a Friedmann expansion particle creation may well be of great cosmological significance, especially since it seems inescapable if one accepts quantum field theory and general relativity."* [158]. Gravitational particle production gained much attention in the 1980s through the work of Mukhanov and Chibisov, who used it to explain the origin of matter perturbations leading to galaxy formation [189]. It has been used in a broader context, including inflationary fluctuations [190–195] as well as the Hawking radiation [47]. But what exactly is GP, and how is it related to dark matter?

Cosmological gravitational particle production can be considered as an analog of a quantum harmonic oscillator when the spring constant changes suddenly [196]. The GP mechanism refers to the particle creation by the violent cosmological expansion. It is viewed as a generic consequence of the behavior of quantum fields in the expanding Universe. Namely, fields that are not invariant under conformal transformation[2] develop a time-dependent dispersion relation due to the coupling with gravity [159]. When the dispersion relation evolves non-adiabatically for some Fourier modes, the field gets excited out of its vacuum state, which, in turn, is interpreted as a particle creation [197, 198]. This implies that the expanding Universe inevitably creates all fields, including dark matter. In the absence of other couplings, which could be responsible for the production of DM, the GP mechanism might provide an

[2]Conformal invariance of a given field operationally boils down to a vanishing trace of its stress-energy tensor.

irreducible source of dark matter particles.

Only recently, it has been realized that DM species might also be created gravitationally from the thermal bath via graviton exchange [152, 153, 199, 200]. Such a scenario can be classified as a UV-dominated freeze-in, which exhibits sensitivity to the initial conditions and is most operative at the highest possible energy scales. It emerges from the universal graviton coupling to the energy-momentum tensors of the DM and SM species.

Even more recently, it has been established that a similar mechanism might also induce DM creation directly from the inflaton field [2, 3, 201–204].

1.6 Introduction

This work emerged from the need to establish and systematize knowledge about purely gravitational vector dark matter. When I began my doctoral studies in 2018, this topic was relatively unexplored in the literature. Of course, the purely gravitational dark matter scenario existed long before I started investigating this topic. However, at that time, the main emphasis was put on scalar dark matter, whose purely gravitational production was discussed in many works, including [120, 162–164, 172]. The very first study of purely gravitational spin-1 field was performed by Graham, Mardon, and Rajendran in 2015 [169]. This analysis assumes a very specific cosmological scenario: the immediate transition from the inflationary into the radiation-dominated Universe. Such a premise is reasonable for light spin-1 particles, but is it also true for heavy vectors? It was precisely this question that became the main motivation for undertaking this work.

As mentioned several times above, the efficiency of non-thermal mechanisms of DM production is the highest at very early times. Hence, such processes exhibit strong dependence on the dynamics of the primordial Universe. According to the well-established cosmic inflationary paradigm, the Universe underwent a phase of accelerated expansion in its early stages [205–210]. Although the inflationary paradigm is incredibly successful, it cannot explain all the puzzles alone. For instance, how the Universe transitioned from the super-cooled stage at the end of inflation into a hot and thermal phase. An additional mechanism is needed to account for the energy injection into the SM sector. It is believed that such processes occurred during the epoch of reheating [122–127, 207, 211–213]. Very little is known about the physics of this phase. Its dynamics is expected to be highly involved and model-dependent. However, it is likely that reheating was not instantaneous, which implies the existence of a new cosmological epoch just after the end of inflation but prior to the onset of the RD era. Its presence might have a significant effect on dark matter production.

Thus, we see that the origin of purely gravitational dark matter is intricately linked to the evolution of the early Universe. Hence, any attempts to disregard or trivialize this fact are *a priori* incomplete and might lead to oversimplified results. The dynamics of the Universe in this scenario cannot be treated only as a background in which particle creation occurs. Instead, it should be viewed as a real source of dark species. This, in turn, means that the evolution of the dark sector is inextricably associated with the dynamics of the Universe itself. Therefore, the key issue to address is to answer the question of how the primordial Universe evolved.

The details of the reheating phase are hardly known. In particular, we have no idea how it

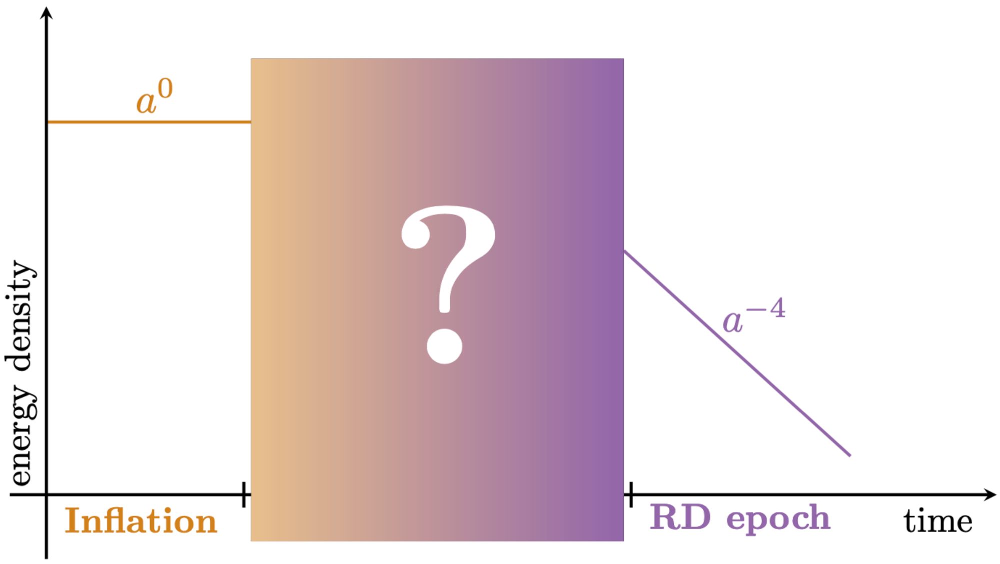

FIGURE 1.7: What happened after the cosmic inflation but before the onset of the Big Bang Nucleosynthesis?

occurred or how long this process lasted. However, we do know that the finite duration of reheating might significantly influence dark matter production, leaving an imprint on its relic abundance. To investigate this effect, we study several perturbative but non-instantaneous reheating scenarios which could give rise to a non-standard cosmology [214–219]. This term refers to an early period (before the Big Bang Nucleosynthesis) that deviates from the standard radiation domination. The existence of non-standard cosmologies might have a significant effect on dark matter production. Moreover, such a scenario has incredibly rich phenomenology, which potentially might be probed in the spectrum of primordial gravitational waves.

Finally, it turns out that purely gravitational particle creation does not exhaust all dark matter production mechanisms. Namely, dark particles can also be produced directly from the inflaton field and the SM quanta due to Planck-suppressed gravitational interactions. The existing literature [152, 153, 199–204] focuses on scalar and fermionic dark matter, and does not fully include subtleties associated to the semi-classical nature of the oscillating inflaton field. However, what is even more important is the fact that in previous works, these three mechanisms were discussed separately without considering their cumulative effect. Such an approach is not well justified since all these processes might generally operate together and are indicative of the same phenomenon - gravity. Hence, a complete picture of purely gravitational dark matter involves not only the incorporation of the early Universe's dynamics but also the discussion of all these effects that inevitably lead to the population of the dark sector.

This thesis is structured as follows. Chapter (2) provides a pedagogical introduction to particle cosmology. The inflationary paradigm is briefly discussed in Chapter (3). Some original results presented in this part are based on [1, 2]. The remaining part of this thesis presents only our original work. Chapter (4) is devoted to non-standard reheating scenarios. Some part of the discussion has already been published [2, 3], while the other part is the subject of ongoing work. In chapter (5), we elaborate on the impact of non-standard cosmologies on the primordial gravitational wave spectrum, relying on Ref.[1]. Finally, in chapter (6), we discuss the production of purely gravitational dark matter vectors in detail. The first part of this chapter, regarding non-perturbative gravitational production, is based on [4], whereas perturbative processes have been partially discussed in Refs. [2, 3]. We conclude in chapter (7).

Chapter 2

Standard Cosmology

In this chapter, we briefly review the fundamentals of the *standard cosmology*, based on several excellent cosmology references, including both classical textbooks [220–225], as well as more recent reviews [19, 226], and lectures notes [227–230]. We commence by providing a concise overview of Einstein's theory of gravity in Sec.(2.1). We accomplish this by introducing fundamental concepts and outlining the mathematical structures that underpin general relativity. Then, in Sec.(2.2), we discuss the isotropic and homogeneous universe whose metric is in the Friedmann–Lemaître–Robertson–Walker (FLRW) form. Section (2.3) is devoted to Einstein's field equations. Here, we derive two fundamental equations for cosmology, i.e., the Friedmann and the Raychaudhuri equations, and study their approximate analytical solutions for a single-component universe. Afterward, in Sec.(2.4), we characterize our Universe by providing the current estimates for some key cosmological parameters describing the ΛCDM model. The quoted values are mostly inferred from the recent Planck 2018 measurements of the CMB anisotropies [13]. In the remaining part of this section, we present some crucial events of the *standard cosmology* and discuss the hot Big Bang (BB) thermodynamics. Finally, in the last section, (2.5), we list some puzzles of the BB paradigm and review the motivation for cosmic inflation.

Disclaimer: The chapter has a pedagogical character and should be viewed as an elementary introduction to more involved topics discussed in this thesis. Readers already familiar with the basic concepts of standard cosmology might skip it.

2.1 Elements of General Relativity

The general theory of relativity (GR) is based on two assumptions:

1. **the principle of equivalence**, which can be formulated in the following manner: "*at every spacetime point in an arbitrary gravitational field it is possible to choose a "locally inertial coordinate system" such that, within a sufficiently small region of the point in question, the laws of nature take the same form as in unaccelerated Cartesian coordinate systems in the absence of gravitation*" [220].

2. **the principle of general covariance**, which states that the form of physical laws is invariant under arbitrary differentiable coordinate transformations.

According to the first postulate, gravitational and inertial masses are equivalent. Moreover, the principle of equivalence states that the effects of gravitation are indistinguishable from the free fall because it is possible to choose a locally inertial frame at each point of space. Finally, it asserts the existence of a locally inertial frame with the structure of the flat Minkowski space.
In addition, the principle of general covariance implies that physical equations hold in a general gravitational field if i) they agree with the laws of special relativity in the absence of

gravity, ii) they preserve their form under a general coordinate transformation, i.e., $x \to x'$. Hence, writing an equation invariant under such transformations essentially boils down to recognizing tensor equations, which are consistent with special relativity in the Minkowski spacetime, substituting the flat metric η_{mn} with the curved one $g_{\mu\nu}$, and replacing ordinary derivatives ∂_μ with covariant ones D_μ.

One of the most relevant concepts in GR is the unification of three spatial dimensions with one dimension of time into a single four-dimensions *spacetime*. In GR, spacetime is a differentiable manifold locally homeomorphic to $\mathbb{R}^4$. This, in particular, implies that one can assign a set of coordinates $x^\mu = \{x^0, x^1, x^2, x^3\}$ to each patch of spacetime. Furthermore, from the *principle of equivalence*, it follows that at each point of spacetime, one can also choose a set of locally inertial coordinates $\xi^m = \{\xi^0, \xi^1, \xi^2, \xi^3\}$. Then, a line element in the vicinity of a given point is

$$ds^2 = \eta_{mn} d\xi^m d\xi^n, \tag{2.1}$$

with $\eta_{mn} = \mathrm{diag}(1, -1, -1, -1)$ being the flat Minkowski metric, while $d\xi^m$ denotes an inertial infinitesimal displacement.
These two sets of coordinates are related to each other through

$$d\xi^m = \frac{\partial \xi^m}{\partial x^\mu} dx^\mu, \tag{2.2}$$

which, in turn, implies

$$ds^2 = g_{\mu\nu} dx^\mu dx^\nu, \qquad\qquad g_{\mu\nu} \equiv \eta_{mn} \frac{\partial \xi^m}{\partial x^\mu} \frac{\partial \xi^n}{\partial x^\nu}. \tag{2.3}$$

Above, we have introduced the symmetric metric tensor $g_{\mu\nu}$, whose inverse is defined by the following relation:

$$g_{\mu\nu} g^{\nu\sigma} = \delta^\sigma_\mu. \tag{2.4}$$

The Minkowski metric is static. In contrast, $g_{\mu\nu}$ is a function of both time and spatial coordinates, i.e., $g_{\mu\nu} = g_{\mu\nu}(t, \vec{x})$. More precisely, the spacetime dependence of the metric tensor involves the effects of gravity, which, in turn, depends on the matter distribution through the Einstein equation, see Sec.(2.3).

Let us now briefly discuss the dynamics of a freely moving particle. According to the first postulate of GR, its equation of motion, or the so-called *geodesic equation*, reads [220]

$$\frac{d^2 x^\lambda}{d\lambda^2} + \Gamma^\lambda_{\mu\nu} \frac{dx^\mu}{d\lambda} \frac{dx^\nu}{d\lambda} = 0 \tag{2.5}$$

with λ being an affine parameter of the particle's trajectory, e.g., its proper time, whose interval is defined as $\Delta\tilde{\tau} = \int \sqrt{ds^2}$. The Christoffel symbols, or the so-called affine connection, are defined as

$$\Gamma^\lambda_{\mu\nu} \equiv \frac{\partial^2 \xi^\alpha}{\partial x^\mu x^\nu} \frac{\partial^\lambda}{\partial x^\alpha}. \tag{2.6}$$

Using the definition of the metric tensor, one obtains

$$\Gamma^\lambda_{\mu\nu} = \frac{1}{2} g^{\rho\lambda} \left(\frac{\partial g_{\mu\rho}}{\partial x^\nu} + \frac{\partial g_{\nu\rho}}{\partial x^\mu} - \frac{\partial g_{\mu\nu}}{\partial x^\rho} \right). \tag{2.7}$$

Note that the affine connection vanishes in flat spacetime, described by the Minkowski metric tensor η_{ab}.

Next, let us consider an arbitrary coordinate transformation of the form $x^\mu \to x'^\mu$. A mixed tensor with upper indices $\mu\nu\dots$ and lower indices $\rho, \sigma\dots$ changes as

$$T^{\mu\nu\cdot}_{\rho\sigma\dots}(x) \to T'^{\mu\nu\cdot}_{\rho\sigma\dots}(x') \equiv \frac{\partial x'^\mu}{\partial x^\lambda}\frac{\partial x'^\nu}{\partial x^\kappa}\dots\frac{\partial x^\alpha}{\partial x'^\rho}\frac{\partial x^\beta}{\partial x'^\sigma}\dots T^{\lambda\kappa\dots}_{\alpha\beta\dots}. \tag{2.8}$$

The metric tensor $g_{\mu\nu}$ transforms as a *covariant tensor*

$$g_{\mu\nu}(x) \to g'_{\mu\nu}(x') \equiv \frac{\partial x^\alpha}{\partial x'^\mu}\frac{\partial x^\beta}{\partial x'^\nu} g_{\alpha\beta}(x), \tag{2.9}$$

whereas its inverse, $g^{\mu\nu}$ behaves as a *contravariant tensor*. However, not all quantities, e.g., the Christoffel symbols, transform as tensors. Hence, it is instructive to define a covariant derivative D_μ, which on *contravariant vector* V^ν acts as

$$D_\mu V^\nu \equiv \frac{\partial V^\nu}{\partial x^\mu} + \Gamma^\mu_{\nu\sigma} V^\sigma. \tag{2.10}$$

Covariant derivatives allow us to assert the effects of gravitation on a physical system. To that end, one should determine a physical equation consistent with special relativity, substitute η_{ab} with $g_{\mu\nu}$, and replace ∂_μ with D_μ.

Next, let us introduce the Riemann curvature tensor

$$R^\rho_{\sigma\mu\nu} := \Gamma^\rho_{\sigma\nu,\mu} - \Gamma^\rho_{\sigma\mu,\nu} + \Gamma^\rho_{\lambda\mu}\Gamma^\lambda_{\sigma\nu} - \Gamma^\rho_{\lambda\nu}\Gamma^\lambda_{\sigma\mu}, \tag{2.11}$$

where the comma notation has been adopted, i.e., $(\dots)_{,\lambda} \equiv \partial(\dots)/\partial x^\lambda$. The Riemann tensor can be viewed as a measure of curvature as it vanishes in a flat metric. From the above expression, one can easily check that it is anti-symmetric under the interchange of $\mu \leftrightarrow \nu$, and $\rho \leftrightarrow \sigma$, at the same time being symmetric under the interchange of $\mu\nu \leftrightarrow \rho\sigma$. Finally, $R^\rho_{\sigma\mu\nu}$ satisfies the following identity:

$$R_{\mu\nu\rho\sigma} + R_{\mu\sigma\nu\rho} + R_{\mu\rho\sigma\nu} = 0. \tag{2.12}$$

Differentiating the above expression with respect to x^λ in a locally inertial frame, one finds

$$R_{\mu\nu\rho\sigma,\lambda} + R_{\mu\nu\lambda\rho,\sigma} + R_{\mu\nu\sigma\lambda,\rho} = 0. \tag{2.13}$$

Since in a locally inertial frame, all Christoffel symbols are zero, in the above expression, one can replace ordinary derivatives with the covariant derivatives, obtaining the so-called Bianchi identities

$$R_{\mu\nu\rho\sigma;\lambda} + R_{\mu\nu\lambda\rho;\sigma} + R_{\mu\nu\sigma\lambda;\rho} = 0, \tag{2.14}$$

where semi-colon denotes the covariant derivative, defined in Eq. (2.10). Finally, contracting the first and third indices of the Riemann tensor, one obtains the symmetric Ricci tensor

$$R_{\mu\nu} \equiv R^\rho_{\mu\rho\nu}, \tag{2.15}$$

and the Ricci scalar through the following contraction:

$$R \equiv g^{\mu\nu} R_{\mu\nu}. \tag{2.16}$$

2.2 Friedmann–Lemaître–Robertson–Walker (FLRW) Universe

As opposed to the anthropocentrism view in which the Earth appears to be a unique place, in the Heliocentric model, it was the Sun that is positioned at the center of the *universe*. Throughout the years, this *local universe* has turned out not to be the whole Universe, so the Sun or even the Solar System has lost their favored position. According to the Copernican principle, human beings are not privileged observers of the Universe, located at its very center. In fact, there is nothing special in our local reference frame. This compelling paradigm provides a guide for studying processes occurring in different regions of the Universe. In particular, the Copernican principle applied to cosmological scales leads us toward the assumption that there are neither favorable directions nor unique places in the Universe. Although the isotropy and homogeneity of the Universe had to be taken as a postulate for a long time, current empirical data strongly support this presupposition on cosmological scales. Despite pretty significant inhomogeneities at small distances, the further one looks into the Universe, the simpler it appears. In particular, the distribution of galaxies and other cosmological structures on large scales ($\sim 100\,\mathrm{Mps}$) is nearly isotropic. From this fact, combined with the Copernican principle, one infers large-scale homogeneity. These two constitute the *cosmological principle* - the foundation of the standard model of cosmology. This principle implies that observations from the Earth are representative of observations from any other vantage point in the Universe and hence legitimate their application to cosmological models. It is worth noting that the homogeneity and isotropy of the Universe are not exact but rather statistical and should be understood as a first approximation. Nevertheless, the *cosmological principle* is widely used in theoretical models nowadays.

2.2.1 The FLRW metric

The *cosmological principle* strongly narrows down the possible form of the spacetime metric compatible with the assumption of isotropy and homogeneity. In particular, isotropic and homogeneous space must have uniform curvature. One demonstrates that there exist only three types of such three-dimensional manifolds: (i) flat space, (ii) sphere with a constant positive curvature, and (iii) hyperbolic space of constant negative curvature. In the spherical coordinates, the most general isotropic and homogeneous metric is given by [226]

$$dl^2 = \frac{dr^2}{1 - kr^2/R_0^2} + r^2 d\Omega^2, \qquad\qquad d\Omega^2 = d\theta^2 + sin^2\theta\, d\phi^2, \tag{2.17}$$

where the azimuthal θ and polar ϕ angles vary in the range $\theta \in [0, \pi]$, $\phi \in [0, 2\pi)$, respectively. The parameter k is related to the curvature of space and takes only three discrete values, i.e., $k \in \{-1, 0, 1\}$, corresponding to a three-dimensional space with negative curvature - a hyperboloid H_3 embedded in four-dimensional Lorentzian space $\mathbb{R}^{1,3}$, the flat Euclidean space E_3, and three-dimensional hypersphere S_3 embedded in four-dimensional Euclidean space, respectively.

Statistical homogeneity and isotropy imply that spacetime can be represented by a sequence of spatial slices ordered in time. The metric is in the form Eq. (2.17) at each three-dimensional piece. Moreover, these two symmetries reduced ten independent components of the metric tensor to a single function of time, such that the line element of four-dimensional spacetime can be written as

$$ds^2 = dt^2 - a^2(t)dl^2, \tag{2.18}$$

where the function $a(t)$ is called the scale factor. Its form can be determined by Einstein's field equations, which will be discussed in Section (2.3).
Inserting Eq.(2.17) into the above expression leads to the most general metric consistent with the *cosmological principle* in four dimensions:

$$ds^2 = dt^2 - a^2 \left(\frac{dr^2}{1 - kr^2/R_0^2} + r^2 d\Omega^2 \right). \tag{2.19}$$

This is the so-called Friedmann–Lemaître–Robertson–Walker (FLRW) metric developed independently by the named authors between 1923 and 1935 [231–234]. It should be emphasized that the FLRW metric does not have the same symmetry as the spacetime itself since it is not homogeneous. Nevertheless, all physical quantities computed from the above metric display all spacetime symmetries.
In what follows, we use the convention in which the scale factor $a(t)$ and the curvature parameter k are dimensionless, whereas the radial coordinate r and the curvature scale R_0 have length dimensions. Such a choice allows us to set $a(t_0) = 1$ at present times. Moreover, the scale R_0 corresponds to the present physical curvature. Let us also stress that for $k \neq 0$, one typically distinguishes two length scales associated with the FLRW metric. Namely, the curvature radius $R_{\text{curv}} \equiv a|k|R_0$, and the so-called Hubble length, defined as $l_H \equiv cH^{-1} = H^{-1}$, with

$$H \equiv \frac{\dot{a}}{a}, \tag{2.20}$$

being the Hubble parameter or the Hubble rate. On the other hand, for $k = 0$, the FLRW metric is characterized fully by the scale of expansion H.

It is convenient to rescale the radial coordinate r according to the following formula [226]:

$$\frac{dr}{\sqrt{1 - kr^2/R_0^2}} = d\chi, \tag{2.21}$$

such that Eq.(2.19) can be recast as

$$ds^2 = dt^2 - a^2 \left(d\chi^2 + S_k^2(\chi) d\Omega^2 \right), \tag{2.22}$$

where the form of the function $S_k^2(\chi)$ is determined by the curvature parameter k. In particular, for $k = 0$, one gets $S_0(\chi) = \chi$, so that the spatial part of metric is in the form of the Euclidean flat metric, i.e.,

$$ds^2 \Big|_{k=0} = dt^2 - a^2 \left(d\chi^2 + \chi^2 d\Omega^2 \right). \tag{2.23}$$

However, the spacetime is curved since the scale factor is a function of time. In particular, its variation accounts for the universe's expansion (or contraction).
On the other hand, for the positive curvature parameter, i.e., $k = 1$, one obtains $S_1(\chi) = R_0 \sin(\chi/R_0)$. In this case, the spatial part of (2.19) has the form of a 3D hypersphere metric

$$ds^2 \Big|_{k=1} = dt^2 - a^2 \left(d\chi^2 + R_0^2 \sin^2(\chi/R_0) \, d\Omega^2 \right). \tag{2.24}$$

Note that the coordinate system described by the metric (2.19) with $k = 1$ is singular for $r = R_0$. Such singularity is removed in the new coordinates Eq. (2.24), implying that such behavior was related to the choice of coordinates, and has no physical meaning. However, since the coordinate singularity divides the hypersphere into two halves, the coordinates $\{t, r, \theta, \phi\}$ cover only one half. Moreover, let us stress that the positive curvature parameter corresponds to a closed spacetime, see Sec.(2.3.4).
Finally, for $k = -1$, one finds $S_{-1} = R_0 \sinh(\chi/R_0)$. In this case, the metric tensor corresponds to infinite and open spacetime, and the line element is

$$ds^2\Big|_{k=-1} = dt^2 - a^2 \left(d\chi^2 + R_0^2 \sinh^2(\chi/R_0)\, d\Omega^2\right). \tag{2.25}$$

The coordinates $\{t, r, \theta, \phi\}$ of the FLRW metric are called the co-moving coordinates. This name reflects that the physical distance between two objects remaining at rest at fixed spatial coordinates changes with time according to the evolution of the scale factor. In particular, the homogeneity of space implies the existence of a unique reference frame, i.e., *the cosmic rest frame* in which the coordinate distance between two such objects remains the same, but the physical distance changes with time. The time coordinate of such a system is called cosmic time.

2.2.2 The Hubble–Lemaître law

The physical distance ℓ_p between two points in the FLRW metric (2.19) measured on a hypersurface with constant t is related to the comoving distance ℓ though the following formula:

$$\ell_p = a(t)\ell. \tag{2.26}$$

In the expanding universe, the physical distance between two objects increases with time since the scale factor is a monotonically growing function of cosmic time t. In contrast, the comoving distance ℓ remains constant in time.
By differentiating the above relation with respect to t, one obtains the Hubble–Lemaître law [12]

$$v \equiv \frac{d\ell_P}{dt} = \dot{a}(t)\ell = H\ell_P. \tag{2.27}$$

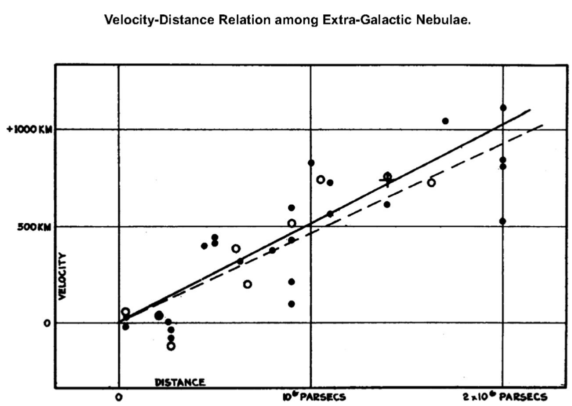

FIGURE 2.1: Velocity–distance relation among extragalactic nebulae, measured by E. Hubble [12].

Edwin Hubble was the first to observe that galaxies move away from the Earth at speeds proportional to their distance. In one of the best recognized scientific articles [12], he published the velocity–distance relation among extragalactic nebulae, which reveals that the velocities of galaxies are directly proportional to their distance, see Fig.(2.1). In other words, the farther they are, the faster they recede away from us. The linear relation between recession velocity and distance indicates a constant expansion of the Universe. Using (2.27), Hubble estimated the present value of the Hubble rate, i.e., the Hubble constant, H_0, to be of the order of 500 km/sec/Mpc [12]. This measurement of this quantity is of great relevance for modern cosmology since it provides valuable information about the rate of cosmic expansion and thus tells us about the matter content of the Universe. As we will discuss in Sec.(2.4), Hubble's estimation contains systematic errors, about seven times that of the present measurements provided, e.g., by the Planck survey. However, it is important to emphasize that there is no consensus on the precise value of the Hubble constant, which remains a topic of ongoing discussion, leading to what is commonly referred to as the *Hubble tension* debate.

2.2.3 Conformal coordinates and redshift

Let us define the conformal time τ through the following transformation of the time coordinate:

$$d\tau := \frac{dt}{a(t)}. \tag{2.28}$$

In conformal coordinates, $\{\tau, r, \theta, \phi\}$, one can factorize the static and dynamical part of the FLRW metric so that the line element becomes

$$ds^2 = a^2(\tau)[d\tau^2 - (d\chi^2 + S_k^2(\phi)d\Omega^2)]. \tag{2.29}$$

The above form is particularly convenient for considering the propagation of light traveling on *null geodesics*, i.e., along the worldlines with $ds^2 = 0$. Isotropy of the background metric allows us to choose coordinates in which the light propagates along the radial direction such that $\theta, \phi = const$. Hence, its path is determined by $d\tau = \pm d\chi$, indicating that in the conformal coordinates, photons move along 45° lines, i.e.,

$$\chi(\tau) = \pm\tau + \text{const.}, \tag{2.30}$$

where the plus (minus) sign corresponds to outgoing (incoming) photons.
Now let us consider the light emitted at a conformal time τ_{emit} at a fixed comoving distance d. Suppose that the signal reaches us at some later moment $\tau_{\text{obs}} = \tau_{\text{emit}} + d$. In conformal coordinates, the duration of the signal $\delta\tau$ is the same at the moment of emission and detection. However, in the comoving coordinates, these two are different. Namely [226],

$$\delta t_{\text{emit}} = a(\tau_{\text{emit}})\delta\tau, \qquad \delta t_{\text{obs}} = a(\tau_{\text{obs}})\delta\tau, \tag{2.31}$$

which implies,

$$\frac{\lambda_{\text{obs}}}{\lambda_{\text{emit}}} = \frac{a(\tau_{\text{obs}})}{a(\tau_{\text{emit}})}, \tag{2.32}$$

where λ_{obs} (λ_{emit}) denotes the wavelength of the observed (emitted) light.
Suppose the signal is detected as the present moment, i.e., $a(\tau_{\text{obs}}) = a_0 = 1$. In this case, the observed wavelength is stretched by the expansion as

$$\lambda_{\text{obs}} = \frac{\lambda_{\text{emit}}}{a(\tau_{\text{emit}})}. \tag{2.33}$$

This effect is called the *cosmological redshift*. The fractional shift of these two wavelengths defines the redshift

$$z := \frac{\lambda_{\text{obs}} - \lambda_{\text{emit}}}{\lambda_{\text{obs}}}, \tag{2.34}$$

which can also be expressed in terms of the scale factor as

$$1 + z = \frac{1}{a(\tau_{\text{emit}})}. \tag{2.35}$$

Redshift z in cosmology is frequently used to label events from the past. From the above definition, it follows that at present, $z_0 = 0$, whereas $z = 1$ corresponds to the Universe half the current size.

2.2.4 Cosmological horizons

Now let us discuss the causal structure of the FLRW metric. In the previous section, we discussed the dynamics of photons propagating along the null geodesics. Particles with non-zero mass travel along timelike worldlines, or *timelike geodesics*, with real proper time, so that $ds^2 > 0$. On the other hand, $ds^2 < 0$ defines the *spacelike geodesics*. Wordlines are called *casual* if they are either lightlike or timelike. According to the *causality principle*, only causal worldlines can represent the motion of a physical object.

The size of causally connected regions of the Universe at some moment t is determined by the maximum comoving distance that light can travel between some initial time t_{BB}, corresponding to the Big Bang singularity and some later time t [226]. It is given by

$$\chi_p(t) := \tau - \tau_{\text{BB}} = \int_{t_{\text{BB}}}^{t} \frac{d\tilde{t}}{a(\tilde{t})}, \tag{2.36}$$

where τ and τ_{BB} denotes the conformal time at t and t_{BB}, respectively. The above expression defines the so-called *(comoving) particle horizon*. The physical size of the particle horizon is

$$d_p(t) := a(t)\chi_p(t). \tag{2.37}$$

Next, let us define the *event horizon* as a surface of the region from which a light ray signal emitted at some moment t_{emit} can be received by an observer in the future [226]. In conformal coordinates, it is given by

$$\chi_{\text{event}} := \int_{\tau}^{\tau_f} d\tilde{\tau} = \tau_f - \tau. \tag{2.38}$$

Hence, χ_{event} can be viewed as a boundary beyond which events cannot affect an observer. Analogously to (2.37), the physical size of the event horizon reads

$$d_{\text{event}}(t) := a(t)\chi_{\text{event}}(t). \tag{2.39}$$

2.3 Einstein's field equations in the FLRW metric

So far, the scale factor $a(t)$ evolution has remained unspecified. The key parameter of the FLRW metric can be determined by the solution to Einstein's field equations - the main subject of this section, which relates the curvature of spacetime to the matter distribution within it.

2.3.1 The Friedmann and Raychaudhuri equations

Let us start with the Einstein–Hilbert action [235–237], which in the presence of a cosmological constant Λ is given as [1]

$$S_{\rm EH} = -\frac{M_{\rm Pl}^2}{2}\int d^4x\sqrt{-g}(R+2\Lambda), \tag{2.40}$$

where $M_{\rm Pl} \equiv \sqrt{c\hbar/(8\pi G)} = (8\pi G)^{-1/2} \simeq 2.435\times 10^{18}$ GeV is the so-called reduced Planck mass, g denotes the determinant of the metric tensor $g_{\mu\nu}$, and R is the Ricci curvature scalar, introduced in Eq. (2.16).
The full action of the theory is a sum of the Einstein–Hilbert term (2.40) and the matter action

$$S_{\rm matter} = \int d^4x\sqrt{-g}\mathcal{L}_{\rm matter}, \tag{2.41}$$

accounting for the dynamics of any matter fields appearing in theory.
The dynamical equations can be found through the principle of least action by demanding the variation of the full action, i.e., $S_{\rm EH}+S_{\rm matter}$, with respect to $g^{\mu\nu}$ to be zero, i.e.,

$$\frac{\delta(S_{\rm EH}+S_{\rm matter})}{\delta g^{\mu\nu}} = 0, \tag{2.42}$$

yielding

$$\frac{M_{\rm Pl}^2}{2}\int d^4x\sqrt{-g}\left[-\frac{\delta R}{\delta g^{\mu\nu}} - \frac{R+2\Lambda}{\sqrt{-g}}\frac{\delta\sqrt{-g}}{\delta g^{\mu\nu}} + \frac{2}{M_{\rm Pl}^2}\frac{1}{\sqrt{-g}}\frac{\delta(\sqrt{-g}\mathcal{L}_{\rm matter})}{\delta g^{\mu\nu}}\right]\delta g^{\mu\nu} = 0. \tag{2.43}$$

The vanishing of the above variation implies

$$\frac{\delta R}{\delta g^{\mu\nu}} + \frac{R+2\Lambda}{\sqrt{-g}}\frac{\delta\sqrt{-g}}{\delta g^{\mu\nu}} = \frac{1}{M_{\rm Pl}^2}T_{\mu\nu}, \tag{2.44}$$

where we have adopted the Belinfante–Rosenfeld definition of the stress-energy tensor

$$T_{\mu\nu} := \frac{2}{\sqrt{-g}}\frac{\delta(\sqrt{-g}\mathcal{L}_{\rm matter})}{\delta g^{\mu\nu}} = 2\frac{\delta\mathcal{L}_{\rm matter}}{\delta g^{\mu\nu}} - g_{\mu\nu}\mathcal{L}_{\rm matter}. \tag{2.45}$$

Note that above, we have used the following identity, see, e.g., [19]:

$$\frac{1}{\sqrt{-g}}\frac{\delta\sqrt{-g}}{\delta g^{\mu\nu}} = -\frac{1}{2}g_{\mu\nu}. \tag{2.46}$$

To calculate the left-hand side of (2.44), one must find the variation of the Ricci scalar w.r.t $g^{\mu\nu}$. This is a standard textbook calculation, which can be found, e.g., in Ref. [19, 224], and gives

$$\frac{\delta R}{\delta g^{\mu\nu}} = R_{\mu\nu}. \tag{2.47}$$

[1] Note that here we have adopted the Landau-Lifshitz "timelike convention" [238], in which the flat metric tensor $\eta_{\mu\nu}$ has the *mostly minuses* signature, i.e., $\eta_{\mu\nu} = \mathrm{diag}(1,-1,-1,-1)$. According to classification developed by Misner, Thorne, and Wheeler [221] other conventions can be categorized according to three signs $\{s_1, s_2, s_3\}$ appearing in the metric tensor $\eta_{\mu\nu} = [s_1]\,\mathrm{diag}(-1,+1,+1,+1)$, the Riemann tensor $R^{\rho}_{\sigma,\mu\nu} = [s_2]\,(\Gamma^{\rho}_{\sigma\nu,\mu} - \Gamma^{\rho}_{\sigma\mu,\nu} + \Gamma^{\rho}_{\lambda\mu}\Gamma^{\lambda}_{\sigma\nu} - \Gamma^{\rho}_{\lambda\nu}\Gamma^{\lambda}_{\sigma\mu})$, and in the Einstein equation $G_{\mu\nu} = [s_3]\,T_{\mu\nu}/M_{\rm Pl}^2$.

Combining all together leads to the well-known Einstein's field equations

$$\boxed{G_{\mu\nu} - \Lambda g_{\mu\nu} = \frac{1}{M_{\text{Pl}}^2} T_{\mu\nu},} \tag{2.48}$$

where the Einstein tensor is defined as

$$G_{\mu\nu} := R_{\mu\nu} - \frac{1}{2} R g_{\mu\nu}. \tag{2.49}$$

Note that $G_{\mu\nu}$ accounts for the curvature of spacetime, whereas the r.h.s. of Eq.(2.48) represents the energy-momentum tensor of the matter content. Hence, one can interpret Eq.(2.48) as a set of ten equations determining the impact of the stress tensor on the curvature of spacetime. Let us also emphasize that out of ten independent components of the symmetric 4×4 tensors, $G_{\mu\nu}$, only six equations are independent. Such reduction follows from the Bianchi identities (2.14).

Now let us work out the two tensors appearing in the Einstein equations, i.e., the Einstein tensor $G_{\mu\nu}$, and the stress-energy tensor $T_{\mu\nu}$. The former is determined by the background metric. In particular, in the FLRW metric (2.19), the only non-vanishing Christoffel symbols (2.7) are

$$\Gamma^0_{ij} = \frac{g^{0\sigma}}{2}[g_{\sigma i,j} + g_{\sigma j,i} - g_{ij,\sigma}] = -\frac{1}{2} g_{ij,t} = \frac{\dot{a}}{a}\tilde{g}_{ij}, \tag{2.50}$$

$$\Gamma^i_{0j} = \frac{g^{i\sigma}}{2}[g_{\sigma 0,j} + g_{\sigma j,0} - g_{0j,\sigma}] = a^{-2}(t)\tilde{g}^{ik}\dot{a}a\tilde{g}_{kj} = \frac{\dot{a}}{a}\delta^i_j, \tag{2.51}$$

$$\Gamma^i_{jk} = \frac{g^{i\sigma}}{2}[g_{\sigma j,k} + g_{\sigma k,j} - g_{jk,\sigma}], \tag{2.52}$$

where we have used the notation $(t, r, \theta, \phi) = (0, 1, 2, 3)$, and indices i and j are for space coordinates. The form of $\tilde{g}_{ij}$ depends on the choice of the spatial coordinates, and in the spherical polar coordinates, one has

$$\tilde{g}_{11} = -\frac{1}{1 - kr^2/R_0^2}, \qquad \tilde{g}_{22} = -r^2, \qquad \tilde{g}_{33} = -r^2 \sin^2\theta. \tag{2.53}$$

From the above Christoffel symbols, one finds (for the detailed calculations see, e.g., [19, 224, 226], and also Sec.(5.1)) that the non-vanishing components of the Ricci tensor are the diagonal ones given by

$$R_{00} = -3\frac{\ddot{a}}{a}, \qquad R_{ij} = a^2\left[\frac{\ddot{a}}{a} + 2\left(\frac{\dot{a}}{a}\right)^2 + 2\frac{k}{a^2R_0^2}\right]\tilde{g}_{ij}. \tag{2.54}$$

Therefore, the Ricci scalar is

$$R = g^{00}R_{00} + g^{ij}R_{ij} = -6\left[\frac{\ddot{a}}{a} + \left(\frac{\dot{a}}{a}\right)^2 + \frac{k}{a^2R_0^2}\right], \tag{2.55}$$

so that the non-zero components of the Einstein tensor are

$$G_{00} = R_{00} - \frac{1}{2}Rg_{00} = 3\left[\left(\frac{\dot{a}}{a}\right)^2 + \frac{k}{a^2R_0^2}\right], \tag{2.56}$$

$$G_{ij} = R_{ij} - \frac{1}{2}Rg_{ij} = \left[2\frac{\ddot{a}}{a} + \left(\frac{\dot{a}}{a}\right)^2 + \frac{k}{a^2R_0^2}\right]g_{ij}. \tag{2.57}$$

Isotropy and homogeneity of spacetime imply that the stress-energy tensor $T_{\mu\nu}$ should exhibit a corresponding structure. Namely, the former symmetry requires the mixed components of the energy-moment tensor to vanish, i.e., $T_{0i} = 0$, whereas spatial components should be of the form $T_{ij} \propto \delta_{ij}$. Furthermore, homogeneity entails the proportionality factor being only a time function. It can be shown that the most generic form of the stress tensor consistent with these symmetries is given by [226]

$$T^{\mu}_{\nu} = \begin{pmatrix} \rho & 0 & 0 & 0 \\ 0 & -p & 0 & 0 \\ 0 & 0 & -p & 0 \\ 0 & 0 & 0 & -p \end{pmatrix}. \tag{2.58}$$

One recognizes in this expression the energy-momentum tensor of a perfect fluid in the reference frame of the comoving observer. Above, ρ and p are only functions of time. In the covariant form, the energy-momentum tensor of the perfect fluid can be written as

$$T_{\mu\nu} = (\rho + p)\, u_\mu u_\nu - p g_{\mu\nu}, \tag{2.59}$$

with u_μ being the four-velocity of the fluid relative to the observer. For the comoving observer, the only non-zero component of the four-velocity is $u_0 = 1$. One interprets ρ and p as the time-dependent energy density and pressure measured in the rest frame of the fluid.
Using (2.56), one finds that $G^0_0 = G_{00}$, which, combined with the 00 component of the energy-momentum tensor, gives the Friedmann equation:

$$\boxed{H^2 = \frac{\rho}{3M_{\rm Pl}^2} - \frac{k}{a^2 R_0^2} + \frac{\Lambda}{3},} \tag{2.60}$$

whereas comparing the spatial components of these two tensors, one gets the Raychaudhuri equation [239]

$$\frac{\ddot{a}}{a} + \frac{1}{2}H^2 + \frac{k}{2a^2 R_0^2} - \frac{\Lambda}{2} = -\frac{1}{2M_{\rm Pl}^2}p, \tag{2.61}$$

which can also be recast as

$$\boxed{\frac{\ddot{a}}{a} = -\frac{1}{6M_{\rm Pl}^2}(\rho + 3p) + \frac{\Lambda}{3}.} \tag{2.62}$$

Note that ρ and p should be understood as the total energy density and pressure of all matter contributions.
By differentiating (2.60) with respect to time,

$$2\frac{\dot{a}}{a}\left[\frac{\ddot{a}}{a} - \frac{\dot{a}^2}{a^2}\right] = \frac{\dot{\rho}}{3M_{\rm Pl}^2} + 2\frac{k}{R_0^2}\frac{\dot{a}}{a^3}, \tag{2.63}$$

and substituting (2.62), one gets

$$2\frac{\dot{a}}{a}\left[-\frac{1}{6M_{\rm Pl}^2}(\rho + 3p) + \frac{\Lambda}{3} - \frac{\dot{a}^2}{a^2}\right] = \frac{\dot{\rho}}{3M_{\rm Pl}^2} + 2\frac{k}{R_0^2}\frac{\dot{a}}{a^3}, \tag{2.64}$$

which combined with (2.60) leads to the continuity equation

$$\dot{\rho} + 3H(\rho + p) = 0. \tag{2.65}$$

The above relations account for the *energy conservation* in the FLRW Universe. It mimics the first law of thermodynamics, $dU = -pdV$, in the expanding spacetime, i.e., for $U = \rho V$ and $V = a^3$. The continuity equation (2.65) together with the Friedmann (2.60) and Raychaudhuri (2.62) constitute a system of three equations, out of which only two are independent. Note that the above formula can also be obtained from the conservation equation for the stress tensor, i.e.,

$$\nabla_\mu T^\mu_\nu = \partial_\mu T^\mu_\nu + \Gamma^\mu_{\mu\lambda} T^\lambda_\nu - \Gamma^\lambda_{\mu\nu} T^\mu_\lambda = 0. \tag{2.66}$$

Namely, for the $\nu = 0$ component of the above expression, one finds the dynamical equation for the energy density

$$\partial_\mu T^\mu_0 + \Gamma^\mu_{\mu\lambda} T^\lambda_0 - \Gamma^\lambda_{\mu 0} T^\mu_\lambda = 0, \tag{2.67}$$

which combined with Christoffel symbols (2.52) gives (2.65).

Before closing this part, let us emphasize that equations (2.60) and (2.62) play a fundamental role in modern cosmology. In particular, the Friedmann equation (2.60) links the evolution of the scale factor $a(t)$ with the matter component of the Universe, its spatial curvature, and a cosmological constant. The Raychaudhuri equation, (2.62), indicates that for the ordinary matter component obeying the *strong energy condition*,

$$\rho + 3p > 0, \tag{2.68}$$

the expansion of the Universe slows down, i.e., $\ddot{a} < 0$. One finds that in the FLRW metric, the negativity of the second time derivative of the scale factor inevitably implies an initial singularity at $t = 0$, since $a \to 0$, and $\rho \propto t^{-2}$ [226]. Stephen Hawking and Roger Penrose have demonstrated that such singularity appears as a universal feature of all Big Bang models [240]. On the other hand, any form of matter violating the *strong energy condition* and dominating the energy budget would cause an acceleration of the scale factor, i.e., $\ddot{a} > 0$. As we will see in the next chapter, such behavior can be observed, e.g., for a scalar field, for which the kinetic energy is much smaller than its potential energy, such that $\rho \simeq -p$. This simple fact lies at the heart of the inflationary paradigm.

2.3.2 Matter components with constant equation of state

To determine the evolution of the scale factor, and thus the dynamics of the Universe, one needs two specify the matter content since different matter components affect the expansion rate differently. A perfect fluid can be characterized by the *equation of state* (e.o.s), i.e., the relation between its pressure and energy density, most often in the form p/ρ. One distinguishes a *barotropic fluid* whose pressure is a function of the energy density only, i.e., $p(\rho)$. The corresponding equation of state is called the *barotropic equation of state*, which for most cosmological fluids can be written in the following form:

$$p = w\rho, \tag{2.69}$$

with w being a constant coefficient, the so-called *equation of state* or *barotropic parameter*. Inserting the above relation into (2.65), one can evaluate the continuity equation, obtaining

$$\frac{d\rho}{\rho} = -3(1+w)\frac{da}{a}, \qquad \Longrightarrow \qquad \rho(a_0) = \left(\frac{a}{a_0}\right)^{-3(1+w)}. \tag{2.70}$$

The above solution shows that as long as $w > -1$, the energy density of a matter dilutes as a power law with the factor. Hence, the dynamics of the cosmological fluids is determined by its equation of state parameter.

It is convenient to rearrange the Friedmann equation (2.60) as follows,

$$H^2 = \frac{1}{3M_{\rm Pl}^2}\rho_{\rm tot}, \qquad\qquad \rho_{\rm tot} \equiv \rho_{\rm matter} + \rho_k + \rho_\Lambda, \tag{2.71}$$

with

$$\rho_k \equiv -M_{\rm Pl}^2 \frac{3k}{a^2 R_0^2}, \qquad\qquad \rho_\Lambda \equiv M_{\rm Pl}^2 \Lambda, \tag{2.72}$$

where we have associated energy density with the curvature term and a cosmological constant. Above, $\rho_{\rm matter}$ refers to the total energy density of all ordinary matter components of the Universe. Since $\rho_k \propto a^{-2}$, from the solution (2.70), one can see that the curvature term mimics a perfect fluid with $w_k = -1/3$. On the other hand, the independence of ρ_Λ on the scale factor indicates that cosmological constant can be viewed as a barotropic fluid with $w_\Lambda = -1$.
Note that along the same lines, one can recast the Raychaudhuri equation (2.62) as

$$\frac{\ddot{a}}{a} = -\frac{1}{6M_{\rm Pl}^2}(\rho_{\rm tot} + 3p_{\rm tot}), \qquad\qquad p_{\rm tot} \equiv p_{\rm matter} + p_k + p_\Lambda, \tag{2.73}$$

where the following identities have been used: $\Lambda/3 = -(\rho_\Lambda + 3p_\Lambda)/(6M_{\rm Pl}^2)$ with $p_\Lambda \equiv -\rho_\Lambda$, and $\rho_k + 3p_k = 0$, with $p_k = -\rho_k/3$.

In the cosmological context, various types of matter are of particular interest. Below we briefly characterize three of them.

i) Non-relativistic, pressureless matter with $w = 0$
The term non-relativistic (NR), pressureless matter, or *dust*, usually refers to a perfect barotropic fluid whose pressure is negligible relative to its energy density, i.e., $|p_{\rm m}| \ll \rho_{\rm m}$, so that one can assume that $w_{\rm m} = 0$. From (2.70), one finds that the energy density of NR matter decreases as $\rho_{\rm m} \propto a^{-3}$. Such behavior results from the fact that the volume V of a given region in space expands as a^3, whereas the energy of particles E making up NR matter remains constant. One typically distinguishes two main types of cosmological dust, i.e., *baryons* constituting an ordinary visible content of the Universe, composed of non-relativistic SM species, and dark matter whose nature remained unknown.

ii) Relativistic matter with $w = 1/3$
The kinetic energy of relativistic particles is so large that, effectively, they can be treated as massless. In particular, a gas of free ultra-relativistic species with $w = 1/3$ is referred to as *radiation*. One can easily find that the energy density of radiation dilutes as $\rho_{\rm r} \propto a^{-4}$. Note that in comparison to $\rho_{\rm r}$, the evolution of $\rho_{\rm r}$ is suppressed by an extra factor of a^{-1}, accounting for the redshift of the radiation energy. There are four main constituents of cosmic radiation: 1) massless SM photons, which now are mostly in the form of the cosmic microwave background, 2) neutrinos, which behaved like relativistic matter in the early Universe, but due to the non-zero mass at some point they decouple and act as matter, 3) gravitons, i.e., a spin-2 massless field mediating gravitational interactions, 4) other (almost) massless species belonging to the SM sector, or any other hidden sector, which mass initially was much smaller

than the temperature of the Universe. Note that, initially, all SM particles behaved as radiation, but as the temperature of the thermal bath dropped below their mass, they became non-relativistic and started to act as dust.

iii) Dark energy $w = -1$
The term dark energy refers to a perfect fluid with e.o.s parameter $w_{\rm de} = -1$. Since the energy density of any matter component is positive, the pressure of such fluid must be negative, which, in turn, generates repulsive gravity. From (2.70), one finds that dark energy density is constant in time, i.e., $\rho_{\rm de} \propto a^0$. Hence, one concludes that the energy increases proportionally to the volume of space. As we have already seen, such a barotropic parameter is characteristic of a cosmological constant. The latter was originally introduced by Einstein to balance the gravitational attraction of matter-energy density and, hence, make the Universe static. A cosmological constant can be viewed either as a geometrical term contributing to the l.h.s. of the Einstein equation or as a new matter component appearing on the r.h.s. of this equation. There are several other candidates for a fluid with constant energy density. The simplest possibility is that of vacuum energy associated with the energy of empty space itself. It can be estimated from the following formula [226]:

$$\rho_{\rm vacuum} = \frac{1}{2}\int_0^\infty \frac{d\vec{k}}{(2\pi)^3}\,\omega_k, \tag{2.74}$$

with $\omega_k \equiv \sqrt{|\vec{k}|^2 + m^2}$ being the zero-point energy associated with fluctuations of the vacuum. One notes that the above quantity exhibits an ultraviolet divergence that can be removed by imposing a UV cut-off scale $k_{\rm max}$, typically assumed to be the Planck scale. After straightforward integration, one finds

$$\rho_{\rm vacuum} \approx \left.\frac{k_{\rm max}^4}{16\pi^2}\right|_{k_{\rm max}=M_{\rm Pl}} \approx 10^{74}\ {\rm GeV}^4. \tag{2.75}$$

Even though conceptually, cosmological constant and vacuum energy are very different, they are observationally indistinguishable. In yet another, more exotic, scenario, a cosmological constant is replaced by a dynamical matter component whose barotropic parameter changes with time.

In particular, there is no profound reason to restrict our attention to matter components with a 'standard' equation of state, i.e., $w \in \{-1, 0, 1/3\}$. In particular, as we will see in the next chapter, *non-standard* values of the e.o.s parameter arise naturally for a scalar field, e.g., if it possesses a non-trivial (neither quadratic nor quartic) potential .

2.3.3 Exact solutions

Now let us discuss the dynamics of the Universe, whose energy budget is dominated by a single barotropic fluid. Different scaling of the energy densities of various matter components implies that the dynamic of the Universe has been determined mainly by a single fluid for most of its history. For the expanding Universe, it has been a matter constituent with the smallest e.o.s parameter at a given time. In this case, assuming that the energy density of a single matter component evolves according to (2.70), from (2.71), one gets

$$a(t) = a_0 \times \begin{cases} \left[1 + \frac{3(1+w)}{2}\sqrt{\frac{\rho(a_0)}{2}}\frac{t-t_0}{M_{\rm Pl}}\right]^{\frac{2}{3(1+w)}}, & w \neq -1, \\ \exp\left[\sqrt{\frac{\rho(a_0)}{3M_{\rm Pl}^2}}(t-t_0)\right], & w = -1, \end{cases} \tag{2.76}$$

matter component	**barotropic parameter w**	$\rho(a)$	$\mathbf{a(t)}$	$a(\tau)$
non-relativistic matter	0	$\propto a^{-3}$	$\propto t^{2/3}$	$\propto \tau^2$
ultra-relativistic radiation	1/3	$\propto a^{-4}$	$\propto t^{1/2}$	$\propto \tau$
spatial curvature	−1/3	$\propto a^{-2}$	$\propto t$	$\propto \exp\left[H_i a_i \tau\right]$
cosmological constant	−1	$\propto a^0$	$\propto \exp\left[Ht\right]$	$\propto \tau^{-1}$

TABLE 2.1: Behaviour of different matter fluids characterized by a constant equation of state parameter w.

or as a function of the conformal time τ (2.28),

$$a(\tau) = a(\tau_0)\begin{cases}\left(1+\frac{1+3w}{2}\frac{a(\tau_0)}{M_{\rm Pl}}\sqrt{\frac{\rho(\tau_0)}{3}}(\tau-\tau_0)\right)^{\frac{2}{1+3w}}, & w \neq -1/3,\\ \exp\left[\sqrt{\frac{\rho(\tau_0)}{3M_{\rm Pl}^2}}a(\tau_0)(\tau-\tau_0)\right], & w=-1/3.\end{cases} \tag{2.77}$$

Above, $a(t_0)$ ($a(\tau_0)$) and t_0 (τ_0) are two integration constants.
Inserting the solution (2.70) into the Friedmann equation, one finds that the relation between the Hubble rate H and the scale factor a takes the power-law formula

$$H(a) = \sqrt{\frac{\rho(a_0)}{3M_{\rm Pl}^2}}\left(\frac{a}{a_0}\right)^{-\frac{3(1+w)}{2}}. \tag{2.78}$$

Hence, for matter fluids with $w > -1$, the Hubble parameter decreases with a, whereas for the special case $w = -1$, it becomes constant in time.
The above results are summarized in Table(2.1).

2.3.4 Critical density

It is instructive to introduce the *dimensionless density parameter* for a given matter component as

$$\Omega_i(t) \equiv \frac{\rho_i(t)}{\rho_{\rm crit}}, \qquad i \in \{{\rm m}, {\rm r}, \Lambda, \dots\}, \tag{2.79}$$

where

$$\rho_{\rm crit}(t) \equiv 3M_{\rm Pl}^2 H^2(t), \tag{2.80}$$

denotes the so-called *critical density*, corresponding to the energy density of a spatially flat universe ($k = 0$) in the absence of a cosmological constant. For convenience, one usually defines also the *curvature density parameter* as [226]

$$\Omega_{\rm k}(t) \equiv -\frac{k}{R_0^2 H^2(t)}, \tag{2.81}$$

which can be positive as well as negative, depending on the curvature parameter k. As explicitly specified above, both $\Omega_i(t)$ and $\Omega_{\rm k}(t)$ are functions of time. Apart from this, one also defines *present density parameters*, which refer to a value of $\Omega(t)$ at the present epoch. To make a distinction between these two, we use the subscript $'0'$ when referring to quantities calculated today, i.e., at t_0. Hence, the present density parameters are

$$\Omega_{i,0}(t) \equiv \frac{\rho_i(t_0)}{\rho_{\text{crit},0}}, \qquad \Omega_{\text{k}}(t) \equiv -\frac{k}{R_0^2 H_0^2}, \tag{2.82}$$

where the critical energy density today is

$$\rho_{\text{crit}}(t) \equiv 3M_{\text{Pl}}^2 H_0^2, \tag{2.83}$$

with $H_0 \equiv H(t_0)$ being the *Hubble constant*.
Isolating contributions from different forms of cosmological fluid, the Friedmann equation (2.60) can be recast to the following compact form:

$$\frac{H^2}{H_0^2} = \Omega_{\text{m},0}\left(\frac{a_0}{a}\right)^3 + \Omega_{\text{r},0}\left(\frac{a_0}{a}\right)^4 + \Omega_{\text{k},0}\left(\frac{a_0}{a}\right)^2 + \Omega_{\Lambda,0}. \tag{2.84}$$

In the current epoch, one finds

$$1 - \Omega_{\text{matter},0} = \Omega_{\text{k},0}, \qquad \Omega_{\text{matter},0} = \Omega_{\text{m},0} + \Omega_{\text{r},0} + \Omega_{\Lambda,0}. \tag{2.85}$$

Hence, measuring the total matter density of the Universe and the Hubble parameter H_0 allows us to determine the present critical energy $\rho_{\text{crit},0}$, and hence establish the present curvature of the Universe. Namely, $\Omega_{\text{matter},0} > 1$ implies positive spatial curvature, $\Omega_{\text{matter},0} = 1$ corresponds to the spatially flat Universe, whereas $\Omega_{\text{matter},0} < 1$ indicates that the spatial curvature is negative, i.e.,

$$\rho_{\text{matter},0} > \rho_{\text{crit},0} \;\Leftrightarrow\; \Omega_{\text{matter},0} > 1 \;\Rightarrow k > 0 \tag{2.86}$$
$$\rho_{\text{matter},0} = \rho_{\text{crit},0} \;\Leftrightarrow\; \Omega_{\text{matter},0} = 1 \;\Rightarrow k = 0, \tag{2.87}$$
$$\rho_{\text{matter},0} < \rho_{\text{crit},0} \;\Leftrightarrow\; \Omega_{\text{matter},0} < 1 \;\Rightarrow k < 0. \tag{2.88}$$

Positive (negative) curvature parameter k corresponds to the closed (open) universe, whereas $k = 0$ implies flat spacetime. Note that the former case corresponds to a decelerated expansion, whereas constant and accelerated expansion only can be admitted for flat and open spacetimes [222]. Hence, an open universe would expand forever as it does not contain enough matter content which could slow down the expansion. On the other hand, a closed universe would possess enough mass to inhibit the expansion and eventually collapses. A flat universe whose matter energy density matches the critical density can be viewed as a balance between these alternatives.

Finally, let us point out that Eq. (2.84) can be rewritten in the following form:

$$\int_{a(t_i)}^{a(t_f)} \frac{da}{\sqrt{\Omega_{\text{r},0}\left(\frac{a_0}{a}\right)^2 + \Omega_{\text{m},0}\left(\frac{a_0}{a}\right) + \Omega_{\text{k},0} + \Omega_{\Lambda,0}\left(\frac{a_0}{a}\right)^{-2}}} = a_0 \cdot H_0 \cdot (t_f - t_i). \tag{2.89}$$

2.4 The Universe

So far, we have provided a general description of the homogeneous and isotropic universe. We have distinguished several types of matter depending on their equation of state parameter and discussed their dynamics and impact on the universe's evolution. Now let us describe our Universe.

The ΛCDM model, based on the pillars of the Standard Model of particle physics and general relativity, is widely regarded as the best established and successful model of cosmology, providing a reasonably good fit to a wide range of empirical data. It is frequently referred to as the *standard model of cosmology* in analogy to its particle physics counterpart. It is dubbed after the two major constituents of the present Universe: dark energy associated with a cosmological constant Λ and cold dark matter CDM. The ΛCDM model emerged at the end of the 1990s as a *concordance model of cosmology* and a descendant of the CDM model, which has not involved the cosmological constant. The former is nowadays widely accepted by the research community primarily because its predictions are in astonishing agreement with various cosmological observations, including the CMB radiation and its temperature fluctuation [13, 241–246], the abundances of the elements [247], the baryon acoustic oscillation (BAO) [248–252], the abundance of galaxy clusters [253, 254], as well as the observed magnitude-distance relation of type Ia supernovae [255–258], which was the original motivation to replace the CDM model by the concordance model.

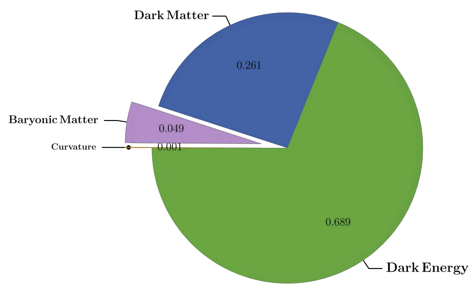

Figure 2.2: The present density parameters of the four dominant matter components of the Universe, i.e., spatial curvature $\Omega_{k,0}$, SM baryonic matter $\Omega_{\mathrm{SM},0}$, dark matter $\Omega_{\mathrm{DM},0}$ and dark energy $\Omega_{\Lambda,0}$.

In its simplest version, ΛCDM involves six independent parameters ingredients [13] (within the 68% confidence limit, and 95% on upper limits): baryon abundance $\Omega_b h^2 = 0.0224 \pm 0.0001$, dark matter abundance $\Omega_{\mathrm{DM}} h^2 = 0.120 \pm 0.001$; the angular acoustic scale $100\theta_{\mathrm{MC}} = 1.0411 \pm 0.0003$; scalar spectral index $n_s = 0.965 \pm 0.004$; the amplitude of curvature perturbations $\ln 10^{10} A_s = 3.043 \pm 0.014$; and reionization optical depth $\tau = 0.054 \pm 0.007$.

The ΛCDM model depicts a flat, increasing Universe whose dynamics is determined by the three major matter component: dark energy Λ ($w_{\mathrm{dE}} \approx -1$) which comprises $\sim 68\%$ of the critical energy density, cold dark matter CDM ($w_{\mathrm{DM}} \approx 0$) which makes up $\sim 27\%$ of the total energy budget, and ordinary baryonic matter which constitutes only a $\sim 5\%$ fraction of the total energy density. The Planck collaboration [13], using the CMB data combined with CMB lensing reconstruction and BAO measurements from recent galaxy surveys such as SDSS, determined the values of the present density parameters of each individual component, i.e., cosmological constant Λ, non-relativistic matter m, spatial curvature k, and ultra-relativistic radiation r, to be

$$\Omega_{\Lambda,0} = 0.6889 \pm 0.0056, \qquad \Omega_{\mathrm{m},0} = 0.3111 \pm 0.0056, \tag{2.90}$$

$$\Omega_{\mathrm{k},0} = 0.001 \pm 0.002, \qquad \Omega_{\mathrm{r},0} \leq 10^{-4}. \tag{2.91}$$

Note that the matter density parameter is a sum of two contributions, i.e., cold dark matter $\Omega_{\mathrm{DM},0} \simeq 0.27$, and the SM baryons (mainly protons) $\Omega_{\mathrm{b},0} \simeq 0.05$.

The relative abundances of the matter components have changed in former times. In particular, as we will have already discussed, in the standard Big Bang cosmology, one distinguishes

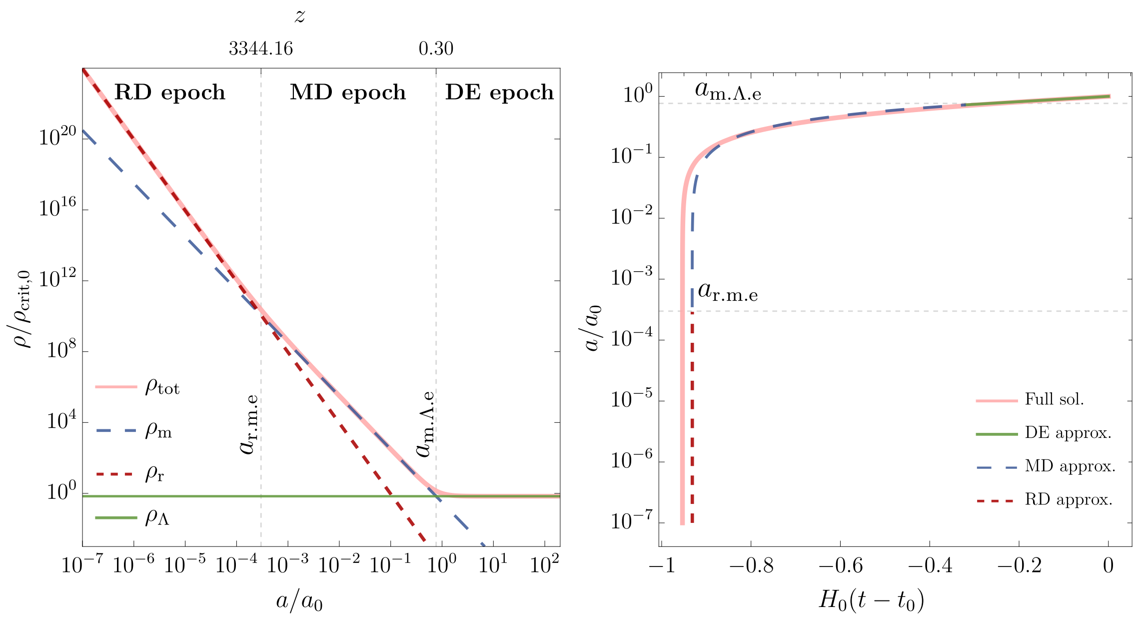

FIGURE 2.3: Left panel: The evolution of energy densities of various components normalized to the present critical energy density. The early radiation-dominated (RD) epoch is followed by the matter-dominated (MD) epoch and the subsequent dark energy (DE) era. At $a_{\rm r.m.e}$ ($a_{\rm m.\Lambda.e}$) the energy density of radiation (matter) equalizes with that of matter (dark energy). Right panel: The corresponding evolution of the scale factor in different cosmological epochs.

the presence of three cosmological epochs in which the total energy budget has been dominated by a single matter component i, such that $\rho_{\rm i} \ll \rho_{\rm j}$. The crossover between different eras occurs around $\Omega_{\rm i}(a_{\rm i.j.e}) \simeq \Omega_{\rm j}(a_{\rm i.j.e})$. Adopting the present values of density parameters (2.90) and (2.91), we can easily convince ourselves that the energy of radiation becomes more and more relevant as one goes back in time, cf. left panel of Fig.(2.3). From the scaling of the radiation and matter energy density with a, one estimates the scale factor corresponding to the radiation-matter equality (r.m.e) as [226]

$$a_{\rm r.m.e} = \frac{\Omega_{\rm r,0}}{\Omega_{\rm m,0}} \approx 2.9 \times 10^{-4}, \tag{2.92}$$

which corresponds to the redshift $z_{\rm r.m.e} \approx 3340$, where we used the following relation

$$z(t) = \frac{a_0}{a(t)} - 1. \tag{2.93}$$

From the fact that $w_{\rm m} > w_{\rm de}$, it follows that the dark energy era should have followed the matter-dominated epoch. Hence, one can determine the scale factor at which dark energy began to dominate over non-relativistic matter

$$a_{\rm m.\Lambda.e} = \left(\frac{\Omega_{\rm m,0}}{\Omega_{\Lambda,0}}\right)^{1/3} \approx 0.77, \tag{2.94}$$

corresponding to $z_{\rm r.m.e} \approx 0.3$.
From relation (2.89), by setting $t_i \to 0$, $a(t_i) \to 0$ and $a(t_f) = a_{\rm r.m.e}$ or $a(t_f) = a_{\rm r.\Lambda.e}$ one obtains $t_{\rm r.m.e} \approx 5 \times 10^4$ years and $t_{\rm r.\Lambda.e} \approx 1.02 \times 10^{10}$ years, respectively. Let us also stress

that one can use (2.89) to estimate the age of the Universe, i.e.,

$$t_0 = 1.38 \times 10^{10} \text{ years}. \tag{2.95}$$

Next, let us make use of the above remarks to find the approximate analytical evolution of the scale factor with time. To that end, we require that both the scale factor as well as the Hubble rate are constant across the transition points, i.e.,

$$a_\Lambda(t_{\rm m.\Lambda.e}) = a_{\rm m}(t_{\rm m.\Lambda.e}), \qquad H_\Lambda(t_{\rm m.\Lambda.e}) = H_{\rm m}(t_{\rm m.\Lambda.e}), \tag{2.96}$$

$$a_{\rm m}(t_{\rm r.m.e}) = a_{\rm r}(t_{\rm r.m.e}), \qquad H_{\rm m}(t_{\rm r.m.e}) = H_{\rm r}(t_{\rm r.m.e}), \tag{2.97}$$

where $a_{\Lambda,\rm m,r}(t)$ $(H_{\Lambda,\rm m,r}(t))$ is the solution describing the scale factor (Hubble rate) evolution in a single-component approximation during DE, MD and RD epochs, respectively. Utilizing Eq. (2.76), one finds that $a(t)$ can be parametrized by the following piecewise function:

$$a(t) = a_0 \begin{cases} \exp\{H_0(t-t_0)\}, & t \gtrsim t_{\rm m.\Lambda.e}, \\ \frac{\left[1+\frac{3}{2}(t-t_{\rm m.\Lambda.e})\right]^{2/3}}{1+z_{\rm m.\Lambda.e}}, & t \in (t_{\rm r.m.e}, t_{\rm m.\Lambda.e}), \\ \frac{\left[1+2\left(\frac{1+z_{\rm r.m.e}}{1+z_{\rm m.\Lambda.e}}\right)^{3/2} H_0(t-t_{\rm r.m.e})\right]^{1/2}}{1+z_{\rm r.m.e}}, & t \lesssim t_{\rm r.m.e}, \end{cases} \tag{2.98}$$

with

$$t_{\rm m.\Lambda.e} = t_0 - \frac{\ln(1+z_{\rm m.\Lambda.e})}{H_0}, \qquad t_{\rm r.m.e} = t_{\rm m.\Lambda.e} - \frac{2}{3H_0} + \frac{2}{3H_0}\left(\frac{1+z_{\rm r.m.e}}{1+z_{\rm m.\Lambda.e}}\right)^{-3/2}, \tag{2.99}$$

and H_0 is the Hubble constant (see below). Note that Eq.(2.98) is not very accurate at the transition points when a single component approximation is not valid.
The right panel of figure (2.3) presents the comparison between the exact numerical solution to the Eq.(2.89) and approximate piecewise evolution found in Eq.(2.98).

For convenience, the value of the Hubble constant is usually parametrized as

$$H_0 = 100\, h \,\text{km}\,\text{s}^{-1}\,\text{Mpc}^{-1}, \tag{2.100}$$

where the scaling factor $h = 0.674 \pm 0.005$ [259].
Hence, the present value of the critical density is [259]

$$\rho_{\rm crit,0} = 3H_0^2 M_{\rm Pl}^2 \simeq (1.053572 \pm 0.000024) \times 10^{-5}\, h^2\, \text{GeV}\,\text{cm}^{-3}. \tag{2.101}$$

It turns out that the current energy density of the Universe is very close to the critical value so that the spatial curvature comprises less than one percent of the total energy budget. Since the energy density $\rho_{\rm k}$ decreases as a^{-2}, the effects of curvature must have been even more negligible in the remote past; for further discussion, see Sec.(2.5).

Finally, let us note that recent studies imply a statistically significant disagreement between late and early Universe measurements of the h parameter. Namely, the expansion rate determined from measurements of distance and redshift seems to be inconsistent with that predicted by the ΛCDM model. For instance, data from the Hubble Space Telescope attains $h = 0.72 \pm 0.2$ [260], whereas the value anchored by the 2018 Planck survey is $h = 0.6737 \pm 0.0054$ [13]. This discrepancy between the locally measured and cosmologically inferred data is known as the famous *Hubble tension*.

Furthermore, the concordance model faces another two difficulties, referred to as the *cosmological constant problem* and the *coincidence problem*.
The former relates to the mindblower discrepancy between the measured value of the energy density associated with a cosmological constant ($\sim 10^{-47}$ GeV^4) and the value of vacuum energy, predicted by the QFT (2.75). The severe incompatibility between these two, estimated to be around 120 orders of magnitude, is considered one of the biggest problems but also a challenge for modern cosmology. Several attempts have been considered to resolve this puzzle, including the dynamical dark energy, modified gravity, the holographic principle, etc., e.g., [261, 262]. Unfortunately, none of them have provided a plausible explanation accepted by a wider cosmological community.
The coincidence problem refers to the fact that dark energy dominated the energy budget surprisingly not so long ago. Since $\Omega_\mathrm{m}/\Omega_\Lambda$ scales as a^{-3}, there is only a short period of time at which these two are comparable. Hence, the coincidence problem is also connected to the question: why values of $\Omega_{\Lambda,0}$ and $\Omega_{\mathrm{m},0}$ are so close to each other at the present epoch, but were and will be very different in the past and future? Given the estimated age of the Universe (2.95), it might seem too much of a coincidence.

2.4.1 The Big Bang cosmology in a nutshell

Let us now give a quick snapshot of the thermal history of the Universe, briefly describing the most important events [19, 222, 226].

Electroweak phase transition $[T \sim 246\,\mathrm{GeV},\ t \sim 10^{-11}\ s]$
Above 246 GeV, electromagnetism and weak interactions were unified into a single electroweak force. At that time, all elementary SM species were massless. When the Universe cooled down below the electroweak scale, the gauge $SU(2) \times U(1)_\mathrm{Y}$ symmetry was spontaneously broken into the $U(1)_\mathrm{em}$ symmetry, see e.g., [263–265]. As a result, the physical degrees of freedom mediating weak and electromagnetic interactions, i.e., the $W^\pm, Z^0$, and the photon γ, were produced. After that, all four fundamental Standard Model interactions have reorganized into their present, low-energy form. In addition, the breaking of electroweak symmetry triggered the Higgs mechanism, causing the Higgs field to develop a vacuum expectation value. As a result, all SM particles that interact with the Higgs boson acquired non-zero masses.

As long as the temperature exceeded the SM species' mass, they remained in thermal equilibrium with the rest of the bath. When the temperature dropped below the mass of the top quark ($\sim$ 173 GeV), it started to annihilate with its own antiparticle, whereas the spontaneous creation of the $t\bar{t}$ pairs became inefficient. Being the heaviest SM states, the top quarks disappeared first. Soon afterward, around $T \sim 10\ GeV$, the annihilation of the Higgs field and three electroweak bosons $W^\pm, Z^0$ took place. The bottom quark disappeared next. This, in turn, was followed by the annihilation of the charm quarks and the tau leptons. The strange quark was next in line; however, its decoupling was interrupted by the QCD phase transition.

QCD phase transition $[T \sim 150\,\mathrm{MeV},\ t \sim 10^{-5}\ s]$
Around the QCD scale, a phase transition associated with the QCD chiral symmetry breaking occurred [266–269]. Free quarks that were too light to decouple prior to that moment clumped together to form hadrons. The conversion of color-charged particles making up a quark–gluon plasma into colorless states is called *confinement*. The newly created hadrons were either mesons (a quark + anti-quark pairs) or baryons (comprising three quarks). Most of them were heavy, so they became non-relativistic below the QCD temperature.

Close to the end of the hadron epoch, the Universe was mainly composed of pions, muons, electrons, neutrinos, and massless photons. The remaining degrees of freedom gradually decoupled from the thermal bath as their interaction rate fell below the Hubble scale. When interactions became inefficient to maintain a thermal equilibrium state, particles decoupled from the rest species, acquiring a relic abundance. The best-established decoupling event is associated with SM neutrinos.

Neutrino decoupling $[T \sim 1\,\text{MeV},\ t \sim 1\,\text{s}]$
When the temperature of the Universe reached $\sim 1\,\text{MeV}$, the interaction rate of the two most common processes involving neutrinos, i.e.,

$$\nu_e + \bar{\nu}_e \leftrightarrow e^+ + e^-, \qquad\qquad e^- + \bar{\nu}_e \leftrightarrow e^- + \bar{\nu}_e, \tag{2.102}$$

drops below the Hubble scale. As a result, relativistic neutrinos decoupled from the SM thermal bath, forming the cosmic neutrino background (CνB).

Electron-positron annihilation $[T \sim 500\,\text{keV},\ t \sim 100\,\text{s}]$
Shortly after the neutrino decoupling, the thermal bath temperature fell below the electron mass. Electrons and positrons became non-relativistic and transferred their energy to photons via the process

$$e^+ + e^- \to \gamma + \gamma, \tag{2.103}$$

but not to SM neutrinos since the latter has already decoupled. In consequence, photons were warmed up relative to cosmic neutrinos, whose temperature T_ν became slightly lower than the temperature of thermal bath T_γ, see Appendix (D).

After the electron-positron annihilation, photons and neutrinos remained the only SM relativistic species.

Big Bang nucleosynthesis $[T \sim 100\,\text{keV},\ t \sim 200\,\text{s}]$
When the hot plasma cooled down below ten billion Kelvin, protons p and neutrons n to started to combine and create certain species of light atomic nuclei, such as helium-4 (^{4}He), deuterium (^{2}H), helium-3 (^{3}He), and lithium-7 (^{7}Li), see, e.g., [270–273]. Apart from these four stable nuclei, two additional unstable or radioactive isotopes were also produced: tritium (^{3}H) and beryllium-7 (^{7}Be), which later decayed into (^{3}He) and (^{7}Li), respectively. Formation of these elements commenced with a deuterium production

$$n + p \leftrightarrow {}^2\text{H} + \gamma. \tag{2.104}$$

The binding energy of deuterium $E_{\text{binding}} = m_p + m_n - m_{^2\text{H}} \approx 2.2$ MeV exceeds the thermal bath temperature $T \lesssim 1$ MeV. Nevertheless, the above process is in equilibrium since it is compensated by the small baryon-to-photon ratio $\eta = n_b/n_\gamma \approx 10^{-9}$ [226]. The Saha equation determines the relative abundance of deuterium

$$\frac{n_{^2\text{H}}}{n_p} = \frac{3}{4} n_n \left(\frac{m_{^2\text{H}}}{m_n m_p} \frac{1}{2\pi T} \right)^{3/2} e^{E_{\text{binding}}/T} \approx \frac{3}{4} \eta \left(\frac{1}{\pi} \frac{T}{m_p} \right)^{3/2} e^{E_{\text{binding}}/T}, \tag{2.105}$$

where we have used the following expressions: $m_n \approx m_{^2\text{H}}/2$, $n_n \approx n_p \approx \eta \cdot n_\gamma$, and $\eta_\gamma \approx T^3$ [226].
One can show that the condition $\frac{n_{^2\text{H}}}{n_p} \simeq 1$ is satisfied for $T \lesssim 0.06$ MeV, prior to the neutrinos

decoupling. Later on, deuterium is sufficiently produced to initiate the helium formation

$$^{2}\mathrm{H} + p \leftrightarrow {}^{3}\mathrm{He} + \gamma, \qquad\qquad {}^{3}\mathrm{He} + {}^{2}\mathrm{H} + p. \tag{2.106}$$

The fraction of helium can be estimated from the following formula [226]:

$$\frac{n_{\mathrm{He}}}{n_p} = \frac{n_n/2}{n_p - n_n} \approx 0.07. \tag{2.107}$$

As the mass of a helium atom is four times larger than a hydrogen atom, the total baryonic mass is mostly comprised of hydrogen (roughly 75%) and helium ($\sim 25\%$). Heavier elements are produced in negligible quantities.

Measurements of the abundances of light elements provide a very precise tool that allows us to test the ΛCDM model and the SM of particle physics [274–276]. This is because the formation of light elements is susceptible to the initial baryon-to-photon ratio η, the rate of expansion, and numbers of relativistic degrees of freedom, and strongly depends on particle properties, e.g., the strength of weak coupling and mass of protons.
The unprecedented agreement between predicted abundances and the observed data can be viewed as the cornerstone of the standard Big Bang model. The only disagreement of the BBN predictions with cosmological data is related to the abundance of ^{7}Li, which should be three times larger than observed according to the BBN paradigm. This puzzle, known as the *lithium problem* [277], remains unsolved.

When the temperature of the Universe reached ~ 0.7eV, the energy density of non-relativistic matter began to dominate over the radiation energy density. The moment when these two matched each other is referred to as *radiation-matter-equality* (r.m.e). After this, the Universe entered the matter-dominated epoch.

Recombination [$T \sim 0.3\,\mathrm{eV}$, $t \sim 370\,000\,\mathrm{years}$]
When the Universe was roughly 370 000 years old, its temperature was sufficiently low for the electrons to combine with the atomic nuclei and form neutral hydrogen. Prior to this, the Universe had been mostly composed of hot and dense plasma, which was effectively opaque to the photons due to the Thomson scattering on free electrons. The corresponding cross-section is quite large, so the mean free path of photons at that time was very short, forbidding their free stream. Everything has changed after the recombination since the cross-section accounting for the photon interactions with the neutral atom is much smaller than the Thomson cross-section. At that moment, photons decoupled from the matter, and the Universe became transparent. The electromagnetic radiation released from the plasma after recombination has streamed freely until today and can be observed as the *cosmic microwave background* (CMB) [25]. It is the farthest and oldest light that we can see. The CMB radiation reaches us today with the same temperature distribution as when it was emitted. It corresponds to a nearly perfect thermal black body spectrum with the present temperature, $T_{\mathrm{CMB},0} \sim 2.72548 \pm 0.00057$ K, redshifted by the factor $z \sim 1100$ since the moment of emission. Such tiny fluctuations, of the order of 10^{-5}, indicate that the Universe at the moment of photon decoupling was homogeneous and isotropic to a large extent, cf. Fig.(2.4). Any deviations from homogeneity provide us with an extremely powerful probe of the early Universe.

Reionization [$T \sim 5\,\mathrm{meV}$, $t \sim (200\ \mathrm{Myr} - 1\ \mathrm{Gyr})$]
About ten million years after the very beginning, the population III stars were created by the gravitational collapse of molecular clouds [278–280]. Then, about one billion years after the Big Bang, the first galaxies started to form. Energetic radiation emitted by such objects

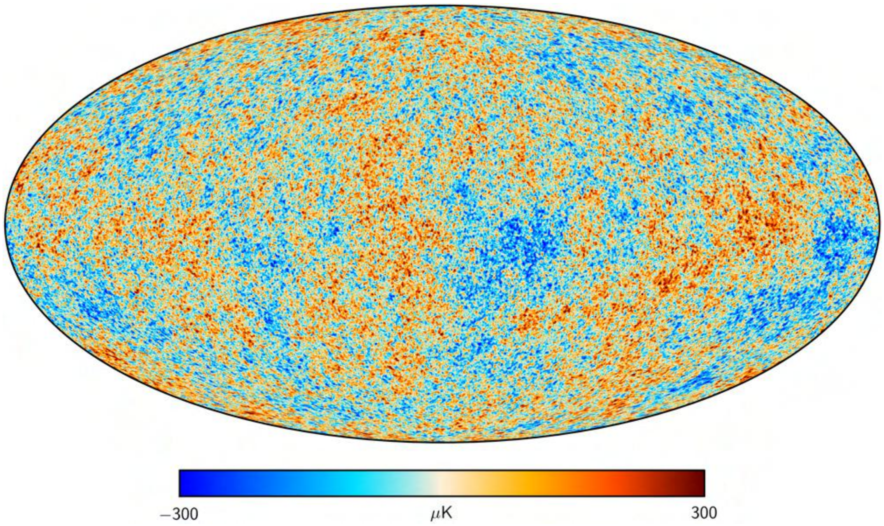

FIGURE 2.4: Map of the CMB temperature fluctuations measured by Planck.
Image credit: ESA and the Planck Collaboration

ionized the neutral hydrogen gas, reionizing the Universe. However, this time, it remained transparent since the matter was much more diluted, as compared to the pre-recombination era, so photon scattering off ionized plasma occurred less often.

Galaxies started coalescing into galaxy clusters ($z = 2.1$) and superclusters ($z = 1.2$), forming the largest known structures in the Universe. This is an ongoing process that is still active at the present epoch.

Matter-Λ equality $[T \sim 0.33\ \text{meV}, \text{t} \sim 9\ \text{Gyr}]$
Roughly nine billion years after the Big Bang, the energy density of matter fell below the dark energy. It commenced the period of the accelerated expansion of the Universe.

2.4.2 Thermal Universe

The early Universe was filled with a hot and dense plasma of high-energy species. The statistical properties of this gas are described by the phase-space distribution function $f(\vec{x}, \vec{p}, t)$, see Appendix B. In general, the distribution function might depend on its position $\vec{x}$, momentum $\vec{p}$, and time. However, the translation invariance of the FLRW metric implies that in the homogeneous Universe, f cannot depend on the position $\vec{x}$, while the isotropy requires f to be only a function of the momentum magnitude $|\vec{p}| \equiv p$. Moreover, to simplify the further discussion, we leave the time dependence of the distribution function implicit.

Although the distribution function provides complete information about a given system, it might seem abstract. The macroscopic description is typically performed in terms of thermodynamical variables. In particular, measurable quantities, such as the number density n, the energy density ρ, and the pressure p of a particle, are related to its distribution function through the following integrals [226]:

$$n := g \int \frac{d^3p}{(2\pi)^3} f(p), \tag{2.108}$$

$$\rho := g \int \frac{d^3p}{(2\pi)^3} E(p) f(p), \tag{2.109}$$

$$p := g \int \frac{d^3p}{(2\pi)^3} \frac{p^2}{3E(p)} f(p), \tag{2.110}$$

where g describes the number of internal degrees of freedom.

In the early Universe, the rate of particle interactions was sufficiently high to maintain the plasma in equilibrium. One distinguished two types of equilibrium, i.e., the *kinetic equilibrium* and the *chemical equilibrium.* The *kinetic equilibrium* is a consequence of the *rapid* energy transfer, i.e., there is an efficient energy and momentum exchange among particles involved in the scattering process. On the other hand, the *chemical equilibrium* follows from the *rapid* number changing events, i.e., particles are efficiently created and destroyed during interactions. A process is referred to as *rapid* if its timescale is much shorter than the scale $1/H$ associated with the expansion of the Universe. Finally, if a system is both in the *kinetic* and *chemical equilibrium*, then a state of *thermal equilibrium* is established. In kinetic equilibrium, constituents of the bath follow the equilibrium distribution described by the equilibrium phase-space function

$$f^{\rm eq}(p,T) = \frac{1}{e^{\frac{E(p)-\mu}{T}} \pm 1}, \tag{2.111}$$

where μ denotes the chemical potential, the plus sign corresponds to the fermionic Fermi-Dirac distribution function, whereas the minus sign corresponds to the bosonic Bose-Einstein distribution function. In the low-temperature limit, $T \ll (E-\mu)$, the above function simplifies to the Maxwell-Boltzmann distribution function, given by the following expression:

$$f^{\rm eq}(p,T) \approx e^{-\frac{E(p)-\mu}{T}}, \qquad\qquad T \ll (E-\mu). \tag{2.112}$$

Moreover, at early times, the chemical potential of all particles is assumed to be negligible compared to their temperature [226]. We adopt this presumption through this thesis.

Neglecting the chemical potential, and using Eqs.(2.108) and (2.109) together with Eq.(2.111), one obtains

$$n^{\rm eq} = \frac{g}{2\pi^2} T^3 I_\pm(x), \qquad\qquad I_\pm(x) \equiv \int_0^\infty \frac{\xi^2}{e^{\sqrt{\xi^2+x^2}} \pm 1} d\xi, \tag{2.113}$$

$$\rho^{\rm eq} = \frac{g}{2\pi^2} T^4 J_\pm(x), \qquad\qquad J_\pm(x) \equiv \int_0^\infty \frac{\xi^2\sqrt{\xi^2+x^2}}{e^{\sqrt{\xi^2+x^2}} \pm 1} d\xi, \tag{2.114}$$

where we have used the dimensionless variables $x \equiv m/T$ and $\xi \equiv p/T$. In general, the above integrals must be done numerically. However, one can compute $I_\pm(x)$ and $J_\pm(x)$ analytically in the two physically relevant regimes, i.e., in the relativistic (R) and non-relativistic (NR) limits. In the former case, i.e., when $x \to 0$, the $I_\pm(x)$ integral simplifies as

$$I_\pm(0) \equiv \int_0^\infty \frac{\xi^2}{e^{\xi} \pm 1} d\xi. \tag{2.115}$$

In the bosonic case ($-$), one can utilize the definition of the Riemann zeta function,

$$\zeta(n) = \frac{1}{\Gamma(n)} \int_0^\infty \frac{x^{n-1}}{e^x - 1} dx, \tag{2.116}$$

which implies $I_-(0) = \Gamma(3)\,\zeta(3) = 2\zeta(3)$.
Whereas for fermions (+ sign), one uses the fact that

$$\int_0^\infty \frac{x^{n-1}}{e^x + 1} dx = \left(1 - \frac{1}{2^{n-1}}\right) \Gamma(n)\zeta(n), \tag{2.117}$$

obtaining $I_+(0) = (1 - 1/4)\,\Gamma(3)\,\zeta(3) = 3\zeta(3)/2$.
Finally, similar computations for the $J_\pm(0)$ integral, leads to

$$J_- = \Gamma(4)\zeta(4) = \frac{\pi^4}{15}, \qquad J_+ = \left(1 - \frac{1}{8}\right) \Gamma(4)\zeta(4) = \frac{7}{8} \cdot \frac{\pi^4}{15}. \tag{2.118}$$

Hence, the number density of relativistic species takes the form

$$n_{\rm R}^{\rm eq} = g\frac{\zeta(3)}{\pi^2} T^3 \cdot \begin{cases} 1 & \text{bosons,} \\ \frac{3}{4} & \text{fermions,} \end{cases} \tag{2.119}$$

whereas their energy density is

$$\rho_{\rm R}^{\rm eq} = g\frac{\pi^2}{30} T^4 \cdot \begin{cases} 1 & \text{bosons,} \\ \frac{7}{8} & \text{fermions.} \end{cases} \tag{2.120}$$

In the non-relativistic limit, i.e., $x \gg 1$, both $I_\pm(x)$ can be approximated by the same integral

$$I_\pm(x) \approx \int_0^\infty \frac{\xi^2}{e^{\sqrt{\xi^2+x^2}}} d\xi \approx \int_0^\infty \frac{\xi^2}{e^{x+\xi^2/(2x)}} d\xi = \sqrt{\frac{\pi}{2}} x^{3/2} e^{-x}, \tag{2.121}$$

where in the second approximation, we have expanded the exponential function in the Taylor series using the fact that the main contribution to the integral comes from $\xi \ll x$.
Inserting the above result into Eq.(2.113), one find the number density of non-relativistic species (both fermions and bosons) is exponentially suppressed, according to the formula

$$n_{\rm NR}^{\rm eq} \equiv \bar{n} = g\left(\frac{mT}{2\pi}\right)^{3/2} e^{-m/T}. \tag{2.122}$$

Let us also notice that in the non-relativistic regime, the energy can be well approximated by $E = \sqrt{p^2 + m^2} = m + p^2/(2m)$, which, in turn, implies the following expression from the energy density:

$$\rho_{\rm NR}^{\rm eq} \approx mn + \frac{3}{2} nT. \tag{2.123}$$

Hence, one observes that the particle contribution to the total energy budget becomes negligible as the temperature T drops below its mass.

Dropping the $\rho_{\rm NR}$ contribution to the total energy density, the latter can be expressed in terms of the *number of relativistic degrees of freedom*, $g_{\star\rho}$, as [226]

$$\rho \simeq \rho_R^{\rm eq} = \frac{\pi^2}{30} g_{\star\rho}(T) T^4, \qquad g_{\star\rho}(T) \approx \sum_{\rm b=\,bosons} g_{\rm b} \left(\frac{T_{\rm b}}{T}\right)^4 + \frac{7}{8} \sum_{\rm f=\,fermions} g_{\rm f} \left(\frac{T_{\rm f}}{T}\right)^4, \tag{2.124}$$

where we have separated the contributions from bosonic (b) and fermionic (f) degrees of freedom and allowed different states to have different temperatures $T_{b,f}$.
At high temperatures, $T \gg 100\,\text{GeV}$, all the SM degrees of freedom were in thermal equilibrium and hence have a common temperature T. Therefore, at early times, the *number of relativistic degrees of freedom* within the SM sector is

$$g_{\star\rho}(T \gg 100 \text{ GeV}) = \sum_{\rm b=\,bosons} \mathrm{g_b} + \frac{7}{8} \sum_{\rm f=\,fermions} \mathrm{g_f} = 106.75. \tag{2.125}$$

As the temperature of the Universe dropped, various particles decoupled from the thermal bath as they became non-relativistic. This leads to the decrease of the $g_{\star\rho}(T)$ function as described in Appendix (D).

Last but not least, let us investigate the evolution of the entropy whose differential is

$$T dS(V,T) \equiv d[\rho(T)V] + p(T)dV = d[(\rho + p)V] - V dp, \tag{2.126}$$

where we have dropped all terms containing chemical potential.
Using the integrability condition, one finds that

$$\frac{\partial^2 S(V,T)}{\partial T \partial V} = \frac{\partial^2 S(V,T)}{\partial V \partial T} \qquad \Longrightarrow \qquad \frac{\partial}{\partial T}\left[\frac{1}{T}(\rho + p)\right] = \frac{\partial}{\partial V}\left[\frac{V}{T}\frac{d\rho}{dT}\right], \tag{2.127}$$

which leads to

$$dp = \frac{p+\rho}{T} dT. \tag{2.128}$$

Inserting the above relations into (2.126), one gets

$$dS = \frac{1}{T} d[V(\rho + p)] - \frac{dT}{T^2} V(\rho + p) = d\left[\frac{V}{T}(\rho + p) + \text{const.}\right]. \tag{2.129}$$

Hence,

$$S(V,T) = \frac{V}{T}\left(\rho(T) + p(T)\right), \tag{2.130}$$

up to an integration constant.

Now let us notice that the continuity equation (2.65) can be recast as

$$a^3 \frac{dp}{dt} = \frac{d}{dt}\left[a^3 (p + \rho)\right], \tag{2.131}$$

which combining with Eq.(2.128) gives us

$$a^3 \frac{1}{T}\frac{dT}{dt}(\rho + p) = \frac{d}{dt}\left[a^3(\rho + p)\right], \tag{2.132}$$

which, in turn, implies

$$\frac{d}{dt}\left[\frac{a^3}{T}(\rho+p)\right]=0. \tag{2.133}$$

Identifying volume V with a^3, one concludes that the entropy density,

$$s(T)=\frac{\rho(T)+p(T)}{T}, \tag{2.134}$$

is conserved in equilibrium. Moreover, by rewriting (2.133) as

$$\frac{d}{dt}(sa^3)=0, \tag{2.135}$$

one concludes that the entropy density decreases as $s \propto a^{-3}$.
The total entropy of a collection of relativistic particles with different temperatures is given by

$$s \equiv \frac{2\pi^2}{45} g_{\star s} T^3, \tag{2.136}$$

where the *number of relativistic degrees of freedom in entropy* is

$$g_{\star s} \approx \sum_{\mathrm{b=\,bosons}} g_{\mathrm{b}}\left(\frac{T_{\mathrm{b}}}{T}\right)^3+\frac{7}{8}\sum_{\mathrm{f=\,fermions}} g_{\mathrm{f}}\left(\frac{T_{\mathrm{f}}}{T}\right)^3. \tag{2.137}$$

Note that if all species are in thermal equilibrium, they have the same temperature T and $g_{\star s}=g_{\star\rho}$. This happens till ~ 1 s after the Big Bang. However, after the e^+e^- annihilation, $g_{\star s}$ becomes slightly larger than $g_{\star\rho}$, which results from the neutrino decoupling.

Moreover, an important consequence of entropy density conservation is that

$$g_{\star s}T^3a^3=\text{const.} \qquad \Longrightarrow\ T\propto g_{\star s}^{-1/3}a^{-1}. \tag{2.138}$$

From the above expression, it follows that

- As long as $g_{\star s}$ remains constant, the temperature T would decrease as $T\sim a^{-1}$.
- Whenever a species becomes non-relativistic, $g_{\star s}$ decreases which implies that $(aT)^3$ increases correspondingly. Since the scale factor is a monotonically growing function, the decline of $g_{\star s}$ presupposes that T must decrease slower than a^{-1}. The entropy of a species that transitions from a relativistic to a non-relativistic state is transferred to the other relativistic particles still present in the thermal bath.

Note that from the second remark, one infers that the present temperature of neutrinos slightly deviates from that of photons. It results from SM neutrinos decoupling from the thermal bath around 1 MeV. After that moment, their temperature dropped as a^{-1}. However, after the e^+e^- annihilation, the thermal bath temperature was heated as the energy density of the electron-positron pairs was transferred to the photons. By counting the effective number of relativistic degrees of freedom in entropy before, $g_{\star s,T\gtrsim 1\,\mathrm{MeV}}=2+(7/8)\cdot 4$, and after, $g_{\star s,T\lesssim 1\,\mathrm{MeV}}=2$, the e^+e^- annihilation, one finds that for the temperature below $\sim 1\,\mathrm{MeV}$, the neutrino temperature T_ν is related to the photon temperature T_γ as

$$T_\nu=\left(\frac{4}{11}\right)^{1/3}T_\gamma. \tag{2.139}$$

2.5 Problems of the hot Big Bang

Despite unquestionable successes and undeniable predictivity, the classical Big Bang paradigm is not the *theory of everything*. Standard cosmology faces many serious problems. Even if some seem not to be impossibility problems, they require serious fine-tuning. Below we list the main open questions and peculiarities of the hot Big Bang model.

2.5.1 The horizon problem

One of the biggest peculiarities of conventional cosmology concerns the observed isotropy of the CMB radiation, which suggests that photons were in causal contact with each other at earlier times. However, as we will demonstrate below, the surface of the last scattering comprises a dozen causally disconnected pieces, which are irreconcilable with observations.

From the discussion in Sec.(2.2.4), we know that the causal structure of space is constrained by the maximum distance from which light can be received. At a given moment t, it can be described by the comoving particle horizon $\chi_p(t)$, which we have introduced in Eq.(2.36). Adopting this formula, one can determine the comoving distance which photons had traveled between the initial BB singularity, i.e., $t_{\rm BB} \to 0$, and the time of last scattering $t_{\rm CMB}$

$$\chi_p^{\rm CMB} = \int_{t_{\rm BB}}^{t_{\rm CMB}} \frac{dt}{a(t)} = \int_{\ln a_{\rm BB}}^{\ln a_{\rm CMB}} (aH)^{-1}\, d\ln a. \tag{2.140}$$

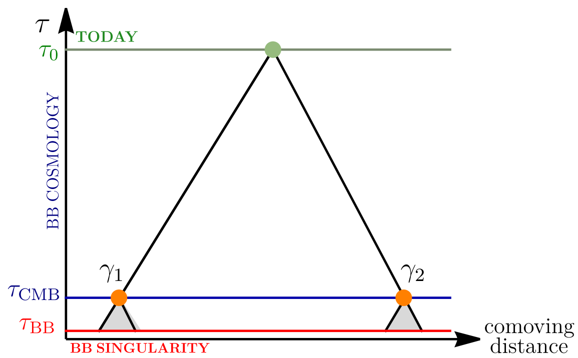

FIGURE 2.5: Conformal diagram for standard Big Bang cosmology. Past light cones of two separated photons γ_1, γ_2 on the surface of the last scattering do not overlap.

Above, $a_{\rm BB} \to 0$ denotes the initial value of the scale factor. Moreover, in Eq.(2.140) we have introduced the *comoving Hubble radius*, or *Hubble horizon* $(aH)^{-1}$. From (2.78), we see that it scales as $a^{(3w+1)/2}$. Therefore, one concludes that for *ordinary matter* obeying the condition (2.68), the Hubble radius is a monotonically growing function of a, and thus, also of the cosmic time t. In particular, this means that the integral (2.140) should be dominated by the upper limit, so thus the contribution to $\chi_p^{\rm CMB}$ from the early times might be neglected. In addition, since $\chi_p \sim \tau$, one infers that the conformal time elapsed between the BB singularity and the emission of the CMB radiation is much shorter than the present conformal age of the Universe. This generates a severe problem for conventional cosmology. Namely, from the conformal diagram Fig.(2.5), we see that past light cones of two photons γ_1, γ_2 located at the CMB surface do not intersect. Therefore, such photons should never have been in casual contact with each other. Consequently, one might expect that the CMB radiation is composed of many causally-disconnected patches, which is manifestly in contradiction with the observed isotropy of the map of relic photons. Such a peculiarity is known as the *horizon problem* and was first realized by Wolfgang Rindler [281] and Charles W. Misner [282].

To make this conclusion more robust, let us estimate the angular distance of the cosmological horizon at the moment of the CMB emission, as seen from the Earth today. At the time of recombination, the angular extension of the horizon can be determined from the following formula [283]:

$$\Delta\Omega_{\text{CMB},0} = \frac{d_p(t_{\text{CMB}})}{a_{\text{CMB}}\,\chi^0_{p,\text{CMB}}}, \qquad \chi^0_{p,\text{CMB}} \equiv \int_{t_{\text{CMB}}}^{t_0} \frac{dt}{a(t)}, \tag{2.141}$$

where $d_p(t_{\text{CMB}}) = a_{\text{CMB}}\,\chi_p^{\text{CMB}}$ defines the physical size of the event horizon at the last scattering surface.
To compute the above integrals, we assume that a single matter component has dominated the Universe at each moment of its evolution. Then, it is possible to solve the Friedmann equation and find the evolution of the scale factor at each period, which we have already done in Eq.(2.98). Utilizing the piecewise approximation Eq.(2.98), one can split the above integrals into several contributions

$$\chi_p^{\text{CMB}} = \int_{t_{\text{BB}}}^{t_{\text{CMB}}} \frac{dt}{a(t)} = \int_{t_{\text{BB}}}^{t_{\text{r.m.e}}} \frac{dt}{a(t)} + \int_{t_{\text{r.m.e}}}^{t_{\text{CMB}}} \frac{dt}{a(t)}, \tag{2.142}$$

and

$$\chi^0_{p,\text{CMB}} = \int_{t_{\text{CMB}}}^{t_0} \frac{dt}{a(t)} = \int_{t_{\text{CMB}}}^{t_{\text{m.}\Lambda\text{.e}}} \frac{dt}{a(t)} + \int_{t_{\text{m.}\Lambda\text{.e}}}^{t_0} \frac{dt}{a(t)}, \tag{2.143}$$

where we have used the fact that $t_{\text{BB}} < t_{\text{r.m.e}} < t_{\text{CMB}} < t_{\text{m.}\Lambda\text{.e}} < t_0$. Using the fact that

$$\int_{t_i}^{t_f} \frac{dt}{a(t)} = -\frac{1}{H_0} \int_{z_i}^{z_f} \frac{dz}{\sqrt{\Omega_{i,0}(1+z)^{-3(1+w_i)}}}, \tag{2.144}$$

after straightforward but tedious calculations, one finds

$$\Delta\Omega_{\text{CMB},0} = \frac{2(1+z_{\text{CMB}})^{-1/2} - (1+z_{\text{r.m.e}})^{-1/2}}{(2+3z_{\text{m.}\Lambda\text{.e}})(1+z_{\text{m.}\Lambda\text{.e}})^{-3/2} - 2(1+z_{\text{CMB}})^{-1/2}} \approx 0.023 \text{ rad}. \tag{2.145}$$

More accurate calculations can be obtained numerically, considering more than one matter component at a time. Employing numerical values of cosmological parameters collected in Table (A.1) together with (2.84), one obtains an even smaller value, i.e., $\Delta\Omega_{\text{CMB},0} \approx 0.0054$ rad. This corresponds to $4\pi^2/(0.0054)^2 \approx 10^6$ causally disconnected patches comprising the surface of the last scattering. Since these pieces have never been in casual contact, how can we explain that the CMB radiation is almost perfectly uniform?

2.5.2 The Flatness Problem

As we have already pointed out in Sec.(2.3.4), the value of $1-\Omega_{\text{matter},0}$ determines the present curvature of the Universe, cf. Eq.(2.85). Since the curvature parameter k is a constant, the sign of $1-\Omega_{\text{matter},0}$ does not change throughout the cosmological evolution. Observational data reveals that the present curvature density parameter $\Omega_{\text{k},0}$ is unexpectedly close to zero; see Eq. (2.91). Now let us explicitly demonstrate why it poses a problem.

As we have learned, the early Universe was dominated by radiation, whose energy density redshifts as a^{-4}. Utilizing Eq.(2.85), one finds that at the early times

$$\Omega_{\text{k}} = 1 - \Omega_{\text{matter}} \simeq \frac{1}{1+\frac{\Omega_{\text{r}}}{\Omega_{\text{k}}}} \simeq \frac{\Omega_{\text{k},0}}{\Omega_{\text{r},0}} \left(\frac{1}{1+z}\right)^2, \tag{2.146}$$

where we have used the following scaling: $\Omega_{\rm r} = \Omega_{\rm r,0}(a_0/a)^4$ and $\Omega_{\rm k} = \Omega_{\rm k,0}(a_0/a)^2$. Using the present values of $\Omega_{\rm r,0}$ (2.90), and $\Omega_{\rm k,0}$ (2.91), one obtains $|\Omega_{\rm k}| \lesssim 7 \cdot 10^{-6}$ at the time of recombination ($z = 1200$), $|\Omega_{\rm k}| \lesssim 6 \cdot 10^{-17}$ during the BBN epoch ($z \simeq 4 \cdot 10^8$), and $|\Omega_{\rm k}| \lesssim 10^{-55}$ during at the GUT scale ($\sim 10^{16}$ GeV, z $\simeq 10^{28}$). Therefore, to explain the abundance of matter components today, the Universe must have been extremely flat in the remote past. Within the standard Big Bang model, this requires fine-tuning and is known as the *flatness problem* [284].

2.5.3 The Monopole Problem

In addition to the horizon and flatness problems, standard cosmology suffers from the so-called *magnetic monopole problem.* Grand Unified Theories (GUT) predict the existence of magnetic monopoles- remnants of the strong and electroweak forces unification, see, e.g., [285, 286]. According to such theories, all three SM gauge interactions were unified as the single electronuclear force at the energies above the GUT scale $\sim 10^{16}$ GeV. Magnetic monopoles are pointlike topological defects constructed as stable knots in the GUT Higgs fields with a mass of the order of $m_{\rm MM} \sim 10^{18}$ GeV. Such superheavy particles with a net magnetic charge are expected to be copiously produced during the GUT phase transition. Their abundance is associated with the misalignment of the GUT Higgs field in different regions of space. The size of the horizon at the GUT scale, i.e., $d_p(t_{\rm GUT})$, sets the upper bound on the mean distance between two monopoles [287]. Since monopoles are stable, their abundance changes only due to expansion. Hence, the mean separation between two neighbor relics increases over time, and at the present moment is given by

$$d_{\rm MM,0} = \frac{d_p(t_{\rm GUT})}{a_{\rm GUT}} = \int_{t_{\rm BB}}^{t_{\rm GUT}} \frac{dt}{a}. \tag{2.147}$$

The above integral can be evaluated assuming that $t_{\rm GUT} \ll t_{\rm r.m.e}$. Then, using the fact that during the RD epoch $a \sim t^{1/2}$, one finds that at the GUT scale, there should have been roughly one magnetic monopole per Hubble volume [287]. The corresponding abundance of magnetic monopoles can be estimated as [283]

$$\Omega_{\rm MM,0} = \frac{m_{\rm MM}}{\rho_{\rm crit,0} d^3_{\rm MM,0}} \simeq 10^{15}, \tag{2.148}$$

which is obviously in contradiction with observational constraints [288, 289]. Hence, if the GUT is correct, which is plausible but not necessarily true, the predicted overabundance of magnetic monopoles is a serious issue for the hot Big Bang cosmology.

2.5.4 On how the standard cosmology has been cured

Although the above-mentioned puzzles have very different natures, they can all be unraveled at once. Namely, the problems of the hot Big Bang can be solved by introducing an early period, i.e., prior to the radiation-dominated epoch, of an accelerated expansion. The idea of the *cosmic inflation* was first proposed by Alan Guth in 1980 [205] and developed by many authors, including Alexei Starobinsky, Andrei Linde, Andreas Albrecht, Paul Steinhardt, Demos Kazanas, etc. [206–210]. The inflationary paradigm should not be considered as a replacement for the standard cosmology. Instead, it is a supplement to the hot Big Bang model, occurring just after the very beginning, before the commencement of the radiation era. Alan Guth realized that the early inflationary phase, during which the scale factor accelerates, i.e., $\ddot{a} > 0$, would account for a number of the observational features of the Universe that are otherwise extremely hard to explain. Let us now demonstrate how the early inflationary phase could cure the Big Bang cosmology.

The horizon problem revisited

Let us first note that the condition for the accelerated expansion $\ddot{a} > 0$ is equivalent to the condition

$$\frac{d}{dt}(aH)^{-1} < 0, \tag{2.149}$$

describing the shrinking of the Hubble sphere.
Suppose that during inflation, the dynamics of the Universe was governed by a single matter component characterized by a generic e.o.s parameter w (2.69). From Eq. (2.78), one finds

$$(aH)^{-1} \propto a^{\frac{3w+1}{2}}, \tag{2.150}$$

which implies that the integral defining the particle horizon $\chi_p(a)$ can be evaluated as

$$\chi_p(a) = \int_{a_{\mathrm{BB}}}^{a} \frac{d\tilde{a}}{\tilde{a}(\tilde{a}H)} = \frac{2\tilde{H}}{1+3w}\left[a^{\frac{1+3w}{2}} - a_{\mathrm{BB}}^{\frac{1+3w}{2}}\right], \tag{2.151}$$

where $\tilde{H} > 0$.

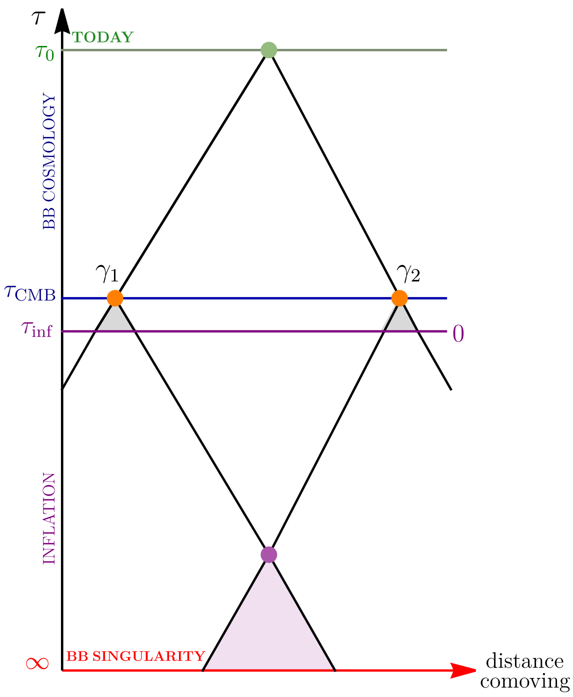

FIGURE 2.6: Conformal diagram for standard BB cosmology supplemented by the cosmic inflation phase. Past light cones of two separated photons γ_1, γ_2 now can overlap. Conformal time τ is negative during inflation and $\tau = 0$ at its very end.

For the ordinary matter obeying the strong energy condition Eq. (2.68), the Hubble sphere grows with time so that the above expression is dominated by the upper limit of the integral, i.e.,

$$\chi_p \approx \frac{2\tilde{H}}{1+3w} a^{\frac{1+3w}{2}}, \qquad \text{for } w > -1/3.$$

Now let us consider a matter component violating the strong energy condition, i.e., whose e.o.s parameter is $w \leq -1/3$. For such a fluid: i) the Hubble radius decreases with time, ii) the particle horizon χ_p receives the main contribution from the early times, such that

$$\chi_p \approx -\frac{2\tilde{H}}{1+3w} a_{\mathrm{BB}}^{\frac{1+3w}{2}}, \qquad \text{for } w \leq -1/3.$$

Note that this corresponds to a negative conformal time at ($a_{\mathrm{BB}} \to 0$)

$$\chi_p \approx -\tau_{\mathrm{BB}} \quad \Longrightarrow \quad \tau_{\mathrm{BB}} \simeq \frac{2\tilde{H}}{1+3w} a_{\mathrm{BB}}^{\frac{1+3w}{2}}. \tag{2.152}$$

The above results imply that for the early inflationary period described by a barotropic parameter $w \leq -1/3$, the Big Bang singularity does not occur at $\tau = 0$. Instead, $\tau_e = 0$ marked merely the end of the cosmic inflation, which does not coincide with the very beginning. The BB singularity, described by $t_{\mathrm{BB}} \to 0$ and $a_{\mathrm{BB}} \to 0$, corresponds to $\tau_{\mathrm{BB}} \to -\infty$.

So how does it solve the horizon problem? The figure (2.6) demonstrates that if the conformal time elapsed between the end and the beginning of inflation $|\tau_e \gg \tau_i|$ is larger than $\tau_0 - \tau_{\rm CCM}$, then all CMB photons γ_1, γ_2 originated from the same casually-connected purple region.

The flatness problem revisited

The shrinking of the Hubble sphere can also rescue the flatness problem. To that end, let us calculate the curvature density parameter at the end of inflation, i.e., $\Omega_{\rm k}^{\rm e}$, assuming that the energy budget of the Universe at that time was dominated by a matter fluid with barotropic parameter $w_{\rm inf}$. Using (2.146), we get

$$\Omega_{\rm k}^{\rm e} \simeq \frac{1}{1+\frac{\Omega_{\rm inf}^{\rm e}}{\Omega_{\rm k}^{\rm e}}} = \frac{1}{1+\frac{\Omega_{\rm inf}^{\rm b}}{\Omega_{\rm k}^{\rm b}}\left(\frac{a_{\rm e}}{a_{\rm b}}\right)^{-1-3w_{\rm inf}}}, \tag{2.153}$$

where $a_{\rm b}(a_{\rm e})$ denotes the scale factor at the beginning (end) of the cosmic inflation, whereas $\Omega_{\rm inf}^{\rm b}(\Omega_{\rm inf}^{\rm e})$ is the density parameter of a matter fluid responsible for inflation at its beginning (end). Note that $a_{\rm b}$ might or might not correspond to the initial singularity $a_{\rm BB}$. In what follows, we, however, assume that $a_{\rm BB} \approx a_{\rm b}$.

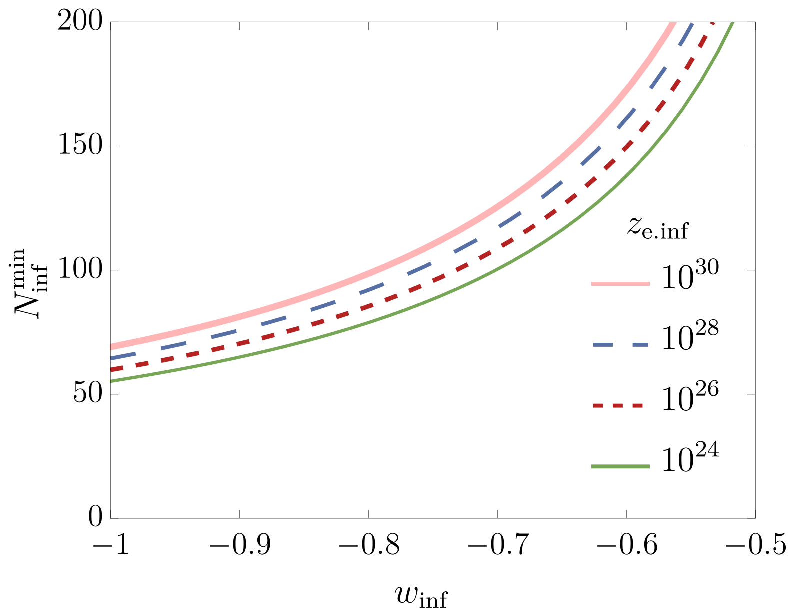

FIGURE 2.7: The minimal number of e-folds required to solve the horizon problem for a given $w_{\rm inf}, z_{\rm e.inf}$ and $\Omega_{\rm k}^{\rm b}/\Omega_{\rm inf}^{\rm b} \sim \mathcal{O}(10^{-1})$.

From the above expression, one can determine the duration of inflation

$$\left(\frac{a_{\rm e}}{a_{\rm b}}\right)^{-1-3w_{\rm inf}} = \frac{\Omega_{\rm k}^{\rm b}}{\Omega_{\rm inf}^{\rm b}}\left(\frac{1}{\Omega_{\rm k}^{\rm e}} - 1\right), \tag{2.154}$$

which, expressed in terms of inflationary e-folds, reads

$$N_{\rm inf} \equiv \ln\left(\frac{a_{\rm e}}{a_{\rm b}}\right) = \frac{-2}{1+3w_{\rm inf}}\left\{\frac{1}{2}\ln\left(\frac{\Omega_{\rm k}^{\rm b}}{\Omega_{\rm inf}^{\rm b}}\right) + \ln\left[\sqrt{\frac{\Omega_{\rm r,0}}{|\Omega_{\rm k,0}|}}(1+z_{\rm e})\right]\right\}, \tag{2.155}$$

where we have assumed that the phase of accelerated expansion was followed by RD epoch and adopted (2.146). To elude fine-tuning of the initial curvature, one could premise that the $\Omega_{\rm k}^{\rm b}/\Omega_{\rm inf}^{\rm b}$ ratio is of the order $\mathcal{O}(10^{-1})$. In this case, $\ln\left[(\Omega_{\rm k}^{\rm b}/\Omega_{\rm inf}^{\rm b})^{-1/(1+3w_{\rm inf})}\right]$ is negative for $w_{\rm inf} < -1/3$. Hence, the flatness problem can be solved, requiring

$$N_{\rm inf} \gtrsim \frac{-2}{1+3w_{\rm inf}} \ln\left(0.3 \cdot z_{\rm e}\right), \tag{2.156}$$

where we have assumed that $1 + z_{\rm e} \approx z_{\rm e}$ and used (2.91). The above condition determines the minimal value of the inflationary number of e-folds, $N_{\rm inf}^{\rm min}$, which resolves the horizon problem for a given $w_{\rm inf}$ and $z_{\rm e}$.

In figure (2.7), we present the relation between $N_{\rm inf}^{\rm min}$ and $w_{\rm inf}$ for several values of $z_{\rm e}$. We see that for $w_{\rm inf} = -1$ the required number of inflationary e-folds is in the range $N_{\rm inf}^{\rm min} \in (50, 70)$ for $z_{\rm e} \in (10^{24}, 10^{30})$.

The monopole problem revisited

Finally, let us elucidate how cosmic inflation might address the magnetic monopole problem. The inflationary paradigm allows for the existence of monopoles as long as they were produced before or during this period. In other words, the early epoch of inflation can help explain the monopole problem, provided that it followed the GUT phase transition. The rapid expansion could have diluted the monopole number density to an unobservably low level. However, such a solution has another limitation. Namely, the maximal temperature reached by the Universe after inflation cannot exceed the GUT scale [283]. Otherwise, unwanted relics might have also been produced after inflation.

Chapter 3

Cosmic inflation

In the previous chapter, we have demonstrated that the hot Big Bang is an incomplete model. It has been shown that its extrapolation back to a BB singularity, i.e., $t_{\rm BB}$, seems inappropriate, as it leads to predictions inconsistent with the observed state of the Universe. In Sec.(2.5.4), we have pointed out that three peculiarities of the hot Big Band, i.e., *the horizon, flatness, and the magnetic monopoles problems*, might be resolved by appending an early period of the accelerated expansion of space, i.e., *cosmic inflation* [205–210].

The inflationary phase is believed to have taken place at a very early time, at the energy scale as high as $\sim 10^{15}$ GeV [226, 228, 290]. Within an extremely tiny fraction of a second after the BB singularity, the Universe might have expanded quasi-exponentially, increasing its initial size roughly $\sim e^{60}$ times. Such energy (and time) scales are poorly understood, as they are far above the energy range of current experiments. Although observations dully constrain this phase, the concept of *cosmic inflation* has become well-established and, nowadays, is it considered rather as a paradigm than just a model.

In Sec.(2.5.4), the conditions for the *cosmic inflation* have been formulated. Namely, three equivalent conditions for that phase are i) the shrinking of the Hubble radius $(aH)^{-1}$, ii) the accelerated expansion of the scale factor $\ddot{a} > 0$, and iii) the violation of the strong energy condition, i.e., $\rho + 3p \leq 0$. However, we have not discussed the specific type of matter that could drive the Universe toward the inflation phase. It turns out that a natural way to archive the accelerated expansion is to introduce a real scalar with flat enough potential. If the energy density of such a field dominates the energy budget at early times, the flatness of its potential lead to a negative pressure, which might automatically guarantee a violation of the strong energy condition. This is why many inflationary models postulate the existence of a spin-0 massive field, the so-called *inflaton*, whose dynamics triggers the *cosmic inflation*. Due to the fact that inflationary energy scales are far beyond our extent, neither the origin nor the nature of the inflaton field is known.

It is worth emphasizing that introducing the scalar field responsible for the accelerated expansion of the Universe not only is a good cure for problems of *standard cosmology* but also provides a mechanism to produce quantum fluctuations that seed the large-scale structures [291–295]. It is considered one of the major successes of the inflationary paradigm as it explains the physical origin of density fluctuations. Quantum fluctuations of the inflaton field also induced tensor perturbations of the metric tensor, which in turn might inevitably lead to the generation of the stochastic background of primordial gravitational waves [192–195]. The detection of such waves might be considered a smoking gun for cosmic inflation.

This chapter is partially based on Ref.[2, 3] and is organized as follows. In Sec.(3.1), we establish the single-field inflationary set-up. In particular, in Sec.(3.1.1), we introduce slow-roll parameters, and then in Sec.(3.1.2), we discuss the slow-roll solutions. In Sec.(3.2), we elaborate on the oscillatory phase of the inflationary paradigm, deriving the approximate oscillatory solutions to the inflaton equation of motion. Subsequently, in Sec.(3.3), we investigate the dynamics of quantum fluctuations induced by the inflaton field and briefly discuss their connection with CMB observables. Next, in Sec.(3.4), we overview the inflationary models. We close this chapter by introducing the $\alpha-$attractor models, which we will adopt in the forthcoming analysis.

3.1 Single-field inflation

The negative pressure condition, obtained from the Raychaudhuri equation Eq.(2.62) can be met by a real spin-0 field ϕ, called *the inflaton field*. This new degree of freedom is assumed to dominate the energy budget of the primordial Universe. The dynamics of the ϕ field is described by the following action:

$$S = S_{\text{EH}} + S_{\phi}, \tag{3.1}$$

where the Einstein-Hilbert action, S_{EH}, was introduced in Eq.(2.40), while the inflaton action is

$$S_{\phi} \equiv \int d^4x\sqrt{-g}\,\mathcal{L}_{\phi}, \qquad \mathcal{L}_{\phi} \equiv \frac{1}{2}g^{\mu\nu}\partial_{\mu}\phi\,\partial_{\nu}\phi - V(\phi). \tag{3.2}$$

In Eq.(3.2), we have assumed that ϕ is minimally coupled to gravity and that its kinetic term is canonically normalized. Above, $V(\phi)$ denotes the potential term for the inflaton, which is left unspecified for the moment.

Next, using the definition for the Belifante–Rosenfeld stress-energy tensor introduced in Eq.(2.45), one finds the energy-momentum tensor for the inflaton field

$$T^{\phi}_{\mu\nu} = \partial_{\mu}\phi\,\partial_{\nu}\phi - g_{\mu\nu}\left[\frac{1}{2}g^{\sigma\rho}\partial_{\sigma}\phi\,\partial_{\rho}\phi - V(\phi)\right]. \tag{3.3}$$

In what follows, we assume that the line element of the background metric is that of the flat ($k=0$) FLRW metric (2.19), and restrict our attention to the homogeneous inflaton field, i.e., $\phi(t,\vec{x}) \equiv \phi(t)$. Then, the 00 component of the energy-momentum tensor, i.e., the energy density, takes the form

$$\rho_{\phi} = T^{0\,\phi}_{0} = \frac{1}{2}\dot{\phi}^2 + V(\phi), \tag{3.4}$$

where the *overdot* denotes derivative with respect to cosmic time t. Moreover, the isotropy of the background metric implies $T^{\phi}_{i0} = T_{0i} = 0$, whereas the diagonal ii (spatial-spatial) component, i.e., the pressure, is

$$p_{\phi} = \frac{1}{2}\dot{\phi}^2 - V(\phi). \tag{3.5}$$

Consequently, the condition for the accelerated expansion, $\rho + 3p < 0$, can be fulfilled only if

$$\dot{\phi}^2 < V(\phi). \tag{3.6}$$

The above condition for the inflationary phase, written in terms of the equation of state parameter $w \equiv p/\rho$, leads to the following inequality: $w < -1/3$, which for the inflaton equation of state,

$$w_\phi = \frac{\frac{1}{2}\dot{\phi}^2 - V(\phi)}{\frac{1}{2}\dot{\phi}^2 + V(\phi)}, \tag{3.7}$$

is automatically guaranteed by Eq.(3.6), since in this case $w_\phi \to -1$.

The Euler-Lagrange equation for the ϕ field reads

$$\partial_\mu \frac{\partial(\sqrt{-g}\mathcal{L}_\phi)}{\partial(\partial_\mu \phi)} - \frac{\partial(\sqrt{-g}\mathcal{L}_\phi)}{\partial \phi} = \partial_\mu \left(\sqrt{-g}\, g^{\mu\nu}\, \partial_\nu \phi\right) + \sqrt{-g}\,\frac{\partial V}{\partial \phi} = 0, \tag{3.8}$$

which can be further recast to the form

$$g^{\mu\nu}\partial_\mu\partial_\nu\phi + \partial_\nu\phi\,\partial_\mu g^{\mu\nu} + \frac{1}{2}g^{\rho\sigma}(\partial_\mu g_{\rho\sigma})g^{\mu\nu}\partial_\nu\phi + \frac{\partial V}{\partial\phi} = 0. \tag{3.9}$$

Thus, neglecting spatial derivatives, the classical equation of motion (EoM) for the inflaton field in the FLRW background can be written in the following form:

$$\ddot{\phi} + 3H\dot{\phi} + V_{,\phi}(\phi) = 0, \tag{3.10}$$

where we have used the shorthand notation $V_{,\phi}(\phi) \equiv \partial V(\phi)/\partial\phi$.
Assuming that the total energy budget is dominated by the inflaton energy density (3.4), the evolution of the Hubble rate, H, is determined by the following Friedmann equation:

$$H^2 = \frac{1}{3M_{\text{Pl}}^2}\left(\frac{1}{2}\dot{\phi}^2 + V(\phi)\right). \tag{3.11}$$

It is worth noting that Eq.(3.10) resembles an EoM for a particle rolling down its potential, subjected to friction via the $3H\dot{\phi}$ term.

3.1.1 Slow-roll parameters

The inflaton EoM (3.10) together with the Friedmann equation (3.11) form a coupled system, which can be solved numerically once the potential $V(\phi)$, and initial conditions $\{\phi_i, \dot{\phi}_i\}$ are specified. Nevertheless, it is instructive to obtain approximate analytical solutions. One can typically distinguish two regimes: the *slow-roll limit* and the *oscillatory solution*, which will be discussed in the next section. The former regime refers to the limit in which the condition (3.6) is satisfied and the acceleration term $\ddot{\phi}$ is subdominant. Let us now discuss these conditions quantitatively [296, 297]. To that end, we first note that

$$\frac{\ddot{a}}{a} = \dot{H} + H^2 \equiv H^2\,(1-\epsilon_H)\,, \qquad \epsilon_H \equiv -\frac{\dot{H}}{H^2} = \frac{d}{dt}\left(\frac{1}{H}\right) = 3\cdot\frac{\dot{\phi}^2/2}{\dot{\phi}^2/2 + V(\phi)}. \tag{3.12}$$

Hence, the condition for accelerated expansion can be formulated in terms of the Hubble slow-roll parameter (HSR) ϵ_H as

$$\ddot{a} > 0 \iff 0 \le \epsilon_H < 1. \tag{3.13}$$

To achieve the required number of e-folds during inflation ($\sim N_{\text{inf}} = 60$ [226]), the above condition should hold for a sufficiently long period. This means that $\epsilon_H \ll 1$ during the cosmic inflation. Such a condition implies that the Hubble rate should change slowly with time, which happens if $V(\phi)$ dominates over the inflaton kinetic energy.

Moreover, accelerated expansion is sustained sufficiently long if the second time derivative of ϕ is small enough: $|\ddot{\phi}| \ll |3H\dot{\phi}|, |V_{,\phi}|$. The condition can be expressed in terms of the second HSR parameter

$$\eta_H \equiv -\frac{\ddot{\phi}}{H\dot{\phi}} = -\frac{d\ln\dot{\phi}}{Hdt} = \epsilon_H - \frac{1}{2}\frac{d\ln\epsilon_H}{Hdt} = \epsilon_H - \frac{1}{2\epsilon_H}\frac{d\epsilon_H}{dN} \ll 1, \tag{3.14}$$

where we have used $dN = Hdt$.
Note that inflation take place when $\epsilon_H < 1$, regardless of the value of η_H. However, the above condition (3.14) ensures that the fractional change of ϵ_H per e-fold is small such that the accelerated phase of expansion last long enough. Moreover, the above constraint allows us to neglect the acceleration term in the inflaton EoM (3.10), which now simplifies to the following form:

$$H \simeq \frac{1}{M_{\rm Pl}}\sqrt{\frac{V(\phi)}{3}}, \qquad \dot{\phi} = -\frac{M_{\rm Pl}}{\sqrt{3}}\frac{V_{,\phi}(\phi)}{\sqrt{V(\phi)}}. \tag{3.15}$$

The above relations indicate that the ϕ field asymptotically approaches an attractor solution [297]. This means that the inflaton promptly converges towards the slow-roll solution for a wide range of initial conditions.

In addition to the HSR parameters, it is instructive to define the potential slow-roll (PSR) parameters through the following expressions:

$$\epsilon_V \equiv \frac{M_{\rm Pl}^2}{2}\left(\frac{V_{,\phi}}{V}\right)^2, \qquad \eta_V \equiv M_{\rm Pl}^2\frac{V_{,\phi\phi}}{V}, \tag{3.16}$$

where $V_{,\phi\phi} \equiv \partial^2 V/\partial\phi^2$.
Note that the smallness of the PSR parameters should allow us to neglect the kinetic term in the Friedmann equation (3.11) and the acceleration term in Eq.(3.10). However, the smallness of ϵ_V and η_V is a necessary but not sufficient condition to guarantee that these terms can be dropped. The PSR parameters can restrict the form of the inflaton potential but are insensitive to the value of $\dot{\phi}$. Hence, the PSR formalism is usually supplemented by the additional constrain $\dot{\phi} \simeq -V_{,\phi}/(3H)$, which assures that ϕ approach to the asymptotic attractor solution.

One can also show that the PSR set can be related to the HSR parameters as [297]

$$\epsilon_V = \epsilon_H\left(\frac{3-\eta_H}{3-\epsilon_H}\right)^2, \tag{3.17}$$

and

$$\eta_V = \sqrt{2M_{\rm Pl}^2\epsilon_H}\frac{\eta_{H,\phi}}{3-\eta_H} + \left(\frac{3-\eta_H}{3-\epsilon_H}\right)(\epsilon_H + \eta_H), \tag{3.18}$$

where the first term in (3.18) is of higher-order. In the lowest-order in slow-roll, one gets $\eta_V \approx \eta_H$, and $\eta_V \approx \eta_H + \epsilon_H$. Consequently, the slow-roll conditions $\epsilon_H, \eta_H \ll 1$ implies $\epsilon_V, \eta_V \ll 1$. Therefore, for the sake of simplicity, we restrict our attention to the PSR parameters in the remaining part of this chapter.

3.1.2 Slow-roll solutions

Now let us note that by differentiating (3.4) with respect to time and implementing EoM for the ϕ field (3.10), we get the continuity equation

$$\dot{\rho_\phi} = \dot{\phi}(\ddot{\phi} + V_{,\phi}) = -3H\dot{\phi}^2 \implies \dot{\rho_\phi} + 3H(p_\phi + \rho_\phi) = 0. \tag{3.19}$$

Since during the slow-roll inflation, $p_\phi \simeq -\rho_\phi$, the conservation equation implies that ρ_ϕ is approximately constant in time. This, in turn, indicates that the Hubble rate is also roughly time-independent. Hence, using the slow-roll version of the Friedmann equation, we find the evolution of the scale factor

$$\frac{d\ln a}{dt} \simeq H_{\rm dS} \equiv \frac{1}{M_{\rm Pl}}\sqrt{\frac{V}{3}} \qquad \implies a_{\rm dS}(t) \simeq a_i \exp\left[H_{\rm dS}(t - t_i)\right], \tag{3.20}$$

where a_i and t_i denote the scale factor and cosmic time corresponding to the onset of the slow-roll phase of inflation, respectively. The constant Hubble parameter leads to exponential expansion, which is a characteristic feature of the de-Sitter (dS) universe. In general, inflationary models slightly deviate from the exact de-Sitter phase ($\epsilon_H^{\rm dS} = 0$), and its deviation is described by the set of slow-roll parameters. In a more realistic scenario, the scale factor grows quasi-exponentially with time, according to the formula

$$a_{\rm I}(t) = a_i \exp\left(-\frac{1}{M_{\rm Pl}^2}\int (\partial_\phi \ln V)^{-1} d\phi\right), \tag{3.21}$$

whereas the evolution of the Hubble rate and the inflaton field feebly depends on time.

Finally, it is also instructive to calculate the inflationary number of e-folds,

$$\begin{aligned} N_{\rm inf} &\equiv \ln\frac{a_e}{a_i} \\ &= \int_{t_i}^{t_e} H\,dt = \int_{\phi_i}^{\phi_e} \frac{H}{\dot{\phi}}\,d\phi \overset{(3.15)}{\approx} -\int_{\phi_i}^{\phi_e} \frac{V}{V_{,\phi}}\,d\phi = \frac{1}{M_{\rm Pl}}\int_{\phi_e}^{\phi_i} \frac{1}{\sqrt{2\epsilon_V}}\,d\phi, \end{aligned} \tag{3.22}$$

where a_e, t_e, and $\phi_e \equiv \phi(t_e)$ correspond to the scale factor, cosmic time, and field value at the end of inflation, defined by the condition,

$$\ddot{a} = 0 \iff \epsilon_H = 1. \tag{3.23}$$

Note that at the end of inflation, one can use (3.17) and (3.18) to eliminate η_H, obtaining

$$\eta_H(a_e) \simeq 1 - 2\sqrt{1 - \eta_V(a_e)}. \tag{3.24}$$

Using the above result, one can show that the condition (3.23) roughly corresponds to [298]

$$\epsilon_V(a_e) \simeq (1 + \sqrt{1 - \eta_V/2})^2. \tag{3.25}$$

The required number of the inflationary e-folds is in the realm of several tens. The horizon and the flatness problems can be resolved providing the total number of e-folds exceeds about $N_{\rm inf} = 60$ [226].

3.2 Oscillatory phase

According to the single-field inflationary scenario delineated in the previous section, the ϕ field rolls down towards the minimum of its potential during the slow-roll phase of inflation. As ϕ evolves towards the smaller values, the slow-roll conditions cease validity, and ϕ enters the oscillatory regime. Its commencement coincides with the termination of the accelerated expansion, defined by the condition (3.23). From Eq.(3.12), we see that the following condition can alternatively define the end of inflation:

$$\dot{\phi}^2(t_e) = V(\phi_e), \tag{3.26}$$

which, in turn, implies

$$\rho_e \equiv \rho_\phi(t_e) = \frac{3}{2}V(\phi_e) \qquad\qquad \Longrightarrow \; w_e = -\frac{1}{3}. \tag{3.27}$$

The inflationary phase ends as the potential steepens and ϕ starts to coherently oscillate around the bottom of its potential with a decaying amplitude. The time scale of oscillations is typically much shorter than the variation of the inflaton amplitude.

During the oscillatory phase, it is convenient to parametrize the inflaton evolution by a product of the following functions [127, 203, 299, 300]:

$$\phi(t) = \varphi(t)\mathcal{P}(t). \tag{3.28}$$

The slowly-varying function $\varphi(t)$, which we refer to as the envelope of the oscillations, accounts mainly for the expansion of the Universe, whereas $\mathcal{P}(t)$ describes the quasi-periodic rapid oscillations. The envelope function is defined by the condition [127, 203, 299, 300]

$$V(\varphi) := \rho_\phi. \tag{3.29}$$

The character of these oscillations strongly depends on the shape of $V(\phi)$ in the vicinity of the minimum. In general, the inflaton potential during the oscillatory epoch can be well approximated by the following monomial:

$$V(\phi) = V(\phi_e)\left|\frac{\phi}{\phi_e}\right|^{2n} = \rho_\phi|\mathcal{P}|^{2n}. \tag{3.30}$$

In the remainder of this thesis, we limit ourselves to potentials steeper than the linear potential during reheating. This implies $n > 1/2$.

Our goal now is to find approximate analytical solutions of (3.10) during the oscillatory phase using the parametrization (3.28) together with the condition (3.29). For this purpose, let us first define a time average of a quantity X over one period of oscillation T, i.e.,

$$\langle X\rangle := \frac{1}{T}\int_t^{t+T} d\tilde{t}\, X(\tilde{t}). \tag{3.31}$$

Furthermore, according to the Leibniz integral rule

$$\frac{d}{dt}\langle X\rangle = \frac{d}{dt}\left(\frac{1}{T}\int_t^{t+T} d\tilde{t}\, X(\tilde{t})\right) = \frac{X(t+T)-X(t)}{T} = \frac{1}{T}\int_t^{t+T} d\tilde{t}\, \dot{X} = \langle\dot{X}\rangle. \tag{3.32}$$

In what follows, we assume that the envelope barely changes during one oscillation. Thanks to (3.29), it means that ρ_ϕ is also almost constant in time, which, in turn, implies that the time variation of H can also be neglected.

Utilizing these remarks, we get

$$\langle\dot{\phi}^2\rangle = \frac{1}{T}\int_t^{t+T} d\tilde{t}\,\dot{\phi}^2(\tilde{t}) \simeq -\langle\phi\ddot{\phi}\rangle \overset{(3.10)}{=} 3H\langle\dot{\phi}\phi\rangle + \langle\phi V_{,\phi}\rangle \simeq \langle\phi V_{,\phi}\rangle, \tag{3.33}$$

where we have integrated by parts in the first and the last steps. Next, using Eqs.(3.4), (3.30) and the above relation, one obtains

$$\begin{aligned}\langle\rho_\phi\rangle &= \frac{1}{2}\langle\phi V_{,\phi}\rangle + \langle V(\phi)\rangle = \frac{1}{2}\left\langle\phi\cdot\frac{2n\,V(\phi)}{\phi}\right\rangle + \langle V(\phi)\rangle = (n+1)\langle V(\phi)\rangle \\ &= (n+1)\langle\rho_\phi|\mathcal{P}|^{2n}\rangle,\end{aligned} \tag{3.34}$$

which indicates that

$$\langle|\mathcal{P}|^{2n}\rangle = \frac{1}{1+n}. \tag{3.35}$$

Hence, the inflaton averaged equation-of-state parameter approaches a constant value during the oscillatory phase

$$\bar{w} \equiv \frac{\langle p_\phi\rangle}{\langle\rho_\phi\rangle} \simeq \frac{(n-1)\langle V(\phi)\rangle}{(1+n)\langle V(\phi)\rangle)} = \frac{n-1}{n+1}. \tag{3.36}$$

The time-averaged version of the continuity equation takes the form

$$\langle\dot{\rho}_\phi\rangle + 3H(1+\bar{w})\langle\rho_\phi\rangle = \frac{d}{dt}\langle\rho_\phi\rangle + 3H(1+\bar{w})\langle\rho_\phi\rangle = 0, \tag{3.37}$$

or simply

$$\boxed{\dot{\rho}_\phi + 3H(1+\bar{w})\rho_\phi = 0,} \tag{3.38}$$

where we have used the fact that $\langle\rho_\phi\rangle = \rho_\phi$.
Lastly, utilizing Eq.(3.36), we see that for the quadratic inflaton potential, i.e., $n=1$, ϕ behaves as a matter, i.e., $\bar{w}=0$, during the oscillatory phase, while for the quartic potential, i.e., $n=2$, inflaton has a radiation-like equation of state, $\bar{w}=1/3$.

3.2.1 The envelope evolution

From Eq.(3.38), one obtains the dynamical equation for the slowly-varying envelope

$$\dot{\varphi} = -\frac{3}{n+1}H\varphi. \tag{3.39}$$

Converting time derivative to derivative with respect to the scale factor a, the above equation can be recast as

$$\frac{d\varphi}{\varphi} = -\frac{3}{n+1}\frac{da}{a}. \tag{3.40}$$

Thus, during the oscillatory phase, the envelope experiences a power-law decrease with the scale factor

$$\varphi(a) = \varphi_e\left(\frac{a_e}{a}\right)^{\frac{3}{n+1}}, \tag{3.41}$$

where φ_e denotes the initial value of the envelope at the onset of the oscillatory phase. By setting $\mathcal{P}_e = 1$, we can relate φ_e to the inflaton field value at the end of inflation ϕ_e, defined by the condition (3.23).

3.2.2 Evolution of the quasi-periodic function

On the other hand, the evolution of the (an)harmonic function $\mathcal{P}$ is described by the following equation:

$$\dot{\phi} = \dot{\varphi}\mathcal{P} + \dot{\mathcal{P}}\varphi \implies \dot{\mathcal{P}} = \frac{\dot{\phi}}{\varphi} - \frac{\dot{\varphi}}{\varphi}\mathcal{P}. \tag{3.42}$$

Using Eq. (3.40), we can further simplify this equation as

$$\dot{\mathcal{P}} = \pm\frac{\sqrt{2\rho_\phi(1-|\mathcal{P}|^{2n})}}{\varphi} + \frac{3}{n+1}H\mathcal{P}, \tag{3.43}$$

where the $\pm$ sign corresponds to $\dot{\phi} > 0$ and $\dot{\phi} < 0$, respectively. Since the time scale associated with the expansion is much longer than the typical time scale of oscillations, we can neglect the second term in the above equation. Consequently, equation (3.43) takes the form of a classical energy integral for a material point characterized by a coordinate x moving in the potential $V(x)$

$$\frac{\dot{x}^2}{2} + V(x) = 0, \tag{3.44}$$

where $x \equiv \mathcal{P}$ and $V(x) \equiv (|x|^{2n}-1)\rho_\phi/\varphi^2$. The ρ_ϕ/φ^2 ratio can be associated with the effective mass of the inflaton field, defined as

$$m_\phi^2 := \left.\frac{\partial^2 V(\phi)}{\partial\phi^2}\right|_{\phi=\varphi} = 2n(2n-1)\frac{\rho_\phi}{\varphi^2}. \tag{3.45}$$

Note that the variation of m_ϕ^2 is negligible in the time scale of oscillations.
The EoM for the $\mathcal{P}$ function can be rewritten as

$$\mathrm{d}t = \pm\frac{\mathrm{d}\mathcal{P}}{\sqrt{A_n(1-|\mathcal{P}|^{2n})}}, \qquad A_n \equiv \frac{m_\phi^2}{n(2n-1)} \simeq const. \tag{3.46}$$

Adopting the initial condition $\mathcal{P}(t_0) = 1$, where $t_0 \simeq t_e$, and choosing the minus sign on the r.h.s. of the above equation, we get

$$-\sqrt{A_n}(t-t_0) = \int_1^{\mathcal{P}(t)} \frac{\mathrm{d}\mathcal{P}}{\sqrt{1-|\mathcal{P}|^{2n}}}. \tag{3.47}$$

Switching to the new variable $u = |\mathcal{P}|^{2n}$, we find

$$-\sqrt{A_n}(t-t_0) = \frac{1}{2n}\int_1^{|\mathcal{P}|^{2n}} \mathrm{d}u\, u^{\frac{1}{2n}-1}(1-u)^{\frac{1}{2}-1}. \tag{3.48}$$

This, in turn, can be rewritten as

$$-\sqrt{A_n}(t-t_0) = \frac{1}{2n}\int_0^{|\mathcal{P}|^{2n}} \mathrm{d}u\, u^{\frac{1}{2n}-1}(1-u)^{\frac{1}{2}-1} - \int_0^1 \mathrm{d}u\, u^{\frac{1}{2n}-1}(1-u)^{\frac{1}{2}-1}, \tag{3.49}$$

which reads to

$$-\sqrt{A_n}(t-t_0) = \frac{1}{2n}B\left(|\mathcal{P}|^{2n}; \frac{1}{2n}, \frac{1}{2}\right) - \frac{\sqrt{\pi}}{2n}\frac{\Gamma\left(\frac{1}{2n}\right)}{\Gamma\left(\frac{1}{2}+\frac{1}{2n}\right)}, \tag{3.50}$$

where $B(x;a,b)$ denotes the incomplete beta functions, defined as

$$B(x;a,b) := \int_0^x \mathrm{d}t\, t^{a-1}(1-t)^{b-1}, \tag{3.51}$$

with $a>0, b>0$ and $0\le x\le 1$, implying

$$0 \le |\mathcal{P}(t)|^{2n} \le 1. \tag{3.52}$$

The period of the inflaton oscillations can be obtained from the following integral:

$$T = 4\int_0^1 \frac{\mathrm{d}x}{\sqrt{2[V(1)-V(x)]}} = \frac{1}{m_\phi}\sqrt{\frac{4\pi(2n-1)}{n}}\frac{\Gamma\left(\frac{1}{2n}\right)}{\Gamma\left(\frac{1}{2}+\frac{1}{2n}\right)}, \tag{3.53}$$

whereas the frequency ω is

$$\omega = m_\phi\sqrt{\frac{\pi n}{2n-1}}\frac{\Gamma\left(\frac{1}{2}+\frac{1}{2n}\right)}{\Gamma\left(\frac{1}{2n}\right)}. \tag{3.54}$$

In order to find an explicit formula for $|\mathcal{P}(t)|$ let us use the beta function, defined as

$$B\left(a,b\right) := \int_0^1 \mathrm{d}t\, t^{a-1}(1-t)^{b-1}. \tag{3.55}$$

Dividing Eq.(3.50) by the beta function, $B\left(\frac{1}{2n},\frac{1}{2}\right) = \sqrt{\pi}\frac{\Gamma\left(\frac{1}{2n}\right)}{\Gamma\left(\frac{1}{2}+\frac{1}{2n}\right)}$, one finds

$$1 - 2n\frac{\Gamma\left(\frac{1}{2}+\frac{1}{2n}\right)}{\Gamma\left(\frac{1}{2n}\right)}\sqrt{\frac{A_n}{\pi}}(t-t_0) = I\left(|\mathcal{P}(t)|^{2n}; \frac{1}{2n}, \frac{1}{2}\right), \tag{3.56}$$

where the following definition of the regularized incomplete beta function has been used

$$I(x;a,b) = B(x;a,b)/B(a,b). \tag{3.57}$$

Thus, the solution for the $|\mathcal{P}(t)|$ function can be expressed in terms of the inverse of the regularized incomplete beta function, i.e.,

$$|\mathcal{P}(t)|^{2n} = I_z^{-1}\left(\frac{1}{2n}, \frac{1}{2}\right), \tag{3.58}$$

where

$$z \equiv 1 - 2n\frac{\Gamma\left(\frac{1}{2}+\frac{1}{2n}\right)}{\Gamma\left(\frac{1}{2n}\right)}\sqrt{\frac{A_n}{\pi}}(t-t_0) = 1 - \frac{4}{T}(t-t_0). \tag{3.59}$$

Finally, let us calculate the time average of $|\mathcal{P}|^{2n}$ over one oscillation period:

$$\begin{aligned}\langle|\mathcal{P}|^{2n}\rangle &= \frac{1}{T}\int_0^T \mathrm{d}t\,|\mathcal{P}(t)|^{2n}\\ &= \frac{4}{T}\int_0^{T/4}\mathrm{d}t\, I^{-1}_{z(t)}\left(\frac{1}{2n},\frac{1}{2}\right), \quad \text{for } n\in\mathbb{R}_+\\ &= \frac{2\Gamma\left(\frac{1}{2}+\frac{1}{2n}\right)}{\sqrt{\pi}\Gamma\left(\frac{1}{2n}\right)}\left[{}_2F_1\left(\frac{1}{2},-\frac{1}{2n};\frac{3}{2};z_0\right)\sqrt{z_0} - {}_2F_1\left(\frac{1}{2},-\frac{1}{2n};\frac{3}{2};z_1\right)\sqrt{z_1}\right], \end{aligned}\tag{3.60}$$

with

$$z_0 \equiv 1 - I_0^{-1}\left(\frac{1}{2n},\frac{1}{2}\right), \qquad z_1 \equiv 1 - I_1^{-1}\left(\frac{1}{2n},\frac{1}{2}\right). \tag{3.61}$$

Relation (3.60) can be further simplified as follows,

$$\langle|\mathcal{P}|^{2n}\rangle = \frac{\Gamma\left(\frac{1}{2}+\frac{1}{2n}\right)\Gamma\left(1+\frac{1}{2n}\right)}{\Gamma\left(\frac{1}{2n}\right)\Gamma\left(\frac{3}{2}+\frac{1}{2n}\right)} = \frac{1}{n+1}, \tag{3.62}$$

which agrees with the result (3.36).

3.2.3 Evolution of slowly-varying variables

Before we conclude this section, let us determine the exact time evolution of several slowly-varying observables. The dynamics of the inflaton energy density is governed by Eq. (3.38), whose solution is takes the power-law form

$$\rho_\phi = \rho_e\left(\frac{a_e}{a}\right)^{3(1+\bar{w})} = \rho_e\left(\frac{a_e}{a}\right)^{\frac{6n}{n+1}}. \tag{3.63}$$

Consequently, from the Friedmann equation, one obtains

$$H = H_e\left(\frac{a_e}{a}\right)^{\frac{3(1+\bar{w})}{2}} = H_e\left(\frac{a_e}{a}\right)^{\frac{3n}{n+1}}, \qquad H_e \equiv \frac{\sqrt{\rho_e}}{\sqrt{3}M_{\rm Pl}}. \tag{3.64}$$

Integrating the above equation, one finds the evolution of the scale factor a with t,

$$a = a_e\left[1+\frac{3n}{n+1}H_e(t-t_e)\right]^{\frac{n+1}{3n}}. \tag{3.65}$$

Then, by inserting solutions (3.41) and (3.63) into Eq. (3.45), one gets

$$m_\phi(a) = m_\phi^e\left(\frac{a_e}{a}\right)^{\frac{3(n-1)}{n+1}}, \qquad m_\phi^e \equiv \sqrt{2n(2n-1)}\frac{\sqrt{\rho_e}}{\phi_e}, \tag{3.66}$$

which indicates that m_ϕ is a monotonically increasing function of the scale factor for $n \in (1/2, 1)$, whereas for $n > 1$ it decreases during the oscillatory phase. Hence, only for $n = 1$, which corresponds to the quadratic inflaton potential, the effective mass is time-independent. Moreover, the time dependency of m_ϕ presupposes that the period of the inflaton oscillations T and the frequency ω also depend on time, provided that $n \neq 1$. In particular, from Eqs.(3.53) and (3.54), we see that for $n \in (1/2, 1)$, $T(\omega)$ decreases (increases), while if $n > 1$ $T(\omega)$ increases (decreases) with the scale factor.

3.3 Constraints on inflationary models

In this section, we revise several inflationary parameters and their corresponding values from the CMB spectrum, following [227]. But before we introduce the principal CMB observables, let us first present a very brief introduction to the topic of quantum fluctuations during inflation.

3.3.1 Primordial perturbations

The inflationary paradigm is so appealing not only because it resolves the hot big bang problems but also because it provides a very natural explanation for tiny inhomogeneities observed in the CMB spectrum. Namely, the primary anisotropies could have originated from the unavoidable zero-point quantum fluctuations of the inflaton ϕ and metric perturbations $\mathcal{R}$. One must go beyond the standard assumption of homogeneity and isotropy to account for primordial fluctuations. To that end, let us define perturbations around the homogeneous background solutions for $\phi(t)$ and the metric $g_{\mu,\nu}(t)$:

$$\tilde{\phi}(t,\vec{x}) = \phi(t) + \delta\phi(t,\vec{x}), \qquad \tilde{g}_{\mu\nu}(t,\vec{x}) = g_{\mu\nu} + \delta g_{\mu\nu}(t,\vec{x}), \tag{3.67}$$

where $\delta\phi \ll \phi$ and $\delta g_{\mu\nu} \ll g_{\mu\nu}$.

To understand the behavior and evolution of primordial perturbations, it is instructive to decompose them into scalar (S), vector (V), and tensor (T) components. This decomposition, known as the SVT decomposition, was introduced by Bardeen in 1980 [301]. At the linear level, perturbations of each type evolve independently of each other. This means that one can track the dynamics of each component separately without significant interference from the others. For instance, scalar perturbations primarily drive the growth of large-scale structures such as galaxies and clusters of galaxies. Vector perturbations, on the other hand, are significantly suppressed during inflation [295]. Tensor perturbations correspond to primordial gravitational waves PGWs and their propagation through space. We focus on tensor (PGWs) and scalar perturbations in the following part of this section, starting from the latter.
In the comoving gauge, the ϕ field is unperturbed, i.e., $\delta\phi = 0$, whereas other scalar degrees of freedom are parameterized by the metric fluctuation $\mathcal{R}(t,\vec{x})$, such that [227]

$$g_{ij} = -a^2[(1-2\mathcal{R})\delta_{ij} + h_{ij}], \tag{3.68}$$

where h_{ij} is the transverse-traceless tensor, i.e, $\partial_i h_{ij} = 0 = h^i_i$. All fluctuations are created on all comoving length scales k^{-1} deep inside the cosmic horizon. Modes with wavelength k^1 much smaller than the comoving Hubble radius $(aH)^{-1}$ are referred to as *subhorizon modes*. Since the comoving Hubble radius shrinks during inflation while the wavenumber k^{-1} of modes remains constant, at some point during inflation, perturbations eventually exit the horizon. We denote this moment as $a_\star = k_\star(H_\star)^{-1}$. Contrarily, modes with wavelength much longer than $(aH)^{-1}$, i.e., $k < aH$, are referred to as *subhorizon modes*. A notable feature of fluctuations is that their amplitude remains constant outside the horizon.

Scalar perturbations

To derive EoM for scalar perturbations one expands the action (3.1) to the second order in $\mathcal{R}$, obtaining [227]

$$\delta S^{(2)} = \int dt d^3x\, a^3 \frac{\dot{\phi}^2}{2H^2}\left[\dot{\mathcal{R}} - \frac{1}{a^2}(\partial_i\mathcal{R})^2\right]. \tag{3.69}$$

Performing the following field redefinition:

$$v \equiv z\mathcal{R}, \qquad z \equiv a\frac{\dot{\phi}}{H}, \tag{3.70}$$

and using the conformal coordinates, one can recast Eq. (3.69) as

$$\delta S^{(2)} = \frac{1}{2}\int d\tau d^3x \left[(v')^2 + (\partial_i v)^2 + \frac{z''}{z}v^2\right], \tag{3.71}$$

where by the prime we have denoted derivative w.r.t. to the conformal time τ, i.e., $' \equiv \partial_\tau$. Hence, the Euler-Lagrange equation for the v field is

$$v'' - \nabla^2 v - \frac{z''}{z}v = 0. \tag{3.72}$$

Now let us promote the classical field v to quantum field operator $\hat{v}$,

$$\hat{v}(\tau,\vec{x}) = \int \frac{d^3k}{(2\pi)^3}\left[v_k(\tau)\hat{a}_{\vec{k}}e^{i\vec{k}\cdot\vec{x}} + v_k^*(\tau)\hat{a}^\dagger_{\vec{k}}e^{-i\vec{k}\cdot\vec{x}}\right], \tag{3.73}$$

and impose the equal time canonical commutation relation (CCR)

$$[\hat{v}(\tau,\vec{x}), \hat{\pi}_v(\tau,\vec{y})] = i\delta^{(3)}(\vec{x}-\vec{y}), \tag{3.74}$$

where $\hat{\pi}_v(\tau,\vec{y}) = \hat{\pi}'_v(\tau,\vec{y})$ denotes the quantum operator describing the momentum conjugate to $\hat{v}$.
The above relation can only be satisfied provided that the creation and annihilation operators obey the following commutation relations:

$$[\hat{a}_{\vec{k}}, \hat{a}^\dagger_{\vec{q}}] = (2\pi)^3\delta^{(3)}(\vec{k}-\vec{q}), \qquad [\hat{a}_{\vec{k}}, \hat{a}_{\vec{q}}] = 0 = [\hat{a}^\dagger_{\vec{k}}, \hat{a}^\dagger_{\vec{q}}], \tag{3.75}$$

whereas the mode functions are normalized such that *the Wronskian* is equal

$$W[v_k, v'_k] \equiv v_k v_k^{*\prime} - v_k^* v'_k = -i. \tag{3.76}$$

From Eq. (3.72), one finds that v_k satisfies the so-called *Mukhanov-Sasaki* equation

$$v''_k + \left[k^2 - \frac{z''}{z}\right]v_k = 0. \tag{3.77}$$

Deep inside the Hubble horizon, the Mukhanov-Sasaki equation simplifies to the harmonic oscillator equation in flat Minkowski spacetime, i.e., $v''_k + k^2 v_k = 0$. Hence, the initial conditions for the mode function can be taken as the Bunch-Davies vacuum, i.e.,

$$\lim_{\tau\to-\infty} v_k = \frac{e^{-ik\tau}}{\sqrt{2k}}, \qquad \lim_{\tau\to-\infty} v'_k = -ik\frac{e^{-ik\tau}}{\sqrt{2k}}. \tag{3.78}$$

Moreover, during the de-Sitter phase of inflation, $H = const.$, which implies that Eq.(3.77) simplifies as

$$v''_k + \left[k^2 - \frac{2}{\tau}\right]v_k = 0. \tag{3.79}$$

The solution to the above equation is given by

$$v_k(\tau) = \frac{e^{-ik\tau}}{\sqrt{2k}}\left(1 - \frac{i}{k\tau}\right). \tag{3.80}$$

To statistically characterize the fluctuations, one introduces the power spectrum using the two-point correlation function [227]

$$\langle \mathcal{R}_k \mathcal{R}_q \rangle = (2\pi)^3 \delta^{(3)}(\vec{k} + \vec{q})\, \mathcal{P}_{\mathcal{R}}(k), \qquad \Delta^2_{\mathcal{R}} \equiv \frac{k^3}{2\pi^2}\mathcal{P}_{\mathcal{R}}(k), \tag{3.81}$$

where $\langle \dots \rangle$ denotes the ensemble average.
Utilizing Eq. (3.70), one can calculate the power spectrum at the horizon crossing, i.e., at $k_\star = a_\star H_\star$, obtaining

$$\langle \mathcal{R}_k \mathcal{R}_q \rangle = (2\pi)^3 \delta^{(3)}(\vec{k} + \vec{q}) \frac{H_\star^2 |v_k(\tau_\star)|^2}{\dot{\phi}_\star^2 a_\star^2} = (2\pi)^3 \delta^{(3)}(\vec{k} + \vec{q}) \frac{1}{2k_\star}\left(1 + \frac{1}{k_\star^2 \tau_\star^2}\right)\frac{H_\star^2}{\dot{\phi}_\star^2 a_\star^2}. \tag{3.82}$$

Note that for superhorizon modes, i.e., $k < aH$, the first term in the above parenthesis is negligible since $|k\tau| < 1$. Hence,

$$\langle \mathcal{R}_k \mathcal{R}_q \rangle \simeq (2\pi)^3 \delta^{(3)}(\vec{k} + \vec{q}) \frac{1}{2k_\star^3}\frac{H_\star^4}{\dot{\phi}_\star^2}. \tag{3.83}$$

Consequently, the dimensionless power spectrum of scalar fluctuations at the horizon crossing is

$$\Delta_s^2(k) \equiv \frac{k^3}{2\pi^2}\mathcal{P}_{\mathcal{R}}(k_\star) = \frac{1}{(2\pi)^2}\frac{H_\star^4}{\dot{\phi}_\star^2} = \frac{1}{8\pi^2}\frac{H_\star^2}{M_{\rm Pl}^2}\frac{1}{\epsilon_H}, \tag{3.84}$$

where we have used the definition of the first HSR parameter Eq. (3.12).

Lastly, let us stress that the scalar power spectrum depends only on k, as Δ_s^2 is evaluated at the horizon crossing $k_\star = a_\star H_\star$. Due to the fact that both H and ϵ_H might slowly vary in time during inflation, one expects that Δ_s^2 could be slightly different for different modes. The deviation from the scale-invariance, i.e., k-independence, can be parametrized by the following expression: [227]

$$\Delta_s^2(k) \equiv A_s\left(\frac{k}{k_\star}\right)^{n_s - 1}, \tag{3.85}$$

where $k_\star$ should be understood as some reference scale, A_s is the amplitude of the scalar spectrum measured at $k = k_\star$, while n_s denotes the scalar spectral index, defined as

$$n_s - 1 \equiv \frac{d\ln \Delta_s^2}{d\ln k}. \tag{3.86}$$

Note that $n_s = 1$ would correspond to a perfect scale-invariance.

Tensor perturbations

Analogously, one can obtain the power spectrum for tensor perturbations. For this purpose, one should expand the Einstein-Hilbert action Eq. (2.40) up to second order [227], obtaining

$$\delta S^{(2)}_{\rm EH} = \frac{M_{\rm Pl}^2}{8}\int d\tau d^3x\, a^2 [|h'_{ij}|^2 - |\partial_l h_{ij}|^2]. \tag{3.87}$$

It is convenient to decompose h_{ij} into the two polarization states

$$h_{ij}(\tau,\vec{x}\,) = \sum_{\lambda=+,\times}\int \frac{d^3k}{(2\pi)^3} h^\lambda_k(\tau)\,\epsilon^\lambda_{ij}(\vec{k}\,)\,e^{i\vec{k}\cdot\vec{x}}, \tag{3.88}$$

where $\epsilon^\lambda_{ij}(\vec{k})$ are symmetric, traceless and transverse spin-2 polarization tensors,

$$\epsilon^\lambda_{ij}(\vec{k}\,) = \epsilon^\lambda_{ji}(\vec{k}\,), \qquad \epsilon^\lambda_{ii}(\vec{k}\,) = 0, \qquad k_i\epsilon^\lambda_{ij}(\vec{k}\,) = 0, \tag{3.89}$$

normalized as

$$\epsilon^\lambda_{ij}(\vec{k})[\epsilon^{\rho,ij}(\vec{k})]^* = \epsilon^\lambda_{ij}(\vec{k})\epsilon^\rho_{ij}(-\vec{k}) = 2\delta^{\lambda\rho}, \tag{3.90}$$

and satisfying the completeness relation

$$\sum_{\lambda=+,\times}\epsilon^\lambda_{ij}(\hat{\vec{k}})\,\epsilon^\lambda_{lm}\,(\hat{\vec{k}}) = P_{il}\,P_{jm} + P_{im}\,P_{jl} - P_{ij}\,P_{lm}\,, \qquad P_{il} = \delta_{il} - \hat{k}_i\,\hat{k}_l, \tag{3.91}$$

where $\hat{\vec{k}}$ denotes the unit vector along the direction of $\vec{k}$.
Inserting decomposition (5.45) into Eq.(3.87), one finds

$$\delta S^{(2)}_{\rm EH} = \frac{M^2_{\rm Pl}}{4}\sum_{\lambda=+,\times}\int d\tau\frac{d^3k}{(2\pi^3)}\,a^2\left[|h^{\lambda\prime}_k|^2 - k^2|h^\lambda_k|^2 + \frac{a''}{a}|h^\lambda_k|^2\right], \tag{3.92}$$

where we have used the orthonormal condition (3.90).
To get a canonically normalized kinetic term, one introduces a new variable

$$\widetilde{h}^\lambda(t,k) \equiv \frac{M_{\rm Pl}}{\sqrt{2}} a\,h^\lambda_k, \tag{3.93}$$

so that the action becomes

$$\delta S^{(2)}_{\rm EH} = \frac{1}{2}\int d\tau d^3x\,\left[|\widetilde{h}^{\lambda\prime}|^2 - k^2|\widetilde{h}^\lambda|^2 + \frac{a''}{a}|\widetilde{h}^\lambda|^2\right]. \tag{3.94}$$

Next, we promote $\widetilde{h}^\lambda$ and its canonically conjugate momenta $\widetilde{\pi}^\lambda = \widetilde{h}^{\lambda\prime}$ to quantum operators $\widehat{\widetilde{h}^\lambda}, \widehat{\widetilde{\pi}^\lambda}$ by imposing the equal time CCR, i.e.,

$$[\widehat{\widetilde{h}^\lambda}(\tau,\vec{x}\,), \widehat{\widetilde{\pi}^\sigma}, (\tau,\vec{y}\,)] = i\delta^{\lambda\sigma}\delta^{(3)}(\vec{x}-\vec{y}), \tag{3.95}$$

with

$$\widehat{\widetilde{h}^\lambda}(\tau,\vec{x}) = \sum_{\sigma=+,\times}\int \frac{d^3k}{(2\pi)^3}\left[\widetilde{h}^\lambda_k(\tau)\hat{b}^\lambda_{\vec{k}}\,e^{i\vec{k}\cdot\vec{x}} + \widetilde{h}^\lambda_k(\tau)\hat{b}^{\lambda\dagger}_{\vec{k}}e^{-i\vec{k}\cdot\vec{x}}\right], \tag{3.96}$$

with the ladder operators satisfying the usual commutation relations

$$[\hat{b}^\lambda_{\vec{k}}, \hat{b}^{\sigma\dagger}_{\vec{q}}] = (2\pi)^3\delta^{\lambda\sigma}\delta^{(3)}(\vec{k}-\vec{q}), \qquad [\hat{b}^\lambda_{\vec{k}}, \hat{b}^\sigma_{\vec{q}}] = 0 = [\hat{b}^{\lambda\dagger}_{\vec{k}}, \hat{b}^{\sigma\dagger}_{\vec{q}}]. \tag{3.97}$$

The mode functions $\widetilde{h}^\lambda_k$ satisfy the

$$\widetilde{h}^{\lambda\prime\prime}_k + \left[k^2 - \frac{a''}{a}\right]\widetilde{h}^\lambda_k = 0, \tag{3.98}$$

which is just the *Mukhanov-Sasaki* equation (3.77), and its Wronskian is normalized to one, i.e., $W[\widetilde{h}_k^\lambda, \widetilde{h}_k^{\lambda\star}] = 1$.

The action (3.94) is equivalent to the action of two real scalar fields (3.71) one can see that the two polarizations of the tensor perturbations behave as a redefined scalar field, $h_k^\lambda = \sqrt{2} v_k/(aM_{\rm Pl})$. Therefore, their two-point function can be calculated as

$$\langle \hat{h}_{ij}(k)\hat{h}_{ij}(q)\rangle = (2\pi)^3\delta^{(3)}(\vec{k}+\vec{q})\frac{4|v_k|^2}{a_\star^2 M_{\rm Pl}^2} \simeq (2\pi)^3\delta^{(3)}(\vec{k}+\vec{q})\frac{1}{k_\star^2}\frac{2H_\star^2}{M_{\rm Pl}^2}, \tag{3.99}$$

where we have utilized the orthonormal relation (3.90), which is responsible for the addition factor of two in the second step.
From the above expression, one infers that the power spectrum of a single polarization is

$$\Delta_h^2 \equiv \frac{k_\star^3}{2\pi^2}\mathcal{P}_h(k_\star) = \frac{1}{\pi^2}\frac{H_\star^2}{M_{\rm Pl}^2}. \tag{3.100}$$

Finally, the dimensionless power spectra for tensor fluctuations is given by

$$\Delta_t^2 = 2\Delta_h^2 = \frac{2}{\pi^2}\frac{H_\star^2}{M_{\rm Pl}^2}, \tag{3.101}$$

so that the tensor-to-scalar ratio is

$$r \equiv \frac{\Delta_t^2}{\Delta_s^2} = 16\epsilon_H(k_\star). \tag{3.102}$$

3.3.2 CMB constraints

Let us now connect the primordial fluctuations to the cosmological observables. To that end, we will establish the link between the newly introduced variables, including the power spectra and the tensor-to-scalar ratio, with the CMB data.

First, we should emphasize that the reference scale $k_\star$ can be related to the pivot scale for the CMB observations measured by Planck, i.e., $k_\star^{\rm CMB} = 0.05\,{\rm Mpc}^{-1}$ [302]. The amplitude of scalar perturbations measured at the pivot scale $k_\star^{\rm CMB}$ is

$$\Delta_s^2(k_\star^{\rm CMB}) = 2.1\times 10^{-9}. \tag{3.103}$$

Utilizing Eq.(3.102), one finds the following upper bound on the tensor-to-scalar ratio:

$$r \leq 0.032, \tag{3.104}$$

at 95% C.L. by the Planck [302] and BICEP/Keck [303] combined analysis [304]. Thus, from Eq. (3.101), we obtain an upper bound on the Hubble scale

$$H_\star \simeq H_e \leq 4.4\times 10^{13}\,{\rm GeV}, \tag{3.105}$$

where we have assumed that the time variation of the Hubble rate in the period between $a_\star$ and a_e is negligible.
Next, it is instructive to quantify the scale-dependence of the power spectra. In analogy with n_s, introduced in Eq.(3.86), one defines the tensor spectral index as

$$n_s - 1 \equiv \frac{d\ln\Delta_s^2}{d\ln k}, \qquad\qquad n_t \equiv \frac{d\ln\Delta_t^2}{d\ln k}. \tag{3.106}$$

From the Planck data [302], we know that the spectral tilt n_s slightly deviates from unity and for the pivot scale is

$$n_s = 0.9649 \pm 0.0042. \tag{3.107}$$

Note that

$$\frac{d\ln\Delta_s^2}{d\ln k} = \frac{d\ln\Delta_s^2}{dN}\left(\frac{d\ln k}{dN}\right)^{-1} = -\left(2\epsilon_H + \frac{d\ln\epsilon_H}{dN}\right)(1-\epsilon_H)^{-1} = -\frac{4\epsilon_H - 2\eta_H}{1-\epsilon_H}, \tag{3.108}$$

and

$$\frac{d\ln\Delta_t^2}{d\ln k} = \frac{d\ln\Delta_t^2}{dN}\left(\frac{d\ln k}{dN}\right)^{-1} = -\frac{2\epsilon_H}{1-\epsilon_H}, \tag{3.109}$$

where we have used Eq. (3.14).
Hence, spectral indices in the leading order in HSR parameters take the form

$$n_s - 1 = 2\eta_H(k_\star) - 4\epsilon_H(k_\star) + \mathcal{O}(\epsilon_H^2, \eta_H^2, \eta_H\epsilon_H), \tag{3.110}$$

$$n_t = -2\eta_H(k_\star) + \mathcal{O}(\epsilon_H^2, \eta_H^2, \eta_H\epsilon_H). \tag{3.111}$$

Now, adopting the slow-roll approximation $\dot\phi \ll V(\phi)$ and the fact that $\eta_V \approx \eta_H$, and $\eta_V \approx \eta_H + \epsilon_H$, one approximates the scalar and tensor power spectra as

$$\Delta^2_{s,\mathrm{SR}} \simeq \frac{1}{24\pi^2}\frac{V}{M_{\mathrm{Pl}}^4}\frac{1}{\epsilon_V}\bigg|_{k_\star = a_\star H_\star}, \qquad \Delta^2_{t,\mathrm{SR}} \simeq \frac{2}{3\pi^2}\frac{V}{M_{\mathrm{Pl}}^4}\bigg|_{k_\star = a_\star H_\star}. \tag{3.112}$$

Consequently,

$$r_{\mathrm{SR}} = 16\epsilon_V(k_\star), \tag{3.113}$$

and

$$n_s^{\mathrm{SR}} - 1 = 2\eta_V(k_\star) - 6\epsilon_V(k_\star), \tag{3.114}$$

$$n_t^{\mathrm{SR}} = -\eta_V(k_\star). \tag{3.115}$$

Now, using Eq. (3.103) and (3.112) we obtain the following constrain on the inflationary scale:

$$V_\star^{1/4} \simeq V_e^{1/4} \leq 1.4 \times 10^{16}\,\mathrm{GeV}. \tag{3.116}$$

3.4 Inflationary models

Once we have discussed the general features of cosmic inflation, we can briefly overview some specific models. Nowadays, there exists a broad diversity of theoretical models aiming to carry out the inflationary process. In fact, inflationary zoology is quite head-spinning, as it contains hundreds of different scenarios. With the passage of time, inflationary models have become more and more sophisticated. The main reason for that is an endeavor to relate the SM of particle physics, i.e., the low-energy effective field theory, with a parent UV theory, which would become relevant at high energy scales. Hence, many models of cosmic inflation originated in beyond the Standard Model theories, including supersymmetry, supergravity, or string theories [305, 306]. An excellent complete review can be found, e.g., in [290, 305].

Below, we restrict ourselves to a very basic outline of inflationary models.
Inflationary models can classify them into several categories, depending on:

- **the number of dynamical fields**
  In addition to the single-field inflation described above, models equipped with more than one slowly-rolling field are also commonly discussed in the literature. Such scenarios are motivated by many high-energy models involving a plethora of spin-0 fields. In particular, one usually considers a model where a pair of scalar fields are responsible for cosmic inflation, see, e.g., [307, 308]; however, the generalization to multi-field inflation is also widely discussed, for a review see, e.g., [309, 310]. The presence of multiple dynamical fields can modify the inflationary dynamics and alter the predictions of single-field models. In particular, multi-field inflationary scenarios predict the generation of non-adiabatic field perturbations during inflation, which could lead, for instance, to detectable non-Gaussianities. Hence, such alternative models are expected to be observationally distinguished from single-field scenarios in the near future.

- **the form of the inflaton potential**
  Different cosmic inflation models vary in a specific form of the inflaton potential $V(\phi)$. Following Ref.[227], one distinguishes two basic types of $V(\phi)$ depending on their behavior during inflation. This classification is based on the displacement of the inflaton field, $\Delta\phi \equiv \phi_{\text{CMB}} - \phi_e$, describing the difference between the inflaton field values at the moment when the CMB fluctuations were created ϕ_{CMB} and the end of inflation ϕ_e, cf. Fig.(3.1).
  The *small-field models*, also known as *new inflation* are typically described by potentials emerging from spontaneous symmetry breaking [207, 208]. In such scenarios, the inflaton, initially located in a false vacuum state, evolves away from an unstable maximum toward a displaced true minimum. Its evolution is sub-Planckian, as ϕ moves over a small distance $\Delta\phi \ll M_{\text{Pl}}$. Small-field potentials can be described by a generic potential of the form [227]

  $$V_{\text{SF}}(\phi) = V_0\left[1 - \left(\frac{\phi}{\mu}\right)^p\right] + \dots \tag{3.117}$$

  where V_0, μ characterized respectively the potential height and width, whereas the dots correspond to higher-order terms. The exponent p is specified in a given model, e.g., for the Higgs-like potential $p = 2$. The Coleman-Weinberg potential [207, 208, 311]

  $$V_{\text{CW}}(\phi) = V_0\left\{\left(\frac{\phi}{\mu}\right)^4\left[\ln\left(\frac{\phi}{\mu}\right) - \frac{1}{4}\right] + \frac{1}{4}\right\} \tag{3.118}$$

  is another example of a small-field model arising from the radiatively-induced symmetry breaking in electroweak and GUT theories. Small-field models are typically characterized by tiny potential slow-roll parameter ϵ_V. The smallness of ϵ_V has observational consequences, implying that the amplitude of the primordial gravitational waves produced during inflation is too small to be detected by future surveys.
  A distinctive feature of the *large-field models* is the super-Planckian evolution of the ϕ field during inflation. Namely, in this type of model, the inflaton field initially has a large field value and then rolls down to a minimum situated at the origin $\phi = 0$. One typically finds $\eta_V \in (-\epsilon_V, \epsilon_V]$ in such scenarios. One of the simplest examples of a large-field inflationary model is the so-called *chaotic inflation* [210], where the inflaton potential has the monomial form

  $$V_{\text{LF}}(\phi) = \lambda\phi^p, \tag{3.119}$$

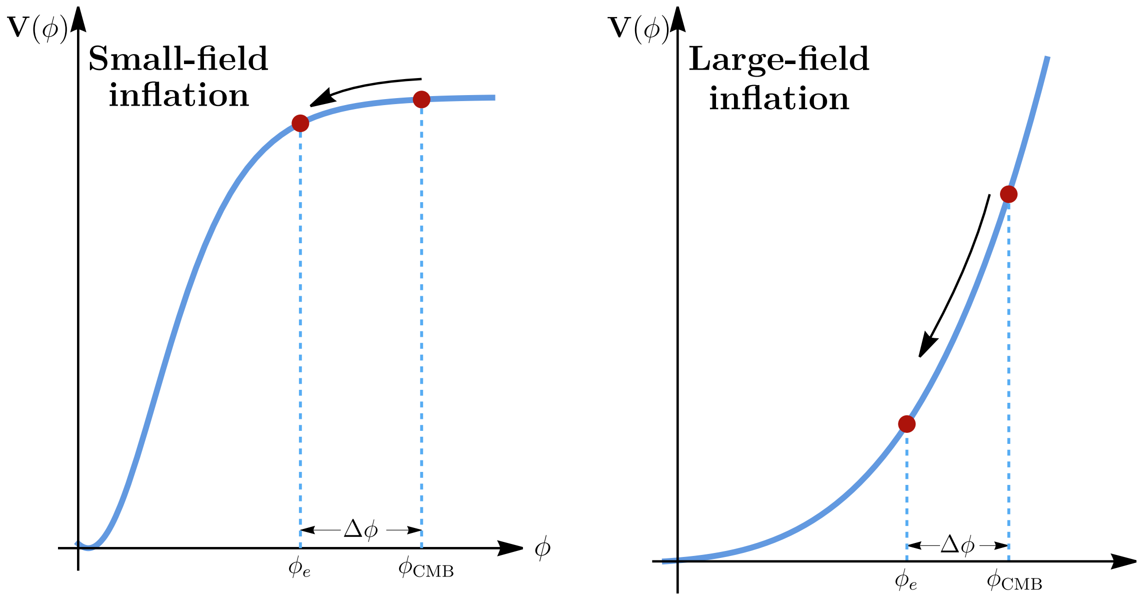

FIGURE 3.1: The schematic evolution of the inflaton field in the small-field (left panel) and the large-field (right panel) inflationary models.

where the inflaton self-coupling λ is typically very small and can be both dimensionless and dimension-full depending on the exponent p. The tensor-to-scalar ratio r might be sufficiently large for this type of inflaton potential to lead to a detectable spectrum of primordial gravitational waves. Another well-established large-field model is the dubbed as the *natural inflation* [311] with the following potential:

$$V_{\mathrm{NI}}(\phi) = V_0 \left[\cos\left(\frac{\phi}{f}\right) + 1\right], \tag{3.120}$$

where the appropriate scales two parameters of the model is respectively $V_0^{1/4} \approx m_{\mathrm{GUT}}$ and $f \approx M_{\mathrm{Pl}}$ [312]. The above potential originates in the BSM theories where the inflaton is associated with the axion field.

In addition to the two above-described scenarios, one sometimes distinguishes yet another class of inflationary model. The third type, dubbed as *hybrid models* [313, 314], where ϕ evolves toward a potential minimum with nonzero vacuum energy. In such a scenario, the accelerated expansion continues forever unless an auxiliary field is added to the theory. A common feature of this model is the following relation between potential slow-roll parameters: $\epsilon_V \in (0, \eta_V)$. The generic type of the inflaton potential in the hybrid models, i.e.,

$$V(\phi) = V_0 \left[1 + \left(\frac{\phi}{\mu}\right)^p\right], \tag{3.121}$$

behaves as a large-field potential in the limit $\phi/\mu \gg 1$, whereas for smaller field values, i.e., $\phi/\mu \ll 1$, it is similar to the small-field potential V_{SF}. However, in this regime, ϕ evolves towards a dynamical fixed point rather than away from it.

- **coupling to gravity**
  In a standard, *minimally-coupled*, scenario, there is no direct coupling between the inflaton and the metric. However, one can consider more exotic scenarios where the non-minimal couplings between ϕ and gravity are present. One of the best-established

examples is the *Higgs inflation* [315], where the SM Higgs doublet $\mathbf{h}$ plays the role of the inflaton field. The action of this model involves a direct coupling of the Higgs field to the Ricci scalar R

$$S_{\mathrm{HI}} = \int d^4\sqrt{-g}\left[-\frac{M_{\mathrm{Pl}}^2}{2}\left(1+\frac{2\xi}{M_{\mathrm{Pl}}^2}\mathbf{h}\mathbf{h}^\dagger\right)R + g^{\mu\nu}(\partial_\mu\mathbf{h})^\dagger\partial_\nu\mathbf{h} - V(\mathbf{h})\right], \qquad (3.122)$$

where ξ denotes the dimensionless non-minimal coupling constant. It turns out that such non-minimally coupled theories can be written as minimally-coupled theories by adopting the appropriate field redefinition. For instance, one can recast the above action as

$$S_{\mathrm{HI}} = \int d^4\sqrt{-\tilde{g}}\left[-\frac{M_{\mathrm{Pl}}^2}{2}\tilde{R} + \tilde{\mathcal{F}}(\mathbf{h})(\partial_\mu\mathbf{h})^\dagger\partial_\nu\mathbf{h} - \tilde{V}(\mathbf{h})\right], \qquad (3.123)$$

performing a conformal transformation $\tilde{g}_{\mu\nu} = \Omega^2(x)g_{\mu\nu}$. From this expression, we see that the price we must pay for this is the appearance of the non-canonical kinetic term $\tilde{\mathcal{F}}(\mathbf{h})(\partial_\mu\mathbf{h})^\dagger\partial_\nu\mathbf{h}$ for the Higgs field.

The original concept of Higgs inflation encounters a unitarity problem since, to reconcile with the CMB data, a sizeable non-minimal coupling is needed [316, 317]. This leads to the violation of unitarity, occurring at a scale comparable to the Hubble scale during inflation. However, as demonstrated in Ref.[318, 319], this problem can be resolved by adding a new degree of freedom coupled to the Higgs boson.

- **modification of the Einstein-Hilbert action**
  In a similar manner, one can also consider the modification of the Einstein-Hilbert action at high energies. Such an attempt was originally investigated by Alexei Starobinsky [206, 206], who wrote down one of the earliest and, at the same time, more elegant models of cosmic inflation, driven by the following purely gravitational action:

$$S_{\mathrm{SI}} = -\frac{M_{\mathrm{Pl}}^2}{2}\int d^4x\sqrt{-g}f(R), \qquad f(r) \equiv R + \frac{R^2}{6M^2}. \qquad (3.124)$$

  The quadratic quantum correction to the Einstein-Hilbert action became relevant in the very early universe when the curvature of spacetime was large. The above action can be put into a standard form under the Weyl transformation $\tilde{g}_{\mu\nu} = \Omega^2(x)g_{\mu\nu}$. In the Einstein frame, the inflaton field emerges as an effective incarnation of the higher curvature correction. The induced inflaton potential is given by

$$V_{\mathrm{SI}} = \frac{3}{4}M_{\mathrm{Pl}}^2M^2\left[1 - \exp - \left(\sqrt{\frac{2}{3}}\frac{\phi}{M_{\mathrm{Pl}}}\right)\right]^2. \qquad (3.125)$$

  The Starobinsky model is in excellent agreement with the Planck data. In particular, the only free parameter of the Starobinsky model, M, is fixed by the observable CMB amplitude as $M \sim 10^{-5}M_{\mathrm{Pl}}$ [302].

- **the form of the kinetic term**
  In inflationary models with canonically-normalized kinetic terms, cosmic inflation can only occur for sufficiently flat potentials. This requirement can be, however, relaxed if one considers a dynamical field whose kinetic term is not canonically normalized, see, e.g., [225, 320, 321]. In such a case, the density Lagrangian of a theory takes the form

$$\mathcal{L} = p(X,\phi) - V(\phi), \qquad X \equiv g^{\mu\nu}\partial_\mu\phi\partial_\nu\phi, \qquad (3.126)$$

where $p(X,\phi)$ is some arbitrary function of the scalar field ϕ and its first derivatives. By varying the above action w.r.t. the metric, one finds that it corresponds to a perfect fluid characterized by the pressure p and energy density $\rho = 2Xp_{,X} - p$ [226].
Note that in this case, the first slow-roll parameter is [226]

$$\epsilon = -\frac{\dot{H}}{H^2} = \frac{3Xp_{,X}}{2Xp_{,X} - p}. \tag{3.127}$$

Hence, for suitable $\mathcal{F}(X)$, one can obtain sufficiently many e-folds of inflation without a flat potential. An interesting feature of that model is the enhancement of the gravitational waves' contribution to the CMB fluctuations, as pointed out in Ref. [225].

3.5 Attractor models

A broad class of inflationary models, including the Starobinsky model [206], the chaotic inflation model with non-minimal coupling to gravity [315, 322], share a common observational prediction for the spectral tilt n_s, and the tensor-to-scalar ratio r [323–329]

$$n_s \simeq 1 - \frac{2}{N_\star}, \qquad\qquad r \simeq \frac{12}{N_\star^2}, \tag{3.128}$$

with $N_\star$ being the number of inflationary e-folds, counted from the horizon existing of the Planck pivot scale $k_\star^{\rm CMB}$ to the end of inflation. The n_s, r prediction (3.128) is an "attractor point" for potentials of the form [330]

$$V(\phi) = V_0 \left[1 - \exp\left(-\sqrt{\frac{2}{3}}\phi\right) + \dots\right], \tag{3.129}$$

in the limit $\phi \to \infty$, where ϕ is canonically normalized inflaton field.
These models can be generalized by introducing an additional parameter α, such that a new generalised potential at large values of ϕ takes the form [330]

$$V(\phi) = V_0 \left[1 - \exp\left(-\sqrt{\frac{2}{3\alpha}}\phi\right) + \dots\right], \tag{3.130}$$

This class of inflationary models, known as the α-attractors, leads to the following prediction of the inflationary observables:

$$n_s \simeq 1 - \frac{2}{N_\star}, \qquad\qquad r \simeq \alpha\frac{12}{N_\star^2}. \tag{3.131}$$

Such models can be embedded in supergravity theories [323, 324]. Without going into technical intricacies, to which we refer the reader to Ref.[323, 324, 330], the $\alpha-$attractor models are described by the following effective Lagrangian [330]:

$$\sqrt{-g}\mathcal{L}_\Phi = \sqrt{-g}\left[\frac{M_{\rm Pl}^2}{2}R + \frac{\alpha}{(1-(\Phi/(\sqrt{3}M_{\rm Pl}))^2)^2}g^{\mu\nu}\partial_\mu\Phi\partial_\nu\Phi - f^2\left(\Phi/(\sqrt{3}M_{\rm Pl})\right)\right], \tag{3.132}$$

where the geometric field Φ is related to the canonically normalized inflaton ϕ through [330]

$$\frac{\Phi}{\sqrt{3}M_{\rm Pl}} = \tanh\left(\frac{\phi}{\sqrt{6\alpha}M_{\rm Pl}}\right). \tag{3.133}$$

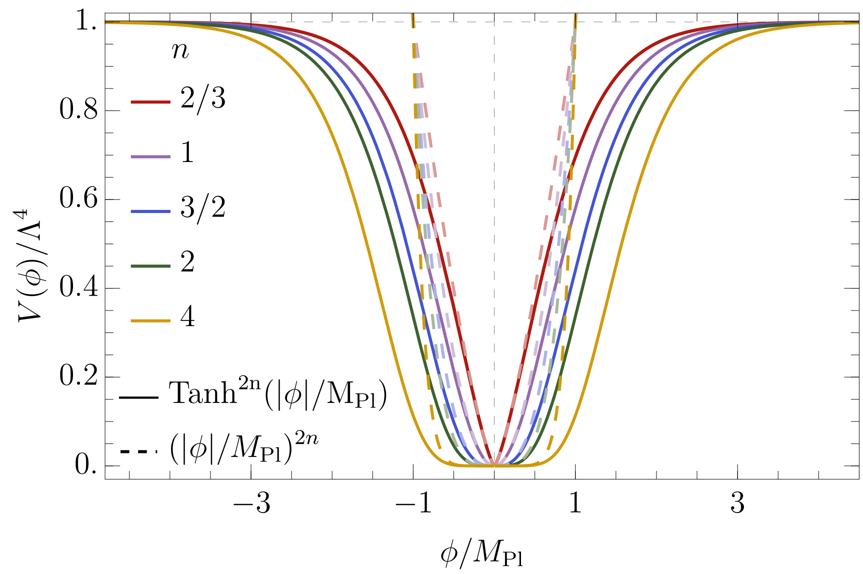

FIGURE 3.2: The $V_T(\phi)/\Lambda^4$ term as a function of $\phi/M_{\rm Pl}$ for different values of n, and $\alpha=1/6$. Solid curves present the full form of $V_T(\phi)$, while dashed curves show the small-field expansion of $V(\phi)$ (the lower line of Eq. (3.136)).

This, in turn, implies that the effective Lagrangian for the ϕ field takes the form

$$\sqrt{-g}\mathcal{L}_\phi = \sqrt{-g}\left[\frac{M_{\rm Pl}^2}{2}R + g^{\mu\nu}\partial_\mu\phi\partial_\nu\phi - f^2\left(\tanh\left\{\frac{\phi}{\sqrt{6\alpha}M_{\rm Pl}}\right\}\right)\right]. \tag{3.134}$$

In the simplest case, i.e., $f = const.$, the above Lagrangian describes the de-Sitter model, where $V(\phi)$ is independent of ϕ and α. On the other hand, for the set of a monomial function $f(z) = \Lambda^2 z^n$, with $n > 0$, one gets

$$V = f^2\left(\tanh\left\{\frac{\phi}{\sqrt{6\alpha}M_{\rm Pl}}\right\}\right) = \Lambda^4\tanh^{2n}\left(\frac{\phi}{\sqrt{6\alpha}M_{\rm Pl}}\right), \tag{3.135}$$

where the parameter Λ has a dimension of mass.

3.5.1 T model

Note that one can distinguish two different regimes of the $\alpha-$attractor T-model

$$V_T \equiv \Lambda^4\tanh^{2n}\left(\frac{|\phi|}{\sqrt{6\alpha}M_{\rm Pl}}\right) \simeq \begin{cases}\Lambda^4, & |\phi| \gg \sqrt{6\alpha}M_{\rm Pl}, \\ \Lambda^4\left(\frac{|\phi|}{\sqrt{6\alpha}M_{\rm Pl}}\right)^{2n}, & |\phi| \ll \sqrt{6\alpha}M_{\rm Pl},\end{cases} \tag{3.136}$$

such that for large field values, i.e., $|\phi| \gg \sqrt{6\alpha}M_{\rm Pl}$, the potential has a plateau $V_T(\phi) \simeq \Lambda^4$, whereas for smaller field values, i.e., $|\phi| \ll \sqrt{6\alpha}M_{\rm Pl}$, it can be well approximated by the power-law form (3.30). Hence, the first regime is suitable for the slow-roll phase of inflation since the flatness of $V_T(\phi)$ guarantees that inflation lasts long enough. Whereas, when ϕ rolls down to the smaller values, below the $\sqrt{6\alpha}M_{\rm Pl}$ scale, inflation ends, and ϕ starts to oscillate around the minimum of its potential. In Fig.(3.2) we show $V(\phi)/\Lambda^4$ as a function of the ϕ field for fixed $\alpha=1/6$, and several benchmark values of the index n.

Now let us calculate the inflationary observables for the $\alpha-$attractor T-model. The PSR parameters (3.16) are

$$\epsilon_V^T(\phi) = \frac{4n^2}{3\alpha}\,\mathrm{csch}^2\left(\sqrt{\frac{2}{3\alpha}}\frac{\phi}{M_{\rm Pl}}\right), \tag{3.137}$$

$$\eta_V^T(\phi) = \frac{4n}{3\alpha}\left[2n - \cosh\left(\sqrt{\frac{2}{3\alpha}}\frac{\phi}{M_{\rm Pl}}\right)\right]\mathrm{csch}^2\left(\sqrt{\frac{2}{3\alpha}}\frac{\phi}{M_{\rm Pl}}\right). \tag{3.138}$$

Hence, the spectral index, and the tensor-to-scalar ratio in the slow-roll approximation, are given by

$$n_S^T(\phi_\star) \simeq 1 - \frac{8n}{3\alpha}\left[n + \cosh\left(\sqrt{\frac{2}{3\alpha}}\frac{\phi_\star}{M_{\rm Pl}}\right)\right]\mathrm{csch}^2\left(\sqrt{\frac{2}{3\alpha}}\frac{\phi_\star}{M_{\rm Pl}}\right), \tag{3.139}$$

$$r^T(\phi_\star) \simeq \frac{64n^2}{3\alpha}\,\mathrm{csch}^2\left(\sqrt{\frac{2}{3\alpha}}\frac{\phi_\star}{M_{\rm Pl}}\right). \tag{3.140}$$

The inflaton field value $\phi_\star$ at the moment when the Planck pivot scale $k_\star^{\rm CMB}$ exits the horizon can be found from Eq. (3.139), and it is given by

$$\begin{aligned}\phi_\star = \sqrt{\frac{3\alpha}{2}}M_P\Bigg\{&-\log\left[3\alpha(1-n_S^T)\right] + \log\Bigg[4n + \sqrt{9\alpha^2(1-n_S^T)^2 + 8n^2(2+3\alpha(1-n_S^T))}\\ &+\sqrt{8n\left[n(4+3\alpha(1-n_S^T)) + \sqrt{8n^2(2+3\alpha(1-n_S^T)) + 9\alpha^2(1-n_S^T)^2}\right]}\Bigg]\Bigg\}.\end{aligned} \tag{3.141}$$

The inflaton field value at the end of inflation, ϕ_e, is determined by the condition (3.23), and can be expressed in terms of the inverse of the hypergeometric function ${}_2F_1(a,b;c;z)$. However, an approximate value of ϕ_e, obtained from Eq. (3.25), is given by

$$\phi_e \simeq \sqrt{\frac{3\alpha}{2}}M_{\rm Pl}\begin{cases}\ln\left[\frac{4n-\sqrt{12\alpha(12\alpha+16n^2-1)}}{1-12\alpha} + \frac{\sqrt{12\alpha-16n\left(\sqrt{3\alpha(12\alpha+16n^2-1)}-12\alpha n-n\right)-1}}{1-12\alpha}\right], & \alpha \le \frac{1}{12},\\[2ex] \ln\left[\frac{4n-\sqrt{12\alpha(12\alpha+16n^2-1)}}{1-12\alpha} - \frac{\sqrt{12\alpha-16n\left(\sqrt{3\alpha(12\alpha+16n^2-1)}-12\alpha n-n\right)-1}}{1-12\alpha}\right], & \alpha > \frac{1}{12},\end{cases} \tag{3.142}$$

while in the lowest order, i.e., by setting $\epsilon_V(a_e) \simeq 1$, one finds

$$\phi_e^{(0)} \simeq \sqrt{\frac{3\alpha}{2}}M_{\rm Pl}\sinh^{-1}\left(\frac{2n}{\sqrt{3\alpha}}\right). \tag{3.143}$$

The number of e-folds between the horizon crossing of the $k_\star$ mode and the end of inflation is

$$\begin{aligned}N_\star &\simeq M_{\rm Pl}\int_{\phi_e}^{\phi_\star}\frac{1}{\sqrt{2\epsilon_V}}d\phi\\ &= \frac{3\alpha}{4n}\left[\cosh\left(\sqrt{\frac{2}{3\alpha}}\frac{\phi_\star}{M_{\rm Pl}}\right) - \cosh\left(\sqrt{\frac{2}{3\alpha}}\frac{\phi_e}{M_{\rm Pl}}\right)\right] \simeq \frac{3\alpha}{4n}\cosh\left(\sqrt{\frac{2}{3\alpha}}\frac{\phi_\star}{M_{\rm Pl}}\right).\end{aligned} \tag{3.144}$$

n	2/3	1	3/2	2	5/2	3	7/2	4	9/2	5
$\bar{w}$	−0.2	0	0.2	1/3	0.429	0.5	0.556	0.6	0.636	0.667
$\phi_\star/M_{\rm Pl}$	3.206	3.409	3.612	3.755	3.867	3.958	4.035	4.102	4.161	4.214
$\phi_e/M_{\rm Pl}$	0.413	0.607	0.805	0.948	1.058	1.149	1.226	1.293	1.351	1.404

TABLE 3.1: Numerical values of the inflaton field for different values of n and fixed $\alpha = 1/6$.

Hence, in the large field limit, we can rewrite the two principal CMB observables as

$$n^T(n,\alpha,N_\star) \simeq 1 - \frac{(3\alpha+4N_\star)}{2N_\star^2}\coth^2\left(\sqrt{\frac{2}{3\alpha}}\frac{\phi_\star}{M_{\rm Pl}}\right) \simeq 1-\frac{2}{N_\star}, \tag{3.145}$$

$$r^T(n,\alpha,N_\star) \simeq \frac{12\alpha}{N_\star^2}\coth^2\left(\sqrt{\frac{2}{3\alpha}}\frac{\phi_\star}{M_{\rm Pl}}\right) \simeq \frac{12\alpha}{N_\star^2}, \tag{3.146}$$

which agree with the prediction (3.131).

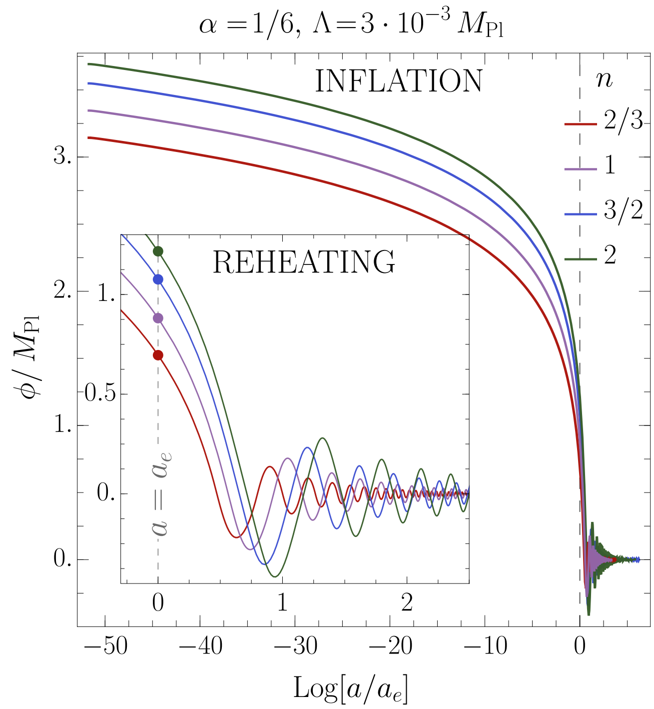

FIGURE 3.3: Numerical solutions for the inflaton EoM (3.10) and (3.11) for various choices on n. The vertical dashed line indicates the end of inflation,i.e., $\epsilon_V(\phi(a_e)) = 1$. Dots present $\phi^{(0)}(a_e)$ Eq.(3.143).

Now let us use the CMB data to constrain the parameters of the $\alpha-$attractor T model. The current upper bound on the tensor-to-scalar ratio (3.104), combined with the measured amplitude of the scalar perturbations (3.131), allows us to express the inflationary scale Λ as

$$\Lambda = \frac{M_{\rm Pl}}{\tanh^{n/2}[\phi_\star/(\sqrt{6\alpha}M_{\rm Pl})]}\left(\frac{3\pi^2}{2}\Delta_s^2 r\right)^{1/4}. \tag{3.147}$$

Note that at $a = a_\star$, the ϕ field is in the large field regime, i.e., $\phi_\star > \sqrt{6\alpha}M_{\rm Pl}$, and the inflaton potential is nearly flat $V(\phi_\star) \approx \Lambda^4$. Hence, from the above condition, one can limit the value of the inflationary scale from above, such that

$$\Lambda \simeq M_{\rm Pl}\left(\frac{3\pi^2}{2}\Delta_s^2 r\right)^{1/4} \lesssim 5.6\times 10^{-3} M_{\rm Pl}. \tag{3.148}$$

Hereinafter, without loss of generality, we fix $\alpha = 1/6$ and consider several values of n, such that $n > 1/2$. The numerical values of $\bar{w}(n)$, and $\phi_\star$, ϕ_e, $\phi_e^{(0)}$ for different values of n are collected in Table (3.1).

Now let us adopt the $\alpha-$attractor potential to determine the full dynamics of the inflaton field. Figure (3.3) presents the numerical solution for ϕ as a function of the scale factor a, obtained after solving two coupled equations (3.10) and (3.11). The rapid oscillations of the quasi-periodic function $\mathcal{P}$ are damped by the decreasing envelope φ due to the redshift of the Universe. The frequency of oscillations, as well as their amplitude, depend on the slope of the inflaton potential n. The approximate analytical solutions for the φ and $\mathcal{P}$ functions are given by Eq. (3.41) and Eq. (3.58), respectively.

Finally, one can also find the evolution of the equation of state w (3.7). Figure (3.4) presents w and its time-averaged $\bar{w}$ as functions of a. During inflation, i.e., for $a < a_e$, the potential energy $V(\phi)$ dominates over the kinetic one, $\dot{\phi}^2/2$, which implies a constant equation-of-state parameter, i.e., $w \simeq 1$. After the end of inflation, i.e., $a > a_e$, w starts to oscillate between -1 and 1, while $\bar{w}$ quickly approaches a constant limit, consistent with the prediction (3.36).

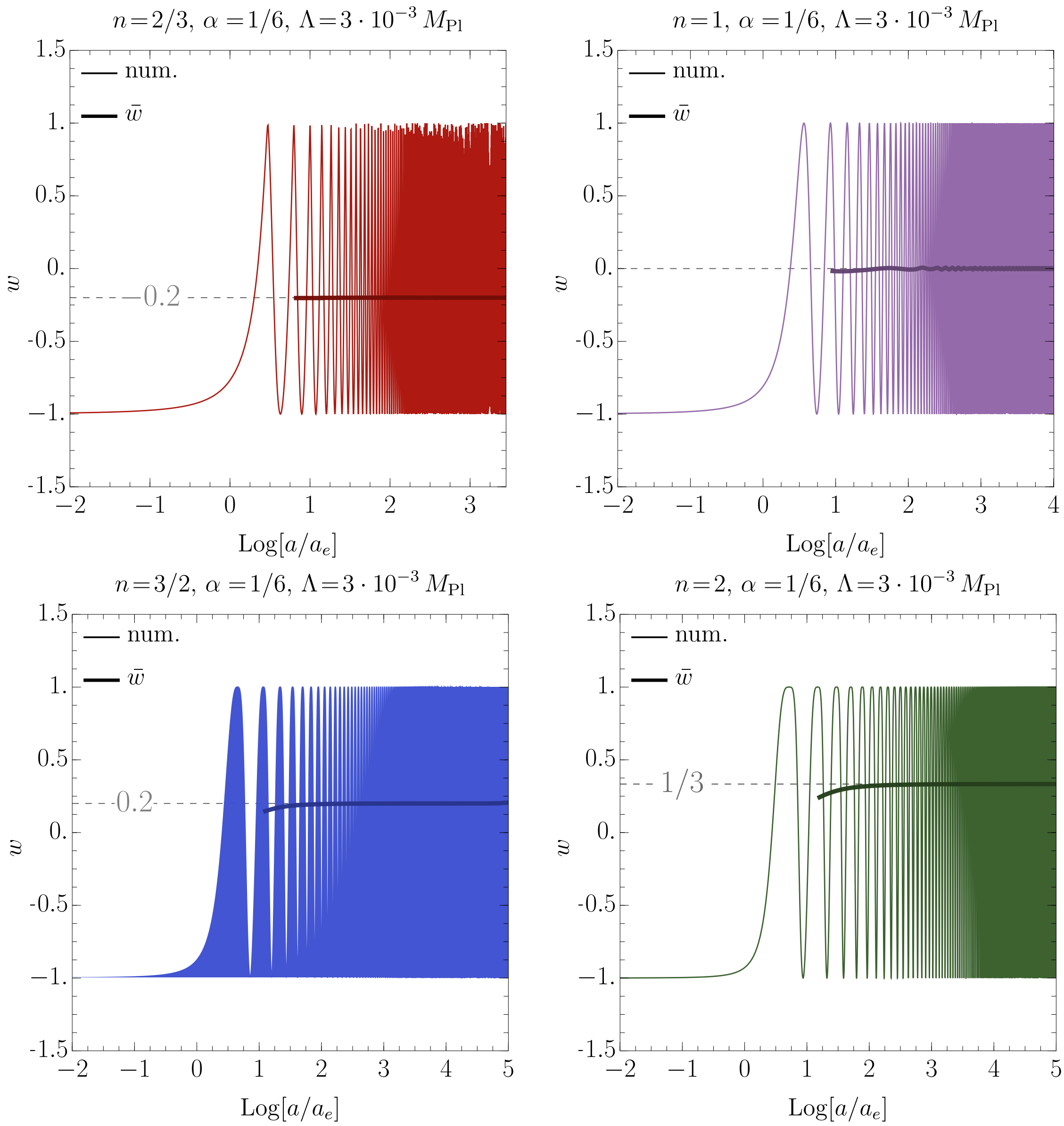

FIGURE 3.4: The equation-of-state parameter, w, and its time-averaged $\bar{w}$ as functions of the scale factor a. Thin colored curves show the full numerical solutions, i.e., p_ϕ/ρ_ϕ (3.7), while thick lines present the time-averaged barotropic parameter, i.e., $\bar{w} = \langle p_\phi \rangle / \langle \rho_\phi \rangle$ (3.36). The horizontal axes are normalized to the scale factor at the end of inflation a_e.

Chapter 4

Reheating

So far, we have developed a qualitative picture of the inflationary period driven by a single scalar field ϕ. [211–213]. The Universe was found to have undergone a phase of accelerated expansion if, at some point, its total energy density was dominated by the slowly evolving inflaton with a nearly constant potential $V(\phi)$. We have demonstrated that the Universe was automatically driven toward flatness and homogeneity during the slow-roll phase of inflation, solving all the puzzles of the standard hot Big Bang at a stroke. Furthermore, it was revealed that the inflaton field could also have sourced primordial perturbations that seed the Universe's large-scale structures. All combine to make the inflationary paradigm extremely attractive and popular. Without a doubt, one can admit that it is so well-established and long-cherished that, over the past decades, it has become more of a scenario than a model. Although observations have not yet confirmed cosmic inflation, several of its predictions have been experimentally verified. Notwithstanding the appealing simplicity and predictability, the inflationary paradigm has a few shortcomings. Namely, as we have already emphasized in the previous chapter, the detailed mechanism responsible for cosmic inflation remains unidentified. Throughout the years, a plethora of inflationary scenarios have been suggested. A cornucopia of models may be considered a curse rather than a good omen. And most importantly, the inflationary paradigm does not alone explain how the Universe became hot and thermal.

In the previous chapter, we have shown that the accelerated phase of expansion terminates as ϕ reaches the end of a flat region of its potential. When the latter becomes steep, the inflaton rolls down towards smaller values and begins to coherently oscillate around the minimum of $V(\phi)$. Due to the large occupation number, it can be effectively treated as a homogeneous scalar condensate with (almost) zero temperature. The Universe plunges into the super-cooled state since the power-law relation between the temperature and scale factor $T \sim a^{-p}$ leads to an exponential decrease of T during inflation. Since rapid expansion inevitably dilutes all matter fields, the Universe becomes not only extremely cold but also virtually empty. Thus, a crucial piece of the story is still missed. The answer to the riddle is relatively straightforward - the energy density accumulated in the inflaton must be somehow transferred to other particles, eventually (re)populating the whole Standard Model sector. The transition from the super-cold state to a hot and thermal Universe is termed *reheating*. At first glance, it might seem that the term *heating* appears to be a more natural choice since it precisely reflects the fact that the primary purpose of this process is to leave the Universe filled with a hot 'soup' of particles. On the other hand, the former term was initially favored because it accentuates that the Universe could have been hot and thermal also prior to inflation so that the reheating process made it hot once again. Although this hypothesis is being debated nowadays, the appellation "reheating" has become widely used.

Connecting the inflationary phase with a hot radiation-dominated Universe requires the inflaton field to couple to other degrees of freedom. The SM species, created either directly or indirectly from the inflaton background, interact with each other and eventually obtain a thermal distribution, providing the required initial conditions for a hot Big Bang scenario. The (re)population of the Universe is highly model-dependent and, unfortunately, barely constrained observationally. This is because the reheating energy scale is far beyond collider experiments, whereas current cosmological experiments cannot directly probe this phase since all the relevant processes had occurred on subhorizon scales and were washed out by the non-linear evolution of cosmic structure later on. Nevertheless, the reheating dynamics is expected to be incredibly rich and complex. It might involve both perturbative as well as highly non-perturbative processes. Therefore, although much effort has been put into developing a consistent theory of reheating in recent years, it remains the least understandable part of the inflationary paradigm.

The original idea of reheating was first proposed by Andrei Linde in 1981 [207]. Then, it has been developed by many authors, e.g., [122–127, 211–213]. Typically, one distinguishes several stages of the reheating period. Its initial phase is usually called *preheating*, during which particles could have been created in violent and explosive non-thermal processes. Preheating might involve various non–linear and non–perturbative effects, including narrow and broad parametric resonances [122, 125, 126] as well as tachyonic production [331–336]. Such phenomena emerge due to the coherent oscillations of the inflaton inducing a time-dependent dispersion relation of daughter fields to which ϕ is coupled. This could lead to an exponential growth of particle occupation in some frequency bands arising from a non-adiabatic change of effective frequencies for selected Fourier modes and generate highly non-thermal final states. The accurate description of resonant processes is quite involved and cannot be incorporated into the standard perturbative expansion framework. Thus, one typically performs lattice simulations. Even though preheating could lead to a rapid population of matter, it is generally insufficient to account for the entire reheating process. Thus, one should also include the perturbative decay of the oscillating inflaton field [211–213]. Generally, the perturbative stage of reheating is prolonged in time; see, e.g., [162, 299, 337–341]. Duration of the reheating phase depends on various factors, e.g., interaction strength or the shape of the inflaton potential during reheating [299, 340, 341]. Finally, during the last reheating stage, matter particles produced from the inflaton reach thermal distribution. It is widely assumed that the thermalization process occurs instantaneously [342]. However, the scenario of non-instantaneous thermalization has also been studied in the literature [343–347].

We begin this chapter by developing a generic framework describing the energy transfer from the coherently oscillating inflaton field into the visible sector in the perturbative reheating scenario. In Sec.(4.1), we specify $\phi -$ SM interactions, considering several direct couplings as well as indirect gravitational interactions between these two sectors. The main result of this section, i.e., the master formulas for the production rates, can be found in Sec.(4.1.3). In Sec.(4.2), we elaborate on Boltzmann equations, accounting for the evolution of the model universe during reheating. Notably, in Sec.(4.2.3), we derive generic solutions to the Boltzmann equation describing the dynamics of the SM radiation in the presence of a time-dependent *inflaton decay with*, whose evolution can be parametrized by a power-law function. We demonstrate that the time-dependency of the *inflaton decay rate* gives rise to a non-standard and non-instantaneous reheating. In Sec.(4.3), we distinguish two types of reheating models, i.e., **standard reheating** driven solely by the direct inflaton-SM interactions, and **mixed scenario**, in which gravitational processes initiate reheating, whereas its completion is controlled by the direct $\phi -$ SM interactions. Here, we also formulate the conditions for the occurrence of these two scenarios. Then, in Sec.(4.4), we present observational constraints on reheating models. The last section is devoted to the *Higgs boson-induced scenario*, induced by the trilinear inflaton interactions with the SM Higgs. Namely, in Sec.(4.5.1), we present the model, demonstrating that such interactions inevitably generate a non-trivial mass term for the SM Higgs doublet. Next, in Sec.(4.5.2), we show that it might cause a kinematic suppression of the radiation production. In Sec.(4.5.3), we find analytical solutions to the Boltzmann equation in two regimes: i) neglecting the mass of the Higgs field, i.e., in the *massless scenario* ii) including the kinematical effects, i.e., in the *massive Higgs scenario*. We show that the non-zero Higgs mass significantly influences the reheating dynamics. Then, in Sec.(4.5.4), we briefly discuss the possibility of the tachyonic Higgs production, and finally, in Sec.(4.5.5), we present the numerical results.

4.1 Inflaton interactions

Let us consider a model universe composed of the inflaton field ϕ and daughter particle F to which ϕ is coupled. The nature and origin of F species remain unspecified in this subsection. In the presented approach, ϕ is treated as a classical, homogeneous background that coherently oscillates in time. As demonstrated in the previous chapter, inflaton undergoes damped quasi-periodic oscillations during reheating. Namely, its evolution is described by the slowly-varying envelope φ and the quasi-periodic function $\mathcal{P}$. Due to the redshift of the Universe, the envelope decreases as a power-law with the scale factor, cf. Eq.(3.41), whereas $\mathcal{P}$ evolves according to Eq.(3.58). Moreover, it has been shown that both functions, i.e., $\varphi(t)$ and $\mathcal{P}(t)$, are determined by the form of the inflaton potential in the oscillatory phase.

Before we develop a consistent approach that allows us to compute the production rate for a given $\phi - F$ interactions, let us first explicitly discuss the underlying assumptions.
First of all, we assume that the inflation occupation number is so high during reheating that the classical treatment of the condensate is justified. Hence, the ϕ field will be regarded as a classical background field, coherently oscillating around the bottom of the $\alpha-$attractor $T-$potential Eq.(3.136). It is instructive to relate the evolution of the envelope with the inflaton energy density according to the following formula:

$$\varphi(t) = M_{\rm Pl} \left(\frac{\rho_\phi(t)}{\Lambda^4}\right)^{\frac{1}{2n}}. \tag{4.1}$$

In what follows, we presume that in the time-scale relevant for the $\phi - F$ interactions, the variation of φ in time can be neglected.
The fast-oscillating function $\mathcal{P}$ is decomposed into the Fourier modes

$$\mathcal{P}(t) = \sum_{k=-\infty}^{\infty} \mathcal{P}_k e^{-ik\omega t}, \tag{4.2}$$

where the Fourier coefficients $\mathcal{P}_k$ are defined by the following integral:

$$\mathcal{P}_k = \frac{\omega(t_0)}{2\pi} \int_{t_0}^{t_0+\frac{2\pi}{\omega(t_0)}} dt\, \mathcal{P}(t) \cdot e^{ik\omega(t)t}, \tag{4.3}$$

with ω being the frequency of the inflaton interactions. Note that according to Eq.(3.54), unless $n = 1$, the inflaton frequency becomes a function of time. However, since φ and thus ω vary in a time-scale much longer than the time-scale of interactions, we assume that $\omega \simeq const.$ in one act of F creation.

The particle production in the oscillating inflaton background can be considered as a quantum process describing a transition from an initial vacuum state $|\alpha\rangle = |0\rangle$ to final state $|\beta\rangle$

in the presence of the time-varying ϕ field. To put it another way, the energy density, initially stored in the coherent oscillations of the ϕ field, is transferred to the F quanta during reheating due to interactions between these two sectors. For the purpose of this analysis, we restrict our attention to the two-particle final state, i.e., $|\beta\rangle = |FF\rangle$. Without going into the details of the UV completion, we consider several direct $\phi - F$ couplings that are linear in the ϕ field

$$\mathcal{L}_{\rm int}^{\rm D} = \mathcal{L}_{\phi SS} + \mathcal{L}_{\phi\Psi\Psi} + \mathcal{L}_{\psi VV} + \mathcal{L}_{\phi AA}\,, \tag{4.4}$$

with

$$\mathcal{L}_{\phi SS} \supset g_{S\phi}\,\phi\, SS\,, \tag{4.5}$$
$$\mathcal{L}_{\phi\Psi\Psi} \supset g_{\Psi\phi}\,\phi\,\Psi\Psi\,, \tag{4.6}$$
$$\mathcal{L}_{\phi\Psi\Psi} \supset g_{V\phi}\,\phi\, V_\mu V^\mu\,, \tag{4.7}$$
$$\mathcal{L}_{\phi AA} \supset h_{A\phi}\,\phi\,(\partial_\mu A)(\partial^\mu A)\,, \tag{4.8}$$

where $S(A)\,, V\,, \Psi$ denote the scalar (pseudoscalar, e.g., axion-like) field, vector boson, and Dirac fermion, whereas coupling constants $g_{S\phi}, g_{V\phi}$ have dimensions of mass, $g_{\Psi\phi}$ is dimensionless, while $h_{A\psi}$ has inverse mass dimension.
In addition, our analysis also includes irreducible gravitational interactions

$$\mathcal{L}_{\rm int}^{\rm grav} = \frac{h^{\mu\nu}}{M_{\rm Pl}}\left[T^{\phi}_{\mu\nu} + T^{S}_{\mu\nu} + T^{\Psi}_{\mu\nu} + T^{V}_{\mu\nu}\right], \tag{4.9}$$

arising from the graviton $h_{\mu\nu}$ couplings to stress-energy tensor (SET) of ϕ

$$T^{\phi}_{\mu\nu} = \partial_\mu\phi\partial_\nu\phi - \eta_{\mu\nu}\left[\frac{1}{2}g^{\alpha\beta}\partial_\alpha\phi\partial_\beta\phi - V(\phi)\right], \tag{4.10}$$

and energy-momentum tensors of the real scalar S,

$$T^{S}_{\mu\nu} = \partial_\mu S\partial_\nu S - \frac{\eta_{\mu\nu}}{2}\left[g^{\alpha\beta}\partial_\alpha S\partial_\beta S - m_S^2 S^2\right], \tag{4.11}$$

Dirac fermion Ψ,

$$\begin{aligned} T^{\Psi}_{\mu\nu} = &\frac{i}{4}\left[\bar\Psi\gamma_\mu\partial_\nu\Psi + \bar\Psi\gamma_\nu\partial_\mu\Psi - (\partial_\mu\bar\Psi)\gamma_\nu\Psi - (\partial_\nu\bar\Psi)\gamma_\mu\Psi\right] \\ &- g_{\mu\nu}\left[\frac{i}{2}\left(\bar\Psi\partial\!\!\!/\Psi - (\partial_\alpha\bar\Psi)\gamma^\alpha\Psi\right) - m_\Psi\bar\Psi\Psi\right], \end{aligned} \tag{4.12}$$

and spin-1 Abelian massive field V,

$$T^{V}_{\mu\nu} = -g^{\alpha\beta}V_{\mu\alpha}V_{\nu\beta} + m_V^2 V_\mu V_\nu - g_{\mu\nu}\left[-\frac{1}{4}g^{\rho\sigma}g^{\alpha\beta}V_{\rho\alpha}V_{\sigma\beta} + \frac{1}{2}m_V^2 g^{\rho\sigma}V_\rho V_\sigma\right], \tag{4.13}$$

respectively.
In the above expressions, we have used the Feynman slash notation $\partial\!\!\!/ \equiv \gamma^\alpha\partial_\alpha$. The mass of the $F \in \{S, \Psi, V, A\}$ states is denoted as m_F. Furthermore, the field strength of the V field is defined as

$$V_{\mu\nu} = \partial_\mu V_\nu - \partial_\nu V_\mu. \tag{4.14}$$

Gravitational particle production in the inflaton background (IG) describes indirect inflaton interactions with quantum fields F, mediated by the spin-2 massless graviton. Diagrams accounting for such processes arise at a dim-6 level and are suppressed by the second power of M_{Pl}. At first glance, IG might seem so feeble that it can be safely neglected. However, there are two important reasons why one should not do this. Firstly, as mentioned above, IG is universal and thus unavoidable. Thus, it provides an irreducible contribution to the particle number density and hence puts lower constraints on various cosmological observables. Furthermore, it turns out that the energy density accumulated in the inflaton field at the onset of reheating is so high that it can counterpoise the Planck suppression.

4.1.1 Free field operators

Particles produced from the inflaton should be interpreted as a quantum excitation of fields. We adopt a standard procedure of canonical quantization by promoting classical fields to quantum operators

$$\hat{S} = \int d\Pi_p \left\{ \hat{a}(\vec{p}) e^{-ip\cdot x} + \hat{a}^\dagger(\vec{p}) e^{ip\cdot x} \right\}, \tag{4.15}$$

$$\hat{\Psi} = \sum_{s=1}^{2} \int d\Pi_p \left\{ \hat{b}^s(\vec{p}) u^s(p) e^{-ip\cdot x} + \hat{c}^{s\dagger}(\vec{p}) v^s(p) e^{ip\cdot x} \right\}, \tag{4.16}$$

$$\hat{\bar{\Psi}} = \sum_{s=1}^{2} \int d\Pi_p \left\{ \hat{b}^{s\dagger}(\vec{p}) \bar{u}^s(p) e^{ip\cdot x} + \hat{c}^s(\vec{p}) \bar{v}^s(p) e^{-ip\cdot x} \right\}, \tag{4.17}$$

$$\hat{V}_\mu = \sum_{\sigma=L,\pm} \int d\Pi_p \left\{ \epsilon^\sigma_\mu(\vec{p}) \hat{d}^\sigma(\vec{p}) e^{-ip\cdot x} + \epsilon^{\sigma *}_\mu(\vec{p}) \hat{d}^{\sigma\dagger}(\vec{p}) e^{ip\cdot x} \right\}, \tag{4.18}$$

$$\hat{h}_{\mu\nu} = \sum_{\lambda=++,--} \int d\Pi_p \left\{ \epsilon^\lambda_{\mu\nu}(\vec{p}) \hat{A}^\lambda(\vec{p}) e^{-ip\cdot x} + \epsilon^{\lambda *}_{\mu\nu}(\vec{p}) \hat{A}^{\lambda\dagger}(\vec{p}) e^{ip\cdot x} \right\}, \tag{4.19}$$

where the following shorthand notation has been used:

$$d\Pi_p \equiv \frac{d^3p}{(2\pi)^3 \sqrt{2p_0}}, \qquad p_0^2 = |\vec{p}|^2 + m_F^2. \tag{4.20}$$

The creation and annihilation operators for the bosonic fields, i.e., $\hat{S}, \hat{V}_\mu$ and $\hat{h}_{\mu\nu}$, obey the standard commutation relations

$$[\hat{a}(\vec{p}), \hat{a}^\dagger(\vec{q})] = (2\pi)^3 \delta^{(3)}(\vec{p} - \vec{q}), \qquad [\hat{d}^\sigma(p), \hat{d}^{\tilde{\sigma}\dagger}(q)] = (2\pi)^3 \delta^{(3)}(\vec{p} - \vec{q}) \delta^{\sigma,\tilde{\sigma}}, \tag{4.21}$$

and

$$[\hat{A}^\lambda(\vec{p}), \hat{A}^{\tilde{\lambda}\dagger}(\vec{q})] = (2\pi)^3 \delta^{(3)}(\vec{p} - \vec{q}) \delta^{\lambda,\tilde{\lambda}}, \tag{4.22}$$

with all other commutators vanishing.
On the other hand, the only non-zero anti-commutators for the fermionic fields are

$$\{\hat{b}^s(\vec{p}), \hat{b}^{r\dagger}(\vec{q})\} = (2\pi)^3 \delta^{(3)}(\vec{p} - \vec{q}) \delta^{sr}, \qquad \{\hat{c}^s(\vec{p}), \hat{c}^{r\dagger}(\vec{q})\} = (2\pi)^3 \delta^{(3)}(\vec{p} - \vec{q}) \delta^{sr}. \tag{4.23}$$

Moreover, the completeness relations for Dirac spinors read

$$\sum_s u^s(p) \bar{u}^s(p) = \not{p} + m_\Psi, \qquad \sum_s v^s(p) \bar{v}^s(p) = \not{p} - m_\Psi, \tag{4.24}$$

whereas the polarization vectors for the spin-1 massive field $\hat{V}_\mu$ satisfy the following relation:

$$\sum_{\sigma=L,\pm}\epsilon^{\sigma}_{\mu}(\vec{p})\epsilon^{\sigma*}_{\nu}(\vec{p}) = -\eta_{\mu\nu}+\frac{p_\mu p_\nu}{m_V^2}, \tag{4.25}$$

while for the spin-2 massless field $\hat{h}_{\mu\nu}$, we have

$$\sum_{\lambda=++,--}\epsilon^{\lambda}_{\mu\nu}(\vec{p})\epsilon^{\lambda*}_{\alpha\beta}(\vec{p}) = \frac{1}{2}[\eta_{\mu\alpha}\eta_{\nu\beta}+\eta_{\mu\beta}\eta_{\nu\alpha}-\eta_{\mu\nu}\eta_{\alpha\beta}] \equiv P_{\mu\nu\alpha\beta}. \tag{4.26}$$

4.1.2 S-matrix elements

Once we have specified ϕ interactions with other fields, we can derive the corresponding S-matrix elements, defined by

$$\begin{aligned} S_{\beta\alpha} &= \Big\langle\beta\Big|\mathcal{T}\Big[\exp\Big(-i\int d^4x\,\mathcal{L}_{\rm int}\Big)\Big]\Big|\alpha\Big\rangle \\ &= \Big\langle\beta\Big|\mathcal{T}\Big[\exp\Big(-i\int d^4x\,(\mathcal{L}^{\rm D}_{\rm int}+\mathcal{L}^{\rm grav}_{\rm int})\Big)\Big]\Big|\alpha\Big\rangle, \end{aligned} \tag{4.27}$$

where $\mathcal{T}$ denotes the time-ordered product.
In the remainder of this subsection, we distinguish two types of the inflaton couplings: direct (D) interactions described by the density Lagrangian (4.4), and indirect interactions (grav) mediated by gravity (4.9).

Direct inflaton interactions

In the case of direct coupling of the inflaton field to F quanta, it is sufficient to expand the S matrix in the lowest non-trivial order, i.e.,

$$\begin{aligned} S^{(1)}_{\beta\alpha} &= -i\int d^4x\,\Big\langle\beta\Big|\mathcal{T}\Big[\mathcal{L}^{\rm D}_{\rm int}(x)\Big]\Big|\alpha\Big\rangle \\ &= -ig_{F\phi}\int d^4x\,\phi(t)\cdot\Big\langle 0\Big|\hat{a}_F(\vec{p}_1)\hat{a}_F(\vec{p}_2)\hat{F}\hat{F}|0\Big\rangle + \\ &\quad - ih_{F\phi}\int d^4x\,\phi(t)\cdot\Big\langle 0\Big|\hat{a}_F(\vec{p}_1)\hat{a}_F(\vec{p}_2)(\partial_\mu\hat{F})(\partial^\mu\hat{F})|0\Big\rangle\,, \end{aligned} \tag{4.28}$$

where $\hat{a}^\dagger_F(\vec{p}_1), \hat{a}^\dagger_F(\vec{p}_2)$ are the ladder operators of the particles in the final state, and $\hat{F}$ represents their quantum field operator. The form of $\hat{F}$ depends on the spin of F particles as in Eqs.(4.15)-(4.18).
Utilizing (4.1) and (4.2), and assuming that $\varphi(t)\simeq const.$ in the time-scale of interactions, one can rewrite the above expression as

$$\begin{aligned} S^{(1)}_{\beta\alpha} &= -ig_{F\phi}M_{\rm Pl}\left(\frac{\rho_\phi}{\Lambda^4}\right)^{\frac{1}{2n}}\sum_k\mathcal{P}_k\int dt\,e^{-ik\omega t}\int d^3\vec{x}\,\Big\langle 0\Big|\hat{a}_F(\vec{p}_1)\hat{a}_F(\vec{p}_2)\hat{F}\hat{F}|0\Big\rangle \\ &\quad - h_{F\phi}M_{\rm Pl}\left(\frac{\rho_\phi}{\Lambda^4}\right)^{\frac{1}{2n}}\sum_k\mathcal{P}_k\int dt\,e^{-ik\omega t}\int d^3\vec{x}\,\Big\langle 0\Big|\hat{a}_F(\vec{p}_1)\hat{a}_F(\vec{p}_2)(\partial_\mu\hat{F})(\partial^\mu\hat{F})|0\Big\rangle \\ &\equiv -iM_{\rm Pl}\left(\frac{\rho_\phi}{\Lambda^4}\right)^{\frac{1}{2n}}\sum_k\mathcal{P}_k\times(1+\delta_F)\mathcal{F}(F)(2\pi)^4\delta(k\omega-p^0_1-p^0_2)\delta^{(3)}(\vec{p}_1+\vec{p}_2), \end{aligned} \tag{4.29}$$

where $\delta_F = 1$ for identical particles in the final state, and $\delta_F = 0$ otherwise. The function $\mathcal{F}(F)$ depends on the form of the inflaton interactions, and it is given by

$$\mathcal{F}(F) = \begin{cases} g_{S\phi}, & F = S, \\ g_{\Psi\phi} \cdot \bar{u}^{s_1}(p_1) v^{s_2}(p_2), & F = \Psi, \\ g_{V\phi} \cdot g^{\mu\nu} \epsilon_\mu^{\sigma,*}(p_1) \epsilon_\nu^{\sigma',*}(p_2), & F = V, \\ h_{A\phi} \cdot (p_1 \cdot p_2), & F = A. \end{cases} \tag{4.30}$$

Indirect inflaton interactions

Now let us calculate the S-matrix element that describes the IG process. To that end, we should expand the S matrix up to the second order, i.e.,

$$\begin{aligned} S^{(2)}_{\beta\alpha} &= \frac{(-i)^2}{2!} \int d^4x \int d^4y \, \langle\beta| \mathcal{T}[\mathcal{L}^{\text{grav}}_{\text{int}}(x) \mathcal{L}^{\text{grav}}_{\text{int}}(y)] \, |\alpha\rangle \,, \\ &= \frac{(-i)^2}{2!} \frac{1}{M^2_{\text{Pl}}} \int d^4x \int d^4y \, \langle\beta| \mathcal{T}[\hat{h}^{\mu\nu}(x) \hat{h}^{\alpha\beta}(y) \left(\widehat{T}^{\phi}_{\mu\nu}(x) \widehat{T}^{F}_{\alpha\beta}(y) + \widehat{T}^{F}_{\mu\nu}(x) \widehat{T}^{\phi}_{\alpha\beta}(y) \right)] \, |\alpha\rangle \,, \end{aligned} \tag{4.31}$$

with $\widehat{T}^F_{\mu\nu}$ being the energy-momentum tensor for the F field.

Gravitational scalar production

Let us first consider the gravitational production of real scalars whose stress-energy tensor is given by (4.10). The $\hat{h}^{\mu\nu}(x)\hat{h}^{\alpha\beta}(y)\widehat{T}^{\phi}_{\mu\nu}(x)\widehat{T}^{S}_{\alpha\beta}(y)$ term takes the form

$$\begin{aligned} & S^{(2)}_{SS} \supset \frac{(-i)^2}{2!} \frac{1}{M^2_{\text{Pl}}} \int d^4x \int d^4y \sqrt{4p^0_1 p^0_2} \Big\langle 0 \Big| \hat{a}(\vec{p}_1) \hat{a}(\vec{p}_2) T[\hat{h}^{\mu\nu}(x) \hat{h}^{\alpha\beta}(y) \widehat{T}^{\phi}_{\mu\nu}(x) \widehat{T}^{S}_{\alpha\beta}(y)] \Big| 0 \Big\rangle \\ & = \frac{(-i)^2}{2!} \frac{1}{M^2_{\text{Pl}}} \sum_{\lambda,\lambda'} \int d^4x \int d^4y \int d\Pi_p \int d\Pi_q \int d\Pi_{k_1} \int d\Pi_{k_2} T^{\phi}_{\mu\nu}(x) \Big\langle 0 \Big| (\epsilon^{\mu\nu,\lambda}(\vec{k}_1) \hat{A}_\lambda(\vec{k}_1) e^{-ik_1x} + \text{h.c.}) \\ & \times (\epsilon^{\alpha\beta,\lambda'}(\vec{k}_2) \hat{A}_{\lambda'}(\vec{k}_2) e^{-ik_2y} + \text{h.c.}) \Big| 0 \Big\rangle \Big\langle 0 \Big| \hat{a}(\vec{p}_1) \hat{a}(\vec{p}_2) \Big[\left(ip_\alpha \hat{a}^\dagger(\vec{p}) e^{ipy} + \text{h.c.} \right) \left(iq_\beta \hat{a}^\dagger(\vec{q}) e^{iqy} + \text{h.c.} \right) \\ & - \frac{\eta_{\alpha\beta}}{2} \left(ip^\rho \hat{a}^\dagger(\vec{p}) e^{+ipy} + \text{h.c.} \right) \left(iq_\rho \hat{a}^\dagger(\vec{q}) e^{iqy} + \text{h.c.} \right) \\ & + \frac{m^2_S}{2} \eta_{\alpha\beta} \left(\hat{a}^\dagger(\vec{p}) e^{+ipy} + \text{h.c.} \right) \left(\hat{a}^\dagger(\vec{q}) e^{+iqy} + \text{h.c.} \right) \Big] \Big| 0 \Big\rangle. \end{aligned} \tag{4.32}$$

Contraction of the graviton operators, e.g., $\hat{A}_\lambda(\vec{k}_1)$ with $\hat{A}^\dagger_{\lambda'}(\vec{k}_2)$, leads to the following propagator:

$$D^{\mu\nu\alpha\beta}(x-y) \equiv \int \frac{d^4\tilde{q}}{(2\pi)^4} \frac{i}{\tilde{q}^2 + i\epsilon} e^{-i(x-y)\tilde{q}} P^{\mu\nu\alpha\beta}, \tag{4.33}$$

where $P^{\mu\nu\alpha\beta}$ was introduced in (4.26).
Using this expression, one finds

$$T^{\phi}_{\mu\nu} P^{\mu\nu\alpha\beta} = \partial^\alpha\phi \partial^\beta\phi - \eta^{\alpha\beta} V(\phi). \tag{4.34}$$

After some tedious but straightforward computations, we get

$$S^{(2)}_{SS} \supset -\frac{(-i)^2}{M^2_{\text{Pl}}} \int d^4x \int d^4y \int \frac{d^4\tilde{q}}{(2\pi)^4} \frac{i}{\tilde{q}^2 + i\epsilon} e^{-i(x-y)\tilde{q}}$$

$$\times \Big[(\partial^\alpha\phi\, p_{1\alpha})(\partial^\beta\phi\, p_{2\beta}) + V(\phi)p_{1\alpha}p_2^\alpha + 2m_S^2 V(\phi) - \frac{1}{2}\partial^\alpha\phi\partial_\alpha\phi(p_1\cdot p_2 + m_S^2)\Big]. \tag{4.35}$$

To further simplify the above result, we take advantage of the homogeneity of the background inflaton field, which implies

$$p_1 \cdot p_2 = \frac{s}{2} - m_F^2, \qquad\qquad p_1^0 = p_2^0 = \frac{\sqrt{s}}{2}, \tag{4.36}$$

where $s \equiv (p_1+p_2)^2$ is the Mandelstam variable. Substitution into (4.35) leads to

$$S_{SS}^{(2)} \supset -\frac{1}{2}\frac{(-i)^2}{M_{\rm Pl}^2}\int d^4x \int d^4y \int \frac{d^4\tilde{q}}{(2\pi)^4}\frac{i}{\tilde{q}^2 + i\epsilon}V(\phi)\Big(s + 2m_S^2\Big)e^{-i(x-y)\tilde{q}}e^{+i(p_1+p_2)y}. \tag{4.37}$$

Note that the power-law inflaton potential can be Fourier expanded as

$$V(\phi) \equiv \rho_\phi \sum_{k=-\infty}^{\infty} \mathcal{P}_k^{2n} e^{-ik\omega t}, \tag{4.38}$$

where we have used the definition of the envelope Eq. (3.29) together with (4.2)-(4.3). Inserting the above decomposition into Eq. (4.37) gives us

$$S_{SS}^{(2)} \supset \frac{i}{2}\frac{\rho_\phi}{M_{\rm Pl}^2}\sum_k \mathcal{P}_k^{2n}\Big(1 + \frac{2m_S^2}{s}\Big)(2\pi)^4\delta(k\omega - p_1^0 - p_2^0)\delta^{(3)}(\vec{p}_1 + \vec{p}_2). \tag{4.39}$$

Hence, the final result, including both contributions to the S-matrix element, is given by

$$S_{SS}^{(2)} = i\frac{\rho_\phi}{M_{\rm Pl}^2}\sum_k \mathcal{P}_k^{2n}\Big(1 + \frac{2m_S^2}{s}\Big)(2\pi)^4\delta(k\omega - p_1^0 - p_2^0)\delta^{(3)}(\vec{p}_1 + \vec{p}_2). \tag{4.40}$$

Gravitational fermion production

Next, we can move on to the fermionic case. The $\hat{h}^{\mu\nu}(x)\hat{h}^{\alpha\beta}(y)\widehat{T}^{\phi}_{\mu\nu}(x)\widehat{T}^{\Psi}_{\alpha\beta}(y)$ term can be recast as

$$\begin{aligned} S_{\Psi\bar{\Psi}}^{(2)} \supset& -\frac{(-i)^2}{M_{\rm Pl}^2}\int d^4x \int d^4y \int \frac{d^4\tilde{q}}{(2\pi)^4}\frac{i}{\tilde{q}^2 + i\epsilon}e^{-i(x-y)\tilde{q}}(\partial^\alpha\phi\partial^\beta\phi - \eta^{\alpha\beta}V(\phi)) \\ &\times \bar{u}^{s_1}(p_1)\left\{\frac{1}{4}\left[\gamma_\alpha(p_2-p_1)_\beta + \gamma_\beta(p_2-p_1)_\alpha\right] - \frac{\eta_{\alpha\beta}}{2}\left(\not{p}_2 - \not{p}_1 + 2m_\Psi\right)\right\}v^{s_2}(p_2). \end{aligned} \tag{4.41}$$

Thanks to the Dirac equations for spinors

$$(\not{p}_1 - m_\Psi)u^s(p_1) = 0, \qquad\qquad (\not{p}_2 + m_\Psi)v^s(p_2) = 0, \tag{4.42}$$

we can get rid off the term $\bar{u}^{s_1}(p_1)\left(\not{p}_2 - \not{p}_1 + 2m_\Psi\right)v^{s_2}(p_2)$.
After some simple algebra, one obtains

$$\begin{aligned} S_{\Psi\bar{\Psi}}^{(2)} \supset& \frac{1}{2}\frac{(-i)^2}{2!}\frac{1}{M_{\rm Pl}^2}\int d^4x \int d^4y \int \frac{d^4\tilde{q}}{(2\pi)^4}\frac{i}{\tilde{q}^2 + i\epsilon}e^{-i(x-y)\tilde{q}}e^{i(p_1+p_2)y} \\ &\times \bar{u}^{s_1}(p_1)\left\{\not{\partial}\phi(\partial^\beta\phi)(p_1-p_2)_\beta - V(\phi)(\not{p}_1 - \not{p}_2)\right\}v^{s_2}(p_2). \end{aligned} \tag{4.43}$$

The homogeneity of the ϕ field implies that the $\not{\partial}\phi(\partial^\beta\phi)(p_1-p_2)_\beta$ term vanishes. Thus, the full S-matrix element describing the gravitational production of Dirac fermions takes the form

$$S^{(2)}_{\Psi\bar{\Psi}} = -\frac{(-i)^2}{2!}\frac{1}{M_{\rm Pl}^2}\int d^4x\int d^4y\int\frac{d^4\tilde{q}}{(2\pi)^4}\frac{i}{\tilde{q}^2+i\epsilon}e^{-(x-y)\tilde{q}}e^{i(p_1+p_2)y}V(\phi)\bar{u}^{s_1}(p_1)(\not{p}_1-\not{p}_2)v^{s_2}(p_2)$$
$$= \frac{i}{2}\frac{\rho_\phi}{M_{\rm Pl}^2}\sum_k\mathcal{P}_k^{2n}\bar{u}^{s_1}(p_1)\frac{\not{p}_1-\not{p}_2}{s}v^{s_2}(p_2)(2\pi)^4\delta(k\omega-p_1^0-p_2^0)\delta^{(3)}(\vec{p}_1-\vec{p}_2). \quad (4.44)$$

Gravitational vector production
Finally, the term $\hat{h}^{\mu\nu}(x)\hat{h}^{\alpha\beta}(y)\widehat{T}^{\phi}_{\mu\nu}(x)\widehat{T}^{V}_{\alpha\beta}(y)$ accounting for the gravitational production of massive spin-1 gauge fields, can be written as

$$S^{(2)}_{VV} \supset \frac{(-i)^2}{2!}\frac{2}{M_{\rm Pl}^2}\int d^4x\int d^4y\int\frac{d^4\tilde{q}}{(2\pi)^4}\frac{i}{\tilde{q}^2+i\epsilon}e^{-i(x-y)\tilde{q}}e^{i(p_1+p_2)y}\Big\{\epsilon_1^*\cdot\epsilon_2^*(\partial^\alpha\phi p_{1\alpha})(\partial^\beta\phi p_{2\beta})+$$
$$-\epsilon_2^*\cdot p_1(\partial^\alpha\phi\epsilon^*_{1\alpha})(\partial^\beta\phi p_{2\beta})-\epsilon_1^*\cdot p_2(\partial^\alpha\phi\epsilon^*_{2\alpha})(\partial^\beta\phi p_{1\beta})+(\partial^\alpha\phi\epsilon^*_{1\alpha})(\partial^\beta\phi\epsilon^*_{2\beta})[p_1\cdot p_2+m_V^2]+$$
$$+\frac{1}{2}\partial^\rho\phi\partial_\rho\phi[(\epsilon_2^*\cdot p_1)(\epsilon_1^*\cdot p_2)-\epsilon_2^*\cdot\epsilon_1^*(p_1\cdot p_2+m_V^2)]+V(\phi)m_V^2\epsilon_1^*\cdot\epsilon_2^*\Big\}$$
$$= \frac{(-i)^2}{2!}\frac{2}{M_{\rm Pl}^2}\int d^4x\int d^4y\int\frac{d^4\tilde{q}}{(2\pi)^4}\frac{i}{\tilde{q}^2+i\epsilon}e^{-i(x-y)\tilde{q}}e^{i(p_1+p_2)y}$$
$$\times\Big[\underbrace{-\frac{\sqrt{s}}{2}\dot{\phi}^2\Big((\epsilon_2^*\cdot p_1)(\epsilon_1^*)^0+(\epsilon_1^*\cdot p_2)(\epsilon_2^*)^0-\sqrt{s}(\epsilon_1^*)^0(\epsilon_2^*)^0\Big)+\frac{\dot{\phi}^2}{2}(\epsilon_2^*\cdot p_1)(\epsilon_1^*\cdot p_2)+V(\phi)m_V^2\epsilon_1^*\cdot\epsilon_2^*}_{\mathcal{A}(4.45)}\Big], \quad (4.45)$$

where in the last equality, we have utilized Eq. (4.36), and the fact that the spatial derivatives of ϕ vanish.
In order to simplify the above result, we use the explicit form of the polarization vectors for the V field. In particular, we choose a frame in which the spin-1 field moves along the z-direction so that

$$p_1^\mu = \Big(\frac{\sqrt{s}}{2},0,0,p_z\Big), \qquad p_2^\mu = \Big(\frac{\sqrt{s}}{2},0,0,-p_z\Big), \quad (4.46)$$

which, in turn, implies the following form of the polarization vectors:

$$(\epsilon^L_{1,(2)})^\mu = \left(\pm\frac{p_z}{m_V},0,0,\frac{\sqrt{s}}{2m_V}\right), \qquad (\epsilon^\pm_{1,(2)})^\mu = \frac{1}{\sqrt{2}}(0,1,\pm i,0). \quad (4.47)$$

Thus, for the two transverse modes, the expression in the square bracket in Eq. (4.45) reduces to,

$$\mathcal{A}^\pm(4.45) = -V(\phi)m_V^2, \quad (4.48)$$

while for the single longitudinally-polarized mode, we have

$$\mathcal{A}^L(4.45) = -V(\phi)\Big(\frac{s}{2}-m_V^2\Big). \quad (4.49)$$

Thus, the total S-matrix element describing the gravitational production of massive spin-1 particles is given by

$$S^{(2)}_{VV} = i\frac{\rho_\phi}{M_{\rm Pl}^2}\sum_k\mathcal{P}_k^{2n}\widetilde{\mathcal{A}}(k)(2\pi)^4\delta(k\omega-p_1^0-p_2^0)\delta^{(3)}(\vec{p}_1+\vec{p}_2), \quad (4.50)$$

with

$$\widetilde{\mathcal{A}}^L(k) \equiv 1 - \frac{2m_V^2}{s}, \qquad\qquad \widetilde{\mathcal{A}}^{\pm}(k) \equiv \frac{2m_V^2}{s}. \tag{4.51}$$

4.1.3 Production rates

Let us now calculate the probability P for the pair production of two particles with four-momenta p_1 and p_2 in the presence of the oscillating inflaton background

$$P(p_1, p_2) = \frac{|S|^2}{\langle 0|0\rangle \langle p_1|p_1\rangle \langle p_2|p_2\rangle}, \tag{4.52}$$

with $\langle 0|0\rangle = 1$, and $\langle p_i|p_i\rangle = (2\pi)^3 2p_i^0 \delta^{(3)}(\vec{0})$ for $i = 1, 2$.
The squared norm of the S-matrix depends on the form of ϕ interactions, i.e.,

(1) for the direct $\phi - F$ interactions, one gets

$$|S^{(1)}_{\phi\to\mathrm{FF}}|^2 = M_{\mathrm{Pl}}^2 \left(\frac{\rho_\phi}{\Lambda^4}\right)^{\frac{1}{n}} \sum_{\mathrm{final}} \Big[\sum_k \mathcal{P}_k \times (1+\delta_F)\mathcal{F}(F)(2\pi)^4 \delta(k\omega - p_1^0 - p_2^0)\delta^{(3)}(\vec{p}_1 + \vec{p}_2)\Big]^2, \tag{4.53}$$

(2) for indirect gravitational production, one finds

$$|S^{(2)}_{\phi\to\mathrm{FF}}|^2 = \frac{\rho_\phi^2}{M_{\mathrm{Pl}}^4} \sum_{\mathrm{final}} \Big[\sum_k \mathcal{P}_k^{2n} \times (1+\delta_F)\tilde{\mathcal{A}}(F)(2\pi)^4 \delta(k\omega - p_1^0 - p_2^0)\delta^{(3)}(\vec{p}_1 + \vec{p}_2)\Big]^2, \tag{4.54}$$

where we have summed over spin/polarization states of F particles.
The above expressions can be further simplified as

$$|S^{(1)}_{\phi\to\mathrm{FF}}|^2 = M_{\mathrm{Pl}}^4 \left(\frac{\rho_\phi}{\Lambda^4}\right)^{\frac{1}{n}} \sum_k |\mathcal{P}_k|^2 (1+\delta_F)^2 |\overline{\mathcal{M}}^{(1)}_{\phi\to\mathrm{FF}}(k)|^2 \Big[(2\pi)^4 \delta(k\omega - p_1^0 - p_2^0)\delta^{(3)}(\vec{p}_1 + \vec{p}_2)\Big]^2, \tag{4.55}$$

and

$$|S^{(2)}_{\phi\to\mathrm{FF}}|^2 = \frac{\rho_\phi^2}{M_{\mathrm{Pl}}^4} \sum_k |\mathcal{P}_k^{2n}|^2 (1+\delta_F)^2 |\overline{\mathcal{M}}^{(2)}_{\phi\to\mathrm{FF}}(k)|^2 \Big[(2\pi)^4 \delta(k\omega - p_1^0 - p_2^0)\delta^{(3)}(\vec{p}_1 + \vec{p}_2)\Big]^2. \tag{4.56}$$

The square of the dimensionless *amplitude* $\mathcal{M}$ summed over spin/polarization states of F particle, accounting for the direct inflaton interactions, is

$$|\overline{\mathcal{M}}^{(1)}_{\phi\to\mathrm{FF}}(k)|^2 \equiv \frac{1}{M_{\mathrm{Pl}}^2} \sum_{\mathrm{final}} |\mathcal{F}(F)|^2 = \begin{cases} (g_{S\phi}/M_{\mathrm{Pl}})^2, & F = S, \\ 2g_{\Psi\phi}^2 [s - 4m_\Psi^2]/M_{\mathrm{Pl}}^2, & F = \Psi, \\ \left(\frac{g_{V\phi}}{M_{\mathrm{Pl}}}\right)^2 \left[2 + \frac{(s-2m_V^2)^2}{4m_V^4}\right], & F = V \text{ and } m_V \neq 0, \\ 4\left(\frac{g_{V\phi}}{M_{\mathrm{Pl}}}\right)^2, & F = V \text{ and } m_V = 0, \\ (h_{A\phi}/M_{\mathrm{Pl}})^2 \cdot \left(\frac{s}{2} - m_A^2\right)^2, & F = A, \end{cases} \tag{4.57}$$

while for gravitational interactions, one finds

$$|\overline{\mathcal{M}}^{(2)}_{\phi\to\mathrm{FF}}(k)|^2 \equiv \sum_{\text{final}} |\tilde{\mathcal{A}}(F)|^2 = \begin{cases} 1 + \frac{4m_S^2}{s} + \frac{4m_S^4}{s^2}, & F = S, \\ \frac{2m_\Psi^2}{s}\left(1 - \frac{4m_\Psi^2}{s}\right), & F = \Psi, \\ 1 - \frac{4m_V^2}{s} + \frac{12m_V^4}{s^2}, & F = V \text{ and } m_V \neq 0, \\ 0, & F = V \text{ and } m_V = 0. \end{cases} \tag{4.58}$$

Let us emphasize that in the limit $m_F \to 0$, only massless scalars S can be gravitationally created in the inflaton background.

To compute the absolute square of the S-matrix element, one has to square two delta functions, appearing in Eqs.(4.55)-(4.56). For that purpose, we assume that the particle creation takes place in a box of volume V in a time duration T. At the end of the computations, the regulators V and T are removed by taking the limit $V, T \to \infty$. Under these assumptions, the square bracket in Eqs.(4.55)-(4.56) can be written as

$$\left[(2\pi)^4\delta(k\omega - p_1^0 - p_2^0)\delta^{(3)}(\vec{p}_1 + \vec{p}_2)\right]^2 = (2\pi)^4\delta(k\omega - p_1^0 - p_2^0)\delta^{(3)}(\vec{p}_1 + \vec{p}_2) \times (2\pi)^4\delta^{(4)}(0), \tag{4.59}$$

with

$$(2\pi)^4\delta^{(4)}(0) = \int \mathrm{d}^4x e^{-i0\cdot x} = VT, \qquad (2\pi)^3\delta^{(3)}(0) = \int \mathrm{d}^3x e^{-i0\cdot\vec{x}} = V. \tag{4.60}$$

Now, Eq. (4.52) simplifies as

$$P^{(1)}_{\phi\to\mathrm{FF}}(p_1, p_2) = M_{\mathrm{Pl}}^4 \left(\frac{\rho_\phi}{\Lambda^4}\right)^{\frac{1}{n}} \sum_k |\mathcal{P}_k|^2 \cdot (1+\delta_F)^2 \frac{|\overline{\mathcal{M}}^{(1)}_{\phi\to\mathrm{FF}}(k)|^2}{2p_1^0 V\, 2p_2^0 V} \times (2\pi)^4\delta(k\omega - p_1^0 - p_2^0)\delta^{(3)}(\vec{p}_1 + \vec{p}_2)VT\,, \tag{4.61}$$

for the direct F production from the inflaton condensate, and

$$P^{(2)}_{\phi\to\mathrm{FF}}(p_1, p_2) = \frac{\rho_\phi^2}{M_{\mathrm{Pl}}^4} \sum_k |\mathcal{P}_k^{2n}|^2 \cdot (1+\delta_F)^2 \frac{|\overline{\mathcal{M}}^{(2)}_{\phi\to\mathrm{FF}}(k)|^2}{2p_1^0 V\, 2p_2^0 V} \times (2\pi)^4\delta(k\omega - p_1^0 - p_2^0)\delta^{(3)}(\vec{p}_1 + \vec{p}_2)VT\,, \tag{4.62}$$

for indirect gravitational production, respectively.
The total probability can be found by summing the above expressions over each outgoing momenta p_1, p_2. In the continuum limit, this reduces to multiplying $P^{(i)}_{\phi\to\mathrm{FF}}(p_1, p_1)/T$ by a factor $V d^3p_1/(2\pi)^3\, V d^3p_2/(2\pi)^3$.
Thus, the rate of particle production in volume V and time $\mathrm{d}t$ can be calculated as

$$\mathrm{d}\mathcal{R}^{(i)}_{\mathrm{FF}} \equiv \frac{V\mathrm{d}^3p_1}{(2\pi)^3}\frac{V\mathrm{d}^3p_2}{(2\pi)^3}\frac{P^{(i)}_{\phi\to\mathrm{FF}}(p_1, p_1)}{T}\mathrm{d}t, \qquad i \in \{1, 2\}, \tag{4.63}$$

whereas, the energy gain of created particles in volume V and time $\mathrm{d}t$ is

$$\mathrm{d}E^{(i)}_{\mathrm{FF}} \equiv (p_1^0 + p_2^0)\frac{V\mathrm{d}^3p_1}{(2\pi)^3}\frac{V\mathrm{d}^3p_2}{(2\pi)^3}\frac{P^{(i)}_{\phi\to\mathrm{FF}}(p_1, p_1)}{T}\mathrm{d}t, \qquad i \in \{1, 2\}. \tag{4.64}$$

Consequently, the total rate $\mathcal{R}^{(i)}_{\rm FF}$ and the energy gain $\mathcal{E}^{(i)}_{\rm FF}$ per volume and time for the considered processes are given by

$$\mathcal{R}^{(1)}_{\rm FF} = M_{\rm Pl}^4 \left(\frac{\rho_\phi}{\Lambda^4}\right)^{\frac{1}{n}} \sum_k |\mathcal{P}_k|^2 \cdot (1+\delta_F)^2\, |\overline{\mathcal{M}}^{(1)}_{\phi\to{\rm FF}}(k)|^2 \\ \times \int \frac{d^3p_1}{(2\pi)^3 2p_1^0} \int \frac{d^3p_2}{(2\pi)^3 2p_2^0} (2\pi)^4 \delta(k\omega - p_1^0 - p_2^0)\delta^{(3)}(\vec{p}_1+\vec{p}_2), \tag{4.65}$$

$$\mathcal{R}^{(2)}_{\rm FF} = \frac{\rho_\phi^2}{M_{\rm Pl}^4} \sum_k |\mathcal{P}^{2n}_k|^2 \cdot (1+\delta_F)^2\, |\overline{\mathcal{M}}^{(2)}_{\phi\to{\rm FF}}(k)|^2 \\ \times \int \frac{d^3p_1}{(2\pi)^3 2p_1^0} \int \frac{d^3p_2}{(2\pi)^3 2p_2^0} (2\pi)^4 \delta(k\omega - p_1^0 - p_2^0)\delta^{(3)}(\vec{p}_1+\vec{p}_2), \tag{4.66}$$

and

$$\mathcal{E}^{(1)}_{\rm FF} = M_{\rm Pl}^4 \left(\frac{\rho_\phi}{\Lambda^4}\right)^{\frac{1}{n}} \sum_k |\mathcal{P}_k|^2 \cdot (1+\delta_F)^2\, |\overline{\mathcal{M}}^{(1)}_{\phi\to{\rm FF}}(k)|^2 \\ \times \int \frac{d^3p_1}{(2\pi)^3 2p_1^0} \int \frac{d^3p_2}{(2\pi)^3 2p_2^0} (p_1^0+p_2^0)(2\pi)^4 \delta(k\omega - p_1^0 - p_2^0)\delta^{(3)}(\vec{p}_1+\vec{p}_2), \tag{4.67}$$

$$\mathcal{E}^{(2)}_{\rm FF} = \frac{\rho_\phi^2}{M_{\rm Pl}^4} \sum_k |\mathcal{P}^{2n}_k|^2 \cdot (1+\delta_F)^2\, |\overline{\mathcal{M}}^{(2)}_{\phi\to{\rm FF}}(k)|^2 \\ \times \int \frac{d^3p_1}{(2\pi)^3 2p_1^0} \int \frac{d^3p_2}{(2\pi)^3 2p_2^0} (p_1^0+p_2^0)(2\pi)^4 \delta(k\omega - p_1^0 - p_2^0)\delta^{(3)}(\vec{p}_1+\vec{p}_2). \tag{4.68}$$

After straightforward computations, we find

$$\mathcal{R}^{(1)}_{\rm FF} = \frac{M_{\rm Pl}^4}{4\pi} \left(\frac{\rho_\phi}{\Lambda^4}\right)^{\frac{1}{n}} \sum_{k=1}^{\infty} |\mathcal{P}_k|^2 \cdot (1+\delta_F)^2 |\overline{\mathcal{M}}^{(1)}_{\phi\to{\rm FF}}(k)|^2 \sqrt{1-\left(\frac{2m_F}{k\omega}\right)^2}, \tag{4.69}$$

$$\mathcal{R}^{(2)}_{\rm FF} = \frac{1}{4\pi}\frac{\rho_\phi^2}{M_{\rm Pl}^4} \sum_{k=1}^{\infty} |\mathcal{P}^{2n}_k|^2 \cdot (1+\delta_F)^2 |\overline{\mathcal{M}}^{(2)}_{\phi\to{\rm FF}}(k)|^2 \sqrt{1-\left(\frac{2m_F}{k\omega}\right)^2}, \tag{4.70}$$

and

$$\mathcal{E}^{(1)}_{\rm FF} = \frac{M_{\rm Pl}^4}{8\pi} \left(\frac{\rho_\phi}{\Lambda^4}\right)^{\frac{1}{n}} \sum_{k=1}^{\infty} k\omega |\mathcal{P}_k|^2 \cdot\ (1+\delta_F)^2 |\overline{\mathcal{M}}^{(1)}_{\phi\to{\rm FF}}(k)|^2 \sqrt{1-\left(\frac{2m_F}{k\omega}\right)^2}, \tag{4.71}$$

$$\mathcal{E}^{(2)}_{\rm FF} = \frac{1}{8\pi}\frac{\rho_\phi^2}{M_{\rm Pl}^4} \sum_{k=1}^{\infty} k\omega |\mathcal{P}^{2n}_k|^2 \cdot\ (1+\delta_F)^2 |\overline{\mathcal{M}}^{(2)}_{\phi\to{\rm FF}}(k)|^2 \sqrt{1-\left(\frac{2m_F}{k\omega}\right)^2}. \tag{4.72}$$

4.2 Boltzmann equations

Now our goal is to trace the evolution of the whole system, taking into account interactions between the inflaton and the SM sector. In this part, we assume that F is part of the visible sector. During the reheating phase, the dynamics of the model universe can be determined by the following set of time-averaged Boltzmann equations (BEqs) for the inflaton and SM radiation energy densities:

$$\dot{\rho}_\phi + \frac{6n}{1+n} H \rho_\phi = -\mathcal{E}_{\mathrm{SM\,SM}}, \tag{4.73}$$

$$\dot{\rho}_{\mathrm{SM}} + 4H\rho_{\mathrm{SM}} = \mathcal{E}_{\mathrm{SM\,SM}}, \tag{4.74}$$

supplemented by the Friedmann equation, which now depends on the evolution of both sectors

$$H^2 = \frac{1}{3M_{\mathrm{Pl}}^2} \left(\rho_\phi + \rho_{\mathrm{SM}}\right). \tag{4.75}$$

Above, $\mathcal{E}_{\phi\to\mathrm{SM\,SM}}(-\mathcal{E}_{\phi\to\mathrm{SM\,SM}})$ denotes the energy gain (lose) of the SM sector (the inflaton) averaged over ϕ oscillations. Note that in general, $\mathcal{E}_{\mathrm{SM\,SM}}$ can be written a sum, i.e.,

$$\mathcal{E}_{\mathrm{SM\,SM}} = \sum_l \mathcal{E}^{\mathrm{l}}_{\mathrm{SM\,SM}}, \tag{4.76}$$

if F has several possible production channels or there are several SM species F_l to which ϕ is coupled. For instance, suppose that the inflaton couples directly only to the SM scalar, i.e., the Higgs doublet **h**, which in the linear parametrization can be written as

$$\boldsymbol{h} = \frac{1}{\sqrt{2}} \begin{pmatrix} h_2 + ih_3 \\ h_0 + ih_1 \end{pmatrix}, \tag{4.77}$$

where h_i $(i=0,1,2,3)$ are the four real components. In this case, ϕ also inevitably interacts with all the particle content of the SM, i.e., fermions $\mathbf{\Psi}$ including six quarks (up, down, charm, strange, top, bottom) as well as six leptons (electron, electron neutrino, muon, muon neutrino, tau, tau neutrino), and massive gauge bosons $\mathbf{V} = \{W^\pm, Z^0\}$, though indirect processes mediated by the graviton exchange.

4.2.1 Inflaton decay rates

Notice that Eq.(4.73) is just the continuity equation for the inflaton field Eq.(3.19), where we have included the fact that ϕ loses its energy not only due to the expansion but also as a result of interactions with the SM sector. Moreover, in Eq.(4.73), we have used the relation between $\bar{w}$ and n derived in Eq.(3.36). The above form of the BEqs indicates that if there are no hidden sectors, the total energy acquired by the SM bath must be counterbalanced by the energy dissipated from the inflaton field. Typically, one parametrizes the r.h.s of BEqs as

$$\mathcal{E}_{\mathrm{SM\,SM}} \equiv (1+\bar{w})\,\rho_\phi \cdot \langle \Gamma_{\phi\to\mathrm{SM\,SM}} \rangle, \tag{4.78}$$

where $\langle \Gamma_{\phi\to\mathrm{SM\,SM}} \rangle$ denotes a *time-averaged inflaton decay rate*. Strictly speaking, $\langle \Gamma_{\phi\to\mathrm{SM\,SM}} \rangle$ cannot be considered as a standard decay width (or a cross-section) accounting for the $\phi-$SM interactions. This is because, in the framework described in the previous section, ϕ is not regarded as a quantum field decaying (annihilating) into other quanta. Instead, it represents a coherently oscillating condensate of zero-momenta particles. Nonetheless, the above parametrization is useful as it allows us to mimic the standard form of Boltzmann equations.

Utilizing Eq.(4.71) together with Eq.(4.57), we find that for the considered direct $\phi-$ SM interactions, the *time-averaged inflaton decay rate* takes the following form:

$$\langle\Gamma^{(1)}_{\phi\to\mathbf{hh}}\rangle = \left\langle g^2_{h\phi}\frac{1+n}{2n}\frac{1}{8\pi}\frac{\omega M^4_{\rm Pl}}{\rho_\phi}\left(\frac{\rho_\phi}{\Lambda^4}\right)^{\frac{1}{n}}\sum_{i=0}^{3}\sum_{k=1}^{\infty}k|\mathcal{P}_k|^2\sqrt{1-\frac{4m^2_{h_i}}{(k\omega)^2}}\right\rangle, \tag{4.79}$$

$$\langle\Gamma^{(1)}_{\phi\to\mathbf{\Psi\bar\Psi}}\rangle = \left\langle g^2_{\Psi\phi}\frac{1+n}{2n}\frac{1}{4\pi}\frac{\omega^3 M^2_{\rm Pl}}{\rho_\phi}\left(\frac{\rho_\phi}{\Lambda^4}\right)^{\frac{1}{n}}\sum_{\mathbf{\Phi}}\sum_{k=1}^{\infty}k^3|\mathcal{P}_k|^2\left(1-\frac{4m^2_{\Psi}}{(k\omega)^2}\right)^{3/2}\right\rangle, \tag{4.80}$$

$$\begin{aligned}\langle\Gamma^{(1)}_{\phi\to\boldsymbol{\mathcal{V}\mathcal{V}}}\rangle = &\left\langle g^2_{\mathcal{V}\phi}\frac{1+n}{2n}\frac{1}{32\pi}\frac{\omega M^4_{\rm Pl}}{\rho_\phi}\left(\frac{\rho_\phi}{\Lambda^4}\right)^{\frac{1}{n}}(1+\delta_{\boldsymbol{\mathcal{V}}})^2\right.\\ &\left.\times\sum_{\boldsymbol{\mathcal{V}}}\sum_{k=1}^{\infty}k|\mathcal{P}_k|^2\left(\frac{k\omega}{m_{\mathcal{V}}}\right)^4\left[1-4\left(\frac{m_{\mathcal{V}}}{k\omega}\right)^2+12\left(\frac{m_{\mathcal{V}}}{k\omega}\right)^4\right]\sqrt{1-\frac{4m^2_{\mathcal{V}}}{(k\omega)^2}}\right\rangle,\end{aligned} \tag{4.81}$$

where we have included all *decay channels* by summing over all the SM scalars, fermions, and vectors to which ϕ is directly coupled. Note that above, we have rescaled the coupling constant, i.e.,

$$g_{S\phi}\to g_{h\phi}\cdot M_{\rm Pl}, \qquad\qquad g_{V\phi}\to g_{\mathcal{V}\phi}\cdot M_{\rm Pl}, \tag{4.82}$$

such that $g_{h\phi}, g_{\Psi\phi}$ and $g_{\mathcal{V}\phi}$ are now dimensionless. Moreover, we have used $\delta_{\mathbf{h}}=1, \delta_{\mathbf{\Psi}}=0$. In the case of the $\phi\to\mathbf{hh}$ interactions, the factor $(1+\delta_{\mathbf{h}})^2=4$ cancels out with the factor of $(1/2)^2$ coming from the normalization of the Higgs doublet.
In addition, one could also consider the derivative coupling with the following *decay width*:

$$\langle\Gamma^{(1)}_{\phi\to\rm AA}\rangle = \left\langle\frac{1+n}{2n}\frac{4}{8\pi}\left(\frac{h_{A\phi}}{M_{\rm Pl}}\right)^2\frac{\omega M^4_{\rm Pl}}{\rho_\phi}\left(\frac{\rho_\phi}{\Lambda^4}\right)^{\frac{1}{n}}\sum_{\rm A}\sum_{k=1}^{\infty}k|\mathcal{P}_k|^2(k\omega)^4\left(1-\frac{2m^2_A}{(k\omega)^2}\right)^2\sqrt{1-\frac{4m^2_A}{(k\omega)^2}}\right\rangle, \tag{4.83}$$

where we have assumed that $\delta_A=1$.
Finally, *inflaton decay rates* describing its indirect gravitational interactions are given by

$$\langle\Gamma^{(2)}_{\phi\to\mathbf{hh}}\rangle = \left\langle\frac{1}{8\pi}\frac{\rho_\phi}{M^4_{\rm Pl}}\sum_{i=0}^{3}\sum_{k=0}^{\infty}k\omega|\mathcal{P}^{2n}_k|^2\left(1+\frac{4m^2_{h_i}}{(k\omega)^2}+\frac{4m^4_{h_i}}{(k\omega)^4}\right)\sqrt{1-\frac{4m^2_{h_i}}{(k\omega)^2}}\right\rangle, \tag{4.84}$$

$$\langle\Gamma^{(2)}_{\phi\to\mathbf{\Psi\bar\Psi}}\rangle = \left\langle\frac{1}{2\pi}\frac{\rho_\phi}{M^4_{\rm Pl}}\sum_{\mathbf{\Psi}}\sum_{k=0}^{\infty}k\omega|\mathcal{P}^{2n}_k|^2\frac{m^2_\Psi}{(k\omega)^2}\left(1-\frac{4m^2_\Psi}{(k\omega)^2}\right)^{3/2}\right\rangle, \tag{4.85}$$

$$\langle\Gamma^{(2)}_{\phi\to\boldsymbol{\mathcal{V}\mathcal{V}}}\rangle = \left\langle\frac{1}{8\pi}\frac{\rho_\phi}{M^4_{\rm Pl}}\sum_{\boldsymbol{\mathcal{V}}}\sum_{k=0}^{\infty}k\omega|\mathcal{P}^{2n}_k|^2\left(1-\frac{4m^2_{\mathcal{V}}}{(k\omega)^2}+\frac{12m^4_{\mathcal{V}}}{(k\omega)^4}\right)\sqrt{1-\frac{4m^2_{\mathcal{V}}}{(k\omega)^2}}\right\rangle. \tag{4.86}$$

4.2.2 Decay widths in the massless limit

Since reheating occurred at the highest available energy scales just after the end of inflation, it is instructive to consider the limit in which masses of SM species are negligible, i.e., $m_{\rm SM}\to 0$. In this regime, the above formulas simplify as

$$\langle\Gamma^{(1)}_{\phi\to\mathbf{hh}}\rangle\Bigg|_{m_h\to 0} = \Gamma^{(1)}_{\phi\to\mathbf{hh}}\Bigg|_{m_h\to 0} = 4\cdot g^2_{h\phi}\frac{1+n}{2n}\frac{\omega}{8\pi}\left(\frac{M_{\rm Pl}}{\Lambda}\right)^4\left(\frac{\rho_\phi}{\Lambda^4}\right)^{\frac{1-n}{n}}\sum_{k=1}^{\infty}k|\mathcal{P}_k|^2\,,$$

$$\langle\Gamma^{(1)}_{\phi\to\mathbf{\Psi\bar\Psi}}\rangle\Bigg|_{m_\Psi\to 0} = \Gamma^{(1)}_{\phi\to\mathbf{\Psi\bar\Psi}}\Bigg|_{m_\Psi\to 0} = \#_{\mathbf{\Psi}}\cdot g^2_{\Psi\phi}\frac{1+n}{2n}\frac{\omega}{4\pi}\left(\frac{\omega M_{\rm Pl}}{\Lambda^2}\right)^2\left(\frac{\rho_\phi}{\Lambda^4}\right)^{\frac{1-n}{n}}\sum_{k=1}^{\infty}k^3|\mathcal{P}_k|^2\,,$$

$$\langle\Gamma^{(1)}_{\phi\to\boldsymbol{\mathcal{V}}\boldsymbol{\mathcal{V}}}\rangle\Big|_{m_{\mathcal{V}}\to 0} = \Gamma^{(1)}_{\phi\to\boldsymbol{\mathcal{V}}\boldsymbol{\mathcal{V}}}\Big|_{m_{\mathcal{V}}\to 0} = \#_{\boldsymbol{\mathcal{V}}}\cdot 2\cdot(1+\delta_{\mathbf{V}})^2\cdot\Gamma_{\phi\to\mathbf{hh}}(g_{h\phi}\leftrightarrow g_{\mathcal{V}\phi})\,,$$
$$\langle\Gamma^{(1)}_{\phi\to\mathrm{AA}}\rangle\Big|_{m_A\to 0} = \Gamma^{(1)}_{\phi\to\mathrm{AA}}\Big|_{m_A\to\to 0} = \#_A\cdot\frac{1+n}{2n}\frac{\omega}{8\pi}\left(\frac{\omega^2 M_{\mathrm{Pl}} h_{A\phi}}{\Lambda^2}\right)^2\left(\frac{\rho_\phi}{\Lambda^4}\right)^{\frac{1-n}{n}}\sum_{k=1}^{\infty}k^5|\mathcal{P}_k|^{,}, \tag{4.87}$$

with $\#_{\boldsymbol{\Psi}}, \#_{\boldsymbol{\mathcal{V}}}, \#_A$ denote the number of SM fermions, vectors, and axion-like particles to which ϕ couples directly. Moreover, it is important to stress that averaging over inflaton oscillations in the massless limit is trivial since the time scale of ρ_ϕ and ω is much longer than the time scale of interactions.
In the case of gravitational interactions, the only open channel in the massless limit, i.e., $m_{\mathrm{SM}}\to 0$, is

$$\langle\Gamma^{(2)}_{\phi\to\mathbf{hh}}\rangle\Big|_{m_h\to 0} = \Gamma^{(2)}_{\phi\to\mathbf{hh}}\Big|_{m_h\to 0} = 4\cdot\frac{\omega}{8\pi}\frac{\rho_\phi}{M_{\mathrm{Pl}}^4}\sum_{k=0}^{\infty}k|\mathcal{P}_k^{2n}|^2. \tag{4.88}$$

Since $\langle\Gamma^{(1)}_{\phi\to\boldsymbol{\Psi}\bar{\boldsymbol{\Psi}}}\rangle$ is proportional to the square mass of SM fermions, in the limit $m_\Psi\to 0$ the corresponding *decay width* vanishes. The same happens to *inflaton decay rate* describing gravitational creation of SM massless vectors, as the corresponding amplitude squared is zero (4.58). Thus, the inflaton field cannot transfer its energy to massless vectors and fermions through gravitational interactions.

The above formulas indicate that in the *massless scenario*, i.e., $m_F\to 0$, *inflaton decay rates* have, in general, two sources of time-dependency, namely, ρ_ϕ and ω. Thus, to determine the evolution of Γ_ϕ, one needs to find the solution for ρ_ϕ during the reheating phase. To that end, we assume that during the early stage of reheating, the role of the interaction term on the r.h.s of (4.73) is subdominant so that the energy density of ϕ decreases approximately according to Eq.(3.63). Furthermore, the evolution of ω is governed by the following power-law solution:

$$\omega = \omega_e\cdot\left(\frac{\rho_\phi}{\Lambda^4}\right)^{\frac{n-1}{2n}} \simeq \omega_e\left(\frac{\rho_e}{\Lambda^4}\right)^{\frac{n-1}{2n}}\left(\frac{a_e}{a}\right)^{\frac{3(n-1)}{n+1}}, \qquad \omega_e\equiv\sqrt{2\,n^2\,\pi}\,\frac{\Gamma\left(\frac{n+1}{2n}\right)}{\Gamma\left(\frac{1}{2n}\right)}\frac{\Lambda^2}{M_{\mathrm{Pl}}}. \tag{4.89}$$

Consequently, the time-dependence of the *inflaton decay rates* can be parametrized as

$$\Gamma_{\phi\to\mathrm{FF}}\equiv\widetilde{\Gamma}^e_{\phi\to\mathrm{FF}}\left(\frac{a_e}{a}\right)^{\beta_F}, \tag{4.90}$$

where

$$\widetilde{\Gamma}^e_{\phi\to\mathbf{hh}} = 4\cdot g_{h\phi}^2\frac{1+n}{2n}\frac{\omega_e}{8\pi}\left(\frac{M_{\mathrm{Pl}}}{\Lambda}\right)^4\left(\frac{\rho_e}{\Lambda^4}\right)^{\frac{1-n}{2n}}\sum_{k=1}^{\infty}k|\mathcal{P}_k|^2\,, \tag{4.91}$$

$$\widetilde{\Gamma}^e_{\phi\to\boldsymbol{\Psi}\bar{\boldsymbol{\Psi}}} = \#_{\boldsymbol{\Psi}}\cdot g_{\Psi\phi}^2\cdot\frac{1+n}{2n}\frac{\omega_e}{4\pi}\left(\frac{\omega_e M_{\mathrm{Pl}}}{\Lambda^2}\right)^2\left(\frac{\rho_e}{\Lambda^4}\right)^{\frac{n-1}{2n}}\sum_{k=1}^{\infty}k^3|\mathcal{P}_k|^2, \tag{4.92}$$

$$\widetilde{\Gamma}^e_{\phi\to\boldsymbol{\mathcal{V}}\boldsymbol{\mathcal{V}}} = \#_{\boldsymbol{\mathcal{V}}}\cdot\frac{1}{2}\cdot(1+\delta_{\mathcal{V}})^2\cdot\widetilde{\Gamma}^e_{\phi\to\mathbf{hh}}(g_{h\phi}\leftrightarrow g_{\mathcal{V}\phi}), \tag{4.93}$$

$$\widetilde{\Gamma}^e_{\phi\to\mathrm{AA}} = \#_A\cdot\frac{1+n}{2n}\frac{\omega_e}{8\pi}\left(\frac{\omega_e^2 M_{\mathrm{Pl}} h_{A\phi}}{\Lambda^2}\right)^2\left(\frac{\rho_e}{\Lambda^4}\right)^{\frac{3n-3}{2n}}\sum_{k=1}^{\infty}k^5|\mathcal{P}_k|^2, \tag{4.94}$$

n	1	3/2	2	5/2	3	7/2	4	9/2	5
$\sum_k k\vert\mathcal{P}_k\vert^2$	1/4	0.2381	0.2294	0.2228	0.2177	0.2135	0.2101	0.2072	0.2047
$\sum_k k^3\vert\mathcal{P}_k\vert^2$	1/4	0.2420	0.2406	0.2418	0.2442	0.2472	0.2504	0.2537	0.2571
$\sum_k k^5\vert\mathcal{P}_k\vert^2$	1/4	0.2782	0.3433	0.4270	0.5254	0.6372	0.7620	0.8994	1.049
$\sum_k k\vert\mathcal{P}_k^{2n}\vert^2$	1/8	0.1816	0.1410	0.1659	0.1458	0.1598	0.1476	0.1566	0.1485

TABLE 4.1: Numerical values of the summation factors appearing in Eqs.(4.91)-(4.94) and Eq.(4.96), for different values of n.

and

$$\beta_{\mathbf{h}} = \frac{3(1-n)}{1+n}, \qquad \beta_{\mathbf{\Psi}} = \frac{3(n-1)}{1+n}, \qquad \beta_{\boldsymbol{\mathcal{V}}} = \beta_{\mathbf{h}}, \qquad \beta_{\mathrm{A}} = \frac{9(n-1)}{1+n}\,, \tag{4.95}$$

whereas for indirect gravitational channels, one finds

$$\widetilde{\Gamma}^{\mathrm{grav},e}_{\phi\to\mathbf{hh}} = 4\cdot\frac{1+n}{2n}\frac{\omega_e}{8\pi}\left(\frac{\Lambda}{M_{\mathrm{Pl}}}\right)^4\left(\frac{\rho_e}{\Lambda^4}\right)^{\frac{3n-1}{2n}}\sum_{k=1}^{\infty}k|\mathcal{P}_k^{2n}|^2\,, \tag{4.96}$$

with

$$\beta^{\mathrm{grav}}_{\mathbf{h}} = \frac{3(3n-1)}{1+n}. \tag{4.97}$$

To obtain time-independent *inflaton decay widths* $\widetilde{\Gamma}^e_{\phi\to\mathrm{FF}}$, one needs to determine the summation factors appearing in the Eqs. (4.91)-(4.94) and Eq.(4.96). For a given monomial potential $|\phi|^{2n}$, Fourier coefficients, $\mathcal{P}_k$, are defined by the integral Eq.(4.3). For the quadratic inflaton potential, i.e., $n=1$, the only non-zero Fourier coefficient is $\mathcal{P}_1 = 1/2$. In general, if $n \in \{1/2, 3/2, \dots\}$ or n is a positive integer greater than 1, all even $\mathcal{P}_k$ coefficient with $k \in \{2, 4, \dots\}$ vanish. Moreover, we observe that values of the $\mathcal{P}_k$ coefficients quickly decrease with k such that the sum $\sum_k k|\mathcal{P}_k|^2$ converges around $k\sim 10$ for $n \leq 10$, and around $k \sim 30$ for larger values of n. For the $\sum_k k^3|\mathcal{P}_k|^2$ and $\sum_k k^5|\mathcal{P}_k|^2$ terms we have summed over several dozen of $\mathcal{P}_k$ coefficients. In each case, the sum is dominated by the contribution from the first non-zero harmonics. In the case of gravitational interactions, if the exponent ^{2n} is odd, i.e., n is a positive half-odd-integers, all even $\mathcal{P}_k^{2n}$ coefficients with $k \in \{2, 4, \dots\}$ are zero. On the other hand, if n is a positive integer greater than 1, odd $\mathcal{P}_k^{2n}$ coefficients with $k \in \{1, 3, \dots\}$ vanish. Moreover, for $n=1$ the only non-zero Fourier coefficient is $\mathcal{P}_2^2 = 1/4$. The numerical values of the $\sum_k k|\mathcal{P}_k|^2$, $\sum_k k^3|\mathcal{P}_k|^2$, $\sum_k k^5|\mathcal{P}_k|^2$, and $\sum_k k|\mathcal{P}_k^{2n}|^2$ terms for different values of n are collected in Table 4.1.

Now we should stress that the above formulas presuppose that in the massless limit *inflaton decay rates* describing direct ϕ interactions with the SM bath are time-independent only if ϕ has a quadratic potential, i.e., $n = 1$. For other types of inflaton potential, $\Gamma_{\phi\to\mathrm{FF}}$ could both decrease and increase with time during reheating, depending on the value of n. Since we have restricted our attention to the class of potentials steeper than the linear potential, i.e., $n > \frac{1}{2}$, for the scalar and vector interactions, $\beta_{\mathbf{h}}$ and $\beta_{\boldsymbol{\mathcal{V}}}$ are positive for $n \in (1/2, 1)$, and negative if $n > 1$. Hence, for $n \in (1/2, 1)$ $(n > 1)$ $\Gamma_{\phi\to\mathbf{hh}}$ and $\Gamma_{\phi\to\boldsymbol{\mathcal{V}}\boldsymbol{\mathcal{V}}}$ are decreasing (increasing) functions of the scale factor. Contrarily, in case of the direct inflaton coupling to SM fermions $\mathbf{\Psi}$, or derivative coupling to axion-like particles A, the corresponding *decay widths* $\Gamma_{\phi\to\mathbf{\Psi}\bar{\mathbf{\Psi}}}$ and $\Gamma_{\phi\to\mathrm{AA}}$ decrease (increase) during reheating for $n > 1\,(n \in (1/2, 1))$, respectively. Decreasing the *inflaton decay rate* means that the energy transfer from the ϕ field to the SM particles becomes less and less efficient during reheating. On the other hand, if $\Gamma_{\phi\to\mathrm{FF}}$ grows with a, the rate of energy injection into the visible sector increases with time, which implies that SM quanta are more effectively produced at the late stages of reheating than at its beginning. Thus, we conclude that for $n > 1$, reheating triggered by the $\phi \to \mathbf{\Psi}\bar{\mathbf{\Psi}}$ or $\phi \to \mathrm{AA}$ interactions is delayed as compared to the models in which reheating is induced by the inflaton-scalars or inflaton-vectors coupling. At this point, it should be stressed that the above statement is valid if all time-independent *decay width* $\widetilde{\Gamma}^e_{\phi\to\mathrm{FF}}$ are of the same order of magnitude. In general, this last condition might not necessarily be met since the considered interactions arise from operations of different dimensions. Finally, $\Gamma^{\mathrm{grav}}_{\phi\to\mathbf{hh}}$ responsible for gravitational interactions among the inflaton and SM Higgs fields always decreases with the scale factor in the range of n considered in this analysis. It is worth noting that the decline of $\Gamma^{\mathrm{grav}}_{\phi\to\mathbf{hh}}$ is always faster than the rate of decrease of *inflaton decay widths* accounting for direct $\phi-\mathrm{SM}$ interactions.

	$n \in (1/2, 1)$	$n = 1$	$n > 1$
$\Gamma_{\phi\to\mathbf{hh}}(a)$	$\searrow$	$\rightarrow$	$\nearrow$
$\Gamma_{\phi\to\mathbf{\Psi}\bar{\mathbf{\Psi}}}(a)$	$\nearrow$	$\rightarrow$	$\searrow$
$\Gamma_{\phi\to\boldsymbol{\nu}\boldsymbol{\nu}}(a)$	$\searrow$	$\rightarrow$	$\nearrow$
$\Gamma_{\phi\to\mathrm{AA}}(a)$	$\nearrow$	$\rightarrow$	$\searrow$
$\Gamma^{\mathrm{grav}}_{\phi\to\mathbf{hh}}(a)$	$\searrow$	$\searrow$	$\searrow$

TABLE 4.2: Evolution of the *inflaton decay rates* with the scale factor. $\searrow$ ($\nearrow$) denotes monotonically decreasing (increasing) function, whereas $\rightarrow$ indicates a constant function.

4.2.3 Generic solutions to the second Boltzmann equation

Now let us find an approximate analytical solution to the second Boltzmann equation, assuming that the inflaton interactions are described by the time-dependent decay rate (4.90). With this end in view, we recast Eq. (4.74) to the form

$$d(a^4\rho_{\mathrm{SM}}) = \frac{2n}{1+n}\frac{a^3}{H(a)}\rho_\phi\langle\Gamma_{\phi\to\mathrm{SM\,SM}}\rangle\, da. \tag{4.98}$$

At the beginning of reheating, the energy density of the SM sector is negligible, i.e., $\rho_{\mathrm{SM}}(a_e) \simeq 0$. To find the solution to the above equation, one has to specify the evolution of the Hubble rate. We assume that at the beginning of reheating, the total energy density of the Universe is dominantly in the form of the inflaton energy density, i.e., $\rho_{\mathrm{tot}}(a_e) \simeq \rho_e$. Hence, from the Friedmann equation, one obtains

$$H_{\mathrm{RH}}(a) \simeq \sqrt{\frac{\rho_\phi(a)}{3M_{\mathrm{Pl}}^2}} = H_e\left(\frac{a_e}{a}\right)^{\frac{3n}{n+1}}, \qquad \text{for } a \in [a_e, a_{\mathrm{rh}}). \tag{4.99}$$

The above solution is valid in the period between the end of inflation and the end of reheating, which we define by the inflaton-radiation equality, i.e.,

$$\rho_\phi(a_{\mathrm{rh}}) = \rho^{\mathrm{RH}}_{\mathrm{SM}}(a_{\mathrm{rh}}) \equiv \rho_{\mathrm{rh}}. \tag{4.100}$$

Inserting the generic form of the *inflaton decay width* (4.90), and using (4.99), enable us to find the following solution to the radiation energy density:

$$\rho^{\mathrm{RH}}_{\mathrm{SM}}(a) \simeq \frac{6n}{1+n}\widetilde{\Gamma}^e_{\phi\to FF}\, H_e M_{\mathrm{Pl}}^2$$

$$\times \begin{cases} \frac{n+1}{n+4-\beta_F(n+1)}\left[\left(\frac{a_e}{a}\right)^{\beta_F+\frac{3n}{1+n}} - \left(\frac{a_e}{a}\right)^4 \right], & \beta_F \neq \frac{n+4}{n+1}, \\ \left(\frac{a_e}{a}\right)^4 \ln\left(\frac{a}{a_e}\right), & \beta_F = \frac{n+4}{n+1}, \end{cases} \quad \text{for } a \in [a_e, a_{\rm rh}]. \tag{4.101}$$

During the early stages of reheating total energy budget of the Universe is dominated by the energy density of oscillating inflaton condensate. Hence, the background dynamics is mainly sensitive to the form of the inflaton potential, which, in turn, is determined by the value of n. On the other hand, the behavior of the radiation bath depends on both n and β_F parameters. Note that if

$$\beta_F < (n+4)/(n+1), \tag{4.102}$$

the first term in the square bracket in Eq. (4.101) quickly dominates over the second. On the other hand, if $\beta_F > (n+4)/(1+n)$ the energy density of the SM radiation decreases as a^{-4}, and becomes insensitive to the value of n.

Let us now discuss the late-time behavior, i.e., for $a \gg a_e$, of the solution (4.101) for a few *massless reheating scenarios*. At first, suppose that reheating is induced by the $\phi \to \mathbf{hh}$ or $\phi \to \boldsymbol{\mathcal{V}\mathcal{V}}$ interactions. In this case, the first term in (4.101) always dominates, since the condition (4.102) is satisfied for $n > 1/2$ if $\beta_F = 3(1+n)/(1+n)$. If reheating occurs as a result of ϕ coupling to (almost) massless SM fermions, then $\beta_F < (n+4)/(n+1)$ as long as $n \in (1/2, 7/2)$. On the other hand, if reheating is triggered by the derivative $\phi \to AA$ interactions, then $\rho_\phi \propto a^{-4}$ provided that $n > 13/8$. Finally, in the purely gravitational scenario, where the energy density of the inflaton field is transferred to the SM sector only via gravitational interactions, the second term in Eq. (4.101) dominates if $n > 7/8$. Therefore, depending on the value of n and the form of the inflaton interactions, one gets a very different evolution of the SM sector. The non-trivial power-law dependence of the radiation energy density on the scale factor during this phase is referred to as *non-standard reheating.*

There are several comments here in order. Firstly, let us specify conditions that must be satisfied to (re)populate the Universe. In order to achieve successful reheating, the energy density of the inflaton field must at some point equalize with the radiation energy density, according to the formula (4.100). Otherwise, SM degrees of freedom never capture the total energy budget of the Universe, and the standard cosmology is spoilt. To quantify this condition, we assume that $\rho_{\rm SM}$ experiences a power-law evolution with the scale factor, i.e., $\rho_{\rm SM} \propto a^s$. Using the solution for the inflaton energy density found in Eq.(3.63), the necessary but not sufficient condition for successful reheating can be formulated as follows:

$$-\frac{6n}{1+n} < s. \tag{4.103}$$

Limiting our attention to $n > 1/2$, and using Eq.(4.101) together with (4.95), one finds that the requirement (4.103) is satisfied:

- for $\phi \to \mathbf{hh}$ and $\phi \to \boldsymbol{\mathcal{V}\mathcal{V}}$ interactions if $n > \frac{1}{2}$,
- for $\phi \to \mathbf{\Psi\bar{\Psi}}$ interaction if $n \in \left(\frac{1}{2}, \frac{7}{2}\right)$, and for $n > \frac{7}{2}$,
- for $\phi \to$ AA interaction if $n \in \left(\frac{1}{2}, \frac{3}{2}\right)$, and for $n > 2$,
- for gravitational interactions $\phi \to h_{\mu\nu} \to \mathbf{hh}$ if $n > 2$.

For other values of n, which do not fulfill the above criterion, the energy density of the SM sector dilutes faster than the inflaton energy density, and since just after the end of inflation $\rho_\phi \gg \rho_{\rm SM}^{\rm RH}$ the inflaton-radiation equality (4.100) is never achieved. It should be highlighted that the above condition alone does not assure successful reheating, e.g., even if the energy density of radiation decreases slower than the inflaton energy density, its initial amount can be too low to overtake ρ_ϕ. Hence, other constraints on the reheating scenario must also be taken into account.

Secondly, we should emphasize that the whole SM sector is assumed here to emerge from the F field, which, in turn, is directly produced through the *inflaton decays*. In other words, once the F particles are created, they decay/scatter to the rest of the SM species and, that way, transfer their energy to other relativistic degrees of freedom.

Thirdly, we assume that the radiation bath thermalizes instantaneously. This assumption seems quite justified since the scattering of F particles should be efficient enough to guarantee instantaneous thermalization.

Finally, let us define the thermal bath temperature T through the following relation:

$$T(a) = \left(\frac{30}{\pi^2 g_{\star\rho}(T)}\right)^{1/4} [\rho_{\rm SM}^{\rm RH}(a)]^{1/4}\,, \tag{4.104}$$

with $g_{\star\rho}(T)$ counting an effective number of relativistic degrees of freedom at the temperature T.

In the light of (4.101), the non-standard evolution of the radiation energy density implies a non-trivial relation between T and a during reheating. More precisely, inserting the solution (4.101) into (4.104), we find

$$\begin{aligned} T_{\rm RH}(a) \approx &\left(\frac{180\cdot n\,\widetilde{\Gamma}^e_{\phi\to {\rm FF}} H_e M_{\rm Pl}^2}{(n+1)\pi^2 g_{\star\rho}(T)}\right)^{1/4} \\ &\times\begin{cases} \left[\frac{n+1}{4+n-\beta_F(1+n)}\right]^{1/4}\left(\frac{a_e}{a}\right)^{\frac{\beta_F}{4}+\frac{3n}{4(n+1)}}, & \beta_F < \frac{n+4}{n+1}, \\ \frac{a_e}{a}[\ln{(a/a_e)}]^{1/4}, & \beta_F = \frac{n+4}{n-1}, \\ \left[\frac{n+1}{\beta_F(1+n)-n-4}\right]^{1/4}\frac{a_e}{a}, & \beta_F > \frac{n+4}{n+1}, \end{cases} \qquad \text{for } a\in[a_e, a_{\rm rh}]. \end{aligned} \tag{4.105}$$

Note that above, we have dropped either the first or the second term in the bracket in Eq.(4.101) depending on the relation between β_F and $(n+4)/(n+1)$. Hence, (4.105) reflects the late-time behavior of the thermal bath temperature and is not applicable at the onset of reheating when both terms of Eq.(4.101) are comparable.

Moreover, from the condition (4.100), we get the scale factor at the end of reheating

$$a_{\rm rh} = a_e\begin{cases} \zeta_1^{\frac{n+1}{3n-\beta_F(n+1)}}, & \beta_F < \frac{n+4}{n+1}, \\ \zeta_2^{\frac{n+1}{2(n-2)}} W^{\frac{n+1}{2(n-2)}}(\zeta_2)\,, & \beta_F = \frac{n+4}{n+1}, \\ (-\zeta_1)^{\frac{n+1}{2(n-2)}}\,, & \beta_F > \frac{n+4}{n+1}, \end{cases} \tag{4.106}$$

with

$$\zeta_1 \equiv \frac{n+4-\beta_F(n+1)}{2n}H_e/\widetilde{\Gamma}^e_{\phi\to{\rm FF}}, \qquad \zeta_2 \equiv \frac{n-2}{n}H_e/\widetilde{\Gamma}^e_{\phi\to{\rm FF}}. \tag{4.107}$$

Above, $W(z)$ denotes the Lambert W function defined as the function satisfying $z = W(z)e^{W(z)}$ [348].

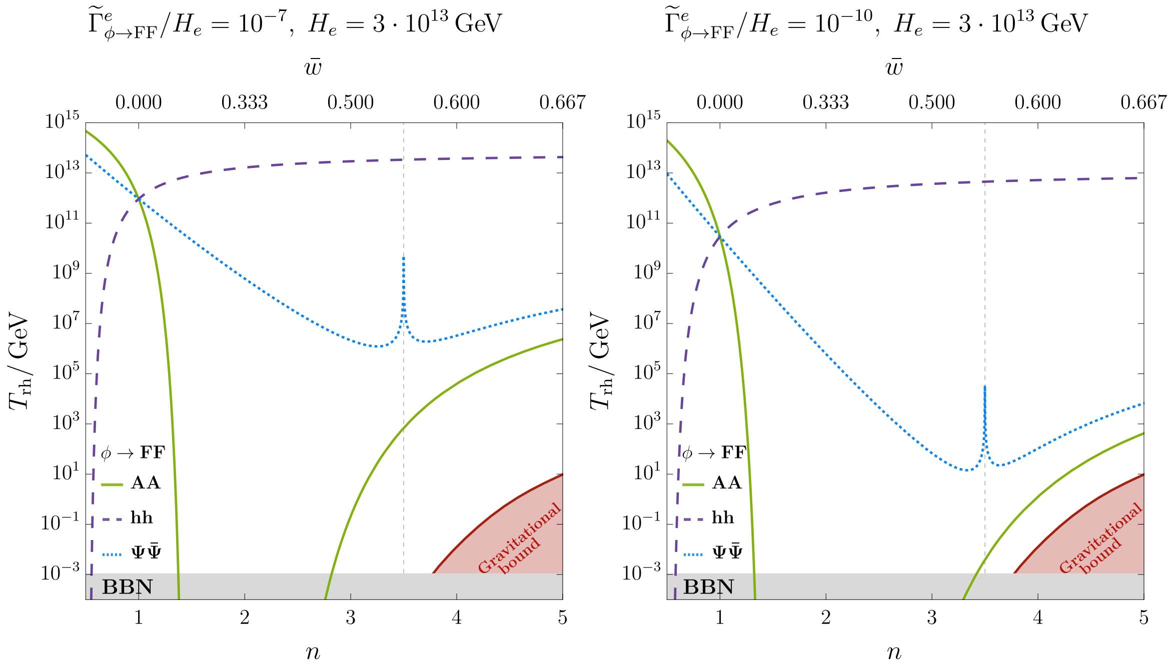

FIGURE 4.1: The reheating temperature as a function of the index n (the averaged equation-of-state parameter $\bar{w}$) in different reheating models, i.e., driven by $\phi - A$ (solid green), $\phi - \mathbf{h}$ (loosely dashed purple), $\phi - \mathbf{\Phi}$ (dashed blue) and gravitational (solid red) interactions. In the left (right) panel, the adopted initial value of the *inflaton decay width* is $\widetilde{\Gamma}_{\phi\to\mathrm{FF}} = 10^{-7}H_e$ ($\widetilde{\Gamma}_{\phi\to\mathrm{FF}} = 10^{-10}H_e$). Note that pale red and gray regions are excluded due to gravitational bound on T_{rh} and the BBN constraint (4.140), respectively.

Consequently, the *reheating temperature*, i.e., the temperature at the end of reheating, is

$$T_{\mathrm{rh}} \simeq \begin{cases} \left(\frac{90\,H_e^2 M_{\mathrm{Pl}}^2}{\pi^2 g_{\star\rho}(T_{\mathrm{rh}})}\right)^{1/4} \zeta_1^{\frac{3n}{2\beta_F(n+1)-6n}}, & \beta_F < \frac{n+4}{n+1}, \\ \left(\frac{90(n-2)H_e^2 M_{\mathrm{Pl}}^2}{(n+1)\pi^2 g_{\star\rho}(T_{\mathrm{rh}})}\right)^{1/4} \zeta_2^{\frac{3n}{4(2-n)}} W^{\frac{n+1}{2(2-n)}}(\zeta_2)\,[\ln \zeta_2^{\frac{n+1}{2(n-2)}} W^{\frac{n+1}{2(n-2)}}(\zeta_2)]^{1/4}, & \beta_F = \frac{n+4}{n-1}, \\ \left(\frac{90\,H_e^2 M_{\mathrm{Pl}}^2}{\pi^2 g_{\star\rho}(T_{\mathrm{rh}})}\right)^{1/4} (-\zeta_1)^{\frac{3n}{4(2-n)}}, & \beta_F > \frac{n+4}{n+1}. \end{cases} \tag{4.108}$$

Analogously, the Hubble rate at the end of reheating is given by

$$H_{\mathrm{rh}} \simeq H_e \begin{cases} \zeta_1^{\frac{3n}{\beta_F(n+1)-3n}}, & \beta_F < \frac{n+4}{n+1}, \\ \zeta_2^{\frac{3n}{2(2-n)}} W^{\frac{3n}{2(2-n)}}(\zeta_2), & \beta_F = \frac{n+4}{n-1}, \\ (-\zeta_1)^{\frac{3n}{2(2-n)}}, & \beta_F > \frac{n+4}{n+1}. \end{cases} \tag{4.109}$$

It is important to stress that T_{rh} is not a maximal temperature that the SM sector could reach during the reheating phase. The thermal bath temperature could rise to several orders of magnitude above T_{RH} [337]. Namely, the temperature of the SM sector has a peak at

$$a_{\max} \equiv a_e \begin{cases} \left[\frac{1}{4}\left(\beta_F + \frac{3n}{n+1}\right)\right]^{\frac{n+1}{\beta_F(n+1)-n-4}}, & \beta_F \neq \frac{n+4}{n+1}, \\ e^{1/4}, & \beta_F = \frac{n+4}{n+1}, \end{cases} \tag{4.110}$$

such that its maximal value can be estimated from the following formula:

$$T_{\max} \equiv T_{\mathrm{RH}}(a_{\max}) \approx \left(\frac{180 \cdot n\, \widetilde{\Gamma}^{e}_{\phi\to\mathrm{FF}} H_e M_{\mathrm{Pl}}^2}{(n+1)\pi^2 g_{\star\rho}(T_{\max})}\right)^{1/4}$$
$$\times \begin{cases} \left[\frac{n+1}{4+n-\beta_F(n+1)}\right]^{1/4} \left[\frac{1}{4}\left(\beta_F + \frac{3n}{n+1}\right)\right]^{\frac{3n+\beta_F(1+n)}{4[4+n-\beta_F(1+n)]}}, & \beta_F < \frac{n+4}{n+1}, \\ \frac{1}{\sqrt{2}} e^{-1/4}, & \beta_F = \frac{n+4}{n+1}, \\ \left[\frac{n+1}{\beta_F(n+1)-4-n}\right]^{1/4} \left[\frac{1}{4}\left(\beta + \frac{3n}{1+n}\right)\right]^{\frac{n+1}{4+n-\beta_F(n+1)}}, & \beta_F > \frac{n+4}{n+1}. \end{cases} \tag{4.111}$$

4.3 Reheating scenarios

All the above results concerning the dynamics of the SM sector during reheating are rather generic. They can be employed in any perturbative reheating model in which the inflaton field oscillates around the minimum of monomial potential $\sim |\phi|^{2n}$, daughter particles are approximately massless, and the evolution of the *inflaton decay rate* can be parametrized by a power-law formula (4.90). As we already have pointed out, ϕ might also transfer its energy to the SM radiation through several direct or indirect channels. In the considered scenario, direct $\phi-$ SM interactions are always accompanied by irreducible gravitational interactions. Depending on the relative relation between $\Gamma_{\phi\to\mathrm{FF}}$ and $\Gamma^{\mathrm{grav}}_{\phi\to\mathrm{FF}}$, reheating is achieved either as a result of the *inflaton decay* into the pairs of the SM bath or via purely gravitational interactions among ϕ and SM species. In the general case, both *decay rates* are time-dependent, implying that the relation between these two might change during reheating. Namely, it is conditioned upon the strength of the $\phi - F$ coupling as well as the form of the inflaton-SM interactions and the shape of the inflaton potential through n. Depending on these factors, one distinguishes two possible scenarios for perturbative reheating:

1. **standard reheating** - energy stored in the oscillations of ϕ condensate is injected into radiation as a result of direct interactions between ϕ and SM species; indirect gravitational interactions are negligible throughout the whole period of reheating,

2. **mixed scenario** - both direct and indirect inflaton interactions partially govern the reheating dynamics.

To determine which case occurs for a given coupling constant $g_{F\phi}$, n, and the inflationary scale Λ, which sets H_e and hence ρ_e, ω_e, one needs to examine the condition,

$$\Gamma_{\phi\to\mathrm{FF}}(a) > \Gamma^{\mathrm{grav}}_{\phi\to\mathbf{hh}}(a). \tag{4.112}$$

4.3.1 Standard reheating

Suppose the above condition holds during the entire reheating phase, i.e., for $a \in (a_e, a_{\mathrm{rh}})$. Then, the **standard reheating** scenario is realized, and the inflaton energy is injected to the visible sector solely through direct $\phi-$ SM interactions. Above, we have restricted our attention to *massless reheating scenario*, in which the inflaton energy density is transferred gravitationally only to the SM scalars, and therefore, $\Gamma^{\mathrm{grav}}_{\phi\to\mathrm{FF}} \simeq \Gamma^{\mathrm{grav}}_{\phi\to,\mathbf{hh}}$. It is worth underlining that for all considered values of n, gravitational *decay rate* $\Gamma^{\mathrm{grav}}_{\phi\to\mathbf{hh}}(a)$ decreases faster than $\Gamma_{\phi\to\mathrm{FF}}(a)$. Hence, one infers that reheating is controlled only by direct $\phi-$ SM interactions, provided that

$$\widetilde{\Gamma}^{e}_{\phi\to\mathrm{FF}} > \widetilde{\Gamma}^{\mathrm{grav,e}}_{\phi\to\mathbf{hh}}. \tag{4.113}$$

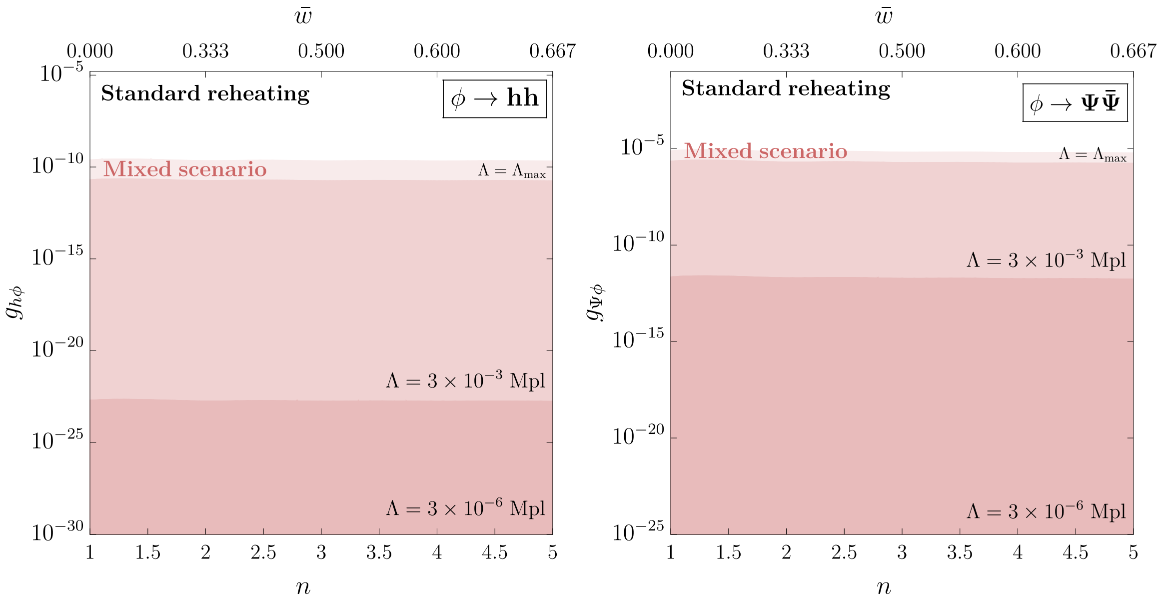

FIGURE 4.2: The relation between the dimensionless coupling constants and n ($\bar{w}$) for which the standard reheating (white region) and the mixed scenario (colored region) are realized for the scalar (left panel) and fermionic (right panel) cases. The adopted values of the inflationary scale Λ are specified in each region. The maximal scale corresponds to $\Lambda_{\max} \simeq 5.6 \times 10^{-3}\, M_{\rm Pl}$, see Eq.(3.148).

Using Eqs.(4.91)-(4.94) together with Eq.(4.96), one finds that it happens if the coupling constants $\{g_{h\phi}, g_{\Psi\phi}, g_{\mathcal{V}\phi}, h_{A\phi}\}$ satisfy

$$g_{h\phi}^2 \gtrsim \left(\frac{\Lambda}{M_{\rm Pl}}\right)^8 \left(\frac{\rho_e}{\Lambda^4}\right)^{\frac{2n-1}{n}} \frac{\sum_k k|\mathcal{P}_k^{2n}|^2}{\sum_k k|\mathcal{P}_k|^2}, \tag{4.114}$$

$$g_{\Psi\phi}^2 \gtrsim \frac{2}{\#_\Psi} \left(\frac{\Lambda}{M_{\rm Pl}}\right)^6 \left(\frac{\Lambda}{\omega_e}\right)^2 \frac{\rho_e}{\Lambda^4} \frac{\sum_k k|\mathcal{P}_k^{2n}|^2}{\sum_k k^3|\mathcal{P}_k|^2}, \tag{4.115}$$

$$g_{\mathcal{V}\phi}^2 \gtrsim \frac{8}{\#_\mathcal{V}(1+\delta_\mathcal{V})^2} \left(\frac{\Lambda}{M_{\rm Pl}}\right)^8 \left(\frac{\rho_e}{\Lambda^4}\right)^{\frac{2n-1}{n}} \frac{\sum_k k|\mathcal{P}_k^{2n}|^2}{\sum_k k|\mathcal{P}_k|^2}, \tag{4.116}$$

$$h_{A\phi}^2 \gtrsim \frac{4}{\#_A} \frac{\Lambda^2}{\omega_e^4} \left(\frac{\Lambda}{M_{\rm Pl}}\right)^6 \left(\frac{\rho_e}{\Lambda^4}\right)^{\frac{1}{n}} \frac{\sum_k k|\mathcal{P}_k^{2n}|^2}{\sum_k k^5|\mathcal{P}_k|^2}. \tag{4.117}$$

Note that the above bounds feebly depend on the exponent n, cf. Fig.(4.2). This is because the ratios of the summation factors and ρ_e/Λ^4 are of order one. Hence, all constraints are mainly sensitive to the inflationary scale Λ (or equivalently, the Hubble rate H_e). Thus, the most stringent limits are obtained for $\Lambda_{\max}$ Eq.(3.148). For instance, in the Higgs boson-induced reheating model (left panel of Fig.(4.2)), triggered by direct $\phi - \mathbf{h}$ coupling, gravitational interactions can be neglected as long as $g_{h\phi} \gtrsim 3 \cdot 10^{-10}$ for $\Lambda_{\max}$, whereas for the lower value of $\Lambda = 1.6 \cdot 10^{-3} M_{\rm Pl}$, used in this analysis, one finds $g_{h\phi} \gtrsim 6.6 \cdot 10^{-12}$. For the fermionic case (right panel of Fig.(4.2)), for a given inflationary scale Λ, the standard reheating scenario occurs for stronger $\phi - \mathbf{\Psi}$ coupling.

4.3.2 Mixed scenario

On the other hand, if Eq.(4.112) is violated at the onset of reheating, but $\Gamma_{\phi\to\mathrm{FF}}$ starts to dominate over $\Gamma^{\mathrm{grav}}_{\phi\to\mathbf{hh}}$ at some point during reheating, then the **mixed scenario** is accomplished. In this case, there exists $a_{\mathbf{c}} \in (a_e, a_{\mathrm{rh}})$, such that

$$\widetilde{\Gamma}_{\phi\to\mathrm{FF}}(a_{\mathbf{c}}) = \widetilde{\Gamma}^{\mathrm{grav}}_{\phi\to\mathbf{hh}}(a_{\mathbf{c}}), \qquad a_{\mathbf{c}} \in (a_e, a_{\mathrm{rh}}). \tag{4.118}$$

Note that above a_{rh} should be understood as $a_{\mathrm{rh}} = \min(a^{\mathrm{F}}_{\mathrm{rh}}, a^{\mathrm{grav}}_{\mathrm{rh}})$, where $a^{\mathrm{F}}_{\mathrm{rh}}$ denotes the scale factor at the end of reheating induced by direct ϕ − SM interactions, whereas $a^{\mathrm{grav}}_{\mathrm{rh}}$ is given by

$$a^{\mathrm{grav}}_{\mathrm{rh}} \equiv a_e \left(\frac{8n-7}{2n} \frac{H_e}{\Gamma^{\mathrm{grav,e}}_{\phi\to\mathbf{hh}}} \right)^{\frac{n+1}{2(n-2)}}, \qquad n > 2. \tag{4.119}$$

For the considered direct inflaton-SM interaction, one finds,

$$a_c^{\mathbf{h}} = a_e \left(\frac{\Lambda}{M_{\mathrm{Pl}}}\right)^{\frac{4(1+n)}{3(2n-1)}} g_{h\phi}^{-\frac{1+n}{3(2n-1)}} \left(\frac{\rho_e}{\Lambda^4}\right)^{\frac{1+n}{6n}} \left[\frac{\sum_k k|\mathcal{P}_k^{2n}|^2}{\sum_k k|\mathcal{P}_k|^2}\right]^{\frac{1+n}{6(2n-1)}}, \tag{4.120}$$

$$a_c^{\mathbf{\Psi}} = a_e \left(\frac{\#_\Psi g^2_{\Psi\phi}}{2}\right)^{-\frac{n+1}{6n}} \left(\frac{\Lambda}{\omega_e}\right)^{\frac{n+1}{3n}} \left(\frac{\Lambda}{M_{\mathrm{Pl}}}\right)^{\frac{n+1}{n}} \left(\frac{\rho_e}{\Lambda^4}\right)^{\frac{n+1}{6n}} \left[\frac{\sum_k k|\mathcal{P}_k^{2n}|^2}{\sum_k k^3|\mathcal{P}_k|^2}\right]^{\frac{1+n}{6n}}, \tag{4.121}$$

$$a_c^{\boldsymbol{\mathcal{V}}} = a_e \left(\frac{\Lambda}{M_{\mathrm{Pl}}}\right)^{\frac{4(1+n)}{3(2n-1)}} \left(\frac{\#_{\mathcal{V}}}{2}(1+\delta_{\mathcal{V}})^2 g^2_{h\phi}\right)^{-\frac{1+n}{6(2n-1)}} \left(\frac{\rho_e}{\Lambda^4}\right)^{\frac{1+n}{6n}} \left[\frac{\sum_k k|\mathcal{P}_k^{2n}|^2}{\sum_k k|\mathcal{P}_k|^2}\right]^{\frac{1+n}{6(2n-1)}}, \tag{4.122}$$

$$a_c^{\mathrm{A}} = a_e \left(\frac{4\Lambda^2}{\#_A \omega_e^4 h^2_{A\phi}}\right)^{\frac{1+n}{8}} \left(\frac{\Lambda}{M_{\mathrm{Pl}}}\right)^{\frac{3(1+n)}{4}} \left(\frac{\rho_e}{\Lambda^4}\right)^{\frac{1+n}{8n}} \left[\frac{\sum_k k|\mathcal{P}_k^{2n}|^2}{\sum_k k^5|\mathcal{P}_k|^2}\right]^{\frac{1+n}{8}}. \tag{4.123}$$

In the **mixed scenario**, reheating is governed initially, i.e., between $a \in (a_e, a_{\mathrm{c}})$, by indirect gravitational interaction. In the vicinity of a_{c}, both *decay channels* are relevant, whereas in the period between a_c and a_{rh}, the inflaton energy is injected into the SM sector mainly via direct interactions. Hence, in this scenario, the completion of reheating is exclusively sparked by the direct $\phi-$SM coupling. Note that the reverse situation, i.e., reheating induced direct ϕ interactions and completed by indirect, gravitational interactions, is not possible since $\Gamma^{\mathrm{grav}}_{\phi\to\mathbf{hh}}$ redshifts faster than $\Gamma_{\phi\to\mathbf{hh}}$ for all considered values of n.

It is worth stressing that in the **mixed scenario**, the maximal temperature of the SM sector is controlled by gravitational interactions. Hence, such processes might provide an ultimate lower bound on the maximum temperature of the thermal bath. Using $\beta^{\mathrm{grav}}_{\mathbf{h}} = 3(3n-1)/(1+n)$ and (4.111), one finds

$$\begin{aligned} T^{\mathrm{grav}}_{\max} \simeq & \left(\frac{45}{\pi^3 g_{\star,\rho}(T_{\max})} \omega_e H_e M^2_{\mathrm{Pl}} \sum_k k|\mathcal{P}_k^{2n}|^2\right)^{1/4} \frac{\Lambda}{M_{\mathrm{Pl}}} \left(\frac{\rho_e}{\Lambda^4}\right)^{\frac{3n-1}{8n}} \\ & \times \begin{cases} \left\{ \left(\frac{n+1}{7-8n}\right) \left[\left(3 - \frac{15}{4(n+1)}\right)^{\frac{3(1-4n)}{8n-7}} - \left(3 - \frac{15}{4(n+1)}\right)^{\frac{4(1+n)}{8n-7}} \right] \right\}^{1/4}, & n \neq 7/8, \\ \frac{1}{\sqrt{2}} e^{-1/4}, & n = \frac{7}{8}. \end{cases} \end{aligned} \tag{4.124}$$

The numerical factors depending on the value of n are of the order $\mathcal{O}(10^{-1})$, and for the quadratic (quartic) inflaton potential, i.e., $n = 1$ ($n = 2$), the above expression gives $T^{\mathrm{grav}}_{\max} \simeq 6.1 \cdot 10^{12}$ GeV ($T^{\mathrm{grav}}_{\max} \simeq 5.5 \cdot 10^{12}$ GeV) for $H_e = 3 \cdot 10^{13}$ GeV, cf. Fig.(4.3). These results agree with estimates found in Ref. [349]. It is important to stress that the above formulas

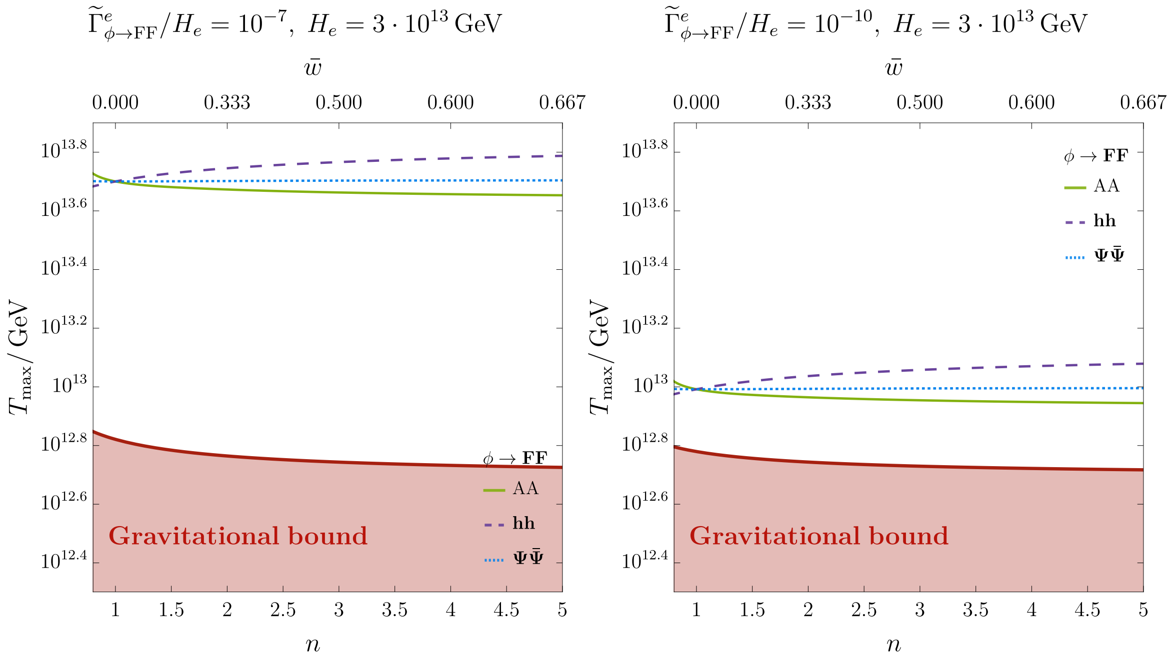

FIGURE 4.3: The maximal temperature obtained by the SM bath as a function of the index n (the averaged equation-of-state parameter $\bar{w}$) in different reheating models, i.e., driven by $\phi - A$ (solid green), $\phi - \mathbf{h}$ (loosely dashed purple), $\phi - \mathbf{\Psi}$ (dashed blue) and gravitational (solid red) interactions. In the left (right) panel, the adopted initial value of the *inflaton decay width* is $\widetilde{\Gamma}_{\phi\to\mathrm{FF}} = 10^{-7}H_e$ ($\widetilde{\Gamma}_{\phi\to\mathrm{FF}} = 10^{-10}H_e$). Note that the pale red region is excluded due to gravitational bound on $T_{\max}$, see Eq. (4.125).

provide an absolute lower bound on the maximal thermal bath temperature for a given n and inflationary scale Λ, which sets H_e, ω_e, and ρ_e. Namely, the following condition:

$$T^{\mathrm{grav}}_{\max} \leq T_{\max}, \tag{4.125}$$

must hold in any perturbative reheating model. This, in principle, means that the Universe must have reached this temperature regardless of the details of the reheating process. Suppose in any considered scenario, the predicted value of $T_{\max}$ is lower than the value obtained from Eq.(4.124). In that case, gravitational interactions should have been taken into account since this process dominates at the onset of reheating and thus determines the maximum temperature of the SM sector.

4.3.3 Purely gravitational reheating

In particular, one could image the third scenario, in which the condition (4.112) is violated throughout the whole reheating, such that

$$\Gamma_{\phi\to\mathrm{FF}}(a^{\mathrm{grav}}_{\mathrm{rh}}) < \Gamma^{\mathrm{grav}}_{\phi\to\mathbf{hh}}(a^{\mathrm{grav}}_{\mathrm{rh}}). \tag{4.126}$$

The above condition defines the **purely gravitational reheating** - extreme scenario, in which direct inflaton interactions with the SM species are so feeble, or even do not exist at all, that reheating can only be achieved the Planck suppressed gravitational interactions. It can be considered as the minimal yet natural mechanism to drive the transition from the inflationary phase to the radiation-dominated epoch. According to the discussion below

(4.103), such a scenario might only be realized for a stiff inflaton potential, i.e., $n > 2$. In this case all reheating observables, i.e., $\{T_{\max}, a_{\rm rh}, T_{\rm rh}, H_{\rm rh}\}$, would be determined solely by the inflationary scale Λ, and the form of the inflaton potential during reheating. However, as pointed out in Ref.[350], the possibility of the **purely gravitational reheating** is excluded by constraints on dark radiation for excessive gravitational waves produced from inflation. At this point, we should stress that in the general case, one could also investigate the *non-minimal gravitational reheating scenario* in which the ϕ and the Higgs fields have non-minimal couplings to the gravity of the form

$$-\frac{\xi_\phi}{2M_{\rm Pl}^2}|\phi|^2\widetilde{\mathcal{R}}, \qquad \text{and} \qquad -\frac{\xi_{\mathbf{h}}}{2M_{\rm Pl}^2}|\mathbf{h}|^2\widetilde{\mathcal{R}}, \tag{4.127}$$

where $\widetilde{\mathcal{R}}$ is the Ricci scalar in the Jordan frame, $|\xi_\phi| \ll M_{\rm Pl}^2/\langle\phi\rangle^2$ [349], $|\xi_{\mathbf{h}}| \lesssim 10^{15}$ [351, 352], and $\xi_{\mathbf{h}} \sim \mathcal{O}(10^{-2})$ [353–355]. Such a scenario has been considered, for instance, by the authors of Ref.[349, 350, 356] who claimed that minimal gravitational interactions dominate over non-minimal ones when [349]

$$12\xi_\phi\,\xi_{\mathbf{h}} + 3\xi_{\mathbf{h}} + 2\xi_\phi < \frac{1}{2}. \tag{4.128}$$

In this work, we, however, focus on the minimal scenario, ignoring the non-minimal contribution, setting $\xi_\phi \to 0$ and $\xi_{\mathbf{h}} \lesssim 1/6$.

In the remaining part of this chapter, we will elaborate on the **Higgs-induced reheating**, governed by the cubic $g_{h\phi}\phi|\mathbf{h}|^2$ coupling. In particular, we will distinguish *massless* and *massive reheating scenarios* and discuss the role of the inflaton-induced mass of the Higgs boson on reheating dynamics. But before we move on to this part, let us first discuss constraints on reheating models.

4.4 Constraints on reheating models

Since existing cosmological experiments cannot directly probe the reheating phase, it might be crucial to look for some indirect imprints of the reheating dynamics, some unique predictions allowing us to disentangle the plethora of post-inflationary models and rule out unreliable scenarios. In this section, we outline the procedure for obtaining constraints on the number of e-folds from the end of inflation to the end of the reheating phase, i.e.,

$$N_{\rm rh} = \ln\left(\frac{a_{\rm rh}}{a_e}\right), \tag{4.129}$$

using the current bounds on the inflationary observables. This will allow us to establish a connection between the physics of reheating determined by the form and strength of the inflaton coupling and the CMB observables.

First, let us note that the CMB pivot scale $k_\star^{\rm CMB} \equiv k_\star$ links the primordial Universe with the late one. More precisely, it relates the inflationary quantities, measured when the $k_\star$ mode crosses the Hubble radius, to the late-time observables corresponding to the moment when the pivot scale re-enters the horizon. In particular, using the fact that the horizon crossing occurs when $k_\star = a_\star H_\star$, we can evolve the scale factor through different epochs, as

$$\frac{k_\star}{H_\star} = \frac{a_\star}{a_e}\frac{a_e}{a_{\rm rh}}\frac{a_{\rm rh}}{a_{\rm r.m.e}}a_{\rm r.m.e}, \tag{4.130}$$

where $a_{\rm r.m.e}$ denotes the scale factor at the radiation-matter equality. By taking the logarithm of the above expression, one gets

$$\ln\left(\frac{k_\star}{H_\star}\right) = -N_\star - N_{\rm rh} - N_{\rm rd} + \ln(a_{\rm r.m.e}), \tag{4.131}$$

where $N_\star \equiv \ln(a_e/a_\star)$ denotes the number of e-folds between the horizon exit of the pivot scale $k_\star$ and the beginning of reheating, which in the slow-roll approximation is determined by the following integral:

$$N_\star \simeq \frac{1}{M_{\rm Pl}} \int_{\phi_e}^{\phi_\star} \frac{1}{\sqrt{2\epsilon_V}} d\phi, \tag{4.132}$$

whereas $N_{\rm RD} \equiv \ln(a_{\rm r.m.e}/a_{\rm rh})$ is the number of e-folds during the radiation-dominated epoch. Using the results obtained in the previous section, one can relate the reheating number of e-folds $N_{\rm rh}$ to the energy density of ϕ at the onset of reheating, i.e., $\rho_e \equiv 3V(\phi_e)/2$. Namely, from Eq. (4.100), one has

$$\rho_{\rm rh} = \rho_e \left(\frac{a_e}{a_{\rm rh}}\right)^{\frac{6n}{1+n}}. \tag{4.133}$$

On the other hand, $\rho_{\rm rh}$ can also be expressed in terms of the reheating temperature as

$$\rho_{\rm rh} = \frac{\pi^2 g_{\star\rho,{\rm rh}}}{30} T_{\rm rh}^4, \tag{4.134}$$

with $g_{\star\rho,{\rm rh}} \equiv g_{\star\rho}(T_{\rm rh})$ being the total number of relativistic d.o.f. at the reheating temperature $T_{\rm rh}$. Assuming no extra relativistic d.o.f. beyond the SM, we set $g_{\star rho,{\rm rh}} \simeq 106.75$.
Hence, the number of e-folds during reheating phase is given by

$$N_{\rm rh} = \frac{1+n}{6n} \ln\left(\frac{45}{\pi^2 g_{\star\rho,{\rm rh}}} \frac{V(\phi_e)}{T_{\rm rh}^4}\right). \tag{4.135}$$

In what follows, we assume that there is no additional entropy injection after the end of reheating. Thus, employing the entropy conservation $g_{\star s}(T)a^3T^3 = const.$, where $g_{\star s}(T)$ counts the number of relativistic d.o.f. contributing to entropy density at temperature T, one obtains the following relation between $T_{\rm rh}$, and the temperature at matter-radiation equality:

$$T_{\rm rh} = \left(\frac{g_{\star s,{\rm r.m.e}}}{g_{\star s,{\rm rh}}}\right)^{1/3} \left(\frac{a_{\rm r.m.e}}{a_{\rm rh}}\right) T_{\rm r.m.e}, \tag{4.136}$$

where $g_{\star s,{\rm r.m.e}} \equiv g_{\star s}(T_{\rm r.m.e})$ and $g_{\star s,{\rm rh}} \equiv g_{\star s}(T_{\rm rh})$.
Inserting the above relation into Eq. (4.135), one finds

$$\begin{aligned} N_{\rm rh} &= \frac{1+n}{6n} \ln\left(\frac{45}{\pi^2 g_{\star,{\rm rh}}} \frac{V(\phi_e)}{T_{\rm r.m.e}^4} \left(\frac{g_{\star s,{\rm rh}}}{g_{\star s,{\rm r.m.e}}}\right)^{4/3} \left(\frac{a_{\rm rh}}{a_{\rm r.m.e}}\right)^4\right), \\ &\simeq 4 \cdot \frac{1+n}{6n}\left[\frac{1}{4}\ln\left(\frac{45}{\pi^2 g_{\star,{\rm rh}}}\right) + \ln\left(\frac{\Lambda}{T_{\rm r.m.e}}\right) + \frac{1}{3}\ln\left(\frac{g_{\star s,{\rm rh}}}{g_{\star s,{\rm r.m.e}}}\right) - N_{\rm rd}\right], \end{aligned} \tag{4.137}$$

where in the last step we have used $V(\phi_e) \approx \Lambda^4$. In general, we could also use a more accurate approximation utilizing Eq.(3.147); however, for the purpose of this analysis, the adopted approximation is sufficient.

Now, one can use Eq. (4.131) to eliminate $N_{\rm rd}$ from the above expression. After simple algebra, we obtain

$$N_{\rm rh} \simeq \frac{2(n+1)}{n-2}\left[\frac{1}{4}\ln\Big(\frac{45}{\pi^2 g_{\star,\rm rh}}\Big) + \frac{1}{3}\ln\Big(\frac{g_{\star s,\rm rh}}{g_{\star s,\rm r.m.e}}\Big) - \ln(a_{\rm r.m.e}) + \ln\Big(\frac{\Lambda}{H_\star}\Big) + \ln\Big(\frac{k_\star}{T_{\rm r.m.e}}\Big) + N_\star\right]. \tag{4.138}$$

The above relation is only valid if $n \neq 2$. This results from the fact that for the quartic inflaton potential, i.e., $n = 2$, the rate of the Universe's expansion is the same during reheating and radiation-dominated epoch.
Adopting $g_{\star,\rm rh} \simeq g_{\star s,\rm rh} = 106.75$, $g_{\star s,\rm r.m.e} = 3.94$, $a_{\rm r.m.e} \simeq 1/3400$, $T_{\rm r.m.e} \simeq 0.8\,\text{eV}$ and $k_\star = 0.05\,\text{Mpc}^{-1}$, we get

$$N_{\rm rh} \approx \frac{2(n+1)}{2-n}\left[61.6 - \ln\Big(\frac{\Lambda}{H_\star}\Big) - N_\star\right], \tag{4.139}$$

Hence, for $n \neq 2$, the above relation limits the duration of the reheating phase from the inflationary observables $\Lambda, N_\star$. Furthermore, another constraint can be imposed by utilizing the BBN lower-bound on the reheating temperature [272, 357–362]

$$T_{\rm rh} \gtrsim T_{\rm BBN} \sim 4\ \text{MeV}. \tag{4.140}$$

Using (4.135) and assuming that $V(\phi_e) \approx \Lambda^4$, one finds the following upper bound on the reheating number of e-folds:

$$N_{\rm rh} \lesssim \frac{2(n+1)}{3n}\left[6.7 + \ln\Big(\frac{\Lambda}{1\ \text{GeV}}\Big)\right]. \tag{4.141}$$

Hence for $\Lambda \lesssim 1.4 \times 10^{16}$ GeV Eq.(3.148), one obtains

$$N_{\rm rh} \lesssim 59 \cdot \frac{n+1}{2n}, \tag{4.142}$$

and for $n = 2$, one finds $N_{\rm rh} \lesssim 44$.
in Table 4.3, we summarize the constraints on $N_{\rm rh}$ for several values of n used in the forthcoming analysis.

α	n	$N_{\rm rh}[n_s : 1\sigma]$	$N_{\rm rh}[n_s : 2\sigma]$
1/6	2/3	13.8	26.1
1/6	1	22.0	41.7
1/6	3/2	48.0	47.8
1	2/3	15.2	27.5
1	1	23.4	43.1
1	3/2	47.8	47.7

TABLE 4.3: Constraints on $N_{\rm rh}$ for different values of α and n. For $n = 2$, the constraint is only from the lower limit on reheating temperature from BBN, which is $N_{\rm rh} \lesssim 44$.

4.5 Higgs boson-induced reheating

Now let us consider the *Higgs boson reheating* triggered by the cubic interaction of the inflaton with the SM Higgs doublet. So far, we have neglected the mass of final states. However, any daughter particles F inevitably acquire a non-zero mass due to their direct coupling to the inflaton fields. The non-zero mass m_F of the F field has a negligible impact on the reheating dynamics provided that $m_F \ll m_\phi$. However, if m_F becomes larger or comparable with m_ϕ, it generates a kinematic suppression of the SM quanta production, which could have non-trivial implications on the evolution of the SM radiation. In what follows, we illustrate this phenomenon on the example of *massive Higgs reheating scenario*, for which the non-zero mass of the **h** field cannot be neglected during reheating.

4.5.1 The model

In our model, the effective density Lagrangian of the Higgs boson during the reheating phase has the form

$$\sqrt{-g}\mathcal{L}_{\mathbf{h}} \supset g^{\mu\nu}\left(\partial_\nu \boldsymbol{h}\right)^\dagger\left(\partial_\mu \boldsymbol{h}\right) - g_{h\phi}M_{\rm Pl}\phi(t)|\boldsymbol{h}|^2 - V(\boldsymbol{h}), \quad V(\boldsymbol{h}) = \lambda_h\left(|\boldsymbol{h}|^2 - \frac{v_{\rm EW}^2}{2}\right)^2, \tag{4.143}$$

where λ_h is the Higgs-boson quartic coupling. At the scale of electroweak interaction $v_{\rm EW} \simeq$ 246 GeV, the value of Higgs quartic coupling is $\lambda_h \simeq 0.13$, corresponding to the Higgs mass $m_{h_0}^{\rm EW} = 125$ GeV. Since the energy scale of inflation and reheating is typically much higher than the electroweak scale, we can neglect the bare mass in $V(\boldsymbol{h})$ and approximate the Higgs potential by

$$V(\boldsymbol{h}) \simeq \lambda_h|\boldsymbol{h}|^4, \qquad \text{for } a < a_{\rm rh}. \tag{4.144}$$

Consequently, during the reheating phase, the Higgs mass parameter is given by

$$\mu_h^2 = g_{h\phi}M_{\rm Pl}\phi(t). \tag{4.145}$$

The above term is responsible for the generation of a non-trivial mass for all four components, h_i, of the Higgs doublet, i.e.,

$$m_{h_i}^2 = g_{h\phi}M_{\rm Pl}\,\varphi\begin{cases}|\mathcal{P}|, & \mathcal{P} > 0,\ i = 0,1,2,3,\\ |\mathcal{P}|, & \mathcal{P} < 0,\ i = 0,\\ \infty, & \mathcal{P} < 0,\ i = 1,2,3.\end{cases} \tag{4.146}$$

This expression shows that $m_{h_i}^2$ is subjected to the short-scale oscillations of the ϕ field through the quasi-periodic function $\mathcal{P}$. During one half of the period, when $\mathcal{P}$ is positive, the electroweak symmetry remains unbroken, and each component of the Higgs doublet receives a non-zero mass $m_{h_i} = \sqrt{g_{\boldsymbol{h}}M_{\rm Pl}\varphi|\mathcal{P}|}$. In the second half of the period, when $\mathcal{P}$ becomes negative, the mass of the physical Higgs component, i.e., $i = 0$, is $m_{h_0} = \sqrt{2g_{\boldsymbol{h}}M_{\rm Pl}\varphi|\mathcal{P}|}$, whereas the remaining three Goldstone bosons $i = 1,2,3$ become the longitudinal components of the SM gauge bosons and decouple from the ϕ field. In the unitary gauge, that corresponds to an infinite mass of h_i for $i = 1,2,3$ since these components are non-dynamical modes in the broken phase.

As a result of a periodic change of a μ_h^2 sign, the Higgs field undergoes rapid phase transitions between phases of broken and unbroken electroweak gauge symmetry and acquires a $\phi(t)$-dependent vev, i.e.,

$$v_h = \begin{cases}0\,, & \phi(t) > 0\,,\\ \sqrt{\dfrac{|\mu_h^2(\phi)|}{\lambda_h}}\,, & \phi(t) < 0,\end{cases} \qquad \text{for } a \in [a_e, a_{\rm rh}]. \tag{4.147}$$

Note that since v_h is a function of the ϕ field, this non-trivial Higgs vev vanishes rapidly around $a \sim a_{\rm rh}$, since after the inflaton-radiation equality ϕ is diluted to a negligible amount. Therefore, after reheating, the Higgs field remains in the symmetric (unbroken) phase until the electroweak phase transition at the temperature scale $\mathcal{O}(100)$ GeV. Furthermore, we should stress that all massive SM particles receive a non-zero mass during reheating as a result of their coupling to the Higgs field, i.e.,

$$m_{\rm SM} = \frac{m_{\rm SM}^{\rm EW}}{v_{\rm EW}} v_h, \qquad \text{for } a \in [a_e, a_{\rm rh}], \tag{4.148}$$

where $m_{\rm SM}^{\rm EW}$ denotes the electroweak mass of the SM species.

Constraints on the inflaton-Higgs coupling

As all the effects discussed above highly depend on the strength of the inflaton-Higgs coupling $g_{h\phi}$, let us now discuss the constraints one should impose on it.
Firstly, the presence of the inflaton-Higgs coupling should not substantially modify the inflationary dynamics not to spoil the prediction of the single-field inflation described in the previous chapter. In particular, we have ignored interaction terms in the EoM for the ϕ field, treating the SM fields as small perturbations. Moreover, we have also neglected possible back-reactions on the inflaton field. To justify this treatment, one must impose a perturbativity limit upon the strength of the $g_{h\phi}$ coupling. For instance, we can require that the amplitude for $\boldsymbol{h}$ scattering in a background of the classical ϕ field with its double insertion is smaller than the corresponding amplitude with a single insertion. This leads to the following upper bound on the inflaton-Higgs coupling:

$$g_{h\phi} \lesssim \left(\frac{\Lambda^2}{\phi M_{\rm Pl}}\right), \tag{4.149}$$

where ϕ denotes the strength of the external inflaton field determined by its EoM Eq.(3.10).
Secondly, the inflaton-Higgs coupling $g_{h\phi}$ must also be limited from below to ensure the stability of the Higgs potential. Namely, due to quantum corrections, within the SM sector, the quartic Higgs coupling λ_h runs down towards negative values at the energy scales $\sim 10^{10}$ GeV making the Higgs potential unstable [363]. However, in the presence of new physics interactions, such as the inflaton-Higgs coupling considered in this thesis, the stability of the Higgs potential can be achieved for larger Higgs field values [363]. In particular, since $|\phi|\sim \mathcal{O}(\text{few})M_{\rm Pl}$ during inflation, the inflaton-dependent mass for the Higgs doublet (4.146) could be quite large, which leads to the stability/positivity of the Higgs potential. The maximal Higgs field strength up to which the potential is stable could be estimated by comparing the cubic term $g_{h\phi}M_{\rm Pl}\phi|\mathbf{h}|^{\mathbf{2}}$ with the quartic term $\lambda_h|\mathbf{h}|^{\mathbf{4}}$. This leads to

$$|\boldsymbol{h}_{\rm max}|^2 \sim \frac{g_{h\phi}}{\lambda_h} M_{\rm Pl}\, \phi, \tag{4.150}$$

Now let us recall that the cosmological constant term Λ^4 well approximates $V(\phi)$ during inflation. Therefore, in order not to jeopardize predictions of the single-field inflation, we exact both $\lambda_h|\boldsymbol{h}|^4$ and $g_{h\phi}M_{\rm Pl}\,\phi\,|\boldsymbol{h}|^2$ terms to be negligible relative to Λ^4 in the whole region of stability, i.e., up to the largest allowed Higgs-field value $\boldsymbol{h} = \boldsymbol{h}_{\rm max}$. This requirement leads to the following condition:

$$g_{h\phi} \lesssim \sqrt{\lambda_h}\left(\frac{\Lambda^2}{\phi M_{\rm Pl}}\right). \tag{4.151}$$

The above result provides a stronger bound on the inflaton-Higgs coupling than Eq. (4.149) for $\lambda_h < 1$. Therefore, we will adopt the (4.151) constraint in the following analysis.

Furthermore, as demonstrated in Ref.[363], if the Higgs mass exceeds the Hubble rate, or more precisely $m_{h_0} > 3H_e/2$, the fluctuations of the h_0 fields are strongly suppressed during inflation, which ensures the stability of the Higgs potential. This remark set the lower limit for $g_{h\phi}$, such that

$$g_{h\phi} \gtrsim \frac{3}{4}\sqrt{6\alpha}\left(\frac{\Lambda^2}{\phi M_{\rm Pl}}\right)^2\left(\frac{\phi}{\sqrt{6\alpha}M_{\rm Pl}}\right). \tag{4.152}$$

For the benchmark values of the inflationary scale $\Lambda = 3\times 10^{-3}M_{\rm Pl}$ and $\alpha = 1/6$, adopted in this analysis, we find the following consistency region for the inflation-Higgs coupling:

$$6\cdot 10^{-11} \lesssim g_{h\phi} \lesssim 7\cdot 10^{-6}, \tag{4.153}$$

where we have used $\phi \sim \sqrt{6\alpha}M_{\rm Pl}$.
Finally, let us notice that the above limits depend on λ_h; increasing λ_h implies larger values of the $g_{h\phi}$ coupling.

4.5.2 The kinematic suppression

Now let us discuss in detail the consequences of the non-zero mass of the Higgs field for the physics of reheating. To that end, we rewrite the *time-averaged inflaton decay rate* accounting for the cubic inflaton-Higgs interactions (4.79) as follows,

$$\langle\Gamma^{(1)}_{\phi\to\mathbf{hh}}\rangle \equiv \langle\Gamma_{\phi\to\mathbf{hh}}\rangle = \frac{1+n}{2n}\frac{g^2_{h\phi}}{32\pi}\frac{M^2_{\rm Pl}}{m_\phi}\gamma_h\,, \tag{4.154}$$

with

$$\gamma_h \equiv \frac{8n\sqrt{\pi n}(2n-1)\Gamma\left(\frac{n+1}{2n}\right)}{\Gamma\left(\frac{1}{2n}\right)}\sum_{i=0}^{3}\sum_{k=1}^{\infty}k|\mathcal{P}_k|^2\left\langle \mathrm{Re}\left[\sqrt{1-\frac{4m^2_{h_i}}{k^2\omega^2}}\right]\right\rangle. \tag{4.155}$$

Note that Eq. (4.154) mimics a standard formula for the decay width describing the decay of a quantum spin-0 massive field into two other massive scalars. The kinematic parameter γ_h introduced above incorporates effects induced by the classical nature of the inflaton. It is important to emphasize that $\langle\Gamma_{\phi\to\mathbf{hh}}\rangle$ has two sources of time dependence. Namely,

(i) the effective mass of the inflaton field m_ϕ Eq.(3.45)

(ii) the inflaton-induced mass of the SM Higgs m_{h_i} (4.146), or more preciesly, the ratio $2m_{h_i}/(k\omega)$ which appears in the square root in Eq. (4.155).

It turns out that $\langle\Gamma_{\phi\to\mathbf{hh}}\rangle$ is time-independent only in the *massless reheating scenario*, i.e., when $m_{h_i} = 0$, with the quadratic inflaton potential $n = 1$. In this special case, $\gamma_h = 4$ since the inflaton field can transfer its energy density to four massless components of the Higgs field, or in other words, ϕ has four equivalent *decay channels*. However, if the inflaton-induced mass of the Higgs field cannot be neglected, then $\langle\Gamma_{\phi\to\mathbf{hh}}\rangle$ develops time-dependence even if ϕ oscillates in the quadratic potential.

One can distinguish two time-scales relevant to the reheating dynamics—namely, the scale of the inflaton oscillations and the scale associated with the expansion of the Universe. As we have already stressed in the previous chapter, the time-scale of m_ϕ evolution is typically longer than that of the inflaton oscillations. On the other hand, the Higgs mass parameter rapidly changes in time due to the violent oscillations of the $\mathcal{P}$ function. The amplitude of these oscillations is damped since the envelope φ decreases with time, according to Eq.(3.41). It is important to stress that to track the evolution of the SM sector, one should consider the Boltzmann equation (4.74) averaged over rapid oscillations of the inflaton. Notice that the inflaton-induced Higgs mass is the only source of the short-scale variation of the *inflaton decay width*. Hence, it is convenient to factorize these two time-scales relevant for the variation of $\langle\Gamma_{\phi\to\mathbf{hh}}\rangle$ and average only the square root in (4.154). More precisely, averaging the inflaton mass is trivial since we have assumed that m_ϕ does not change in one period of ϕ oscillations. Nevertheless, the summation and averaging performed in (4.154) deserve an explanation. In particular, let us point out that the adopted procedure takes into account the fact that in the unbroken phase, i.e., when $\mathcal{P} > 0$, the inflaton field 'decays' into four real components of the Higgs doublet, while in the second half of the period, when $\mathcal{P}$ becomes negative, the energy can only be injected to h_0, since the remaining components $h_{1,2,3}$ decouple from the inflaton. Furthermore, we should stress that the kinematic suppression is only relevant if the energy $k\omega$ of the inflaton mode k is negligible compared to the factor $2m_{h_i}$. In addition, for all values of n, the sum over inflaton modes k is dominated by the contribution from the first Fourier mode, i.e., $k = 1$, as the Fourier coefficients $\mathcal{P}_k$ drops quickly for larger mode numbers.

Time-averaging over the inflaton oscillations

Now we aim to find an approximate analytical formula for the $\langle\sqrt{1-(2m_{h_i}/k\omega)^2}\rangle$ term appearing in (4.155). It is the crucial factor in calculating the inflaton width, capturing the kinematic phase-space suppression generated by the non-zero Higgs mass. As a first step towards this goal, let us note that the time average of the inflaton-induced Higgs mass is given by

$$\langle m_{h_i}\rangle = \sqrt{g_{h\phi}M_{\rm Pl}\,\varphi}\,\frac{\Gamma\left(\frac{3}{4n}\right)\Gamma\left(\frac{n+1}{2n}\right)}{\Gamma\left(\frac{2n+3}{4n}\right)\Gamma\left(\frac{1}{2n}\right)}\begin{cases}\frac{1+\sqrt{2}}{2}, & i=0,\\ \frac{1}{2}, & i=1,2,3.\end{cases} \tag{4.156}$$

Note that $\langle m_{h_i}\rangle$ is approximately constant during one period of oscillation; however, it varies in a longer time-scale according to the φ evolution. It is also instructive to write the $\langle m_h\rangle/(k\omega)$ ratio for the dominant $k = 1$ mode

$$\frac{\langle m_h\rangle}{\omega} \simeq \frac{\sqrt{g_{h\phi}M_{\rm Pl}\,\varphi}}{m_\phi}\sqrt{\frac{2n-1}{\pi\, n}}\,\frac{\Gamma\left(\frac{3}{4n}\right)}{\Gamma\left(\frac{2n+3}{4n}\right)} = \frac{\sqrt{g_{h\phi}}}{\sqrt{2\pi}\,n}\frac{M_{\rm Pl}^2}{\Lambda^2}\frac{\Gamma\left(\frac{3}{4n}\right)}{\Gamma\left(\frac{2n+3}{4n}\right)}\left(\frac{\varphi_e}{M_{\rm Pl}}\right)^{\frac{3-2n}{2}}\left(\frac{a}{a_e}\right)^{\frac{3(2n-3)}{2(n+1)}}, \tag{4.157}$$

where for brevity we have neglected the Higgs field h_i component-dependent contribution $(1+\sqrt{2})/2$ for $i = 0$ and $1/2$ for $i = 1, 2, 3$. Moreover, in the second line of Eq. (4.157), we have employed the solution for the envelope Eq.(3.41). The time-dependence of the $\langle m_h\rangle/\omega$ factor disappears for $n=3/2$, whereas for $n<3/2$ ($n>3/2$) it decreases (increases) with the scale factor during the reheating phase. Therefore, we can conclude that the phase-space suppression amplifies with time for $n > 3/2$ and stays constant for $n = 3/2$. However, if $n < 3/2$, the role of the non-zero mass of the Higgs field generated by its coupling to the inflaton becomes less and less important.

Next, we find that the average of the phase-space factor can be written as

$$\left\langle\sqrt{1-\frac{4m_{h_i}^2}{k^2\omega^2}}\right\rangle \approx \left\lceil\frac{9\,\kappa_i\, n\Gamma\left(\frac{n+1}{2n}\right)}{16\sqrt{\pi}\,\Gamma\left(\frac{1}{2n}\right)}\frac{k^2\omega^2}{g_{h\phi}M_{\rm Pl}\varphi}\right\rceil = \left\lceil\frac{9\sqrt{\pi}\kappa_i n^2\Gamma\left(\frac{n+1}{2n}\right)^3}{16(2n-1)\Gamma\left(\frac{1}{2n}\right)^3}\frac{k^2m_\phi^2}{g_{h\phi}M_{\rm Pl}\varphi}\right\rceil, \tag{4.158}$$

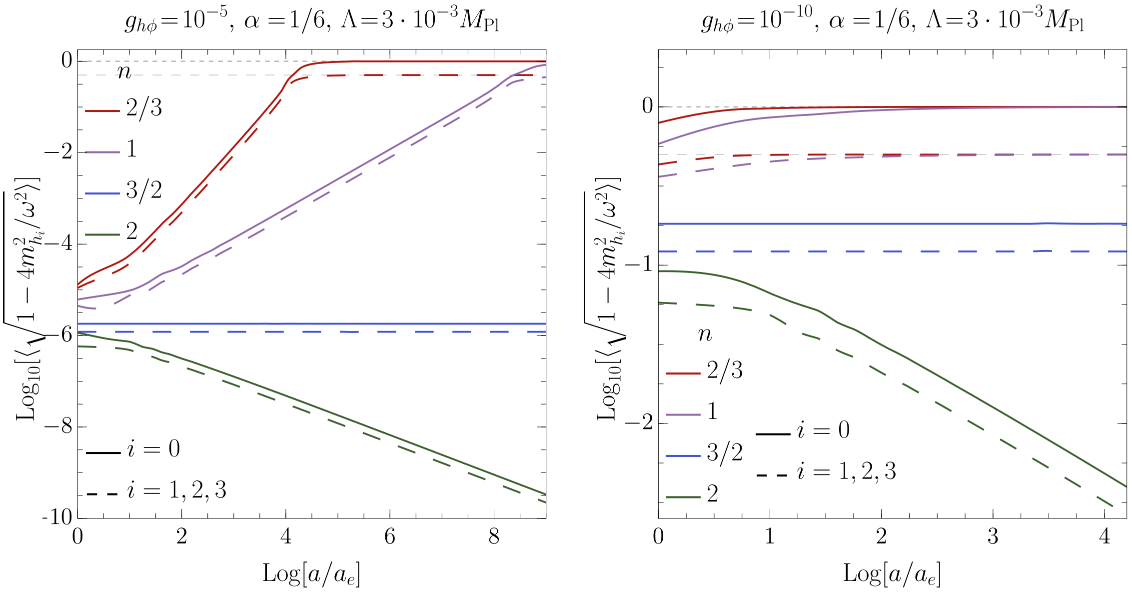

FIGURE 4.4: Evolution of the phase-space factor $\langle\sqrt{1-4m_{h_i}^2/(k^2\omega^2)}\rangle$ as a function of the scale factor a for $k=1$ and two values of the inflaton-Higgs coupling $g_{h\phi}=10^{-5}$ and 10^{-10} in the left and right panel, respectively. Solid (dashed) lines are for the $i=0$ $(1,2,3)$ components of the Higgs doublet.

with for the physical component of the Higgs field $\kappa_0=1$, whereas $\kappa_{1,2,3}=1/2$ due to the fact that the $i=1,2,3$ components become Goldstone modes in the broken phase. Above, we have introduced the 'ceiling' function $\lceil\cdots\rceil$, defined as

$$\lceil x\rceil=\begin{cases}1, & x\geq 1,\\ x, & x<1.\end{cases} \tag{4.159}$$

Consequently, $\lceil\cdots\rceil=1$ implies no kinematic suppression, whereas $\lceil\cdots\rceil\neq 1$ indicates that the inflaton-induced Higgs mass becomes of the order of the energy $k\omega$ of the oscillating mode. Note that the time-dependence of the phase-space factor enters through the envelope Eq.(3.41), and the inflaton mass Eq.(3.66). Hence, we can also rewrite Eq. (4.158) as an explicit function of the scale factor, i.e.,

$$\left\langle\sqrt{1-\frac{4m_{h_i}^2}{k^2\omega^2}}\right\rangle\approx\left\lceil\frac{g_k}{g_{h\phi}}\left(\frac{a_e}{a}\right)^{\frac{3(2n-3)}{(n+1)}}\right\rceil, \tag{4.160}$$

with

$$g_k\equiv\frac{9\sqrt{\pi}\kappa_i k^2 n^3\Lambda^4\,\Gamma\left(\frac{n+1}{2n}\right)^3}{8\,M_{\rm Pl}^4\,\Gamma\left(\frac{1}{2n}\right)^3}. \tag{4.161}$$

Above, we have assumed that $\varphi_e\sim M_{\rm Pl}$. From Eq. (4.160), we see that the phase-space factor increases (decreases) with time for $n<3/2$ $(n>3/2)$, whereas for $n=3/2$ it is time-independent, as we have already deduced above.
Next, we can estimate the value of the scale factor a_k at which the 'ceiling' function approaches unity. We find

$$a_k\equiv a_e\left(\frac{g_k}{g_{h\phi}}\right)^{\frac{(n+1)}{3(2n-3)}},\qquad n\neq 3/2. \tag{4.162}$$

Note that the condition $\lceil\cdots\rceil = 1$ indicates that the kinetic effects become irrelevant (relevant) for $n < 3/2$ ($n > 3/2$). On the other hand, if $n = 3/2$ the phase-space factor (4.160) is a time-independent when $g_{h\phi} > g_k$ for $k = 1$. Moreover, we should also stress that for $n < 3/2$, the effects of the non-zero Higgs mass could become irrelevant before the end of reheating if $a_k < a_{\rm rh}$. In this case, in the period between $a_k < a \leq a_{\rm rh}$, the reheating dynamics becomes insensitive to the inflaton-induced Higgs mass. Contrarily, for $n > 3/2$, the role of the kinematic suppression increases with time. This is because even if the Higgs mass is negligible at the onset of the reheating phase, it would soon become of the order of the inflaton energy $k\omega$, and hence the kinematic effects might be important until the end of reheating.

Lastly, let us stress that utilizing the above definition of a_k, one can rewrite the phase-phase factor (4.160) as

$$\left\langle\sqrt{1-\frac{4m_{h_i}^2}{k^2\omega^2}}\right\rangle \approx \begin{cases} \left\lceil \left(\frac{a_k}{a}\right)^{\frac{3(2n-3)}{(n+1)}} \right\rceil, & n\neq 3/2, \\ \left\lceil \frac{g_k}{g_{h\phi}} \right\rceil, & n=3/2. \end{cases} \tag{4.163}$$

Numerical results

The evolution of $\left\langle\sqrt{1-\frac{4m_{h_i}^2}{k^2\omega^2}}\right\rangle$ as a function of the scale factor a for two values of the inflaton-Higgs coupling $g_{h\phi} = 10^{-5}$ (left panel) and 10^{-10} and $k = 1$ obtained numerically, is shown in Fig. 4.4. This figure indicates that if the inflaton-induced mass of the Higgs field is small compared to the inflaton energy $k\omega$, the factor $\langle\sqrt{1-(2m_{h_i}/k\omega)^2}\rangle = 1$ and kinetic effects are no longer relevant. In particular, we observe that for $n < 3/2$ and $g_{h\phi} = 10^{-5}$, the phase-space factor initially grows with time until $2m_{h_i}$ drops below $k\omega$, which coincide with $a \simeq a_k$. More precisely, from the left panel of Fig. 4.4, we see that the number of the reheating e-folds during which kinematic suppression is present can be estimated as $N_k \sim 4$ and 9 for $n = 2/3$ and $n = 1$, respectively. We should highlight that the Higgs production is not completely terminated even if $2m_{h_i}$ exceeds the inflaton energy $k\omega$. This happens because, during each oscillation, ϕ goes through zero, which implicates the vanishing of the Higgs mass. In these short time intervals when $m_{h_i} \to 0$, the "inflaton decays" are kinematically allowed, so that $\langle\sqrt{1-(2m_{h_i}/k\omega)^2}\rangle = 1$ is non-zero. Furthermore, we see that the phase-space factor is time-independent for $n = 3/2$ and can be approximated by $\langle\sqrt{1-(2m_{h_i}/k\omega)^2}\rangle \sim \lceil \kappa_i\Lambda^4/(4g_{h\phi}M_{\rm Pl}^4)\rceil$. In this case, kinetic suppression is present during the entire reheating phase unless $g_{h\phi}$ is tiny and the ceiling function approaches one. Finally, for $n > 3/2$, the ratio $2m_{h_i}/k\omega)^2$ grows during reheating, which means that the role of non-zero Higgs mass becomes more and more relevant so that $\langle\sqrt{1-(2m_{h_i}/k\omega)^2}\rangle$ decreases as the scale factor increases. This, in particular, means that even if the Higgs mass is negligible at the commencement of the reheating phase, kinetic suppression grows with time. Last of all, let us emphasize that numerical results for the phase-space factor evolution presented in Fig. 4.4 agree to a large extent with our approximate analytic estimations (4.160). In Fig. 4.5, we have plotted the evolution of the mass of the 0-component of the Higgs doublet, m_{h_0} (4.146), its average $\langle m_{h_0}\rangle$ (4.156), as well as the inflaton frequency ω Eq.(4.89) as functions of the scale factor for two values of n, namely $n = 2/3$ (left panel) and $3/2$ (right panel), and two values of $g_{h\phi} = 10^{-5}$ (red curve) and 10^{-10} (blue curve). These two figures confirm our analytical predictions that the kinematic suppression is relevant in the region where $\langle m_{h_0}\rangle \gtrsim m_\phi$. In particular, by comparing left panels of Fig. 4.4 with Fig. 4.5, we see that for $n = 2/3$, $\langle m_{h_0}(a)\rangle$ matches with ω around $a \simeq a_k$.

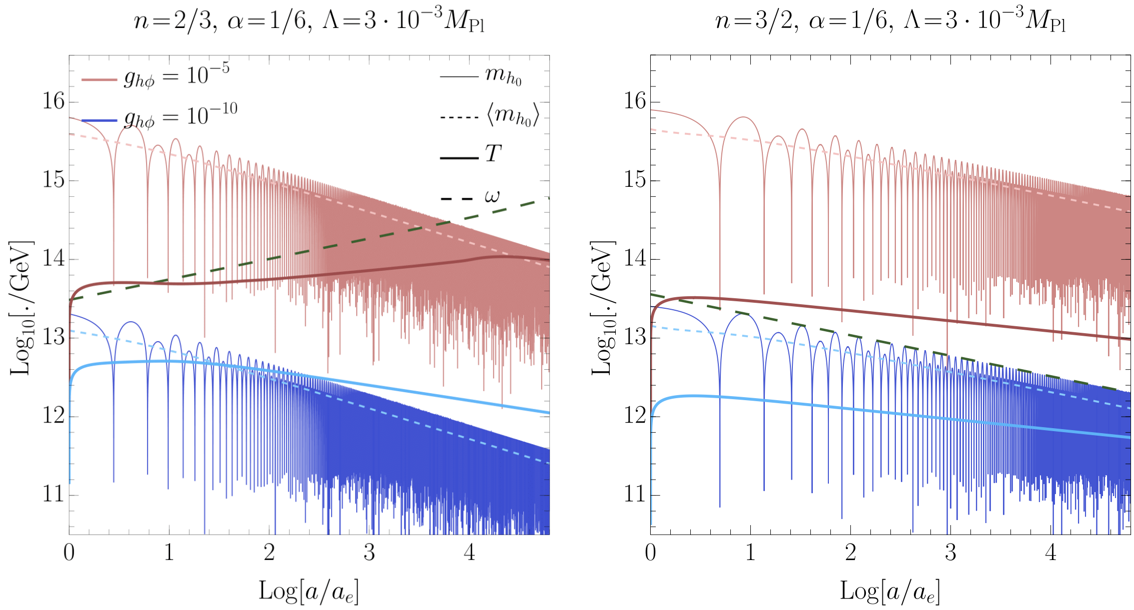

FIGURE 4.5: The evolution of the Higgs mass $m_{h_0}(a)$ for two values of the inflaton-Higgs coupling $g_{h\phi}=10^{-5}$ (blue) and $g_{h\phi}=10^{-7}$ (red) for $n=2/3$ and $3/2$ in the left and right panel, respectively. Thin dashed curves show the evolution of the averaged Higgs mass, i.e., $\langle m_{h_0}(a)\rangle$, whereas thick solid curves present the evolution of the thermal bath temperature. The loosely dashed green lines illustrate the evolution of the inflaton mass m_ϕ.

4.5.3 Analytical solutions to the Boltzmann equations

In the previous subsection, we have established the impact of the inflaton-induced Higgs mass on the evolution of the phase-space factor $\left\langle\sqrt{1-\frac{4m_{h_i}^2}{k^2\omega^2}}\right\rangle$. In particular, it has been shown that non-zero mass of the Higgs field could engender a kinematic suppression that affects the energy transfer from the inflaton to SM sector and might generate a non-trivial scaling of the phase-space factor with a (4.163). Such behavior is observed if the mass $2m_{h_i}$ is at least comparable with the energy $k\omega$, which, in turn, depends on the strength of the inflaton-Higgs coupling. One may distinguish two regimes:

(i) **massless scenario** where the inflaton-induced mass of the SM Higgs is negligible compared to the energy $k\omega$ so that one can employ the limit $m_{h_i}\to 0$,

(ii) **massive scenario** in which the non-trivial kinematic effects influence the reheating dynamics.

Now let us consider both cases in detail. As we will explicitly demonstrate below, there are significant differences between these two scenarios.

Massless case

The **massless reheating scenario** has been discussed in Sec.(4.2), where we have neglected the contribution to the Higgs boson mass originating from the cubic interaction term $g_{h\phi}M_{\rm Pl}\phi|\boldsymbol{h}|^2$. This is, of course, merely a reference point introduced to illustrate the effects of kinetic suppression in the realistic case, i.e., with $m_{h_i}\neq 0$. In the limit $m_{h_i}\to 0$, the only source of time-dependence of the *inflaton decay rate* (4.154) is through the effective inflaton mass m_ϕ Eq.(3.66). In particular, for $n<1$, $\Gamma_{\phi\to\mathbf{hh}}$ decreases during reheating, whereas for $n>1$ it increases with time. Therefore, one expects that for fixed values of the model parameters, i.e., $\{g_{h\phi},\alpha,\Lambda\}$, reheating in the *massless scenario* is the most efficient for $n>1$, while for $n<1$ its duration is prolonged. Moreover, let us stress that for quadratic inflaton potential, i.e., $n=1$, we reproduce the well-known expression for the time-independent decay width, i.e., $\Gamma_{\phi\to\mathbf{hh}} \overset{n=1}{=} (g_{h\phi}M_{\rm Pl})^2/(8\pi m_\phi)$, with $m_\phi=\sqrt{2}\Lambda^2/M$ and $\mathcal{P}_k=\delta_{1k}/2$.

From Eq.(4.101), one obtains the following solution for the SM radiation energy density in the *Higgs massless reheating scenario*:

$$\begin{aligned}\rho_{\rm SM}^{\rm RH,(0)}(a) &= \frac{6n}{4n+1} M_{\rm Pl}^2 H_e\, \widetilde{\Gamma}^e_{\phi\to\mathbf{hh}} \left[\left(\frac{a_e}{a}\right)^{\frac{3}{n+1}} - \left(\frac{a_e}{a}\right)^4\right] \\ &\simeq \frac{6n}{4n+1} M_{\rm Pl}^2 H_e\, \widetilde{\Gamma}^e_{\phi\to\mathbf{hh}} \left(\frac{a_e}{a}\right)^{\frac{3}{n+1}}, \qquad \text{for } a\in[a_e, a_{\rm rh}]. \end{aligned} \tag{4.164}$$

Consequently, the temperature of the thermal bath evolves as

$$T_{\rm RH}^{(0)}(a) \simeq \left[\frac{180 n M_{\rm Pl}^2 H_e\, \widetilde{\Gamma}^e_{\phi\to\mathbf{hh}}}{(4n+1)\pi^2\, g_{\star\rho}(T)}\right]^{1/4} \left(\frac{a_e}{a}\right)^{\frac{3}{4(n+1)}}. \tag{4.165}$$

For the quadratic inflaton potential, i.e., $n=1$, we reproduce the well-known result i.e., $T\propto a^{-3/8}$. The scaling of the SM energy density $\rho_{\rm SM}^{(0)}$ with a for several values of n is collected in Table 4.4.

Another quantity of physical importance is the maximum temperature

$$T_{\rm max}^{(0)} = \left[\frac{180 M_{\rm Pl}^2 H_e\, \widetilde{\Gamma}^e_{\phi\to\mathbf{hh}}}{(4n+1)\pi^2\, g_{\star\rho}(T_{\rm max})}\right]^{1/4} \left(\frac{3}{4(n+1)}\right)^{\frac{3}{4(4n+1)}}, \tag{4.166}$$

and the reheating temperature

$$T_{\rm rh}^{(0)} = \left(\frac{90 H_e^2 M_{\rm Pl}^2}{\pi^2 g_{\star\rho}(T_{\rm rh})}\right)^{1/4} \left(\frac{4n+1}{2n}\,\frac{H_e}{\widetilde{\Gamma}^e_{\phi\to\mathbf{hh}}}\right)^{\frac{n}{2(1-2n)}}. \tag{4.167}$$

We should highlight that in the considered range of $g_{h\phi}$ variation, i.e., $g_{h\phi}\in(10^{10},10^{-5})$, the entire reheating dynamics in the *massless scenario* is dominated by the direct inflaton-Higgs coupling, such that irreducible gravitational interactions are subdominant, cf. Fig.(4.2).

Massive case

Next, we consider the effects of the inflaton-induced Higgs mass on the reheating dynamics, considering the **massive reheating scenario**. The crucial difference of this scenario as compared to the reheating with the massless Higgs, discussed above, is the presence of the kinetic suppression in $\langle\Gamma_{\phi\to\mathbf{hh}}\rangle$ (4.154) through γ_h (4.155). In particular, the main difference emerges due to non-trivial averaging of the phase-space factor $\langle\sqrt{1-(2m_{h_i}/k\omega)^2}\rangle$ over inflaton oscillations, which generates a suppression due to the non-zero Higgs mass Eq. (4.160). Furthermore, as it has been pointed out above, the γ_h factor is time-independent only if $n=3/2$, whereas for $n<3/2$ ($n>3/2$), it increases (decreases) during the reheating period. In particular, for $n<3/2$, the $(2m_{h_i}/k\omega)$ ratio decreases with time, and the kinetic suppression gradually disappears around $a\sim a_k$. Note that, in principle, the kinematic suppression can be present throughout the whole reheating if $a_k>a_{\rm rh}$, or it may at some point become irrelevant if $a_k<a_{\rm rh}$. In the latter case, the inflaton-induced mass of the Higgs field suppresses the radiation production in the period between $a_e<a\le a_k$, while for $a_k<a\le a_{\rm rh}$ the reheating dynamics follows the same evolution as in the *massless scenario*. Contrarily, for $n>3/2$ the non-trivial Higgs mass could have a negligible impact on the reheating dynamics for sufficiently small inflaton-Higgs coupling $g_{h\phi}$. However, in this case, $(2m_{h_i}/k\omega)$ increases with time so that the kinetic suppression becomes relevant at some point, affecting the reheating dynamics until the end of reheating.

The time-averaged inflaton decay width Eq. (4.154), including the non-zero mass term of the Higgs field, can be written in the following form:

$$\langle \Gamma_{\phi\to\mathbf{hh}}\rangle \simeq \Gamma^e_{\phi\to\mathbf{hh}}\left(\frac{a_e}{a}\right)^{\frac{3(1-n)}{n+1}} \times \sum_{k=1}^{\infty} k|\mathcal{P}_k|^2 \begin{cases} \left\lceil \left(\dfrac{a_k}{a}\right)^{\frac{3(2n-3)}{(n+1)}} \right\rceil, & n\neq 3/2, \\ \left\lceil \dfrac{g_k}{g_{h\phi}} \right\rceil, & n=3/2, \end{cases} \tag{4.168}$$

with

$$\Gamma^e_{\phi\to\mathbf{hh}} \equiv \frac{\widetilde{\Gamma}^e_{\phi\to\mathbf{hh}}}{\sum_{k=1}^{\infty} k|\mathcal{P}_k|^2}. \tag{4.169}$$

In what follows, we find the SM energy density and thermal bath temperature evolution in three cases, i.e., $n \lessgtr 3/2$, and $n = 3/2$. Note that if $n \lessgtr 3/2$ and $a \gtrless a_k$ the *inflaton decay width*, accounting for the inflaton-Higgs interactions, has no phase-space suppression and coincides with that of the massless Higgs boson case. Hence, in this case, the evolution of the SM energy density follows Eq. (4.164). On the other hand, for $n \lessgtr 3/2$ and $a \lessgtr a_k$, the phase-space kinematic suppression affects the reheating dynamics, and, therefore, the evolution of the SM energy density is modified relative to the massless case Eq. (4.164). In addition, for $n = 3/2$, we observe a constant suppression proportional to $\lceil g_k/g_{h\phi}\rceil$ throughout the reheating period. Therefore, if $n = 3/2$, the relation between $\rho_{\rm SM}$ and T with the scale factor in the *massive scenario* is the same as in the massless case; however, due to constant suppression, the maximal temperature of the SM sector is reduced. The solution of the second Boltzmann equation (4.74) in the *massive reheating scenario* takes the form

$$\begin{aligned}\rho^{\rm RH}_{\rm SM}(a) \simeq{}& \frac{6n}{n+1} M^2_{\rm Pl} H_e \widetilde{\Gamma}^e_{\phi\to\mathbf{hh}} \\ &\times \begin{cases} \dfrac{n+1}{2(5-n)}\left[\left(\dfrac{a_e}{a}\right)^{\frac{6(n-1)}{n+1}} - \left(\dfrac{a_e}{a}\right)^4\right] \displaystyle\sum_{k=1}^{\infty} k|\mathcal{P}_k|^2 \left(\dfrac{a_k}{a_e}\right)^{\frac{3(2n-3)}{(n+1)}}, & a\lessgtr a_k,\ n\lessgtr 3/2, \\ \dfrac{n+1}{4n+1}\left[\left(\dfrac{a_e}{a}\right)^{\frac{3}{n+1}} - \left(\dfrac{a_e}{a}\right)^4\right] \displaystyle\sum_{k=1}^{\infty} k|\mathcal{P}_k|^2, & a\gtrless a_k,\ n\lessgtr 3/2, \\ \dfrac{n+1}{4n+1}\left[\left(\dfrac{a_e}{a}\right)^{\frac{3}{n+1}} - \left(\dfrac{a_e}{a}\right)^4\right] \displaystyle\sum_{k=1}^{\infty} k|\mathcal{P}_k|^2 \left\lceil \dfrac{g_k}{g_{h\phi}}\right\rceil, & n=3/2. \end{cases}\end{aligned} \tag{4.170}$$

Thus, during the kinematical suppression phase, i.e., $a \lessgtr a_k$ for $n \lessgtr 3/2$, the energy density of the SM sector and its temperature scale as

$$\rho^{\rm RH}_{\rm SM} \propto a^{\frac{6(1-n)}{n+1}}, \qquad T_{\rm RH} \propto a^{\frac{3(1-n)}{2(n+1)}}, \qquad a\lessgtr a_k,\ n\lessgtr 3/2. \tag{4.171}$$

Whereas, in the region where the kinematic suppression is absent, we get the scaling as that of the massless Higgs case, i.e.,

$$\rho^{\rm RH}_{\rm SM} \sim \rho^{\rm RH,(0)}_{\rm SM} \propto a^{\frac{-3}{n+1}}, \qquad T_{\rm RH} \sim T^{(0)}_{\rm RH} \propto a^{\frac{-3}{4(n+1)}}, \qquad a\gtrless a_k,\ n \lesseqgtr 3/2. \tag{4.172}$$

n	$\langle\Gamma^{(0)}_{\phi\to\mathbf{hh}}\rangle$	$\rho^{\mathrm{RH},(0)}_{\mathrm{SM}}$	$T^{(0)}_{\mathrm{RH}}$	$\langle\Gamma_{\phi\to\mathbf{hh}}\rangle$	$\rho^{\mathrm{RH}}_{\mathrm{SM}}$	T_{RH}
$2/3$	$a^{-3/5}$	$a^{-9/5}$	$a^{-9/20}$	$a^{12/5}$	$a^{6/5}$	$a^{3/10}$
1	a^{0}	$a^{-3/2}$	$a^{-3/8}$	$a^{3/2}$	a^{0}	a^{0}
$3/2$	$a^{3/5}$	$a^{-6/5}$	$a^{-3/10}$	$a^{3/5}$	$a^{-6/5}$	$a^{-3/10}$
2	a^{1}	a^{-1}	$a^{-1/4}$	a^{0}	a^{-2}	$a^{-1/2}$

TABLE 4.4: Approximate scaling of the averaged inflaton decay width, $\langle\Gamma_{\phi\to\mathbf{hh}}\rangle$, energy density of the SM sector, ρ_{SM}, and thermal bath temperature, T, with the scale factor, a, in the *massless* (with superscript (0)) and *massive Higgs boson-induced reheating.*

It is important to emphasize that the behavior of the SM energy density with the scale factor is very unusual. It turns out that in the *massive scenario* for $n = 2/3$, both ρ_{SM} and T increase with time, whereas for the quadratic inflaton potential, i.e., $n = 1$, they are nearly constant. Moreover, as we have discussed earlier on, for $n = 3/2$, the inflaton decay rate depends on time only though m_ϕ and thus, in both *massless* and *massive* cases, we obtain the same dependence on the scale factor a. Finally, for $n > 3/2$, the scaling of ρ_{SM} with a is steeper in the *massive reheating scenario* in comparison to the massless Higgs case. The approximate scalings of the *time-averaged inflaton decay width*, the SM energy density, ρ_{SM}, and the temperature, T, with a, are collected in Table 4.4 for both considered scenarios.

4.5.4 Tachyonic resonant production of Higgs bosons

Before we present the complete numerical analysis of the reheating dynamics in the Higgs boson-induced scenario, it is convenient to comment on the non-perturbative tachyonic Higgs production during the early stages of reheating. Such a possibility emerges from the fact that the inflaton-induced Higgs mass parameter μ_h^2 (4.145) could exceed the inflaton effective mass m_ϕ^2 Eq.(3.45) for values of $g_{h\phi}$ satisfying (4.151) and (4.152) limits, i.e.,

$$\sqrt{\lambda_h}\left(\frac{\Lambda^2}{\phi M_{\mathrm{Pl}}}\right) \gtrsim g_{h\phi} \gtrsim \frac{3}{4}\left(\frac{\Lambda^2}{\phi M_{\mathrm{Pl}}}\right)^2\left(\frac{\phi}{M_{\mathrm{Pl}}}\right), \tag{4.173}$$

at the commencement of reheating phase, when $\phi = \phi_e \sim M_{\mathrm{Pl}}$. In this case, tachyonic resonant production of the Higgs boson can constitute an efficient source of (p)reheating [333, 334].

To discuss this phenomenon in more detail, let us find the equation of motion for the Higgs field. From Eq. (4.143), one gets the following EoM in the unitary gauge:

$$\left(\frac{d^2}{dt^2} - \frac{\nabla^2}{a^2} + 3H\frac{d}{dt} + g_{h\phi}M_{\mathrm{Pl}}\phi\right)h_0 = -\lambda_h h_0^3, \tag{4.174}$$

where the non-linear term on the r.h.s. of the above equation is present due to Higgs self-interactions. In the expanding background, a general solution of (4.174) is difficult to handle and typically requires lattice simulations. However, to develop some intuition and make analytical predictions, we employ the so-called Hartree approximation, which allows us to replace the non-linear term with a linear counterpart, according to

$$\lambda_h h_0^3 \to 3\lambda_h\langle h_0^2\rangle h_0, \tag{4.175}$$

with $\langle h_0^2\rangle$ being the variance of the Higgs field. The latter can be found using the linear solution (or iteratively in orders of the quartic coupling λ_h) for the Higgs mode function $h_{0,k}$

with mode momentum k as

$$\left\langle h_0^2 \right\rangle (t) = \frac{1}{2\pi^2} \int_0^\infty dk\, k^2 \left|h_{0,k}(t)\right|^2 , \tag{4.176}$$

where

$$h_0(t, \vec{x}) = \int \frac{d^3k}{(2\pi)^3} h_{0,k}(t, \vec{k}) e^{i\vec{k}\cdot\vec{x}}, \tag{4.177}$$

with $h_{0,k}(t, \vec{k}) = h^*_{0,k}(t, \vec{k}) \equiv h_{0,k}$.

Inserting decomposition (4.177) into Eq. (4.174), we obtain the following mode equation:

$$\ddot{h}_{0,k} + 3H\dot{h}_{0,k} + \left(\frac{k^2}{a^2} + g_{h\phi} M_{\rm Pl}\phi + 3\lambda_h \left\langle h_0^2 \right\rangle\right) h_{0,k} = 0, \tag{4.178}$$

where we have adopted the Hartree approximation (4.175). Applying the field redefinition

$$\tilde{h}_{0,k} \equiv a^{3/2} h_{0,k}, \tag{4.179}$$

we can recast the above equation to the harmonic oscillator form

$$\ddot{\tilde{h}}_{0,k} + \omega_k^2 \tilde{h}_{0,k} = 0, \tag{4.180}$$

with the time-dependent dispersion relation

$$\omega_k^2 \equiv \frac{k^2}{a^2} + g_{h\phi} M_{\rm Pl}\phi + 3\lambda_h \langle h_0^2 \rangle - \frac{3}{2}\frac{\ddot{a}}{a} - \frac{3}{4}\left(\frac{\dot{a}}{a}\right)^2 . \tag{4.181}$$

The two last terms can be combined into

$$-\frac{3}{2}\frac{\ddot{a}}{a} - \frac{3}{4}\left(\frac{\dot{a}}{a}\right)^2 = \frac{9}{4} H^2 w, \tag{4.182}$$

where we have used the fact that

$$\frac{\ddot{a}}{a} = -\frac{1}{2}\frac{1}{3M_{\rm Pl}^2}(1+3w)\rho. \tag{4.183}$$

Thus,

$$\omega_k^2 \equiv \frac{k^2}{a^2} + \frac{9}{4} H^2 w + g_{h\phi} M_{\rm Pl}\phi + 3\lambda_h \left\langle h_0^2 \right\rangle . \tag{4.184}$$

Note that the first and the fourth term are always positive, whereas the equation-of-state parameter $w = p/\rho$ during reheating varies in the range $w \in [-1, 1]$. Since the second and the third terms oscillate for half of the period, they provide a negative contribution to ω_k^2. If the positivity of the remaining components of ω_k^2 does not compensate for the negative input, the solution of the (4.180) has no longer an oscillatory form. Instead, if ω_k^2 becomes negative, the mode function grows exponentially, and the Higgs field experience tachyonic growth. Hence, we conclude that the cubic inflaton interactions might source the non-perturbative production of Higgs modes, i.e., preheating dynamics. At this point, we should stress that the second term, proportional to $H^2 w$, is subdominant compared to the third one if $g_{h\phi}$ is in the range (4.173), and the amplitude of the inflaton oscillation is of the of $\sim M_{\rm Pl}$. Therefore, tachyonic production of the Higgs field is mainly driven by the large negative mass term. However, the positive contribution from the self-interaction term $\lambda_h \langle h_0^2 \rangle$ could shut off the resonant production provided that

$$3\lambda_h \left\langle h_0^2 \right\rangle \gtrsim |\mu_h^2|. \tag{4.185}$$

Note that if the above condition is satisfied, then it guarantees that the tachyonic enhancement of the Higgs production does not occur for any momentum mode k; hence, the non-perturbative effects are irrelevant for the reheating dynamics. To put it another way, Eq.(4.185) defines a lower bound on the Higgs quartic coupling for which the tachyonic production is irrelevant for $\mu_h^2 < 0$.

To find the lower limit on λ_h, one needs to determine the variance of the Higgs field (4.176) for $\mu_h^2 < 0$ since resonant production can only occur for negative values of the ϕ field. This can be done by employing the leading linear solution for the mode function $h_{0,k}(t)$, i.e., neglecting the λ_h term in the mode equation (4.178), see also [333], as

$$\langle h_0^2 \rangle \sim \frac{|\mu_h|\Lambda^2}{16\pi^2 M_{\rm Pl}} \exp\left(\frac{4|\mu_h| M_{\rm Pl}}{\Lambda^2}\right). \tag{4.186}$$

Inserting the above expression into (4.185), we find

$$\lambda_h \gtrsim \frac{16\pi^2}{3} \frac{\sqrt{g_{h\phi}|\phi|} M_{\rm Pl}^{3/2}}{\Lambda^2} \exp\left(-\frac{4\sqrt{g_{h\phi}|\phi|} M_{\rm Pl}^{3/2}}{\Lambda^2}\right). \tag{4.187}$$

For the values of Higgs quartic coupling employed throughout this thesis, i.e., $\lambda_h \sim 0.1$, the lower bound on $g_{h\phi}$ to block the resonant production reads

$$g_{h\phi} \gtrsim \frac{4\Lambda^4}{M_{\rm Pl}^3 |\phi|}. \tag{4.188}$$

Note that the above lower limit for $g_{h\phi}$ is slightly stronger than the one in (4.173). Hence, for

$$\frac{3}{4}\left(\frac{\Lambda^4}{M_{\rm Pl}^3|\phi|}\right) \lesssim g_{h\phi} \lesssim 4\left(\frac{\Lambda^4}{M_{\rm Pl}^3|\phi|}\right), \tag{4.189}$$

and $\lambda_h \sim 0.1$ tachyonic resonant production of Higgs modes is possible. A detailed analysis of this phenomenon is an interesting possibility; however, it is beyond the scope of this thesis.

To summarize, our analysis presented above (with an order of magnitude approximations) indicates that in the parameter space considered in this work (with $g_{h\phi}$ respecting lower bound (4.188)), the tachyonic resonant production of the SM Higgs field is inefficient due to Higgs self-interactions, and does not affect the reheating dynamics. Therefore, in the following numerical analysis, we only focus on the perturbative production of Higgs bosons according to the discussion that has been held in the previous section.

4.5.5 Numerical analysis

Finally, let us present a numerical analysis of the reheating dynamics induced by the cubic inflaton-Higgs interactions in the *massless and massive scenarios*. In this subsection, we provide complete numerical solutions of the Boltzmann equations for the inflaton $\rho_\phi(a)$ and SM radiation $\rho_{\rm SM}(a)$ energy densities during and after reheating. In the considered model, the reheating dynamics depends only on the form of the inflaton potential and the strength of its interactions with the Higgs field. In the numerical study, we use the following benchmark values of the α-attractor T-model parameters: $\alpha = 1/6$, $\Lambda = 3 \times 10^{-3} M_{\rm Pl}$, and consider four different values of n, namely $n \in \{2/3, 1, 3/2, 2\}$ which correspond to the equation of state during the reheating phase $\bar{w} = \{-1/5, 0, 1/5, 1/3\}$, respectively. Furthermore, we consider two values for the inflaton-Higgs coupling $g_{h\phi} = 10^{-5}$ and 10^{-10}, which are close to its upper and lower bounds, see Eq. (4.153).

In the upper panels of Fig.(4.6) and (4.7), we have plotted numerical solutions for the inflaton (orange) and radiation (purple) energy densities for fixed $g_{h\phi} = 10^{-5}$ and $g_{h\phi} = 10^{-10}$ in Fig. 4.6 and Fig. 4.7, respectively. The lower panel of each figure presents the evolution of the thermal bath temperature (blue), the Hubble rate (green), and the *time-averaged inflaton decay width* (red) as functions of the scale factor a. The solid and dashed curves correspond to the *m*assive and *m*assless reheating scenario. White (black) dots indicate the end of the reheating phase, i.e., the moment at which the inflaton energy density matches with the SM energy density in the *massless* (*massive*) scenario. Note that the inflaton-radiation equality roughly coincides with $\langle \Gamma_{\phi \to \mathbf{hh}} \rangle \simeq H$ in both considered scenarios.

There are several comments here in order. First, let us stress that in both considered reheating scenarios, the inflaton energy density scales as $a^{-6n/(n+1)}$ during the reheating phase. After the inflaton-radiation equality, ρ_ϕ sharply drops for $n \geq 1$. On the other hand, if $n \in (1/2, 1)$, the decline of the inflaton energy density is far more gentle. This behavior springs from the fact that the *averaged inflaton decay width* decreases with the scale factor for $n \in (1/2, 1)$. Hence, in this case, the ϕ field does not entirely transfer its energy into the SM sector around $a_{\rm rh}$; instead, it slowly redshifts below the radiation energy density. Nevertheless, the total energy density of the Universe after the end of reheating is dominated by the energy of the relativistic SM species, and the contribution from the inflaton field soon becomes subdominant. Secondly, the SM energy density evolution during the reheating phase is dramatically different in the *massive reheating scenario* compared to the case where the inflaton-induced Higgs mass has been neglected. Not only does the non-zero Higgs mass change the evolution of the radiation energy density, but it also affects the duration of the reheating phase. Next, let us stress that in the *massive scenario*, the energy density of the SM species is reduced compared to the *massless case*, which, in turn, leads to the elongation of reheating in the former scenario. As seen from Fig. 4.6 and Fig. 4.7, such effects are more significant for relatively large inflaton–Higgs coupling. Furthermore, let us highlight that the presented numerical results are in good agreement with our analytic estimations Eq. (4.164) for *massless* and Eq. (4.170) for *massive reheating cases*. Finally, it should be emphasized that after the end of reheating, i.e., $a > a_{\rm rh}$, we reproduce the prediction of the standard cosmology, namely the energy density of the Universe redshifts as radiation, i.e., $\rho \propto a^{-4}$ in both considered scenarios.

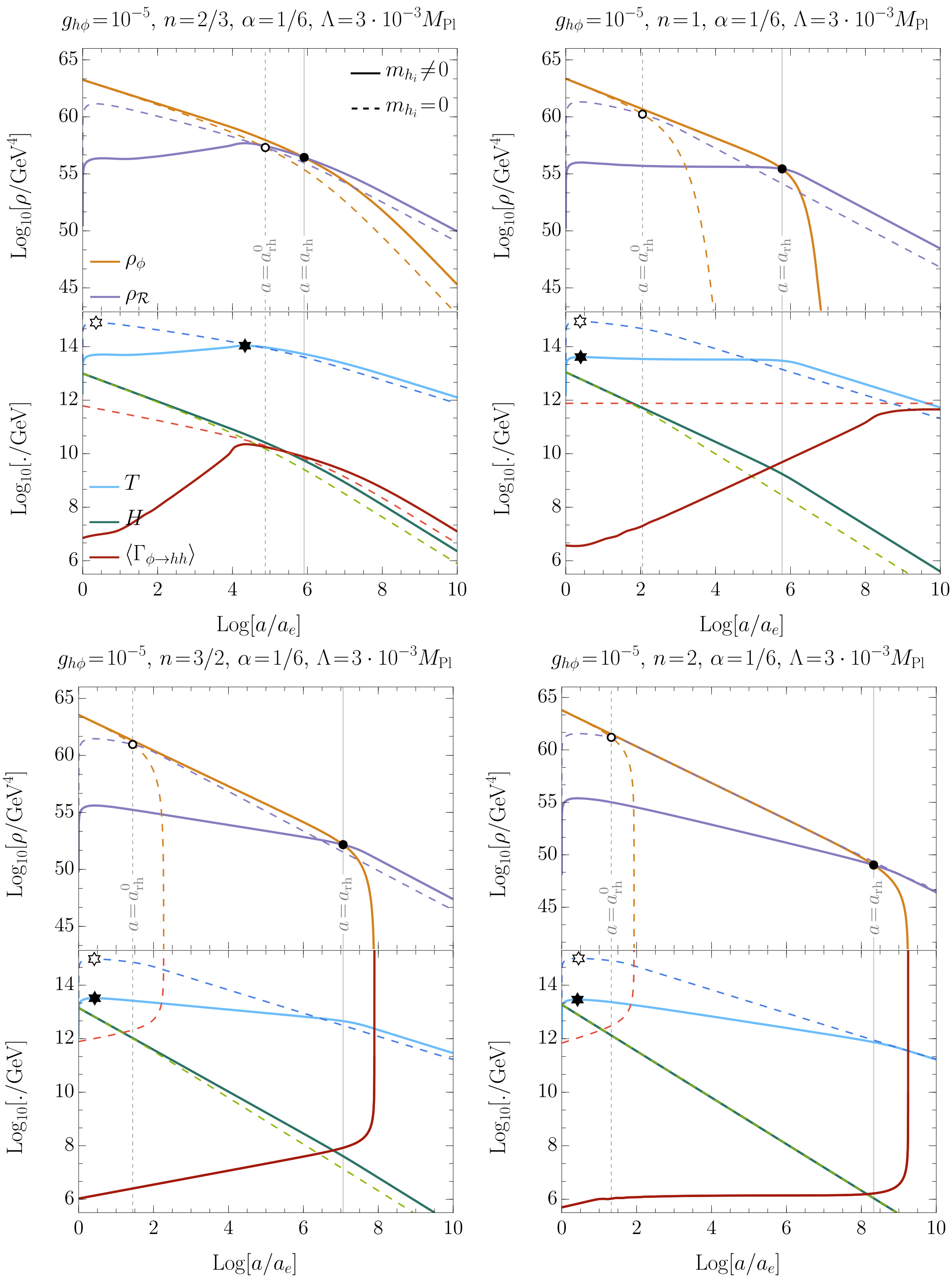

FIGURE 4.6: The upper panels present the evolution of the inflaton ρ_ϕ (orange line) and radiation $\rho_{\rm SM}$ (purple line) energy densities as functions of a in the *massless* (dashed) and *massive reheating scenario* (solid curves). The position of white and black dots indicate the inflaton-radiation equality in the *massless* and *massive scenarios*, respectively. The lower panels show the evolution of the thermal bath temperature T (blue), the Hubble parameter H (green), and *averaged inflaton decay width* $\langle\Gamma_{\phi\to\mathbf{hh}}\rangle$ (red). White and black stars signalize the maximal temperature obtained by the SM sector during reheating for massless and massive final states, respectively.

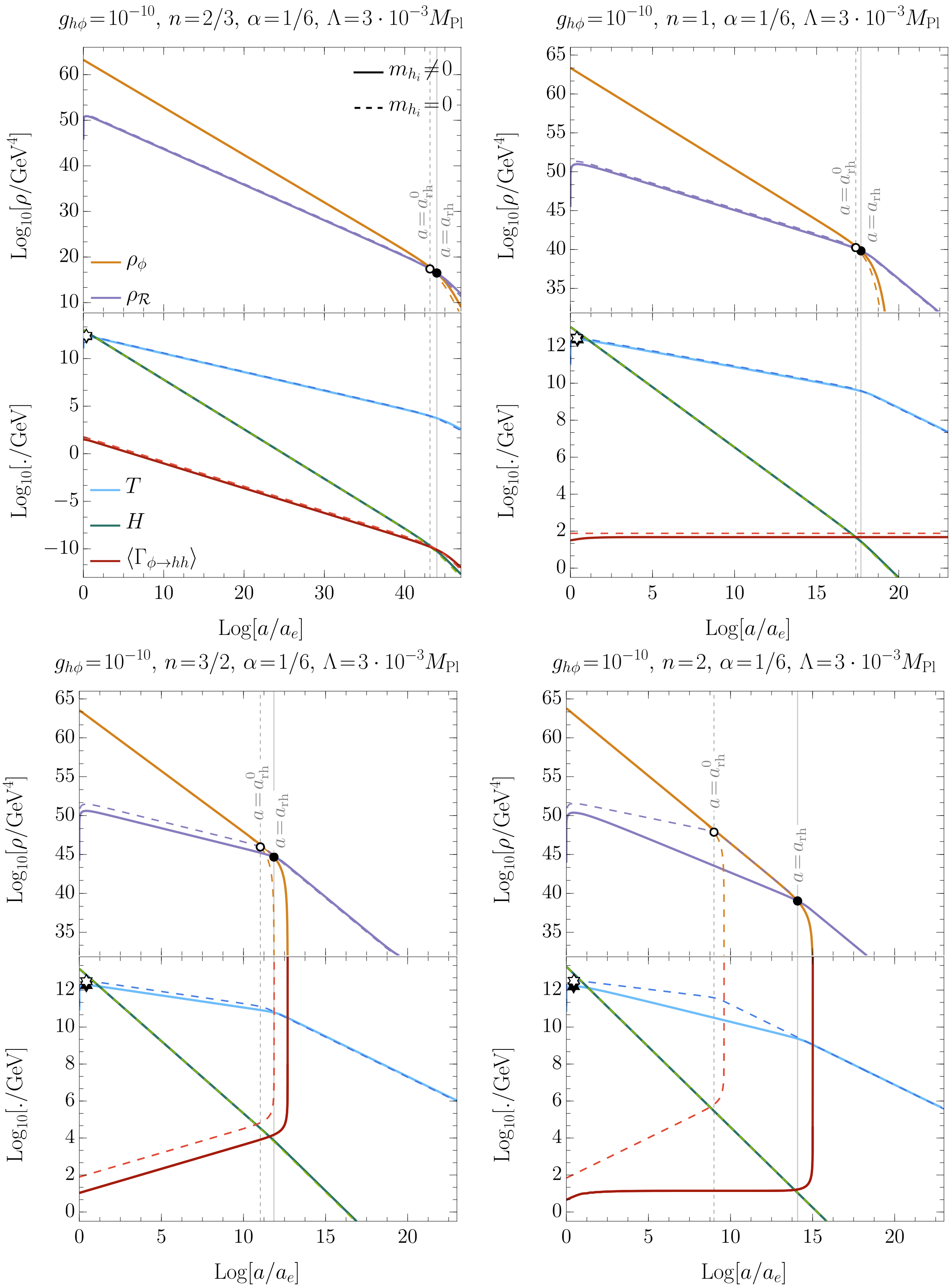

FIGURE 4.7: Same as in Fig. 4.6 except for $g_{h\phi} = 10^{-10}$.

Moreover, as it is shown in the lower panel of the figures (4.6) and (4.7), the Hubble rate H decreases as $a^{-3n/(n+1)}$ during reheating, and as a^{-2} afterward, independent on the considered reheating scenario. The most significant effect of the non-trivial Higgs mass during reheating is on the *inflaton decay width*. The evolution of $\langle\Gamma_{\phi\to\mathbf{hh}}\rangle$ with a is very sensitive to the strength of the inflaton-Higgs coupling constant as the latter determines the role of kinematic effects. Namely, in all considered cases, we observe that $\langle\Gamma_{\phi\to\mathbf{hh}}\rangle$ is suppressed relative to its massless counterpart $\langle\Gamma^{(0)}_{\phi\to\mathbf{hh}}\rangle$. Since the role of kinematic suppression decreases with time for $n \leq 3/2$, the *inflaton decay width* in the *massive scenario* initially grows with the scale factor up to the moment when the Higgs mass becomes negligible and $\langle\Gamma_{\phi\to\mathbf{hh}}\rangle$ roughly approaches $\langle\Gamma^{(0)}_{\phi\to\mathbf{hh}}\rangle$. The convergence of these two quantities is not perfect as in the *massless scenario* the inflaton "decays" to four massless Higgs components. Contrarily, in the *massive reheating* (even if the kinematic effects are tiny), during one half of the oscillation period, i.e., when$\mathcal{P}<0$ and the electroweak symmetry is broken, inflaton can only transfer its energy to one final state - h_0, while during the other half ($\mathcal{P}>0$) the final state is made of four massive Higgs components h_i degenerate in mass. Therefore, eventually, the averaged inflaton decay rate $\langle\Gamma_{\phi\to\mathbf{hh}}\rangle$ for the *massive case*, in the limit, when mass effects are negligible, is a factor 5/8 smaller than that of the massless case, see Fig. 4.6 and Fig. 4.7. On the other hand, for $n = 3/2$, we observe a constant kinematic suppression of $\langle\Gamma_{\phi\to\mathbf{hh}}\rangle$, which results in a shift of the *inflaton decay width* towards smaller values. Whereas, for $n \geq 3/2$, the impact of the non-zero Higgs mass on $\langle\Gamma_{\phi\to\mathbf{hh}}\rangle$ is the largest and leads to completely different evolution with the scale factor than in the massless case. Our numerical results illustrating the *averaged inflaton decay rate* in the presence of the kinematic suppression agree well with analytic result (4.168). At this point, we should stress that our analytical estimations are only valid during the reheating period, i.e., for $a \in [a_e, a_{\rm rh}]$, when the inflaton energy density is analytically calculated. Since after the end of reheating $a > a_{\rm rh}$ the inflaton energy sharply vanishes for $n \geq 1$, the corresponding *decay width*, which is proportional to $\rho^{(1-n)/n}$, becomes divergent for $n > 1$, which is indeed seen in Fig. 4.6 and Fig. 4.7 for $n = \{3/2, 2\}$. Finally, we see that the Higgs mass effects are relevant for the large inflaton-Higgs coupling, e.g., $g_{h\phi} = 10^{-5}$. However, as we have emphasized above, even for relatively weak coupling, e.g., $g_{h\phi} = 10^{-10}$, the kinematic suppression might still be significant for $n > 3/2$.

To summarize this section, we have demonstrated that the consequences of the inflaton-induced mass of the SM Higgs field can be dramatic for the reheating dynamics. Not only does it change the evolution of the radiation energy density and hence, the thermal bath temperature, but it also affects the duration of the reheating period, cf. the left panel of Fig. 4.8, where we have compared the relation between $N_{\rm rh}$ and $g_{h\phi}$, in both considered scenarios. We see that in the *massive scenario*, reheating is not only delayed but also strongly suppressed. Moreover, in this case, the production of the SM species is less efficient than in the *massless case*. Therefore, the thermal bath temperature, measured by the energy density of the SM radiation, in the *massive scenario* is reduced compared to the *massless case*, which is explicitly shown in the right panel of Fig. 4.8. This figure shows that the most considerable discrepancy between the *massless* and *massive scenarios* is observed for the $n=2$ curve. It is also worth noting that in the standard scenario with massless Higgs, the maximal temperature, $T_{\rm max}$, is typically attained shortly after the end of inflation. However, in the *massive scenario* and for $n \in (1/2, 1)$ it is reached after a few e-folds of reheating when kinematic suppression becomes irrelevant and $\langle\Gamma_{\phi\to\mathbf{hh}}\rangle$ approaches $\langle\Gamma^{(0)}_{\phi\to\mathbf{hh}}\rangle$. As the strength of the inflaton-Higgs interactions decreases, the role of the non-zero mass of the Higgs boson becomes less and less relevant for the dynamics of reheating. As shown in the left panel of Fig. 4.8, all solid curves slowly approach the corresponding dashed lines. For the small value of the inflaton-Higgs coupling, e.g., $g_{h\phi} = 10^{-10}$, the discrepancy between solid and corresponding dashed lines is

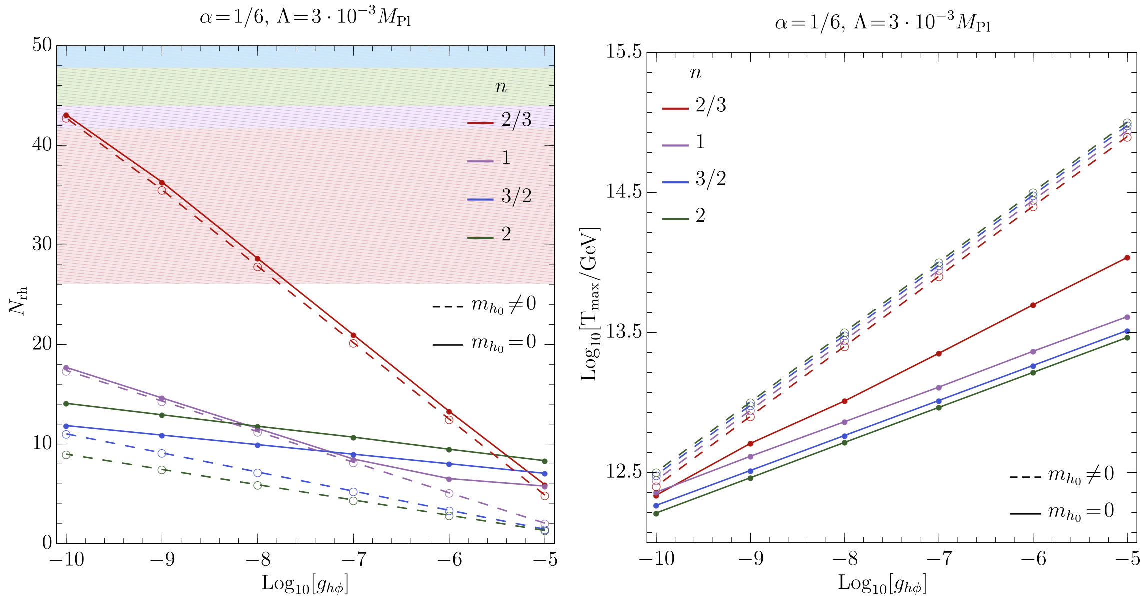

FIGURE 4.8: Left panel: Relation between the reheating numbers of e-folds $N_{\rm rh}$ and the inflaton-Higgs coupling constant $g_{h\phi}$. Right panel: Relation between the maximal temperature, $T_{\rm max}$, obtained during reheating and $g_{h\phi}$. Filled (empty) dotes present pairs of $(g_{h\phi}, N_{\rm rh})$ obtained assuming the massive (massless) reheating scenario, whereas solid (dashed) curves show corresponding linear interpolations to the data. In the upper panel, colored regions show constraints on $N_{\rm rh}$ for different values of n, see Table (4.3).

tiny. However, the $n=2$ curve is an exception to this rule, and even for $g_{h\phi} = 10^{-10}$, we observe a non-negligible deviation from the massless case. This is caused by the fact that for the $n=2$ case, the slope of $\rho_{\rm SM}$ as a function of a is steeper in the *massive scenario*, and thus it takes more e-folds of reheating to drop ρ_ϕ below $\rho_{\rm SM}$.

Chapter 5

Primordial gravitational waves

The primordial gravitational waves (PGWs) are considered one of the key predictions of the inflationary paradigm, as they originated from quantum fluctuations of the inflation field [192–195]. Such fluctuations caused the perturbations of the metric tensor through Einstein's field equations. Tiny quantum fluctuations, with wavelength much shorter than the inflationary Hubble radius, were stretched to the super-horizon scales as a result of the accelerated expansion of the Universe. After horizon-crossing, the quantum nature of PGWs disappeared as primordial fluctuations became classical. Later on, in the subsequent post-inflationary epochs, these perturbations eventually became sub-horizon as they crossed the Hubble radius. When tensor modes re-enter the horizon, they transition into a coherent background of gravitational waves (GWs). This background exhibits stochastic behavior while maintaining its classical nature and constitutes an irreducible source of GWs.

In a conventional post-inflationary scenario, tensor modes re-entered the horizon during the radiation-dominated epoch, giving rise to an almost scale-invariant spectrum of PGWs. However, the presence of *non-standard cosmologies* might alter this prediction and breaks a scale-invariance of a PGWs spectrum. For instance, it is well known that the existence of an early stiff era before the RD epoch could lead to a blue-tilted spectrum for modes crossing the horizon during this phase [364–378]. In addition, in such a scenario, the amplitude of the tensor power spectrum becomes significantly enhanced compared to the standard case. The *non-standard cosmologies* arise if the onset of the RD epoch is delayed, e.g., due to a non-instantaneous reheating. As demonstrated in the previous chapter, this might happen, e.g., when the inflaton oscillates in a non-trivial potential during reheating, which inevitably results in a time-dependent interaction rate.

Motivated by the above arguments, we investigate the impact of the non-standard reheating dynamics on the PGWs spectrum. We focus on two *massless reheating scenarios* induced by the direct inflaton coupling to the SM scalars and fermions[1] This chapter is based on Ref.[1] and it is organized as follows. In Sec.(5.1), we derive the equation of motion for GWs in the presence of anisotropic tensor. Then we discuss the evolution of GWs in the super- and sub-horizon regimes and provide the generic solution to their EoM. We end this section by obtaining the master formula for the spectral energy density of the primordial gravitational waves. In Sec.(5.2), we find the present energy density of PGWs re-entering the horizon during the RD epoch as well as during the non-standard reheating phase. The existing observational constraints are discussed in Sec.(5.3). Finally, we present our results in Sec.(5.4).

[1] More extended analysis can be found in Ref.[1], where we have also discussed the reheating scenario induced by derivative interactions as well as elaborated on the impact of the *time-dependent inflaton decay width* on the UV freeze-in DM production and its connection with GWs dynamics.

5.1 Gravitational waves

The perturbed FLRW metric in the conformal Newtonian gauge reads [379]

$$ds^2 = a^2(\tau)\left\{(1+2\Psi)d\tau^2 - \left[(1+2\Phi)\delta_{ij} + \frac{1}{2}\left(\partial_i\epsilon_j + \partial_j\epsilon_i\right) + h_{ij}\right]dx^i dx^j\right\}, \tag{5.1}$$

where Ψ, Φ denote the gauge-invariant Bardeen variables responsible for the perturbations in the scalar sector, whereas $\frac{1}{2}\left(\partial_i\epsilon_j + \partial_j\epsilon_i\right)$ and h_{ij} are vector and tensor perturbations, respectively.

Note that in the presence of perturbations, the energy density ρ, the pressure p, and the fluid four-velocity u_μ become functions of the position, i.e.,

$$\rho(\tau,\vec{x}) = \bar{\rho}(\tau) + \delta\rho(\tau,\vec{x}), \quad p(\tau,\vec{x}) = \bar{p}(\tau) + \delta p(\tau,\vec{x}), \quad u_\mu(\tau,\vec{x}) = \bar{u}_\mu(\tau) + \delta u_\mu(\tau,\vec{x}), \tag{5.2}$$

where quantities with a bar denote homogeneous background values. Including a contribution from the anisotropic stress (AS) tensor Σ_μ^ν, the perturbed energy-momentum tensor can be decomposed as [379]

$$\delta T_\mu^\nu = (\delta\rho + \delta p)\bar{u}^\mu\bar{u}_\nu + (\bar{\rho} + \bar{p})(\delta u^\mu \bar{u}_\nu + \bar{u}^\mu \delta u_\nu) - \delta p \delta_\nu^\mu - \Sigma_\nu^\mu. \tag{5.3}$$

The spatial part of the AS tensor contains scalar, vector, and tensor components

$$\Sigma_{ij} \equiv \Sigma_{ij}^{\mathrm{s}} + \Sigma_{ij}^{\mathrm{v}} + \Pi_{ij}^{\mathrm{TT}}, \tag{5.4}$$

where Π_{ij}^{TT} is chosen to be transverse T and traceless T, i.e.,

$$\partial_i \Pi_{ij}^{\mathrm{TT}} = 0, \qquad \delta^{ij}\Pi_{ij}^{\mathrm{TT}} = 0. \tag{5.5}$$

Restricting our attention to tensor perturbations, we consider the following line element:

$$ds^2 = a^2(\tau)[d\tau^2 - (\delta_{ij} + h_{ij})dx^i dx^j], \tag{5.6}$$

where the h_{ij} tensor is symmetric, traceless, and transverse, i.e.,

$$h_{ij} = h_{ji}, \qquad \delta^{ij}h_{ij} = 0, \qquad \partial^j h_{ij} = 0, \tag{5.7}$$

and hence contains two independent modes.

To study the evolution of tensor perturbations, one should find the perturbed Einstein equation

$$\delta G_\mu^\nu = M_{\mathrm{Pl}}^{-2}\,\delta T_\mu^\nu. \tag{5.8}$$

To find the l.h.s. of Eq.(5.8), let us first compute the affine connection of the perturbed metric (5.6). From the definition (2.7), one finds that up to the linear order, the non-vanishing Christoffel symbols are

$$\Gamma_{00}^0 = \frac{g^{0\sigma}}{2}[g_{\sigma 0,\tau} + g_{\sigma 0,\tau} - g_{00,\sigma}] = \frac{a'}{a} = \mathcal{H}, \tag{5.9}$$

$$\begin{aligned}\Gamma_{ij}^0 &= \frac{g^{0\sigma}}{2}[g_{\sigma i,j} + g_{\sigma j,i} - g_{ij,\sigma}] = \frac{a^{-2}}{2}\partial_\tau(a^2(\delta_{ij} + h_{ij})) = \frac{a'}{a}\delta_{ij} + \frac{a'}{a}h_{ij} + h'_{ij} \\ &= \mathcal{H}\left[\delta_{ij} + h_{ij}\right] + h'_{ij},\end{aligned} \tag{5.10}$$

$$\Gamma_{j0}^i = \frac{g^{i\sigma}}{2}[g_{\sigma j,\tau} + g_{\sigma 0,j} - g_{j0,\sigma}] = \frac{a^{-2}(\delta^{ik} - h^{ik})}{2}\partial_\tau(a^2(\delta_{kj} + h_{kj}))$$

$$= \mathcal{H}\delta^i_j + \frac{1}{2}h^{i\prime}_j + \mathcal{O}(h^2), \tag{5.11}$$

$$\Gamma^i_{jk} = \frac{g^{i\sigma}}{2}[g_{\sigma j,k} + g_{\sigma k,j} - g_{jk,\sigma}] = \frac{a^{-2}(\delta^{il} - h^{il})}{2}a^2\left[h_{lj,k} + h_{lk,j} - h_{jk,l}\right]$$

$$= \frac{1}{2}\left(h^i_{j,k} + h^i_{k,j} - \delta^{il}h_{jk,l}\right) + \mathcal{O}(h^2). \tag{5.12}$$

Hence, the non-zero components of the Ricci tensor (2.15) are

$$R_{00} = \partial_\lambda\Gamma^\lambda_{00} - \partial_\tau\Gamma^\lambda_{0\lambda} + \Gamma^\lambda_{\lambda\rho}\Gamma^\rho_{00} - \Gamma^\rho_{0\lambda}\Gamma^\lambda_{0\rho}$$

$$= -3\mathcal{H}' - \frac{1}{2}h^{i\prime\prime}_i + \mathcal{H}\left(3\mathcal{H} + \frac{1}{2}h^{i\prime}_i\right) - \left(\mathcal{H}\delta^i_j + \frac{1}{2}h^{i\prime}_j\right)\left(\mathcal{H}\delta^j_i + \frac{1}{2}h^{j\prime}_i\right)$$

$$= \underbrace{-3\mathcal{H}'}_{\text{the background value}} + \mathcal{O}(h^2), \tag{5.13}$$

and

$$R_{ij} = \partial_\lambda\Gamma^\lambda_{ij} - \partial_j\Gamma^\lambda_{i\lambda} + \Gamma^\lambda_{\lambda\rho}\Gamma^\rho_{ij} - \Gamma^\rho_{j\lambda}\Gamma^\lambda_{i\rho}$$

$$= \mathcal{H}'\delta_{ij} + \mathcal{H}'h_{ij} + \mathcal{H}h'_{ij} + \frac{1}{2}h''_{ij} - \frac{1}{2}\nabla^2 h_{ij} + 4\mathcal{H}^2 h_{ij} + 2\mathcal{H}h'_{ij} + 4\mathcal{H}^2\delta_{ij} - 2\mathcal{H}^2\delta_{ij}$$

$$- 2\mathcal{H}^2 h_{ij} - \mathcal{H}\delta_{jk}h^{k\prime}_i - 2\mathcal{H}h_{jk}h^{k\prime}_i - \mathcal{H}h'_{ij} - h'_{jk}h^{k\prime}_i$$

$$+ \frac{1}{4}(h^k_{j,m} + h^k_{m,j} - \delta^{kl}h_{jm,l})(h^m_{i,k} + h^m_{k,i} - \delta^{ml}h_{ik,l})$$

$$= \underbrace{(\mathcal{H}' + 2\mathcal{H}^2)\delta_{ij}}_{\text{the background value}} + \underbrace{\frac{1}{2}\left(h''_{ij} - \nabla^2 h_{ij} + 2\mathcal{H}h'_{ij} + 2\mathcal{H}'h_{ij} + 4\mathcal{H}^2 h_{ij}\right)}_{\text{1st order perturbation}} + \mathcal{O}(h^2). \tag{5.14}$$

Note that at the linear order, the Ricci scalar R (2.16) does not receive any contribution from tensor perturbations. This results from the fact that all terms are either of the second order, e.g., $h_{ij}h^{ij}$, or vanish because h_{ij} is transverse, and traceless (5.7). Thus, the Ricci scalar takes its homogeneous value,

$$R = a^{-2}\left[-3\mathcal{H}' - \delta^{ij}\left(\mathcal{H}' + 2\mathcal{H}^2\right)\delta_{ij}\right] = -6a^{-2}\left[\mathcal{H}' + \mathcal{H}^2\right]. \tag{5.15}$$

Now we can calculate the non-zero components of the Einstein tensor

$$G_{00} = R_{00} - \frac{1}{2}g_{00}R = -3\mathcal{H}' + \frac{a^2}{2}\frac{6}{a^2}\left[\mathcal{H}' + \mathcal{H}^2\right] = 3\mathcal{H}^2, \tag{5.16}$$

$$G_{ij} = R_{ij} - \frac{1}{2}g_{ij}R$$

$$= (\mathcal{H}' + 2\mathcal{H}^2)\delta_{ij} + \frac{1}{2}\left(h''_{ij} - \nabla^2 h_{ij} + 2\mathcal{H}h'_{ij} + 2\mathcal{H}'h_{ij} + 4\mathcal{H}^2 h_{ij}\right)$$

$$- \frac{a^2(\delta_{ij} + 2h_{ij})}{2}\frac{6}{a^2}\left[\mathcal{H}' + \mathcal{H}^2\right]$$

$$= -(2\mathcal{H}' + \mathcal{H}^2)\delta_{ij} + \frac{1}{2}\left(h''_{ij} - \nabla^2 h_{ij} + 2\mathcal{H}h'_{ij} - 4\mathcal{H}'h_{ij} - 2\mathcal{H}^2 h_{ij}\right). \tag{5.17}$$

Hence,

$$\delta G^j_i = -\frac{a^{-2}}{2}\delta^{jk}\left(h''_{ik} - \nabla^2 h_{ik} + 2\mathcal{H}h'_{ik} - 4\mathcal{H}'h_{ik} - 2\mathcal{H}^2 h_{ik}\right). \tag{5.18}$$

To compute the r.h.s of (5.8), we use the fact that the background value of the spatial part of SET is $T_i^j = -\bar{p}\delta_i^j$. Moreover, perturbations of the energy-momentum tensor in the tensor sector take the form

$$\delta T_i^{j,\mathrm{t}} = -\Pi_i^{j,\mathrm{TT}}. \tag{5.19}$$

In the conformal coordinates, the background Einstein equation reads

$$(00): \qquad 3\mathcal{H}^2 = M_{\mathrm{Pl}}^{-2} a^2 \bar{\rho}, \tag{5.20}$$

$$(ij): \qquad 2\mathcal{H}' + \mathcal{H}^2 = -M_{\mathrm{Pl}}^{-2} a^2 \bar{p}, \tag{5.21}$$

whereas the equation for perturbation is

$$h_{ij}'' - \nabla^2 h_{ij} + 2\mathcal{H}h_{ij}' - 4\mathcal{H}' h_{ij} - 2\mathcal{H}^2 h_{ij} = 2M_{\mathrm{Pl}}^{-2} a^2 (\bar{p}\, h_{ij} + \Pi_{ij}^{\mathrm{TT}}). \tag{5.22}$$

Utilizing the background equation (5.21), one obtains

$$\boxed{h_{ij}'' + 2\mathcal{H}h_{ij}' - \nabla^2 h_{ij} = 2M_{\mathrm{Pl}}^{-2} a^2\, \Pi_{ij}^{\mathrm{TT}}.} \tag{5.23}$$

It is instructive to decompose Π_{ij}^{TT} into Fourier modes

$$\Pi_{ij}^{\mathrm{TT}}(\tau, \vec{x}\,) = \sum_{\lambda=+,\times} \int \frac{d^3k}{(2\pi)^3} \Pi_k^\lambda(\tau)\, \epsilon_{ij}^\lambda(\vec{k}\,)\, e^{i\vec{k}\cdot\vec{x}}, \tag{5.24}$$

where the two polarisation tensors $\epsilon_{ij}^\lambda(\vec{k})$ are symmetric, traceless and transverse Eq.(3.91), and have the orthonormal Eq.(3.90), and completeness relations (3.90).

Then, by utilizing Eq.(5.45), one finds that in the momentum space the EoM for the mode function h_k^λ becomes

$$h_k^{\lambda\prime\prime} + 2\mathcal{H}h_k^{\lambda\prime} + k^2 h_k^\lambda = 2M_{\mathrm{Pl}}^{-2} a^2 \Pi_k^\lambda. \tag{5.25}$$

To track the propagation of the tensor perturbations, one can neglect the r.h.s. of the above equation. In other words, the mode equation

$$h_k^{\lambda\prime\prime} + 2\mathcal{H}h_k^{\lambda\prime} + k^2 h_k^\lambda \simeq 0, \tag{5.26}$$

describes the evolution of the PGWs in the FLRW background after the source, responsible for their generation, has been switched off.
Note that by redefining the h_k field, according to

$$\widetilde{h}_k^\lambda \equiv \frac{\sqrt{2}}{M_{\mathrm{Pl}}} \frac{h_k^\lambda}{a}, \tag{5.27}$$

one obtains the *Mukhanov-Sasaki* equation for the tensor perturbations, which we have introduced in (3.98).

Now let us consider the solution to the mode equation (3.98) in two regimes, i.e., when modes enter the horizon and become super-Hubble ($(aH)^{-1} \ll k^{-1}$), and in the sub-horizon limit ($(aH)^{-1} \gg k^{-1}$) when modes eventually re-enter the horizon after the cosmic inflation.

5.1.1 The super-horizon regime

In the far past, all modes were inside the horizon. All curvature fluctuations were stretched as the comoving horizon $(aH)^{-1}$ shrank during inflation. At some point the comoving wavelength k^{-1} crossed the Hubble radius, i.e., $k_\star^{-1} = (a_\star H_\star)^{-1}$, and modes became super-Hubble. In the super-horizon regime, $(aH)^{-1} \ll k^{-1}$, the EoM for tensor perturbations (5.26) simplifies as

$$h_k^{\lambda\prime\prime} + 2\,\frac{a'}{a} h_k^{\lambda\prime} \approx 0\,, \qquad\qquad \Longrightarrow\ a^{-2}\left(a^2\, h^{\lambda\prime}\right)' \approx 0\,. \tag{5.28}$$

The above equation has a solution

$$h_\lambda(\tau, \vec{k}) = \mathcal{C}_1 + \mathcal{C}_2 \int \frac{d\tau'}{a(\tau')^2}\,, \tag{5.29}$$

where $\mathcal{C}_{1,2}$ are constants of integration. The second term in the above expression quickly decays and, thus, becomes negligible. Hence, one can ignore it, obtaining a constant solution. Therefore, the amplitude of tensor perturbations remains constant in the super-horizon scale [380, 381].

5.1.2 The sub-horizon regime

Tensor modes that exit the horizon during inflation eventually re-enter it in the following cosmological epochs. To analyze the behavior of GWs in the sub-horizon regime, $(aH)^{-1} \gg k^{-1}$, let us note that the $\frac{a''}{a}$ ratio scales as $\sim (aH)^2$, and therefore, in the sub-horizon limit it is subdominant. In this regime, the solution to the mode equation (3.98) is well-approximated by the following expression:

$$\widetilde{h}_k^\lambda(\tau) \simeq \mathcal{C}_3 \exp{(ik\tau)} + \mathcal{C}_4 \exp{(-ik\tau)}.$$

Hence, tensor perturbations undergo damped oscillations

$$h_k^\lambda(\tau) \simeq \frac{\sqrt{2}\,\mathcal{C}_3}{M_{\rm Pl}} \frac{\exp{(ik\tau)}}{a} + \frac{\sqrt{2}\,\mathcal{C}_4}{M_{\rm Pl}} \frac{\exp{(-ik\tau)}}{a}. \tag{5.30}$$

5.1.3 The generic solution

Once we have discussed the asymptotic behavior of the tensor perturbations in the super- and sub-horizon regimes, let us elaborate on the generic solution to the equation (5.26). To that end, let us note that

$$\mathcal{H} = \frac{a'}{a} = \frac{2}{1+3w} \frac{\tau^{\frac{2}{1+3w}-1}}{\tau^{\frac{2}{1+3w}}} = \frac{2}{1+3w}\frac{1}{\tau}. \tag{5.31}$$

Hence, the mode equation (5.26) can be rewritten as

$$\ddot{h}_k^\lambda + \frac{4}{1+3w}\frac{1}{x}\dot{h}_k^\lambda + h_k^\lambda \simeq 0, \tag{5.32}$$

where $\dot{()} \equiv \partial/\partial x$, and $x \equiv k\tau$. Adopting the field redefinition

$$e_k^\lambda = x^{3/2} h_k^\lambda, \tag{5.33}$$

one finds

$$x^2\ddot{e}_k^\lambda + \left(\underbrace{\frac{-12w}{1+3w}}_{\equiv 2p} +1\right) x\dot{e}_k^\lambda + \left(x^2 + \underbrace{\frac{15}{4} - \frac{6}{1+3w}}_{\equiv \beta^2}\right) e_k^\lambda = 0, \tag{5.34}$$

which is a transformed version of the Bessel equation

$$x^2\ddot{y} + (2p+1)x\dot{y} + (\alpha^2 x^{2r} + \beta^2)y = 0. \tag{5.35}$$

The solution to the above equation takes the following form:

$$y = x^{-p}\left[C_1 J_{q/r}\left(\frac{\alpha}{r}x^r\right) + C_2 Y_{q/r}\left(\frac{\alpha}{r}x^r\right)\right], \qquad q = \sqrt{p^2-\beta^2}. \tag{5.36}$$

Hence, the tensor perturbations evolve as

$$h_k^\lambda(\tau) = x^{-3/2}e_k^\lambda = (k\tau)^{-\frac{3}{2}+\frac{6w}{1+3w}}\left[C_1 J_q(k\tau) + C_2 Y_q(k\tau)\right], \tag{5.37}$$

with

$$q \equiv \sqrt{\frac{6}{1+3w}\left[1+\frac{w^2}{1+3w}\right] - \frac{15}{4}}. \tag{5.38}$$

Utilizing solution (5.37) during, e.g., matter-dominated phase $w_{\rm MD} = 0$, one finds

$$h_k^{\lambda,\rm MD}(\tau) = (k\tau)^{3/2}\left[C_1 J_{3/2}(k\tau) + C_2 Y_{3/2}(k\tau)\right],$$

where

$$J_{3/2}(x) = \sqrt{\frac{2}{\pi x}}\left(\frac{\sin(x)}{x} - \cos(x)\right), \tag{5.39}$$

$$Y_{3/2}(x) = -\sqrt{\frac{2}{\pi x}}\left(\frac{\cos(x)}{x} + \sin(x)\right). \tag{5.40}$$

The asymptotic behavior of the Bessel function,

$$J_{3/2}(x) \overset{x\to 0}{\simeq} \frac{1}{3}\sqrt{\frac{2}{\pi}}x^{3/2}, \qquad Y_{3/2}(x) \overset{x\to 0}{\simeq} -\sqrt{\frac{2}{\pi}}x^{-3/2}, \tag{5.41}$$

$$J_{3/2}(x) \overset{x\to \infty}{\simeq} -\sqrt{\frac{2}{\pi}}\cos(x)\, x^{-1/2}, \qquad Y_{3/2}(x) \overset{x\to \infty}{\simeq} -\sqrt{\frac{2}{\pi}}\sin(x) x^{-1/2}, \tag{5.42}$$

indicates that $C_2 = 0$.

5.1.4 The energy spectrum of PGWs

To obtain the energy-momentum tensor of GWs, one needs to expand the Ricci tensor to the second order in tensor perturbations. The results reads [372, 380–383]

$$T_{\mu\nu}^{\rm GW} = \frac{M_{\rm Pl}^2}{4}\langle \partial_\mu h_{\alpha\beta}\, \partial^\mu h^{\alpha\beta}\rangle, \tag{5.43}$$

where $\langle \dots \rangle$ denotes an average over a length-scale l and/or time-scale $\tilde{t}$, where $\lambda \ll l \ll L_B$, with λ (L_B) being the length-scale of GWs (the background), whereas $1/f_{GW} \ll \tilde{t} \ll 1/f_B$

with f_{GW} and f_B denoting the frequency of GWs and the characteristic frequency of the background variation, respectively [372].
Hence, the energy density carried by the GWs is given by

$$\rho_{\rm GW} \equiv T_{00}^{\rm GW} = \frac{M_{\rm Pl}^2}{4}\langle \dot{h}_{ij}\,\dot{h}^{ij}\rangle, \tag{5.44}$$

Inserting

$$h_{ij}(\tau,\vec{x}\,) = \sum_{\lambda=+,\times}\int \frac{d^3k}{(2\pi)^3} h_k^\lambda(\tau)\,\epsilon_{ij}^\lambda(\vec{k}\,)\,e^{i\vec{k}\cdot\vec{x}}, \tag{5.45}$$

one finds

$$\begin{aligned}\rho_{\rm GW} &= \frac{M_{\rm Pl}^2}{4}\sum_\lambda\sum_\sigma\int\frac{d^3k}{(2\pi)^3}\int\frac{d^3q}{(2\pi)^3}\langle \dot{h}_k^\lambda(\tau)\,\epsilon_{ij}^\lambda(\vec{k}\,)\,e^{i\vec{k}\cdot\vec{x}}\dot{h}_q^\lambda(\tau)\,\epsilon^{\sigma,ij}(\vec{q}\,)\,e^{i\vec{q}\cdot\vec{x}}\rangle\\ &= \frac{M_{\rm Pl}^2}{2}\sum_\lambda\int\frac{d^3k}{(2\pi)^3}|\dot{h}_k^\lambda|^2,\end{aligned} \tag{5.46}$$

where we have utilized Eq.(3.90) and the fact that the spatial average $\langle\ldots\rangle$ is equivalent to the ensemble average in the momentum space [380], i.e.,

$$\langle \dot{h}_k^\lambda \dot{h}_q^\sigma\rangle = (2\pi)^3\delta^{\lambda\sigma}\delta^{(3)}(\vec{k}+\vec{q})|\dot{h}_k^\lambda|^2. \tag{5.47}$$

In the following steps, we assume that the primordial GWs are unpolarized, which means that $|h_k^+|= |h_k^\times|$.

It is convenient to parametrize the dynamics of PGWs after their first horizon-crossing by introducing the transfer function, $\mathcal{T}(\tau,k)$, as follows [381, 384],

$$h_k^\lambda(\tau) = h_k^{\lambda,\star}\mathcal{T}(\tau,k), \tag{5.48}$$

with $h_k^{\lambda,\star}$ being the value of the mode function evaluated at the moment when the k mode exits the horizon, i.e., $h_k^\lambda(\tau_\star)$, where $\tau_\star$ is defined by the condition $k_\star = a_\star(\tau_\star)H_\star(\tau_\star)$. As we have explicitly demonstrated in Sec.(5.1.1), the amplitude of PGWs remains constant on super-horizon scales, which implies that $\mathcal{T}(\tau,k)\to 1$, for $(aH)^{-1}\ll k^{-1}$. Hence, the non-trivial part of $\mathcal{T}(\tau,k)$ accounts for the post-inflationary sub-horizon evolution of gravitational waves. This means that the transfer function connects the primordial with the late-time behavior of the mode function.
Inserting Eq.(5.48) into Eq.(5.46), we find

$$\rho_{\rm GW} = \frac{M_{\rm Pl}^2}{2a^2}\int\frac{d^3k}{(2\pi)^3}|h_k^{\lambda,\star}|^2[\mathcal{T}(\tau,k)']^2 \equiv \frac{M_{\rm Pl}^2}{4a^2}\int d\ln k\Delta_t^2[\mathcal{T}'(\tau,k)]^2, \tag{5.49}$$

with

$$\Delta_t^2 \equiv \frac{k_\star^3}{\pi^2}|h_k^{\lambda,\star}|^2 = \frac{2}{\pi^2}\frac{H_\star^2}{M_{\rm Pl}^2}, \tag{5.50}$$

where we have used Eq.(3.101).
Now let us introduce the spectral density, defined by the ratio of the GWs energy density per

logarithmic wavenumber, normalized to the critical density $\rho_{\rm crit} = 3\,H^2 M_{\rm Pl}^2$, i.e.,

$$\Omega_{\rm GW}(\tau,k) = \frac{1}{\rho_c}\frac{d\rho_{\rm GW}}{d\ln k}\,. \tag{5.51}$$

Using Eq.(5.49), one gets

$$\Omega_{\rm GW}(\tau,k) = \frac{1}{12}\frac{\Delta_t^2}{a^2H^2}[\mathcal{T}'(\tau,k)]^2. \tag{5.52}$$

Thus to find the spectral density of PGWs, one needs to determine $\mathcal{T}'(\tau,k)$. To that end, we take advantage of the fact that the GWS amplitude stays constant on super-horizon scales and decreases as a^{-1} once tensor perturbations re-enter the Hubble horizon. Using the sub-horizon solution (5.30), one infers that

$$\mathcal{T}' \sim \frac{a^{\rm hc}}{a}(k - Ha)e^{ik\tau}, \tag{5.53}$$

where $a^{\rm hc}$ denotes the scale factor at the second (after inflation) horizon-crossing. In the sub-horizon regime, one can neglect the second term in the parenthesis, obtaining [219, 375, 385]

$$|\mathcal{T}'(\tau,k)|^2 = \frac{k^2}{2}\left(\frac{a^{\rm hc}}{a}\right)^2, \tag{5.54}$$

where the factor 1/2 is responsible for the average of the tensor mode functions oscillations [381, 386, 387]. The above equation indicates that $\mathcal{T}(\tau\,,k)$ characterizes the expansion history between the moment of the second horizon-crossing $\tau^{\rm hc}$ of a given mode k, and some later moment $\tau > \tau^{\rm hc}$.

Inserting Eq.(5.54) into (5.52), we finally obtain

$$\Omega_{\rm GW}(\tau,k) = \frac{1}{24}\left(\frac{k}{aH}\right)^2 \Delta_t^2 \left(\frac{a^{\rm hc}}{a}\right)^2. \tag{5.55}$$

5.2 Present energy density of PGWs

The energy density parameter of PGWs at the present epoch can be calculated from the following formula:

$$\Omega_{\rm GW}^{(0)}h^2(k) = \frac{1}{24}\left(\frac{k}{a_0H_0}\right)^2 \Delta_t^2 \left(\frac{a^{\rm hc}}{a_0}\right)^2 h^2\,. \tag{5.56}$$

Our goal now is to determine the $a^{\rm hc}/a_0$ ratio. For this purpose, we assume that modes re-enter the Hubble horizon when the averaged equation-of-state parameter of the Universe is equal $\bar{w}$. From (2.150) we already known that

$$a^{\rm hc} = k^{-\frac{2}{1+3\bar{w}}}\,. \tag{5.57}$$

Hence, one anticipates that $\Omega_{\rm GW}^{(0)}h^2$ has a power-law dependence on k.
Utilizing (5.57) together with (5.56), one finds

$$\Omega_{\rm GW}^{(0)}(k) \propto k^{\frac{2(3\bar{w}-1)}{1+3\bar{w}}}\,. \tag{5.58}$$

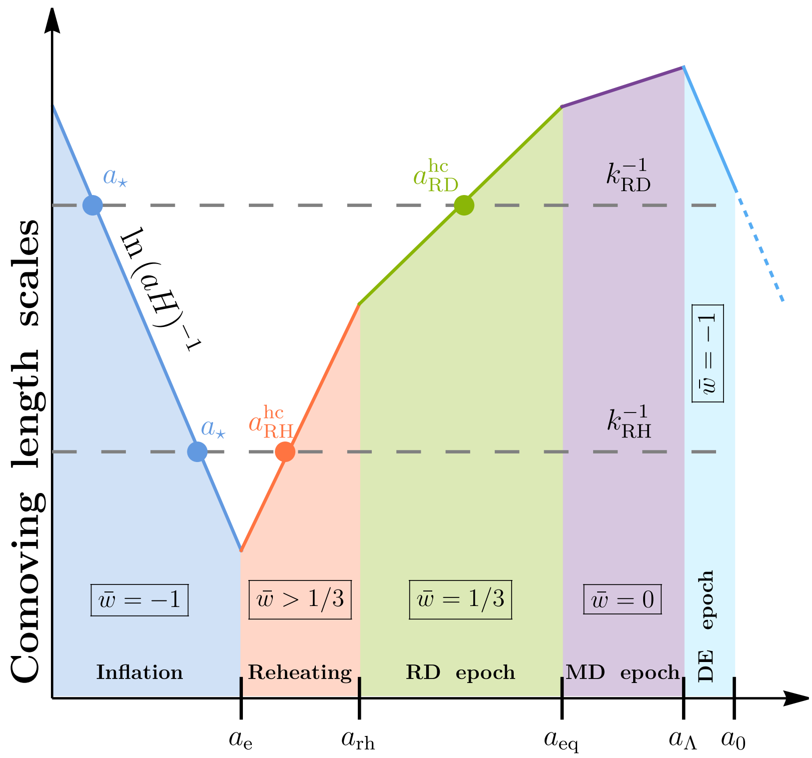

FIGURE 5.1: The evolution of cosmological comoving length scales with the scale factor at different cosmological epochs. Here "RD" stands for radiation domination, "MD" implies matter domination, and "DE" corresponds to dark energy domination. The $(aH)^{-1}$ curve shows the evolution of the Hubble horizon, which shrinks during inflation and grows in the subsequent cosmological eras. Modes with wavenumber $k_{\rm RD}^{-1}$ $(k_{\rm RH}^{-1})$ exit the horizon at $a_\star$, and re-enter it during RD (reheating) phase.

In the remaining part of this section, we aim to find the proportionality coefficient in the above expression. One expects that this coefficient should somehow depend on the expansion history at the moment of the second horizon-crossing after the end of inflation. Therefore, it might be different for modes reentering the horizon at different cosmological epochs, e.g., during reheating or later on during the RD epoch.

5.2.1 The horizon-crossing during the RD era

At first, let us find the spectrum of GWs reentering the horizon during the RD epoch after the end of reheating, i.e., $a_{\rm RD}^{\rm hc} \in (a_{\rm rh}, a_{\rm r.m.e})$, cf. the $k_{\rm RH}^{-1}$ mode in Fig.(5.1). In this case, the present fractional energy density of PGWs is given by

$$\Omega_{\rm GW}^{(0),{\rm RD}} h^2(k) = \frac{\Delta_t^2}{24}\left(\frac{H_{\rm RD}^{\rm hc}}{H_0}\right)^2\left(\frac{a_{\rm RD}^{\rm hc}}{a_0}\right)^4 h^2\,. \tag{5.59}$$

The Hubble rate at the horizon-crossing $H_{\rm RD}^{\rm hc}$ can be related to its present value through the following formula [381]:

$$\left(\frac{H_{\rm RD}^{\rm hc}}{H_0}\right)^2 = \frac{\frac{\pi^2}{30} g_{\star\rho,{\rm RD}}^{\rm hc} (T_{\rm RD}^{\rm hc})^4}{\rho_{{\rm crit},0}} = \frac{\frac{\pi^2}{15} T_{\gamma,0}^4}{\rho_{{\rm crit},0}} \frac{g_{\star\rho,{\rm RD}}^{\rm hc}}{2}\left(\frac{T_{\rm RD}^{\rm hc}}{T_{\gamma,0}}\right)^4 = \Omega_{\gamma,0}\frac{g_{\star\rho,{\rm RD}}^{\rm hc}}{2}\left(\frac{g_{\star s,{\rm RD}}^{\rm hc}}{g_{\star s,fin}}\right)^{-4/3}\left(\frac{a_0}{a_{\rm RD}^{\rm hc}}\right)^4, \tag{5.60}$$

where in the last step, we have used the entropy conservation, i.e., $g_{\star s}a^3T^3 = \text{const}$. Note that $\Omega_{\gamma,0} = \rho_{\gamma,0}/\rho_{\text{crit},0} = 2.47 \times 10^{-5}\, h^{-2}$, and $g_{\star s,fin}$ is evaluated after the neutrino decoupling. Substituting Eq.(5.60) into (5.59), one finds the standard *scale-invariant* result for the spectral GW energy density

$$\Omega_{\text{GW}}^{(0),\text{RD}} h^2(k) = \frac{\Delta_t^2}{24} \frac{g_{\star\rho,\text{RD}}^{\text{hc}}}{2} \left(\frac{g_{\star s,\text{RD}}^{\text{hc}}}{g_{\star s,fin}}\right)^{-4/3} \Omega_{\gamma,0} h^2. \tag{5.61}$$

The above expression implies that the spectrum of GWs which re-enter the horizon during the RD phase is approximately flat.

5.2.2 The horizon-crossing during reheating

Now let us investigate the spectrum of GWs reentering the horizon just after the end of inflation, during the reheating phase, i.e., $a_{\text{RH}}^{\text{hc}} \in (a_e, a_{\text{rh}})$. In Fig.(5.1), such case is represented by the mode with wavenumber k_{RH}^{-1}.
For the monomial inflaton potential, the averaged equation-of-state parameter $\bar{w}$ during reheating can be related to the index n, parametrizing the inflaton potential Eq.(3.30), though (3.36). Utilizing Eq.(5.56), one finds

$$\Omega_{\text{GW}}^{(0),\text{RH}} h^2(k) = \frac{\Delta_t^2}{24} \left(\frac{H_{\text{RH}}^{\text{hc}}}{H_0}\right)^2 \left(\frac{a_{\text{RH}}^{\text{hc}}}{a_0}\right)^4 = \Omega_{\text{GW}}^{(0),\text{RD}} h^2(k) \left[\left(\frac{g_{\star\rho,\text{rh}}}{g_{\star\rho,\text{RD}}^{\text{hc}}}\right)^{\frac{3}{4}} \frac{g_{\star s,\text{RD}}^{\text{hc}}}{g_{\star s,\text{rh}}}\right]^{\frac{4}{3}} \left(\frac{a_{\text{RH}}^{\text{hc}}}{a_{\text{rh}}}\right)^{\frac{4-2\,n}{n+1}}, \tag{5.62}$$

where we have used the following relations:

$$\left(\frac{a_{\text{rh}}}{a_{\text{RH}}^{\text{hc}}}\right)^4 \left(\frac{H_{\text{rh}}}{H_{\text{RD}}^{\text{hc}}}\right)^2 = \frac{g_{\star\rho,\text{rh}}}{g_{\star\rho,\text{RD}}^{\text{hc}}} \left(\frac{g_{\star s,\text{RD}}^{\text{hc}}}{g_{\star s,\text{rh}}}\right)^{4/3}, \tag{5.63}$$

$$\left(\frac{a_{\text{RH}}^{\text{hc}}}{a_{\text{rh}}}\right)^4 \left(\frac{H_{\text{RH}}^{\text{hc}}}{H_{\text{rh}}}\right)^2 = \left(\frac{a_{\text{RH}}^{\text{hc}}}{a_{\text{rh}}}\right)^{\frac{4-2\,n}{n+1}}, \tag{5.64}$$

assuming entropy conservation after the end of reheating, and relating the Hubble rate at the horizon crossing $H_{\text{RH}}^{\text{hc}}$ to its value at the end of reheating using Eq.(4.99).

The frequency f of PGWs crossing the horizon during reheating is [381]

$$f = \frac{k}{2\pi} \frac{1}{a_0} = \frac{H_{\text{RH}}^{\text{hc}}}{2\,\pi} \frac{a_{\text{RH}}^{\text{hc}}}{a_0} = \frac{1}{2\pi} \sqrt{\frac{\rho_{\text{rh}}}{3M_{\text{Pl}}^2}} \frac{a_{\text{RH}}^{\text{hc}}}{a_0} \left(\frac{a_{\text{rh}}}{a_{\text{RH}}^{\text{hc}}}\right)^{\frac{3\,n}{n+1}}. \tag{5.65}$$

Let us stress that the frequencies of PGWs cannot be arbitrarily large. Oppositely, there exists an upper bound,

$$f_{\max} = \frac{H_e}{2\pi} \frac{a_e}{a_0} = \frac{H_e}{2\pi} \frac{g_{\star s,0}^{1/3}\, T_0}{g_{\star s,\text{rh}}^{1/3}\, T_{\text{rh}}} \frac{a_e}{a_{\text{rh}}}, \tag{5.66}$$

determined by the frequency of modes that re-enter the horizon just after the end of inflation. Note that modes with frequencies $f > f_{\max}$ are never produced.
The ratio a_e/a_{rh} can be estimated from Eq.(4.106), as a function of the index n, $\beta_F(n)$, $\widetilde{\Gamma}^e_{\phi\to FF}$, and the Hubble scale at the end inflation H_e. Alternatively, one can relate $f_{\max}$ to

the inflationary scale Λ as follows

$$f_{\max} = \frac{1}{2\sqrt{2}\pi}\frac{\Lambda^2}{M_{\rm Pl}}\frac{g_{\star s,0}^{1/3}\,T_0}{g_{\star s,{\rm rh}}^{1/3}\,\rho_{\rm rh}^{1/4}}\left(\frac{30}{\pi^2 g_{\star\rho,{\rm rh}}}\right)^{-1/4}\times\begin{cases}\xi_1^{\frac{n+1}{\beta_F(n+1)-3n}}, & \beta_F<\frac{n+4}{n+1},\\ \xi_2^{\frac{n+1}{2(2-n)}}\,W^{\frac{n+1}{2(2-n)}}(\xi_2)\,, & \beta_F=\frac{n+4}{n+1},\\ (-\xi_1)^{\frac{n+1}{2(2-n)}}\,, & \beta_F>\frac{n+4}{n+1},\end{cases} \tag{5.67}$$

where ξ_1, ξ_2 are now expressed as a function of Λ, i.e.,

$$\xi_1 \simeq \frac{n+4-\beta_F(n+1)}{2n}\frac{\Lambda^2}{\sqrt{2}M_{\rm Pl}\,\widetilde{\Gamma}^e_{\phi\to FF}}, \qquad \xi_2 \simeq \frac{n-2}{n}\frac{\Lambda^2}{\sqrt{2}M_{\rm Pl}\,\widetilde{\Gamma}^e_{\phi\to FF}}. \tag{5.68}$$

Note that above, we have used the following approximation:

$$H_e \simeq \frac{1}{\sqrt{2}}\frac{\Lambda^2}{M_{\rm Pl}}, \tag{5.69}$$

neglecting the $\tanh^{2n}(\phi_e/(\sqrt{6\alpha}M_{\rm Pl}))$ factor.
From Eq. (5.65), one finds

$$\frac{a^{\rm hc}_{\rm RH}}{a_{\rm rh}} = f^{\frac{1+n}{1-2n}}\left[2\sqrt{3}\pi\left(\frac{g_{\star s,{\rm rh}}}{g_{\star s,0}}\right)^{1/3}\left(\frac{30}{\pi^2 g_{\star\rho,{\rm rh}}}\right)^{1/4}\frac{M_{\rm Pl}}{T_0\rho_{\rm rh}^{-1/4}}\right]^{\frac{1+n}{1-2n}}. \tag{5.70}$$

Substituting the above formula into Eq. (5.62), one obtains

$$\Omega^{(0),{\rm RH}}_{\rm GW}h^2 = \Omega^{(0),{\rm RD}}_{\rm GW}h^2\,\widetilde{\mathcal{F}}(g_\star)\left[\frac{1}{2\pi\sqrt{3}}\frac{T_0}{M_{\rm Pl}}\left(\frac{30}{\pi^2\,g_{\star\rho,{\rm rh}}}\right)^{-\frac{1}{4}}\right]^{\frac{4-2n}{2n-1}}\rho_{\rm rh}^{\frac{2-n}{4n-2}}\,f^{\frac{2n-4}{2n-1}}\,, \tag{5.71}$$

with

$$\widetilde{\mathcal{F}}(g_\star) \equiv \frac{g_{\star\rho,{\rm rh}}}{g^{\rm hc}_{\star\rho,{\rm RD}}}\left(\frac{g^{\rm hc}_{\star s,{\rm RD}}}{g_{\star s,{\rm rh}}}\right)^{\frac{4}{3}}\left(\frac{g_{\star s,{\rm rh}}}{g_{\star s,0}}\right)^{\frac{4-2n}{3-6n}}. \tag{5.72}$$

Let us stress that Eq.(5.71) reveals the blue-tilted behavior of the GWs spectrum for $\bar{w} > 1/3$, which indicates a stiff inflaton potential, i.e., $n > 2$.
Using, Eqs.(4.101) and (4.106), one finds that

$$\rho_{\rm rh} \simeq \frac{1}{\sqrt{2}}\frac{6n}{1+n}\widetilde{\Gamma}^e_{\phi\to FF}\Lambda^2 M_{\rm Pl} \times\begin{cases}\frac{n+1}{n+4-\beta_F(n+1)}\,\xi_1^{\frac{\beta_F(n+1)+3n}{\beta_F(n+1)-3n}}, & \beta_F<\frac{n+4}{n+1},\\ \xi_2^{\frac{2n+2}{2-n}}\,W^{\frac{2n+2}{2-n}}(\xi_2)\ln\left[\xi_2^{\frac{n+1}{2(n-2)}}\,W^{\frac{n+1}{2(n-2)}}(\xi_2)\right], & \beta_F=\frac{n+4}{n+1},\\ \frac{n+1}{\beta_F(n+1)-(n+4)}\,(-\xi_1)^{\frac{2n+2}{2-n}}\,, & \beta_F>\frac{n+4}{n+1}.\end{cases} \tag{5.73}$$

Hence, one can substitute the above expression into (5.71), and explicitly express $\Omega^{(0),{\rm RH}}_{\rm GW}$ as a function of $\{\widetilde{\Gamma}^e_{\phi\to FF}, \Lambda, \beta_F, n\}$, obtaining

$$\Omega^{(0),{\rm RH}}_{\rm GW}h^2(f) \simeq \Omega^{(0),{\rm RD}}_{\rm GW}h^2\,\widetilde{\mathcal{F}}(g_\star)\left[\frac{1}{2\pi\sqrt{3}}\frac{T_0}{M_{\rm Pl}}\left(\frac{30}{\pi^2\,g_{\star\rho,{\rm rh}}}\right)^{-\frac{1}{4}}\right]^{\frac{4-2n}{2n-1}} f^{\frac{2n-4}{2n-1}}$$

$$
\times \left[\frac{6\,n}{\sqrt{2}(n+1)}\,\widetilde{\Gamma}^{e}_{\phi\to FF}\Lambda^2 M_{\rm Pl}\right]^{\frac{2-n}{4\,n-2}}
$$

$$
\times \begin{cases}
\left[\frac{n+1}{n+4-\beta_F(n+1)}\left(\frac{n+4-\beta_F(n+1)}{2n}\frac{\Lambda^2}{\sqrt{2}M_{\rm Pl}\,\widetilde{\Gamma}^{e}_{\phi\to FF}}\right)^{\frac{\beta_F(n+1)+3n}{\beta_F(n+1)-3n}}\right]^{\frac{2-n}{4\,n-2}}, & \beta_F < \frac{n+4}{n+1},\\
\left[\theta^4 \ln\left[\theta^{-1}\right]\right]^{\frac{2-n}{4\,n-2}}, & \beta_F = \frac{n+4}{n+1},\\
\left[\frac{n+1}{\beta_F(n+1)-(n+4)}\left(\frac{\beta_F(n+1)-(n+4)}{2n}\frac{\Lambda^2}{\sqrt{2}M_{\rm Pl}\,\widetilde{\Gamma}^{e}_{\phi\to FF}}\right)^{\frac{2n+2}{2-n}}\right]^{\frac{2-n}{4\,n-2}}, & \beta_F > \frac{n+4}{n+1},
\end{cases}
\tag{5.74}
$$

with

$$
\theta = \left(\frac{n-2}{n}\frac{\Lambda^2}{\sqrt{2}M_{\rm Pl}\,\widetilde{\Gamma}^{e}_{\phi\to FF}}\right)^{\frac{n+1}{2(2-n)}} W^{\frac{n+1}{2(2-n)}}\left(\frac{n-2}{n}\frac{\Lambda^2}{\sqrt{2}M_{\rm Pl}\,\widetilde{\Gamma}^{e}_{\phi\to FF}}\right). \tag{5.75}
$$

The above expressions explicitly show how the proportionality coefficient of Eq. (5.58) depends on the model of reheating, determined by the form of $\widetilde{\Gamma}^{e}_{\phi\to FF}$ and β_F. The form of $\Omega^{(0),\rm RH}_{\rm GW}h^2$ reflects the non-standard evolution of the scale factor a with n during reheating and encapsulates the dynamics of this phase encoded in $\rho_{\rm rh}$. In the non-instantaneous reheating model, the behavior of the scale factor a depends solely on the form of the inflaton potential. On the other hand, the $\Omega^{(0),\rm RH}_{\rm GW}h^2$ dependency on $\rho_{\rm rh}$ can be viewed as a measure of the inflaton-SM interactions, which triggers the completion of reheating. The above result relies on two assumptions: i) that H evolves according to Eq.(4.99), and ii) that time evolution of the *inflaton decay rate*, responsible for the successful accomplishment of reheating is described by the generic power-law formula (4.90). Note that even if the indirect gravitational processes initiate reheating, its ending is governed always[2] by the direct inflaton interactions with the SM bath. Hence, we should highlight that Eq.(5.74) is valid in both the **standard reheating** as well as in the **mixed scenario**, discussed in Sec.(4.3).

From Eq.(5.71), we see that the only frequency dependence of $\Omega^{(0),\rm RH}_{\rm GW}h^2(f)$ is through $f^{\frac{2\,n-4}{2\,n-1}}$, which, in turn, implies that the present spectrum of GWs can be approximated by the following piecewise function:

$$
\Omega^{(0)}_{\rm GW}(f) \sim \Omega^{(0),\rm RD}_{\rm GW}\begin{cases}
1\,, & f < f_{\rm rh},\\
f^{\frac{2\,n-4}{2\,n-1}}\,, & f_{\rm rh} < f < f_{\rm max},\\
0\,, & f > f_{\rm max},
\end{cases}
\tag{5.76}
$$

where $f_{\rm rh}$ denotes the frequency of the mode which re-enters the horizon at the very end of reheating, i.e.,

$$
\begin{aligned}
f_{\rm rh} &= \frac{H_{\rm rh}}{2\pi}\frac{a_{\rm rh}}{a_0} = \frac{1}{2\pi}\sqrt{\frac{\rho_{\rm rh}}{3M_{\rm Pl}^2}}\left(\frac{g_{\star s,0}}{g_{\star s,\rm rh}}\right)^{1/3}\frac{T_0}{\rho_{\rm rh}^{1/4}}\left(\frac{30}{\pi^2 g_{\star\rho,\rm rh}}\right)^{-1/4}\\
&= \frac{1}{2\pi\sqrt{3}}\left(\frac{g_{\star s,0}}{g_{\star s,\rm rh}}\right)^{1/3}\left(\frac{30}{\pi^2 g_{\star\rho,\rm rh}}\right)^{-1/4}\frac{T_0}{M_{\rm Pl}}\left[\frac{1}{\sqrt{2}}\frac{6n}{1+n}\widetilde{\Gamma}^{e}_{\phi\to FF}\Lambda^2 M_{\rm Pl}\right]^{1/4}
\end{aligned}
$$

[2]As pointed out in Ref.[350], purely gravitational reheating is ruled out, since it is inconsistent with BBN constraints.

$$\times \begin{cases} \left[\frac{n+1}{n+4-\beta_F(n+1)}\,\xi_1^{\frac{\beta_F(n+1)+3n}{\beta_F(n+1)-3n}}\right]^{1/4}, & \beta_F < \frac{n+4}{n+1}, \\ \left[\xi_2^{\frac{2n+2}{2-n}}\,W^{\frac{2n+2}{2-n}}(\xi_2)\ln\left[\xi_2^{\frac{n+1}{2(n-2)}}\,W^{\frac{n+1}{2(n-2)}}(\xi_2)\right]\right]^{1/4}, & \beta_F = \frac{n+4}{n+1}, \\ \left[\frac{n+1}{\beta_F(n+1)-(n+4)}\,(-\xi_1)^{\frac{2n+2}{2-n}}\right]^{1/4}, & \beta_F > \frac{n+4}{n+1}. \end{cases} \tag{5.77}$$

Note that the total energy density parameter for gravitational waves $\Omega^{(0)}_{\rm GW}h^2(f)$ is a sum of the energy carried by modes reentering the horizon during the reheating phase, and the constant contribution coming from modes with $f \lesssim f_{\rm rh}$, which become sub-horizon during the RD epoch, i.e.,

$$\Omega^{(0)}_{\rm GW}(f)h^2 \simeq \Omega^{(0),\rm RH}_{\rm GW}h^2(f) + \Omega^{(0),\rm RD}_{\rm GW}h^2(f). \tag{5.78}$$

5.3 Constraints on the model parameters

So far, we have elaborated on the connection between the present spectral energy density of PGWs and the reheating dynamics. The latter was determined by the index n, characterizing inflaton potential during reheating, β_F, parametrizing inflaton interactions with the SM bath responsible for the completion of reheating, and $\widetilde{\Gamma}^e_{\phi\to FF}$. Now let us review existing experimental constraints on the model parameter space.

5.3.1 Constraints on the effective number of relativistic degree of freedom

The energy density of gravitational waves redshifts as $\rho_{\rm GW} \propto a^{-4}$, i.e., the same way as the energy density of ultrarelativistic matter. Therefore, the stochastic background of the primordial gravitational waves acts as an additional source of radiation, which contributes to the evolution of the Hubble rate as [372]

$$H^2 \simeq H_0^2\left[\left(\Omega^{(0)}_{\rm GW} + \Omega_{r,0}\right)\left(\frac{a_0}{a}\right)^4 + \Omega_{m,0}\left(\frac{a_0}{a}\right)^2 + \Omega_{\Lambda,0}\right]. \tag{5.79}$$

The above formula indicates that in order not to spoil predictions of the standard cosmology, the extra radiation component should not significantly modify the expansion history of the Universe. In particular, two cosmological events providing highly accurate measurements of the expansion rate are Big Bang Nucleosynthesis and the process of photon decoupling. Below, we demonstrate how the amount of radiation can constrain the present spectral energy density of GWs at the time of BBN and CMB decoupling. To that end, let us notice that the present density parameter of GWs can be related to the photon energy density, $\rho_\gamma(T) = \pi^2T^4/15$, though the formula

$$\Omega^{(0)}_{\rm GW} = \frac{\rho_{\rm GW}(T)}{\rho_{\rm crit,0}}\left(\frac{g_{\star s,0}^{1/3}\,T_0}{g_{\star s}^{1/3}(T)\,T}\right)^4 = \Omega_{\gamma,0}\left(\frac{g_{\star s,0}}{g_{\star s}(T)}\right)^{4/3}\frac{\rho_{\rm GW}(T)}{\rho_\gamma(T)}. \tag{5.80}$$

Hence, to ensure that the radiation abundance during BBN and CMB decoupling remains within permissible limits, the spectral energy density of GWs needs to be constrained. Typically, any additional source of radiation can be expressed in terms of the *effective number of relativistic degrees of freedom* $N_{\rm eff}$. Namely, separating the contributions from bosonic (b) and fermionic (f) degrees of freedom, the total energy density of relativistic species can be expressed as in Eq.(2.124). For $T \lesssim m_e$, after the electron-positron annihilation, the *effective* *number of relativistic degrees of freedom* is

$$g_{\star\rho}(T \lesssim m_e) = 2 + \frac{7}{8}\, 2 \cdot N_{\rm eff} \left(\frac{4}{11}\right)^{4/3}, \tag{5.81}$$

where we have used the fact that after e^+e^- annihilation, the neutrino temperature is related to the photon temperature as $T_\nu = T_\gamma\,(4/11)^{1/3}$, see Appendix (D).
In the presence of the primordial GWs, the total radiation energy density at $T \lesssim m_e$ can be written as a sum of three contributions:

$$\rho_r(T \lesssim m_e) = \rho_\gamma + \rho_\nu + \rho_{\rm GW} = \frac{\pi^2}{30}\left[2 + \frac{7}{4} N_{\rm eff}\left(\frac{4}{11}\right)^{4/3}\right] T_\gamma^4 = \rho_\gamma \left[1 + \frac{7}{8} N_{\rm eff}\left(\frac{4}{11}\right)^{4/3}\right], \tag{5.82}$$

which, in turn, implies

$$\frac{\rho_\nu}{\rho_\gamma} + \frac{\rho_{\rm GW}}{\rho_\gamma} \equiv \frac{7}{8}\left[N_{\rm eff}^{\rm SM} + \Delta N_{\rm eff}\right]\left(\frac{4}{11}\right)^{4/3}, \tag{5.83}$$

where the excess of radiation constituents, $\Delta N_{\rm eff}$, can be expressed as

$$\Delta N_{\rm eff} = N_{\rm eff} - N_{\rm eff}^{\rm SM} = \frac{8}{7}\left(\frac{11}{4}\right)^{4/3} \frac{\rho_{\rm GW}(T)}{\rho_\gamma(T)}. \tag{5.84}$$

Instantaneous decoupling of the SM neutrinos would have led to $N_{\rm eff}^{\rm SM} = 3$. However more precise value, taking into account non-instantaneous decoupling and the fact that the spectrum of SM neutrinos after decoupling deviates slightly from the Fermi-Dirac distribution, is $N_{\rm eff}^{\rm SM} = 3.044$ [388–396].
Then, one can utilize the above expression to impose the upper bound on the energy density of GWs today [372]

$$\Omega_{\rm GW}^{(0)} h^2 \leq \Omega_\gamma^{(0)}\, h^2 \left[\frac{g_{\star s,0}}{g_{\star s}(T)}\right]^{4/3} \frac{7}{8}\, \Delta N_{\rm eff} \simeq 5.6 \times 10^{-6}\, \Delta N_{\rm eff}\,, \tag{5.85}$$

where

$$\Omega_{\rm GW}^{(0)} h^2 = \int_{f_{\rm BBN}}^{f_{\rm max}} \frac{df}{f}\, \Omega_{\rm GW}^{(0)}(f) h^2\,, \tag{5.86}$$

and we have used $\Omega_\gamma^{(0)}\, h^2 = 2.47 \times 10^{-5}$, $g_{\star s}(T = {\rm MeV}) \simeq 10.75$, $g_{\star s,0} \simeq 3.91$.
Note that the upper limit of the integral (5.86), $f_{\rm max}$ (5.66), corresponds to the frequency of modes that match the size of the horizon at the very end of inflation, whereas the lower limit, $f_{\rm BBN}$, denotes the frequency of modes that re-enter the horizon at the time of BBN. The integration (5.86) can be performed analytically using Eq. (5.74). For all $f_{\rm BBN} < f < f_{\rm max}$ and $n > 2$ it gives us [368, 372, 374, 397]

$$\Omega_{\rm GW}^{(0)}\, h^2(f) \lesssim 2 \times 5.62 \times 10^{-6} \left(\frac{n-2}{2\,n-1}\right) \Delta N_{\rm eff} \lesssim 5.62 \times 10^{-6}\, \Delta N_{\rm eff}. \tag{5.87}$$

Utilizing Eq. (5.71), one finds that for $n > 2$, $\Omega_{\rm GW}^{(0),{\rm RH}} h^2$ is inversely proportional to $\rho_{\rm rh}$. Hence, an increase of $\rho_{\rm rh}$ leads to the less stringent bound on $\Omega_{\rm GW}^{(0)}$ coming from $\Delta N_{\rm eff}$. In the remaining part of this chapter, we explicitly demonstrate that if reheating efficiency is high GWs energy density is diluted, and in such the case, one easily evades the $\Delta N_{\rm eff}$ constraints. Let us also stress that the bound in Eq.(5.85) applies only to GWs produced before the BBN or CMB decoupling.

Finally, we review the current experimental constraints and prospects for $\Delta N_{\rm eff}$ measurements. Within the framework of ΛCDM, the Planck data gives $N_{\rm eff,Planck} = 2.99 \pm 0.34$ at 95% CL [13]. Once the baryon acoustic oscillation (BAO) data are included, the estimation becomes more stringent, i.e., $N_{\rm eff,Planck+BAO} = 2.99 \pm 0.17$. The combined BBN+CMB analysis reveals $N_{\rm eff,BBN+CMB} = 2.880 \pm 0.144$ [398]. The forthcoming CMB surveys such as CMB-S4 [399] and CMB-HD [400] are expected to achieve a level of precision $\Delta N_{\rm eff} \simeq 0.06$ and $\Delta N_{\rm eff} \simeq 0.027$, respectively. In the next era of satellite missions, including COrE [401] and Euclid [402], these limits might be further improved up to $\Delta N_{\rm eff} \lesssim 0.013$.

5.3.2 BBN bounds on the reheating temperature

Yet another constraint on the model parameter space originates from the BBN bounds on the thermal bath temperature at the end of reheating, which now can be expressed in terms of the inflationary scale $\Lambda, \widetilde{\Gamma}^e_{\phi\to FF}, \beta_F$ and n, as follows

$$T_{\rm rh} \simeq \left[\frac{30}{\sqrt{2}\pi^2 g_{\star\rho,\rm rh}}\frac{6n}{1+n}\widetilde{\Gamma}^e_{\phi\to FF}\Lambda^2 M_{\rm Pl}\right]^{1/4} \times \begin{cases} \left[\frac{n+1}{n+4-\beta_F(n+1)}\,\xi_1^{\frac{\beta_F(n+1)+3n}{\beta_F(n+1)-3n}}\right]^{1/4}, & \beta_F < \frac{n+4}{n+1}, \\ \left\{\xi_2^{\frac{2n+2}{2-n}}\,W^{\frac{2n+2}{2-n}}(\xi_2)\ln\left[\xi_2^{\frac{n+1}{2(n-2)}}\,W^{\frac{n+1}{2(n-2)}}(\xi_2)\right]\right\}^{1/4}, & \beta_F = \frac{n+4}{n+1}, \\ \left[\frac{n+1}{\beta_F(n+1)-(n+4)}\,(-\xi_1)^{\frac{2n+2}{2-n}}\right]^{1/4}, & \beta_F > \frac{n+4}{n+1}. \end{cases} \tag{5.88}$$

Let us stress that once the reheating scenario is specified, β_F is set by the index n, according to (4.95). However, it is worth noting that $T_{\rm rh}$ in the middle case, i.e., for $\beta_F = (n+4)/(n+1)$, is independent of β_F. For example, in the case of Yukawa interaction (4.6), this corresponds to $n = 7/2$, while the uppermost and lowermost cases are realized for $n \ll 7/2$ and $n \gg 7/2$, respectively.

As we have already stressed in Sec.(4.4), to maintain the agreement with the BBN predictions, one should impose the lower bound on reheating temperature so that $T_{\rm rh} \gtrsim 4\,{\rm MeV}$ [272, 357–362]. From the above expression, we see that the BBN bound puts a constraint on the inflaton couplings (through $\widetilde{\Gamma}^e_{\phi\to FF}$) and inflaton potential parameters, i.e., Λ and n.

5.3.3 Bounds on the inflationary scale

Finally, according to our discussion in Sec.(3.3), from the CMB measurement of the inflationary observables, i.e., the tensor-to-scalar ratio r and the spectral index n_s, one could infer the upper limit on the Hubble rate at the end of inflation (3.105), which for the $\alpha-$attractor T-model is equivalent to the constrain on the inflationary scale Λ (3.148), i.e., $\Lambda \lesssim 1.4 \times 10^{16}\,{\rm GeV}$.

5.4 Results and Discussion

In this section, we present the results for the spectrum of primordial gravitational waves in the presence of a non-standard reheating phase. As it has already been noted in the previous section, the enhancement of $\Omega^{(0)}_{\rm GW}h^2$ is expected for a stiff inflaton potential, i.e., $n > 2$. Below, we restrict our attention to two possible scenarios, focusing on reheating models induced by the direct inflaton interactions with SM scalars and fermions, parametrized by $g_{S\phi}$[3] (4.5) and dimensionless $g_{\Phi\phi}$ (4.6) coupling constants, respectively. We assume that direct inflaton-SM interactions are weak so that the inflaton-induced mass of the final states can be neglected and the kinematic effects, discussed in Sec.(4.5.2), do not affect the reheating dynamics. In other words, SM quanta are here treated as massless states. Moreover, we assume that they thermalize instantaneously after being produced. Let us also stress that for the considered values of the coupling constant gravitational interactions can be relevant at the beginning of reheating. However, its completion is triggered solely by the direct inflaton-SM interactions, parametrized by $\widetilde{\Gamma}^e_{\phi\to FF}$. Since $\Omega^{(0)}_{\rm GW}h^2$ does not depend on observables that are sensitive to conditions on the onset of reheating, e.g., $T_{\rm max}$, in the remaining part of this chapter, we neglect the gravitational contribution to the reheating process.

5.4.1 Bosonic scenario

Let us begin with the cubic inflaton-scalar interaction (4.5), for which $\beta_S = 3(1-n)/(1+n)$. The strength of the inflaton-Higgs coupling, and hence the duration of the reheating phase, is determined by the coupling constant $g_{S\phi}$ having a mass dimension. Note that the same coupling also controls the spectral energy density of PGWs through Eq. (5.74). Hence, detecting a signal from the stochastic GWs background would give us a unique opportunity to test models of reheating. Thus, the main purpose of the presented analysis is to find the range of the model parameters for which there exist detection prospects for the GWs spectrum satisfying the inflationary, BBN, and $\Delta N_{\rm eff}$ constraints.

To that end, we first fixed the inflationary scale $\Lambda = 10^{16}\,$GeV, and choose four benchmark values of the $g_{S\phi}$ coupling, i.e., $g_{S\phi} \in \{10^{-10}, 10^{-12}, 10^{-14}, 10^{-16}\}\,$GeV for which we plot $T_{\rm rh}$ as a function of n (top left panel of Fig. 5.2). From this figure, we see that for $g_{S\phi} \gtrsim 10^{-12}$ GeV, the reheating temperature exceeds the BBN bound for all considered values of n and evades the $\Delta N_{\rm eff}$ constraints. On the other hand, for weaker inflaton-Higgs coupling and large values of n, one observes that a significant amount of dark radiation is created in the form of PGWs which is inconsistent with the $\Delta N_{\rm eff}$ bound. This region corresponds to the red part of the curves.
Moreover, according to Eq. (5.74), the spectral energy density of PGWs scales as $\Omega^{(0)}_{\rm GW} \propto \left(\Lambda^{8\,n-7}/g_{S\phi}^{n-2}\right)^{\frac{2n}{(1-2\,n)^2}}$. Hence, for fixed inflaton-Higgs coupling and $n > 7/8$, the energy density carried by GWs could exceed the present bounds on dark radiation if the inflationary scale Λ is high enough. This is demonstrated in the top right panel of Figure 5.2, from which we see that large values of Λ can potentially be in conflict with the $\Delta N_{\rm eff}$ constraint. The $\Delta N_{\rm eff}$ red region represents the collective present and future bounds on the $N_{\rm eff}$ excess. Namely, the solid red line corresponds to the Planck data, i.e., $N_{\rm eff} = 2.99 \pm 0.34$ at 95% CL [13]. The dashed red line represents a combined BBN+CMB analysis, providing $N_{\rm eff} = 2.880 \pm 0.144$ [398]. The dot-dashed and dotted red lines are for the upcoming CMB experiments, i.e., CMB-S4 [399] and CMB-HD [400] for which $\Delta N_{\rm eff} \simeq 0.06$ and $\Delta N_{\rm eff} \simeq 0.027$, respectively. Finally, the loosely dashed red line corresponds to the predictions of the next generation of satellite missions, such as COrE [401] and Euclid [402], giving $\Delta N_{\rm eff} \lesssim 0.013$. Note that as seen from the left bottom panel, for fixed n and Λ, the aforementioned bounds set stronger constraints for the prolonged reheating models, with a weak inflaton-Higgs coupling.

[3]Note that to keep the consistency with Ref.[1] in this chapter, we use a mass dimensional parameter $g_{S\phi}$ instead of dimensionless $g_{h\phi}$.

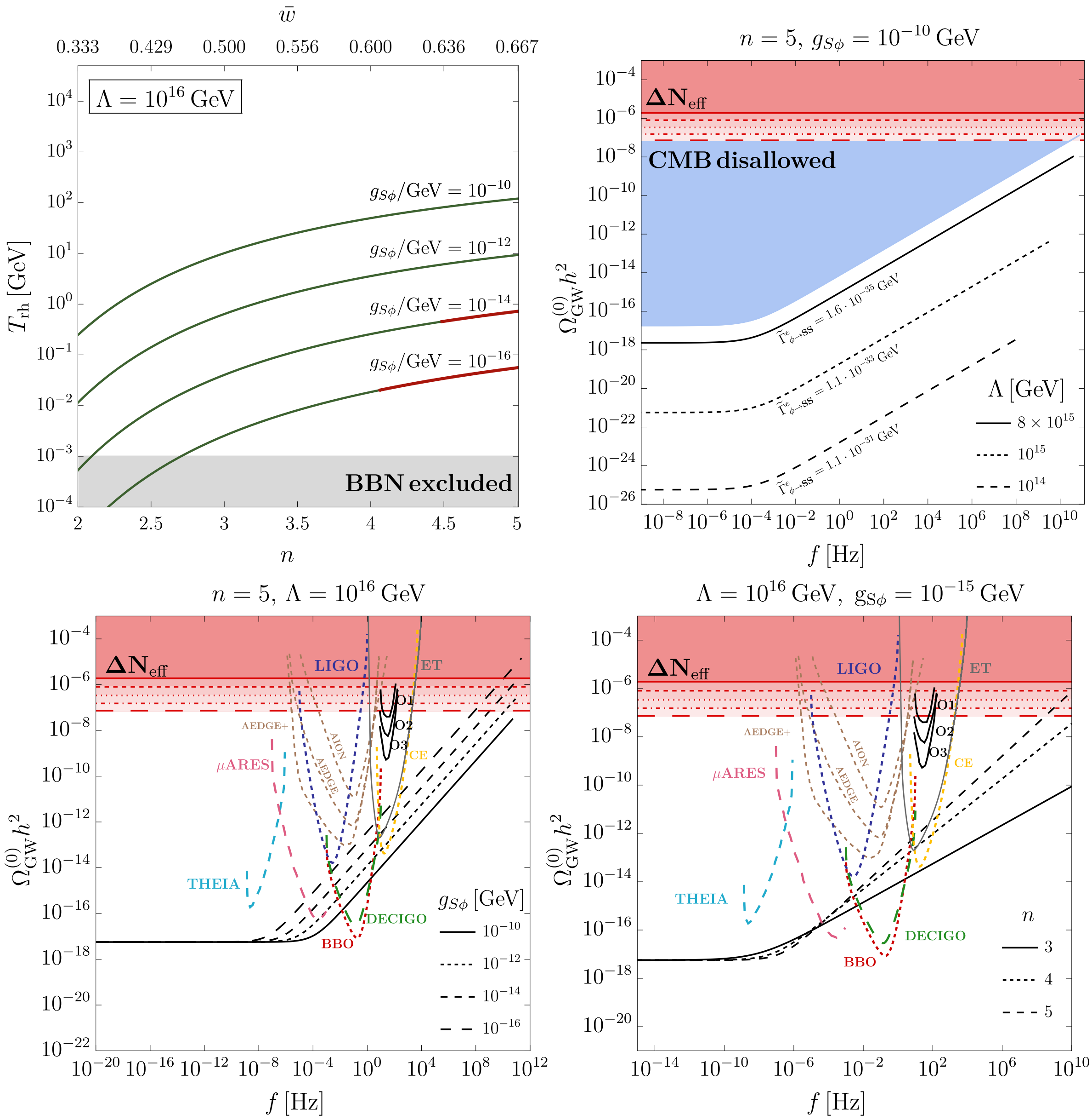

FIGURE 5.2: $\phi \to SS$ scenario. *Top Left:* The reheating temperature $T_{\rm rh}$ as a function of the index n for four benchmark values of $g_{S\phi}$. The thick red part of the curves is excluded by the present bound on $\Delta N_{\rm eff}$ [13]. The BBN bound on $T_{\rm rh}$ disregards the grey-shaded region. *Top Right:* The relation between $\Omega^{(0)}_{\rm GW}h^2$ and the frequency f for a fixed $n = 5$ and $g_{S\phi} = 10^{-10}$ GeV. Different curves correspond to different choices of the inflationary scale Λ. In the pale red regions GWs are overproduced, i.e., this part is ruled out by the $\Delta N_{\rm eff}$ bounds. *Bottom Left:* Same as the top right, but for fixed Λ and n, with different choices of $g_{S\phi}$. Colored curves correspond to different sensitivities of future GWs experiments. *Bottom Right:* Same as the bottom left but for a fixed Λ and $g_{S\phi}$, and three different choice of n.

The bottom right panel illustrates the behaviour of $\Omega^{(0)}_{\rm GW}h^2(f)$ for different inflaton potentials, i.e., $n \in \{3, 4, 5\}$. From this figure, we see that for such a choice of n, the spectral energy density of GWs lies within reach of the proposed GWs detectors while remaining beyond the probe of the future $\Delta N_{\rm eff}$ experiments. In particular, we show the existing and expected sensitivity of several GWs experiments,[4] including LIGO [404–409],

[4]Here we use sensitivity curves derived in Ref. [403].

LISA [410, 411], CE [412, 413], ET [414, 415], BBO [416, 417], DECIGO [418–422], μ-ARES [423], THEIA [424], AEDGE [425, 426] and AION [426–429].

5.4.2 Fermionic scenario

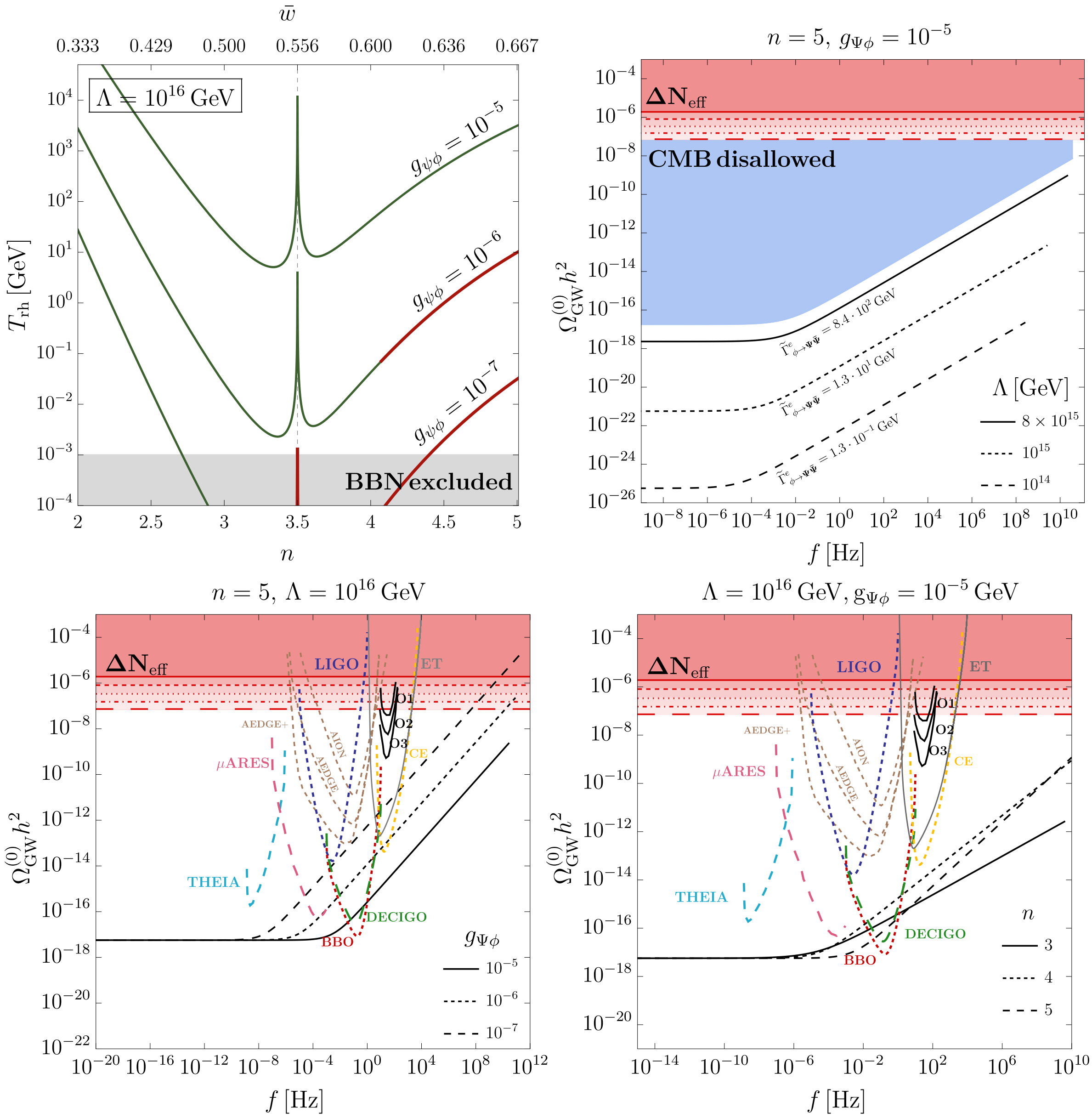

FIGURE 5.3: Same as Fig.(5.2) but for the $\phi \to \Psi\bar{\Psi}$ scenario.

Next, we consider the fermionic reheating triggered by the direct $\phi - \Psi$ interaction (4.6). In such the case, $\beta_\Psi = 3\,(n-1)/(n+1)$, so that $\beta_\psi \gtrless (n+4)/(n+1)$ for $n \gtrless 7/2$, and $\beta_\psi = (n+4)/(n+1)$ if $n = 7/2$. This implies a different relation between $T_{\rm rh}$ and n in these two regions. This effect is shown in the top left panel of figure 5.3, from which we see that the reheating temperature exhibits a different behavior around the transition point $n = 7/2$. In particular, the reheating temperature decreases with n for $n < 7/2$, whereas for $n > 7/2$, it starts to grow with n. Similar to the $\phi - S$ scenario discussed above, for a fixed $n = 5$, small couplings are disregarded by the present $\Delta N_{\rm eff}$ constraints on the GWs spectrum. Lastly, the lower right panel shows a range in the parameter space for which the fermionic reheating scenario might be probed in future GWs detectors.

5.4.3 Combined limits

In Fig. 5.4, we show the model's parameter space that remains allowed after imposing several observational bounds discussed before. Pink regions are forbidden by the BBN bound on reheating temperature. Different shadings correspond to different choices of coupling constants. For instance, the darkest pink region in the left panel, corresponding to $g_{S\phi} = 10^{-15}$ GeV, is disallowed by the BBN bounds. In the region below the reheating temperature for a fixed $g_{S\phi} = 10^{-15}$ GeV, and a given value of Λ, n exceeds $T_{\rm BBN}$, hence for the adopted inflaton-Higgs coupling this part of the parameter space is allowed. On the other hand, this region is forbidden by for weak $g_{S\phi} = 10^{-18}$ GeV. The gray meshed region parallel to the horizontal axes shows the CMB bound on the inflationary scale Λ, which feebly depends on the index n. The blue areas are disallowed by the $\Delta N_{\rm eff}$ bound from PLANCK on GWs overproduction.

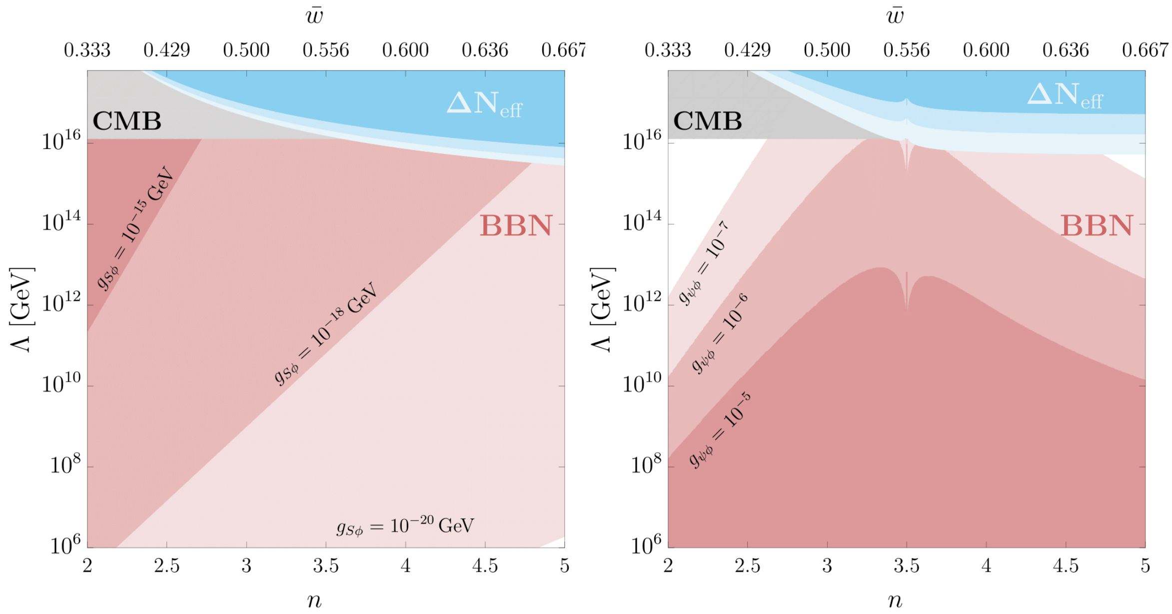

FIGURE 5.4: $\phi \to SS$ (left panel) and $\phi \to \Psi\bar{\Psi}$ (right panel) reheating scenarios. In both cases, pink regions corresponding to a given coupling constant, i.e., either $g_{S\phi}$ or $g_{\Psi\psi}$, are disallowed by the BBN bound on reheating temperature $T_{\rm rh} < 4$ MeV. Blue regions are forbidden by the PLANCK observed $\Delta N_{\rm eff}$ constraint on $\Omega^{(0)}_{\rm GW}h^2$ at $f = f_{\rm max}$. Note that different shadings correspond to different values of $g_{F\phi}$; the darkest tone is for the $g_{S\phi} = 10^{-15}$ GeV (left panel) and $g_{\Psi\phi} = 10^{-5}$ (right panel). The gray meshed part is ruled out by the CMB bound on the scale of inflation $\Lambda \gtrsim 1.4 \times 10^{16}$ GeV.

Chapter 6

Purely gravitational dark matter

After a long and arduous journey, we have finally gotten through the very last chapter of this thesis, devoted to the main protagonist of this work - dark matter.

Here we explore a model where a stable spin-1 massive field serves as a candidate for dark matter. In particular, as we have mentioned in Sec.(1.6), we focus on minimal, and in some sense extreme, dark matter model, assuming that dark species interact with other particles only via gravity. Such scenarios have a well-motivated theoretical background since, so far, all evidence supporting the existence of a dark sector has been inferred from purely gravitational effects. However, even though such a scenario appears very natural, it has only recently gained attention. The reasons for this might be twofold. The first one is related to another well-established DM scenario, which was considered a paradigm rather than a model for a long time. Dark matter in the form of WIMPs (see Sec.(1.4.2)) seems to be attractive not only due to the beautiful and simple physics leading to the so-called *"WIMP miracle"* but also because it bears some resemblance to the SM particles, building up the visible part of the Universe. WIMP DM could be easily accommodated by virtue of the latter in some extension of the SM of particle physics. In addition, the potential possibility of probing WIMP DM in colliders, underground detectors, and telescopes was considered an appealing feature of this scenario. The second reason concerns the challenges the purely gravitational DM model must face. Namely, the weakness of gravitational interactions significantly reduces the experimental prospects for verifying such a model. Hence, it is a real nightmare for experimental physicists. In addition, naively, one could expect that gravitational phenomena might not be efficient enough to saturate the observed abundance. Fortunately, this last concern turns out to be completely misconceived.

As we will demonstrate below, the *minimal* DM scenario cannot be looked down on as oversimplistic. Contrarily, its phenomenology is incredibly rich and involved. What makes this model particularly attractive is its sophisticated simplicity. Namely, the fact that gravitational phenomena might be so powerful at early times that alone could create the whole dark Universe. In this model, the origin of dark matter is inevitably related to the cosmic inflation paradigm, providing an ideal environment for gravitational processes, which under 'normal circumstances' cannot lead to such a conspicuous particle production. It is also worth appreciating the complementarity of this model with inflationary observables, including the scale of inflation, the tensor-to-scalar ratio, etc.

Gravitational phenomena, which we elaborate on in this chapter, can be considered a consequence of general relativity and the behavior of matter fields in curved spacetime. It turns out that even in such an extreme scenario, one distinguishes several mechanisms that might be responsible for DM production in the early Universe. We will focus our attention on three different processes of gravitational origin leading to dark matter production. Namely, we will investigate DM production induced by the non-adiabatic evolution of matter in the rapidly expanding Universe, non-thermal gravitational production from the inflaton field, and finally, gravitational freeze-in from the SM bath.

The former mechanism, i.e., the so-called **purely gravitational particle production (GP)**, is an example of non-perturbative processes occurring at the transition from the inflationary to the post-inflationary Universe. It can be viewed as semi-classical since describing such phenomena involves the behavior of quantum fields in the classical gravitational background. It is well-known that matter fields that are not invariant under a Weyl conformal transformation are copiously produced purely by expansion. This is because fields that are not conformally coupled to gravity develop a time-dependent dispersion relation. This relation could evolve non-adiabatically in the expanding Universe due to the tachyonic instability, mixing the positive and negative frequency modes. As a result, the vacuum state is not stable, but it varies over time. This very effect is interpreted as particle production by the inflating Universe. Let us notice that the description of the GP mechanism cannot be incorporated in a standard Boltzmann framework and requires careful analysis of equations of motion supplemented by the Friedmann equation determining the background evolution.

In addition, DM species can also be created perturbatively in processes mediated by a massless spin-2 graviton $h_{\mu\nu}$. Such interactions arise as a result of $h_{\mu\nu}$ coupling to the energy-momentum tensors of the inflaton $T^{\phi}_{\mu\nu}$, SM particles $T^{\rm SM}_{\mu\nu}$, and DM sector $T^{\rm DM}_{\mu\nu}$. In the lowest order, this coupling gives rise to a tree-level s-channel scattering leading to the **pair production of dark particles in the inflaton background (IG)**, and **DM gravitational freeze-in production from the SM species (SMG)** via the process $\mathrm{SM\,SM} \to h_{\mu\nu} \to \mathrm{DM\,DM}$. Typically, for these two mechanisms, DM evolution is investigated by solving the Boltzmann equations, which seem to be an appropriate tool for studying particle production in a post-inflationary Universe.

It is worth remarking that these mechanisms occur in slightly different moments and have different natures. The GP mechanism is mostly relevant during inflation and transitioning from the inflationary phase into a reheating era. DM particles are created here from the vacuum due to the quasi-exponentially expansion of the Universe. On the other hand, the perturbative treatment is justified when the Universe undergoes a power expansion, and the Minkowski metric can approximate a background metric. More precisely, in this case, one assumes that in the time-scale of interactions, the variation of the background geometry is negligible so that all processes occur in the flat spacetime. The perturbative treatment of the gravitational interaction can be used if the scale factor, a, is a power-law function of time. Hence, it cannot be justified during inflation, when a grows exponentially with time. Moreover, perturbative DM production from the inflaton field requires high energy. Thus it can only exist during reheating when ρ_ϕ contributes dominantly to the total energy density of the Universe. After the inflaton-radiation equality, the inflaton is depleted, and its energy density decreases quasi-exponentially. The gravitational production from the SM bath being in thermal equilibrium also involves high energy (temperature), but in contrast with the IG process, it can, in principle, exist after reheating.

This chapter is structured as follows. In Sec.(6.1), the evolution of the background is specified based on our results from Chapter (5). In Sec.(6.2), we elaborate on the origin of the mass term for a vector DM field. Section (6.3) is devoted to the description of a massive vector field in the expanding FLRW Universe. In Sec.(6.4), the dynamics of longitudinal modes during cosmic inflation is discussed, whereas Sec.(6.5) focuses on their post-inflationary evolution. Then, in Sec.(6.6), we present our final results regarding the GP dark matter production and comment on isocurvature perturbations. Perturbative DM production mechanisms are discussed in Sec. (6.7). Finally, in the last section (6.8), we show are final results where all discussed processes are included.

6.1 Background evolution

In this chapter, we aim to investigate the implications of non-standard reheating on the gravitational production of DM species. To maintain compliance with the notation used in Ref.[4], we parametrize the post-inflationary dynamics by the following four parameters: the averaged equation-of-state parameter of the inflaton $\bar{w}$, the Hubble scale at the end of inflation H_e, the coefficient β_F accounting for the time-dependency of the inflaton decay width Eq.(4.90), and the reheating efficiency γ, defined as

$$\gamma^2 \equiv \frac{H_{\rm rh}}{H_e}. \tag{6.1}$$

Note that $\gamma \in (0, 1]$, such that $\gamma = 1$ corresponds to instantaneous reheating, whereas any deviation from this value indicates a finite duration of the reheating phase.
We investigate the production of dark matter in the early Universe, where two crossovers took place, i.e., the transition from the inflationary to the reheating phase and the subsequent transition to the RD epoch. We require the scale factor and the Hubble rate to be continuous functions across these two crossovers,

$$a_{\rm I}(\tau_e) = a_{\rm rh}(\tau_e), \qquad H_e(\tau_e) = H_{\rm rh}(\tau_e), \tag{6.2}$$

$$a_{\rm rh}(\tau_{\rm rh}) = a_{\rm RD}(\tau_{\rm rh}), \qquad H_{\rm rh}(\tau_{\rm rh}) = H_{\rm RD}(\tau_{\rm rh}), \tag{6.3}$$

where the subscripts $\{\mathrm{I}, \mathrm{RH}, \mathrm{RD}\}$ correspond to the solutions during inflation, reheating, and RD era, respectively. The continuity of a and H imply [1]

$$a(\tau) = \begin{cases} \dfrac{-1}{H_e(\tau - \frac{3}{2}\tau_e(1+\bar{w}))}, & \tau \le \tau_e, \\ \dfrac{2}{H_e(1+3\bar{w})} \tau_e^{\frac{-3(1+\bar{w})}{1+3\bar{w}}} \tau^{\frac{2}{1+3\bar{w}}}, & \tau_e < \tau \le \tau_{\rm rh}, \\ \dfrac{1}{H_e}\left(\dfrac{2}{1+3\bar{w}}\right)^2 \tau_e^{-\frac{3(1+\bar{w})}{1+3\bar{w}}} \tau_{\rm rh}^{\frac{1-3\bar{w}}{1+3\bar{w}}} \Big(\tau - \dfrac{1}{2}\tau_{\rm rh}(1-3\bar{w})\Big), & \tau_{\rm rh} < \tau, \end{cases} \tag{6.4}$$

and

$$H(\tau) = \begin{cases} H_e, & \tau \le \tau_e, \\ H_e\, \tau_e^{\frac{3(1+\bar{w})}{1+3\bar{w}}} \tau^{-\frac{3(1+\bar{w})}{1+3\bar{w}}}, & \tau_e < \tau \le \tau_{\rm rh}, \\ \dfrac{H_e}{4}\left(\dfrac{1+3\bar{w}}{\tau - \frac{1}{2}\tau_{\rm rh}(1-3\bar{w})}\right)^2 \tau_e^{\frac{3(1+\bar{w})}{1+3\bar{w}}} \tau_{\rm rh}^{\frac{-1+3\bar{w}}{1+3\bar{w}}}, & \tau_{\rm rh} < \tau\,. \end{cases} \tag{6.5}$$

As we will explicitly demonstrate below, both GP and IG are not influenced by the parameter β_F. This is because these two mechanisms are primarily determined by the inflaton field, whose dynamics barely depend on β_F. More precisely, the independence on β_F follows from the fact that both processes are (almost) insensitive to the evolution of the SM sector

[1] In order to satisfy the continuity conditions, we utilize the freedom to shift the conformal time by a constant and adjust the normalization of the scale factor independently in each region under consideration.

at the onset of reheating. On the other hand, the proper description of thermal freeze-in requires knowledge of thermal bath temperature evolution, which generally is a function of β_F.

In what follows, we assume that the energy budget $\rho_{\rm tot}$ during inflation and early stages of reheating is mainly in the form of the inflaton energy, whereas after the end of reheating, the Universe becomes dominated by radiation. Hence,

$$\rho_{\rm tot}(a) \simeq \begin{cases} \rho_\phi(a), & a \leq a_{\rm rh}, \\ 3M_{\rm Pl}^2 H_e^2 \gamma^4 \left(\frac{a_{\rm rh}}{a}\right)^4, & a \in [a_{\rm rh}, a_{\rm r.m.e}], \end{cases} \tag{6.6}$$

where the evolution of ρ_ϕ during inflation and following reheating is described by Eq.(3.4) Eq.(3.63), respectively.

From the above expression, it follows that the Hubble rate behaves as

$$H(a) \simeq \begin{cases} H_e, & a < a_e, \\ H_e \left(\frac{a_e}{a}\right)^{3(1+\bar{w})/2}, & a \in [a_e, a_{\rm rh}], \\ \gamma^2 H_e \left(\frac{a_{\rm rh}}{a}\right)^2, & a \in [a_{\rm rh}, a_{\rm r.m.e}], \end{cases} \tag{6.7}$$

Note that the scale factor at the end of reheating can be expressed as

$$a_{\rm rh} = a_e \gamma^{\frac{-4}{3(1+\bar{w})}}, \tag{6.8}$$

whereas the reheating temperature is given by

$$T_{\rm rh} = \gamma \left(\frac{90 M_{\rm Pl}^2 H_e^2}{\pi^2 g_{\star\rho,\rm rh}} \right)^{1/4}. \tag{6.9}$$

During reheating, the temperature dependence on the scale factor can be approximated by the following formula:

$$T_{\rm RH}(a) = T_{\rm rh} \begin{cases} \left(\frac{a_{\rm rh}}{a}\right)^{\frac{\beta_F}{4} + \frac{3(1+\bar{w})}{8}} & \beta_F < 5(1-3\bar{w})/2, \\ \frac{a_{\rm rh}}{a}, & \beta_F > 5(1-3\bar{w})/2, \end{cases} \qquad a \in [a_e, a_{\rm rh}], \tag{6.10}$$

where we have assumed that $g_{\star\rho}(T)$ do not change during reheating, i.e., $g_{\star\rho,\rm rh}/g_{\star\rho}(T) \simeq 1$.

It is worth emphasizing that γ can be related to $\widetilde{\Gamma}^e_{\phi\to FF}$, which we have used to parameterize the perturbative inflaton-SM interactions Eq. (4.90), through the following expression:

$$\widetilde{\Gamma}^e_{\phi\to FF} = H_e \begin{cases} \frac{5-3\bar{w}-2\beta_F}{2} \cdot \gamma^{2-\frac{4\beta_F}{3(1+\bar{w})}}, & \beta_F < (5-3\bar{w})/2, \\ \frac{3\bar{w}+2\beta_F-5}{2} \cdot \gamma^{\frac{4(3\bar{w}-1)}{3(1+\bar{w})}}, & \beta_F > (5-3\bar{w})/2. \end{cases} \tag{6.11}$$

Lastly, we would like to mention that from the BBN bound on the reheating temperature, i.e., $T_{\rm BBN} \simeq 4\,\text{MeV}$ [272, 357–362], and the CMB limit on the Hubble scale at the end of inflation, i.e., $H_e \leq 4.4 \cdot 10^{13}$ GeV (3.105), one infers the lower bound on the reheating efficiency:

$$\gamma \gtrsim 10^{-15}. \tag{6.12}$$

6.2 Mass term for a spin-1 field

Let us first describe how a dark spin-1 field $X_\mu(x)$ becomes massive. To that end, we consider the de Broglie-Proca action for a vector field in a generic background metric [430, 431]

$$S = \int d^4x\sqrt{-g}\,\mathcal{L}_X, \qquad \mathcal{L}_X = -\frac{1}{4}g^{\mu\alpha}g^{\nu\beta}X_{\mu\nu}X_{\alpha\beta} + \frac{1}{2}m_X^2 g^{\mu\nu}X_\mu X_\nu, \tag{6.13}$$

with

$$X_{\mu\nu} \equiv \partial_\mu X_\nu - \partial_\nu X_\mu, \tag{6.14}$$

being the (dark) field strength.
Although the above Lagrangian density, $\mathcal{L}_X$, is Lorentz-invariant, it does not describe a gauge theory since the mass term explicitly spoils the gauge invariance, i.e., it is not invariant under a local $U_X(1)$-transformations of the form

$$X_\mu(x) \to X_\mu(x) + \partial_\mu\alpha(x). \tag{6.15}$$

However, the Proca action can be viewed as the effective theory, i.e., the low-energy limit of the gauge-invariant Stueckelberg action equipped with a real scalar field $\Phi_{\rm DM}$ restoring the symmetry. The Stueckelberg Lagrangian density is given by [432, 433]

$$\mathcal{L}_S = -\frac{1}{4}g^{\mu\alpha}g^{\nu\beta}X_{\mu\nu}X_{\alpha\beta} + \frac{1}{2}g^{\mu\nu}(\partial_\mu\Phi_{\rm DM} - m_X X_\mu)(\partial_\nu\Phi_{\rm DM} - m_X X_\nu). \tag{6.16}$$

The above Lagrangian density is invariant under the following transformations:

$$X_\mu(x) \to X_\mu(x) - \partial_\mu\chi(x), \qquad \Phi_{\rm DM}(x) \to \Phi_{\rm DM}(x) + m_X\chi(x). \tag{6.17}$$

Note that the $\Phi_{\rm DM}$ field can be eliminated by choosing the gauge $\chi = -\Phi/m_X$, so that the Stueckelberg Lagrangian (6.16) becomes equivalent to the Proca Lagrangian (6.13).
We can also view the Stuckelberg mechanism as a limit of the Abelian-Higgs model. In the Higgs mechanism one introduces a complex scalar field $\boldsymbol{\Phi}_{\rm DM}$ with a non-zero vacuum expectation value $\langle\boldsymbol{\Phi}_{\rm DM}\rangle = \mathbf{v}_{\rm DM}$, such that [434]

$$\mathcal{L}_H = -\frac{1}{4}g^{\mu\alpha}g^{\nu\beta}X_{\mu\nu}X_{\alpha\beta} + g^{\mu\nu}(\mathcal{D}_\mu\boldsymbol{\Phi}_{\rm DM})(\mathcal{D}_\nu\boldsymbol{\Phi}_{\rm DM})^\dagger - \lambda\left(\boldsymbol{\Phi}_{\rm DM}\boldsymbol{\Phi}_{\rm DM}^\dagger - \mathbf{v}_{\rm DM}^2\right)^2, \tag{6.18}$$

where the covariant derivative is

$$\mathcal{D}_\mu\boldsymbol{\Phi}_{\rm DM} = (\partial_\mu - ig_X X_\mu)\boldsymbol{\Phi}_{\rm DM}, \tag{6.19}$$

and

$$X_\mu(x) \to X_\mu(x) - \partial_\mu\chi(x), \qquad \boldsymbol{\Phi}_{\rm DM}(x) \to \boldsymbol{\Phi}_{\rm DM}(x)e^{ig_X\chi(x)}. \tag{6.20}$$

After $U_X(1)$ symmetry breaking, initially massless field X_μ acquires a non-zero mass

$$m_X = g_X\mathbf{v}_{\rm DM}. \tag{6.21}$$

However, in contrast to the Stuckelberg mechanism, $\boldsymbol{\Phi}_{\rm DM}$ cannot be entirely eliminated by the gauge transformation [434]. On the other term, the Stuckelberg model can be considered as the limit of the Higgs mechanism, corresponding to the case

$$\mathbf{v}_{\rm DM} \to \infty, \qquad g_X \to 0, \tag{6.22}$$

such that the product $g_X \mathbf{v}_{\rm DM}$ is preserved, and the vector mass is finite. Note that dark Higgs is effectively integrated out in this limit since its mass becomes divergent.

6.3 Massive vector field in the FLRW metric

Then, let us consider the dark abelian massive gauge field X_μ, described by the Proca action Eq. (6.13), in the spatially-flat Friedmann-Lemaître–Robertson–Walker metric, with the line element introduced in Eq.(2.19) with $k = 0$. To analyze particle production in the expanding Universe, switching to conformal coordinates in which the line element takes the form (2.29) is convenient. Hence, in these coordinates, the determinant of the metric is $g = -a^8$. We should also remind that $-\infty < \tau < +\infty$, while $\tau = 0$ is a typical choice for the end of inflation.

Before describing the vector field dynamics, it is beneficial to comment on the possible non-minimal interactions of the X_μ field. The Proca action accounts for the dynamics of the spin-1 massive field, minimally coupled to gravity. However, the minimal setup might be extended in several ways. In particular, one could consider the following dimension-4 operators involving the Ricci scalar R and Ricci tensor $R_{\mu\nu}$ [435]:

$$\xi_1 R g^{\mu\nu} X_\mu X_\nu, \qquad\qquad \xi_2 g^{\mu\nu} R_{\mu\nu} g^{\rho\sigma} X_\rho X_\sigma, \tag{6.23}$$

describing non-minimal interactions of the vector field X_μ with gravity. Analogously to the mass term, the non-minimal couplings (6.23) are not gauge invariant. However, both terms might arise from the Stuckelberg mechanism. One should also notice that introducing non-minimal couplings induces a ghost-like action for the longitudinal component of the vector field [435, 436]. Hence, to avoid ghost instability, we set $\xi_1 = 0 = \xi_2$ in the rest of this thesis. In addition, one could also consider the non-canonical kinetic couplings of the form [437–441]

$$f(\phi) X_{\mu\nu} X^{\mu\nu}, \qquad\qquad f(\phi) X_{\mu\nu} \tilde{X}^{\mu\nu}, \tag{6.24}$$

where $f(\phi)$ denotes some function of a scalar field ϕ, which might or might not play a role of the inflaton, and $\tilde{X}^{\mu\nu} \equiv \epsilon^{\mu\nu\rho\sigma} X_{\rho\sigma}/2$ with $\epsilon^{\mu\nu\rho\sigma}$ being the completely anti-symmetric tensor. Such couplings emerge in various well-motivated theoretical frameworks, such as axion inflation [442]. As we will explicitly demonstrate below, transversely-polarized modes of a minimally coupled vector field generate scale-invariant density fluctuations during inflation and hence cannot constitute all the observed dark matter, see also [168, 169, 443, 444]. On the other hand, it has been shown that the presence of the non-minimal coupling to the scalar field ϕ (6.24) leads to a tachyonic production of one of the transverse components of the vector field [437–441]. Thus, the existence of direct interactions among the ϕ and X_μ fields would inevitably give rise to another production channel of spin-1 particles. Finally, in the non-minimal framework, one might postulate the existence of a small mixing between the dark and visible vectors via the dark $U_X(1)$ kinetic mixing with the SM hypercharge $U_Y(1)$, i.e., $\epsilon/2\, B^{\mu\nu} X_{\mu\nu}$, with ϵ being the mixing parameter, and $B^{\mu\nu}$ denoting the field strength tensor for the SM $U_Y(1)$, gauge boson B_μ. In all of the above-mentioned non-minimal scenarios, there would be at least two sources of dark vectors, which, in turn, would imply non-trivial phenomenology of the dark sector. However, for the purpose of this thesis, we restrict our attention to the simplest albeit viable model, assuming that the dark matter candidate X_μ couples minimally to gravity and has no other interactions with the visible or hidden sectors. Interestingly, even in such an extreme scenario, the phenomenology of the dark sectors turns out to be rich and involved.

6.3.1 EoM for the dark vector field

From the Proca action (6.13) one gets the following EoM for the $\beta-$ component of the vector field:

$$\frac{1}{\sqrt{-g}}\partial_\alpha(\sqrt{-g}g^{\alpha\mu}g^{\beta\nu}X_{\mu\nu}) + m_X^2 g^{\mu\beta}X_\mu = 0. \tag{6.25}$$

The above expression comprises four equations for the time $\beta = 0$ and spatial $\beta = i$ components of the X_μ field. In particular, for the $\beta = 0$ component, one finds

$$\partial_i \dot{X}_i - \partial_i^2 X_0 + m_X^2 a^2 X_0 = 0, \tag{6.26}$$

or in the conformal time,

$$\partial_i X_i' - \partial_i^2 X_0 + m_X^2 a^2(\tau) X_0 = 0, \tag{6.27}$$

whereas for the spatial components $\beta = i$, one gets

$$\ddot{X}_i + H\dot{X}_i - a^{-2}\partial_l(\partial_l X_i - \partial_i X_l) + m_X^2 X_i = \partial_i(\dot{X}_0 + HX_0), \tag{6.28}$$

or equivalently, in conformal coordinates

$$X_i'' - \partial_l(\partial_l X_i - \partial_i X_l) + m_X^2 a^2(\tau) X_i = \partial_i X_0'. \tag{6.29}$$

In the above equations, overdots denote derivatives with respect to the cosmic time t, primes stand for derivatives w.r.t the conformal time τ, whereas $\partial_i \equiv \partial/\partial x_i$ corresponds to the spatial derivatives. Note that X_0 does not have a kinetic term and can be considered a non-dynamical, auxiliary field. As we will shortly demonstrate, it does not mix longitudinal and transverse modes and, thus, can be isolated from the remaining three physical components of the X_μ field. To get rid of the spurious degree of freedom, we differentiate (6.25) with respect to ∂_β, obtaining

$$\partial_\beta\left[\frac{1}{\sqrt{-g}}\partial_\alpha(\sqrt{-g}g^{\alpha\mu}g^{\beta\nu}X_{\mu\nu}) + m_X^2 g^{\mu\beta}X_\mu\right] = 0, \tag{6.30}$$

from which it follows that

$$\dot{X}_0 = \frac{1}{a^2}\partial^i X_i - 2HX_0 + \frac{H}{a^2 m_X^2}\left(\partial^i \dot{X}_i - \partial_i^2 X_0\right), \tag{6.31}$$

or equivalently, in conformal coordinates,

$$X_0' = \partial^i X_i - 2\mathcal{H}X_0. \tag{6.32}$$

In the Fourier space, the X_μ field can be written as

$$X_0(t,\vec{x}) = \int \frac{d^3k}{(2\pi)^3} X_0(t,\vec{k})e^{i\vec{k}\cdot\vec{x}}, \qquad \vec{X}(t,\vec{x}) = \int \frac{d^3k}{(2\pi)^3}\vec{X}(t,\vec{k})e^{i\vec{k}\cdot\vec{x}}. \tag{6.33}$$

Inserting the above decomposition into Eq.(6.26), we find

$$X_0(t,\vec{k}) = -\frac{i\vec{k}\cdot\dot{\vec{X}}(t,\vec{k})}{k^2 + a^2 m_X^2}, \qquad \text{or} \qquad X_0(\tau,\vec{k}) = -\frac{i\vec{k}\cdot\vec{X}'(\tau,\vec{k})}{k^2 + a^2(\tau)m_X^2}, \tag{6.34}$$

in the second expression, we have used analogous Fourier decomposition in conformal coordinates. Furthermore, utilizing expansion (6.33), we can recast Eqs. (6.31) and (6.32) as

$$\dot{X}_0(t,\vec{k}) = \frac{i}{a^2}\vec{k}\cdot\vec{X}(t,\vec{k}) - 2HX_0(t,\vec{k}) + \frac{H}{a^2 m_X^2}[i\vec{k}\cdot\vec{X}(t,\vec{k}) + k^2 X_0(t,\vec{k})], \tag{6.35}$$

and

$$X_0'(\tau,\vec{k}) = i\vec{k}\cdot\vec{X}(\tau,\vec{k}) - 2\mathcal{H}X_0(\tau,\vec{k}), \tag{6.36}$$

respectively.
In the above equations, we have employed the shorthand notation $|\vec{k}|\equiv k$ for the magnitude of the comoving momentum. Moreover, we should also stress that the reality of the DM gauge field implies $X_\mu^*(\tau,\vec{k}) = X_\mu(\tau,-\vec{k})$.

Now, it is instructive to decompose $\vec{X}$ into a basis of helicity states, i.e.,

$$\vec{X}(\tau,\vec{k}) = \sum_{\lambda=\pm,L} \vec{\epsilon}_\lambda(\vec{k})X_\lambda(\tau,k), \tag{6.37}$$

where

$$\vec{k}\cdot\vec{X}(\tau,\vec{k}) = kX_L(\tau,k). \tag{6.38}$$

The polarization vectors $\vec{\epsilon}_\lambda$ satisfy the following relations:

$$\vec{k}\cdot\vec{\epsilon}_\pm(\vec{k}) = 0, \qquad \vec{k}\cdot\vec{\epsilon}_L(\vec{k}) = k, \tag{6.39}$$

$$\vec{k}\times\vec{\epsilon}_\pm(\vec{k}) = \mp ik\vec{\epsilon}_\pm(\vec{k}), \qquad \vec{k}\times\vec{\epsilon}_L(\vec{k}) = 0, \tag{6.40}$$

$$\vec{\epsilon}_\lambda^{\,*}(\vec{k}) = \vec{\epsilon}_\lambda(-\vec{k}), \qquad \vec{\epsilon}_\lambda(\vec{k})\cdot\vec{\epsilon}_{\tilde{\lambda}}^{\,*}(\vec{k}) = \delta_{\lambda,\tilde{\lambda}}. \tag{6.41}$$

Note that by virtue of the isotropy of the background FLRW metric, mode functions $X_\lambda(\tau,\vec{k})$ can only depend on the magnitude of the comoving momentum k, i.e., $X_\lambda(\tau,k)$.
Substituting (6.38) into (6.34), we conclude that X_0 does not contain a contribution from the transverse modes, i.e.,

$$X_0(t,k) = -\frac{ik\dot{X}_L(t,k)}{k^2 + a^2 m_X^2}, \qquad \text{or} \qquad X_0(\tau,k) = -\frac{ikX_L'(\tau,k)}{k^2 + a^2(\tau)m_X^2}. \tag{6.42}$$

Moreover, using Eq.(6.35) and its conformal counterpart Eq.(6.36) we can express the time derivative of the X_0 field as

$$\dot{X}_0(t,k) = ik\left(\frac{1}{a^2}X_L(t,k) + \frac{3H}{k^2 + a^2 m_X^2}\dot{X}_L(t,k)\right), \tag{6.43}$$

or equivalently,

$$X_0'(\tau,k) = ik\left(X_L(\tau,k) + 2\mathcal{H}\frac{X_L'(\tau,k)}{k^2 + a^2(\tau)m_X^2}\right). \tag{6.44}$$

Inserting (6.43) into Eq.(6.28), we get the following equation of motion for the longitudinal and two transverse components of the vector field:

$$\ddot{X}_L(t,k) + \frac{3k^2 + a^2 m_X^2}{k^2 + a^2 m_X^2} H\dot{X}_L(t,k) + \left(\frac{k^2}{a^2} + m_X^2\right) X_L(t,k) = 0, \tag{6.45}$$

$$\ddot{X}_\pm(t,k) + H\dot{X}_\pm(t,k) + \left(\frac{k^2}{a^2} + m_X^2\right) X_\pm(t,k) = 0, \tag{6.46}$$

whereas, in conformal coordinates, one finds

$$X_L''(\tau,k) + 2\mathcal{H}\frac{k^2}{k^2 + a^2(\tau)m_X^2} X_L'(\tau,k) + \left(k^2 + m_X^2 a^2(\tau)\right) X_L(\tau,k) = 0, \tag{6.47}$$

$$X_\pm''(\tau,k) + (k^2 + a^2(\tau)m_X^2) X_\pm(\tau,k) = 0. \tag{6.48}$$

6.3.2 Harmonic oscillator with a time-dependent dispersion relation

In the previous section, we found a set of decoupled second-order differential equations (6.47) and (6.48), one for each Fourier mode $X_\lambda(\tau,k)$. It is worth noting that Eq. (6.48) governing the transversely-polarized modes $X_\pm$ takes the form of a harmonic oscillator (HO) equation with a time-dependent frequency $\omega_\pm^2 \equiv k^2 + a^2(\tau)m_X^2$. On the other hand, Eq.(6.47) can be recast into the harmonic oscillator form by employing the following field redefinition:

$$X_L(\tau,k) = \frac{\sqrt{k^2 + a^2(\tau)m_X^2}}{a(\tau)m_X} A_L(\tau,k), \tag{6.49}$$

which, in turn, allows us to rewrite (6.47) as

$$A_L''(\tau,k) + \omega_L^2 A_L(\tau,k) = 0, \tag{6.50}$$

with

$$\omega_L^2 \equiv k^2 + a^2(\tau)m_X^2 + a^2(\tau)\frac{k^2}{k^2 + a^2(\tau)m_X^2}\left(\frac{\mathcal{R}}{6} + \frac{3m_X^2}{k^2 + a^2(\tau)m_X^2}\mathcal{H}^2\right), \tag{6.51}$$

where we have used the fact that the Ricci scalar in the flat FLRW metric is given by (5.15).

The HO equations such as Eqs.(6.48) and (6.50) have a two-dimensional space of solutions, spanned by a linearly-independent solution $X_\pm^{(1)}$, $X_\pm^{(2)}$ and $A_L^{(1)}$, $A_L^{(2)}$, respectively. The general solution can be written as a superposition of two (yet undetermined) solutions

$$X_\pm(\tau,k) = a_\pm^-(\vec{k})\mathcal{X}_\pm(\tau,k) + a_\pm^+(-\vec{k})\mathcal{X}_\pm^*(\tau,k), \tag{6.52}$$

$$A_L(\tau,k) = a_L^-(\vec{k})\mathcal{X}_L(\tau,k) + a_L^+(-\vec{k})\mathcal{X}_L^*(\tau,k), \tag{6.53}$$

where

$$\mathcal{X}_\pm(\tau,k) = X_\pm^{(1)}(\tau,k) + iX_\pm^{(2)}(\tau,k), \qquad \mathcal{X}_L(\tau,k) = A_L^{(1)}(\tau,k) + iA_L^{(2)}(\tau,k), \tag{6.54}$$

whereas $a_\lambda^-(\vec{k})$, $a_\lambda^+(-\vec{k})$ are complex, time-independent coefficients.
The reality of the $X_\mu(\tau,k)$ field implies

$$a_\lambda^+(\vec{k}) = (a_\lambda^-)^*(\vec{k}). \tag{6.55}$$

Combining (6.52) and (6.53) with Eq. (6.33), one obtains

$$\vec{X}(\tau,\vec{x}) = \sum_{\lambda=\pm,L} \int \frac{d^3k}{(2\pi)^3} \vec{\epsilon}_\lambda(\vec{k}) e^{i\vec{k}\cdot\vec{x}} \left[a_\lambda^-(\vec{k}) \mathcal{X}_\lambda(\tau,k) + a_\lambda^+(-\vec{k}) \mathcal{X}_\lambda^*(\tau,k) \right], \tag{6.56}$$

where $\mathcal{X}_\pm(\tau,k)$ and $\mathcal{X}_L(\tau,k)$ satisfy Eqs.(6.48) and (6.50), respectively.

Note that the *Wronskian*, $W[x_1,x_2] \equiv x_1' x_2 - x_2' x_1$, of two solutions x_1, x_2 of a generic HO equation is time-independent, $W'[x_1,x_2] = 0$. Moreover, $W[x_1,x_2]$ vanishes if solutions x_1 and x_2 are not linearly independent, which follows from the fact that, in this case, one of the solutions is proportional to the second one. On the other hand, for two linearly independent solutions, the *Wronskian* is a non-zero constant.

6.3.3 Quantization

The theory can be quantized in a standard way, i.e., by promoting constants of integration $a_\lambda^-(\vec{k})$ and $a_\lambda^+(-\vec{k})$ appearing in Eqs.(6.52) and (6.53), to quantum operators $\hat{a}_\lambda(\vec{k})$, $\hat{a}_\lambda^\dagger(-\vec{k})$, respectively. Next, we introduce a canonical vector field variable

$$\hat{\vec{X}}(\tau,\vec{x}) = \sum_{\lambda=\pm,L} \int \frac{d^3k}{(2\pi)^3} \vec{\epsilon}_\lambda(\vec{k}) e^{i\vec{k}\cdot\vec{x}} \left[\hat{a}_\lambda(\vec{k}) \mathcal{X}_\lambda(\tau,k) + \hat{a}_\lambda^\dagger(-\vec{k}) \mathcal{X}_\lambda^*(\tau,k) \right]. \tag{6.57}$$

Analogously to the quantization procedure in flat Minkowski spacetime, we define the conjugate momentum operator $\hat{\vec{\Pi}}_\lambda \equiv \delta\mathcal{L}_X / \delta\vec{X}'$

$$\hat{\vec{\Pi}}(\tau,\vec{x}) = \sum_{\lambda=\pm,L} \int \frac{d^3k}{(2\pi)^3} \vec{\epsilon}_\lambda(\vec{k}) e^{i\vec{k}\cdot\vec{x}} \left[\hat{a}_\lambda(\vec{k}) \mathcal{X}_\lambda'(\tau,k) + \hat{a}_\lambda^\dagger(-\vec{k}) \mathcal{X}_\lambda'^*(\tau,k) \right]. \tag{6.58}$$

Then, one imposes the equal-time canonical commutation relations (CCR) on components of the canonical quantum variables

$$[\hat{X}_\lambda(\tau,\vec{x}), \hat{\Pi}_{\lambda'}(\tau,\vec{y})] = i\delta^{(3)}(\vec{x}-\vec{y})\delta_{\lambda,\lambda'}, \quad [\hat{X}_\lambda(\tau,\vec{x}), \hat{X}_\lambda(\tau,\vec{y})] = 0, \quad [\hat{\Pi}_\lambda(\tau,\vec{x}), \hat{\Pi}_\lambda(\tau,\vec{y})] = 0. \tag{6.59}$$

The annihilation and creation operators satisfy the following commutation relation:

$$[\hat{a}_\lambda(\vec{k}), \hat{a}_{\tilde{\lambda}}^\dagger(\vec{\tilde{k}})] = (2\pi)^3 \delta_{\lambda\tilde{\lambda}} \delta^{(3)}(\vec{k}-\vec{\tilde{k}}), \qquad [\hat{a}_\lambda(\vec{k}), \hat{a}_{\tilde{\lambda}}(\vec{\tilde{k}})] = 0, \qquad [\hat{a}_\lambda^\dagger(\vec{k}), \hat{a}_{\tilde{\lambda}}^\dagger(\vec{\tilde{k}})] = 0. \tag{6.60}$$

The ladder operators $\hat{a}_\lambda(\vec{k}), \hat{a}_\lambda^\dagger(\vec{k})$ are used to construct a particle spectrum of the underlying theory. The vacuum $|0\rangle$ is defined as the eigenstate of the annihilation operator $\hat{a}_\lambda(\vec{k})$ with zero eigenvalue, i.e.,

$$\forall_{\vec{k}}\ \hat{a}_\lambda(\vec{k})\,|0\rangle = 0\,|0\rangle\,, \tag{6.61}$$

whereas the set of excited states is created by the repeated action of the creation operator on the vacuum state

$$|m_{k_1} n_{k_2} \ldots\rangle = \frac{1}{\sqrt{m!\,n!\ldots}} (\hat{a}_\lambda^\dagger(\vec{k}_1))^m (\hat{a}_\lambda^\dagger(\vec{k}_1))^n \ldots |0\rangle\,, \tag{6.62}$$

where m_{k_1} and $n_{k_1}\ldots$ denote the occupation numbers in the modes $\mathcal{X}_\lambda(\tau,k_1), \mathcal{X}_\lambda(\tau,k_2)\ldots$, respectively.

Substituting (6.57) and (6.58) into (6.59) and using (6.60), one finds

$$
\begin{aligned}
[\hat{X}_\lambda(\tau,\vec{x}),\hat{\Pi}_{\lambda'}(\tau,\vec{y})] &= \int \frac{d^3k}{(2\pi)^3}\int\frac{d^3\tilde{k}}{(2\pi)^3}e^{i\vec{k}\cdot\vec{x}}e^{i\vec{\tilde{k}}\cdot\vec{y}} \\
&\times\left[\hat{a}_\lambda(\vec{k})\mathcal{X}_\lambda(\tau,k)+\hat{a}^\dagger_\lambda(-\vec{k})\mathcal{X}^*_\lambda(\tau,k),\hat{a}_{\tilde{\lambda}}(\vec{\tilde{k}})\mathcal{X}'_{\tilde{\lambda}}(\tau,\tilde{k})+\hat{a}^\dagger_{\tilde{\lambda}}(-\vec{\tilde{k}})\mathcal{X}^{*\prime}_{\tilde{\lambda}}(\tau,\tilde{k})\right] \\
&= \delta_{\lambda,\tilde{\lambda}}\int\frac{d^3k}{(2\pi)^3}e^{i\vec{k}\cdot(\vec{x}-\vec{y})}\left[\mathcal{X}_\lambda\mathcal{X}^{*\prime}_\lambda-\mathcal{X}^*_\lambda\mathcal{X}'_\lambda\right]. \qquad (6.63)
\end{aligned}
$$

Since,

$$
\delta^{(3)}(\vec{x}-\vec{y}) = \int\frac{d^3k}{(2\pi)^3}e^{i\vec{k}\cdot(\vec{x}-\vec{y})}, \qquad (6.64)
$$

the mode functions $\mathcal{X}_\pm$ and $\mathcal{X}_L$ are supposed to be normalized such that their Wronskian is

$$
W[\mathcal{X}_\lambda,\mathcal{X}^*_\lambda] = \mathcal{X}'_\lambda\mathcal{X}^*_\lambda-\mathcal{X}^{*\prime}_\lambda\mathcal{X}_\lambda = -i. \qquad (6.65)
$$

It is important to emphasize that the quantum Hamiltonian

$$
\hat{H}_\lambda(\tau) = \frac{1}{2}\int d^3x\left[\hat{\Pi}^2_\lambda+(\nabla\hat{X}_\lambda)^2+m^2_{\text{eff},\lambda}(\tau)\hat{X}^2_\lambda\right], \qquad (6.66)
$$

with

$$
m^2_{\text{eff},\pm}\equiv a^2(\tau)m^2_X,\quad m^2_{\text{eff},L}\equiv a^2(\tau)m^2_X+a^2(\tau)\frac{k^2}{k^2+a^2(\tau)m^2_X}\left(\frac{\mathcal{R}}{6}+\frac{3m^2_X}{k^2+a^2(\tau)m^2_X}\mathcal{H}^2\right), \qquad (6.67)
$$

receives a time-dependence through the effective mass $m^2_{\text{eff},\lambda}(\tau)$.
Note that the Hamiltonian of a system can be written as

$$
\begin{aligned}
\hat{H}_\lambda(\tau) &= \frac{1}{2}\int d^3x\, e^{i(\vec{k}+\vec{\tilde{k}})\cdot\vec{x}}\int\frac{d^3k}{(2\pi)^3}\int\frac{d^3\tilde{k}}{(2\pi)^3}\Big\{\hat{a}_\lambda(\vec{k})\hat{a}_{\tilde{\lambda}}(\vec{\tilde{k}})F+\hat{a}^\dagger_\lambda(-\vec{k})\hat{a}^\dagger_{\tilde{\lambda}}(-\vec{\tilde{k}})F^* \\
&\quad+[\hat{a}_\lambda(\vec{k})\hat{a}^\dagger_{\tilde{\lambda}}(-\vec{\tilde{k}})+\hat{a}^\dagger_\lambda(-\vec{k})\hat{a}_{\tilde{\lambda}}(\vec{\tilde{k}})]E\Big\} \\
&= \frac{1}{2}\int\frac{d^3k}{(2\pi)^3}\left\{\hat{a}_\lambda(\vec{k})\hat{a}_\lambda(-\vec{k})F+\hat{a}^\dagger_\lambda(-\vec{k})\hat{a}^\dagger_\lambda(\vec{k})F^*+[\hat{a}_\lambda(\vec{k})\hat{a}^\dagger_\lambda(\vec{k})+\hat{a}^\dagger_\lambda(-\vec{k})\hat{a}_\lambda(-\vec{\tilde{k}})]E\right\}, \qquad (6.68)
\end{aligned}
$$

with

$$
F\equiv F_\lambda(\tau,k) = [\mathcal{X}'_\lambda(\tau,k)]^2+\omega^2_\lambda\mathcal{X}^2_\lambda(\tau,k),\quad E\equiv E_\lambda(\tau,k) = |\mathcal{X}'_\lambda(\tau,k)|^2+\omega^2_\lambda|\mathcal{X}_\lambda(\tau,k)|^2. \qquad (6.69)
$$

Let us now determine how $\hat{H}_\lambda(\tau)$ acts on the vacuum state, defined in Eq.(6.61)

$$
\hat{H}_\lambda(\tau)\left|0\right\rangle = \frac{1}{2}\int\frac{d^3k}{(2\pi)^3}\left\{F^*\hat{a}^\dagger_\lambda(-\vec{k})\hat{a}^\dagger_\lambda(\vec{k})+\delta^{(3)}(\vec{k}-\vec{k})(2\pi)^3E\right\}\left|0\right\rangle. \qquad (6.70)
$$

The state $|0\rangle$ is the eigenstate of $\hat{H}_\lambda$ with the lowest possible eigenvalue if and only if the first term in the above parenthesis vanishes. However, even if this condition is initially satisfied, it may be violated later due to the time dependence of ω^2_λ. Consequently, no time-independent eigenstates exist that could serve as a vacuum. The eigenstate of the quantum Hamiltonian with the lowest possible energy evolves with time which can be interpreted as a particle production in the curved spacetime. The amount of produced species is determined by their dispersion relation. In the considered case, the dispersion relation $\omega_\pm^2$ for two transversely-polarized modes is positive for all Fourier modes. Conversely, there is some region in the parameter space where the frequency ω_L^2 is negative. More precisely, the third term in (6.51) proportional to $\mathcal{R}(\tau)$ is negative when

$$\mathcal{R} = \frac{(3w-1)\rho(\tau)}{M_{\rm Pl}^2} < 0, \implies w < \frac{1}{3}. \tag{6.71}$$

It should be noted that while $w < 1/3$ is a necessary condition, it is not sufficient to guarantee that $\omega_L^2 < 0$. The square of the frequency ω_L^2 becomes negative if and only if the following condition is satisfied:

$$\omega_L^2 < 0 \qquad \Leftrightarrow \qquad \left(\frac{k^2 + a^2(\tau)m_X^2}{k^2}\right)^2 + \mathcal{H}^2 \frac{3a^2(\tau)m_X^2}{k^2 + a^2(\tau)m_X^2} < \frac{1-3w}{2}\mathcal{H}^2. \tag{6.72}$$

As we will demonstrate later in this chapter, the negativity of ω_L^2 gives rise to the tachyonic resonant production of longitudinal modes.

6.3.4 The energy density of the DM spin-1 field

Using the Belifante–Rosenfeld definition of the stress-energy tensor Eq.(2.45), one finds

$$T^X_{\mu\nu} = -g^{\sigma\beta}X_{\mu\sigma}X_{\nu\beta} + m_X^2 X_\mu X_\nu - g_{\mu\nu}\left(-\frac{1}{4}g^{\rho\alpha}g^{\sigma\beta}X_{\rho\sigma}X_{\alpha\beta} + \frac{1}{2}m_X^2 g^{\rho\sigma}X_\rho X_\sigma\right). \tag{6.73}$$

The energy density of a spin-1 dark field, $\rho \equiv g^{00}T_{00} = T_0^0$ is given by

$$\rho_X = \frac{1}{2a^2}\left(\dot{X}_i - \partial_i X_0\right)^2 + \frac{1}{4a^4}(\partial_i X_j - \partial_j X_i)^2 + \frac{1}{2}\frac{m_X^2}{a^2}X_i^2 + \frac{1}{2}m_X^2 X_0^2, \tag{6.74}$$

or in conformal coordinates

$$\rho_X = \frac{1}{2a^4(\tau)}\left(X_i' - \partial_i X_0\right)^2 + \frac{1}{4a^4(\tau)}(\partial_i X_j - \partial_j X_i)^2 + \frac{1}{2a^2(\tau)}m_X^2 X_i^2 + \frac{1}{2a^2(\tau)}m_X^2 X_0^2. \tag{6.75}$$

Using decomposition (6.33), one finds

$$\begin{aligned}\rho_X(\tau,\vec{x}) = \frac{1}{2a^4(\tau)}\int\frac{d^3k}{(2\pi)^3}\int\frac{d^3\tilde{k}}{(2\pi)^3}e^{i(\vec{k}+\vec{\tilde{k}})\cdot\vec{x}}\Big\{&\vec{X}'(\tau,\vec{k})\cdot\vec{X}'(\tau,\vec{\tilde{k}}) - i\vec{k}\cdot\vec{X}'(\tau,\vec{\tilde{k}})X_0(\tau,\vec{k}) \\ -i\vec{\tilde{k}}\cdot\vec{X}'(\tau,\vec{k})X_0(\tau,\vec{\tilde{k}}) - [\vec{k}\cdot\vec{\tilde{k}}][X_0(\tau,\vec{k})\cdot X_0(\tau,\vec{\tilde{k}})] - [\vec{k}\cdot\vec{\tilde{k}}][\vec{X}(\tau,\vec{k})\cdot\vec{X}(\tau,\vec{\tilde{k}})] \\ +[\vec{k}\cdot\vec{X}(\tau,\vec{\tilde{k}})][\vec{\tilde{k}}\cdot\vec{X}(\tau,\vec{k})] + a^2(\tau)m_X^2\left[X_0(\tau,\vec{k})X_0(\tau,\vec{\tilde{k}}) + \vec{X}(\tau,\vec{k})\cdot\vec{X}(\tau,\vec{\tilde{k}})\right]\Big\}&.\end{aligned} \tag{6.76}$$

Now, we can substitute Eq.(6.34) into (6.76), obtaining

$$\begin{aligned}\rho_X = \frac{1}{2a^4(\tau)}\int\frac{d^3k}{(2\pi)^3}\int\frac{d^3\tilde{k}}{(2\pi)^3}e^{i(\vec{k}+\vec{\tilde{k}})\cdot\vec{x}}\Bigg\{&\vec{X}'(\tau,\vec{k})\cdot\vec{X}'(\tau,\vec{\tilde{k}}) - \vec{k}\cdot\vec{X}'(\tau,\vec{\tilde{k}})\frac{\vec{k}\cdot\vec{X}'(\tau,\vec{k})}{k^2+a^2(\tau)m_X^2} \\ -\vec{\tilde{k}}\cdot\vec{X}'(\tau,\vec{k})\frac{\vec{\tilde{k}}\cdot\vec{X}'(\tau,\vec{\tilde{k}})}{\tilde{k}^2+a^2(\tau)m_X^2} + [\vec{k}\cdot\vec{\tilde{k}}]\frac{\vec{k}\cdot\vec{X}'(\tau,\vec{k})}{k^2+a^2(\tau)m_X^2}\frac{\vec{\tilde{k}}\cdot\vec{X}'(\tau,\vec{\tilde{k}})}{\tilde{k}^2+a^2(\tau)m_X^2} - [\vec{k}\cdot\vec{\tilde{k}}][\vec{X}(\tau,\vec{k})\cdot\vec{X}(\tau,\vec{\tilde{k}})]&\end{aligned}$$

$$
\begin{aligned}
&+ [\vec{k}\cdot\vec{X}(\tau,\tilde{\vec{k}})][\tilde{\vec{k}}\cdot\vec{X}(\tau,\vec{k})] + a^2(\tau)m_X^2\left[-\frac{\vec{k}\cdot\vec{X}'(\tau,\vec{k})}{k^2+a^2(\tau)m_X^2}\frac{\tilde{\vec{k}}\cdot\vec{X}'(\tau,\tilde{\vec{k}})}{\tilde{k}^2+a^2(\tau)m_X^2} + \vec{X}(\tau,\vec{k})\cdot\vec{X}(\tau,\tilde{\vec{k}})\right]\Bigg]\Bigg\} \\
&= \frac{1}{2a^4(\tau)}\sum_{\lambda,\tilde{\lambda}}\int\frac{d^3k}{(2\pi)^3}\int\frac{d^3\tilde{k}}{(2\pi)^3}e^{i(\vec{k}+\tilde{\vec{k}})\cdot\vec{x}}\Bigg\{X'_\lambda(\tau,k)X'_{\tilde{\lambda}}(\tau,\tilde{k})\Bigg[\vec{\epsilon}_\lambda(\vec{k})\cdot\vec{\epsilon}_{\tilde{\lambda}}(\tilde{\vec{k}}) - \frac{[\vec{k}\cdot\vec{\epsilon}_{\tilde{\lambda}}(\tilde{\vec{k}})][\vec{k}\cdot\vec{\epsilon}_\lambda(\vec{k})]}{k^2+a^2(\tau)m_X^2} + \\
&-\frac{[\tilde{\vec{k}}\cdot\vec{\epsilon}_\lambda(\vec{k})][\tilde{\vec{k}}\cdot\vec{\epsilon}_{\tilde{\lambda}}(\tilde{\vec{k}})]}{\tilde{k}^2+a^2(\tau)m_X^2} + [\vec{k}\cdot\tilde{\vec{k}}]\frac{\vec{k}\cdot\vec{\epsilon}_\lambda(\vec{k})}{k^2+a^2(\tau)m_X^2}\frac{\tilde{\vec{k}}\cdot\vec{\epsilon}_{\tilde{\lambda}}(\tilde{\vec{k}})}{\tilde{k}^2+a^2(\tau)m_X^2} - a^2(\tau)m_X^2\frac{\vec{k}\cdot\vec{\epsilon}_\lambda(\vec{k})}{k^2+a^2(\tau)m_X^2}\frac{\tilde{\vec{k}}\cdot\vec{\epsilon}_{\tilde{\lambda}}(\tilde{\vec{k}})}{\tilde{k}^2+a^2(\tau)m_X^2}\Bigg] \\
&+X_\lambda(\tau,k)X_{\tilde{\lambda}}(\tau,\tilde{k})\left[\vec{\epsilon}_\lambda(\vec{k})\cdot\vec{\epsilon}_{\tilde{\lambda}}(\tilde{\vec{k}})[a^2(\tau)m_X^2 - \vec{k}\cdot\tilde{\vec{k}}] + [\vec{k}\cdot\vec{\epsilon}_{\tilde{\lambda}}(\tilde{\vec{k}})][\tilde{\vec{k}}\cdot\vec{\epsilon}_\lambda(\vec{k})]\right]\Bigg\}. \qquad (6.77)
\end{aligned}
$$

At this point, it is convenient to introduce the power spectrum $\mathcal{P}_X$ and $P_{X'}$ through the following relation:

$$
\begin{aligned}
\langle\vec{X}(\tau,\vec{k})\cdot\vec{X}(\tau,\tilde{\vec{k}})\rangle &= (2\pi)^3\delta^{(3)}(\vec{k}+\tilde{\vec{k}})\frac{2\pi^2}{k^3}\mathcal{P}_X(\tau,k), \\
\langle\vec{X}'(\tau,\vec{k})\cdot\vec{X}'(\tau,\tilde{\vec{k}})\rangle &= (2\pi)^3\delta^{(3)}(\vec{k}+\tilde{\vec{k}})\frac{2\pi^2}{k^3}\mathcal{P}_{X'}(\tau,k). \qquad (6.78)
\end{aligned}
$$

In the position space, the classical two-point correlation functions are given by

$$
\begin{aligned}
\langle\vec{X}^2(\tau,\vec{x})\rangle &= \int\frac{d^3k}{(2\pi)^3}\int\frac{d^3\tilde{k}}{(2\pi)^3}e^{i(\vec{k}+\tilde{\vec{k}})\cdot\vec{x}}\langle\vec{X}(\tau,k)\cdot\vec{X}(\tau,\tilde{k})\rangle = \int\frac{d^3k}{(2\pi)^3}\frac{2\pi^2}{k^3}\mathcal{P}_X(\tau,k) \\
&= \int d\ln k\,\mathcal{P}_X(\tau,k), \qquad (6.79) \\
\langle(\vec{X}'(\tau,\vec{x}))^2\rangle &= \int\frac{d^3k}{(2\pi)^3}\int\frac{d^3\tilde{k}}{(2\pi)^3}e^{i(\vec{k}+\tilde{\vec{k}})\cdot\vec{x}}\langle\vec{X}'(\tau,k)\cdot\vec{X}'(\tau,\tilde{k})\rangle = \int\frac{d^3k}{(2\pi)^3}\frac{2\pi^2}{k^3}\mathcal{P}_{X'}(\tau,k) \\
&= \int d\ln k\,\mathcal{P}_{X'}(\tau,k). \qquad (6.80)
\end{aligned}
$$

Thus, the ensemble average of ρ_X is

$$
\begin{aligned}
\langle\rho_X(\tau)\rangle = \frac{1}{2a^4(\tau)}\sum_\lambda\int\frac{d^3k}{(2\pi)^3}\frac{2\pi^2}{k^3}&\left\{\mathcal{P}_{X'_\lambda}\left[1-\frac{[\vec{k}\cdot\vec{\epsilon}_\lambda(\vec{k})][\vec{k}\cdot\vec{\epsilon}_\lambda(-\vec{k})]}{k^2+a^2(\tau)m_X^2}\right]\right. \\
&\left.+\mathcal{P}_{X_\lambda}\left[k^2+a^2(\tau)m_X^2-[\vec{k}\cdot\vec{\epsilon}_\lambda(-\vec{k})][\vec{k}\cdot\vec{\epsilon}_\lambda(\vec{k})]\right]\right\}. \qquad (6.81)
\end{aligned}
$$

Using Eq.(6.41), one can then separate the above expression into two independent contributions for the transverse

$$
\langle\rho_{X_\pm}(\tau)\rangle = \frac{1}{2a^4(\tau)}\int d\ln k\left\{\mathcal{P}_{X'_\pm}+\mathcal{P}_{X_\pm}[k^2+a^2(\tau)m_X^2]\right\}, \qquad (6.82)
$$

and the longitudinal modes

$$
\langle\rho_{X_L}(\tau)\rangle = \frac{1}{2a^4(\tau)}\int d\ln k\left\{\frac{a^2(\tau)m_X^2}{k^2+a^2(\tau)m_X^2}\mathcal{P}_{X'_L}+a^2(\tau)m_X^2\mathcal{P}_{X_L}\right\}, \qquad (6.83)
$$

respectively.

Afterward, one can also introduce the two-point correlation function for the quantum operator $\hat{\vec{X}}_\lambda(\tau, k)$ (6.57) as

$$\langle \hat{\vec{X}}^2(\tau,\vec{x})\rangle \equiv \langle 0|\,\hat{\vec{X}}^2(\tau,\vec{x})\,|0\rangle = \sum_{\lambda,\tilde{\lambda}} \int \frac{d^3k}{(2\pi)^3} \int \frac{d^3\tilde{k}}{(2\pi)^3} e^{i(\vec{k}+\vec{\tilde{k}})\cdot\vec{x}}\,\vec{\epsilon}_\lambda(\vec{k})\cdot\vec{\epsilon}_{\tilde{\lambda}}(\vec{\tilde{k}})$$
$$\times \langle 0|\,[\hat{a}_\lambda(\vec{k})\mathcal{X}_\lambda + \hat{a}^\dagger_\lambda(-\vec{k})\mathcal{X}^*_\lambda][\hat{a}_{\tilde{\lambda}}(\vec{\tilde{k}})\mathcal{X}_{\tilde{\lambda}} + \hat{a}^\dagger_{\tilde{\lambda}}(-\vec{\tilde{k}})\mathcal{X}^*_{\tilde{\lambda}}]\,|0\rangle$$
$$= \int \frac{d^3k}{(2\pi)^3}\left\{|\mathcal{X}_L|^2+|\mathcal{X}_+|^2+|\mathcal{X}_-|^2\right\}. \tag{6.84}$$

Note that in the above expression, $\mathcal{X}_L$ denotes the mode function of the redefined longitudinal field A_L, i.e., which is related to the physical longitudinal component of the dark vector field through (6.49) and (6.53).

The vacuum expectation value of the total energy density can be written as a sum of two terms, accounting for the energy density of two transversely-polarized modes

$$\langle \hat{\rho}_{X_\pm}\rangle \equiv \langle 0|\,\hat{\rho}_{X_\pm}\,|0\rangle = \frac{1}{2a^4(\tau)}\int \frac{d^3k}{(2\pi)^3}\left\{|\mathcal{X}'_\pm|^2+|\mathcal{X}_\pm|^2\Big[k^2+a^2(\tau)m_X^2\Big]\right\}, \tag{6.85}$$

and the energy density of the single longitudinal mode

$$\langle \hat{\rho}_{X_L}\rangle \equiv \langle 0|\,\hat{\rho}_{X_L}\,|0\rangle = \frac{1}{2a^4(\tau)}\int \frac{d^3k}{(2\pi)^3}\left\{|\mathcal{X}'_L|^2+|\mathcal{X}_L|^2\left[k^2+a^2(\tau)m_X^2+\mathcal{H}^2\frac{k^4}{(k^2+a^2(\tau)m_X^2)^2}\right]\right.$$
$$\left. -(\mathcal{X}'_L\mathcal{X}^*_L+\mathcal{X}^{*\prime}_L\mathcal{X}_L)\mathcal{H}\frac{k^2}{k^2+a^2(\tau)m_X^2}\right\}. \tag{6.86}$$

The energy density of the dark vector field at a given moment is determined by solutions of the HO equations (6.48) and (6.50), and the background dynamics through $a(\tau)$ and its (conformal) time derivatives. It is instructive to recall that the gravitational production of longitudinal modes receives the tachyonic enhancement if dark vector mass m_X satisfies condition (6.72). In this case, the production of $\mathcal{X}_L$ modes is expected to be parametrically larger than that of the transverse modes, see also [169, 173, 445]. Therefore, in the following, we focus solely on the gravitational production of the longitudinal modes in the expanding Universe, assuming that

$$\langle \hat{\rho}_{X_\pm}\rangle \ll \langle \hat{\rho}_{X_L}\rangle \qquad \Longrightarrow \qquad \langle \hat{\rho}_X\rangle \simeq \langle \hat{\rho}_{X_L}\rangle. \tag{6.87}$$

6.4 The inflationary evolution of longitudinal modes

This section aims to determine the evolution of longitudinal modes during cosmic inflation. Specifically, our goal is to obtain solutions to the mode equation for the longitudinal component of the dark field, allowing us to find its energy density through (6.86). As demonstrated in Chapter (3), the Hubble parameter is a slowly-varying function of time during the slow-roll phase of inflation. Hence, we assume that during inflation, $H \simeq H_e$. Consequently, during the de Sitter stage of inflation, the frequency ω_L^2 (6.51) can be written as

$$\omega_L^2(\tau\le\tau_e) \equiv \omega_{\rm I}^2(\tau) = k^2 + a_{\rm I}^2(\tau)m_X^2 - \frac{2k^4 - k^2a_{\rm I}^2(\tau)m_X^2}{(k^2+a_{\rm I}^2(\tau)m_X^2)^2}a_{\rm I}^2(\tau)H_e^2\,, \tag{6.88}$$

where we have used the following relations:

$$\left(\frac{a'}{a}\right)^2 = a_{\mathrm{I}}^2(\tau)H_e^2, \qquad \frac{a''}{a} = 2a_{\mathrm{I}}^2(\tau)H_e^2.$$

By examining the above equation, one observes that for heavy DM species with a mass much greater than the Hubble parameter during inflation, $m_X \gg H_e$, the dispersion relation ω_L^2 remains positive. On the other hand, if $m_X \ll H_e$ there is some region in the parameter space, where $\omega_L^2 < 0$, which leads to tachyonic enhancement of $\mathcal{X}_L$ modes. Yet another reason to focus on relatively light DM species, i.e., $m_X < H_e \ll \Lambda$, is not to spoil the single-field inflation. Namely, we assume that the inflaton energy density $3M_{\mathrm{Pl}}^2 H_e^2 \approx \Lambda^4$ dominates the energy budget of the Universe during inflation. In the remaining part, we restrict ourselves to DM vectors with masses $m_X \lesssim H_e$.

In the far past, all vector modes were deep inside the Hubble horizon, so that $a_{\mathrm{I}}(\tau)m_X \ll a_{\mathrm{I}}(\tau)H_e \ll k$. In the subhorizon limit, ω_L^2 is nearly constant, and the EoM for longitudinal modes simplifies as

$$\mathcal{X}_L''(\tau) + k^2\mathcal{X}_L(\tau) = 0. \tag{6.89}$$

The unique solution that minimizes the energy is the Bunch-Davies state (3.78)

$$\lim_{\tau\to-\infty} \mathcal{X}_L(\tau) \equiv \mathcal{X}_{\mathrm{L}}^{\mathrm{BD}}(\tau) = \frac{1}{\sqrt{2k}}e^{-ik\tau}. \tag{6.90}$$

In what follows, we use the above solution as the initial condition.
We can distinguish two scales relevant to this analysis. Namely, the comoving Compton wavelength $(am_X)^{-1}$ and the Hubble horizon $(aH)^{-1}$. The relation between these three scales determines the evolution of the longitudinal mode with wavenumber $1/k$. During the de-Sitter stage of inflation, apart from the Bunch-Davies solution, one distinguishes two other regimes:

(*a*) *Intermediate-wavelength inflationary regime* ($a_{\mathrm{I}}(\tau)m_X \ll k \ll a_{\mathrm{I}}(\tau)H_e$), such that

$$\omega_{\mathrm{I}}^2 \approx k^2 - 2a_{\mathrm{I}}^2(\tau)H_e^2. \tag{6.91}$$

(*b*) *Long-wavelength inflationary regime* ($k \ll a_{\mathrm{I}}(\tau)m_X \ll a_{\mathrm{I}}(\tau)H_e$), such that

$$\omega_{\mathrm{I}}^2 \approx a_{\mathrm{I}}^2(\tau)m_X^2 + \frac{k^2}{a_{\mathrm{I}}^2(\tau)m_X^2}a_{\mathrm{I}}^2(\tau)H_e^2. \tag{6.92}$$

Figure Fig. 6.1 shows the evolution of length-scales $(am_X)^{-1}$, $(aH)^{-1}$, and $1/k$ for heavy $H_{\mathrm{rh}} \le m_X < H_e$ (left panel) and light $m_X < H_{\mathrm{rh}}$ (right panel) DM vectors. This section focuses on the first part of these two diagrams accounting for the inflationary dynamics. During this phase, heavy and light DM vectors behave the same way. Based on the discussion above, one identifies three different inflationary solutions to the longitudinal mode equation. In the remote past, all modes evolved in the red sub-horizon region, the so-called Bunch-Davies vacuum, where the solution to the mode equation has the oscillatory form (6.90). Modes with wavenumber $1/k \gg 1/k_e$, where $k_e \equiv a_e H_e$, cross the Hubble horizon $(a_{\mathrm{I}}H_e)^{-1}$ at some point during inflation, and enter the *purple* region '(*a*)'. In the *intermediate-wavelength inflationary regime* (purple region (a)), their dispersion relation is approximated by (6.91). Finally, long-wavelength modes with $1/k \gg 1/k_m$, where $k_m \equiv a_e H_e$, cross the Compton wavelength curve $(am_X)^{-1}$, and enter the blue *long-wavelength inflationary regime* before the end of inflation, where ω_L^2 is in the form (6.92). Thus, three distinct types of inflationary

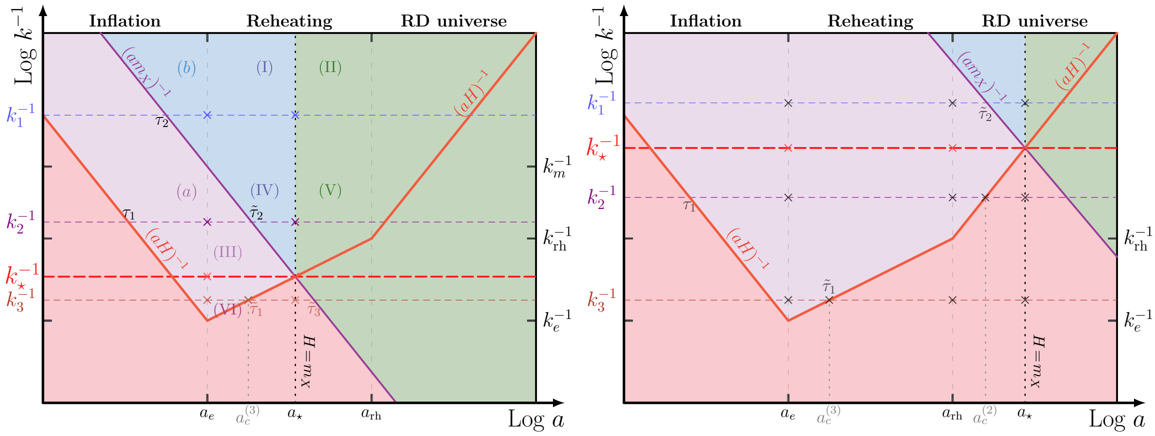

FIGURE 6.1: Evolution of various cosmological distances during and after inflation for heavy vector DM i.e. $H_{\rm rh} \leq m_X < H_{\rm e}$ (left diagram), and light vector DM $m_X < H_{\rm rh}$ (right diagram). In the red subhorizon regions $am_X, aH \ll k$, in ther purple part $am_X < k < aH$, blue region corresponds to $k < am_X < aH$, whereas in the green region $aH, k \ll am_X$. Here $a_c = k/H$ denotes the second (after inflation0 *horizon crossing*, $k_m \equiv a_e m_X$, $k_\star = a_\star m_X$, $k_e \equiv a_e H_e$, and $k_{\rm rh} \equiv a_{\rm rh} H_{\rm rh}$.

evolution for longitudinal modes can be distinguished. *Short-wavelength modes* remain in the red sub-horizon region throughout the whole period of inflation. *Intermediate-wavelength modes* end their inflationary evolution in the purple region. Finally, *long-wavelength modes* pass through all these regions and end up in the blue region '(b)'. The *intermediate-* and *long-wavelength* modes are represented in the left panel of Fig. 6.1 by k_2^{-1} (dashed purple horizontal line) such that $k_2^{-1} \in (k_e^{-1}, k_m^{-1})$, and k_1^{-1} (dashed blue horizontal line), such that $k_1^{-1} > k_m^{-1}$, respectively.

6.4.1 Intermediate-wavelength regime

In the (a) *intermediate-wavelength regime*, the EoM for longitudinal modes takes the form

$$\frac{d^2}{d\eta^2}\mathcal{X}_L + \left(k^2 - \frac{2}{\eta^2}\right)\mathcal{X}_L = 0, \qquad \text{where} \quad \eta \equiv \tau - \frac{3}{2}(1+\bar{w})\tau_e, \tag{6.93}$$

where τ_e denotes the conformal time at the end of inflation. The solution to the above equation is given by

$$\mathcal{X}_L^{(a)}(\eta) = \sqrt{\frac{2}{\pi k}}\, C_1^{(a)} \left[\frac{\sin(k\eta)}{k\eta} - \cos(k\eta)\right] - \sqrt{\frac{2}{\pi k}}\, C_2^{(a)} \left[\frac{\cos(k\eta)}{k\eta} + \sin(k\eta)\right], \tag{6.94}$$

where the integration constants $C_1^{(a)}$ and $C_2^{(a)}$ are fixed by the Bunch-Davies initial condition (6.90), as

$$C_1^{(a)} = -\frac{\sqrt{\pi}}{2} e^{ik\left(\frac{3}{2}(1+\bar{w})\tau_e\right)}, \qquad\qquad C_2^{(a)} = -iC_1^{(a)}\,. \tag{6.95}$$

Hence, Eq. (6.94) can be recast to the form

$$\begin{aligned}\mathcal{X}_L^{(a)}(\tau) &= \frac{1}{\sqrt{2k}}\left(1 - \frac{i}{k(\tau - \frac{3}{2}(1+\bar{w})\tau_e)}\right)e^{-ik\tau} \\ &\overset{k \ll a_I H_e}{\approx} \frac{-i}{\sqrt{2k}}\frac{1}{k(\tau - \frac{3}{2}(1+\bar{w})\tau_e)}e^{-ik\tau} = \frac{i}{2\sqrt{k}}\frac{a_{\rm I}(\tau)H_e}{k}e^{-ik\tau}\,.\end{aligned} \tag{6.96}$$

The above solution indicates that in the *intermediate-wavelength inflationary regime*, longitudinal modes grow linearly with the scale factor $a_{\rm I}(\tau)$. The behavior of the dark matter vectors in this region exhibits similarities to that of a massless scalar, as discussed in [169].

6.4.2 Long-wavelength regime

In the (b) *long-wavelength regime*, the mode equation is given by

$$\frac{d^2}{d\eta^2}\mathcal{X}_L + \left(\frac{m_X^2}{H_e^2\eta^2} + \frac{k^2H_e^2}{m_X^2}\right)\mathcal{X}_L = 0, \tag{6.97}$$

with the following solution:

$$\mathcal{X}_L^{(b)}(\eta) = \sqrt{\eta}\left[C_1^{(b)}J_n\left(\frac{H_e}{m_X}k\eta\right) + C_2^{(b)}Y_n\left(\frac{H_e}{m_X}k\eta\right)\right], \tag{6.98}$$

where $J_n(x)$ and $Y_n(x)$ denote the Bessel functions of the first and second kind, respectively, with

$$n = \frac{1}{2}\sqrt{1-\frac{4m_X^2}{H_e^2}} \approx \frac{1}{2}. \tag{6.99}$$

Adopting the above approximation, we can simplify $\mathcal{X}_L^{(b)}$ as

$$\mathcal{X}_L^{(b)}(\tau) = -C_1^{(b)}\sqrt{\frac{2m_X}{\pi kH_e}}\sin\left(\frac{k}{a_{\rm I}(\tau)m_X}\right) - C_2^{(b)}\sqrt{\frac{2m_X}{\pi kH_e}}\cos\left(\frac{k}{a_{\rm I}(\tau)m_X}\right). \tag{6.100}$$

To set $C_1^{(b)}$ and $C_2^{(b)}$ coefficients, we match the solutions in the *intermediate-* and *long-wavelength* regions, such that the mode function $\mathcal{X}_L$, as well as its time derivative $\mathcal{X}_L'$ are continuous. Hence, at the crossover, we require

$$\mathcal{X}_L^{(b)}(\tau_2) = \mathcal{X}_L^{(a)}(\tau_2), \qquad \mathcal{X}_L^{(b)\prime}(\tau_2) = \mathcal{X}_L^{(a)\prime}(\tau_2), \tag{6.101}$$

where τ_2 denotes the conformal time at which mode with wavenumber $1/k$ crosses the Compoton wavelength $(a_{\rm I}(\tau_2)m_X)^{-1}$, i.e.,

$$\tau_2 = \frac{3}{2}\tau_e(1+\bar{w}) - \tilde{b}\frac{m_X}{kH_e}, \tag{6.102}$$

In the above formula, $\tilde{b}$ is an auxiliary parameter introduced to improve the agreement between numerical and analytical solutions. In the following calculations, we set $\tilde{b} = 1.2$. Then, from Eq. (6.101), one obtains

$$C_1^{(b)} = \sqrt{\frac{\pi}{H_e m_X}}\frac{(iH_e^2+\tilde{b}H_em_X - i\tilde{b}^2m_X^2)\cos(\tilde{b}) - \tilde{b}(iH_e^2+\tilde{b}H_em_X)\sin(\tilde{b})}{2\tilde{b}^2m_X}e^{-ik\tau_2}, \tag{6.103}$$

$$C_2^{(b)} = -\sqrt{\frac{\pi}{H_e m_X}}\frac{(iH_e^2+\tilde{b}H_em_X - i\tilde{b}^2m_X^2)\sin(\tilde{b}) + \tilde{b}(iH_e^2+\tilde{b}H_em_X)\cos(\tilde{b})}{2\tilde{b}^2m_X}e^{-ik\tau_2}. \tag{6.104}$$

Next, expanding the above result in the *long-wavelength* limit, i.e., $k \ll a_{\rm I}(\tau)m_X \ll a_{\rm I}(\tau)H_e$, one finds that Eq. (6.100) can be well approximated by a constant solution, i.e.,

$$\mathcal{X}_L^{(b)} \approx \frac{i}{\sqrt{2k}}\frac{H_e}{m_X}\frac{(\sin(\tilde{b})+\tilde{b}\cos(\tilde{b}))}{\tilde{b}^2}\, e^{-ik\left(\frac{3}{2}(1+\bar{w})\tau_e - \tilde{b}\frac{m_X}{kH_e}\right)}. \tag{6.105}$$

Note that for the adopted value of $\tilde{b} = 1.2$, the factor $(\sin(\tilde{b}) + \tilde{b}\cos(b))/\tilde{b}^2 \approx 0.95$ for $\tilde{b} = 1.2$ can be safely neglected. Let us also emphasize that the above solution implies that the tachyonic growth of longitudinal modes is terminated in the *long-wavelength region*. Furthermore, from Eq. (6.105) one notices that the amplitude $|\mathcal{X}_L^{(b)}|^2$ scales as k^{-1} in the *long-wavelength region*, whereas the amplitude of massive scalars is proportional to $k^{-3/2}$ [169].

6.4.3 Numerical results

In Fig. 6.2 we have plotted the inflationary evolution of *intermediate-* (e.g. k_2^{-1} mode in Fig. (6.1)) and *long-wavelength* modes (e.g. k_1^{-1} mode in Fig. (6.1)). These two figures present the comparison between approximate analytical solutions Eq. (6.90) (dashed red curve), Eq. (6.96) (dashed purple), and (Eq. (6.105)) (dashed navy) with exact numerical results (solid cyan). The agreement between the two is excellent, as evident from this comparison. The vertical dashed gray lines indicate the moment at which longitudinal modes exit the horizon, marked by the condition $a = k/H_e$, and when their wavenumber $1/k$ matches with the Compton wavelength, i.e., $a = k/m_X$.

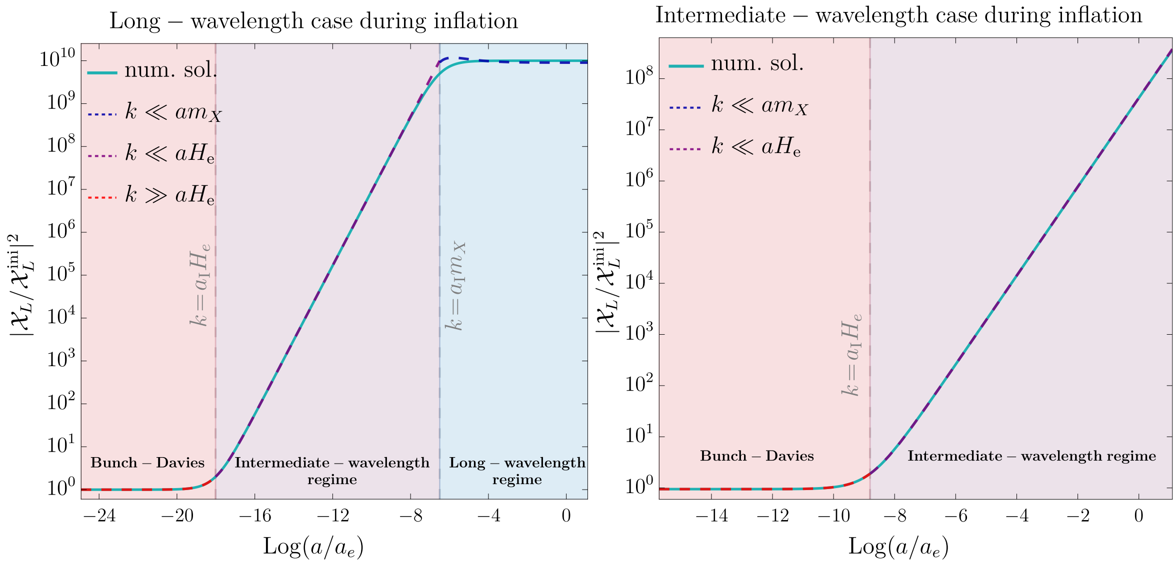

FIGURE 6.2: Evolution of the mode functions $\mathcal{X}_L$ normalized to the initial value $\mathcal{X}_L^{\rm ini}$ with the scale factor a during inflation for $k \ll a_e m_X \ll a_e H_e$ (left-panels) and $a_e m_X \ll k \ll a_e H_e$ (right-panels). Solid cyan curves correspond to numerical solutions, while dashed red, purple, and blue curves show analytical solutions (6.90), (6.96), and (6.105), respectively. Here $m_X = 10^8$ GeV, $H_e = 10^{13}$ GeV, $\bar{w} = 0$ and $k = 10^{-8}$ GeV ($k = 10^{-4}$ GeV) for the left (right) panel.

6.4.4 The expectation value of energy density

Finally, let us use the inflationary solutions obtained above to determine the expectation value of the energy density for longitudinal modes. Note that $\langle\hat{\rho}_L\rangle$ is calculated with respect to the Bunch-Davies vacuum. Utilizing Eq. (6.86) together with (6.90), one finds that the fraction energy density per log momentum for sub-horizon modes is

$$\frac{d\langle\hat{\rho}_L(a)\rangle}{d\ln k} = \frac{k^4}{4\pi^2 a^4} + \frac{k^2\left(H_e^2 + m_X^2\right)}{8\pi^2 a^2} - \frac{H_e^2 m_X^2}{4\pi^2} + \frac{3a^2 H_e^2 m_X^4}{8\pi^2 k^2} + \mathcal{O}\left(\left(\frac{am_X}{k}\right)^2, \left(\frac{aH_e}{k}\right)^4\right). \quad (6.106)$$

It is worth noting that for large values of k, the first three terms in the above expression diverge. To eliminate divergent contributions from sub-horizon modes, we adopt the following cut-off scale $\Lambda = k_e \equiv a_e H_e$, which truncates the energy density integral to super-horizon modes that exit the Hubble horizon during inflation.

Next, for *intermediate-wavelength* modes, one finds

$$\frac{d\langle\hat{\rho}_L(a)\rangle}{d\ln k} = \frac{1}{2}\left(\frac{k}{a}\right)^2\left(\frac{H_e}{2\pi}\right)^2\left\{1 + \mathcal{O}\Big(\Big(\frac{m_X}{H_e}\Big)^2, \Big(\frac{k}{aH_e}\Big)^2\Big)\right\}, \tag{6.107}$$

where we have used (6.96).

Finally, for *long-wavelength* modes, one gets

$$\frac{d\langle\hat{\rho}_L(a)\rangle}{d\ln k} = \frac{1}{2}\left(\frac{k}{a}\right)^2\left(\frac{H_e}{2\pi}\right)^2\left\{1 + \mathcal{O}\Big(\Big(\frac{k}{am_X}\Big)^2, \Big(\frac{k}{am_X}\Big)^4 \cdot \Big(\frac{H_e}{m_X}\Big)^2\Big)\right\}. \tag{6.108}$$

Hence, at the very end of inflation, the fractional energy density of longitudinal modes scales as

$$\frac{d\langle\hat{\rho}_L(a_e)\rangle}{d\ln k} \approx \begin{cases} \dfrac{k^4}{4\pi^2 a_e^4}, & \text{sub-horizon modes } k \gg a_e H_e, \\ \dfrac{1}{2}\left(\dfrac{k}{a_e}\right)^2\left(\dfrac{H_e}{2\pi}\right)^2, & \text{super-horizon modes } k \ll a_e H_e. \end{cases} \tag{6.109}$$

The above expression indicates that the main contribution to $d\langle\hat{\rho}_L(a_e)\rangle/d\ln k$ comes from modes with a wavenumber of the order of $1/k_e$.

6.5 The post-inflationary evolution of longitudinal modes

Once we have found solutions to EoM for longitudinal modes during the de-Sitter stage of inflation, we can analyze their post-inflationary evolution. To that end, one needs to specify the background dynamics. In this subsection, we aim to investigate the impact of non-instantaneous reheating on gravitational DM production. Namely, we assume that the crossover between inflation and the RD epoch is not immediate. Instead, we explore a more generic scenario, which we elaborated on in Chapter (4). In this case, the background dynamics can be solely determined by the averaged equation-of-state parameter $\bar{w}$ and the reheating efficiency γ. Let us recall that for the power-law inflaton potential ϕ^{2n}, $\bar{w}$ is related to the index n through Eq.(3.36). For a given reheating model, the reheating efficiency γ is specified by the inflaton equation-of-state parameter, the form, and the strength of the $\phi -$ SM interactions. In this chapter, we do not consider any specific reheating model; instead, we develop a generic description adopting a non-standard post-inflationary scenario. Moreover, we assume that the Universe enters the RD epoch after reheating.

After inflation, i.e., for $a > a_e$, the dispersion relation for the longitudinal modes can be recast as

$$\omega_L^2(\tau) \simeq k^2 + a^2 m_X^2 - \frac{k^2}{k^2 + a^2 m_X^2}\left(\frac{1 - 3\bar{w}}{2} - \frac{3a^2 m_X^2}{k^2 + a^2 m_X^2}\right) a^2 H^2\,. \tag{6.110}$$

It is worth noting that the term in Eq. (6.5) involving $a'' \simeq a^2 H^2 (1 - 3\bar{w})/2$ is discontinuous across the transition points τ_e and $\tau_{\rm rh}$. Consequently, the frequency ω_L^2 also has a jump at these two points. This discontinuity is not physical, as its presence results from the fact that in the adopted approximations, $\bar{w}$ is not continuous across these two crossovers, e.g., during inflation $\bar{w} \approx -1$, whereas immediately after its end $\bar{w} \neq -1$. Hence, the discontinuity can be removed if one considers the full dynamics of the inflaton field. As shown in Sec.(3.5), in such a case, the equation-of-state parameter is a continuous function of a. At this point, we should emphasize that the energy density of longitudinal modes depends on the field value $\mathcal{X}_L$ and its derivative $\mathcal{X}_L'$, and contains only terms proportional to a and a'. Since the scale factor and the Hubble rate are continuous across the transition points, to ensure the continuity of ρ_L, we require the mode functions to match at τ_e and $\tau_{\rm rh}$:

$$\mathcal{X}_L^{(-)}(\tau_{e,\rm rh}) = \mathcal{X}_L^{(+)}(\tau_{e,\rm rh}), \qquad \mathcal{X}_L^{(-)\prime}(\tau_{e,\rm rh}) = \mathcal{X}_L^{(+)\prime}(\tau_{e,\rm rh}), \tag{6.111}$$

with $\mathcal{X}_L^{(-/+)}$ being the *left/right* limits of the solutions to the mode equation, i.e., $\mathcal{X}_L^{(-/+)}(\tau_{e,\rm rh}) = \lim\limits_{\tau\to\tau_{e,\rm rh}^{-/+}} \mathcal{X}_L(\tau)$.

To analyze the post-inflationary behavior of the longitudinal modes, it is instructive to examine the following four regimes (see Fig. 6.1):

$$\omega_L^2 \approx \begin{cases} k^2, & a(\tau)m_X, a(\tau)H(\tau) \ll k, & (6.112\text{a}) \\ -\left(\dfrac{1-3\bar{w}}{2} - \dfrac{3a^2(\tau)m_X^2}{k^2}\right)a^2(\tau)H^2(\tau), & a(\tau)m_X \ll k \ll a(\tau)H(\tau), & (6.112\text{b}) \\ \dfrac{k^2}{a^2(\tau)m_X^2}\left(\dfrac{5+3\bar{w}}{2}\right)a^2(\tau)H^2(\tau), & k \ll a(\tau)m_X \ll a(\tau)H(\tau), & (6.112\text{c}) \\ a^2(\tau)m_X^2, & a(\tau)H(\tau), k \ll a(\tau)m_X. & (6.112\text{d}) \end{cases}$$

In the remaining part, we focus on longitudinal modes that exit the Hubble horizon during inflation. As demonstrated in the previous section, only these modes receive tachyonic enhancement. Additionally, it is important to emphasize that the post-inflation evolution of DM vectors depends on the wavenumber $1/k$, as well as the relationship between their mass m_X and the Hubble scale at the end of reheating $H_{\rm rh}$. Below, we will explicitly show that the dynamics of light DM species (with mass $m_X \ll H_{\rm rh}$) differ from those with a mass of $m_X \gg H_{\rm rh}$.

6.5.1 Dynamics of heavy DM vectors

For heavy DM vectors, i.e., $H_{\rm rh} \leq m_X < H_e$, one distinguishes three types of post-inflationary evolution.

Long-wavelength modes

Longitudinal modes with wavenumber $1/k \gg 1/k_m \equiv a_e m_X$ (e.g., the k_1^{-1} mode in the left panel of Fig. 6.1) start their post-inflationary evolution in the blue region, and then enter the green area at some point after inflation, where they eventually re-enter the Hubble horizon. At the early times, their dispersion relation is $\omega_L^2 \to 0$, so that the solution to the mode equation takes the form

$$\mathcal{X}_L^{(\rm I)}(a) = C_1^{(\rm I)} + C_2^{(\rm I)} a^{\frac{1+3\bar{w}}{2}}. \tag{6.113}$$

Longitudinal modes with wavenumber $1/k \gg 1/k_m$ (e.g., k_1^{-1} curve in Fig. 6.1) start their post-inflationary evolution in the blue region, and at some point, they enter the green area, where they eventually re-enter the Hubble horizon. At the early times, their dispersion relation is $\omega_L^2 \to 0$, so that the solution to the mode equation takes the form

$$C_1^{(\mathrm{I})} = \frac{i}{\sqrt{2k}} \frac{H_e}{m_X} e^{-ik\left(\frac{3}{2}\tau_e(1+\bar{w}) - \tilde{b}\frac{m_X}{kH_e}\right)}, \qquad C_2^{(\mathrm{I})} = 0.$$

Therefore, the growing solution proportional to $a^{\frac{1+3\bar{w}}{2}}$ is suppressed, and one obtains a constant solution for the mode function

$$\mathcal{X}_L^{(\mathrm{I})} = \frac{i}{\sqrt{2k}} \frac{H_e}{m_X} e^{-ik\left(\frac{3}{2}\tau_e(1+\bar{w}) - \tilde{b}\frac{m_X}{kH_e}\right)}, \tag{6.114}$$

which indicates that the amplitude $|\mathcal{X}^{(\mathrm{I})}|^2$ scales as k^{-1}.

Next, at $\tau_\star = (\tilde{b}m_X/H_e)^{-\frac{1+3\bar{w}}{3(1+\bar{w})}}$, indicating the moment at which the Compton wavelength $(a(\tau_\star)m_X)^{-1}$ crosses with Hubble horizon $a(\tau_\star)H(\tau_\star)$, longitudinal modes enter the green region, in which $\omega_L^2 \approx a^2 m_X^2$. The change of ω_L^2 is slow (i.e., adiabatic) if

$$2\pi|\omega_L'| \ll \omega_L^2, \tag{6.115}$$

implying

$$2\pi H \ll m_X\,. \tag{6.116}$$

The above condition is satisfied in the green region, except for a short period after $\tau = \tau_\star$. Hence, the solution to the mode equation in the green area II can be written as

$$\mathcal{X}_L^{(\mathrm{II})}(\tau) = \frac{C_1^{(\mathrm{II})}}{\sqrt{2a(\tau)m_X}} \exp\Big(i\int_{\tau_\star}^{\tau} d\tau'\, a(\tau')m_X\Big) + \frac{C_2^{(\mathrm{II})}}{\sqrt{2a(\tau)m_X}} \exp\Big(-i\int_{\tau_\star}^{\tau} d\tau'\, a(\tau')m_X\Big). \tag{6.117}$$

Coefficients $C_1^{(\mathrm{II})}, C_2^{(\mathrm{II})}$ are determined by the following conditions:

$$\mathcal{X}_L^{(\mathrm{II})}(\tau_\star) = \mathcal{X}_L^{(\mathrm{I})}(\tau_\star), \qquad \mathcal{X}_L^{(\mathrm{II})\prime}(\tau_\star) = \mathcal{X}_L^{(\mathrm{I})\prime}(\tau_\star), \tag{6.118}$$

setting

$$C_{1,2}^{(\mathrm{II})} = \frac{H_e}{2}\sqrt{\frac{a(\tau_\star)}{m_X k}}\left[\frac{\tilde{b}}{2}\left(\frac{\tilde{b}m_X}{H_e}\right)^{-\frac{2}{3(w+1)}} \frac{a_e}{a(\tau_\star)} \pm i\right] \exp\Big[-ik\Big(\frac{3}{2}\tau_e(1+\bar{w}) - \frac{\tilde{b}m_X}{kH_e}\Big)\Big]. \tag{6.119}$$

We see that longitudinal modes in green region II oscillate in time with decreasing amplitude. The comparison between analytical and numerical solutions (left panel of Fig. 6.3) indicates good agreement between these two results.

Intermediate-wavelength modes:

Intermediate-wavelength modes, i.e., $k_m < k < k_\star$, (e.g., the k_2^{-1} mode in the left panel of Fig. 6.1) pass through three regions, i.e., purple III, blue IV, and green V during reheating. Since in the purple region $a^2m_X^2/k^2 \ll 1$, the second term in the parenthesis in Eq. (6.112b) is small and thus can be neglected in analytical estimations. Hence, the solution to the mode equation in this region is given by

$$\mathcal{X}_L^{(\mathrm{III})}(a) = C_1^{(\mathrm{III})}a + C_2^{(\mathrm{III})}a^{-\frac{(1-3\bar{w})}{2}} \simeq C_1^{(\mathrm{III})}a.$$

Note that the first term proportional to a grows with time, whereas the second one is decaying since $\bar{w} > -1/3$ after the end of inflation. Moreover, as long as $\bar{w} < 1$, it is small compared to the growing solution, and hence, it can be neglected in analytical estimations. We fix $C_1^{(\mathrm{III})}$ by requiring

$$\mathcal{X}_L^{(\mathrm{III})}(\tau_e) = \mathcal{X}_L^{(a)}(\tau_e), \qquad \mathcal{X}_L^{(\mathrm{III})\prime}(\tau_e) = \mathcal{X}_L^{(a)\prime}(\tau_e), \tag{6.120}$$

which leads to the following solution:

$$\mathcal{X}_L^{\mathrm{III}}(a) = \frac{iH_e}{\sqrt{2}k^{3/2}}\, e^{-ik\tau_e}\ a. \tag{6.121}$$

The above solution indicates that longitudinal modes grow linearly with the scale factor a in the purple region, whereas their amplitude $|\mathcal{X}_L^{\mathrm{III}}|^2$ is proportional to k^{-3}.

Next, at $\tilde{\tau}_2 = \tau_e(\tilde{b}\, a_e m_X/k)^{-(1+3\bar{w})/2}$ such that $k = \tilde{b}a(\tilde{\tau}_2)m_X$ with $\tilde{b} \simeq \mathcal{O}(1)$ longitudinal modes enter the blue region IV, where the solution of the mode equation is in the form (6.113). Coefficients, parametrizing this solution, can be obtained by merging (6.113) with (6.121) at $\tilde{\tau}_2$. Contrary to the constant solution for long-wavelength modes, $\mathcal{X}_L^{-}(\tau_e)$ grows with time. Therefore, one could naively expect that the growing term in (6.113), proportional to $a^{(1+3\bar{w})/2}$, might dominate the solution in the blue region, following (6.121). However, the exact numerical solution presented in the upper-middle panel of Fig. 6.3 indicates that even in this case, the growing part of the solution (6.113) is subdominant, such that the amplitude of intermediate-wavelength modes in the blue region IV remains constant

$$\mathcal{X}_L^{(\mathrm{IV})} = C_1^{(\mathrm{IV})} = \frac{iH_e}{\sqrt{2}k^{1/2}}\,\frac{e^{-ik\tau_e}}{m_X}\,. \tag{6.122}$$

Let us also note that the amplitude in this region scales as $|\mathcal{X}_L^{(\mathrm{IV})}|^2 \propto k^{-1}$.

Finally, intermediate-wavelength modes at $\tau_\star$ enter the green region V, where the approximate solution takes the form (6.117). The constants of solutions $C_1^{(\mathrm{V})}, C_2^{(\mathrm{V})}$ are determined by matching Eq. (6.117) with Eq. (6.122) at $\tau_\star$. We find that the solution to the mode equation in the green region V is in the form given by (6.117) with $C_1^{(\mathrm{II})}, C_2^{(\mathrm{II})}$ replaced by

$$C_{1,2}^{(\mathrm{V})} = \frac{C_1^{(\mathrm{III})}}{\sqrt{2}}\sqrt{m_X a(\tau_\star)}\left[1 \mp i\frac{a_e}{a(\tau_\star)}\frac{H_e}{2m_X}\left(\frac{\tilde{b}m_X}{H_e}\right)^{\frac{3\bar{w}+1}{3(\bar{w}+1)}}\right]. \tag{6.123}$$

Short-wavelength modes:

After inflation, both intermediate- and short-wavelength, i.e., $k_\star < k < k_\mathrm{e}$, modes are in the purple region, where their amplitude grows in time according to Eq. (6.121). At $\tilde{\tau}_1$, the latter crosses the Hubble horizon and re-enters the red sub-horizon region, where k is the dominant energy scale. It is convenient to consider the purple and red areas collectively to analyze the dynamics of short-wavelength modes. In this case, one can neglect the mass term $a^2 m_X^2$ in the dispersion relation, obtaining

$$\mathcal{X}_L^{\prime\prime(\mathrm{VI})} + \left(k^2 - \frac{1-3\bar{w}}{2}a^2H^2\right)\mathcal{X}_L^{(\mathrm{VI})} = 0. \tag{6.124}$$

The solution to the above equation is in the form

$$\mathcal{X}_L^{(\mathrm{VI})}(a) = \sqrt{\frac{2}{(1+3\bar{w})aH(a)}}\left[C_1^{(\mathrm{VI})}J_\nu\Big(\frac{2k}{(1+3\bar{w})aH(a)}\Big) + C_2^{(\mathrm{VI})}Y_\nu\Big(\frac{2k}{(1+3\bar{w})aH(a)}\Big)\right], \tag{6.125}$$

with $\nu \equiv \frac{-3(1-\bar{w})}{2(1+3\bar{w})}$.

Merging the above solution with the inflationary solution $\mathcal{X}_L^{(a)}(\tau_e)$ at the end of inflation, one finds

$$C_1^{(\mathrm{VI})} = \frac{i\pi\exp\Big(\frac{-2ik}{(1+3\bar{w})k_e}\Big)}{2\sqrt{2(1+3\bar{w})k/k_e}}\left[Y_{\nu-1}\Big(\frac{2k}{(1+3\bar{w})k_e}\Big) + iY_\nu\Big(\frac{2k}{(1+3\bar{w})k_e}\Big)\right], \tag{6.126}$$

$$C_2^{(\mathrm{VI})} = \frac{-i\pi\exp\Big(\frac{-2ik}{(1+3\bar{w})k_e}\Big)}{2\sqrt{2(1+3\bar{w})k/k_e}}\left[J_{\nu-1}\Big(\frac{2k}{(1+3\bar{w})k_e}\Big) + iJ_\nu\Big(\frac{2k}{(1+3\bar{w})k_e}\Big)\right]. \tag{6.127}$$

Then, at $\tilde{\tau}_3$ short-wavelength modes enter the green region, where their solution is given by Eq. (6.117). After some straightforward but tedious calculation, we find that both constant coefficients parametrizing (6.117) are non-zero, so that the solution oscillates in time, as shown in the right-panel of Fig. 6.3.

Finally, let us notice that for sub-horizon modes, the solution (6.125) can be approximated by the following function:

$$\mathcal{X}_L^{(\mathrm{VI})}(k \gg aH) \approx \frac{3i\Gamma(-\nu)(1-\bar{w})(1+3\bar{w})^{\frac{1-3\bar{w}}{1+3\bar{w}}}}{4\sqrt{\pi k}}\Big(\frac{k}{k_e}\Big)^{-\frac{3(1+\bar{w})}{1+3\bar{w}}}\sin\Big(\frac{2\pi}{1+3\bar{w}}\Big)\sin\Big(\frac{2k+\pi aH(a)}{aH(1+3\bar{w})}\Big), \tag{6.128}$$

6.5.2 Light vector dark matter

The solutions to the mode equation obtained in the previous section can also be applied for light DM vectors with mass $m_X < H_{\mathrm{rh}}$. In particular, light DM species also experience a tachyonic growth in the purple region, where their mode function evolves according to Eq. (6.121). As we have demonstrated above, this growth is eventually terminated at the moment when modes go outside of the region. Modes with wavenumber $1/k \ll 1/k_{\mathrm{rh}} \equiv (a_{\mathrm{rh}}H_{\mathrm{rh}})^{-1}$ re-enter the Hubble horizon during reheating. Such modes follow the evolution of heavy DM vectors with short wavelengths. On the other hand, light modes with wavenumber $1/k_{\mathrm{rh}} \ll 1/k \ll 1/k_\star$ (see right panel of Fig. 6.1) grow in amplitude throughout the whole period of reheating and enter the red subhorizon region only during the RD epoch. Finally, light modes, characterized by wavenumber $1/k \gg 1/k_m^{rh} \equiv (a_{\mathrm{rh}}m_X)^{-1}$, follow the evolution of heavy DM vectors with long-wavelength.

6.5.3 Numerical results

Figure (6.3) presents the post-inflationary evolution of the *long-* (e.g. k_1), *intermediate-* (e.g. k_2) and *short-wavelength* (e.g. k_3) modes. Numerical results (solid cyan curves) are in accord with analytical approximations. The dashed navy constant solution in the left panel was found in Eq.(6.114), whereas Eq.(6.117) gives the oscillating dashed green function. In the middle panel, dashed purple, navy, and green solutions are described respectively by the functions Eqs.(6.121), (6.122) and (6.117) with $C_{1,2}^{\mathrm{II}} \to C_{1,2}^{\mathrm{V}}$ given by (6.123). Finally, the analytical formula for the dashed purple and red curves was found in Eqs.(6.125).

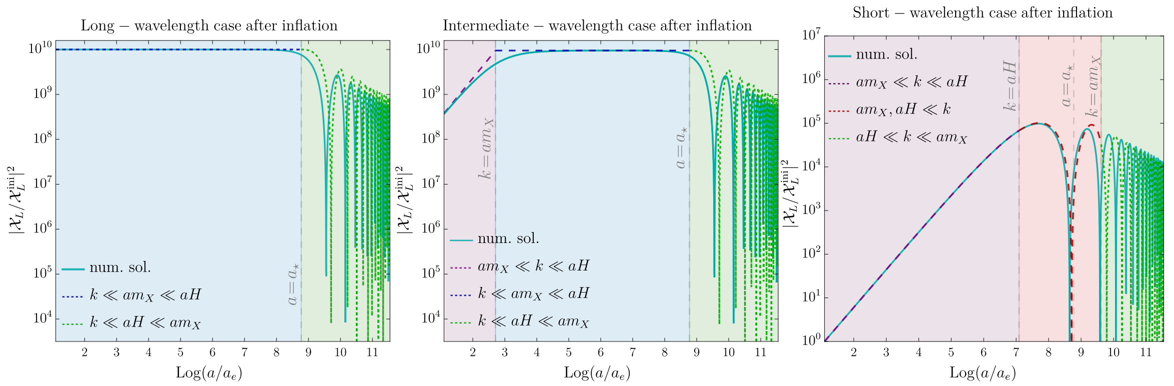

FIGURE 6.3: The post-inflationary evolution of the longitudinal modes normalized to the initial value as a function of the scale factor for *long-* $k < k_m$ (left-panel), *intermediate* $k_m < k < k_\star$ (middle panel), and *short-wavelength modes* $k_\star < k < k_e$ (right-panel). The solid cyan curves correspond to the exact numerical solution, while dashed colored curves show analytical predictions. The following benchmark values are adopted in these figures: $m_X = 10^8$ GeV, $H_e = 10^{13}$ GeV, $\bar{w} = 0$ with $k = 10^{-8}\,\text{GeV}, 10^{-4}\,\text{GeV}, 10^{-1}\,\text{GeV}$ for the left, center, and right panel, respectively.

6.5.4 Energy density scaling

Before ending this section, let us utilize the results obtained above to determine the scaling of the energy density with k and a in each considered region. With this end in view, we employ approximate solutions for the mode function $\mathcal{X}_L$ to identify the dominant contribution to $\langle \hat{\rho}_L \rangle$.

In the red (R) subhorizon region, where k is the dominant energy scale, one can insert the solution (6.128) into Eq. (6.86), obtaining

$$\frac{d\langle \hat{\rho}_L^{(\rm R)} \rangle}{d\ln k} \approx \frac{9\Gamma^2(-\nu)(1-\bar{w})^2(1+3\bar{w})^{\frac{2(1-3\bar{w})}{1+3\bar{w}}}}{32\pi^3} \frac{k^4}{a^4} \left(\frac{k}{k_e}\right)^{-\frac{3(1+\bar{w})}{1+3\bar{w}}} \propto k^{-\frac{2(1-3\bar{w})}{1+3\bar{w}}} a^{-4} \,. \tag{6.129}$$

In the purple (P) region, where $am_X \ll k \ll aH$, the solution to the mode equation can be approximated by Eq. (6.121), which, in turn, implies the following scaling:

$$\frac{d\langle \rho_L^{(\rm P)} \rangle}{d\ln k} \approx \frac{k^5}{4\pi^2 a^2} |C_1^{(\rm III)}|^2 \propto k^2 a^{-2} \,. \tag{6.130}$$

Note that one obtains the same scaling using (6.125) in the limit $k \ll aH$.
Next, in the blue (B) region, using Eq. (6.113) with $C_2^{(\rm I)} \approx 0$, one finds

$$\frac{d\langle \hat{\rho}_L^{(\rm B)} \rangle}{d\ln k} \approx \frac{k^3}{4\pi^2 a^4} \left(\frac{k^4}{a^4 m_X^4} a^2 H^2 + k^2 + a^2 m_X^2 \right) |C_1^{(\rm I)}|^2 \propto k^2 a^{-2} \,. \tag{6.131}$$

It is important to stress that the above relation, which reveals that $\langle \hat{\rho}_L \rangle$ scales as a^{-2} in the region where $k \ll am_X \ll aH$, can be considered a distinct characteristic of vector dark matter, see also [169, 435]. In particular, this fact distinguishes DM vectors from massive scalars whose energy density is nearly constant (w.r.t. to a) in the blue region. The scaling $\langle \hat{\rho}_L \rangle \propto a^0$, observed for massive spin-0 field, leads to an amplification of isocurvature perturbations at large scales, which is currently strongly constrained by the CMB data [302]. Hence, damping the DM vector energy density $\propto a^{-2}$ is a desirable feature, suppressing unwanted isocurvature perturbations at large scales.

Finally, in the green region, where am_X is the dominant energy scale, we find that the

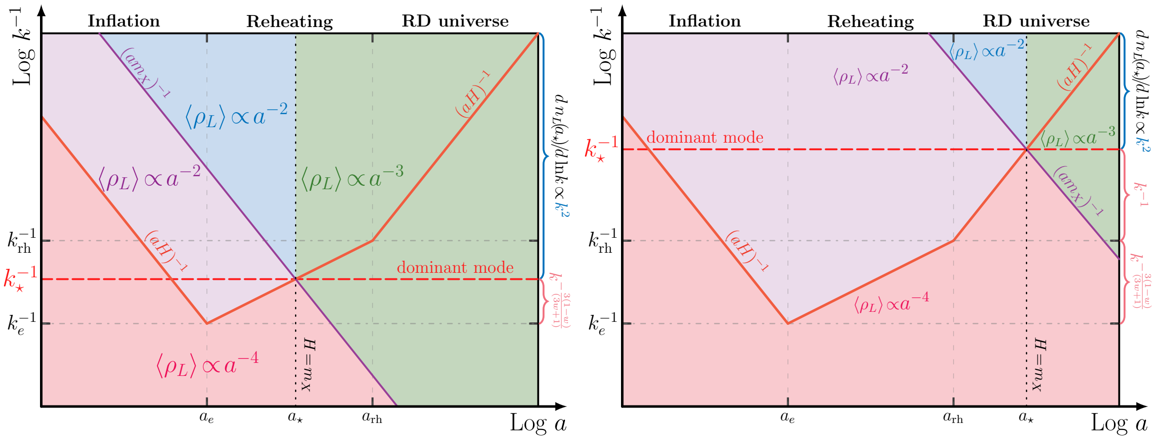

FIGURE 6.4: The scaling of the fractional energy density with a in various regions for heavy vector DM, i.e., $m_X > H_{\rm rh}$ (left diagram) and light vector DM $m_X < H_{\rm rh}$ (right diagram). The main contribution to the total energy density comes from the $k_\star \equiv a_\star m_X$ mode. Here $k_e \equiv a_e H_e$ and $k_{\rm rh} \equiv a_{\rm rh} H_{\rm rh}$.

energy density of DM vectors scales as matter, i.e.,

$$\frac{d\langle\hat{\rho}_L^{(\rm G)}\rangle}{d\ln k} \approx \frac{a m_X\, k^3}{4\pi^2 a^4}\left(|C_1^{(\rm II)}|^2 + |C_2^{(\rm II)}|^2\right) \propto k^2 a^{-3}\,,$$

where the oscillatory terms proportional to $\exp\left[\pm i\int d\tau a(\tau) m_X\right]$ have been neglected.

The above results can be summarized as

$$\frac{d\langle\hat{\rho}_L\rangle}{d\ln k} \propto \begin{cases} k^{-\frac{2(1-3\bar{w})}{1+3\bar{w}}}\, a^{-4}, & a(\tau)m_X, a(\tau)H(\tau) \ll k, \\ k^2 a^{-2}, & a(\tau)m_X, k \ll a(\tau)H(\tau), \\ k^2 a^{-3}, & a(\tau)H(\tau), k \ll a(\tau)m_X\,. \end{cases} \tag{6.132}$$

Let us recall that at the very end of inflation, the main contribution to the total energy density comes from modes with the shortest wavelength ($1/k \sim 1/k_e$). However, as evident from the expression mentioned above, such modes receive the strongest suppression proportional to a^{-4} in the subhorizon region. On the other hand, longitudinal modes with longer wavelengths initially have a smaller contribution to the total energy density, but their energy is also redshifted to a lesser extent.

6.6 Purely gravitational production - results

This section aims to evaluate the present number or energy density of DM vectors produced via the GP mechanism. Following the approach developed in the previous part of this chapter, we restrict our attention to super-horizon modes, i.e., with wavenumber $1/k \gg 1/k_e$, which exit the Hubble horizon during inflation.

The expectation value of the fractional number density of DM vectors can be expressed as

$$\frac{d\,\langle\hat{n}_L\rangle}{d\ln k} = \frac{1}{E_L}\frac{d\,\langle\hat{\rho}_L\rangle}{d\ln k}, \tag{6.133}$$

with $E_L \equiv \sqrt{m_X^2 + (k/a)^2}$ being the energy of a single DM particle.
The present energy or number density of DM species can be related to their energy or number

density at $a_\star$ when the $1/k_\star$ modes re-enter the Hubble horizon, and the Hubble rate equalizes with the DM mass, i.e., $H(a_\star) = m_X$. Using the above formula, one finds

$$\frac{d\langle \hat{n}_L(a_\star)\rangle}{d\ln k} = \frac{1}{\sqrt{m_X^2 + k^2/a_\star^2}} \frac{d\langle \hat{\rho}_L(a_\star)\rangle}{d\ln k}. \tag{6.134}$$

In Fig. 6.4, we present the scaling of $d\langle\hat{\rho}_L(a_\star)\rangle/d\ln k$ with momentum k for heavy (left panel) and light (right panel) DM vectors. In both mass regimes, the dominant contribution to the total energy density comes from modes with wavenumber $1/k_\star$ (dashed, red curve). After exiting the Hubble horizon during inflation, such modes become subhorizon and experience a tachyonic growth in the purple region, where their energy density decreases as a^{-2}. Then, at $a = a_\star$, the $k_\star$ modes re-enter the horizon, and their energy density starts to redshift as a matter, i.e., $\langle\hat{\rho}_L\rangle \propto a^{-3}$. Modes with longer wavelengths, $1/k \gg 1/k_\star$, contribute less to the total energy (or number) density, since in the blue and purple regions $d\langle\hat{\rho}_L(a_\star)\rangle/d\ln k \propto k^2$, see Eq. (6.132). As we will demonstrate later, such behavior of long-wavelength modes prevents a generation of 'dangerous' isocurvature perturbations at the CMB scales. Finally, short-wavelength modes of heavy vectors re-enter the horizon before the $k_\star$ modes and receive a strong suppression in the red region. Namely, in the subhorizon regime, the energy density of dark vectors decreases as radiation, i.e., $\langle\hat{\rho}_L\rangle \propto a^{-4}$. For heavy DM species, modes with wavenumber $1/k < 1/k_\star$ re-enter the horizon during reheating when the Hubble rate scales as $a^{-3(1+\bar{w})/2}$, which, as we will see, implies that their number density is proportional to $k^{-\frac{3(1-\bar{w})}{(3\bar{w}+1)}}$. Consequently, if $\bar{w}<1$, the fractional number density per $\ln k$ at $a_\star$ for heavy DM species has a peak structure centered around the characteristic momentum scale $k_\star$. This unique feature of massive spin-1 field produced gravitationally has been first established in [169] for instantaneous reheating, i.e., an immediate transition from inflationary to radiation-dominated Universe. Here, we extend this observation for non-instantaneous and non-standard reheating, parametrized by a generic equation of state $\bar{w} < 1$. On the other hand, in the case of light DM vectors, modes with wavenumber $1/k_{\rm rh} < 1/k < 1/k_\star$ re-enter the Hubble horizon during reheating so that their fractional number density at $a_\star$, i.e., $d\langle\hat{n}_L(a_\star)\rangle/d\ln k$, scales as k^{-1}. However, light modes with wavenumber $1/k_e < 1/k < 1/k_{\rm rh}$ re-enter the horizon after reheating during the RD epoch, and as we will show below $d\langle\hat{n}_L(a_\star)\rangle/d\ln k \propto k^{-\frac{3(1-\bar{w})}{(3\bar{w}+1)}}$. Hence, provided that $\bar{w} < 1$, the number density per logarithmic momentum for both heavy and light DM vectors also has a peak structure. In what follows, we will present a detailed numerical analysis of this qualitative discussion.

6.6.1 Number density of the heavy DM vectors

For heavy vectors, i.e., with mass in the range $H_{\rm rh} \leq m_X < H_e$, there are two important regimes:

(a) $k_\star < k < k_e$,

(b) $k < k_\star$.

The expectation value of the fractional number density for short-wavelength heavy modes at $a_\star$ can be estimated as

$$\left.\frac{d\langle\hat{n}_L(a_\star)\rangle}{d\ln k}\right|_{k_\star<k<k_e} \approx \frac{a_\star}{k}\frac{d\langle\hat{\rho}_L(a_\star)}{d\ln k} = \frac{a_\star}{k}\frac{d\langle\hat{\rho}_L(a_e)\rangle}{d\ln k}\left(\frac{a_e}{a_{\rm hc}}\right)^2\left(\frac{a_{\rm hc}}{a_\star}\right)^4, \tag{6.135}$$

where we have used the fact that at $a_\star$, $m_X^2 \ll (k/a_\star)^2$, such that $E_L \simeq k/a_\star$. Moreover, $a_{\rm hc}$ denotes the scale factor corresponding to the second (after inflation) horizon crossing, i.e.,

$a_{\rm hc} = h/H(a_{\rm hc})$. Since short-wavelength modes re-enter the Hubble horizon during reheating, using Eq.(6.7) (middle case), one finds

$$a_{\rm hc}\big|_{k_\star<k<k_e} = a_e \left(\frac{H_e\, a_{\rm hc}}{k}\right)^{\frac{2}{3(1+\bar{w})}},$$

which, in turn, implies

$$a_{\rm hc}\big|_{k_\star<k<k_e} = a_e^{\frac{3(1+\bar{w})}{1+3\bar{w}}} \left(\frac{H_e}{k}\right)^{\frac{2}{1+3\bar{w}}}. \tag{6.136}$$

Inserting, the above formula into (6.135), we obtain

$$\frac{d\langle\hat{n}_L(a_\star)\rangle}{d\ln k}\bigg|_{k_\star<k<k_e} \approx \frac{H_e^3}{8\pi^2}\left(\frac{m_X}{H_e}\right)^{\frac{2}{1+\bar{w}}}\left(\frac{k_e}{k}\right)^{\frac{3(1-\bar{w})}{1+3\bar{w}}} \tag{6.137}$$

For long-wavelength modes, one finds

$$\frac{d\langle\hat{n}_L(a_\star)\rangle}{d\ln k}\bigg|_{k<k_\star} \approx \frac{1}{m_X}\frac{d\langle\hat{\rho}_L(a_\star)}{d\ln k} = \frac{1}{m_X}\frac{d\langle\hat{\rho}_L(a_e)\rangle}{d\ln k}\left(\frac{a_e}{a_\star}\right)^2 = \frac{H_e^3}{8\pi^2}\left(\frac{m_X}{H_e}\right)^{\frac{1-3\bar{w}}{3(1+\bar{w})}}\left(\frac{k}{k_e}\right)^2 \tag{6.138}$$

where we have used the fact that the crossing of the Hubble horizon with the Compton wavelength ($H(a_\star){=}m_X$) for heavy vectors occurs during the reheating phase, such that

$$a_\star = a_e\left(\frac{H_e}{m_X}\right)^{\frac{2}{3(1+\bar{w})}}. \tag{6.139}$$

6.6.2 Number density of the light DM vectors

For light DM vectors, $m_X < H_{\rm rh}$, one should consider the following three cases:

(a) $k_{\rm rh} < k < k_e$,

(b) $k_\star < k < k_{\rm rh}$,

(c) $k < k_\star$.

The expectation value of DM vector number density in the case (a) is given by

$$\frac{d\langle\hat{n}_L(a_\star)\rangle}{d\ln k}\bigg|_{k_{\rm rh}<k<k_e} \approx \frac{a_\star}{k}\frac{\langle\hat{\rho}_L(a_\star)\rangle}{d\ln k} = \frac{a_\star}{k}\frac{\langle\hat{\rho}_L(a_e)\rangle}{d\ln k}\left(\frac{a_e}{a_{\rm hc}}\right)^2\left(\frac{a_{\rm hc}}{a_{\rm rh}}\right)^4\left(\frac{a_{\rm rh}}{a_\star}\right)^4. \tag{6.140}$$

Short-wavelength light modes re-enter the horizon during reheating so that $a_{\rm hc}$ is given by Eq.(6.136), which, in turn, implies

$$\frac{d\langle\hat{n}_L(a_\star)\rangle}{d\ln k}\bigg|_{k_{\rm rh}<k<k_e} \approx \frac{H_e^3}{8\pi^2}\left(\frac{m_X}{H_e}\right)^{3/2}\gamma^{\frac{1-3\bar{w}}{1+\bar{w}}}\left(\frac{k_e}{k}\right)^{\frac{3(1-\bar{w})}{1+3\bar{w}}}. \tag{6.141}$$

Evolving the number density of intermediate-wavelength light modes, one finds

$$\frac{d\langle\hat{n}_L(a_\star)\rangle}{d\ln k}\bigg|_{k_\star<k<k_{\rm rh}} \approx \frac{a_\star}{k}\frac{d\langle\hat{\rho}_L(a_\star)\rangle}{d\ln k} = \frac{a_\star}{k}\frac{d\langle\hat{\rho}_L(a_e)\rangle}{d\ln k}\left(\frac{a_e}{a_{\rm rh}}\right)^2\left(\frac{a_{\rm rh}}{a_{\rm hc}}\right)^2\left(\frac{a_c}{a_\star}\right)^4. \tag{6.142}$$

Such modes re-enter the horizon during the RD epoch. Hence, utilizing Eq.(6.7) (the third line), one obtains

$$a_{\rm hc}\big|_{k_\star<k<k_{\rm rh}} = a_e \left(\frac{H_e}{H_{\rm rh}}\right)^{\frac{2}{3(1+w)}} \left(\frac{H_{\rm rh}a_{\rm hc}}{k}\right)^{1/2}, \tag{6.143}$$

which can also be expressed in terms of the reheating efficiency γ as

$$a_{\rm hc}\big|_{k_\star<k<k_{\rm rh}} = a_e^2 \gamma^{-\frac{2(1-3\bar{w})}{3(1+\bar{w})}} \frac{H_e}{k}. \tag{6.144}$$

Hence,

$$\frac{d\langle \hat{n}_L(a_\star)\rangle}{d\ln k}\bigg|_{k_\star<k<k_{\rm rh}} \approx \frac{H_e^3}{8\pi^2}\left(\frac{m_X}{H_e}\right)^{3/2} \gamma^{\frac{-1+3\bar{w}}{3(1+\bar{w})}} \frac{k_e}{k}. \tag{6.145}$$

Finally, for the longitudinal modes (c) with $k<k_\star$, we have

$$\begin{aligned}\frac{d\langle \hat{n}_L(a_\star)\rangle}{d\ln k}\bigg|_{k<k_\star} &\approx \frac{1}{m_X}\frac{\langle\hat{\rho}_L(a_\star)\rangle}{d\ln k} = \frac{1}{m_X}\frac{\langle\hat{\rho}_L(a_e)\rangle}{d\ln k}\left(\frac{a_e}{a_{\rm rh}}\right)^2\left(\frac{a_{\rm rh}}{a_\star}\right)^2, \\ &= \frac{H_e^3}{8\pi^2}\gamma^{\frac{2(1-3\bar{w})}{3(1+\bar{w})}}\left(\frac{k}{k_e}\right)^2,\end{aligned} \tag{6.146}$$

where we have used the fact that long-wavelength modes re-enter the horizon at

$$a_\star = a_e \gamma^{\frac{3w-1}{3(1+w)}}\left(\frac{H_{\rm I}}{m_X}\right)^{1/2}. \tag{6.147}$$

Our findings regarding the expectation value of the fractional number density for longitudinal modes in both mass regimes can be summarized as follows:

- For heavy vector DM mass $H_{\rm rh}\leq m_X<H_{\rm I}$,

$$\frac{d\langle \hat{n}_L(a_\star)\rangle}{d\ln k} = \frac{H_e^3}{8\pi^2}\begin{cases}\left(\frac{m_X}{H_e}\right)^{\frac{2}{1+\bar{w}}}\left(\frac{k_e}{k}\right)^{\frac{3(1-\bar{w})}{1+3\bar{w}}}, & k_\star<k<k_e, \quad (6.148a)\\ \left(\frac{m_X}{H_e}\right)^{\frac{1-3\bar{w}}{3(1+\bar{w})}}\left(\frac{k}{k_e}\right)^2, & k<k_\star. \quad (6.148b)\end{cases}$$

- For light vector DM mass $m_X<H_{\rm rh}$,

$$\frac{d\langle \hat{n}_L(a_\star)\rangle}{d\ln k} = \frac{H_e^3}{8\pi^2}\begin{cases}\left(\frac{m_X}{H_e}\right)^{3/2}\gamma^{\frac{1-3\bar{w}}{1+\bar{w}}}\left(\frac{k_e}{k}\right)^{\frac{3(1-\bar{w})}{1+3\bar{w}}}, & k_{\rm rh}<k<k_e, \quad (6.149a)\\ \left(\frac{m_X}{H_e}\right)^{3/2}\gamma^{\frac{-1+3\bar{w}}{3(1+\bar{w})}}\frac{k_e}{k}, & k_\star<k<k_{\rm rh}, \quad (6.149b)\\ \gamma^{\frac{2(1-3\bar{w})}{3(1+\bar{w})}}\left(\frac{k}{k_e}\right)^2, & k<k_\star. \quad (6.149c)\end{cases}$$

In Fig. 6.5, we present the expectation value of the fractional number density as a function of $k/k_\star$ at $a_\star$ for heavy (left panel) and light (right panel) DM vectors. Numerical results confirm the peak structure of the power spectrum, such that $d\langle\hat{n}_L(a_\star)\rangle/d\ln k$ is dominated by modes with a wavenumber of the order of $1/k_\star$. Moreover, in Fig. 6.6, we compare the exact numerical results (solid curves) with analytical approximations Eqs.(6.149a)-(6.149c) (dashed curves) for two values of the equation of state parameter $\bar{w}=\{0,1/3\}$.

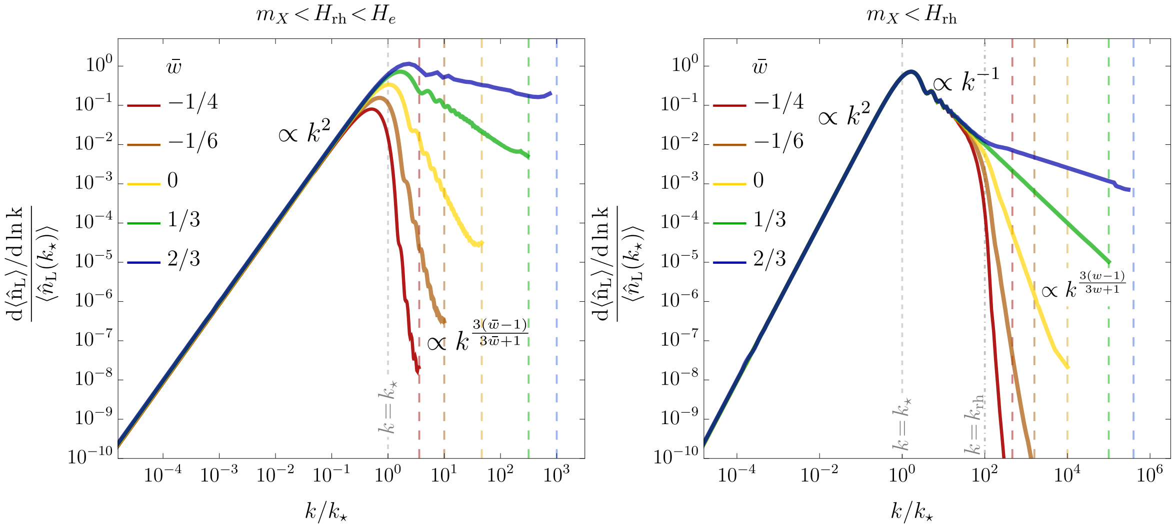

FIGURE 6.5: The expectation value of the number density per $\ln k$ normalized to its value for the $k_\star$ mode as a function of $k/k_\star$. The left (right) panel presents the spectrum for heavy $H_{\rm rh} \leq m_X < H_{\rm I}$ (light $m_X < H_{\rm rh}$) DM vectors. Dashed (Dotted) grey vertical lines indicate $k = k_\star (k_{\rm rh})$, while dashed colored lines show $k = k_e$ for corresponding value of $\bar{w}$. Both spectra are calculated at $a = a_\star$. Here we take: $H_e = 10^{13}$ GeV, $\gamma = 10^{-3}$, $m_X = 10^8$ GeV (left panel), $m_X = 10^3$ GeV (right panel).

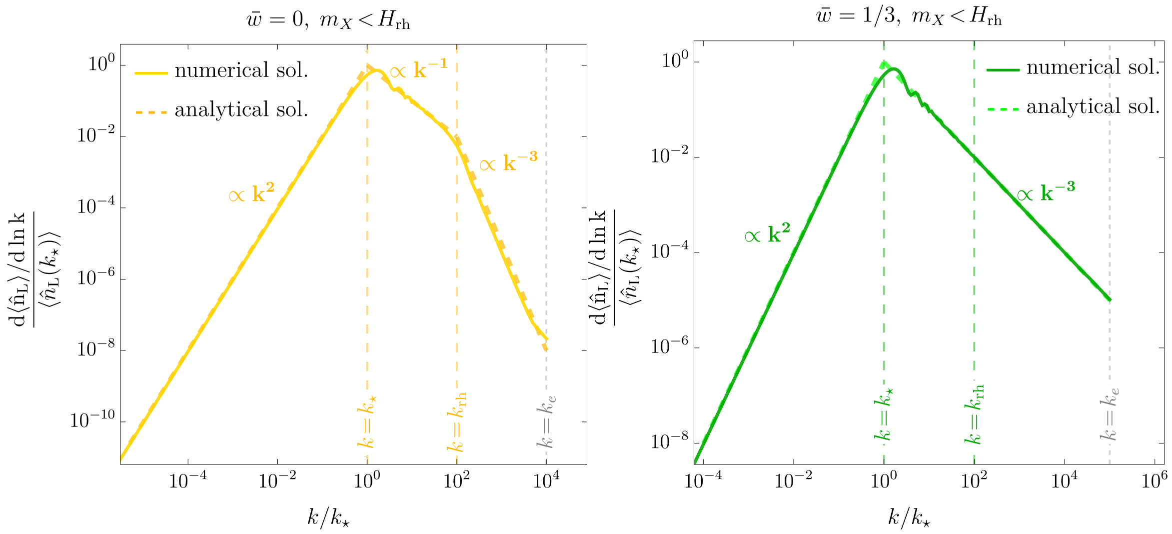

FIGURE 6.6: Comparison between numerical results (solid curves) and analytical predictions (dashed curves) for the fractional number density at $a = a_\star$. The same parameters as in Fig. 6.5 have been adopted.

It is worth noting that similar behavior was observed in the previous study Ref. [169] focusing on the instantaneous reheating scenario, as well as in Ref. [435] for a non-instantaneous matter-dominated reheating with $\bar{w} = 0$.

Finally, let us determine the total number density of DM species at $a_\star$. For heavy vectors, one finds

$$\langle \hat{n}_L^{\rm hDM}(a_\star)\rangle = \frac{H_e^3}{8\pi^2}\left[\left(\frac{m_X}{H_e}\right)^{\frac{1-3\bar{w}}{3(1+\bar{w})}} k_e^{-2}\int_0^{k_\star} k dk + \left(\frac{m_X}{H_e}\right)^{\frac{2}{1+\bar{w}}} k_e^{\frac{3(1-\bar{w})}{(1+3\bar{w})}} \int_{k_\star}^{k_e} k^{\frac{-4}{1+3\bar{w}}} dk\right]$$

$$
\begin{aligned}
&= \frac{H_e^3}{8\pi^2}\left[\frac{1}{2}\frac{m_X}{H_e} + \frac{1+3\bar{w}}{3(\bar{w}-1)}\left(\frac{m_X}{H_e}\right)^{\frac{2}{1+\bar{w}}}\left(1-\left(\frac{m_X}{H_e}\right)^{\frac{\bar{w}-1}{1+\bar{w}}}\right)\right] \\
&\approx \frac{m_X H_e^2}{8\pi^2}\left[\frac{1}{2} + \frac{1+3\bar{w}}{3(1-\bar{w})}\right], \qquad (6.150)
\end{aligned}
$$

where in the last line, we have used the fact for $\bar{w} \in (-1/3, 1)$, the ratio $\left(\frac{H_e}{m_X}\right)^{\frac{1-\bar{w}}{1+\bar{w}}} \gg 1$. Furthermore, it should also be stressed that above a cut-off limit $k_{\max} = k_e$ has been adopted so that only super-horizon modes that exit the horizon during inflation and re-enter it during reheating contribute to the total number density. Note that subhorizon modes, i.e., $k > k_e$, never exit the Hubble horizon; thus, they do not receive any tachyonic enhancement. Therefore, the contribution from such modes is significantly suppressed.
The total number density of light DM species is, in turn, given by

$$
\begin{aligned}
\langle \hat{n}_L^{\mathrm{lDM}}(a_\star)\rangle &= \frac{H_e^3}{8\pi^2}\Bigg[\gamma^{\frac{2(1-3\bar{w})}{3(1+\bar{w})}} k_e^{-2}\int_0^{k_\star} k\,dk + \left(\frac{m_X}{H_e}\right)^{3/2}\gamma^{\frac{-1+3\bar{w}}{3(1+\bar{w})}} k_e \int_{k_\star}^{k_{\mathrm{rh}}} k^{-2}dk \\
&\quad + \left(\frac{m_X}{H_e}\right)^{3/2}\gamma^{\frac{1-3\bar{w}}{1+\bar{w}}} k_e^{\frac{3(1-\bar{w})}{1+3\bar{w}}}\int_{k_{\mathrm{rh}}}^{k_e} k^{\frac{-4}{1+3\bar{w}}}dk\Bigg] \\
&= \frac{H_e^3}{8\pi^2}\Bigg[\frac{1}{2}\frac{m_X}{H_e} - \left(\frac{m_X}{H_e}\right)^{3/2}\gamma^{-1}\left(1-\gamma\left(\frac{H_e}{m_X}\right)^{1/2}\right) \\
&\quad - \frac{1+3\bar{w}}{3(1-\bar{w})}\left(\frac{m_X}{H_e}\right)^{3/2}\gamma^{\frac{1-3\bar{w}}{1+\bar{w}}}\left(1-\gamma^{\frac{2(\bar{w}-1)}{1+\bar{w}}}\right)\Bigg] \\
&\approx \frac{m_X H_e^2}{8\pi^2}\left[\frac{3}{2} + \frac{1+3\bar{w}}{3(1-\bar{w})}\sqrt{\frac{m_X}{H_{\mathrm{rh}}}}\right], \qquad (6.151)
\end{aligned}
$$

where we have assumed that $\bar{w} \in (-1/3, 1)$, which implies $\gamma^{\frac{2(\bar{w}-1)}{1+\bar{w}}} \gg 1$.

6.6.3 Isocurvature density perturbations

Before we present the final result regarding the gravitationally-produced vector DM, let us comment on the isocurvature density perturbations.

As we have explicitly demonstrated above, the number (and energy) density of both heavy ($H_{\mathrm{rh}} < m_X < H_e$) and light ($m_X < H_{\mathrm{rh}}$) dark vectors is dominated by the contribution from longitudinal modes with characteristic comoving momentum,

$$
k_\star = a_{\mathrm{r.m.e}}\sqrt{m_X H_{\mathrm{r.m.e}}}\begin{cases}\left(\dfrac{H_{\mathrm{rh}}}{m_X}\right)^{\frac{1-3\bar{w}}{6(1+\bar{w})}}, & H_{\mathrm{rh}} \le m_X < H_e\,, \\ 1\,, & H_{\mathrm{r.m.e}} \le m_X < H_{\mathrm{rh}}\,. \end{cases} \qquad (6.152)
$$

It also has been established that the fractional number density of long-wavelength modes, $1/k_\star < 1/k$, drops as k^2., cf. Eqs.(6.148b) and (6.149c). We should emphasize that this result is independent of the details of reheating and remains robust in non-standard and instantaneous reheating models. Now, let us discuss the effect of the observed infrared behavior on the isocurvature perturbations.

First of all, we should stress that due to the fact that our DM candidate couples to the SM species only through gravity, the corresponding density fluctuations are of the isocurvature type [169]. Hence, density perturbations induced by DM vectors with wavelengths of the order of the pivot CMB scale, i.e., $k \sim k_\star^{\rm CMB} \approx 0.05\,{\rm Mpc}^{-1}$ may induce large isocurvature perturbations. The latter is, in turn, highly constrained by the Planck data [13]. This limit concerns only modes with a wavelength of cosmological size. As first demonstrated in Ref. [169], the power spectrum of longitudinal vector DM density fluctuations drops as k^3 for the long-wavelength modes with $k < k_\star$. Such a result was derived for the instantaneous reheating model. However, this outcome is also valid in the considered case since the presence of a prolonged non-standard reheating phase only affects the scaling behavior of the short-wavelengths modes $k > k_\star$ (in both mass regimes). Therefore, owing to the k^3 suppression, DM vectors would not produce problematic isocurvature perturbations, provided that the $k_\star$ scale corresponds to cosmological scales much smaller than the CMB pivot scale $k \sim k_\star^{\rm CMB}$. Utilizing (6.152), one finds

$$k_\star \approx 1400\,{\rm pc}^{-1}\sqrt{\frac{m_X}{10^{-14}\ {\rm GeV}}}\begin{cases}\left(\dfrac{H_{\rm rh}}{m_X}\right)^{\frac{1-3\bar{w}}{6(1+\bar{w})}}\,, & H_{\rm rh} \leq m_X < H_e\,,\\ 1\,, & H_{\rm r.m.e} \leq m_X < H_{\rm rh}\,.\end{cases} \tag{6.153}$$

If $m_X \geq 10^{-14}$ GeV, the characteristic wavenumber $1/k_\star$ for light DM vectors is tiny relative to the CMB pivot scale. As a result, these species are unaffected by isocurvature constraints and can be considered viable dark matter candidates.
Contrarily, the $k_\star$ scale for heavy dark vectors non-trivially depends as a power-law on the $H_{\rm rh}/m_X$ ratio, which can be recast as

$$\left(\frac{H_{\rm rh}}{m_X}\right)^{\frac{1-3\bar{w}}{6(1+\bar{w})}} = \begin{cases}\left(\dfrac{m_X}{H_{\rm rh}}\right)^{[0,\,1/6)} \geq 1\,, & \bar{w} = [1/3,\ 1)\,,\\ \left(\dfrac{H_{\rm rh}}{m_X}\right)^{(1/2,\,0)} < 1\,, & \bar{w} = (-1/3,\ 1/3)\,.\end{cases} \tag{6.154}$$

The above estimations imply that, for a stiff equation of state, i.e., $\bar{w} \geq 1/3$, the characteristic wavelength scale of heavy dark vectors corresponds to tiny cosmological scales. Hence, in this case, gravitationally produced spin-1 particles evade isocurvature constraints. On the other hand, for $\bar{w} = (-1/3, 1/3)$, the $k_\star$ scale of heavy dark vectors might be of the order of the CMB pivot scale, and hence potentially might lead to dangerous isocurvature perturbations. To safely avoid the isocurvature constraints, we establish the following criterion for the reheating scale $H_{\rm rh}$:

$$m_X \geq H_{\rm rh} \geq 10^{-14}\ {\rm GeV}\left(\frac{10^{-14}\ {\rm GeV}}{m_X}\right)^{\frac{2(1+3\bar{w})}{(1-3\bar{w})}}\,, \qquad \text{with} \qquad \bar{w} = (-1/3, 1/3). \tag{6.155}$$

The above result sets the most stringent bound on the reheating scale, i.e., $H_{\rm rh} \geq 10^{-14}$ GeV for $\bar{w} \simeq -1/3$. Consequently, isocurvature perturbations produced by heavy dark vectors are significantly suppressed at cosmological scales provided that $m_X \geq H_{\rm rh} \geq 10^{-14}$ GeV.

Hence, we conclude that isocurvature perturbations do not pose a concern for gravitationally-produced vector DM with masses exceeding 10^{-14} GeV. It is worth emphasizing that our findings are also valid within various reheating scenarios, including those involving non-standard cosmological models.

6.6.4 Present abundance of DM vectors

The present abundance of dark matter is usually expressed in terms of the critical energy density $\rho_{\text{crit},0}$ as follows

$$\Omega_{\text{DM},0}h^2 = \frac{\rho_{\text{DM}}(a_0)}{\rho_{\text{crit},0}}h^2 = \frac{m_{\text{DM}}\, n_{\text{DM}}(a_0)}{\rho_{\text{crit},0}}h^2, \tag{6.156}$$

where $\rho_{\text{crit},0} = 1.88\, h^2 \times 10^{-29}\,\text{g}\,\text{cm}^{-3}$.
Within a given model, the predicted amount of DM species $\Omega_X h^2$ today should saturate the observed value

$$\Omega^{\text{obs}}_{\text{DM}}h^2 = 0.120 \pm 0.001, \qquad (68\%, \textit{Planck}\ \text{TT, TE, EE} + \text{lowE} + \text{lensing}) \tag{6.157}$$

measured by the Planck Collaboration [13]

The present number density $n_X(a_0)$ of DM vectors produced gravitationally is related to their number density at $a_\star$, i.e., $n_\star \equiv \langle \hat{n}_L(a_\star)\rangle$. More precisely, the comoving number density $n_X(a)a^3$ becomes approximately constant after reentering the Hubble horizon of the $k_\star$ modes. Hence, the number density at the present epoch can be determined by rescaling the number density of dark vectors at $a_\star$. Namely,

$$n_X(a_0) = n_\star \left(\frac{a_\star}{a_0}\right)^3 = n_\star \frac{s_0}{s_{\text{rh}}}\left(\frac{a_\star}{a_{\text{rh}}}\right)^3, \tag{6.158}$$

where $s_0 = 2970\ \text{cm}^{-3}$. Note that above, we have assumed that the entropy density s is conserved after the end of reheating.
Since, the scale factor $a_\star$ is defined by the $H(a_\star) = m_X$ equality, the ratio $a_\star/a_{\text{rh}}$ depends on the relation between m_X and H_{rh}. The above condition is satisfied for heavy vectors during the reheating phase, while it is met during the RD epoch for light species. Employing the relation Eq.(6.7), one finds

$$n_X(a_0) = \frac{s_0}{s_{\text{rh}}}\frac{H^2_{\text{rh}}}{m^2_X}\begin{cases} \left(\dfrac{m_X}{H_{\text{rh}}}\right)^{\frac{2\bar{w}}{1+\bar{w}}} \langle \hat{n}^{\text{hDM}}_L(a_\star)\rangle\,, & H_{\text{rh}} \le m_X < H_e, \\ \sqrt{\dfrac{m_X}{H_{\text{rh}}}}\ \langle \hat{n}^{\text{lDM}}_L(a_\star)\rangle\,, & H_{\text{r.m.e}} \le m_X < H_{\text{rh}}, \end{cases} \tag{6.159}$$

The entropy density at the end of reheating is given by

$$s_{\text{rh}} = 4\gamma^3\left(\frac{\pi^2 g_{\star s,\text{rh}}}{90}\right)^{1/4}(M_{\text{Pl}}H_e)^{3/2}. \tag{6.160}$$

In what follows, we adopt $g_{\star,s,\text{rh}} \approx 106.75$, assuming no extra relativistic d.o.f. beyond the SM.
Utilizing Eq.(6.159), one estimates the present-day abundance of gravitationally produced DM vectors as

$$\Omega^{\text{GP}}_X h^2 = \gamma\left(\frac{90}{\pi^2 g_{\star\rho,\text{rh}}}\right)^{1/4}\frac{s_0\, h^2}{4M^2_{\text{Pl}}\,\rho_c}\frac{\sqrt{M_{\text{Pl}}H_e}}{m_X}\begin{cases} \gamma^{-\frac{4\bar{w}}{1+\bar{w}}}\left(\dfrac{m_X}{H_e}\right)^{\frac{2\bar{w}}{1+\bar{w}}}\langle \hat{n}^{\text{hDM}}_L(a_\star)\rangle, & H_{\text{rh}} \le m_X < H_e, \\ \gamma^{-1}\sqrt{\dfrac{m_X}{H_e}}\ \langle \hat{n}^{\text{lDM}}_L(a_\star)\rangle, & m_X < H_{\text{rh}}, \end{cases} \tag{6.161}$$

Employing the approximate results for the total number density $\langle \hat{n}_L(a_\star)\rangle$ from Eqs. (6.150)-(6.151), one can simplify the above formula as

$$\Omega_X^{\rm GP} h^2 \approx 10^{-20} \times \begin{cases} \left(\dfrac{1}{2} + \dfrac{1+3\bar{w}}{3(1-\bar{w})}\right) \left(\dfrac{m_X}{H_e}\right)^{\frac{2\bar{w}}{1+\bar{w}}} \gamma^{\frac{1-3\bar{w}}{1+\bar{w}}} \left(\dfrac{H_e}{1\,\mathrm{GeV}}\right)^{5/2}, & H_{\rm rh} \leq m_X < H_e, \\ \left(\dfrac{3}{2} + \dfrac{1+3\bar{w}}{3(1-\bar{w})}\sqrt{\dfrac{m_X}{\gamma^2 H_e}}\right) \sqrt{\dfrac{m_X}{1\,\mathrm{GeV}}} \left(\dfrac{H_e}{1\,\mathrm{GeV}}\right)^2, & m_X < H_{\rm rh}, \end{cases} \tag{6.162}$$

Let us now highlight several important remarks concerning our final result. First of all, we should emphasize that the abundance of light DM vectors barely depends on the details of reheating, since for $m_X \ll H_{\rm rh}$ and $\bar{w} \in (-1/3, 1)$, one finds $3/2 \gg 1+3\bar{w}/(3-3\bar{w})\sqrt{m_X/H_{\rm rh}}$. In this case, the current relic density of dark vectors is sensitive only to the mass of DM species and the inflationary scale H_e. Intuitively one can understand this result as follows, the energy density of DM vectors is dominated by the $k_\star$ modes, which cross the Hubble horizon after reheating, during the RD era (see Fig. 6.4 right-panel). Hence, the dependence on the non-standard cosmological evolution during reheating is less significant for such modes, and one gets the same results as for instantaneous reheating. In particular, we should stress that our findings for light DM are consistent with Ref. [169], where an instantaneous transition from the inflationary to the radiation-dominated period was assumed. On the other hand, from the above expressions, one infers that the abundance of heavy DM vectors strongly depends on the physics of reheating through γ and $\bar{w}$. In particular, we observe that for the matter-dominated reheating, i.e.,$\bar{w} = 0$, the predicted value of $\Omega_X^{\rm GP} h^2$ does not depend on DM mass, provided that $m_X \in (\gamma^2 H_e, H_e)$. In this case, our result agrees with Refs. [173, 435], where a non-instantaneous phase of reheating with a matter dominated ($\bar{w}=0$) Universe was considered. Let us also stress that the power-law dependence of $\Omega_X^{\rm GP} h^2$ on $\bar{w}$ implies that for a stiff equation-of-state parameter and a given DM mass m_X a lower value of H_e is needed to saturate the observed value of DM abundance.

In Fig. 6.7, we show the parameter space in the $H_e - m_X$ plane, which is consistent with the observed DM abundance (solid curves), i.e., $\Omega_X^{\rm GP} h^2 = \Omega_{\rm DM}^{\rm obs} h^2$, and gives 10% of the relic density (dashed curves), i.e., $\Omega_X^{\rm GP} h^2 = 0.1 \times \Omega_{\rm DM}^{\rm obs} h^2$, for four choices of the reheating efficiency $\gamma = 10^{-1}, 10^{-3}, 10^{-5}$, and 10^{-10}, and various values of $\bar{w} \in \{-1/4, -1/6, 0, 1/3, 2/3\}$. The hatched gray region corresponding to $H_e \geq 4.4 \times 10^{13}$ GeV is excluded by the Planck satellite at 95% C.L. [13], see the discussion around Eq.(3.105). The correct abundance is produced for light DM vectors for $m_X \approx 4 \times 10^{-15}$ $(4.4 \times 10^{13}\ \mathrm{GeV}/H_e)^4$ GeV. Our numerical results confirm that the impact of non-standard reheating is negligible for DM species with mass below $H_{\rm rh}$. However, non-instantaneous reheating characterized by a generic equation of state $\bar{w}$ significantly affects the relic abundance of heavy vectors. Furthermore, for the efficient reheating, e.g., $\gamma = 10^{-1}$, the GP production of DM vectors provides the observed relic density for spin-1 particles with mass $m_X \approx [10^{-14}, 10^9]$ GeV for $H_e \approx [10^{14}, 10^8]$ GeV, respectively. On the other hand, we see that for $\gamma = 10^{-10}$, vectors with mass $m_X \approx [10^{-14}, 10^{12}]$ GeV can account for the total observed DM abundance provided that the inflationary scale is in the range $H_e \approx [10^{14}, 10^6]$ GeV. Therefore, one concludes that there is a wide range of parameter space within which gravitationally produced massive spin-1 species can serve as viable DM candidates.

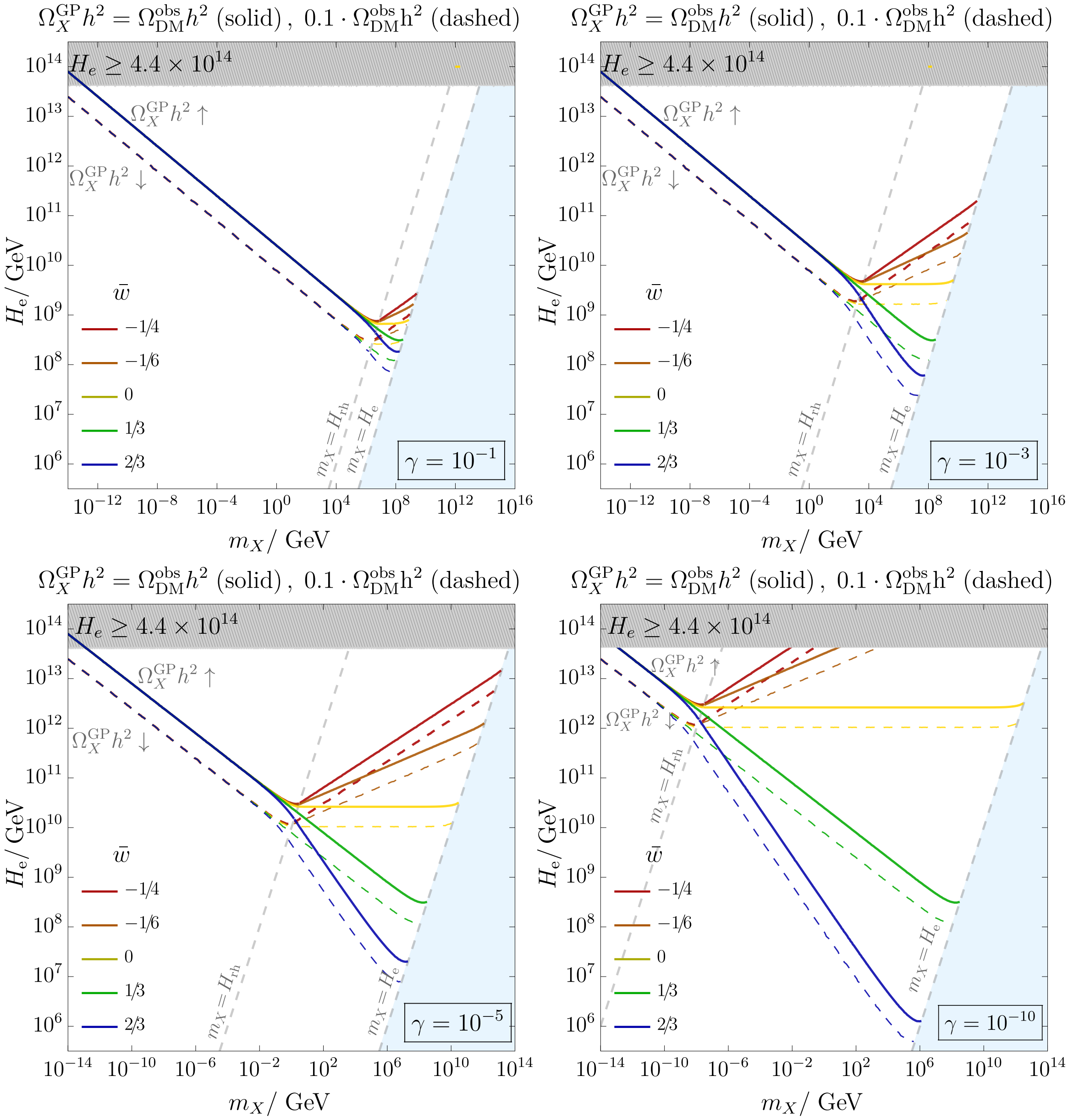

FIGURE 6.7: The value of the Hubble rate at the end inflation H_e as a function of the dark vector mass m_X that reproduces the observed relic abundance $\Omega_{\rm DM}^{\rm obs}h^2$ (solid curves) and 10% of the observed density (dashed curves) for different values of the equation of state parameter $\bar{w}$. In the pale blue region, the mass of DM species exceeds the Hubble scale H_e Eq.(3.105), whereas the hatched gray region is excluded by the Planck satellite at 95% C.L. [13].

6.7 Perturbative DM production

Apart from purely gravitational production originating in cosmic inflation, two additional primordial sources of dark species could be considered irreducible. Namely, DM particles might also be created perturbatively in the process of gravitational scattering, invoking the graviton exchange. Such interactions emerge from the graviton $h_{\mu\nu}$ coupling to the energy-momentum tensors of matter fields $T^{\mu\nu}$ associated with the visible, dark, or other hidden sectors. In the simplest scenario considered in this thesis, dark vectors are created non-thermally in the classical background of the inflaton field (such processes have been discussed in Sec.(4.3) as a source of gravitational reheating) and thermally due to the gravitational freeze-in of SM quanta. Both mechanisms are universal and unavoidable, providing, together with the GP mechanism, the ultimate lower bound on the abundance of dark species. Since the amplitude of gravitational scattering is suppressed by the second power of the Planck mass, efficient particle production might only occur at the highest available energy scales, which can partly compensate for the weakness of gravitational interactions.

It is worth noting that the discussion of gravitational scattering is typically developed in the so-called *Boltzmann approach* [446], based on the solution of the Boltzmann equation, obtained in the framework of quantum field theory (QFT) in flat spacetime. This approach is justified after the end of inflation when the timescale of interactions is typically much shorter than the timescale of expansion, such that one can adopt a Minkowskian geometry. In particular, the perturbative analysis of gravitational scattering is applicable when the scale factor is a power-law function of time t. Hence, such treatment cannot be justified during cosmic inflation, when a grows exponentially with time. This assumption, together with a prerequisite for the existence of a universal and time-independent vacuum state, distinguish this mechanism from the GP particle production discussed earlier. In particular, these two processes have distinct natures and are active in slightly different moments. Moreover, to some extent, they are independent of each other, and we will discuss them in this way.

6.7.1 Inflaton-induced gravitational DM production

We start with a description of the IG mechanism of particle production in the early, but post-inflationary Universe.

Gravitational DM production from the inflaton field involves indirect interactions of ϕ with dark fields, mediated by the single graviton exchange in the s-channel. Such processes emerge from the following Lagrangian density:

$$\mathcal{L}_{\phi X} \supset \frac{h^{\mu\nu}}{M_{\mathrm{Pl}}} \left[T^{\phi}_{\mu\nu} + T^{X}_{\mu\nu} \right], \tag{6.163}$$

containing the contraction of $h^{\mu\nu}$ with the stress tensor of the inflaton $T^{\phi}_{\mu\nu}$ Eq.(4.10), and the energy-momentum tensor of the dark sector $T^{X}_{\mu\nu}$, which for the spin-1 massive DM candidate takes the form Eq.(6.73). Hence, the diagram responsible for dark matter production arises at a dimension-6 level and is proportional to M_{Pl}^{-2}. Although the Planck suppression significantly reduces the strength of gravitational interactions, the energy density accumulated in the inflaton field is so high, especially at the commencement of reheating, that it can counterpoise the Planck damping. As we have already stressed, this mechanism strongly resembles gravitational reheating, discussed in Sec.(4.2.3). The only fundamental difference between these two is the nature of particles in the final states, i.e., the latter case ϕ transfers its energy into the SM sector. Moreover, in the presented analysis, we always include the mass of dark fields, which, as we will see, leads to non-trivial mass effects.

The production rate

To investigate DM gravitational production in the background of the inflaton field, we adopt the *Boltzmann approach* [446], in which the following equation describes the dynamics of the dark sector:

$$\dot{n}_X + 3Hn_X = \mathcal{R}_{\phi X}. \tag{6.164}$$

The production rate of spin-1 dark particles takes the form

$$\mathcal{R}_{\phi X} = \frac{2}{8\pi}\frac{\rho_\phi^2}{M_{\rm Pl}^4}\sum_{k=1}|\mathcal{P}_k^{2n}|^2\cdot\left(1-\frac{4m_X^2}{(k\omega)^2}+12\frac{m_X^4}{(k\omega)^4}\right)\sqrt{1-\frac{4m_X^2}{(k\omega)^2}}, \tag{6.165}$$

where we have used Eq.(4.70) with $|\mathcal{M}^{(2)}_{\phi\to XX}|^2$ given by Eq.(4.58).
Let us recall that the inflaton frequency ω Eq.(4.89) is, in the general case, a function of the scale factor, and only for a matter-like equation of state, i.e., $\bar{w}=0$ $(n=1)$, is time-independent. Moreover, we should also stress that the $\mathcal{P}_k^{2n}$ coefficients decrease with k. Consequently, the sum $\sum_k|\mathcal{P}_k^{2n}|^2$ quickly converges. For the quadratic inflaton potential, Eq. (6.165) simplifies as follows,

$$\mathcal{R}_{\phi X} \overset{\bar{w}=0}{=} \frac{2}{128\pi}\frac{\rho_\phi^2}{M_{\rm Pl}^4}\left(1-\frac{m_X^2}{m_\phi^2}+\frac{3m_X^4}{m_\phi^4}\right)\sqrt{1-\frac{m_X^2}{m_\phi^2}}, \tag{6.166}$$

where we have used the fact that for $\bar{w}=0$, the only non-zero Fourier coefficient is $\mathcal{P}_2^2=1/4$, so that from the summation factor in Eq.(6.165) one gets $\sum_k|\mathcal{P}_k^{2n}|^2=1/16$. In this case, the source term receives time dependence only through ρ_ϕ. On the other hand, if $\bar{w}\neq 0$, the production rate $\mathcal{R}_{\phi X}$ also has another source of time-dependency, namely, the frequency ω. For light DM vectors, the dependency of $\mathcal{R}_{\phi X}$ on ω is quite mild; hence, the rate of DM production is expected to be the highest at the onset of the reheating phase, when ρ_ϕ is the largest. Note that the time-independence of ω for $\bar{w}=0$ implies the existence of a standard constant mass threshold, i.e., $m_X<m_\phi$, during the whole period of reheating. This means that DM vectors with masses exceeding the effective mass of the ϕ field cannot be produced from the inflaton background. Contrarily, for $\bar{w}\neq 0$, there are typically infinitely many non-zero coefficients $\mathcal{P}_k^{2n}$ contributing to the source term. Hence, in such a case, one cannot define a threshold in an ordinary sense since higher harmonics might compensate for the smallness of ω. In particular, by increasing the value of the denominator in the phase-space factor $\sqrt{1-(m_X/k\omega)^2}$, we circumvent the standard kinematical suppression. However, one should also take into account the fact that $\mathcal{R}_{\phi X}$ receives quasi-exponential suppression coming from the Fourier coefficients $\mathcal{P}_k^{2n}$ accounting for higher harmonics. It turns out that the main contribution to the $\mathcal{R}_{\phi X}$ term comes from the first non-zero harmonic $k_{\rm min}$.

Since, for $\bar{w}>0$ $(n>1)$, the frequency ω drops with time, the mass threshold for a given harmonics also decreases during reheating. Therefore, the production of DM vectors with mass in the range $m_X\in[k_{\rm min}\,\omega_e/2, k_{\rm min}\,\omega_{\rm rh}/2]$ might be kinematically terminated at some point during reheating. Contrarily, for $\bar{w}<0$ $(n<1)$, one observes a growth of the inflaton frequency during reheating. This fact does not have a direct impact on the gravitational creation of light DM vectors, i.e., with mass $m_X\ll k_{\rm min}\omega_e$, since in this case, the evolution of $\mathcal{R}_{\phi X}$ is mainly driven by ρ_ϕ. On the other hand, the increase of ω has pronounced consequences for heavy DM vectors. Namely, even if their production was kinematically disfavoured at the onset of reheating, at some point during reheating, $k_{\rm min}\omega(a)$ could exceed $2m_X$, allowing DM vectors to be gravitationally pair produced from the lowest harmonic of the inflaton field. Such behavior is observed for heavy dark vectors, with mass $m_X\in[k_{\rm min}\,\omega_e/2, k_{\rm min}\,\omega_{\rm rh}/2]$, for which the source term is maximized at the scale factor a_X when $k_{\rm min}\omega(a_X)\sim 2m_X$. It is instructive to find an analytic expression for a_X. From the definition: $k_{\rm min}\omega(a_X)=2m_X$, one gets

$$a_X = a_e \begin{cases} \left\lfloor \dfrac{2m_X}{\omega_e} \right\rfloor^{-\frac{1}{3\bar{w}}}, & \bar{w} < 0, \\ 1, & \bar{w} \geq 0. \end{cases} \tag{6.167}$$

In the above formula, we have used the 'floor' function $\lfloor \cdots \rfloor$, defined as

$$\lfloor x \rfloor = \begin{cases} 1, & x \leq 1, \\ x, & x > 1. \end{cases} \tag{6.168}$$

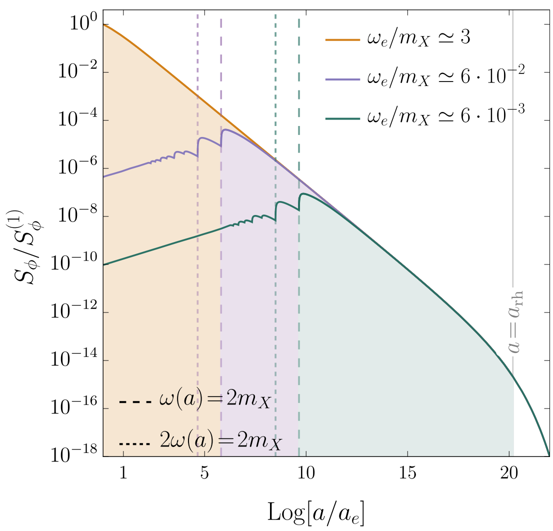

FIGURE 6.8: The evolution of the $S_\phi \equiv a^2\mathcal{R}_{\phi X}/H^2$ term normalized to its initial value $S_\phi^{(1)}$ as a function of the scale factor for $\bar{w} = -0.2$.

The relation (6.167) explicitly demonstrates that the maximum of $\mathcal{R}_{\phi X}$ might not necessarily coincide with the maximum of ρ_ϕ.

This effect is shown in Fig. (6.8), where we have plotted the evolution of the $S_\phi \equiv a^2\mathcal{R}_{\phi X}/H^2$ term as a function of a for light (orange curve), i.e., $m_X < \omega_e/2$, and heavy DM vectors (purple and green curves), i.e., $m_X \in [\omega_e/2, \omega_{\rm rh}/2]$. The orange curve reaches a peak at the onset of reheating, whereas the purple and green curves are peaked at $a = a_X$. One observes that for $\bar{w} < 0$, the gradual growth of ω might provide the phase for the production of heavy DM vectors before the end of reheating.

Relic abundance of DM vectors produced via the IG mechanism

Now, let us come back to the Boltzmann equation Eq. (6.164), which determines the number density of DM species produced gravitationally in the inflaton background, i.e.,

$$n_X(a) = \frac{1}{a^3}\int_{a_e}^{a} d\tilde{a}\, \frac{\tilde{a}^2}{H(\tilde{a})}\mathcal{R}_{\phi X}(\tilde{a}). \tag{6.169}$$

The comoving number density,

$$N_X \equiv n_X(a)a^3, \tag{6.170}$$

approaches a constant limit around the end of reheating, which results from the fact that shortly after this moment, ϕ is significantly depleted, and hence, the contribution from ρ_ϕ to the total energy budget becomes negligible. Consequently, the number density of DM particles at the present epoch can be approximated by the solution of (6.169) with the upper limit of the integral taken as $a = a_{\rm rh}$. Inserting solutions for $H(a)$ Eq.(6.7) and $\rho_\phi(a)$ (3.63), one finds

$$n_X(a_0) \simeq H_e^3 \frac{2}{1+3\bar{w}} \frac{3}{8\pi} \sum_{k=1}^{\infty} |\mathcal{P}_k^{2n}|^2 \Big(\frac{a_e}{a_X}\Big)^{\frac{3(1+3\bar{w})}{2}} \Big(\frac{a_e}{a_0}\Big)^3 \Big[1 - \Big(\frac{a_X}{a_{\rm rh}}\Big)^{\frac{3(1+3\bar{w})}{2}}\Big]. \tag{6.171}$$

Note that we have neglected the phase space factor $m_X^2/(k\omega)^2$ in the above solution. Moreover, we have also assumed that the comoving number density of DM species is conserved after the end of reheating, i.e., $N_X(a_{\rm rh}) \simeq N_X(a_0)$.

Let us stress that for $\bar{w} > -1/3$ ($n > 1/2$), the second factor in the squared bracket in Eq. (6.171) is subdominant, i.e., $(a_X/a_{\rm rh})^{3(1+3\bar{w})/2} \ll 1$. Thus, utilizing Eq. (6.167), one can recast the above solution as

$$n_X(a_0) \simeq H_e^3 \frac{2}{1+3\bar{w}} \frac{3}{8\pi} \sum_{k=1}^{\infty} |\mathcal{P}_k^{2n}|^2 \Big(\frac{a_e}{a_0}\Big)^3 \times \begin{cases} \Big\lceil \dfrac{\omega_e}{2m_X} \Big\rceil^{-\frac{1+3\bar{w}}{2\bar{w}}}, & \bar{w} < 0, \\ 1, & \bar{w} \geq 0. \end{cases} \tag{6.172}$$

Using Eq. (6.156), one estimates the present amount of DM vectors produced gravitationally from the inflaton field as

$$\Omega_X^{\rm IG} h^2 = \frac{3}{16\pi} \frac{1}{1+3\bar{w}} \left(\frac{90}{\pi^2 g_{\star\rho,\rm rh}}\right)^{1/4} \sqrt{\frac{H_e^3}{M_{\rm Pl}^3}} \frac{m_X s_0\, h^2}{\rho_c} \gamma^{\frac{1-3\bar{w}}{1+\bar{w}}} \sum_k |\mathcal{P}_k^{2n}|^2 \times \begin{cases} \Big\lceil \dfrac{\omega_e}{2m_X} \Big\rceil^{-\frac{1+3\bar{w}}{2\bar{w}}}, & \bar{w} < 0, \\ 1, & \bar{w} \geq 0. \end{cases} \tag{6.173}$$

Note that in the above expression, we have used the entropy conservation after the end of reheating, i.e., $s_{\rm rh}/s(a_0) \simeq a_0^3/a_{\rm rh}^3$, and utilized Eq. (6.160).

Let us take a closer look at the above formula. In particular, one finds that for $\bar{w} = -0.2$ ($n = 2/3$), the 'floor' function for heavy DM vectors simplifies as $\omega_e/(2m_X)$. This, in turn, results in a very peculiar behavior of $\Omega_X^{\rm IG} h^2$. Namely, in this case, the predicted abundance of vector DM particles with mass in the range $\omega_e \lesssim 2m_X \lesssim \omega_{\rm rh}$ does not depend on m_X. Moreover, one notices that $\Omega_X^{\rm IG} h^2$ is insensitive to the evolution of thermal bath but depends on the duration of the reheating period through γ. Since for non-instantaneous reheating $\gamma < 1$, the predicted DM relic density is suppressed by the reheating efficiency parameter for $\bar{w} < 1/3$ ($n < 2$). On the other hand, for a stiff inflaton equation of state $\bar{w} > 1/3$ ($n > 2$), one observes the enhancement of $\Omega_X^{\rm IG} h^2$, since, in this case, the slope of the γ dependence on $\bar{w}$ changes its sign, and $\gamma^{\frac{1-3\bar{w}}{1+\bar{w}}} > 1$. Finally, for a radiation-like equation of state $\bar{w} = 1/3$ ($n = 2$), the amount of DM vectors produced gravitationally from the inflaton field is independent of the reheating dynamics while being only a function of the Hubble scale at the end of inflation. In other words, the present abundance of DM species in this scenario is determined solely by their mass and the initial energy density accumulated in the inflaton field at the onset of reheating. Therefore, in this case, one expects that there exists a unique limit on DM mass, above which the predicted abundance of dark species $\Omega_X^{\rm IG} h^2$ exceeds the observed relic density $\Omega_{\rm DM}^{\rm obs} h^2$. Similar behavior has been established by the authors of Ref.[203] in the case of spin-0 DM species. In general, comparing the predicted value of $\Omega_X^{\rm IG} h^2$ for a given m_X and two choices of the inflaton equation of state $\bar{w}_1 < \bar{w}_2$, the reheating efficiency parameter γ must be smaller for a stiffer barotropic parameter to match with the observed DM relic abundance.

Figure (6.9) illustrates the region in the $H_e - m_X$ parameter space for which the amount of dark vectors produced via the IG mechanism saturates the observed abundance $\Omega_{\rm DM}^{\rm obs} h^2$. Solid color curves correspond to $\Omega_X^{\rm IG} h^2 = \Omega_{\rm DM}^{\rm obs} h^2$, while in the region above (below), the

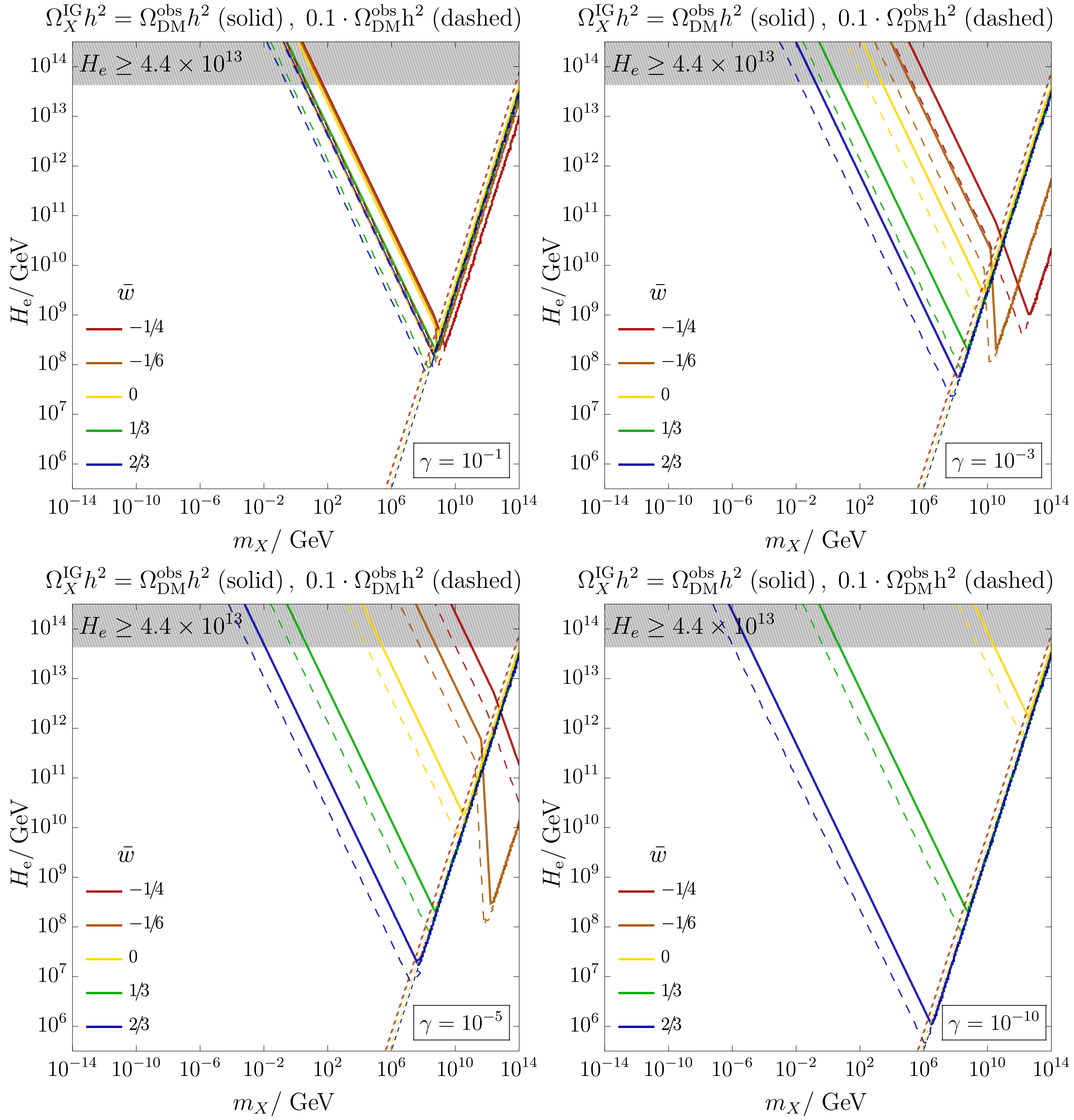

FIGURE 6.9: The value of the Hubble rate at the end inflation H_e as a function of the dark vector mass m_X that saturates the observed relic abundance $\Omega_{DM}^{obs}h^2$ (solid curves) and 10% of the observed density (dashed curves) assuming DM production only through the IG mechanism. In the pale blue region, the mass of DM species exceeds the Hubble scale H_e Eq.(3.105), whereas the hatched gray region is excluded by the Planck satellite at 95% C.L. [13].

predicated abundance overproduced (underestimates) the DM relic density. Different panels are for different reheating efficiency, as specified in the lower right corner of each figure.
Our numerical results warrant that decreasing γ leads to a shrinkage (an enlargement) of the allowed parameter space for $\bar{w} < 1/3$ ($\bar{w} > 1/3$). One also observes that the position of the green curves remains unchanged with varying the value of γ, demonstrating that for this choice of $\bar{w}$, the produced amount of DM vectors does not depend on the reheating efficiency. For all considered values of $\bar{w}$ we see that for light vectors, i.e., $m_X \lesssim \omega_e$, a smaller H_e is needed to match $\Omega_{DM}^{obs}h^2$ for heavier species. Moreover, the $-1/4$ and $-1/6$ curves change their slope around $m_X \sim \omega_e$ (dashed diagonal lines) as a result of the kinematic effects discussed above.

6.7.2 Gravitational freeze-in from thermal bath

Gravitational freeze-in is a universal phenomenon describing the annihilation of the SM degrees of freedom into the pairs of DM particles. Indirect interactions between the visible and dark sectors arise through the coupling of the graviton $h^{\mu\nu}$ to the energy-momentum tensor of the SM and DM fields. Massive dark vectors can be created gravitationally from SM scalars, fermions, and vectors, and the amplitude of such processes depends on the spin of SM particles. Let us emphasize that the SM quanta are assumed to be in thermal equilibrium. Hence, one anticipates that the abundance of DM vectors, in this scenario, should be sensitive to the thermal history of the Universe.

Furthermore, it should be stressed that the description of the SMG processes, as opposed to the IG production, can be performed in a standard QFT framework. Namely, gravitational freeze-in can be considered a purely quantum process in which the initial state $|i\rangle$ comprises quantum fields representing SM species. Therefore, the collision term $\mathcal{S}_{\text{SM DM}}$, accounting for DM production from the thermal bath, can be computed in a standard way. This subsection presents the final results of the multi-stage analysis performed in Appendix (C).

Production rates

The following Boltzmann equation governs the dynamics of dark vectors produced via the gravitational freeze-in:

$$\frac{dN_X}{da} = \frac{a^2}{H}\mathcal{S}_{\text{SM DM}} \simeq \frac{a^2}{H}\bar{n}_X^2\langle\sigma|v|\rangle_{XX\to h_{\mu\nu}\to\text{SM SM}}, \tag{6.174}$$

where N_X is the comoving number density of DM species (6.170).
The source term is defined as

$$\mathcal{S}_{\text{SM DM}} \equiv (\bar{n}_X^2 - n_X^2)\langle\sigma|v|\rangle_{XX\to h_{\mu\nu}\to\text{SM SM}}, \tag{6.175}$$

where equilibrium number density of dark vector X_μ the zero chemical potential is given by

$$\bar{n}_X \simeq \frac{3}{2\pi^2}m_X^2 T K_2\left(\frac{m_X}{T}\right), \tag{6.176}$$

where $K_2(x)$ is the modified Bessel function of the second kind.
Note that in Eq. (6.174) we have assumed that $\bar{n}_X^2 \gg n_X^2$. The adopted simplification follows from the fact that DM vectors having only gravitational interactions with the SM sector are not in equilibrium with the thermal bath. It results from the fact that gravitational interactions suppressed by the Planck mass scale are so weak that the interaction efficiency $\langle\sigma|v|\rangle n_X/H \ll 1$, indicating a lack of equilibrium among the dark sector.

The thermally averaged cross-section $\langle\sigma|v|\rangle_{XX\to h_{\mu\nu}\to\text{SM SM}}$ for the gravitational DM-SM interactions can be calculated from the standard formula [2] [447],

$$\langle\sigma|v|\rangle_{ii\to FF} = \frac{(2J_i+1)^2}{\bar{n}_i^2}\frac{T}{32\pi^4}\int_{4m_{\max}^2}^{\infty} ds\,\sqrt{s}(s-4m_i^2)\,\sigma_{ii\to FF}(s)K_1\left(\frac{\sqrt{s}}{T}\right), \tag{6.177}$$

where $\sigma_{ii\to FF}$ is the cross-section averaged over possible spin states of the DM particles in the initial state i and summed over spins of the SM particles in the final state f, J_i denotes the spin of the initial states, whereas $m_{\max} \equiv \max(m_i, m_F)$, with m_i (m_F) being the mass

[2] Note that for convenience we compute here the thermally-averaged cross-section describing the annihilation of DM particles into the SM species. However, the result remains the same if one considers the production process, i.e., the pair-annihilation of SM quanta into dark particles.

of particles in the initial (final) state.

The SMG production of spin-1 dark particles occurs though the following four channels:

$$\sigma_{XX\to h_{\mu\nu}\to h_i h_i} = \frac{1}{9}\frac{1}{480\pi s^3 M_{\rm Pl}^4}\frac{\sqrt{s-4m_{h_i}^2}}{\sqrt{s-4m_X^2}}\Big[2m_{h_i}^4\left(84m_X^4+68m_X^2 s+19s^2\right) - 2m_{h_i}^2 s(6m_X^2+s)(2m_X^2+7s)+3s^2(6m_X^4+2m_X^2 s+s^2)\Big], \tag{6.178}$$

$$\sigma_{XX\to h_{\mu\nu}\to \bar\Psi\Psi} = \frac{1}{9}\frac{1}{960\pi s^2 M_{\rm Pl}^4}\frac{\sqrt{s-4m_{\Psi}^2}}{\sqrt{s-4m_X^2}}\Big(1-\frac{4m_\Psi^2}{s}\Big)\Big[2m_{\Psi}^2\left(84m_X^4+68m_X^2 s+19s^2\right) +s(48m_X^4+56m_X^2 s+13s^2)\Big], \tag{6.179}$$

$$\sigma_{XX\to h_{\mu\nu}\to VV} = \frac{1}{9}\frac{1}{480\pi s^3 M_{\rm pl}^4}\frac{\sqrt{s-4m_{V}^2}}{\sqrt{s-4m_X^2}}\Big[m_V^4(504m_X^4+408m_X^2 s+114s^2) + m_V^2(408m_X^4 s+536m_X^2 s^2+118s^3)+114m_X^4 s^2+118m_X^2 s^3+29s^4\Big], \tag{6.180}$$

$$\sigma_{XX\to h_{\mu\nu}\to \gamma\gamma} = \frac{1}{9}\frac{1}{240\pi M_{\rm Pl}^4}\frac{48m_X^4+56m_X^2 s+13s^2}{\sqrt{s(s-4m_X^2)}}, \tag{6.181}$$

accounting for the annihilation of SM scalars, fermions, massive and massless vectors, respectively.

In the limit $m_{\rm SM}\to 0$, the corresponding thermally-averaged cross-sections are given by

$$\langle\sigma|v|\rangle_{XX\to h_{\mu\nu}\to h_i h_i} = \frac{9}{32\pi^4}\frac{1}{120\pi M_{\rm Pl}^4}\frac{m_X^6 T^2}{\bar n_X^2}\Big\{3K_1^2\Big(\frac{m_X}{T}\Big)+2K_2^2\Big(\frac{m_X}{T}\Big)\Big[1+4\Big(\frac{T}{m_X}\Big)^2\Big] + 4\frac{T}{m_X}K_1\Big(\frac{m_X}{T}\Big)K_2\Big(\frac{m_X}{T}\Big)\Big\}, \tag{6.182}$$

$$\langle\sigma|v|\rangle_{XX\to h_{\mu\nu}\to \bar\Psi\Psi} = \frac{9}{32\pi^4}\frac{1}{90\pi M_{\rm Pl}^4}\frac{m_X^6 T^2}{\bar n_X^2}\Big\{11K_1^2\Big(\frac{m_X}{T}\Big)+K_2^2\Big(\frac{m_X}{T}\Big)\Big[9+26\Big(\frac{T}{m_X}\Big)^2\Big] + 13\frac{T}{m_X}K_1\Big(\frac{m_X}{T}\Big)K_2\Big(\frac{m_X}{T}\Big)\Big\}, \tag{6.183}$$

$$\langle\sigma|v|\rangle_{XX\to h_{\mu\nu}\to \gamma\gamma} = \frac{9}{32\pi^4}\frac{3}{135\pi M_{\rm Pl}^4}\frac{m_X^6 T^2}{\bar n_X^2}\Big\{11K_1^2\Big(\frac{m_X}{T}\Big)+K_2^2\Big(\frac{m_X}{T}\Big)\Big[9+26\Big(\frac{T}{m_X}\Big)^2\Big] + 13\frac{T}{m_X}K_1\Big(\frac{m_X}{T}\Big)K_2\Big(\frac{m_X}{T}\Big)\Big\}. \tag{6.184}$$

Contrarily, if masses of SM species are not negligible, i.e., $m_{\rm SM}\neq 0$, the integral over s in Eq. (6.177) must be performed numerically, see [2].

The source term $\mathcal{S}_{\rm SMDM}$, in general, can be written as a sum of four contributions:

$$\mathcal{S}_{\rm SM\,DM} = N_{h_i}\mathcal{S}_{h_i h_i}+N_\Psi\mathcal{S}_{\bar\Psi\bar\Psi}+N_V\mathcal{S}_{VV}+N_\gamma\mathcal{S}_{\gamma\gamma}, \tag{6.185}$$

where we have separated contributions from SM scalars, fermions, and massive and massless vectors. Above, $N_{\rm SM}$ denotes the number of SM species of a given spin, i.e., $N_{h_i}=4$ for four real components of the Higgs doublet, $N_\Psi=45$ for six (anti)quarks with three colors (36), three charged (anti)lepton (6) and three left-handed neutrinos, $N_V = 3$ for three electroweak massive gauge bosons, $N_\gamma = 9$ for eight gluons and one photon.

Note that in the non-relativistic (NR) limit, i.e., $m_X \gg T$, and for $m_{\rm SM} \to 0$, the source terms behaves as

$$\mathcal{S}^{\rm NR}_{\rm SM\,SM} \equiv \mathcal{S}_{\rm SM\,SM}\Bigg|_{m_X \gg T} \simeq \frac{\mathcal{B}^{\rm NR}_{\rm SM\,SM}}{32\pi^4}\left(\frac{m_X}{M_{\rm Pl}}\right)^4 m_X T^3 e^{-2m_X/T}, \tag{6.186}$$

with

$$\mathcal{B}^{\rm NR}_{h_i h_i} = \frac{3}{16}, \qquad \mathcal{B}^{\rm NR}_{\bar\Psi\Psi} = 1, \qquad \mathcal{B}^{\rm NR}_{\gamma\gamma} = 2. \tag{6.187}$$

In the relativistic (R) limit $m_X \ll T$, the $\mathcal{S}_{\rm SM\,SM}$ term can be approximated as

$$\mathcal{S}^{\rm R}_{\rm SM\,SM} \equiv \mathcal{S}_{\rm SM\,SM}\Bigg|_{m_X \ll T} \simeq \frac{1}{32\pi^5}\frac{T^8}{M^4_{\rm Pl}}\mathcal{B}^{\rm R}_{\rm SM\,SM}, \tag{6.188}$$

with

$$\mathcal{B}^{\rm R}_{h_i h_i} = \frac{12}{5}, \qquad \mathcal{B}^{\rm R}_{\bar\Psi\Psi} = \frac{52}{5}, \qquad \mathcal{B}^{\rm R}_{\gamma\gamma} = \frac{104}{5}. \tag{6.189}$$

The asymptotic behavior of the source term implies that efficient freeze-in DM production occurs only when the temperature of the thermal bath exceeds the mass of DM vectors. In particular, the production of DM vectors with mass $m_X > T_{\rm max}$ is exponentially suppressed.

Based on the above discussion, it can be concluded that the SMG processes are an example of the ultraviolet (UV) freeze-in mechanism, in which the abundance of DM species is highly sensitive to the initial conditions. In particular, one observes a strong dependence of the source term $\mathcal{S}^{\rm R}_{\rm SM\,SM}$ on T, namely $\mathcal{S}^{\rm R}_{\rm SM\,SM} \propto T^8$. Such behavior indicates that the efficiency of this process depends not only on the maximal temperature of the thermal bath but also on its evolution in time. As a result, the amount of dark species produced via this mechanism should be determined predominantly by the dynamics of the SM sector at the highest energy scales. Hence, one expects that the present abundance of DM particles might be sensitive to the course of reheating if the transition from the inflationary to the RD epoch was not instantaneous. On the other hand, in the scenario with instantaneous reheating, it might depend solely on the reheating temperature.

6.7.3 Present abundance of DM vectors produced from the thermal bath

The efficiency of the gravitational freeze-in production is determined by the relation between the thermal bath temperature T and the mass of DM vectors m_X. In particular, we consider the following three regimes:

1. **Heavy vectors, with mass $T_{\rm max} \lesssim m_X$**
   Such species have never become relativistic so that the source term $\mathcal{S}_{\rm SM\,SM}$ could be approximated by $\mathcal{S}^{\rm NR}_{\rm SM\,SM}$. Hence, dropping post-reheating contribution to the freeze-in DM production, the present value of the comoving number density can be found from the following formula:

$$N_X(a_0) \simeq \frac{\mathcal{B}^{\rm NR}_{\rm SM\,SM}}{32\pi^4}\left(\frac{m_X}{M_{\rm Pl}}\right)^4 \frac{m_X}{H_e} a_e^{-\frac{3(1+\bar w)}{2}} \int_{a_e}^{a_{\rm rh}} da\, a^{\frac{7+3\bar w}{2}} T^3_{\rm RH}(a) e^{-2m_X/T_{\rm RH}(a)}, \tag{6.190}$$

where the evolution of $T_{\rm RH}(a)$ is described by (6.10).
After some straightforward but tedious computations, one obtains

$$N_X(a_0) \approx \widetilde{T}_{\rm rh}^3 \frac{\mathcal{B}^{\rm NR}_{\rm SM\,SM}}{32\pi^4}\left(\frac{m_X}{M_{\rm Pl}}\right)^4 \frac{\widetilde{T}_{\rm rh}}{H_e} e^{-2m_X/\widetilde{T}_{\rm rh}} a_e^3 \times \begin{cases} \dfrac{4}{2\beta_F + 3\bar{w} + 3}, & \beta_F < (5-3\bar{w})/2, \\ \dfrac{1}{2}, & \beta_F > (5-3\bar{w})/2. \end{cases} \tag{6.191}$$

with

$$\widetilde{T}_{\rm rh} \equiv T_{\rm rh} \begin{cases} \gamma^{-\frac{1}{2}-\frac{\beta_F}{3(1+\bar{w})}}, & \beta_F < (5-3\bar{w})/2, \\ \gamma^{-\frac{4}{3(1+\bar{w})}}, & \beta_F > (5-3\bar{w})/2. \end{cases} \tag{6.192}$$

Using the fact that $n_X(a_0) = N_X(a_0)/a_0^3$ together with (6.9) and (6.160), one finds the following formula for the relic abundance of heavy DM vectors:

$$\Omega^{\rm SMG}_{X,({\rm h})} h^2 = \left(\frac{90}{\pi^2 g_{\star s,{\rm rh}}}\right)^{5/4} \frac{\mathcal{B}^{\rm NR}_{\rm SM\,SM}}{128\pi^4}\left(\frac{m_X}{M_{\rm Pl}}\right)^4 \frac{m_X M_{\rm Pl}^2 H_e}{\rho_c} h^2 \frac{s_0}{(M_{\rm Pl}H_e)^{3/2}} \gamma^{\frac{3-\bar{w}}{1+\bar{w}}} h^2$$
$$\times\, e^{-2m_X/\widetilde{T}_{\rm rh}} \cdot \begin{cases} \dfrac{4}{2\beta_F + 3\bar{w} + 3}\gamma^{-\frac{4\beta_F}{3(1+\bar{w})}}, & \beta_F < (5-3\bar{w})/2, \\ \dfrac{1}{2}\gamma^{2-\frac{16}{3(1+\bar{w})}}, & \beta_F > (5-3\bar{w})/2. \end{cases} \tag{6.193}$$

2. **Vectors with intermediate mass** $m_X \in (T_{\rm rh}, T_{\rm max})$
Dark vectors with mass in the range $m_X \in (T_{\rm rh}, T_{\rm max})$ becomes non-relativistic during reheating when the temperature of the thermal bath drops below their mass. This happens at $a_{\rm NR}$, such that $T(a_{\rm NR}) \sim m_X$. Using (6.10), one finds

$$a_{\rm NR} = a_{\rm rh} \times \begin{cases} (T_{\rm rh}/m_X)^{\frac{8}{2\beta_F + 3(1+\bar{w})}}, & \beta_F < 5(1-3\bar{w})/2, \\ T_{\rm rh}/m_X, & \beta_F > 5(1-3\bar{w})/2. \end{cases} \tag{6.194}$$

Hence, the present comoving number density can be approximated by the sum of two integrals:

$$N_X(a_0) \simeq N_X(a_{\rm rh}) \approx \frac{\mathcal{B}^{\rm R}_{\rm SM\,SM}}{32\pi^5}\frac{1}{M_{\rm Pl}^4}\frac{a_e^{-\frac{3(1+\bar{w})}{2}}}{H_e}\int_{a_e}^{a_{\rm NR}} da\, a^{\frac{7+3\bar{w}}{2}} T_{\rm RH}^8(a)$$
$$+ \frac{\mathcal{B}^{\rm NR}_{\rm SM\,SM}}{32\pi^4}\left(\frac{m_X}{M_{\rm Pl}}\right)^4 \frac{m_X}{H_e} a_e^{-\frac{3(1+\bar{w})}{2}} \int_{a_{\rm NR}}^{a_{\rm rh}} da\, a^{\frac{7+3\bar{w}}{2}} T_{\rm RH}^3(a) e^{-2m_X/T_{\rm RH}(a)}. \tag{6.195}$$

Neglecting the exponentially suppressed contribution from the second term, one obtains

$$N_X(a_0) \approx \frac{\mathcal{B}^{\rm R}_{\rm SM\,SM}}{32\pi^5}\frac{T_{\rm rh}^8}{H_e M_{\rm Pl}^4} a_e^3$$
$$\times \begin{cases} \frac{2}{3(1-\bar{w})-4\beta_F}\left[\gamma^{\frac{-2(\bar{w}+3)}{1+\bar{w}}}\left(\frac{T_{\rm rh}}{m_X}\right)^{\frac{12(1-\bar{w})-16\beta_F}{2\beta_F+3(1+\bar{w})}} - \gamma^{-4-\frac{8\beta_F}{3(1+\bar{w})}}\right], & \beta_F < 5(1-3\bar{w})/2, \\ \frac{2}{3\bar{w}-7}\left[\left(\frac{T_{\rm rh}}{m_X}\right)^{\frac{3(3+\bar{w})}{2}}\gamma^{-2\frac{3+\bar{w}}{1+\bar{w}}} - \gamma^{\frac{-32}{3(1+\bar{w})}}\right], & \beta_F > 5(1-3\bar{w})/2. \end{cases} \tag{6.196}$$

Therefore, the relic abundance of dark vectors with intermediate mass can be found from the following formula:

$$
\Omega^{\rm SMG}_{X,({\rm i})}h^2 = \frac{\mathcal{B}^{\rm R}_{\rm SM\,SM}}{128\pi^5}\left(\frac{90}{\pi^2 g_{\star,{\rm rh}}}\right)^{9/4}\gamma^{\frac{9+5\bar{w}}{1+\bar{w}}}\frac{s_0}{(M_{\rm Pl}H_e)^{3/2}}\frac{m_X H_e^3}{\rho_c}h^2
$$
$$
\times\begin{cases}\frac{2}{3(1-\bar{w})-4\beta_F}\left[\gamma^{\frac{-2(\bar{w}+3)}{1+\bar{w}}}\left(\frac{T_{\rm rh}}{m_X}\right)^{\frac{12(1-\bar{w})-16\beta_F}{2\beta_F+3(1+\bar{w})}}-\gamma^{-4-\frac{8\beta_F}{3(1+\bar{w})}}\right], & \beta_F<5(1-3\bar{w})/2,\\ \frac{2}{3\bar{w}-7}\left[\left(\frac{T_{\rm rh}}{m_X}\right)^{\frac{3(3+\bar{w})}{2}}\gamma^{-2\frac{3+\bar{w}}{1+\bar{w}}}-\gamma^{\frac{-32}{3(1+\bar{w})}}\right], & \beta_F>5(1-3\bar{w})/2.\end{cases}
\tag{6.197}
$$

3. **Light vectors** $m_X \ll T_{\rm rh}$
In this case, the solution to the Boltzmann equation can be separated into the following three relevant contributions:

$$
\begin{aligned}
N_X(a_0) \simeq\ & \frac{\mathcal{B}^{\rm R}_{\rm SM\,SM}}{32\pi^5}\frac{1}{M_{\rm Pl}^4}\frac{a_e^{-\frac{3(1+\bar{w})}{2}}}{H_e}\int_{a_e}^{a_{\rm rh}} da\, a^{\frac{7+3\bar{w}}{2}}T^8_{\rm RH}(a)\\
&+\frac{\mathcal{B}^{\rm R}_{\rm SM\,SM}}{32\pi^5}\frac{1}{H_e M_{\rm Pl}^4}\frac{\gamma^{\frac{2(1-3\bar{w})}{3(1+\bar{w})}}}{a_e^2}\int_{a_{\rm rh}}^{\tilde{a}_{\rm NR}} da\, a^4\, T^8_{\rm RD}(a)\\
&+\frac{\mathcal{B}^{\rm NR}_{\rm SM\,SM}}{32\pi^4}\left(\frac{m_X}{M_{\rm Pl}}\right)^4\frac{m_X}{H_e}\frac{\gamma^{\frac{2(1-3\bar{w})}{3(1+\bar{w})}}}{a_e^2}\int_{\tilde{a}_{\rm NR}}^{a_{\rm r.m.e}} da\, a^4 T^3_{\rm RD}(a)e^{-2m_X/T_{\rm RD}(a)}.
\end{aligned}
\tag{6.198}
$$

The first term, in the above expression, accounts for the gravitational freeze-in during reheating, the second describes production in the relativistic regime during the radiation-dominated epoch, whereas the last one is responsible for the gravitation producation of non-relativistic dark vectors during the RD era. Note that $\tilde{a}_{\rm NR}$ corresponds to the scale factor, at which $T_{\rm RD}(\tilde{a}_{\rm NR}) = m_X$, and can be calaculated from the following expression:

$$
\tilde{a}_{\rm NR} = a_e\gamma^{-\frac{4}{3(1+\bar{w})}}\frac{T_{\rm rh}}{m_X}\left(\frac{g_{\star s,{\rm rh}}}{g_{\star s}(T(\tilde{a}_{\rm NR}))}\right)^{1/4}.
\tag{6.199}
$$

The main contribution to $N_X(a_0)$ comes from the first integral, and is given by

$$
N_X(a_0) \approx \frac{\mathcal{B}^{\rm R}_{\rm SM\,SM}}{32\pi^5}\frac{T^8_{\rm rh}}{H_e M^4_{\rm Pl}}a_e^3
\times\begin{cases}\frac{2}{3(1-\bar{w})-4\beta_F}\left[\gamma^{\frac{-2(3+\bar{w})}{1+\bar{w}}}-\gamma^{-4-\frac{8\beta_F}{3(1+\bar{w})}}\right], & \beta_F<5(1-3\bar{w})/2,\\ \frac{2}{3\bar{w}-7}\left[\gamma^{-2\frac{3+\bar{w}}{1+\bar{w}}}-\gamma^{\frac{-32}{3(1+\bar{w})}}\right], & \beta_F>5(1-3\bar{w})/2.\end{cases}
\tag{6.200}
$$

Consequently, we arrive at the following expression for relic abundance

$$
\Omega^{\rm SMG}_{X,({\rm l})}h^2 = \frac{\mathcal{B}^{\rm R}_{\rm SM\,SM}}{128\pi^5}\left(\frac{90}{\pi^2 g_{\star\rho,{\rm rh}}}\right)^{9/4}\gamma^{\frac{9+5\bar{w}}{1+\bar{w}}}\frac{s_0}{(M_{\rm Pl}H_e)^{3/2}}\frac{m_X H_e^3}{\rho_c}h^2
\times\begin{cases}\frac{2}{3(1-\bar{w})-4\beta_F}\left[\gamma^{\frac{-2(3+\bar{w})}{1+\bar{w}}}-\gamma^{-4-\frac{8\beta_F}{3(1+\bar{w})}}\right], & \beta_F<5(1-3\bar{w})/2,\\ \frac{2}{3\bar{w}-7}\left[\gamma^{-2\frac{3+\bar{w}}{1+\bar{w}}}-\gamma^{\frac{-32}{3(1+\bar{w})}}\right], & \beta_F>5(1-3\bar{w})/2.\end{cases}
\tag{6.201}
$$

Note that the above formula for $\Omega^{\rm SMG}_{X,(\rm l)}h^2$ resembles the expression for $\Omega^{\rm SMG}_{X,(\rm i)}h^2$. The only difference between these two is the appearance of the suppression factor $\left(\frac{T_{\rm rh}}{m_X}\right)^{\frac{12(1-\bar{w})-16\beta_F}{2\beta_F+3(1+\bar{w})}}$ in Eq.(6.197).

In all discussed cases, $\Omega^{\rm SMG}_X h^2$ exhibits a complicated dependence on the reheating efficiency. To clarify the above results, let us consider two specific reheating scenarios, driven by a massless scalars S and fermions Φ. In this case, the coefficient β_F, parametrizing the $\Gamma_{\phi\to\rm FF}$ evolution Eq.(4.90), is given by $\beta_{\rm S} = -3\bar{w}$, and $\beta_\Psi = 3\bar{w}$, respectively. Hence, for the bosonic reheating, i.e., triggered by $\phi \to SS$ interactions, one finds[3] that both $\Omega^{\rm SMG}_{X,(\rm l)}h^2$ and $\Omega^{\rm SMG}_{X,(\rm i)}h^2$ scale as $\propto \gamma^3$. For the fermionic case, one finds the same scaling, i.e., $\Omega^{\rm SMG}_X h^2 \propto \gamma^3$, provided that $\bar{w} < 1/5$, whereas if $\bar{w} > 1/5$ the predicted relic density is proportional to $\propto \gamma^{(15+3\bar{w}-8\beta_F)/(3+3\bar{w})}$, thus, for a radiation-like equation-of-state one finds $\Omega^{\rm SMG}_X h^2 \propto \gamma^2$.

In Fig. (6.10), we present the relation between the inflationary Hubble scale H_e and mass of DM vectors m_X for which gravitational freeze-in from the SM bath correctly predicts the observed abundance of DM species. In the upper panel of these figures, we have adopted the massless bosonic reheating scenario, controlled by $\phi \to SS$ interactions, whereas in the lower panels, we have assumed that reheating is triggered by direct $\phi - \Psi$ interactions. One can see that the gravitational freeze-in strongly depends on the parameter γ. For efficient reheating, the range of viable DM masses is quite large. However, as γ decreases, all curves move toward larger values of H_e, and the allowed range in parameter space shrinks significantly. It turns out that for $\gamma \lesssim 10^{-3}$ SMG mechanism is almost not operative for any value of $\bar{w}$ in the bosonic reheating scenario. The same conclusion was come by the authors of Ref. [199] who considered only a matter-like reheating $\bar{w} = 0$. However, we observe that in the fermionic case for $\gamma \lesssim 10^{-3}$, there is some mass window in which SMG can be considered as a viable mechanism of DM production provided that ϕ has a stiff e.o.s parameter, i.e., $\bar{w} > 1/3$, cf. right panel of Fig. (6.11). By comparing the position of different colored curves, we see that in the bosonic reheating, for a given mass, the larger value of H_e is needed for a stiff inflaton e.o.s parameter (blue curve corresponding to $n = 2/3$). On the other hand, a reversed ordering is observed for the fermionic case. Such behavior results from the fact that $\beta_S = -\beta_\Psi$, hence only for $\bar{w} = 0$, these two scenarios give the same result. For light vectors, $\Omega^{\rm SMG}_{X,(\rm l)}h^2$ is proportional to m_X (6.201), hence, for heavier species smaller value of H_e is needed to saturate the observed abundance. On the other hand, for dark vectors with a mass exceeding $T_{\rm rh}$, the Hubble rate must be larger to counterbalance Boltzmann suppression.

Lastly, in Fig.(6.10), we compare our results for two choices of $\bar{w}$, i.e., $\bar{w} = 0$ (yellow curves), and $\bar{w} = 1/3$ (green curves), and two reheating scenarios, i.e., triggered by $\phi \to SS$ (left panel) and $\phi \to \Psi\bar{\Psi}$ (right panel) interactions. These two figures show that the massless bosonic and fermionic reheating scenario predictions are indistinguishable if ϕ has a matter-like equation of state. On the other hand, these two models give very different results for $\bar{w} = 1/3$. In this case, one observed that the allowed parameter space is larger if reheating is achieved by the inflaton coupling to fermions. Moreover, in this case, one observes weaker dependence on the reheating efficiency parameter γ. Namely, in the bosonic case, one observes that $\Omega^{\rm SM}_X h^2 \propto \gamma^3$ for both considered values of $\bar{w}$. On the other hand, in the fermionic scenario one gets the same scaling for a matter-like e.o.s, whereas for $\bar{w} = 1/3$, $\Omega^{\rm SM}_X h^2 \propto \gamma^2$.

[3]To obtain this result, one should use the first line of Eq. (6.197) and Eq. (6.201), i.e., the $\beta_F < 5(1-3\bar{w})/2$ case, and neglected the second factor in the square bracket.

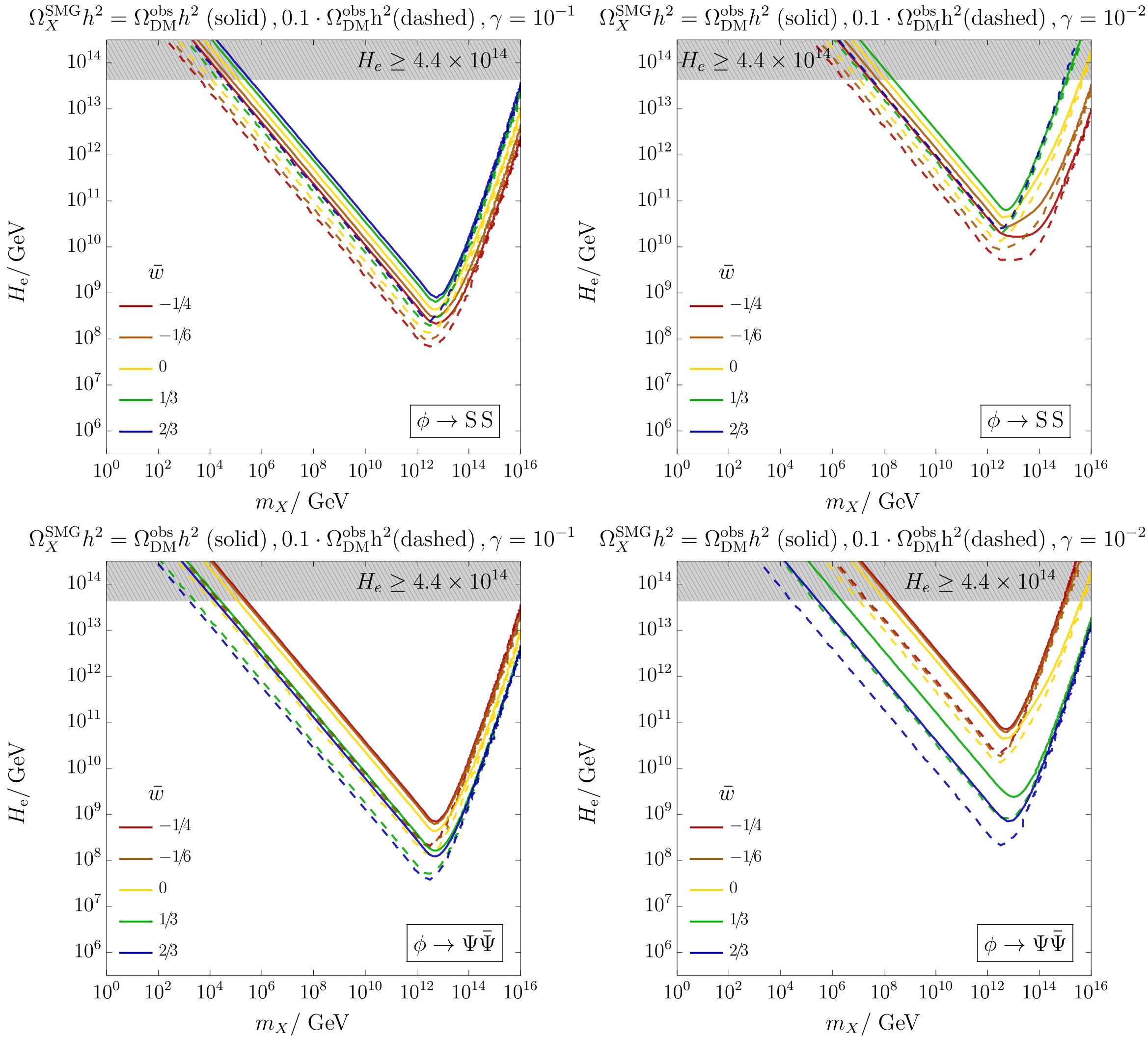

FIGURE 6.10: The value of the Hubble rate at the end inflation H_e as a function of the dark vector mass m_X that saturates the observed relic abundance $\Omega_{\rm DM}^{\rm obs}h^2$ (solid curves) and 10% of the observed density (dashed curves) assuming DM production only through the gravitational freeze-in from the thermal bath. In the upper (lower) panels, the bosonic (fermionic) reheating scenario is adopted. The hatched gray region is excluded by the Planck satellite at 95% C.L. [13].

6.8 Final results and discussion

So far, we have discussed each production mechanism separately. For each considered process, we have derived approximate formulas which allow us to calculate the predicted abundance of dark vectors as a function of three parameters γ, H_e, and m_X. Now let us combine our findings, accounting for all gravitational production channels for the two most established reheating scenarios, i.e., for a matter-like and radiation-like equation of states.

Dark vectors with mass smaller than the inflationary scale H_e are dominantly produced via the GP mechanism, cf. Fig.(6.12). Considering the CMB constraints on the Hubble scale at the end of inflation, we see that vectors as light as $\sim 10^{13}$ GeV can be created gravitationally due to non-adiabatic expansion of the Universe during inflation. To understand this observation quantitatively, let us compare expressions for the final abundance of dark vectors.

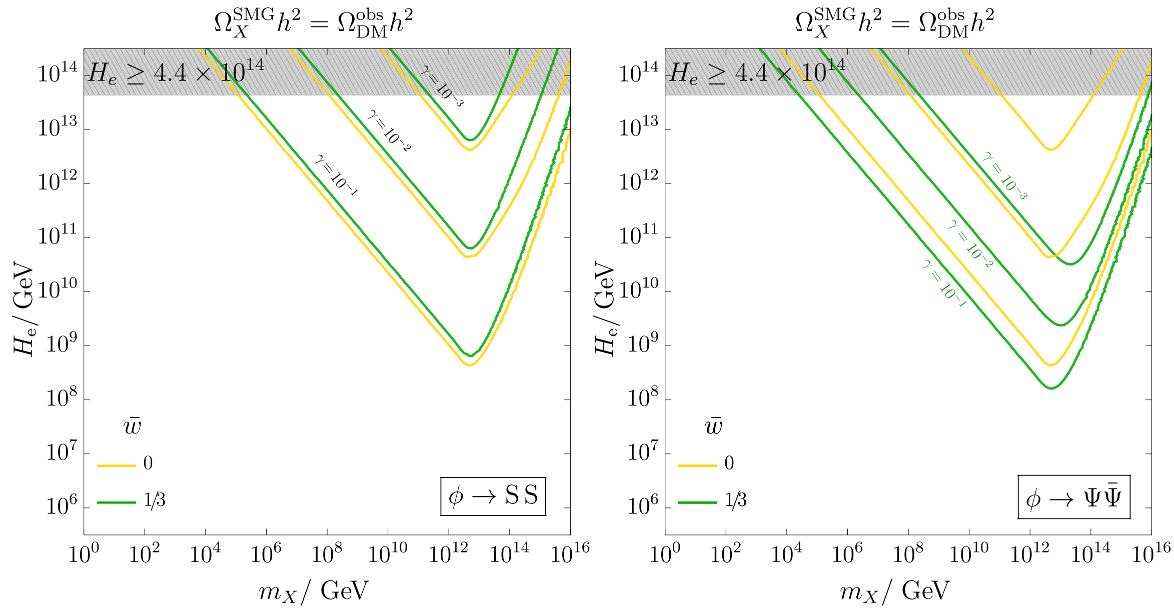

FIGURE 6.11: Comparison between bosonic (left panel) and fermionic (right panel) cases.

Utilizing Eq.(6.201) and (6.173) and neglecting numerical factors, one finds

$$\frac{\Omega_X^{\rm IP}h^2}{\Omega_{X,(\rm l)}^{\rm SMG}h^2} \sim \gamma^{-2\frac{1+6\bar{w}}{1+3\bar{w}}}, \tag{6.202}$$

in the bosonic reheating scenario for $\bar{w} \geq 0$, and fermionic case for $\bar{w} \in [0, 1/5)$. Note that the exponent $-2\frac{1+6\bar{w}}{1+3\bar{w}}$ is negative for $\bar{w} > -1/6$. Since $\gamma \ll 1$, it implies the thermal freeze-in DM production is inefficient in such cases. Similarly, for $\bar{w} > 1/5$ in the fermionic scenario, one obtains

$$\frac{\Omega_X^{\rm IP}h^2}{\Omega_{X,(\rm l)}^{\rm SMG}h^2} \sim \gamma^{-4+\frac{8\beta_F}{3(1+\bar{w})}}. \tag{6.203}$$

The exponent $-4 + \frac{8\beta_F}{3(1+\bar{w})}$ for $\beta_F < \frac{5}{2}(1-3\bar{w})$ and $\bar{w} > 1/5$ is always negative, which leads to the similar conclusion as above.
In addition, from Eqs.(6.161) and (6.173), and for $\bar{w} \geq 0$, one finds

$$\frac{\Omega_X^{\rm GP}h^2}{\Omega_X^{\rm IP}h^2} \sim \left(\frac{H_e}{m_X}\right)^{\frac{1-\bar{w}}{1+\bar{w}}}, \tag{6.204}$$

where we have neglected numerical factors of order one. Note that the above result is independent of the reheating efficiency γ. For $\bar{w} \in [0, 1)$, the index $(1-\bar{w})/(1+\bar{w})$ is always positive, which implies that for $m_X \ll H_e$ the GP process is the main source of particle production. The GP and IP mechanisms might provide a comparable contribution to the abundance of dark vectors only in a narrow window, i.e., when $m_X \sim H_e$.

Since the inflaton mass, or more precisely the energy $k_{\rm min}\omega_e$ of the oscillating modes, is naturally of the order of H_e, DM vectors with a mass exceeding H_e cannot be abundantly produced in the inflaton background. However, dark vectors with a mass in the range $H_e, T_{\rm max}$ can still be created gravitationally from the thermal bath. However, this process, in contrast with non-thermal production mechanisms, is susceptible to the γ parameter, which controls the temperature of the thermal bath, and, thus, the efficiency of SMG. From Fig.(6.12), we see that thermal freeze-in significantly enlarges the allowed parameter space provided that $\gamma \gtrsim 10^{-1}$. For prolonged reheating, the contribution from SMG to the total DM relic abundance is less relevant, and for $\gamma \sim 10^{-4}$, it can be neglected in both considered scenarios.

Another important conclusion is that stable spin-1 massive particles are, in general, copiously created in the primordial Universe, even if they do not have any other interactions with other species. Namely, there is a large region in the $H_e - m_X$ parameter space (colored part of Fig.(6.12)), where purely gravitational processes inevitably overestimate the observed DM relic density. Similar conclusions also apply to stable scalars, as pointed out in Ref. [448, 449]

As a final remark, let us comment on the observational prospects of the purely gravitational DM. In principle, one could consider two possibilities. The first one is much more optimistic - dark species might have other interactions that do not participate in its creation. In this case, one expects that DM species might variously manifest its presence, including direct detection in ongoing and planned experiments. However, it is not the case considered in this thesis. The second option is significantly more poignant and pessimistic. Namely, DM particles might be stable due to the imposed discrete $\mathbb{Z}_2$ symmetry and have only gravitational interactions with themselves and the visible sector. In such a case, detecting purely gravitational dark species in laboratory experiments is rather unlikely. However, it is not necessary for dark matter to be absolutely stable as long as its lifetime is longer than the age of the Universe. A small mixing between dark vectors and the SM photons can be allowed through dark $U_X(1)$ kinetic mixing with the SM hypercharge $U_Y(1)$, i.e., $\epsilon/2B^{\mu\nu}X_{\mu\nu}$, with $B_{\mu\nu}$ being the field strength for the SM $U_Y(1)$ gauge boson B_μ. If the mixing parameter ϵ is very small, dark vectors remain stable over the timescales of the Universe's age, and there is a possibility of direct detection [169]. In addition, a cosmological signature of DM might involve a generation of non-Gaussianity in the curvature perturbations, provided that there exists a small direct coupling between dark species and the inflaton [186, 187]. Finally, let us stress that although the observed blue-tilted spectrum of vector DM suppresses isocurvature perturbations, it can enhance the formation of primordial black holes, which could potentially be tested in the future [450].

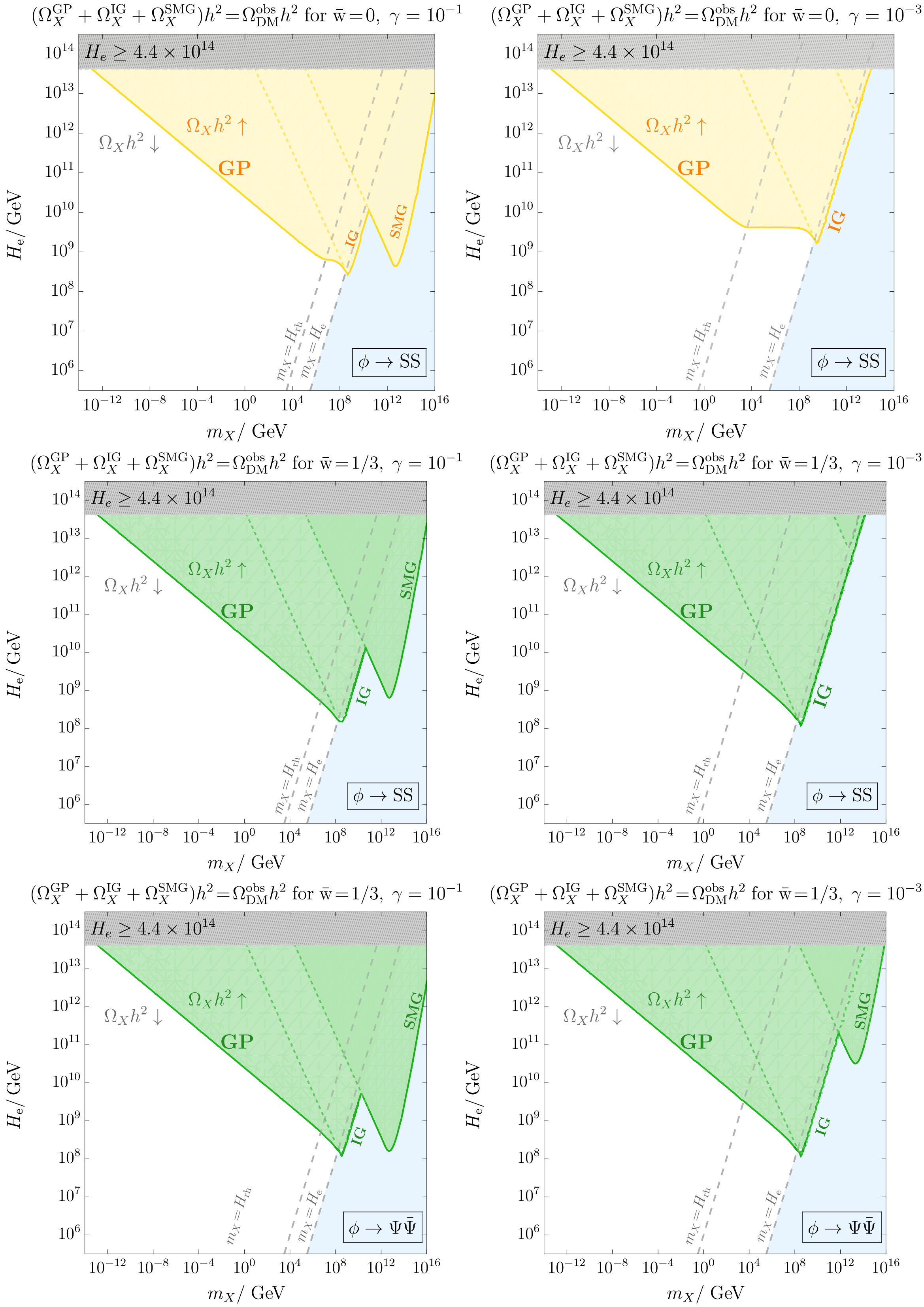

FIGURE 6.12: The $H_e - m_X$ parameter space for which gravitational processes lead to overproduction (colored regions) and underestimates the present DM abundance (white part). Here we have included all considered production mechanisms, i.e., purely gravitational production (GP), production from the inflaton field (IG), and gravitational freeze-in (SMG). Solid colored curves present the relation between H_e and m_X which for a given reheating scenario, e.o.s parameter $\bar{w}$, and reheating efficiency γ saturates $\Omega_{\rm DM}^{\rm obs}h^2$. In the blue region, DM vectors are solely produced by the IG and SMG mechanisms.

Chapter 7

Concluding remarks

This thesis is not about dark matter in the early Universe. Instead, it is about dark matter and the early Universe. These two play an equally important role in this work and are intricately coupled with each other. In particular, understanding the evolution of the dark sector requires a thorough understanding of the role of the early-Universe dynamics in dark matter production.

In this work, we have applied Occam's razor by considering the simplest possible scenario for the dark sector. Namely, we have assumed that it is comprised of spin-1 massive particles having only gravitational interactions with the visible or hidden sectors. Such a model is well motivated by the observations and appears as a relatively natural explanation for the DM puzzle. Interestingly, despite its undeniable simplicity and elegance, it also offers us an incredibly rich phenomenology. Furthermore, this scenario can be regarded as truly universal, unavoidable, and complementary to models of the primordial Universe.

The main goal of this thesis was to describe various phenomena of gravitational origin that might contribute to the creation of DM species. In the purely gravitational DM scenario, such processes might be most operative at the highest available energy scales, i.e., during and after cosmic inflation. Hence, one should first specify the background dynamics to investigate DM production in the primordial Universe. We employ the $\alpha-$attractor T model, a viable cosmic inflation model consistent with the CMB constraints. In chapter (3), we have provided a detailed description of the inflaton dynamics during the slow-roll and the oscillatory phase, assuming that a monomial function can approximate the inflaton potential after inflation. Furthermore, we have demonstrated that depending on its form quantities characterizing the inflaton dynamics, such as its effective mass or the period of oscillations, might become functions of time.

In chapter (4), we have included the effect of the inflaton interactions on its post-inflationary dynamics. Namely, we have elaborated on several perturbative but non-instantaneous reheating scenarios induced by the direct inflaton coupling to the SM species and indirect gravitational interactions mediated by massless graviton. In this part, we have developed a framework that allows us to determine the energy transfer between the inflaton and the SM sector, considering the semi-classical nature of the former. In particular, our analysis takes into account that during reheating, the inflaton coherently oscillates around the minimum of its potential. Then, it has been shown that the non-trivial, i.e., non-quadratic, inflaton potential inevitably generates a time-dependence of the *inflaton decay rate*, which generally takes a power-law form. We have presented a detailed analysis of this effect by obtaining approximate analytical solutions to the Boltzmann equations. Two different reheating scenarios have been analyzed, i.e., the **standard scenario** in which the energy injection into the SM sector is controlled by direct inflaton interactions with the visible sector, and the **mixed scenario** where reheating is initiated by gravitational processes, while direct $\phi-SM$ interactions trigger its completion. Furthermore, we have described in detail **the Higgs boson-induced scenario**, where reheating occurs due to cubic inflaton-Higgs coupling. Such interactions generate the ϕ- dependent mass term for the Higgs field, leading to a kinematical suppression of the Higgs boson production. We have demonstrated that the inflaton-induced mass of the daughter field can be another source of time-dependence of the *inflaton decay width*. A comparison between the predictions of the *massive scenario* (taking into account the non-zero Higgs mass) and the *massless Higgs model* (neglecting kinetic effects) was presented, indicating that considering the non-zero Higgs mass has an important impact on the dynamics of the visible sector.

Then, in chapter (5), we have discussed the impact of the non-standard and non-instantaneous reheating scenario on the propagation of primordial gravitational waves generated during cosmic inflation. Here, we have demonstrated that the presence of an early stiff era (before the onset of the radiation-dominated phase) might significantly enhance the signal, leading to the blue-tilted behavior of the PGWs spectrum. Furthermore, our results show that there might be a possibility of probing inflaton couplings to the SM sector by measuring a signal from the stochastic background gravitational waves of the inflationary origin. In particular, we have shown that future gravitational wave detectors might be sensitive to the weak inflaton-SM couplings, implying prolonged reheating.

Finally, in Chapter (6), we have utilized our findings to discuss the evolution of the dark sector. Three different mechanisms of gravitational origin have been studied. Namely, purely gravitational production in the expanding Universe as well as two perturbative processes involving DM creation in the inflaton background and gravitational freeze-in from the SM bath. We have demonstrated that a complete description of non-thermal DM production mechanisms only requires specifying four parameters, i.e., its mass, the inflationary Hubble scale, the equation of state of the Universe during reheating, and the reheating efficiency parameter. On the other hand, to compute the amount of dark matter species created gravitationally from the SM sector in addition one needs to know how time-evolution of the temperature, which is determined by the form of the inflaton interactions and its potential. For each mechanism, we have found regions in the parameter space providing the observed relic abundance of DM species assuming different reheating scenarios. In particular, it has been shown that purely gravitational production of light vectors is insensitive to the details of reheating. However, determining the dynamics of the reheating phase is crucial for heavy dark vectors with a mass exceeding the Hubble rate at the end of reheating. In this case, one gets very different results depending on the adopted model. Similar conclusions also applied to gravitation DM production from the inflaton field, which turns out to be independent of the details of reheating only for the quartic inflaton potential. On the other hand, gravitational freeze-in production strongly depends on the efficiency of reheating and becomes nonoperative in prolonged reheating models. Lastly, we have discussed the net effect of all these mechanisms, showing that purely gravitational particle production dominantly produces DM vectors in a vast mass range. In contrast, gravitational freeze-in might only be relevant for very heavy dark vectors with a mass exceeding the Hubble rate at the end of inflation but below the maximal temperature obtained by the thermal bath.

Now the time has come to encapsulate the title of this thesis. The role of gravitational interactions during reheating and dark matter production cannot be overestimated. Namely, gravity has manifested itself in at least three ways in this thesis. First and foremost, different phenomena of gravitational origin have been demonstrated to serve as a viable mechanism for dark matter production. It is worth emphasizing that this is not a single process that leads to the population of the dark sectors. Instead, gravity is a source of various phenomena that might occur at slightly different moments of time and have different natures but act coherently, such that the final abundance of dark species should be viewed as a net effect of all of them. In addition, gravitational interactions might also be relevant in the reheating process, initiating its onset. Hence, such interactions put the ultimate lower bound on reheating observables. Finally, gravity might also provide a tool to probe the early Universe, as the spectrum of primordial gravitational waves might reflect the reheating dynamics.

Appendix A

Cosmological parameters

Parameter	Symbol	Value
Dark energy density	$\Omega_{\Lambda,0}$	0.6889 ± 0.0056
Matter density	$\Omega_{m,0}$	0.3111 ± 0.0056
Baryon density	$\Omega_{m,0}$	0.0493 ± 0.0006
Neutrino density	$\Omega_{\nu,0}$	$\lesssim 0.003$
Spatial curvature	$\|\Omega_{k,0}\|$	$\lesssim 10^{-4}$
Radiation density	$\Omega_{\mathrm{r},0}$	$(9.02 \pm 0.21) \times 10^{-5}$
Photon density	$\Omega_{\gamma,0}$	$(5.38 \pm 0.15) \times 10^{-5}$
Hubble constant	H_0	67.74 ± 0.46 km s^{-1} Mpc^{-1}
Critical density	$\rho_{\mathrm{crit},0}$	$(8.62 \pm 0.12) \times 10^{-27}$ kg m^{-3}
Entropy density	s_0	2970 cm^{-3}
Age of the Universe	t_0	1.38×10^{10} years
Matter-dark energy equality	$t_{\mathrm{m.\Lambda.e}}$	1.02×10^{10} years
Radiation-matter equality	$t_{\mathrm{r.m.e}}$	5×10^4years
Scale factor at radiation-matter equality	$a_{\mathrm{r.m.e}}$	$\approx 2.9 \times 10^{-4}$
Scale factor at matter-dark energy equality	$a_{\mathrm{r.\Lambda.e}}$	≈ 0.77
Redshift at radiation-matter equality	$z_{\mathrm{r.m.e}}$	≈ 3340
Redshift at matter-dark energy equality	$z_{\mathrm{r.\Lambda.e}}$	≈ 0.3

TABLE A.1: Numerical values of the cosmological parameters [13].

Appendix B

Phase-space distribution function

To statistically describe a gas of particles, let us introduce the *phase-space distribution function* $f(\vec{x}, \vec{p}, t)$, containing the information about the distribution of particles in the phase-space $\{\vec{x}, \vec{p}\}$. The distribution function can be related to the macroscopic properties of a gas by summing over all particles' momentum states and weighting them by the corresponding probabilities. To that end, let us treat a gas of particles as a quantum system. According to Heisenberg's uncertainty principle, the simultaneous measurement of the particle position and momentum cannot be performed with arbitrary accuracy. Instead, in quantum mechanics, particles can be localized within a volume $V = h^3$ so that their density of states is $1/h^3$, with h being the Planck constant. Furthermore, if a particle possesses g internal degrees of freedom, e.g., the spin, then the density of states is g/h^3 ($g/(2\pi)^3$ in natural units)[226].

The probability distribution to find a particle k with position $\vec{x}_k$ and momentum $\vec{p}_k$ at a given moment of time t, i.e.,

$$d\mathcal{P} = \frac{g_k}{(2\pi)^3} d^3x_k \, d^3p_k \; f_k(\vec{x}_k, \vec{p}_k, t),$$

where g_k denotes the internal degrees of the species k.

Now let us restrict our attention to the homogeneous, i.e., position-independent, distribution function. [1] The macroscopic description of the species k can be described by the $n-$moment of its phase-space distribution function, defined as

$$M^n(f_k) := g_k \int \frac{d^3p_k}{(2\pi)^3} (\vec{p}_k)^n f_k(\vec{p}_k), \tag{B.1}$$

where we have left the time dependence of the distribution function implicit.
Specifically, the zeroth moment of f_k defines the k particle number density [222]

$$n_k := g_k \int \frac{d^3p_k}{(2\pi)^3} f_k(\vec{p}_k). \tag{B.2}$$

The above expression can be then used to define the averaged value of a quantity $\mathcal{O}_k$, i.e.,

$$\langle \mathcal{O}_k \rangle = \frac{g_k \int \frac{d^3p_k}{(2\pi)^3} \mathcal{O}_k(\vec{p}_k) f_k(\vec{p}_k)}{g_k \int \frac{d^3p_k}{(2\pi)^3} f_k(\vec{p}_k)} = \frac{g_k}{n_k} \int \frac{d^3p_k}{(2\pi)^3} \mathcal{O}_k(\vec{p}_k) f_k(\vec{p}_k). \tag{B.3}$$

Hence, the energy density of the species k can be related to the first moment of f_k as [222]

$$\rho_k := n_k \langle E_k \rangle = g_k \int \frac{d\vec{p}_k}{(2\pi)^3} E_k(|\vec{p}_k|) f_k(\vec{p}_k), \tag{B.4}$$

[1] More generic treatment can be found, e.g., in Ref.[223].

whereas the pressure is associated with second moment of f_k through the following formula [222]:

$$P_k := g_k \int \frac{d\vec{p}_k}{(2\pi)^3} \frac{|\vec{p}_k|^2}{3E_k(|\vec{p}_k|)}(\vec{p}_k) f_k(\vec{p}_k). \tag{B.5}$$

Appendix C

Boltzmann equation

The Boltzmann equation is a formal tool that allows us to investigate processes beyond the thermal equilibrium, involving the creation or destruction of particles, decoupling, freeze-out, freeze-in, etc. Hence, It is handy for tracking the evolution of particles whose distribution starts to depart from equilibrium at some point.

The particle distribution might change for two reasons, i.e., due to the Universe's expansion and particle-number changing events. Interactions among different species would alter the particle abundance only if the corresponding interaction rate Γ is small compared to the expansion rate H. Otherwise, if Γ is high, i.e., $\Gamma \gg H$, the equilibrium state is established as interactions take place with equal probability in both directions, e.g., the A, B species involved in the $A \leftrightarrow B$ process are produced with the same rate as a result of the B, A destruction. In this case, the particle abundance dilutes only due to the expansion.

The Boltzmann equation formalizes the above remarks. It can be expressed as follows [222, 451–453]

$$\mathbf{L}[f_k] = \boldsymbol{\mathcal{C}}[f_k], \tag{C.1}$$

where $\mathbf{L}[f_k]$ is the Liouville operator, whereas $\boldsymbol{\mathcal{C}}[f_k]$ is the collision operator.
The covariant version of the Liouville operator is given by [222]

$$\mathbf{L}[f_k] := p_k^\mu \frac{\partial f_k}{\partial x_k^\mu} - \Gamma^\mu_{\nu\rho}\, p_k^\nu\, p_k^\rho\, \frac{\partial f_k}{\partial p_k^\mu}. \tag{C.2}$$

The symmetries of the FLRW metric constrain the form of the distribution function. Namely, f_k can only depend on the momentum magnitude $|\vec{p}_k| = p_k$, and time t, i.e., $f_k = f_k(p_k, t)$. Hence, in the spatially-flat FLRW metric, Eq.(C.2) can be recast as

$$\mathbf{L}[f_k] := E_k \frac{\partial f_k}{\partial t} - \frac{\dot{a}}{a}\, p_k^2 \frac{\partial f_k}{\partial E_k}, \tag{C.3}$$

so that the Boltzmann equation (C.1) becomes

$$\frac{\partial f_k}{\partial t} - H(t)\, p_k \frac{\partial f_k}{\partial p_k} = \frac{\boldsymbol{\mathcal{C}}[f_k]}{E_k}. \tag{C.4}$$

C.1 Collisionless Boltzmann equation

Let us now focus on the collisionless Boltzmann equation,

$$\frac{\partial f_k}{\partial t} - H(t)\, p_k \frac{\partial f_k}{\partial p_k} = 0. \tag{C.5}$$

assuming that the collision operator $\boldsymbol{\mathcal{C}}[f_k]$ vanishes. In this case, the above equation describes the evolution of f_k in the expanding Universe when the species k does not interact with other particles. By integrating Eq.(C.5) over all the possible momenta (in a quantum phase-space), one finds

$$g_k \int \frac{d\vec{p}_k}{(2\pi)^3} \frac{\partial f_k}{\partial t} - g_k H(t) \int \frac{d\vec{p}_k}{(2\pi)^3}\, p_k \frac{\partial f_k}{\partial p_k} = 0. \tag{C.6}$$

The first integral can be written as a time derivative of the zeroth moment of f_k, see (B.2). It is convenient to integrate the second term by parts, obtaining

$$\int \frac{d\vec{p}_k}{(2\pi)^3}\, p_k \frac{\partial f_k}{\partial p_k} = -3 \int \frac{d\vec{p}_k}{(2\pi)^3} f_k, \tag{C.7}$$

where we have dropped the boundary term.
The collisionless Boltzmann equation becomes

$$\boxed{\dot{n}_k + 3Hn_k = 0,} \qquad\qquad \Longrightarrow \frac{d(na^3)}{dt} = 0. \tag{C.8}$$

Note that the above formula reflects the fact that in the absence of interactions, the number density of the species k remains conserved in a volume $V \propto a^3$.
The evolution of the energy density of the interactionless species k is obtained in the same manner. Namely, to that end one multiply Eq.(C.5) by the energy E_k and integrate over momenta,

$$g_k \int \frac{d\vec{p}_k}{(2\pi)^3} E_k \frac{\partial f_k}{\partial t} - g_k H(t) \int \frac{d\vec{p}_k}{(2\pi)^3}\, p_k E_k \frac{\partial f_k}{\partial p_k} = 0. \tag{C.9}$$

From the definition (B.4), one sees that the first term stands for the time derivative of the energy density, while the second can be recast as

$$\int \frac{d\vec{p}_k}{(2\pi)^3}\, p_k E_k \frac{\partial f_k}{\partial p_k} = -3 \int \frac{d\vec{p}_k}{(2\pi)^3} \left(E_k + \frac{p_k^2}{3E_k} \right) f_k = -3(\rho_k + p_k), \tag{C.10}$$

where in the last equality we have used Eqs.(B.4) and (B.5).
Hence, in the absence of interactions, the evolution of the k species energy density follows the following equation:

$$\boxed{\dot{\rho}_k + 3H(1 + w_k)\rho_k = 0,} \tag{C.11}$$

with $w_k \equiv p_k/\rho_k$. The above version of the Boltzmann equation implies that the energy density of matter, $w_k = 0$, redshifts as a^{-3}, whereas the energy density of radiation,$w_k = 1/3$, decreases as a^{-4}.

C.2 Collision operator

The presence of the collision operator in Eq.(C.4) might non-trivially influence the evolution of the distribution function. In particular, the number (or energy density) of a given species k changes due to energy and momentum transfer via interactions with other species. All the physics underlying these processes are encapsulated in the action of the $\boldsymbol{\mathcal{C}}$ operator on the phase-space distribution function f_k.

The most general formula for the collision operator describing the evolution of the species k

involved in the $\mathrm{I} \to \mathrm{F}$ interaction, where I(F) represents the initial (final) state composed of one or more particles labeled by the index $i(f)$, takes the following form [222, 451–453]:

$$\mathcal{C}[f_k] = \pm \frac{1}{\mathcal{S}_\mathrm{I}\,\mathcal{S}_\mathrm{F}} \int \prod_{i\in\mathrm{I},\, f\in\mathrm{F}} \left[d\widetilde{\Pi}_{k\neq i} d\widetilde{\Pi}_{k\neq f} \left(|\overline{\mathcal{M}}_{\mathrm{I}\to\mathrm{F}}|^2 \Phi_i(f_i, f_f) - |\overline{\mathcal{M}}_{\mathrm{F}\to\mathrm{I}}|^2 \Phi_f(f_i, f_f) \right) \right] \times (2\pi)^4 \delta^{(4)} \left(\sum_i p_i - \sum p_f \right), \tag{C.12}$$

with

$$d\widetilde{\Pi}_j \equiv g_j \frac{d^3 p_j}{(2\pi)^2 2E_j}, \qquad j \in \{i, f\}. \tag{C.13}$$

The overall plus sign corresponds to the k particle production, i.e., the species k belongs to the final state, $k \in \mathrm{F}$, whereas the minus sign holds for the k particle destruction, i.e., the species k belongs to the initial state, $k \in \mathrm{I}$.
Above $\mathcal{S}_\mathrm{I}(\mathcal{S}_\mathrm{F})$ denotes the symmetrization factor, i.e.,

$$\mathcal{S}_{\mathrm{I(F)}} \equiv \prod_{i(f)\,\in\,\mathrm{I(F)}} n_{i(f)}!\,, \tag{C.14}$$

which accounts for identical particles in the initial (final) state. The mean of the amplitude square, $|\overline{\mathcal{M}}_{\mathrm{I(F)}\to\mathrm{F(I)}}|^2$, is averaged over the initial and final spin states, i.e.,

$$|\overline{\mathcal{M}}_{\mathrm{I(F)}\to\mathrm{F(I)}}|^2 \equiv \prod_{i\in\mathrm{I}, f\in\mathrm{F}} \frac{1}{g_i} \frac{1}{g_f} |\mathcal{M}_{\mathrm{I(F)}\to\mathrm{F(I)}}|^2. \tag{C.15}$$

The delta function enforces the energy-momentum conservation, and finally, the phase-space factor is defined as

$$\Phi_{i(f)}(f_i, f_f) \equiv \pm f_{i(f)} (1 \pm f_{f(i)}), \tag{C.16}$$

where the plus (minus) sign is for Φ_i (Φ_f), while f_i and f_f denote distribution functions for the species in the initial and final states, respectively. Moreover, the $\pm$ sign accounts for the quantum effects, i.e., the Pauli blocking (plus sign) occurring for fermions and the Bose enhancement (minus sign) concerning bosons.

In the remaining part, we assume the CP invariance in all considered reactions. In this case, the matrix elements are the same for the $\mathrm{I} \to \mathrm{F}$ reaction and their inverses $\mathrm{F} \to \mathrm{I}$. Hence, with the assumed CP invariance, Eq.(C.17) becomes

$$\mathcal{C}[f_k] = \pm \frac{1}{\mathcal{S}_\mathrm{I}\,\mathcal{S}_\mathrm{F}} \int \prod_{i\in\mathrm{I},\, f\in\mathrm{F}} \left[d\widetilde{\Pi}_{k\neq i} d\widetilde{\Pi}_{k\neq f} |\overline{\mathcal{M}}_{\mathrm{I}\to\mathrm{F}}|^2 \Phi_{if}(f_i, f_f) \right] (2\pi)^4 \delta^{(4)} \left(\sum_i p_i - \sum p_f \right), \tag{C.17}$$

with

$$\Phi_{if}(f_i, f_f) \equiv f_i (1 \pm f_f) - f_f (1 \pm f_i). \tag{C.18}$$

Note that if all species in the initial and final states are in thermal equilibrium, their distribution functions follow the equilibrium distribution

$$f^{\text{eq}}(p_k, T) = \frac{1}{e^{\frac{E_k - \mu_k}{T}} \pm 1}, \tag{C.19}$$

where μ_k denotes the chemical potential of the species k, T is the common temperature for all particles in the equilibrium, whereas the $+\,(-)$ sign is for fermions (bosons).

The vanishing of the $\boldsymbol{\mathcal{C}}$ operator can serve as a tool to define different equilibrium states. Namely,

- if $\boldsymbol{\mathcal{C}}[f_k] = 0$ for the number conserving processes, i.e., in which the number of all species in the initial and final states are the same, the system is in **kinetic equilibrium**;
- it $\boldsymbol{\mathcal{C}}[f_k] = 0$ for the number changing interactions, i.e., in which the number of species in the initial state is not the same as in the final state, the system is in **chemical equilibrium**; in this case, in addition to the energy conservation, the chemical potential conservation:

  $$\sum_{i \in \text{I}} \mu_i = \sum_{f \in \text{F}} \mu_f, \tag{C.20}$$

  also holds.
- **thermal equilibrium** prevails when both **kinetic** and **chemical equilibrium** are present; it is characterized by the the detailed-balance equation:

  $$\prod_{i \in \text{I},\, f \in \text{F}} f_i^{\text{eq}}(1 \pm f_f^{\text{eq}}) = \prod_{i \in \text{I},\, f \in \text{F}} f_f^{\text{eq}}(1 \pm f_i^{\text{eq}}) \tag{C.21}$$

Finally, let us define the **collision** or **source term**

$$\mathcal{R}_k := g_k \int \frac{d^3 p_k}{(2\pi^3)} \frac{\boldsymbol{\mathcal{C}}[f_k]}{E_k}, \tag{C.22}$$

and the **energy gain**

$$\mathcal{E}_k := g_k \int \frac{d^3 p_k}{(2\pi^3)} \boldsymbol{\mathcal{C}}[f_k], \tag{C.23}$$

appearing on the r.h.s. of the number density (C.8) and energy density equations (C.11), respectively.

C.3 Binary processes

In this thesis, we restrict our attention exclusively to the two body scattering:

$$i\,j \leftrightarrow \text{AB}.$$

Let us consider the collision operator describing the production of the A particles, which for the above interactions takes the following form:

$$\boldsymbol{\mathcal{C}}_{ij \leftrightarrow \text{AB}} = +\frac{1}{\mathcal{S}_{ij}\, \mathcal{S}_{\text{AB}}} \int d\widetilde{\Pi}_i\, d\widetilde{\Pi}_j\, d\widetilde{\Pi}_{\text{B}} |\overline{\mathcal{M}}_{ij \leftrightarrow \text{AB}}|^2 \Phi_{ij\text{AB}} (2\pi)^4 \delta^{(4)}\left(p_i + p_j - p_{\text{A}} - p_{\text{B}}\right), \tag{C.24}$$

with

$$\Phi_{ij\mathrm{AB}} \equiv \left[f_i f_j (1 \pm f_\mathrm{A})(1 \pm f_\mathrm{B}) - f_\mathrm{A} f_\mathrm{B} (1 \pm f_i)(1 \pm f_j)\right]. \tag{C.25}$$

We focus on the class of processes in which A species is produced from particles i, j comprising thermal bath. In this case, their distribution functions f_i, f_j follows the equilibrium distribution (C.19), i.e., $f_i = f_i^{\mathrm{eq}} = f_j^{\mathrm{eq}}$. Moreover, we assume that the chemical potential is negligible and consider the low-energy limit of Eq.(C.19) so that i) the Fermi-Dirac and Bose-Einstein distributions can be well approximated by the classical Maxwell-Boltzmann distribution,

$$f_k^{\mathrm{eq}} \approx e^{-\frac{E_k}{T}}, \tag{C.26}$$

and ii) and the quantum effects (Bose enhancement and Pauli blocking) are not relevant, i.e., $1 \pm f_{ij} \approx 1$. Hence,

$$\Phi_{ij\mathrm{AB}} \approx f_i^{\mathrm{eq}} f_j^{\mathrm{eq}} - f_\mathrm{A} f_\mathrm{B} = f_A^{\mathrm{eq}} f_B^{\mathrm{eq}} - f_\mathrm{A} f_\mathrm{B}, \tag{C.27}$$

where in the second equality we have used Eq.(C.21).
Consequently, the collision operator (C.24) simplifies as

$$\begin{aligned}\mathcal{C}_{ij\leftrightarrow\mathrm{AB}} \simeq & \frac{1}{g_\mathrm{A}} \frac{1}{\mathcal{S}_{ij}\,\mathcal{S}_\mathrm{AB}} \\ & \int \frac{d\widetilde{\Pi}_i}{g_i} \frac{d\widetilde{\Pi}_j}{g_j} \frac{d\widetilde{\Pi}_\mathrm{B}}{g_\mathrm{B}} |\mathcal{M}_{ij\leftrightarrow\mathrm{AB}}|^2 (f_A^{\mathrm{eq}} f_B^{\mathrm{eq}} - f_\mathrm{A} f_\mathrm{B})(2\pi)^4 \delta^{(4)}\left(p_i + p_j - p_\mathrm{A} - p_\mathrm{B}\right).\end{aligned} \tag{C.28}$$

The collision operator (C.22) of the A species can be written as

$$\begin{aligned}\mathcal{R}_\mathrm{A} = & \frac{1}{\mathcal{S}_{ij}\,\mathcal{S}_\mathrm{AB}} \\ & \int \frac{d\widetilde{\Pi}_i}{g_i} \frac{d\widetilde{\Pi}_j}{g_j} \frac{d\widetilde{\Pi}_\mathrm{A}}{g_\mathrm{A}} \frac{d\widetilde{\Pi}_\mathrm{B}}{g_\mathrm{B}} |\mathcal{M}_{ij\leftrightarrow\mathrm{AB}}|^2 (f_A^{\mathrm{eq}} f_B^{\mathrm{eq}} - f_\mathrm{A} f_\mathrm{B})(2\pi)^4 \delta^{(4)}\left(p_i + p_j - p_\mathrm{A} - p_\mathrm{B}\right).\end{aligned} \tag{C.29}$$

Using the balance equation, one can recast the above expression as

$$\mathcal{R}_\mathrm{A} \equiv (n_A^{\mathrm{eq}} n_B^{\mathrm{eq}} - n_A n_B) \langle \sigma |v| \rangle_{AB\to ij}, \tag{C.30}$$

where the thermally-averaged cross-section is defined as [454]

$$\begin{aligned}\langle \sigma |v| \rangle_{AB\to ij} := & \frac{1}{n_A^{\mathrm{eq}} n_B^{\mathrm{eq}}} \\ & \times \frac{1}{\mathcal{S}_{ij}\,\mathcal{S}_\mathrm{AB}} \int d\Pi_i\, d\Pi_j\, d\Pi_\mathrm{A}\, d\Pi_\mathrm{B} |\mathcal{M}_{AB\leftrightarrow\mathrm{ij}}|^2 f_A^{\mathrm{eq}} f_B^{\mathrm{eq}} (2\pi)^4 \delta^{(4)}\left(p_i + p_j - p_\mathrm{A} - p_\mathrm{B}\right),\end{aligned} \tag{C.31}$$

where $d\Pi_j \equiv \frac{d^3 p_j}{(2\pi)^3 2E_j}$.
Hence,

$$\mathcal{R}_\mathrm{A} \equiv \left(1 - \frac{n_A n_B}{n_A^{\mathrm{eq}} n_B^{\mathrm{eq}}}\right) n_A^{\mathrm{eq}} n_B^{\mathrm{eq}} \langle \sigma |v| \rangle_{AB\to ij}. \tag{C.32}$$

C.3.1 Thermally-averaged cross-section

Now let us compute the thermally-averaged cross-section defined in expression (C.31). Utilizing Eq.(C.26), we get

$$\langle\sigma|v|\rangle_{AB\to ij} := \frac{1}{n_A^{\rm eq} n_B^{\rm eq}} \frac{1}{\mathcal{S}_{ij}\,\mathcal{S}_{\rm AB}} \int d\Pi_i\, d\Pi_j\, d\Pi_{\rm A}\, d\Pi_{\rm B} |\mathcal{M}_{AB\leftrightarrow {\rm ij}}|^2 (2\pi)^4 \delta^{(4)}\left(p_i + p_j - p_{\rm A} - p_{\rm B}\right) e^{-(E_A+E_b)/T}. \tag{C.33}$$

The above integral can be expressed in terms of the spin-averaged annihilation cross-section

$$\bar{\sigma}_{AB\to ij} := \frac{1}{g_A}\frac{1}{g_B}\frac{\mathcal{S}_{ij}\,\mathcal{S}_{\rm AB}}{4F(p_A,p_B)} \int d\Pi_i\, d\Pi_j |\mathcal{M}_{AB\leftrightarrow {\rm ij}}|^2 (2\pi)^4 \delta^{(4)}\left(p_i + p_j - p_{\rm A} - p_{\rm B}\right), \tag{C.34}$$

where

$$F(p_A,p_B) \equiv \sqrt{(p_A\cdot p_B)^2 - p_A^2 p_B^2}, \tag{C.35}$$

as follows,

$$\langle\sigma|v|\rangle_{AB\to ij} := \frac{g_A\, g_B}{n_A^{\rm eq} n_B^{\rm eq}} \int \frac{d^3p_A}{(2\pi)^3}\frac{d^3p_B}{(2\pi)^3}\frac{F(p_A,p_B)}{E_A E_B}\bar{\sigma}_{AB\to ij} e^{-(E_A+E_b)/T}. \tag{C.36}$$

It is instructive to use the following identity [454]:

$$\int d\Pi_A\, d\Pi_B = \frac{1}{8}\frac{1}{(2\pi)^4}\int_{(m_A+m_A)^2}^{\infty} ds \int_{\sqrt{s}}^{\infty} dE_+ \int_{\epsilon_-}^{\epsilon_+} dE_-, \tag{C.37}$$

where $s \equiv (p_A + p_B)^2$ is the Mandelstam, $E_\pm = E_A \pm E_B$, whereas

$$\epsilon_\pm = |m_A^2 - m_B^2|\frac{E_+}{s} \pm \sqrt{\frac{\lambda(s,m_A^2,m_B^2)}{s}}\sqrt{\frac{E_+^2}{s}-1}, \tag{C.38}$$

with

$$\lambda(x,y,z) \equiv x^2 + y^2 + z^2 - 2xy - 2xz - 2yz, \tag{C.39}$$

being the Källén function.

Note that if $\bar{\sigma}_{AB\to ij}$ depends only on the Mandelstam variable s, the other two integrals over $E_\pm$ can be performed analytically, leaving [454]

$$\langle\sigma|v|\rangle_{AB\to ij} := \frac{g_A\, g_B}{n_A^{\rm eq} n_B^{\rm eq}} \times \frac{T}{32\pi^4}\int_{(m_A+m_B)^2}^{\infty} ds \frac{[s-(m_A+m_B)^2][s-(m_A-m_B)^2]}{\sqrt{s}} K_1\left(\frac{\sqrt{s}}{T}\right)\bar{\sigma}_{AB\to ij}. \tag{C.40}$$

Note that if A and B particles are identical, the above expression simplifies as follows,

$$\boxed{\langle\sigma|v|\rangle_{AB\to ij} := \left(\frac{g_A}{n_A^{\rm eq}}\right)^2 \frac{T}{32\pi^4}\int_{4m_A^2}^{\infty} ds\sqrt{s}(s-4m_A^2)K_1\left(\frac{\sqrt{s}}{T}\right)\bar{\sigma}_{AB\to ij}.} \tag{C.41}$$

C.4 Freeze-in DM production

Let us apply the above results to freeze-in (FI) DM production. Such a scenario presupposes interactions between the visible and dark sectors are so weak that DM particles never reach thermal equilibrium. Hence, in this case, the evolution of the DM species, the following Boltzmann equation drives X:

$$\dot{n}_X + 3Hn_X = \mathcal{R}_X^{(\mathrm{FI})}, \tag{C.42}$$

where the collision term is given by

$$\begin{aligned}\mathcal{R}_X^{(\mathrm{FI})} &\simeq n_X^{\mathrm{eq}} n_X^{\mathrm{eq}} \langle \sigma |v| \rangle_{XX\to ij} \\ &= g_X^2 \frac{T}{32\pi^4} \int_{4m_X^2}^{\infty} ds \sqrt{s}(s - 4m_X^2) K_1\left(\frac{\sqrt{s}}{T}\right) \bar{\sigma}_{XX\to ij}.\end{aligned} \tag{C.43}$$

Appendix D

The number of relativistic degree of freedom

The total energy density of the Universe can be expressed in terms of *the number of relativistic degree of fredom* as

$$\rho = \frac{\pi^2}{30} g_{\star\rho}(T) T^4, \qquad g_{\star\rho}(T) \equiv \sum_i g_i \left(\frac{T_i}{T}\right)^4 \frac{J_\pm(x_i)}{J_-(0)}, \tag{D.1}$$

with T being the common temperature of the thermal bath constituents, while

$$J_\pm(x) \equiv \int_0^\infty \frac{\xi^2\sqrt{\xi^2+x^2}}{e^{\sqrt{\xi^2+x^2}} \pm 1} d\xi, \tag{D.2}$$

and $x_i \equiv m_i/T$, $\xi_i \equiv p_i/T$.
Utilizing the fact that $J_-(0) = \frac{\pi^4}{15}$ and separating the contribution from bosons and fermions, one gets

$$g_{\star\rho}(T) \equiv \frac{15}{\pi^4} \left[\sum_{b\,=\,\mathrm{bosons}} g_b \left(\frac{T_b}{T}\right)^4 J_\pm(x_b) + \frac{7}{8} \sum_{f\,=\,\mathrm{fermions}} g_f \left(\frac{T_f}{T}\right)^4 J_\pm(x_f) \right]. \tag{D.3}$$

Analogously, the total entropy density of relativistic species can be expressed in terms of *the number of relativistic degree of freedom in entropy* as

$$s = \frac{2\pi^2}{34} g_{\star s}(T) T^3, \tag{D.4}$$

with

$$g_{\star s}(T) \equiv \frac{15}{\pi^4} \left[\sum_{b\,=\,\mathrm{bosons}} g_b \left(\frac{T_b}{T}\right)^3 J_\pm(x_b) + \frac{7}{8} \sum_{f\,=\,\mathrm{fermions}} g_f \left(\frac{T_f}{T}\right)^3 J_\pm(x_f) \right]. \tag{D.5}$$

As the Universe cools down, different particles decouple from the thermal bath. The decoupling of species occurs when the interaction rate per particle,

$$\Gamma \equiv n^{\mathrm{eq}} \langle \sigma |v| \rangle, \tag{D.6}$$

drops below the expansion rate, i.e., when

$$\Gamma \lesssim H. \tag{D.7}$$

Particles can decouple being relativistic or non-relativistic, comprising *hot* or *cold relics*, respectively.

Within the SM of particle species, at high temperatures, i.e., $T \gtrsim 100$ GeV, all species were relativistic and belonged to the thermal bath. Hence,

$$\begin{aligned}g_{\star\rho}(T \gtrsim 100\,\mathrm{GeV}) &= g_{\star\rho}(T \gtrsim 100\,\mathrm{GeV}) \\ &= 2 + (3\times 3) + (8\times 2) + 1 + \frac{7}{8}\left[(6\times 12) + (3\times 4) + (3\times 2)\right] = 107.75,\end{aligned} \tag{D.8}$$

where we have included two polarization states of photons γ, three polarization states of massive gauge bosons $W^{\pm}, Z^{0}$, two internal degrees of freedom of eight massless gluons, the Higgs field, and two spin-1 states of six flavors of quarks multiplied by the three colors and the factor of two for the antiparticles, two spin states of 6 charged leptons and their antiparticles, and two one internal degree of freedom for three neutrinos and their antiparticles.
Then, when the temperature drops to ~ 30 GeV, the top quark decouples first. Both numbers reduce to

$$g_{\star\rho}(T \gtrsim 30\,\mathrm{GeV}) = g_{\star\rho}(T \gtrsim 30\,\mathrm{GeV}) = 107.75 - \frac{7}{8}\times 12 = 96.25. \tag{D.9}$$

The Higgs boson, together with three massive gauge bosons, decouple next. At the temperature ~ 10 GeV, one finds

$$g_{\star\rho}(T \gtrsim 10\,\mathrm{GeV}) = g_{\star\rho}(T \gtrsim 30\,\mathrm{GeV}) = 96.25 - (3\times 3) - 1 = 86.25. \tag{D.10}$$

Shortly after that moment, the decoupling of the bottom and charm quarks occur, followed by the annihilation of the tau lepton. Then, around $\sim 150\,\mathrm{MeV}$, the QCD phase transition occurs. After that, the total number of relativistic degrees of freedom is a sum of the three types of pions (spin-0 particles), electrons, muons, neutrinos, and photons

$$g_{\star\rho}(T \lesssim T_{\mathrm{QCD}}) = g_{\star s}(T \lesssim T_{\mathrm{QCD}}) = 2 + 3 + \frac{7}{8}\left[(4\times 2) + (3\times 2)\right] = 17.25. \tag{D.11}$$

Subsequently, pions and muons decouple, leading to

$$g_{\star\rho}(T \sim 10\,\mathrm{MeV}) = g_{\star s}(T \sim 10\,\mathrm{MeV})) = 2 + \frac{7}{8}\left[(2\times 2) + (3\times 2)\right] = 10.75. \tag{D.12}$$

Finally, when the temperature of the Universe reaches ~ 1 MeV, SM neutrinos decoupled as hot relics, which to the slightly different evolution of $g_{\star\rho}$ and $g_{\star s}$. Namely, shortly after neutrino decoupling, electrons, and positrons start to annihilate into the pairs of photons. Their energy and entropy are injected into photons but not into neutrinos which are no longer in the thermal bath. Thermal equilibrium is maintained in this process, and the entropy density is conserved separately for particles comprising the thermal bath and decoupled neutrinos. Using the fact that $g_{\star s}a^3T^3$ =const., before, i.e., $T_1 \gtrsim m_e$, and after, i.e.,$T_2 \lesssim m_e$ electron-positron decoupling, one finds for the thermal bath

$$\frac{11}{2}a_1^3T_{\gamma,1}^3 = 2a_2^3T_{\gamma,2}^3, \tag{D.13}$$

and for the neutrino background

$$a_1^3T_{\nu,1}^3 = a_2^3T_{\nu,2}^3, \tag{D.14}$$

which, in turn, implies that at late times, i.e., $T \lesssim m_e$, neutrino temperature, T_ν, is slightly lower than the photon temperature, T_γ, i.e.,

$$T_\nu = \left(\frac{4}{11}\right)^{1/3} T_\gamma. \tag{D.15}$$

At temperatures below the electron mass threshold, the numbers of relativistic degrees of freedom are different,

$$g_{\star\rho} = 2 + \frac{7}{8} \times 2 \times N_{\text{eff}} \times \left(\frac{4}{11}\right)^{4/3}, \tag{D.16}$$

$$g_{\star s} = 2 + \frac{7}{8} \times 2 \times N_{\text{eff}} \times \left(\frac{4}{11}\right), \tag{D.17}$$

where the *number of neutrino species* N_{eff} accounts for the non-instantaneous decoupling of the SM neutrinos and is equal to $N_{\text{eff}} \simeq 3.046$.

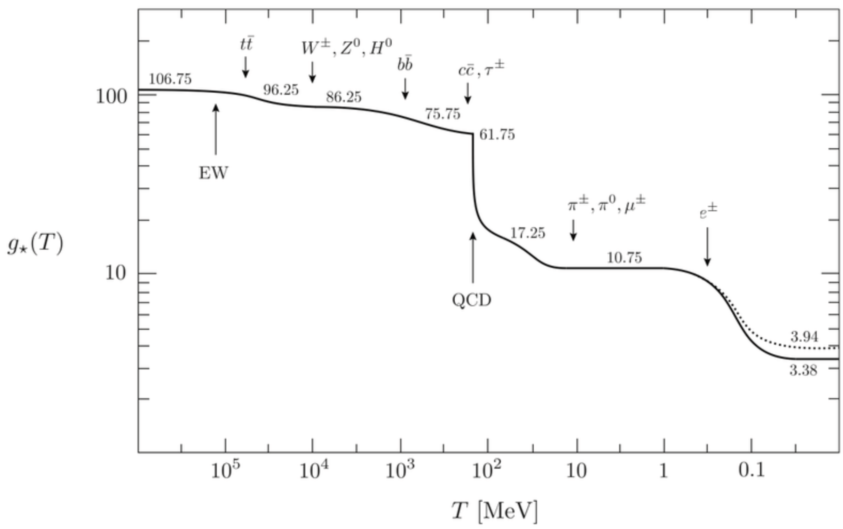

FIGURE D.1: The evolution of the number of relativistic degree of freedom $g_{\star\rho}$ (solid curve) and the number of relativistic degree of freedom in entropy $g_{\star s}$ (solid curve).
Image credit: Daniel Baumann, Cosmology

References

[1] B. Barman, A. Ghoshal, B. Grzadkowski and A. Socha, *Measuring Inflaton Couplings via Primordial Gravitational Waves*, 2305.00027.

[2] A. Ahmed, B. Grzadkowski and A. Socha, *Higgs boson induced reheating and ultraviolet frozen-in dark matter*, *JHEP* **02** (2023) 196 [2207.11218].

[3] A. Ahmed, B. Grzadkowski and A. Socha, *Implications of time-dependent inflaton decay on reheating and dark matter production*, *Phys. Lett. B* **831** (2022) 137201 [2111.06065].

[4] A. Ahmed, B. Grzadkowski and A. Socha, *Gravitational production of vector dark matter*, *JHEP* **08** (2020) 059 [2005.01766].

[5] A. Ahmed, B. Grzadkowski and A. Socha, *Higgs Boson-Induced Reheating and Dark Matter Production*, *Symmetry* **14** (2022) 306.

[6] A. Ahmed, B. Grzadkowski and A. Socha, *Production of Purely Gravitational Vector Dark Matter*, *Acta Phys. Polon. B* **50** (2019) 1809.

[7] V.C. Rubin and W.K. Ford, Jr., *Rotation of the Andromeda Nebula from a Spectroscopic Survey of Emission Regions*, *Astrophys. J.* **159** (1970) 379.

[8] Particle Data Group collaboration, *Review of Particle Physics*, *Phys. Rev. D* **98** (2018) 030001.

[9] B. Gold et al., *Seven-Year Wilkinson Microwave Anisotropy Probe (WMAP) Observations: Galactic Foreground Emission*, *Astrophys. J. Suppl.* **192** (2011) 15 [1001.4555].

[10] Planck collaboration, *Planck 2013 results. XVI. Cosmological parameters*, *Astron. Astrophys.* **571** (2014) A16 [1303.5076].

[11] D. Clowe, M. Bradac, A.H. Gonzalez, M. Markevitch, S.W. Randall, C. Jones et al., *A direct empirical proof of the existence of dark matter*, *Astrophys. J. Lett.* **648** (2006) L109 [astro-ph/0608407].

[12] E. Hubble, *A relation between distance and radial velocity among extra-galactic nebulae*, *Proc. Nat. Acad. Sci.* **15** (1929) 168.

[13] Planck collaboration, *Planck 2018 results. VI. Cosmological parameters*, *Astron. Astrophys.* **641** (2020) A6 [1807.06209].

[14] G. Bertone, D. Hooper and J. Silk, *Particle dark matter: Evidence, candidates and constraints*, *Phys. Rept.* **405** (2005) 279 [hep-ph/0404175].

[15] G. Bertone and D. Hooper, *History of dark matter*, *Rev. Mod. Phys.* **90** (2018) 045002 [1605.04909].

[16] T. Lin, *Dark matter models and direct detection*, *PoS* **333** (2019) 009 [1904.07915].

[17] B. Carr and F. Kuhnel, *Primordial black holes as dark matter candidates*, *SciPost Phys. Lect. Notes* **48** (2022) 1 [2110.02821].

[18] A.M. Green, *Dark matter in astrophysics/cosmology*, *SciPost Phys. Lect. Notes* **37** (2022) 1 [2109.05854].

[19] Y. Mambrini, *Particles in the Dark Universe*, Springer Ed. (9, 2021), 10.1007/978-3-030-78139-2.

[20] B. Thomson, *Baltimore Lectures on Molecular Dynamics and the Wave Theory of Light* (03, 2012), 10.1017/CBO9780511694523.

[21] H. Poincare, *The Milky Way and the Theory of Gases*, *Popular Astronomy* **14** (1906) 475.

[22] J.H. Oort, *The force exerted by the stellar system in the direction perpendicular to the galactic plane and some related problems*, **6** (1932) 249.

[23] F. Zwicky, *Die Rotverschiebung von extragalaktischen Nebeln*, *Helv. Phys. Acta* **6** (1933) 110.

[24] R.A. Alpher and R.C. Herman, *On the Relative Abundance of the Elements*, *Phys. Rev.* **74** (1948) 1737.

[25] A.A. Penzias and R.W. Wilson, *A Measurement of excess antenna temperature at 4080-Mc/s*, *Astrophys. J.* **142** (1965) 419.

[26] D.J. Fixsen, *The Temperature of the Cosmic Microwave Background*, *Astrophys. J.* **707** (2009) 916 [0911.1955].

[27] W. Hu and S. Dodelson, *Cosmic Microwave Background Anisotropies*, *Ann. Rev. Astron. Astrophys.* **40** (2002) 171 [astro-ph/0110414].

[28] T. Treu, *Strong Lensing by Galaxies*, *Ann. Rev. Astron. Astrophys.* **48** (2010) 87 [1003.5567].

[29] M. Kilbinger, *Cosmology with cosmic shear observations: a review*, *Rept. Prog. Phys.* **78** (2015) 086901 [1411.0115].

[30] N. Kaiser and G. Squires, *Mapping the dark matter with weak gravitational lensing*, *Astrophys. J.* **404** (1993) 441.

[31] N. Kaiser, G. Squires and T.J. Broadhurst, *A Method for weak lensing observations*, *Astrophys. J.* **449** (1995) 460 [astro-ph/9411005].

[32] J.A. Tyson, G.P. Kochanski and I.P. Dell'Antonio, *Detailed mass map of CL0024+1654 from strong lensing*, *Astrophys. J. Lett.* **498** (1998) L107 [astro-ph/9801193].

[33] B. Paczynski, *Gravitational microlensing by the galactic halo*, *Astrophys. J.* **304** (1986) 1.

[34] Macho collaboration, *MACHO project limits on black hole dark matter in the 1-30 solar mass range*, *Astrophys. J. Lett.* **550** (2001) L169 [astro-ph/0011506].

[35] MACHO collaboration, *The MACHO project: Microlensing results from 5.7 years of LMC observations*, *Astrophys. J.* **542** (2000) 281 [astro-ph/0001272].

[36] EROS-2 collaboration, *Limits on the Macho Content of the Galactic Halo from the EROS-2 Survey of the Magellanic Clouds*, *Astron. Astrophys.* **469** (2007) 387 [astro-ph/0607207].

[37] E. Aubourg et al., *Evidence for gravitational microlensing by dark objects in the galactic halo*, *Nature* **365** (1993) 623.

[38] A. Udalski, M. Szymanski, J. Kaluzny, M. Kubiak, W. Krzeminski, M. Mateo et al., *The optical gravitational lensing experiment. Discovery of the first candidate microlensing event in the direction of the Galactic Bulge*, *Acta Astron.* **43** (1993) 289.

[39] L. Wyrzykowski et al., *Black Hole, Neutron Star and White Dwarf Candidates from Microlensing with OGLE-III*, *Mon. Not. Roy. Astron. Soc.* **458** (2016) 3012 [1509.04899].

[40] DES collaboration, *Dark Energy Survey Year 1 Results: Methodology and Projections for Joint Analysis of Galaxy Clustering, Galaxy Lensing, and CMB Lensing Two-point Functions*, *Phys. Rev. D* **99** (2019) 023508 [1802.05257].

[41] DES collaboration, *Dark Energy Survey Year 3 results: Cosmological constraints from galaxy clustering and weak lensing*, *Phys. Rev. D* **105** (2022) 023520 [2105.13549].

[42] K. Griest, *Galactic Microlensing as a Method of Detecting Massive Compact Halo Objects*, **366** (1991) 412.

[43] B. Carr and F. Kuhnel, *Primordial Black Holes as Dark Matter: Recent Developments*, *Ann. Rev. Nucl. Part. Sci.* **70** (2020) 355 [2006.02838].

[44] Y.B. Zel'dovich and I.D. Novikov, *The Hypothesis of Cores Retarded during Expansion and the Hot Cosmological Model*, *Soviet Astron. AJ (Engl. Transl.),* **10** (1967) 602.

[45] S. Hawking, *Gravitationally collapsed objects of very low mass*, *Mon. Not. Roy. Astron. Soc.* **152** (1971) 75.

[46] B.J. Carr and S.W. Hawking, *Black holes in the early Universe*, *Mon. Not. Roy. Astron. Soc.* **168** (1974) 399.

[47] S.W. Hawking, *Black hole explosions*, *Nature* **248** (1974) 30.

[48] G.F. Chapline, *Cosmological effects of primordial black holes*, *Nature* **253** (1975) 251.

[49] P. Meszaros, *Primeval black holes and galaxy formation*, *Astron. Astrophys.* **38** (1975) 5.

[50] B. Carr, K. Kohri, Y. Sendouda and J. Yokoyama, *Constraints on primordial black holes*, *Rept. Prog. Phys.* **84** (2021) 116902 [2002.12778].

[51] M. Milgrom, *A Modification of the Newtonian dynamics as a possible alternative to the hidden mass hypothesis*, *Astrophys. J.* **270** (1983) 365.

[52] P. van Dokkum et al., *A galaxy lacking dark matter*, *Nature* **555** (2018) 629 [1803.10237].

[53] S. Dodelson, *The Real Problem with MOND*, *Int. J. Mod. Phys. D* **20** (2011) 2749 [1112.1320].

[54] J.D. Bekenstein, *Relativistic gravitation theory for the MOND paradigm*, *Phys. Rev. D* **70** (2004) 083509 [astro-ph/0403694].

[55] S. Boran, S. Desai, E.O. Kahya and R.P. Woodard, *GW170817 Falsifies Dark Matter Emulators*, *Phys. Rev. D* **97** (2018) 041501 [1710.06168].

[56] E.P. Verlinde, *On the Origin of Gravity and the Laws of Newton*, *JHEP* **04** (2011) 029 [1001.0785].

[57] E.P. Verlinde, *Emergent Gravity and the Dark Universe*, *SciPost Phys.* **2** (2017) 016 [1611.02269].

[58] K. Pardo, *Testing Emergent Gravity with Isolated Dwarf Galaxies*, *JCAP* **12** (2020) 012 [1706.00785].

[59] Super-Kamiokande collaboration, *Evidence for oscillation of atmospheric neutrinos*, *Phys. Rev. Lett.* **81** (1998) 1562 [hep-ex/9807003].

[60] SNO collaboration, *Direct evidence for neutrino flavor transformation from neutral current interactions in the Sudbury Neutrino Observatory*, *Phys. Rev. Lett.* **89** (2002) 011301 [nucl-ex/0204008].

[61] KamLAND collaboration, *First results from KamLAND: Evidence for reactor anti-neutrino disappearance*, *Phys. Rev. Lett.* **90** (2003) 021802 [hep-ex/0212021].

[62] J. Lesgourgues and S. Pastor, *Neutrino mass from Cosmology*, *Adv. High Energy Phys.* **2012** (2012) 608515 [1212.6154].

[63] F. Capozzi, E. Di Valentino, E. Lisi, A. Marrone, A. Melchiorri and A. Palazzo, *Global constraints on absolute neutrino masses and their ordering*, *Phys. Rev. D* **95** (2017) 096014 [2003.08511].

[64] S. Tremaine and J.E. Gunn, *Dynamical Role of Light Neutral Leptons in Cosmology*, *Phys. Rev. Lett.* **42** (1979) 407.

[65] J. Alvey, N. Sabti, V. Tiki, D. Blas, K. Bondarenko, A. Boyarsky et al., *New constraints on the mass of fermionic dark matter from dwarf spheroidal galaxies*, *Mon. Not. Roy. Astron. Soc.* **501** (2021) 1188 [2010.03572].

[66] T. Kobayashi, R. Murgia, A. De Simone, V. Iršič and M. Viel, *Lyman-α constraints on ultralight scalar dark matter: Implications for the early and late universe*, *Phys. Rev. D* **96** (2017) 123514 [1708.00015].

[67] E. Armengaud, N. Palanque-Delabrouille, C. Yèche, D.J.E. Marsh and J. Baur, *Constraining the mass of light bosonic dark matter using SDSS Lyman-α forest*, *Mon. Not. Roy. Astron. Soc.* **471** (2017) 4606 [1703.09126].

[68] E.W. Kolb, D.J.H. Chung and A. Riotto, *WIMPzillas!*, *AIP Conf. Proc.* **484** (1999) 91 [hep-ph/9810361].

[69] R. Ding and Y. Liao, *Spin 3/2 Particle as a Dark Matter Candidate: an Effective Field Theory Approach*, *JHEP* **04** (2012) 054 [1201.0506].

[70] C.-F. Chang, X.-G. He and J. Tandean, *Exploring Spin-3/2 Dark Matter with Effective Higgs Couplings*, *Phys. Rev. D* **96** (2017) 075026 [1704.01904].

[71] M.A.G. Garcia, Y. Mambrini, K.A. Olive and S. Verner, *Case for decaying spin- 3/2 dark matter*, *Phys. Rev. D* **102** (2020) 083533 [2006.03325].

[72] K. Aoki and K.-i. Maeda, *Condensate of Massive Graviton and Dark Matter*, *Phys. Rev. D* **97** (2018) 044002 [1707.05003].

[73] L. Marzola, M. Raidal and F.R. Urban, *Oscillating Spin-2 Dark Matter*, *Phys. Rev. D* **97** (2018) 024010 [1708.04253].

[74] J.M. Armaleo, D. López Nacir and F.R. Urban, *Binary pulsars as probes for spin-2 ultralight dark matter*, *JCAP* **01** (2020) 053 [1909.13814].

[75] M. Asorey and D. García-Álvarez, *Higher spin dark matter*, *AIP Conf. Proc.* **1241** (2010) 1192.

[76] M. Kulaxizi and R. Rahman, *Higher-Spin Modes in a Domain-Wall Universe*, *JHEP* **10** (2014) 193 [1409.1942].

[77] S. Alexander, L. Jenks and E. McDonough, *Higher spin dark matter*, *Phys. Lett. B* **819** (2021) 136436 [2010.15125].

[78] A. Higuchi, *Forbidden Mass Range for Spin-2 Field Theory in De Sitter Space-time*, *Nucl. Phys. B* **282** (1987) 397.

[79] E.G.M. Ferreira, *Ultra-light dark matter*, *Astron. Astrophys. Rev.* **29** (2021) 7 [2005.03254].

[80] W. Hu, R. Barkana and A. Gruzinov, *Cold and fuzzy dark matter*, *Phys. Rev. Lett.* **85** (2000) 1158 [astro-ph/0003365].

[81] L. Hui, J.P. Ostriker, S. Tremaine and E. Witten, *Ultralight scalars as cosmological dark matter*, *Phys. Rev. D* **95** (2017) 043541 [1610.08297].

[82] L. Berezhiani and J. Khoury, *Theory of dark matter superfluidity*, *Phys. Rev. D* **92** (2015) 103510 [1507.01019].

[83] R.D. Peccei and H.R. Quinn, *CP Conservation in the Presence of Instantons*, *Phys. Rev. Lett.* **38** (1977) 1440.

[84] R.D. Peccei and H.R. Quinn, *Constraints Imposed by CP Conservation in the Presence of Instantons*, *Phys. Rev. D* **16** (1977) 1791.

[85] S. Weinberg, *A New Light Boson?*, *Phys. Rev. Lett.* **40** (1978) 223.

[86] F. Wilczek, *Problem of Strong P and T Invariance in the Presence of Instantons*, *Phys. Rev. Lett.* **40** (1978) 279.

[87] I.G. Irastorza, *An introduction to axions and their detection*, *SciPost Phys. Lect. Notes* **45** (2022) 1 [2109.07376].

[88] A. Arvanitaki, S. Dimopoulos, S. Dubovsky, N. Kaloper and J. March-Russell, *String Axiverse*, *Phys. Rev. D* **81** (2010) 123530 [0905.4720].

[89] A. Boyarsky, M. Drewes, T. Lasserre, S. Mertens and O. Ruchayskiy, *Sterile neutrino Dark Matter*, *Prog. Part. Nucl. Phys.* **104** (2019) 1 [1807.07938].

[90] S. Dodelson and L.M. Widrow, *Sterile-neutrinos as dark matter*, *Phys. Rev. Lett.* **72** (1994) 17 [hep-ph/9303287].

[91] X.-D. Shi and G.M. Fuller, *A New dark matter candidate: Nonthermal sterile neutrinos*, *Phys. Rev. Lett.* **82** (1999) 2832 [astro-ph/9810076].

[92] K. Abazajian, G.M. Fuller and M. Patel, *Sterile neutrino hot, warm, and cold dark matter*, *Phys. Rev. D* **64** (2001) 023501 [astro-ph/0101524].

[93] T. Asaka, S. Blanchet and M. Shaposhnikov, *The nuMSM, dark matter and neutrino masses*, *Phys. Lett. B* **631** (2005) 151 [hep-ph/0503065].

[94] T. Asaka and M. Shaposhnikov, *The νMSM, dark matter and baryon asymmetry of the universe*, *Phys. Lett. B* **620** (2005) 17 [hep-ph/0505013].

[95] R.N. Mohapatra and J.C. Pati, *Left-Right Gauge Symmetry and an Isoconjugate Model of CP Violation*, *Phys. Rev. D* **11** (1975) 566.

[96] A. Kusenko, F. Takahashi and T.T. Yanagida, *Dark Matter from Split Seesaw*, *Phys. Lett. B* **693** (2010) 144 [1006.1731].

[97] T. Asaka, M. Laine and M. Shaposhnikov, *Lightest sterile neutrino abundance within the nuMSM*, *JHEP* **01** (2007) 091 [hep-ph/0612182].

[98] L. Lello and D. Boyanovsky, *Cosmological Implications of Light Sterile Neutrinos produced after the QCD Phase Transition*, *Phys. Rev. D* **91** (2015) 063502 [1411.2690].

[99] F. Bezrukov, D. Gorbunov and M. Shaposhnikov, *On initial conditions for the Hot Big Bang*, *JCAP* **06** (2009) 029 [0812.3622].

[100] L. Lello, D. Boyanovsky and R.D. Pisarski, *Production of heavy sterile neutrinos from vector boson decay at electroweak temperatures*, *Phys. Rev. D* **95** (2017) 043524 [1609.07647].

[101] M. Shaposhnikov and I. Tkachev, *The nuMSM, inflation, and dark matter*, *Phys. Lett. B* **639** (2006) 414 [hep-ph/0604236].

[102] K. Petraki and A. Kusenko, *Dark-matter sterile neutrinos in models with a gauge singlet in the Higgs sector*, *Phys. Rev. D* **77** (2008) 065014 [0711.4646].

[103] M. Pospelov, A. Ritz and M.B. Voloshin, *Secluded WIMP Dark Matter*, *Phys. Lett. B* **662** (2008) 53 [0711.4866].

[104] C. Boehm and P. Fayet, *Scalar dark matter candidates*, *Nucl. Phys. B* **683** (2004) 219 [hep-ph/0305261].

[105] J.L. Feng, H. Tu and H.-B. Yu, *Thermal Relics in Hidden Sectors*, *JCAP* **10** (2008) 043 [0808.2318].

[106] N. Arkani-Hamed, D.P. Finkbeiner, T.R. Slatyer and N. Weiner, *A Theory of Dark Matter*, *Phys. Rev. D* **79** (2009) 015014 [0810.0713].

[107] L. Roszkowski, E.M. Sessolo and S. Trojanowski, *WIMP dark matter candidates and searches—current status and future prospects*, *Rept. Prog. Phys.* **81** (2018) 066201 [1707.06277].

[108] J.L. Feng, *The WIMP Paradigm: Theme and Variations*, in *Les Houches summer school on Dark Matter*, 12, 2022 [2212.02479].

[109] K. Griest and M. Kamionkowski, *Unitarity Limits on the Mass and Radius of Dark Matter Particles*, *Phys. Rev. Lett.* **64** (1990) 615.

[110] B.W. Lee and S. Weinberg, *Cosmological Lower Bound on Heavy Neutrino Masses*, *Phys. Rev. Lett.* **39** (1977) 165.

[111] G. Steigman and M.S. Turner, *Cosmological Constraints on the Properties of Weakly Interacting Massive Particles*, *Nucl. Phys. B* **253** (1985) 375.

[112] Q.-H. Cao, C.-R. Chen, C.S. Li and H. Zhang, *Effective Dark Matter Model: Relic density, CDMS II, Fermi LAT and LHC*, *JHEP* **08** (2011) 018 [0912.4511].

[113] M. Beltran, D. Hooper, E.W. Kolb, Z.A.C. Krusberg and T.M.P. Tait, *Maverick dark matter at colliders*, *JHEP* **09** (2010) 037 [1002.4137].

[114] Y. Bai, P.J. Fox and R. Harnik, *The Tevatron at the Frontier of Dark Matter Direct Detection*, *JHEP* **12** (2010) 048 [1005.3797].

[115] R.J. Gaitskell, *Direct detection of dark matter*, *Ann. Rev. Nucl. Part. Sci.* **54** (2004) 315.

[116] A.H.G. Peter, V. Gluscevic, A.M. Green, B.J. Kavanagh and S.K. Lee, *WIMP physics with ensembles of direct-detection experiments*, *Phys. Dark Univ.* **5-6** (2014) 45 [1310.7039].

[117] T. Marrodán Undagoitia and L. Rauch, *Dark matter direct-detection experiments*, *J. Phys. G* **43** (2016) 013001 [1509.08767].

[118] J. Conrad, J. Cohen-Tanugi and L.E. Strigari, *WIMP searches with gamma rays in the Fermi era: challenges, methods and results*, *J. Exp. Theor. Phys.* **121** (2015) 1104 [1503.06348].

[119] J.M. Gaskins, *A review of indirect searches for particle dark matter*, *Contemp. Phys.* **57** (2016) 496 [1604.00014].

[120] D.J.H. Chung, E.W. Kolb and A. Riotto, *Superheavy dark matter*, *Phys. Rev. D* **59** (1998) 023501 [hep-ph/9802238].

[121] D.J.H. Chung, E.W. Kolb and A. Riotto, *Nonthermal supermassive dark matter*, *Phys. Rev. Lett.* **81** (1998) 4048 [hep-ph/9805473].

[122] L. Kofman, A.D. Linde and A.A. Starobinsky, *Reheating after inflation*, *Phys. Rev. Lett.* **73** (1994) 3195 [hep-th/9405187].

[123] S.Y. Khlebnikov and I.I. Tkachev, *Classical decay of inflaton*, *Phys. Rev. Lett.* **77** (1996) 219 [hep-ph/9603378].

[124] L.A. Kofman, *The Origin of matter in the universe: Reheating after inflation*, 5, 1996 [astro-ph/9605155].

[125] L. Kofman, A.D. Linde and A.A. Starobinsky, *Towards the theory of reheating after inflation*, *Phys. Rev. D* **56** (1997) 3258 [hep-ph/9704452].

[126] J.H. Traschen and R.H. Brandenberger, *Particle Production During Out-of-equilibrium Phase Transitions*, *Phys. Rev. D* **42** (1990) 2491.

[127] Y. Shtanov, J.H. Traschen and R.H. Brandenberger, *Universe reheating after inflation*, *Phys. Rev. D* **51** (1995) 5438 [hep-ph/9407247].

[128] F.E. Schunck and E.W. Mielke, *General relativistic boson stars*, *Class. Quant. Grav.* **20** (2003) R301 [0801.0307].

[129] H. Zhang, *Axion Stars*, *Symmetry* **12** (2019) 25 [1810.11473].

[130] A. Kusenko and M.E. Shaposhnikov, *Supersymmetric Q balls as dark matter*, *Phys. Lett. B* **418** (1998) 46 [hep-ph/9709492].

[131] M.G. Alford, A. Schmitt, K. Rajagopal and T. Schäfer, *Color superconductivity in dense quark matter*, *Rev. Mod. Phys.* **80** (2008) 1455 [0709.4635].

[132] Y. Bai, A.J. Long and S. Lu, *Dark Quark Nuggets*, *Phys. Rev. D* **99** (2019) 055047 [1810.04360].

[133] D.P. Finkbeiner and N. Weiner, *Exciting Dark Matter and the INTEGRAL/SPI 511 keV signal*, *Phys. Rev. D* **76** (2007) 083519 [astro-ph/0702587].

[134] J.L. Feng and J. Kumar, *The WIMPless Miracle: Dark-Matter Particles without Weak-Scale Masses or Weak Interactions*, *Phys. Rev. Lett.* **101** (2008) 231301 [0803.4196].

[135] K. Griest and D. Seckel, *Three exceptions in the calculation of relic abundances*, *Phys. Rev. D* **43** (1991) 3191.

[136] R.T. D'Agnolo and J.T. Ruderman, *Light Dark Matter from Forbidden Channels*, *Phys. Rev. Lett.* **115** (2015) 061301 [1505.07107].

[137] Y. Hochberg, E. Kuflik, T. Volansky and J.G. Wacker, *Mechanism for Thermal Relic Dark Matter of Strongly Interacting Massive Particles*, *Phys. Rev. Lett.* **113** (2014) 171301 [1402.5143].

[138] Y. Hochberg, E. Kuflik, H. Murayama, T. Volansky and J.G. Wacker, *Model for Thermal Relic Dark Matter of Strongly Interacting Massive Particles*, *Phys. Rev. Lett.* **115** (2015) 021301 [1411.3727].

[139] D.E. Kaplan, M.A. Luty and K.M. Zurek, *Asymmetric Dark Matter*, *Phys. Rev. D* **79** (2009) 115016 [0901.4117].

[140] K.M. Zurek, *Asymmetric Dark Matter: Theories, Signatures, and Constraints*, *Phys. Rept.* **537** (2014) 91 [1308.0338].

[141] R.T. D'Agnolo, D. Pappadopulo and J.T. Ruderman, *Fourth Exception in the Calculation of Relic Abundances*, *Phys. Rev. Lett.* **119** (2017) 061102 [1705.08450].

[142] L.J. Hall, K. Jedamzik, J. March-Russell and S.M. West, *Freeze-In Production of FIMP Dark Matter*, *JHEP* **03** (2010) 080 [0911.1120].

[143] F. Elahi, C. Kolda and J. Unwin, *UltraViolet Freeze-in*, *JHEP* **03** (2015) 048 [1410.6157].

[144] V. Silveira and A. Zee, *SCALAR PHANTOMS*, *Phys. Lett. B* **161** (1985) 136.

[145] J. McDonald, *Gauge singlet scalars as cold dark matter*, Phys. Rev. D **50** (1994) 3637 [hep-ph/0702143].

[146] C.P. Burgess, M. Pospelov and T. ter Veldhuis, *The Minimal model of nonbaryonic dark matter: A Singlet scalar*, Nucl. Phys. B **619** (2001) 709 [hep-ph/0011335].

[147] B. Kors and P. Nath, *Aspects of the Stueckelberg extension*, JHEP **07** (2005) 069 [hep-ph/0503208].

[148] M. Pospelov, A. Ritz and M.B. Voloshin, *Bosonic super-WIMPs as keV-scale dark matter*, Phys. Rev. D **78** (2008) 115012 [0807.3279].

[149] J. Redondo and M. Postma, *Massive hidden photons as lukewarm dark matter*, JCAP **02** (2009) 005 [0811.0326].

[150] E. Babichev, L. Marzola, M. Raidal, A. Schmidt-May, F. Urban, H. Veermäe et al., *Bigravitational origin of dark matter*, Phys. Rev. D **94** (2016) 084055 [1604.08564].

[151] E. Babichev, L. Marzola, M. Raidal, A. Schmidt-May, F. Urban, H. Veermäe et al., *Heavy spin-2 Dark Matter*, JCAP **09** (2016) 016 [1607.03497].

[152] M. Garny, M. Sandora and M.S. Sloth, *Planckian Interacting Massive Particles as Dark Matter*, Phys. Rev. Lett. **116** (2016) 101302 [1511.03278].

[153] Y. Tang and Y.-L. Wu, *Pure Gravitational Dark Matter, Its Mass and Signatures*, Phys. Lett. B **758** (2016) 402 [1604.04701].

[154] T. Bringmann, P.F. Depta, M. Hufnagel, J.T. Ruderman and K. Schmidt-Hoberg, *Dark Matter from Exponential Growth*, Phys. Rev. Lett. **127** (2021) 191802 [2103.16572].

[155] A. Hryczuk and M. Laletin, *Dark matter freeze-in from semi-production*, JHEP **06** (2021) 026 [2104.05684].

[156] J.L. Feng, A. Rajaraman and F. Takayama, *Superweakly interacting massive particles*, Phys. Rev. Lett. **91** (2003) 011302 [hep-ph/0302215].

[157] N. Bernal, M. Heikinheimo, T. Tenkanen, K. Tuominen and V. Vaskonen, *The Dawn of FIMP Dark Matter: A Review of Models and Constraints*, Int. J. Mod. Phys. A **32** (2017) 1730023 [1706.07442].

[158] L. Parker, *Particle creation in expanding universes*, Phys. Rev. Lett. **21** (1968) 562.

[159] L. Parker, *Quantized fields and particle creation in expanding universes. 1.*, Phys. Rev. **183** (1969) 1057.

[160] L.H. Ford, *Gravitational Particle Creation and Inflation*, Phys. Rev. D **35** (1987) 2955.

[161] V. Kuzmin and I. Tkachev, *Ultrahigh-energy cosmic rays, superheavy long living particles, and matter creation after inflation*, JETP Lett. **68** (1998) 271 [hep-ph/9802304].

[162] D.J.H. Chung, E.W. Kolb and A. Riotto, *Production of massive particles during reheating*, Phys. Rev. D **60** (1999) 063504 [hep-ph/9809453].

[163] D.J.H. Chung, E.W. Kolb, A. Riotto and I.I. Tkachev, *Probing Planckian physics: Resonant production of particles during inflation and features in the primordial power spectrum*, Phys. Rev. D **62** (2000) 043508 [hep-ph/9910437].

[164] G.F. Giudice, I. Tkachev and A. Riotto, *Nonthermal production of dangerous relics in the early universe*, JHEP **08** (1999) 009 [hep-ph/9907510].

[165] R. Kallosh, L. Kofman, A.D. Linde and A. Van Proeyen, *Gravitino production after inflation*, Phys. Rev. D **61** (2000) 103503 [hep-th/9907124].

[166] G.F. Giudice, A. Riotto and I. Tkachev, *Thermal and nonthermal production of gravitinos in the early universe*, JHEP **11** (1999) 036 [hep-ph/9911302].

[167] D.J.H. Chung, L.L. Everett, H. Yoo and P. Zhou, *Gravitational Fermion Production in Inflationary Cosmology*, Phys. Lett. B **712** (2012) 147 [1109.2524].

[168] K. Dimopoulos, *Can a vector field be responsible for the curvature perturbation in the Universe?*, Phys. Rev. D **74** (2006) 083502 [hep-ph/0607229].

[169] P.W. Graham, J. Mardon and S. Rajendran, *Vector Dark Matter from Inflationary Fluctuations*, *Phys. Rev. D* **93** (2016) 103520 [1504.02102].

[170] T. Markkanen, A. Rajantie and T. Tenkanen, *Spectator Dark Matter*, *Phys. Rev. D* **98** (2018) 123532 [1811.02586].

[171] M. Fairbairn, K. Kainulainen, T. Markkanen and S. Nurmi, *Despicable Dark Relics: generated by gravity with unconstrained masses*, *JCAP* **04** (2019) 005 [1808.08236].

[172] Y. Ema, K. Nakayama and Y. Tang, *Production of Purely Gravitational Dark Matter*, *JHEP* **09** (2018) 135 [1804.07471].

[173] Y. Ema, K. Nakayama and Y. Tang, *Production of purely gravitational dark matter: the case of fermion and vector boson*, *JHEP* **07** (2019) 060 [1903.10973].

[174] Y. Ema, R. Jinno, K. Mukaida and K. Nakayama, *Gravitational Effects on Inflaton Decay*, *JCAP* **05** (2015) 038 [1502.02475].

[175] Y. Ema, R. Jinno, K. Mukaida and K. Nakayama, *Gravitational particle production in oscillating backgrounds and its cosmological implications*, *Phys. Rev. D* **94** (2016) 063517 [1604.08898].

[176] N. Bernal, A. Chatterjee and A. Paul, *Non-thermal production of Dark Matter after Inflation*, *JCAP* **12** (2018) 020 [1809.02338].

[177] T. Tenkanen, *Dark matter from scalar field fluctuations*, *Phys. Rev. Lett.* **123** (2019) 061302 [1905.01214].

[178] O. Lebedev, F. Smirnov, T. Solomko and J.-H. Yoon, *Dark matter production and reheating via direct inflaton couplings: collective effects*, *JCAP* **10** (2021) 032 [2107.06292].

[179] C. Cosme, J.a.G. Rosa and O. Bertolami, *Scalar field dark matter with spontaneous symmetry breaking and the* 3.5 *keV line*, *Phys. Lett. B* **781** (2018) 639 [1709.09674].

[180] C. Cosme, J.a.G. Rosa and O. Bertolami, *Scale-invariant scalar field dark matter through the Higgs portal*, *JHEP* **05** (2018) 129 [1802.09434].

[181] O. Lebedev, T. Solomko and J.-H. Yoon, *Dark matter production via a non-minimal coupling to gravity*, *JCAP* **02** (2023) 035 [2211.11773].

[182] N.F. Bell and R.R. Volkas, *Mirror matter and primordial black holes*, *Phys. Rev. D* **59** (1999) 107301 [astro-ph/9812301].

[183] T. Fujita, M. Kawasaki, K. Harigaya and R. Matsuda, *Baryon asymmetry, dark matter, and density perturbation from primordial black holes*, *Phys. Rev. D* **89** (2014) 103501 [1401.1909].

[184] I. Masina, *Dark matter and dark radiation from evaporating primordial black holes*, *Eur. Phys. J. Plus* **135** (2020) 552 [2004.04740].

[185] A. Cheek, L. Heurtier, Y.F. Perez-Gonzalez and J. Turner, *Primordial black hole evaporation and dark matter production. II. Interplay with the freeze-in or freeze-out mechanism*, *Phys. Rev. D* **105** (2022) 015023 [2107.00016].

[186] N. Arkani-Hamed and J. Maldacena, *Cosmological Collider Physics*, 1503.08043.

[187] L.-T. Wang and Z.-Z. Xianyu, *Gauge Boson Signals at the Cosmological Collider*, *JHEP* **11** (2020) 082 [2004.02887].

[188] E. Schrodinger, *The proper vibrations of the expanding universe*, *Physica* **6** (1939) 899.

[189] V.F. Mukhanov and G.V. Chibisov, *Quantum Fluctuations and a Nonsingular Universe*, *JETP Lett.* **33** (1981) 532.

[190] H. Kodama and M. Sasaki, *Cosmological Perturbation Theory*, *Prog. Theor. Phys. Suppl.* **78** (1984) 1.

[191] V.F. Mukhanov, *Quantum Theory of Gauge Invariant Cosmological Perturbations*, *Sov. Phys. JETP* **67** (1988) 1297.

[192] L.P. Grishchuk, *Amplification of gravitational waves in an istropic universe*, *Zh. Eksp. Teor. Fiz.* **67** (1974) 825.

[193] A.A. Starobinsky, *Spectrum of relict gravitational radiation and the early state of the universe*, *JETP Lett.* **30** (1979) 682.

[194] V.A. Rubakov, M.V. Sazhin and A.V. Veryaskin, *Graviton Creation in the Inflationary Universe and the Grand Unification Scale*, *Phys. Lett. B* **115** (1982) 189.

[195] R. Fabbri and M.d. Pollock, *The Effect of Primordially Produced Gravitons upon the Anisotropy of the Cosmological Microwave Background Radiation*, *Phys. Lett. B* **125** (1983) 445.

[196] E.W. Kolb and A.J. Long, *Superheavy dark matter through Higgs portal operators*, *Phys. Rev. D* **96** (2017) 103540 [1708.04293].

[197] N.D. Birrell and P.C.W. Davies, *Quantum Fields in Curved Space*, Cambridge Monographs on Mathematical Physics, Cambridge Univ. Press, Cambridge, UK (2, 1984), 10.1017/CBO9780511622632.

[198] V. Mukhanov and S. Winitzki, *Introduction to quantum effects in gravity*, Cambridge University Press (6, 2007).

[199] M. Garny, A. Palessandro, M. Sandora and M.S. Sloth, *Theory and Phenomenology of Planckian Interacting Massive Particles as Dark Matter*, *JCAP* **02** (2018) 027 [1709.09688].

[200] Y. Tang and Y.-L. Wu, *On Thermal Gravitational Contribution to Particle Production and Dark Matter*, *Phys. Lett. B* **774** (2017) 676 [1708.05138].

[201] Y. Mambrini and K.A. Olive, *Gravitational Production of Dark Matter during Reheating*, *Phys. Rev. D* **103** (2021) 115009 [2102.06214].

[202] M.R. Haque and D. Maity, *Gravitational dark matter: Free streaming and phase space distribution*, *Phys. Rev. D* **106** (2022) 023506 [2112.14668].

[203] S. Clery, Y. Mambrini, K.A. Olive and S. Verner, *Gravitational portals in the early Universe*, *Phys. Rev. D* **105** (2022) 075005 [2112.15214].

[204] M.R. Haque and D. Maity, *Gravitational Reheating*, 2201.02348.

[205] A.H. Guth, *The Inflationary Universe: A Possible Solution to the Horizon and Flatness Problems*, *Phys. Rev. D* **23** (1981) 347.

[206] A.A. Starobinsky, *A New Type of Isotropic Cosmological Models Without Singularity*, *Phys. Lett. B* **91** (1980) 99.

[207] A.D. Linde, *A New Inflationary Universe Scenario: A Possible Solution of the Horizon, Flatness, Homogeneity, Isotropy and Primordial Monopole Problems*, *Phys. Lett. B* **108** (1982) 389.

[208] A. Albrecht and P.J. Steinhardt, *Cosmology for Grand Unified Theories with Radiatively Induced Symmetry Breaking*, *Phys. Rev. Lett.* **48** (1982) 1220.

[209] D. Kazanas, *Dynamics of the Universe and Spontaneous Symmetry Breaking*, *Astrophys. J. Lett.* **241** (1980) L59.

[210] A.D. Linde, *Chaotic Inflation*, *Phys. Lett. B* **129** (1983) 177.

[211] A.D. Dolgov and A.D. Linde, *Baryon Asymmetry in Inflationary Universe*, *Phys. Lett. B* **116** (1982) 329.

[212] L.F. Abbott, E. Farhi and M.B. Wise, *Particle Production in the New Inflationary Cosmology*, *Phys. Lett. B* **117** (1982) 29.

[213] A. Albrecht, P.J. Steinhardt, M.S. Turner and F. Wilczek, *Reheating an Inflationary Universe*, *Phys. Rev. Lett.* **48** (1982) 1437.

[214] S. Hamdan and J. Unwin, *Dark Matter Freeze-out During Matter Domination*, *Mod. Phys. Lett. A* **33** (2018) 1850181 [1710.03758].

[215] M. Drees and F. Hajkarim, *Dark Matter Production in an Early Matter Dominated Era*, *JCAP* **02** (2018) 057 [1711.05007].

[216] L. Visinelli, *(Non-)thermal production of WIMPs during kination*, *Symmetry* **10** (2018) 546 [1710.11006].

[217] K. Dimopoulos and T. Markkanen, *Non-minimal gravitational reheating during kination*, *JCAP* **06** (2018) 021 [1803.07399].

[218] P. Arias, N. Bernal, A. Herrera and C. Maldonado, *Reconstructing Non-standard Cosmologies with Dark Matter*, *JCAP* **10** (2019) 047 [1906.04183].

[219] R. Allahverdi et al., *The First Three Seconds: a Review of Possible Expansion Histories of the Early Universe*, 2006.16182.

[220] S. Weinberg, *Gravitation and Cosmology: Principles and Applications of the General Theory of Relativity*, John Wiley and Sons, New York (1972).

[221] C.W. Misner, K.S. Thorne and J.A. Wheeler, *Gravitation*, W. H. Freeman, San Francisco (1973).

[222] E.W. Kolb and M.S. Turner, *The Early Universe*, vol. 69 (1990), 10.1201/9780429492860.

[223] S. Dodelson, *Modern Cosmology*, Academic Press, Amsterdam (2003).

[224] S.M. Carroll, *Spacetime and Geometry*, Cambridge University Press (7, 2019).

[225] V.F. Mukhanov and A. Vikman, *Enhancing the tensor-to-scalar ratio in simple inflation*, *JCAP* **02** (2006) 004 [astro-ph/0512066].

[226] D. Baumann, *Cosmology*, Cambridge University Press (7, 2022), 10.1017/9781108937092.

[227] D. Baumann, *Inflation*, in *Theoretical Advanced Study Institute in Elementary Particle Physics: Physics of the Large and the Small*, pp. 523–686, 2011, DOI [0907.5424].

[228] D. Baumann, *The physics of inflation*, 2011.

[229] D. Baumann, *Cosmology*, 2019.

[230] D. Tong, *Cosmology*, 2019.

[231] A. Friedmann, *On the Possibility of a world with constant negative curvature of space*, *Z. Phys.* **21** (1924) 326.

[232] G. Lemaitre, *A Homogeneous Universe of Constant Mass and Growing Radius Accounting for the Radial Velocity of Extragalactic Nebulae*, *Annales Soc. Sci. Bruxelles A* **47** (1927) 49.

[233] H.P. Robertson, *Kinematics and World-Structure*, *Astrophys. J.* **82** (1935) 284.

[234] A.G. Walker, *On the formal comparison of Milne's kinematical system with the systems of general relativity*, *Mon.Not.Roy.Astron.Soc..* **95** (1935) 263–269.

[235] A. Einstein, *The Field Equations of Gravitation*, *Sitzungsber. Preuss. Akad. Wiss. Berlin (Math. Phys.)* **1915** (1915) 844.

[236] A. Einstein, *Zur Allgemeinen Relativitätstheorie*, *Sitzungsber. Preuss. Akad. Wiss. Berlin (Math. Phys.)* **1915** (1915) 778.

[237] D. Hilbert, *Die Grundlagen der Physik. 1.*, *Gott. Nachr.* **27** (1915) 395.

[238] L.D. Landau and E.M. Lifschits, *The Classical Theory of Fields*, vol. Volume 2 of *Course of Theoretical Physics*, Pergamon Press, Oxford (1975).

[239] A. Raychaudhuri, *Relativistic cosmology. 1.*, *Phys. Rev.* **98** (1955) 1123.

[240] S.W. Hawking and R. Penrose, *The Singularities of gravitational collapse and cosmology*, *Proc. Roy. Soc. Lond. A* **314** (1970) 529.

[241] WMAP collaboration, *First year Wilkinson Microwave Anisotropy Probe (WMAP) observations: Determination of cosmological parameters*, *Astrophys. J. Suppl.* **148** (2003) 175 [astro-ph/0302209].

[242] WMAP collaboration, *Wilkinson Microwave Anisotropy Probe (WMAP) three year results: implications for cosmology*, *Astrophys. J. Suppl.* **170** (2007) 377 [astro-ph/0603449].

[243] WMAP collaboration, *Five-Year Wilkinson Microwave Anisotropy Probe (WMAP) Observations: Data Processing, Sky Maps, and Basic Results*, *Astrophys. J. Suppl.* **180** (2009) 225 [0803.0732].

[244] WMAP collaboration, *Seven-Year Wilkinson Microwave Anisotropy Probe (WMAP) Observations: Cosmological Interpretation*, *Astrophys. J. Suppl.* **192** (2011) 18 [1001.4538].

[245] Planck collaboration, *Planck 2013 results. I. Overview of products and scientific results*, *Astron. Astrophys.* **571** (2014) A1 [1303.5062].

[246] Planck collaboration, *Planck 2018 results. I. Overview and the cosmological legacy of Planck*, *Astron. Astrophys.* **641** (2020) A1 [1807.06205].

[247] A. Coc and E. Vangioni, *Primordial nucleosynthesis*, *Int. J. Mod. Phys. E* **26** (2017) 1741002 [1707.01004].

[248] SDSS collaboration, *Detection of the Baryon Acoustic Peak in the Large-Scale Correlation Function of SDSS Luminous Red Galaxies*, *Astrophys. J.* **633** (2005) 560 [astro-ph/0501171].

[249] 2dFGRS collaboration, *The 2dF Galaxy Redshift Survey: Power-spectrum analysis of the final dataset and cosmological implications*, *Mon. Not. Roy. Astron. Soc.* **362** (2005) 505 [astro-ph/0501174].

[250] F. Beutler, C. Blake, M. Colless, D.H. Jones, L. Staveley-Smith, L. Campbell et al., *The 6dF Galaxy Survey: Baryon Acoustic Oscillations and the Local Hubble Constant*, *Mon. Not. Roy. Astron. Soc.* **416** (2011) 3017 [1106.3366].

[251] C. Blake et al., *The WiggleZ Dark Energy Survey: mapping the distance-redshift relation with baryon acoustic oscillations*, *Mon. Not. Roy. Astron. Soc.* **418** (2011) 1707 [1108.2635].

[252] L. Anderson et al., *The clustering of galaxies in the SDSS-III Baryon Oscillation Spectroscopic Survey: Baryon Acoustic Oscillations in the Data Release 9 Spectroscopic Galaxy Sample*, *Mon. Not. Roy. Astron. Soc.* **427** (2013) 3435 [1203.6594].

[253] SDSS collaboration, *A MaxBCG Catalog of 13,823 Galaxy Clusters from the Sloan Digital Sky Survey*, *Astrophys. J.* **660** (2007) 239 [astro-ph/0701265].

[254] A. Vikhlinin et al., *Chandra Cluster Cosmology Project III: Cosmological Parameter Constraints*, *Astrophys. J.* **692** (2009) 1060 [0812.2720].

[255] Supernova Search Team collaboration, *Observational evidence from supernovae for an accelerating universe and a cosmological constant*, *Astron. J.* **116** (1998) 1009 [astro-ph/9805201].

[256] A.G. Riess et al., *BV RI light curves for 22 type Ia supernovae*, *Astron. J.* **117** (1999) 707 [astro-ph/9810291].

[257] Supernova Cosmology Project collaboration, *Measurements of Ω and Λ from 42 high redshift supernovae*, *Astrophys. J.* **517** (1999) 565 [astro-ph/9812133].

[258] SNLS collaboration, *The Supernova Legacy Survey: Measurement of Ω_M, Ω_Λ and $\sqsupseteq$ from the first year data set*, *Astron. Astrophys.* **447** (2006) 31 [astro-ph/0510447].

[259] Particle Data Group collaboration, *Review of Particle Physics*, *PTEP* **2020** (2020) 083C01.

[260] J. Soltis, S. Casertano and A.G. Riess, *The Parallax of ω Centauri Measured from Gaia EDR3 and a Direct, Geometric Calibration of the Tip of the Red Giant Branch and the Hubble Constant*, *Astrophys. J. Lett.* **908** (2021) L5 [2012.09196].

[261] S. Weinberg, *The Cosmological Constant Problem*, *Rev. Mod. Phys.* **61** (1989) 1.

[262] M. Li, X.-D. Li, S. Wang and Y. Wang, *Dark Energy*, *Commun. Theor. Phys.* **56** (2011) 525 [1103.5870].

[263] S. Weinberg, *Gauge and Global Symmetries at High Temperature*, *Phys. Rev. D* **9** (1974) 3357.

[264] L. Dolan and R. Jackiw, *Symmetry Behavior at Finite Temperature*, *Phys. Rev. D* **9** (1974) 3320.

[265] M. Dine, R.G. Leigh, P.Y. Huet, A.D. Linde and D.A. Linde, *Towards the theory of the electroweak phase transition*, *Phys. Rev. D* **46** (1992) 550 [hep-ph/9203203].

[266] K.A. Olive, *The Thermodynamics of the Quark - Hadron Phase Transition in the Early Universe*, *Nucl. Phys. B* **190** (1981) 483.

[267] E. Suhonen, *The Quark - Hadron Phase Transition in the Early Universe*, *Phys. Lett. B* **119** (1982) 81.

[268] J.H. Applegate and C.J. Hogan, *Relics of Cosmic Quark Condensation*, *Phys. Rev. D* **31** (1985) 3037.

[269] G.M. Fuller, G.J. Mathews and C.R. Alcock, *The Quark - Hadron Phase Transition in the Early Universe: Isothermal Baryon Number Fluctuations and Primordial Nucleosynthesis*, *Phys. Rev. D* **37** (1988) 1380.

[270] R.A. Alpher, H. Bethe and G. Gamow, *The origin of chemical elements*, *Phys. Rev.* **73** (1948) 803.

[271] R.V. Wagoner, W.A. Fowler and F. Hoyle, *On the Synthesis of elements at very high temperatures*, *Astrophys. J.* **148** (1967) 3.

[272] S. Sarkar, *Big bang nucleosynthesis and physics beyond the standard model*, *Rept. Prog. Phys.* **59** (1996) 1493 [hep-ph/9602260].

[273] D.N. Schramm and M.S. Turner, *Big Bang Nucleosynthesis Enters the Precision Era*, *Rev. Mod. Phys.* **70** (1998) 303 [astro-ph/9706069].

[274] A. Coc, E. Vangioni-Flam, P. Descouvemont, A. Adahchour and C. Angulo, *Updated Big Bang nucleosynthesis confronted to WMAP observations and to the abundance of light elements*, *Astrophys. J.* **600** (2004) 544 [astro-ph/0309480].

[275] G. Steigman, *Primordial Nucleosynthesis in the Precision Cosmology Era*, *Ann. Rev. Nucl. Part. Sci.* **57** (2007) 463 [0712.1100].

[276] F. Iocco, G. Mangano, G. Miele, O. Pisanti and P.D. Serpico, *Primordial Nucleosynthesis: from precision cosmology to fundamental physics*, *Phys. Rept.* **472** (2009) 1 [0809.0631].

[277] B.D. Fields, *The primordial lithium problem*, *Ann. Rev. Nucl. Part. Sci.* **61** (2011) 47 [1203.3551].

[278] J.E. Gunn and B.A. Peterson, *On the Density of Neutral Hydrogen in Intergalactic Space*, *Astrophys. J.* **142** (1965) 1633.

[279] SDSS collaboration, *Evidence for Reionization at $Z \sim 6$: Detection of a Gunn-Peterson trough in a $Z = 6.28$ Quasar*, *Astron. J.* **122** (2001) 2850 [astro-ph/0108097].

[280] R. Barkana and A. Loeb, *In the beginning: The First sources of light and the reionization of the Universe*, *Phys. Rept.* **349** (2001) 125 [astro-ph/0010468].

[281] W. Rindler, *Visual horizons in world-models*, *Mon. Not. Roy. Astron. Soc.* **116** (1956) 662.

[282] C.W. Misner, *The Isotropy of the universe*, *Astrophys. J.* **151** (1968) 431.

[283] V. Mukhanov, *Physical Foundations of Cosmology*, Cambridge University Press, Oxford (2005), 10.1017/CBO9780511790553.

[284] R. Dicke, *Gravitation and the Universe: The Jayne Lectures for 1969*, American Philosophical Institute, Philadelphia (1970).

[285] H. Georgi and S.L. Glashow, *Unity of All Elementary Particle Forces*, *Phys. Rev. Lett.* **32** (1974) 438.

[286] J.C. Pati and A. Salam, *Lepton Number as the Fourth Color*, *Phys. Rev. D* **10** (1974) 275.

[287] T.W.B. Kibble, *Topology of Cosmic Domains and Strings*, *J. Phys. A* **9** (1976) 1387.

[288] Y.B. Zeldovich and M.Y. Khlopov, *On the Concentration of Relic Magnetic Monopoles in the Universe*, *Phys. Lett. B* **79** (1978) 239.

[289] J. Preskill, *Cosmological Production of Superheavy Magnetic Monopoles*, *Phys. Rev. Lett.* **43** (1979) 1365.

[290] J. Martin, C. Ringeval and V. Vennin, *Encyclopædia Inflationaris*, *Phys. Dark Univ.* **5-6** (2014) 75 [1303.3787].

[291] A.H. Guth and S.Y. Pi, *Fluctuations in the New Inflationary Universe*, *Phys. Rev. Lett.* **49** (1982) 1110.

[292] A.A. Starobinsky, *Dynamics of Phase Transition in the New Inflationary Universe Scenario and Generation of Perturbations*, *Phys. Lett. B* **117** (1982) 175.

[293] S.W. Hawking, *The Development of Irregularities in a Single Bubble Inflationary Universe*, *Phys. Lett. B* **115** (1982) 295.

[294] J.M. Bardeen, P.J. Steinhardt and M.S. Turner, *Spontaneous Creation of Almost Scale - Free Density Perturbations in an Inflationary Universe*, *Phys. Rev. D* **28** (1983) 679.

[295] V.F. Mukhanov, H.A. Feldman and R.H. Brandenberger, *Theory of cosmological perturbations. Part 1. Classical perturbations. Part 2. Quantum theory of perturbations. Part 3. Extensions*, *Phys. Rept.* **215** (1992) 203.

[296] E.J. Copeland, E.W. Kolb, A.R. Liddle and J.E. Lidsey, *Reconstructing the inflation potential, in principle and in practice*, *Phys. Rev. D* **48** (1993) 2529 [hep-ph/9303288].

[297] A.R. Liddle, P. Parsons and J.D. Barrow, *Formalizing the slow roll approximation in inflation*, *Phys. Rev. D* **50** (1994) 7222 [astro-ph/9408015].

[298] J. Ellis, M.A.G. Garcia, D.V. Nanopoulos and K.A. Olive, *Calculations of Inflaton Decays and Reheating: with Applications to No-Scale Inflation Models*, *JCAP* **07** (2015) 050 [1505.06986].

[299] M.A.G. Garcia, K. Kaneta, Y. Mambrini and K.A. Olive, *Inflaton Oscillations and Post-Inflationary Reheating*, *JCAP* **04** (2021) 012 [2012.10756].

[300] K. Ichikawa, T. Suyama, T. Takahashi and M. Yamaguchi, *Non-Gaussianity, Spectral Index and Tensor Modes in Mixed Inflaton and Curvaton Models*, *Phys. Rev. D* **78** (2008) 023513 [0802.4138].

[301] J.M. Bardeen, *Gauge Invariant Cosmological Perturbations*, *Phys. Rev. D* **22** (1980) 1882.

[302] Planck collaboration, *Planck 2018 results. X. Constraints on inflation*, *Astron. Astrophys.* **641** (2020) A10 [1807.06211].

[303] BICEP, Keck collaboration, *Improved Constraints on Primordial Gravitational Waves using Planck, WMAP, and BICEP/Keck Observations through the 2018 Observing Season*, *Phys. Rev. Lett.* **127** (2021) 151301 [2110.00483].

[304] M. Tristram et al., *Improved limits on the tensor-to-scalar ratio using BICEP and Planck data*, *Phys. Rev. D* **105** (2022) 083524 [2112.07961].

[305] D.H. Lyth and A. Riotto, *Particle physics models of inflation and the cosmological density perturbation*, *Phys. Rept.* **314** (1999) 1 [hep-ph/9807278].

[306] D. Baumann and L. McAllister, *Inflation and String Theory*, Cambridge Monographs on Mathematical Physics, Cambridge University Press (5, 2015), 10.1017/CBO9781316105733, [1404.2601].

[307] C.T. Byrnes and D. Wands, *Curvature and isocurvature perturbations from two-field inflation in a slow-roll expansion*, *Phys. Rev. D* **74** (2006) 043529 [astro-ph/0605679].

[308] C.M. Peterson and M. Tegmark, *Testing Two-Field Inflation*, *Phys. Rev. D* **83** (2011) 023522 [1005.4056].

[309] J.M. Cline, *String Cosmology*, in *Les Houches Summer School - Session 86: Particle Physics and Cosmology: The Fabric of Spacetime*, 12, 2006 [hep-th/0612129].

[310] L. Senatore and M. Zaldarriaga, *The Effective Field Theory of Multifield Inflation*, *JHEP* **04** (2012) 024 [1009.2093].

[311] Q. Shafi and V.N. Senoguz, *Coleman-Weinberg potential in good agreement with wmap*, *Phys. Rev. D* **73** (2006) 127301 [astro-ph/0603830].

[312] E. Silverstein and A. Westphal, *Monodromy in the CMB: Gravity Waves and String Inflation*, *Phys. Rev. D* **78** (2008) 106003 [0803.3085].

[313] E.J. Copeland, A.R. Liddle, D.H. Lyth, E.D. Stewart and D. Wands, *False vacuum inflation with Einstein gravity*, *Phys. Rev. D* **49** (1994) 6410 [astro-ph/9401011].

[314] A.D. Linde, *Axions in inflationary cosmology*, *Phys. Lett. B* **259** (1991) 38.

[315] F.L. Bezrukov and M. Shaposhnikov, *The Standard Model Higgs boson as the inflaton*, *Phys. Lett. B* **659** (2008) 703 [0710.3755].

[316] C.P. Burgess, H.M. Lee and M. Trott, *Power-counting and the Validity of the Classical Approximation During Inflation*, *JHEP* **09** (2009) 103 [0902.4465].

[317] J.L.F. Barbon and J.R. Espinosa, *On the Naturalness of Higgs Inflation*, *Phys. Rev. D* **79** (2009) 081302 [0903.0355].

[318] G.F. Giudice and H.M. Lee, *Unitarizing Higgs Inflation*, *Phys. Lett. B* **694** (2011) 294 [1010.1417].

[319] J.L.F. Barbon, J.A. Casas, J. Elias-Miro and J.R. Espinosa, *Higgs Inflation as a Mirage*, *JHEP* **09** (2015) 027 [1501.02231].

[320] C. Armendariz-Picon, T. Damour and V.F. Mukhanov, *k - inflation*, *Phys. Lett. B* **458** (1999) 209 [hep-th/9904075].

[321] J. Garriga and V.F. Mukhanov, *Perturbations in k-inflation*, *Phys. Lett. B* **458** (1999) 219 [hep-th/9904176].

[322] D.S. Salopek, J.R. Bond and J.M. Bardeen, *Designing Density Fluctuation Spectra in Inflation*, *Phys. Rev. D* **40** (1989) 1753.

[323] R. Kallosh and A. Linde, *Universality Class in Conformal Inflation*, *JCAP* **07** (2013) 002 [1306.5220].

[324] R. Kallosh and A. Linde, *Multi-field Conformal Cosmological Attractors*, *JCAP* **12** (2013) 006 [1309.2015].

[325] S. Ferrara, R. Kallosh, A. Linde and M. Porrati, *Minimal Supergravity Models of Inflation*, *Phys. Rev. D* **88** (2013) 085038 [1307.7696].

[326] R. Kallosh and A. Linde, *Superconformal generalization of the chaotic inflation model $\frac{\lambda}{4}\phi^4 - \frac{\xi}{2}\phi^2 R$*, *JCAP* **06** (2013) 027 [1306.3211].

[327] R. Kallosh and A. Linde, *Superconformal generalizations of the Starobinsky model*, *JCAP* **06** (2013) 028 [1306.3214].

[328] R. Kallosh and A. Linde, *Non-minimal Inflationary Attractors*, *JCAP* **10** (2013) 033 [1307.7938].

[329] R. Kallosh, A. Linde and D. Roest, *Universal Attractor for Inflation at Strong Coupling*, *Phys. Rev. Lett.* **112** (2014) 011303 [1310.3950].

[330] R. Kallosh, A. Linde and D. Roest, *Superconformal Inflationary α-Attractors*, *JHEP* **11** (2013) 198 [1311.0472].

[331] B.R. Greene, T. Prokopec and T.G. Roos, *Inflaton decay and heavy particle production with negative coupling*, *Phys. Rev. D* **56** (1997) 6484 [hep-ph/9705357].

[332] N. Shuhmaher and R. Brandenberger, *Non-perturbative instabilities as a solution of the cosmological moduli problem*, *Phys. Rev. D* **73** (2006) 043519 [hep-th/0507103].

[333] J.F. Dufaux, G.N. Felder, L. Kofman, M. Peloso and D. Podolsky, *Preheating with trilinear interactions: Tachyonic resonance*, *JCAP* **07** (2006) 006 [hep-ph/0602144].

[334] A.A. Abolhasani, H. Firouzjahi and M.M. Sheikh-Jabbari, *Tachyonic Resonance Preheating in Expanding Universe*, *Phys. Rev. D* **81** (2010) 043524 [0912.1021].

[335] G.N. Felder, J. Garcia-Bellido, P.B. Greene, L. Kofman, A.D. Linde and I. Tkachev, *Dynamics of symmetry breaking and tachyonic preheating*, *Phys. Rev. Lett.* **87** (2001) 011601 [hep-ph/0012142].

[336] G.N. Felder, L. Kofman and A.D. Linde, *Tachyonic instability and dynamics of spontaneous symmetry breaking*, *Phys. Rev. D* **64** (2001) 123517 [hep-th/0106179].

[337] G.F. Giudice, E.W. Kolb and A. Riotto, *Largest temperature of the radiation era and its cosmological implications*, *Phys. Rev. D* **64** (2001) 023508 [hep-ph/0005123].

[338] M.A.G. Garcia, Y. Mambrini, K.A. Olive and M. Peloso, *Enhancement of the Dark Matter Abundance Before Reheating: Applications to Gravitino Dark Matter*, *Phys. Rev. D* **96** (2017) 103510 [1709.01549].

[339] S.-L. Chen and Z. Kang, *On UltraViolet Freeze-in Dark Matter during Reheating*, *JCAP* **05** (2018) 036 [1711.02556].

[340] N. Bernal, F. Elahi, C. Maldonado and J. Unwin, *Ultraviolet Freeze-in and Non-Standard Cosmologies*, *JCAP* **11** (2019) 026 [1909.07992].

[341] M.A.G. Garcia, K. Kaneta, Y. Mambrini and K.A. Olive, *Reheating and Post-inflationary Production of Dark Matter*, *Phys. Rev. D* **101** (2020) 123507 [2004.08404].

[342] K. Harigaya and K. Mukaida, *Thermalization after/during Reheating*, *JHEP* **05** (2014) 006 [1312.3097].

[343] S. Davidson and S. Sarkar, *Thermalization after inflation*, *JHEP* **11** (2000) 012 [hep-ph/0009078].

[344] K. Harigaya, M. Kawasaki, K. Mukaida and M. Yamada, *Dark Matter Production in Late Time Reheating*, *Phys. Rev. D* **89** (2014) 083532 [1402.2846].

[345] K. Mukaida and M. Yamada, *Thermalization Process after Inflation and Effective Potential of Scalar Field*, *JCAP* **02** (2016) 003 [1506.07661].

[346] M.A.G. Garcia and M.A. Amin, *Prethermalization production of dark matter*, *Phys. Rev. D* **98** (2018) 103504 [1806.01865].

[347] K. Harigaya, K. Mukaida and M. Yamada, *Dark Matter Production during the Thermalization Era*, *JHEP* **07** (2019) 059 [1901.11027].

[348] R.M. Corless, G.H. Gonnet, D.E.G. Hare, D.J. Jeffrey and D.E. Knuth, *On the LambertW function*, *Adv. Comput. Math.* **5** (1996) 329.

[349] S. Clery, Y. Mambrini, K.A. Olive, A. Shkerin and S. Verner, *Gravitational portals with nonminimal couplings*, *Phys. Rev. D* **105** (2022) 095042 [2203.02004].

[350] B. Barman, S. Cléry, R.T. Co, Y. Mambrini and K.A. Olive, *Gravity as a portal to reheating, leptogenesis and dark matter*, *JHEP* **12** (2022) 072 [2210.05716].

[351] M. Atkins and X. Calmet, *Bounds on the Nonminimal Coupling of the Higgs Boson to Gravity*, *Phys. Rev. Lett.* **110** (2013) 051301 [1211.0281].

[352] Z.-Z. Xianyu, J. Ren and H.-J. He, *Gravitational Interaction of Higgs Boson and Weak Boson Scattering*, *Phys. Rev. D* **88** (2013) 096013 [1305.0251].

[353] J.R. Espinosa, G.F. Giudice and A. Riotto, *Cosmological implications of the Higgs mass measurement*, *JCAP* **05** (2008) 002 [0710.2484].

[354] M. Herranen, T. Markkanen, S. Nurmi and A. Rajantie, *Spacetime curvature and the Higgs stability during inflation*, *Phys. Rev. Lett.* **113** (2014) 211102 [1407.3141].

[355] T. Markkanen, S. Nurmi, A. Rajantie and S. Stopyra, *The 1-loop effective potential for the Standard Model in curved spacetime*, *JHEP* **06** (2018) 040 [1804.02020].

[356] R.T. Co, Y. Mambrini and K.A. Olive, *Inflationary Gravitational Leptogenesis*, 2205.01689.

[357] M. Kawasaki and T. Moroi, *Gravitino production in the inflationary universe and the effects on big bang nucleosynthesis*, *Prog. Theor. Phys.* **93** (1995) 879 [hep-ph/9403364].

[358] M. Kawasaki, K. Kohri and N. Sugiyama, *MeV scale reheating temperature and thermalization of neutrino background*, *Phys. Rev. D* **62** (2000) 023506 [astro-ph/0002127].

[359] S. Hannestad, *What is the lowest possible reheating temperature?*, *Phys. Rev. D* **70** (2004) 043506 [astro-ph/0403291].

[360] F. De Bernardis, L. Pagano and A. Melchiorri, *New constraints on the reheating temperature of the universe after WMAP-5*, *Astropart. Phys.* **30** (2008) 192.

[361] P.F. de Salas, M. Lattanzi, G. Mangano, G. Miele, S. Pastor and O. Pisanti, *Bounds on very low reheating scenarios after Planck*, *Phys. Rev. D* **92** (2015) 123534 [1511.00672].

[362] T. Hasegawa, N. Hiroshima, K. Kohri, R.S.L. Hansen, T. Tram and S. Hannestad, *MeV-scale reheating temperature and thermalization of oscillating neutrinos by radiative and hadronic decays of massive particles*, *JCAP* **12** (2019) 012 [1908.10189].

[363] J.R. Espinosa, G.F. Giudice, E. Morgante, A. Riotto, L. Senatore, A. Strumia et al., *The cosmological Higgstory of the vacuum instability*, *JHEP* **09** (2015) 174 [1505.04825].

[364] M. Giovannini, *Gravitational waves constraints on postinflationary phases stiffer than radiation*, *Phys. Rev. D* **58** (1998) 083504 [hep-ph/9806329].

[365] M. Giovannini, *Production and detection of relic gravitons in quintessential inflationary models*, *Phys. Rev. D* **60** (1999) 123511 [astro-ph/9903004].

[366] A. Riazuelo and J.-P. Uzan, *Quintessence and gravitational waves*, *Phys. Rev. D* **62** (2000) 083506 [astro-ph/0004156].

[367] N. Seto and J. Yokoyama, *Probing the equation of state of the early universe with a space laser interferometer*, *J. Phys. Soc. Jap.* **72** (2003) 3082 [gr-qc/0305096].

[368] L.A. Boyle and A. Buonanno, *Relating gravitational wave constraints from primordial nucleosynthesis, pulsar timing, laser interferometers, and the CMB: Implications for the early Universe*, *Phys. Rev. D* **78** (2008) 043531 [0708.2279].

[369] A. Stewart and R. Brandenberger, *Observational Constraints on Theories with a Blue Spectrum of Tensor Modes*, *JCAP* **08** (2008) 012 [0711.4602].

[370] B. Li and P.R. Shapiro, *Precision cosmology and the stiff-amplified gravitational-wave background from inflation: NANOGrav, Advanced LIGO-Virgo and the Hubble tension*, *JCAP* **10** (2021) 024 [2107.12229].

[371] M. Artymowski, O. Czerwinska, Z. Lalak and M. Lewicki, *Gravitational wave signals and cosmological consequences of gravitational reheating*, *JCAP* **04** (2018) 046 [1711.08473].

[372] C. Caprini and D.G. Figueroa, *Cosmological Backgrounds of Gravitational Waves*, *Class. Quant. Grav.* **35** (2018) 163001 [1801.04268].

[373] D. Bettoni, G. Domènech and J. Rubio, *Gravitational waves from global cosmic strings in quintessential inflation*, *JCAP* **02** (2019) 034 [1810.11117].

[374] D.G. Figueroa and E.H. Tanin, *Ability of LIGO and LISA to probe the equation of state of the early Universe*, *JCAP* **08** (2019) 011 [1905.11960].

[375] T. Opferkuch, P. Schwaller and B.A. Stefanek, *Ricci Reheating*, *JCAP* **07** (2019) 016 [1905.06823].

[376] N. Bernal, A. Ghoshal, F. Hajkarim and G. Lambiase, *Primordial Gravitational Wave Signals in Modified Cosmologies*, 2008.04959.

[377] R. Caldwell et al., *Detection of early-universe gravitational-wave signatures and fundamental physics*, *Gen. Rel. Grav.* **54** (2022) 156 [2203.07972].

[378] Y. Gouttenoire, G. Servant and P. Simakachorn, *Kination cosmology from scalar fields and gravitational-wave signatures*, 2111.01150.

[379] M. Maggiore, *Gravitational Waves. Vol. 2: Astrophysics and Cosmology*, Oxford University Press (3, 2018).

[380] Y. Watanabe and E. Komatsu, *Improved Calculation of the Primordial Gravitational Wave Spectrum in the Standard Model*, *Phys. Rev. D* **73** (2006) 123515 [astro-ph/0604176].

[381] K. Saikawa and S. Shirai, *Primordial gravitational waves, precisely: The role of thermodynamics in the Standard Model*, *JCAP* **05** (2018) 035 [1803.01038].

[382] M. Maggiore, *Gravitational Waves. Vol. 1: Theory and Experiments*, Oxford University Press (2007), 10.1093/acprof:oso/9780198570745.001.0001.

[383] M. Maggiore, *Gravitational wave experiments and early universe cosmology*, *Phys. Rept.* **331** (2000) 283 [gr-qc/9909001].

[384] L.A. Boyle and P.J. Steinhardt, *Probing the early universe with inflationary gravitational waves*, *Phys. Rev. D* **77** (2008) 063504 [astro-ph/0512014].

[385] S. Kuroyanagi, T. Chiba and N. Sugiyama, *Precision calculations of the gravitational wave background spectrum from inflation*, *Phys. Rev. D* **79** (2009) 103501 [0804.3249].

[386] G. Choi, R. Jinno and T.T. Yanagida, *Probing PeV scale SUSY breaking with satellite galaxies and primordial gravitational waves*, *Phys. Rev. D* **104** (2021) 095018 [2107.12804].

[387] D.G. Figueroa and E.H. Tanin, *Inconsistency of an inflationary sector coupled only to Einstein gravity*, *JCAP* **10** (2019) 050 [1811.04093].

[388] S. Dodelson and M.S. Turner, *Nonequilibrium neutrino statistical mechanics in the expanding universe*, *Phys. Rev. D* **46** (1992) 3372.

[389] S. Hannestad and J. Madsen, *Neutrino decoupling in the early universe*, *Phys. Rev. D* **52** (1995) 1764 [astro-ph/9506015].

[390] A.D. Dolgov, S.H. Hansen and D.V. Semikoz, *Nonequilibrium corrections to the spectra of massless neutrinos in the early universe*, *Nucl. Phys. B* **503** (1997) 426 [hep-ph/9703315].

[391] G. Mangano, G. Miele, S. Pastor, T. Pinto, O. Pisanti and P.D. Serpico, *Relic neutrino decoupling including flavor oscillations*, *Nucl. Phys. B* **729** (2005) 221 [hep-ph/0506164].

[392] P.F. de Salas and S. Pastor, *Relic neutrino decoupling with flavour oscillations revisited*, *JCAP* **07** (2016) 051 [1606.06986].

[393] M. Escudero Abenza, *Precision early universe thermodynamics made simple: $N_{\rm eff}$ and neutrino decoupling in the Standard Model and beyond*, *JCAP* **05** (2020) 048 [2001.04466].

[394] K. Akita and M. Yamaguchi, *A precision calculation of relic neutrino decoupling*, *JCAP* **08** (2020) 012 [2005.07047].

[395] J. Froustey, C. Pitrou and M.C. Volpe, *Neutrino decoupling including flavour oscillations and primordial nucleosynthesis*, *JCAP* **12** (2020) 015 [2008.01074].

[396] J.J. Bennett, G. Buldgen, P.F. De Salas, M. Drewes, S. Gariazzo, S. Pastor et al., *Towards a precision calculation of $N_{\rm eff}$ in the Standard Model II: Neutrino decoupling in the presence of flavour oscillations and finite-temperature QED*, *JCAP* **04** (2021) 073 [2012.02726].

[397] S. Kuroyanagi, T. Takahashi and S. Yokoyama, *Blue-tilted Tensor Spectrum and Thermal History of the Universe*, *JCAP* **02** (2015) 003 [1407.4785].

[398] T.-H. Yeh, J. Shelton, K.A. Olive and B.D. Fields, *Probing physics beyond the standard model: limits from BBN and the CMB independently and combined*, *JCAP* **10** (2022) 046 [2207.13133].

[399] K. Abazajian et al., *CMB-S4 Science Case, Reference Design, and Project Plan*, 1907.04473.

[400] CMB-HD collaboration, *Snowmass2021 CMB-HD White Paper*, 2203.05728.

[401] COrE collaboration, *COrE (Cosmic Origins Explorer) A White Paper*, 1102.2181.

[402] EUCLID collaboration, *Euclid Definition Study Report*, 1110.3193.

[403] K. Schmitz, *New Sensitivity Curves for Gravitational-Wave Experiments*, 2002.04615.

[404] LIGO Scientific, Virgo collaboration, *Observation of Gravitational Waves from a Binary Black Hole Merger*, *Phys. Rev. Lett.* **116** (2016) 061102 [1602.03837].

[405] LIGO Scientific, Virgo collaboration, *GW151226: Observation of Gravitational Waves from a 22-Solar-Mass Binary Black Hole Coalescence*, *Phys. Rev. Lett.* **116** (2016) 241103 [1606.04855].

[406] LIGO Scientific, VIRGO collaboration, *GW170104: Observation of a 50-Solar-Mass Binary Black Hole Coalescence at Redshift 0.2*, *Phys. Rev. Lett.* **118** (2017) 221101 [1706.01812].

[407] LIGO Scientific, Virgo collaboration, *GW170608: Observation of a 19-solar-mass Binary Black Hole Coalescence*, *Astrophys. J. Lett.* **851** (2017) L35 [1711.05578].

[408] LIGO Scientific, Virgo collaboration, *GW170814: A Three-Detector Observation of Gravitational Waves from a Binary Black Hole Coalescence*, *Phys. Rev. Lett.* **119** (2017) 141101 [1709.09660].

[409] LIGO Scientific, Virgo collaboration, *GW170817: Observation of Gravitational Waves from a Binary Neutron Star Inspiral*, *Phys. Rev. Lett.* **119** (2017) 161101 [1710.05832].

[410] LISA collaboration, *Laser Interferometer Space Antenna*, *arXiv e-prints* (2017) arXiv:1702.00786 [1702.00786].

[411] J. Baker et al., *The Laser Interferometer Space Antenna: Unveiling the Millihertz Gravitational Wave Sky*, 1907.06482.

[412] LIGO Scientific collaboration, *Exploring the Sensitivity of Next Generation Gravitational Wave Detectors*, *Class. Quant. Grav.* **34** (2017) 044001 [1607.08697].

[413] D. Reitze et al., *Cosmic Explorer: The U.S. Contribution to Gravitational-Wave Astronomy beyond LIGO*, *Bull. Am. Astron. Soc.* **51** (2019) 035 [1907.04833].

[414] M. Punturo et al., *The Einstein Telescope: A third-generation gravitational wave observatory*, *Class. Quant. Grav.* **27** (2010) 194002.

[415] S. Hild et al., *Sensitivity Studies for Third-Generation Gravitational Wave Observatories*, *Class. Quant. Grav.* **28** (2011) 094013 [1012.0908].

[416] J. Crowder and N.J. Cornish, *Beyond LISA: Exploring future gravitational wave missions*, *Phys. Rev. D* **72** (2005) 083005 [gr-qc/0506015].

[417] V. Corbin and N.J. Cornish, *Detecting the cosmic gravitational wave background with the big bang observer*, *Class. Quant. Grav.* **23** (2006) 2435 [gr-qc/0512039].

[418] N. Seto, S. Kawamura and T. Nakamura, *Possibility of direct measurement of the acceleration of the universe using 0.1-Hz band laser interferometer gravitational wave antenna in space*, *Phys. Rev. Lett.* **87** (2001) 221103 [astro-ph/0108011].

[419] H. Kudoh, A. Taruya, T. Hiramatsu and Y. Himemoto, *Detecting a gravitational-wave background with next-generation space interferometers*, *Phys. Rev. D* **73** (2006) 064006 [gr-qc/0511145].

[420] K. Nakayama and J. Yokoyama, *Gravitational Wave Background and Non-Gaussianity as a Probe of the Curvaton Scenario*, *JCAP* **01** (2010) 010 [0910.0715].

[421] K. Yagi and N. Seto, *Detector configuration of DECIGO/BBO and identification of cosmological neutron-star binaries*, *Phys. Rev. D* **83** (2011) 044011 [1101.3940].

[422] S. Kawamura et al., *Current status of space gravitational wave antenna DECIGO and B-DECIGO*, *PTEP* **2021** (2021) 05A105 [2006.13545].

[423] A. Sesana et al., *Unveiling the gravitational universe at μ-Hz frequencies*, *Exper. Astron.* **51** (2021) 1333 [1908.11391].

[424] A. Vallenari, *The future of astrometry in space*, *Frontiers in Astronomy and Space Sciences* **5** (2018) .

[425] AEDGE collaboration, *AEDGE: Atomic Experiment for Dark Matter and Gravity Exploration in Space*, *EPJ Quant. Technol.* **7** (2020) 6 [1908.00802].

[426] L. Badurina, O. Buchmueller, J. Ellis, M. Lewicki, C. McCabe and V. Vaskonen, *Prospective sensitivities of atom interferometers to gravitational waves and ultralight dark matter*, *Phil. Trans. A. Math. Phys. Eng. Sci.* **380** (2021) 20210060 [2108.02468].

[427] P.W. Graham, J.M. Hogan, M.A. Kasevich and S. Rajendran, *Resonant mode for gravitational wave detectors based on atom interferometry*, *Phys. Rev. D* **94** (2016) 104022 [1606.01860].

[428] MAGIS collaboration, *Mid-band gravitational wave detection with precision atomic sensors*, 1711.02225.

[429] L. Badurina et al., *AION: An Atom Interferometer Observatory and Network*, *JCAP* **05** (2020) 011 [1911.11755].

[430] L. de Broglie, *Black radiation and light quantum*, *J. Phys. Radium* **3** (1922) 422.

[431] A. Proca, *Sur la theorie ondulatoire des electrons positifs et negatifs*, J. Phys. Radium **7** (1936) 347.

[432] H. Ruegg and M. Ruiz-Altaba, *The Stueckelberg field*, Int. J. Mod. Phys. A **19** (2004) 3265 [hep-th/0304245].

[433] H. van Hees, *The Renormalizability for massive Abelian gauge field theories revisited*, hep-th/0305076.

[434] M. Duch, B. Grzadkowski and J. Wudka, *Classification of effective operators for interactions between the Standard Model and dark matter*, JHEP **05** (2015) 116 [1412.0520].

[435] E.W. Kolb and A.J. Long, *Completely dark photons from gravitational particle production during the inflationary era*, JHEP **03** (2021) 283 [2009.03828].

[436] K. Nakayama, *Vector Coherent Oscillation Dark Matter*, JCAP **10** (2019) 019 [1907.06243].

[437] J.A. Dror, K. Harigaya and V. Narayan, *Parametric Resonance Production of Ultralight Vector Dark Matter*, Phys. Rev. D **99** (2019) 035036 [1810.07195].

[438] P. Agrawal, N. Kitajima, M. Reece, T. Sekiguchi and F. Takahashi, *Relic Abundance of Dark Photon Dark Matter*, Phys. Lett. B **801** (2020) 135136 [1810.07188].

[439] R.T. Co, A. Pierce, Z. Zhang and Y. Zhao, *Dark Photon Dark Matter Produced by Axion Oscillations*, Phys. Rev. D **99** (2019) 075002 [1810.07196].

[440] M. Bastero-Gil, J. Santiago, L. Ubaldi and R. Vega-Morales, *Vector dark matter production at the end of inflation*, JCAP **04** (2019) 015 [1810.07208].

[441] M. Bastero-Gil, J. Santiago, R. Vega-Morales and L. Ubaldi, *Dark photon dark matter from a rolling inflaton*, JCAP **02** (2022) 015 [2103.12145].

[442] E. Pajer and M. Peloso, *A review of Axion Inflation in the era of Planck*, Class. Quant. Grav. **30** (2013) 214002 [1305.3557].

[443] A.E. Nelson and J. Scholtz, *Dark Light, Dark Matter and the Misalignment Mechanism*, Phys. Rev. D **84** (2011) 103501 [1105.2812].

[444] P. Arias, D. Cadamuro, M. Goodsell, J. Jaeckel, J. Redondo and A. Ringwald, *WISPy Cold Dark Matter*, JCAP **06** (2012) 013 [1201.5902].

[445] G. Alonso-Álvarez, T. Hugle and J. Jaeckel, *Misalignment \& Co.: (Pseudo-)scalar and vector dark matter with curvature couplings*, JCAP **02** (2020) 014 [1905.09836].

[446] K. Kaneta, S.M. Lee and K.-y. Oda, *Boltzmann or Bogoliubov? Approaches Compared in Gravitational Particle Production*, 2206.10929.

[447] G.B. Gelmini and P. Gondolo, *Neutralino with the right cold dark matter abundance in (almost) any supersymmetric model*, Phys. Rev. D **74** (2006) 023510 [hep-ph/0602230].

[448] O. Lebedev and J.-H. Yoon, *Challenges for inflaton dark matter*, Phys. Lett. B **821** (2021) 136614 [2105.05860].

[449] O. Lebedev, *Scalar overproduction in standard cosmology and predictivity of non-thermal dark matter*, JCAP **02** (2023) 032 [2210.02293].

[450] B. Carr, T. Tenkanen and V. Vaskonen, *Primordial black holes from inflaton and spectator field perturbations in a matter-dominated era*, Phys. Rev. D **96** (2017) 063507 [1706.03746].

[451] S.R. De Groot, *Relativistic Kinetic Theory. Principles and Applications* (1980).

[452] J. Bernstein, L.S. Brown and G. Feinberg, *The Cosmological Heavy Neutrino Problem Revisited*, Phys. Rev. D **32** (1985) 3261.

[453] J. Bernstein, *KINETIC THEORY IN THE EXPANDING UNIVERSE*, Cambridge Monographs on Mathematical Physics, Cambridge University Press, Cambridge, U.K. (1988), 10.1017/CBO9780511564185.

[454] P. Gondolo and G. Gelmini, *Cosmic abundances of stable particles: Improved analysis*, Nucl. Phys. B **360** (1991) 145.